Techi

1. Report No.	2. Government Accession No.	3. Recipients
FHWA/TX-92+1209-2F		

4. Title and Subtitle
ENHANCING THE STRENGTH AND DUCTILITY OF POST-TENSIONED SEGMENTAL BOX-GIRDER BRIDGES

5. Report Date
April 1991

6. Performing Organization Code

7. Author(s)
A. N. A. Hindi, M. E. Kreger, and J. E. Breen

8. Performing Organization Report No.
Research Report 1209-2F

9. Performing Organization Name and Address
Center for Transportation Research
The University of Texas at Austin
Austin, Texas 78712-1075

10. Work Unit No. (TRAIS)

11. Contract or Grant No.
Research Study 3-5-89/0-1209

12. Sponsoring Agency Name and Address
Texas State Department of Highways and Public Transportation; Transportation Planning Division
P. O. Box 5051
Austin, Texas 78763-5051

13. Type of Report and Period Covered
Final

14. Sponsoring Agency Code

15. Supplementary Notes
Study conducted in cooperation with the U. S. Department of Transportation, Federal Highway Administration. Research Study Title: "Effect of Improved Bonding of External Tendons and the Use of Supplemental Continuous Bonded Tendons in External Post-Tensioned Bridges"

16. Abstract

An investigation was conducted to determine the effect of using external tendons, discretely bonded at intermediate diaphragms, and supplemental, grouted internal tendons on the strength and ductility of post-tensioned segmental box-girder bridges. In the current research program, additional experimental testing, performed on an existing three-span bridge model that was constructed and tested during an earlier study, and an analytical study were performed to examine the influence of improved bonding of external tendons and supplemental internal tendons on the behavior of segmental box-girder bridges.

Both the experimental and the analytical portion of the study were carried out in three phases. Results of the tests and computer model indicated that both discrete bonding of external tendons and use of supplemental, grouted internal tendons improved the strength and ductility of segmental box girder construction. Design recommendations for predicting the ultimate external tendon stress and for enhancing the strength and ductility of segmental box girder construction are presented in this report.

17. Key Words	18. Distribution Statement
external tendons, bonded, internal tendons, bonded, grouted, strength, ductility, post-tensioned segmental box-girder bridges, diaphragms, flexural tests, analytical model	No restrictions. This document is available to the public through the National Technical Information Service, Springfield, Virginia 22161.

19 Security Classif. (of this report)	20. Security Classif. (of this page)	21. No. of Pages	22. Price
Unclassified	Unclassified	378	

Form DOT F 1700.7 (8-72) Reproduction of completed page authorized

ENHANCING THE STRENGTH AND DUCTILITY OF POST-TENSIONED SEGMENTAL BOX-GIRDER BRIDGES

by

A.N.A. Hindi, M.E. Kreger and J.E. Breen

Research Report No. 1209-2F
Research Project 3-5-89-/0-1209

"Effect of Improved Bonding of External Tendons and the Use of Supplemental Continuous Bonded Tendons in External Post-Tensioned Bridge"

Conducted for

Texas
State Department of Highways and Public Transportation

in Cooperation with the

U.S. Department of Transportation
Federal Highway Administration

by

CENTER FOR TRANSPORTATION RESEARCH
BUREAU OF ENGINEERING RESEARCH
THE UNIVERSITY OF TEXAS AT AUSTIN

April 1991

NOT INTENDED FOR CONSTRUCTION,
BIDDING OR PERMIT PURPOSES

M. E. Kreger, P.E. (Texas No. 65541)
J. E. Breen, P.E. (Texas No. 18479)

Research Supervisors

The contents of this report reflect the views of the authors, who are responsible for the facts and the accuracy of the data presented herein. The contents do not necessarily reflect the official views or policies of the Federal Highway Administration. This report does not constitute a standard, specification, or regulation.

There was no invention or discovery conceived or first actually reduced to practice in the course of or under this contract, including any art, method, process, machine, manufacture, design or composition of matter, or any new and useful improvement thereof, or any variety of plant which is or may be patentable under the patent laws of the United States of America or any foreign country.

PREFACE

This report is the second in a series which summarizes an investigation of the effect of using external post-tensioning tendons, discretely bonded at intermediate diaphragm locations, and grouted, supplemental internal tendons on the strength and ductility of segmental box-girder construction. This report summarizes a series of tests on a three-span post-tensioned box-girder bridge model, as well as the development of a finite element model and the comprehensive analytical study that followed.

This work is part of Research Project 3-5-89/0-1209, entitled "*Effect of Improved Bonding of External Tendons and the Use of Supplemental Continuous Bonded Tendons in External Post-Tensioned Bridges.*" The research was conducted by the Phil M. Ferguson Structural Engineering Laboratory as part of the overall research programs of the Center for Transportation Research of The University of Texas at Austin. The work was sponsored jointly by the Texas State Department of Highways and Public Transportation and the Federal Highway Administration under an agreement with The University of Texas at Austin and the State Department of Highways and Public Transportation.

Liaison with the State Department of Highways and Public Transportation was maintained through the contact representative, Mr. Alan Matejowsky, who provided valuable suggestions and practical insight throughout all phases of the research project.

This portion of the overall study was co-directed by Michael E. Kreger, Associate Professor of Civil Engineering, and John E. Breen, who holds the Nasser I. Al-Rashid Chair in Civil Engineering. The conduct of the testing program and analytical study were the direct responsibility of Mr. Azez N.A. Hindi, Assistant Research Engineer. He was assisted by Mr. Brock J. Radloff during the experimental phase of the research program.

SUMMARY

An investigation was conducted to determine the effect of using external tendons, discretely bonded at intermediate diaphragms, and supplemental, grouted internal tendons on the strength and ductility of post-tensioned segmental box-girder bridges. In the current research program additional experimental testing, performed on an existing three-span bridge model that was constructed and tested during an earlier study, and an analytical study were performed to examine the influence of improved bonding of external tendons and supplemental internal tendons on the behavior of segmental box-girder bridges.

The experimental study was performed in three phases. In the first phase, a structural evaluation and repair procedure were carried out to determine the condition of the previously overloaded bridge model and to restore the model to a condition that came as close as practical to resembling the original condition of the structure. In the second phase, flexural tests were conducted on the model to examine the effect of incremental discrete bonding of external tendons to intermediate diaphragms on the overall behavior of the structure. In the third phase flexural strength tests were performed to examine the effect of supplementary ungrouted or grouted internal tendons on the strength and ductility of the bridge model.

The analytical portion of the study was also carried out in three phases. In the first phase a non-linear finite element program, which modeled the effects of concrete cracking and slipping of external and internal tendons, was developed. In the second phase the analytical model was verified by comparing responses calculated using the analytical model to experimental results from this program and tests reported in the literature. In the third phase a pametric study of a number of variables associated with segmental box girder construction was performed.

Results of the tests and computer model indicated that both discrete bonding of external tendons and use of supplemental, grouted internal tendons improved the strength and ductility of segmental box girder construction. Design recommendations for predicting the ultimate external tendon stress and for enhancing the strength and ductility of segmental box girder construction are presented in this report.

IMPLEMENTATION

This report provides a detailed description of an experimental program, involving a three-span segmental box-girder bridge model, and of a comprehensive analytical study. Specific recommendations for evaluating the effective tendon stress in external tendons of segmental construction, and for bonding external tendons at intermediate diaphragm locations in order to improve the strength and ductility of the box girder are presented. The primary use of this report will be to provide bride design engineers with a method for assessing the strength of post-tensioned segmental box-girder construction with external tendons, and to provide practical guidance for increasing the strength and ductility of existing box-girder structures.

TABLE OF CONTENTS

LIST OF TABLES

LIST OF FIGURES

CHAPTER ONE
INTRODUCTION

1.1 Background

The technological development and the utilization of post-tensioned concrete box girder bridges in the U.S. have progressed at a remarkable rate (2). The introduction of segmental technology, with its time-saving and economic advantages, has resulted in the predominance of segmental prestressed box girder construction for medium to moderate long-span bridges. Use of external post-tensioning is an important recent development in U.S. box girder structures. Long Key bridge, completed in 1980, was the first externally post-tensioned box girder bridge in the United States. At the present time, the Texas State Department of Highways and Public Transportation is involved in a very extensive four-part project in San Antonio using segmental precast box girder bridges with external tendons.

"Internal post-tensioning" refers to the practice of embedding tendon ducts in straight or draped patterns, as required by design, within the concrete webs and flanges of the box girder section. This practice requires time-consuming placing and securing of the ducts inside the box girder reinforcing cage. Congestion and interference with the reinforcing cage can result if multiple ducts are present. After the concrete is placed and cured, and after the precast segments are assembled, tendons are pulled through the embedded ducts and then stressed. The ducts are normally cement grouted which bonds the tendon to the duct and provides corrosion protection for the tendon.

"External post-tensioning" implies that the tendons are removed from the webs and flanges of the concrete section, and are relocated inside the void of the box girder or between the webs of non-box girders (See Figure 1.1). The draped profile is maintained by passing the tendons through deviation devices cast monolithically with webs and/or flanges at discrete points along the span. Different shape and size deviators are used, although the most common form is a small block or saddle located at the junction of the flange and web of the box girder section. Anchorages for the external tendons are usually placed in the pier segments in thick diaphragms. Blister anchorages are sometimes used at intermediate points in the span. Tendons often overlap at diaphragm anchorages for continuity. The external tendon is positively connected to the concrete only at the anchorages and the deviators. Between these points of attachment, the external tendon is enclosed in sheathing, typically polyethylene tubing which is not attached to the concrete section. In U.S. practice, the tendon is usually grouted for protection against corrosion.

1.1.1 Historical Developments. The use of external prestressing tendons is a construction technique almost as old as the use of prestressed concrete. Freyssinet clearly recognized the nature of losses in prestressed concrete with regard to creep and shrinkage, but Dischinger (3) first proposed a mathematical model for calculating the effects of those losses. Dischinger suggested using external tendons for two reasons: the possibility of restressing the tendons if undesirable deflections occurred, and the longer life of such tendons due to the reduced influence of fatigue loadings. A number of structures with external tendons were built by Dischinger(3) in the late nineteen thirties and early nineteen forties.

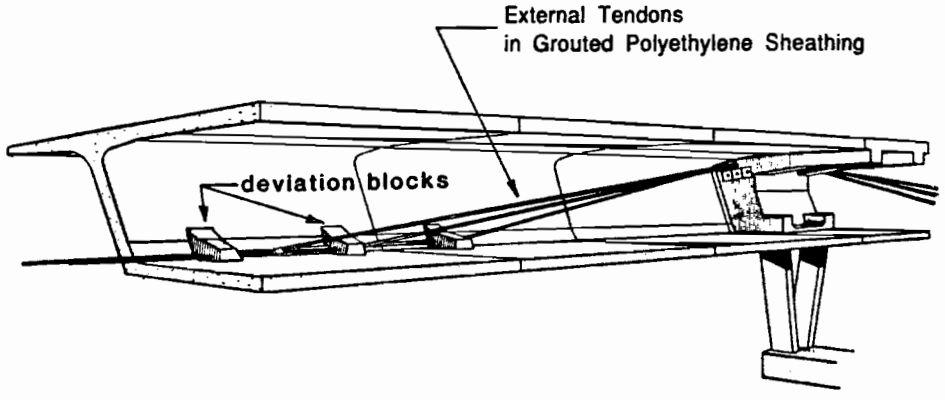

Figure 1.1 External post-tensioning components [From Ref. (2)].

However, external post-tensioning was discarded for some time because Freyssinet and other engineers emphasized the advantages of structures with bonded tendons. The advantages of bonded-tendon construction characteristics include higher utilization of bonded prestressing steel strength under ultimate loads, the general possibility of higher tendon eccentricity with internal tendons, and the greater ductility which is attainable when steel stresses increase above the yield strength. External post-tensioning did not disappear completely. Several externally post-tensioned bridges were constructed in post-WWII Europe. However, in some of these cases, external tendons had to be replaced prematurely due to inadequate corrosion protection systems (3).

A rebirth of external post-tensioning was observed in the mid-seventies. With the advent of segmentally precast box-girder construction, placement of internal tendons caused severe congestion problems in webs and flanges, and external tendons were seen as a logical way of reducing such congestion. External post-tensioning was very well suited to the span-by-span construction process. The French engineer, Muller, introduced external post-tensioning in the United States to speed the construction process and to reduce cost.

Since 1980 many bridges have been designed and constructed in the United States and in France using either external tendons or a combination of internal and external tendons. Long-span structures can be built with this latter method when the structure is constructed by the cantilever method using internal tendons, and then has external tendons added for continuity and for service loads. In addition, external tendons have been used in the growing trend for mixed systems in which combinations of concrete and steel have been used to form composite systems.

External tendons can be used for new structures as well as for strengthening existing structures. Any material with reasonable compression characteristics can be combined with external tendons. Applications of external tendons in structural steel and in composite steel-concrete structures are known (3).

An external post-tensioning tendon system consists of prestressing steel, mechanical end anchorages, a corrosion protection system, and deviation saddles as shown in Fig 1.1.

1.1.2 Rehabilitation of Existing Structures. Generally, external tendons can be used in deficient structures to increase the axial stress component and to provide uplift if deviators can be added to the structures. External tendons have been used in strengthening of bridges, parking structures, and circular structures such as silos and reservoirs (3).

The modern development of external prestressing can be traced to repair and retrofit of prestressed concrete bridges. Additional prestressing can be done by two methods: differential jacking of supports and adding of prestressing tendons. Jacking of supports has the advantage of being easy, economical, and fast. However, creep induces force redistributions over time and reduces the additional prestressing. The second method involves additional prestressing with external tendons. This method is a more permanent solution but it involves technical considerations concerning tendon layout, anchorages, deviation devices, and tendon protection.

Straight and draped tendons can be used for repair and retrofit of bridges. Straight tendons eliminate the need for deviators and reduce friction losses. However, the result is not efficient for flexural strengthening, and straight tendons will not help in carrying shear. Draped tendons, which follow the moment diagram, are more efficient for flexural resistance and, in addition, can increase the shear resistance due to the contribution of the inclined tendons. In this case, deviators must be used to achieve the tendon profile. The deviators are clamped to the webs or flanges. They introduce local stress concentrations and increase friction losses in tendons.

Anchoring the tendons to the existing structure presents the most difficult problem. Several methods have been used successfully. A large beam may be cast at the ends of the bridge section as shown in Fig 1.2(a). The beam can be designed to transfer the concentrated forces to the existing structure. In this case, tendons as long as the bridge must be used. They are anchored at the ends of the existing structure. This procedure will most likely disrupt traffic flow while demolishing the abutment and constructing the beams.

Tendons can be anchored at an existing diaphragm as shown in Fig. 1.2(b) if analysis verifies that the diaphragm can provide adequate resistance. In this case, a core must be drilled in the existing diaphragm and the anchorage hardware must be embedded in the anchorage block which is cast against the diaphragm face.

A concrete boss can be prestressed to the webs or flanges of the existing structure (Figure 1.2(c)). In this case, tendon anchorages can be distributed along the structure length. The effect of force diffusion creates considerable localized stresses which are added to the existing state of stress. Localized stresses can be reduced by stressing the anchor boss to the web-flange junction. Anchorage bosses have been designed conservatively by designing for clamping forces which are double the prestress force. The stressing procedure to attach the anchor boss to the existing structure should be studied thoroughly to reduce the prestress losses in the generally very short threaded bar lengths. A thorough analysis of the stresses between the anchor boss and the existing structure must be made since the stresses do not distribute uniformly over the contact area.

Two types of deviators for draped tendons have been used successively. The first type is the deviator boss which is similar to the anchor boss as shown in Figure 1.3(a). The second type of deviator is a reinforced concrete rib positively attached to the web with

reinforcement or adhesives and dowels as shown in Figure 1.3(b). In this case, the stresses are reduced due to the large contact area between the rib and the existing structure. Ducts located within anchorages and deviators isolate the tendons from the concrete and guide the tendon properly. Metal conduit and high density polyethylene tubing filled with cement grout after stressing have worked well for protection against corrosion between attachment points. The French have experimented with lubricated external tendons to allow easy replacement.

1.1.3 Advantages and Disadvantages. External tendons can be used for new structures as well as for existing structures needing strengthening. In designing a new bridge superstructure, a designer may opt for external tendons, internal tendons, or a combination of both. There are many good reasons to choose external tendons. Some of the arguments which previously seemed weighted in favor of the internal tendons are now weighted differently (3).

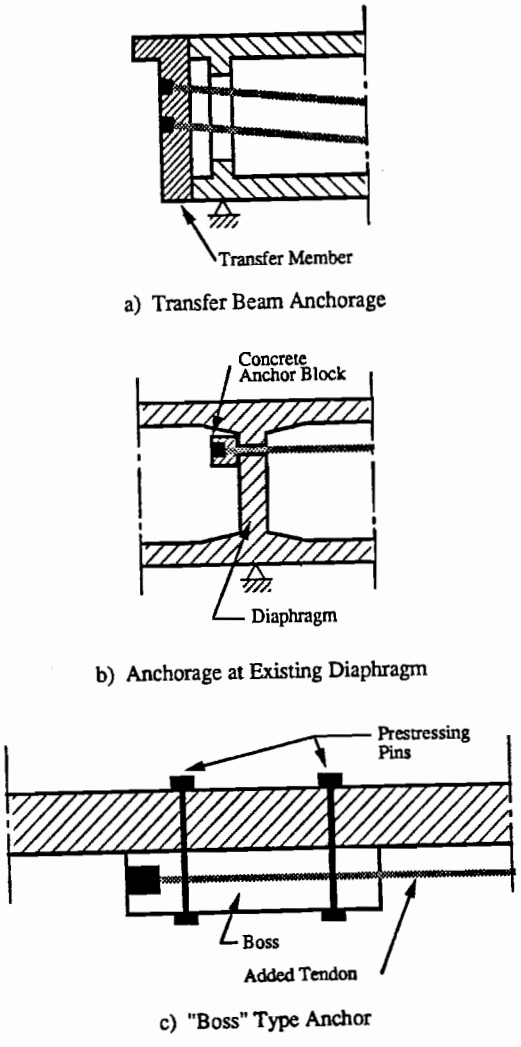

a) Transfer Beam Anchorage

b) Anchorage at Existing Diaphragm

c) "Boss" Type Anchor

Figure 1.2 Anchorage schemes for retrofit external tendons [From Ref. (2)].

In some cases, degradation of the internal prestressing tendons by corrosion attack has resulted from:

i) Low quality concrete which exhibited high porosity and excessive carbonation.

ii) Missing or deteriorated bridge deck protection which allows free attack by de-icing chemicals.

iii) Badly cracked concrete resulting from inadequate design and/or insufficient minimum bonded reinforcement.

iv) Incomplete filling of the tendon duct by cement grout.

It is very difficult to assess the degree of degradation in internal tendons because no reliable non-destructive inspection method is available. On the other hand, external tendons provide the possibility of inspecting the corrosion protection and replacing the tendon if necessary.

A detailed discussion of advantages and disadvantages of external post-tensioning is given by Powell(2). Among the most important advantages are:

a) Eliminating Ducts in the Cross Section. Removing the ducts and tendons from the concrete section allows reduction in web thickness which results in possible reduction in dead load. The absence of ducts in the web improves the calculated shear resistance because all codes base the resistance to shear on an effective web thickness by deducting the duct diameter. Elimination of the ducts leads to improved concreting. Eliminating the interface between the ducts and passive reinforcement results in simpler and quicker assembly of segment cages. This will lead to "assembly line" efficiency.

b) Access to the external tendon ducts is greatly improved which eases the grouting procedure.

c) The overall loss of prestress due to friction is reduced due to reduction in horizontal angle changes.

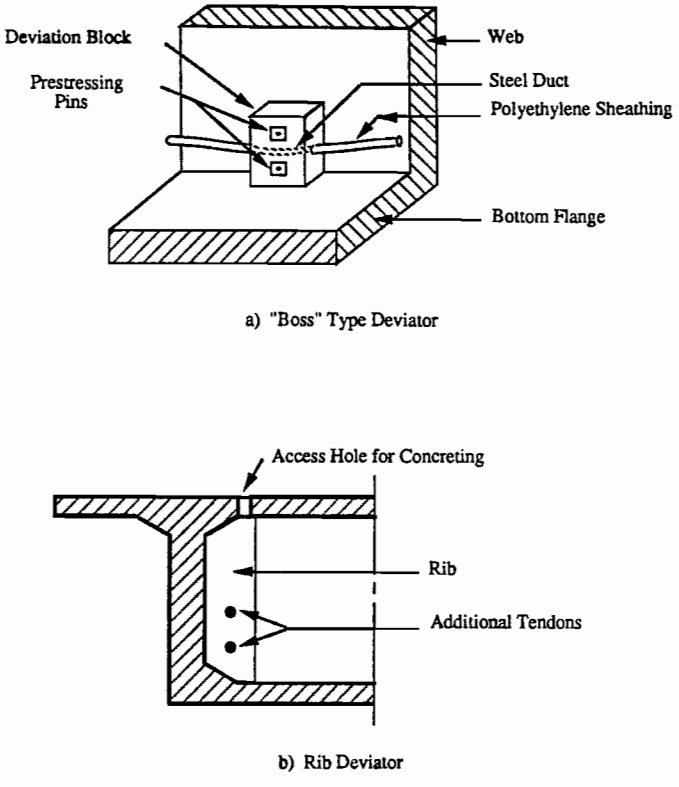

Figure 1.3 Deviators for retrofit external tendons [From Ref. (2)].

d) Concern for conventional fatigue is minimized because of low service load stress reversals in unbonded tendons.

e) Misalignment of the internal tendon ducts is eliminated.

f) Corrosion protection is improved due to continuous-sheath duct instead of epoxied joints where internal tendons pass between segments.

g) Rapid construction is possible with the span-by-span erection method.

The disadvantages include the following:

a) Vibrations of long free external tendons have been experienced several times.

b) Reduction in available eccentricity of prestress forces is a negative aspect of external post-tensioning. The range of possible eccentricity is limited due to the need for attaching the tendon between the top and bottom flanges.

c) Concentration of forces at attachments such as anchorages and deviation blocks can cause a catastrophic distress or failure.

d) Shear behavior of the system may be changed upon opening of cracks or joints. The shear strength at an opening joint may be limited by the tensile capacity of the web reinforcement which is lower than that of monolithic construction.

e) External tendons are attached to the concrete sections at discrete points along the span. As a result, tendon strain is not compatible with the adjacent concrete strains. In fact, the tendon strain is averaged over the unbonded length of the tendon. The large tendon elongations which are required to increase tendon stress much above the effective prestress level result in mechanism behavior with large rotations concentrated at the critical joints along the span. Due to the limited rotation capacity of the joint, the change in external tendon stress is considerably less than that of internal tendons.

d) Failure of the structure is governed by the rotation capacity of the joint. Concentration of rotations at few joints may result in early failure with a reduction in ductility and strength.

1.1.4 Corrosion Protection System. This subsection is a summary of material presented in Reference (3). High-strength prestressing steel needs careful protection against various types of corrosion attack.

Table 1.1 Environmental Class (From Ref. (3))

Environmental Class	Environmental Conditions
1 Modest	Structural elements always dry or under water
2 Moderate	Structural elements subject to moist conditions
3 Severe	Structural elements subject to permanent humid conditions and/or changing wetting and drying conditions
4 Aggressive	Structural elements subject to aggressive conditions

1.1.4.1 Internal Tendons. Protection is provided by the alkaline environment of the cement grout and the surrounding concrete. The protection works if attention is given to several aspects in design and construction. In Ref. (3) a corrosion protection strategy is proposed which is summarized in Tables 1.1 and 1.2. In addition to the design measures, adequate materials and good workmanship are needed. Experience has shown that improvements in concrete quality, detailing, and amount of reinforcement are necessary.

1.1.4.2 External Tendons. As with internal tendons, the external tendon corrosion strategy is based on environmental conditions and safety considerations such as fire and strand failure. Different methods used for external tendon corrosion protection are:

i) Zinc Coating. The corrosion resistance depends on the type of galvanizing and the applied thickness. Zinc coated prestressing steel has been used in France. As reported (3), zinc coatings have been damaged during handling and installation.

Table 1.2 Corrosion Protection Strategy for Internal Tendons [From Ref. (3)]

Environmental Class (See Table 1.1)	Prestressing Steel in Tension Zone under Sustained Load		Special Protection Measures Necessary		Allowable Design Crack Width (mm) under * Sustained Loads			Concrete Cover (mm)		
	Post-Tensioning	Pre-tensioning	Post-tensioning	Pre-tensioning	Post-tensioning	Pre-tensioning	Reinforced Concrete	Post-tensioning	Pre-tensioning	Reinforced Concrete
1	Yes		No		0.2	0.1	0.4	40*	35	25
2	Yes		No		0.2	0.1	0.4	50*	45	35
3	Yes	Yes	No	Yes	0.2	**	0.25	50	**	45
		No		No		0.1			55	
4	Yes		Yes		**	**		**	**	
	No		No		0.2***	0.1***	0.25	60	65	55

*) Corrosion protection not relevant for cover of sheathing
**) Not relevant for corrosion protection
***) Under rare load combinations

Another problem arose when zinc accumulated in the stressing anchorage inside the wedges.

ii) Polymer Coating. Bonding polymer to the steel by fusion has been developed in the United States primarily for the protection of reinforcing steel. A number of applications for polymer-coated strands using a much tougher polymer coating have been reported (3). It remains to be seen whether this system will prove to be a viable solution for prestressing steel. Problems could occur due to the fact that only the outer strand surface is protected, while the king wire and inner surfaces of the six surrounding wires have no coatings. The coating may be locally interrupted by the indentations of the wedge teeth at the anchorages.

iii) Protective Sheathing. Protective sheathing represents an envelope around the prestressing steel. Steel or plastic tubes (polypropylene or polyethylene) are suitable materials. Proper couplings for joining these tubes with each other and with the anchorages or the saddles are required to achieve an effective protection system. Injection of the voids inside the sheathing with cement grout has proved to be economical and reliable. Grease and wax products have been used when the tendon needs to be replaced or restressed. These materials are more expensive, difficult to inject, and have a possibility of leakage. Individually greased and plastic-sheathed monostrands offer many advantages because they are manufactured under factory conditions and their use is growing.

1.1.5 Behavioral Aspects. Figure 1.4 (3) shows moment-curvature relationships for a bridge section with three types of tendon systems. The amount of steel in each case is calculated to give the same ultimate moment. There is no difference in behavior between girders with bonded or unbonded tendons below the decompression moment. The section with unbonded tendons has substantially more area of steel, a higher initial prestress and, therefore, higher decompression moment than the section with bonded tendons. The behavior of the girders above the decompression moments is as follows:

a) Girder with Bonded Tendons: The tendon force increases up to the yield strength. The increase in tendon force and the increase in the internal lever arm of the section provide a yield strength moment substantially higher than the decompression moment. Due to the bond of steel and concrete, flexural strength of the section is more or less independent of the adjacent girder zones.

b) Girder with Unbonded Tendons: Due to the relative displacement between the concrete and the steel which is caused by the absence of bond, the steel stress increases only slightly due to deformation of the total structure. The tendon force increase depends on the geometry, the total deformation of the structure, and the tendon profile. The change in unbonded tendon stress will be relatively small for long and slender structures and hence the ultimate moment is basically equal to the decompression moment. Unless friction and/or bond at closely spaced deviators and/or bonded tendons are provided, the ultimate moment is equal to the decompression moment. In order to obtain the same ultimate moment for the structure with bonded tendons, a substantially increased area of prestressing steel (here 25% more) is required. The strength of an externally post-tensioned structure at one section depends on the behavior of the entire structure, or at least a

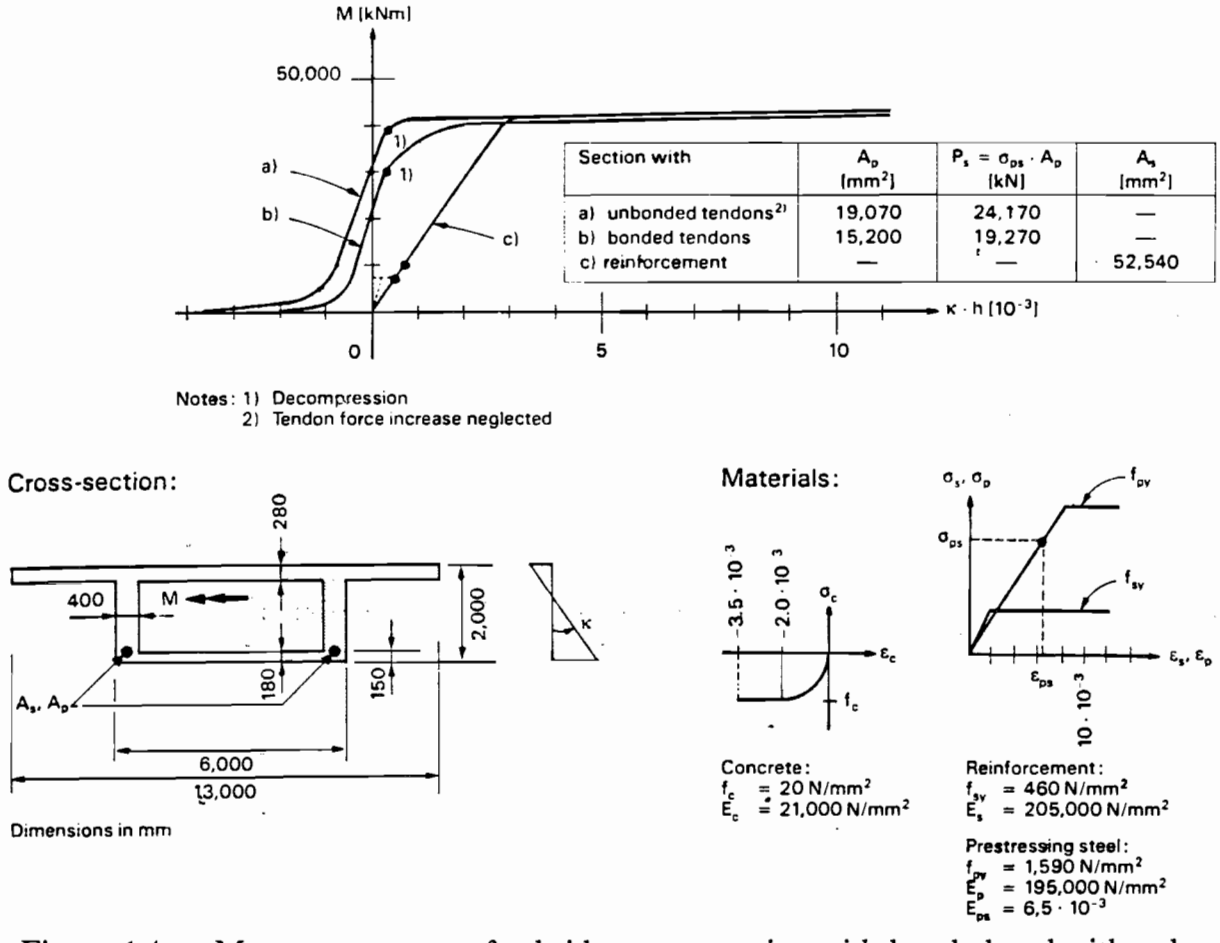

Figure 1.4 Moment-curvature for bridge cross section with bonded and with unbonded prestressing [From Ref. (3)].

substantial part of the structure, even if bonding at intermediate deviators is provided.

A good crack distribution can be obtained if the ultimate resistance of the critical section is higher than the cracking moment of the adjacent sections. This principle is used to calculate the minimum percentage of reinforcement. In segmental construction, the ultimate moment of the critical joint should be higher than the cracking moment or joint-opening moment of the adjacent joints.

Ungrouted internal tendons behave similarly to an external tendon. Finally, continuous bonded tendons and/or external tendons bonded at intermediate deviators should increase the flexural resistance of the structure.

1.2 Previous Studies

1.2.1 Experimental Research.

1.2.1.1 University of Texas. The first part of this overall study which was sponsored by the Texas State Department of Highways and Public Transportation was conducted in the Ferguson Structural Engineering Laboratory at the Balcones Research Center of the University of Texas at Austin. In that portion of the study, the behavior of a multi-span segmental box-girder bridges with external tendons was examined. The study focused on the results of tests on a reduced scale model of a span-by-span constructed structure similar to those of the San Antonio 'Y' project. A 1/4-scale three span bridge model using conventional external tendon details was tested for flexural and shear strength. The main objectives of that study were to determine the strength and ductility of usual segmentally, precast bridges with external tendons(1).

The girder was match cast and erected using the span-by-span procedure. One exterior span of the model was constructed with dry joints while the other two spans had epoxy joints. Each of the spans was loaded separately to determine the effect of epoxy joints on the flexural strength, ductility, and shear strength. In the flexural strength tests, the critical joint opened and continued to open until the support joint opened. The tendon stress did not increase significantly until the critical joint opened. A primary mechanism formed after the critical and the support joints opened. As the critical joint rotation increased, inclined cracks formed and propagated in the compression region.

The primary effect of the epoxy joints on the ultimate flexural strength of the model was to concentrate the midspan rotation at a single joint. This difference led to lower ultimate flexural strength and ductility in the span with epoxy joints than in the span with dry joints where a larger number of joints opened near ultimate load.

The possible advantage of epoxy joints is that the shear transfer at the match-cast joint has the additional component of adhesion between the segments. The adhesion component is in addition to the friction and shear key strength in the dry joints.

1.2.1.2 C.E.B.T.P. Tests (France). Eleven simple-span beams were tested to investigate the behavior of externally prestressed concrete beams especially near failure (4). The different parameters which were considered are the following:

a) Construction process for the beams, which was either monolithic (cast-in-place) or made of precast segments (match cast with dry joints).

b) Tendon layout, either totally external, mixed, or totally internal.

c) Amount of ordinary reinforcement.

d) Type of tendon sheath injection, which consisted of cement grout or wax.

Table 1.3 shows the different parameters for each beam, while Figures 1.5 through 1.7 show the dimensions, cross section, and tendon layout.

Table 1.3 CEBTP Experimental program (From Ref. (4))

	Specimen	Tendon Layout	Ordinary Reinforcement	Injection
Precast Segments	NM1	External	1.05%	None
	NM2	External	1.05%	Cement
	NM3	External	1.05%	Wax
	NM4	Mixed	1.05%	Cement
	NM5	Internal	1.05%	Cement
Cast in Place	NM6	External	0.02%	Cement
	NM9	External	0.02%	Wax
	NM8	External	0.5%	Cement
	NM11	External	0.5%	Wax
	NM10	External	0.77%	Cement
	NM7	Mixed	0.02%	Cement

It is clear that the ductility at failure increases when the amount of internal tendons increases. Another important fact observed is that the concentration of compressive strain in the joint section where crushing occurs, is higher than the strain in the middle of the segments.

Figure 1.9 shows the behavior of monolithic beams with external tendons and with different amounts of passive reinforcement. It is clear that the passive reinforcement greatly improves ductility. The ultimate strength is also increased largely due to the additional resisting moment of the passive reinforcement and partly because of the higher external tendon forces developed due to larger deflections. The amount of passive reinforcement improved ductility up to a certain extent but did not improve it further. There is little difference in behavior between the cement grouted external tendons and the wax-injected external tendons (NM6 vs NM9 and NM8 vs NM11). Both are clearly unbonded tendons. The deformability is a little larger in the wax-injected external tendon girder due to greater slip of the tendons at the deviators.

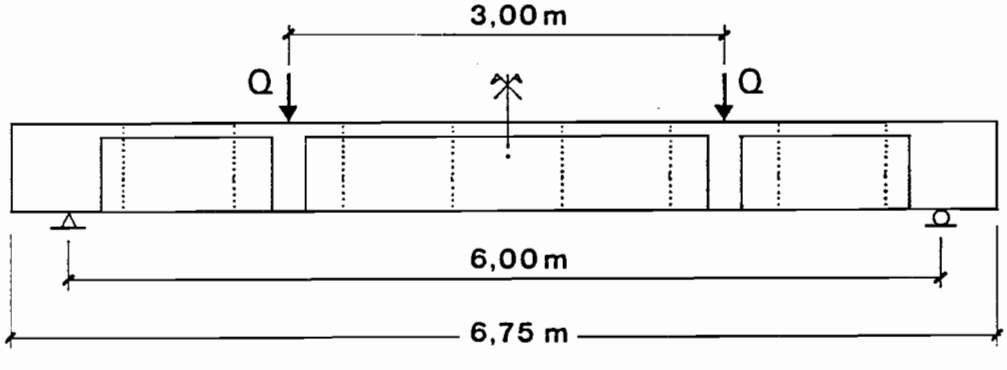

Figure 1.5 Girder elevation [From Ref. (4)].

Figure 1.10 shows the behavior of monolithic beams with different tendon layouts. Ductility is clearly increased by increasing the amount of internal tendons (NM7 vs NM6). However, the ductility of a beam with mixed internal and external tendons and very little passive reinforcement (0.02% for NM7) is smaller than the case for the external tendon girder with a large amount of passive reinforcement (0.5% for NM8) producing the same ultimate moment as the beam with mixed tendons (NM7 vs NM8).

1.2.1.3 Construction Technology Laboratory Tests. CTL constructed and tested three simply supported segmental girders at the request of Figg and Muller Engineers, Inc. (22). One girder had conventional bonded internal tendons, a second girder had unbonded external tendons, and a third girder had external tendons encased in a secondary cast making it modified unbonded. The main objective was to compare the behavior of the three types of post-tensioning systems(1).

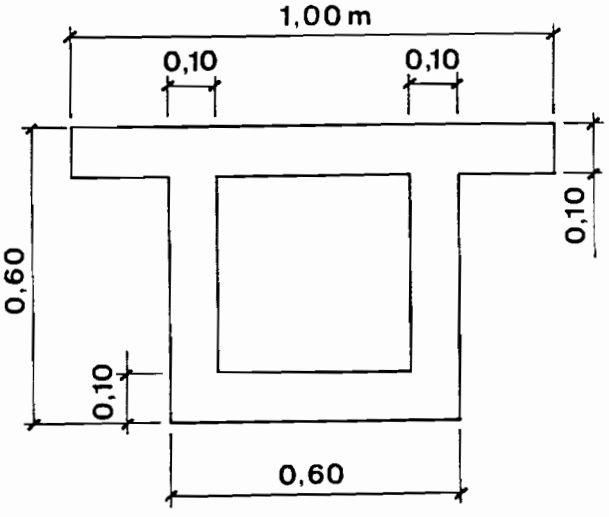

Figure 1.6 Cross section [From Ref. (4)].

The girders were loaded statically in two cycles. The first cycle of loading increased until the mid-span deflection reached 3 inches (span/120), then the girders were unloaded. To simulate an anchorage loss in the case of an earthquake, the wedges of some of the strands were burned and removed. The girders were then loaded to failure.

The "bonded girder" mode of failure was flexural with concrete crushing in the compression zone and strands fracturing in the tension zone. The "unbonded" and "modified unbonded" girders were experienced a shear compression failure in the web at the top flange interface.

Figure 1.11 shows the load deflection behavior of the three girders in the two loading cycles and a comparison with the theoretical analysis for the bonded girder. The reduced capacity in strength and ductility of unbonded system was evident.

1.2.2 Analytical Research.

1.2.2.1 University of Texas. Several programs have been developed to analyze externally post-tensioned box girders. Finite element formulations are usually implemented in these programs. El Habr (5) coded and tested a program based on the following finite elements:

Figure 1.8 shows the comparison of load-deflection behavior in the precast segmental beams with different tendon layouts.

a) Fibrous Strip Beam Elements. The bridge segments were modeled with a fibrous beam element which takes into consideration the layers of steel and concrete in the segment. Inelastic material stress-strain relations were incorporated for concrete, passive reinforcement, and active reinforcement.

b) Joint Element. A finite joint element was used to connect two segments together. The joint element transfers compressive forces and takes into consideration the difference between dry and epoxy joints.

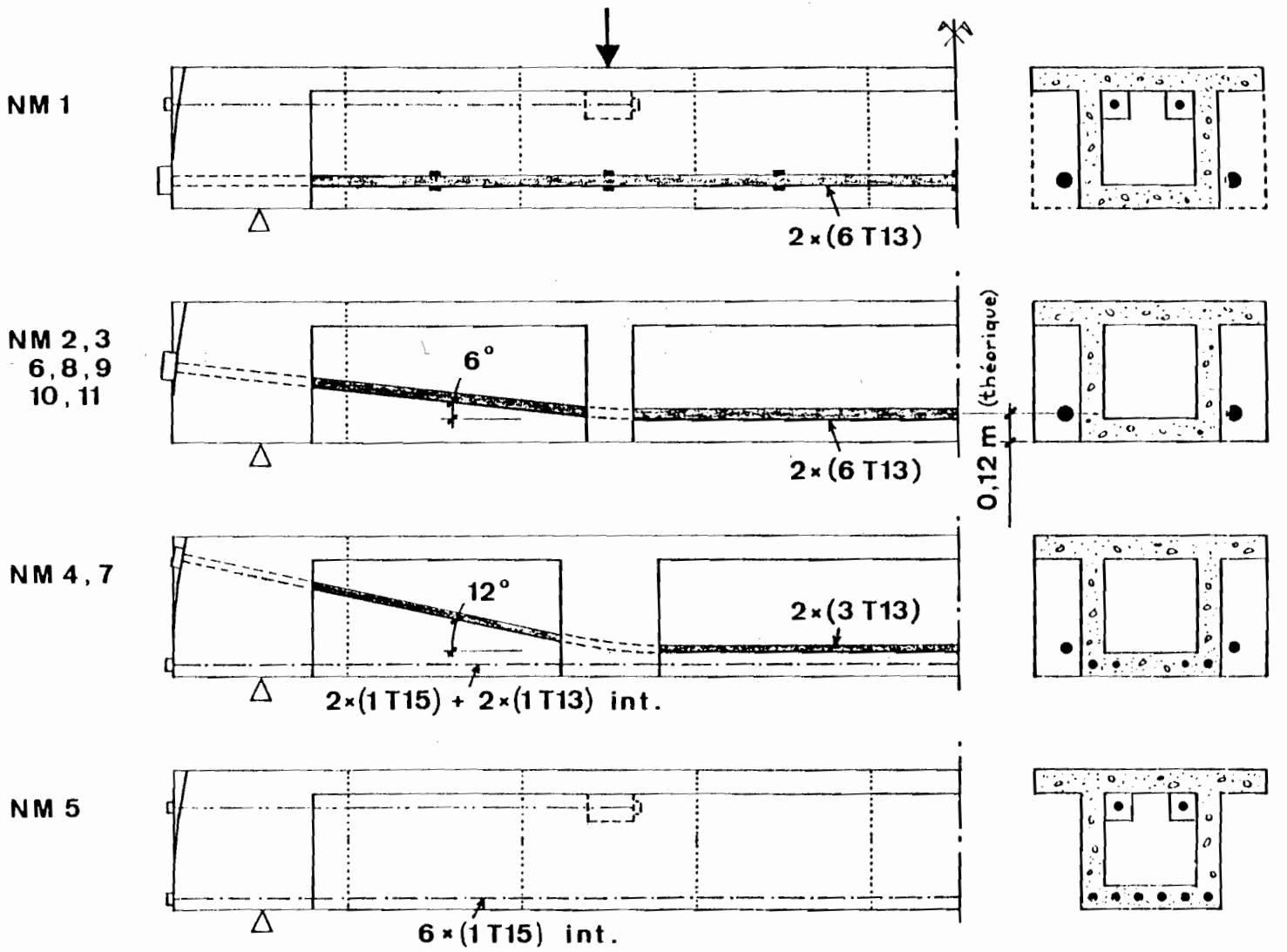

Figure 1.7 Tendon layout [From Ref. (4)].

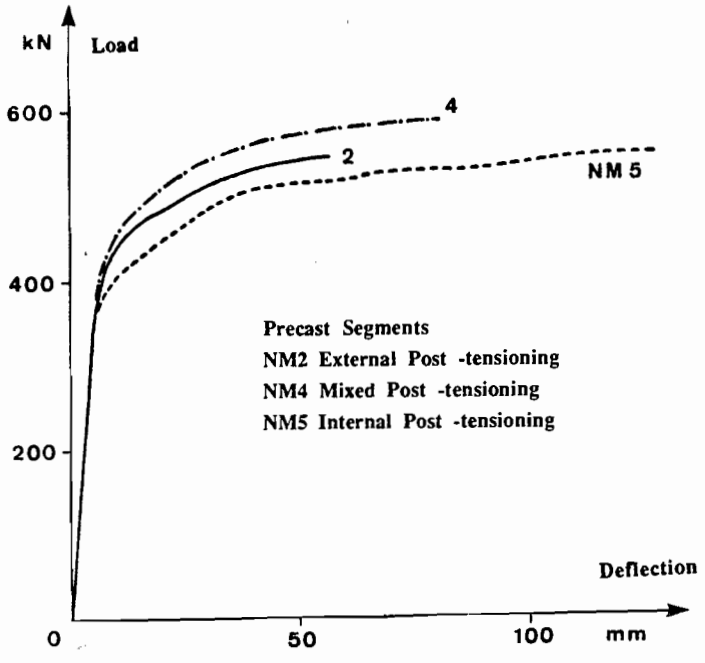

Figure 1.8 Load-deflection curve, precast segmental beams with different tendons layouts [From Ref. (4)].

c) External Tendon Element. The external tendons were modeled with a direct tension element connected to the nodes by rigid links. These elements do not take into consideration the slip between the tendon and concrete.

1.2.2.2 Jean Muller International Inc. A computer program (Deflect) (6) has been developed to analyze the structures prestressed by external tendons. The program takes into consideration the change in segment rigidity by using moment curvature relationships constructed by using finite element analysis for the bridge segment. All analysis is carried out on the segments assuming that the stress distribution is linear elastic, the joint section remains plane, and concrete in tension between two joints is uncracked. A non-linear prestressing steel stress-strain relationship is assumed. The program takes into consideration the tendon profile and bonding conditions of the tendons at the deviators. The stress distribution is calculated by iteration until satisfactory results are obtained.

The finite element analysis to construct moment curvature relationships for the segments is carried out assuming that the material is linear elastic. Because there is no failure limit on the concrete in compression, the moment curvature relationship extends to a very large curvature of about 450 times the curvature when the segment is totally under compression.

The program was tested by comparing the program analytical results with CEBTP tests and CTL tests. Figure 1.12 shows the comparison between the program results and a CEBTP test. Two cases were run for the beam with the same geometry and prestress tendons. One run assumed that the tendons were external tendons while the second run

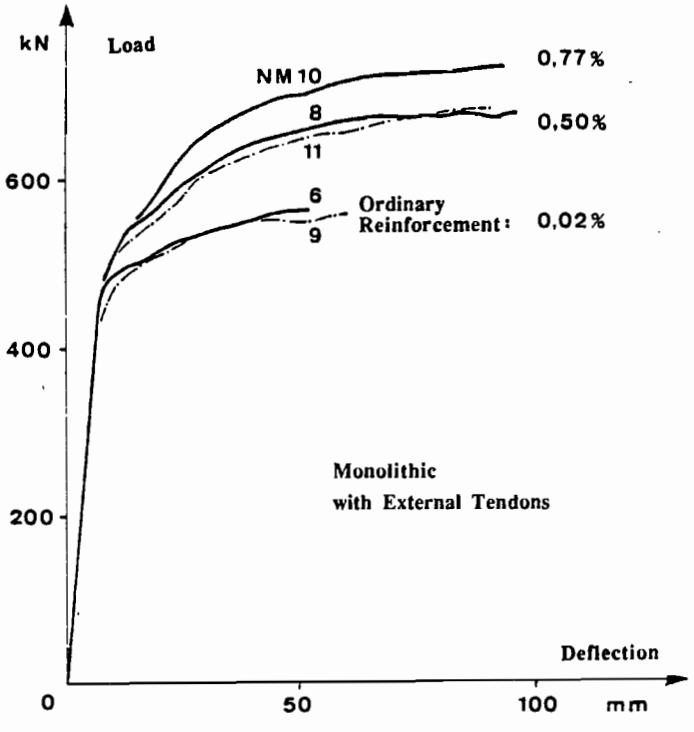

Figure 1.9 Load-deflection curve, cast-in-place beams [From Ref. (4)] (influence of the Percentage of Ordinary Reinforcement).

assumed that the tendons were fully bonded over the whole length. The difference between the three cases (CEBTP test and the two runs) was very small up to ultimate capacity. The program shows a similar agreement with the CTL tests.

The program results indicate that there is very little difference in behavior up to the ultimate load between structures prestressed by either external or internal tendons. The tests (4) had shown that in external-tendon structures, rotations are concentrated in a few joints which failed prematurely by concrete crushing. Program Deflect did not take the concrete crushing into consideration since it assumed that the concrete material is linear elastic with no stress or strain limit on the concrete.

1.2.2.3 C.E.B.T.P. (France). In addition to the experimental tests on the eleven beams reported in this chapter, a computer program was implemented to analyze structures prestressed with external post-tensioning (4). The program used the moment-area method and was restricted to simply supported beams. The program used the model for concrete strain distribution in a cracked element proposed by Giuriani (7) which was also used in the program developed in this study. The program was tested by comparing its results with the experimental tests performed in the same study. The program results were in close agreement with the tests but in some cases the program did not trace the load up to failure.

1.2.3 Additional Research. The strength and ductility of segmental construction with external tendons should be improved if the external tendons are bonded at intermediate diaphragm locations (3). An investigation of the adequacy and efficiency of the bond mechanism between the strands, the deviators, and the intermediate 'pass-through' diaphragms was also investigated by Radloff (10) in Ferguson Laboratory at the University of Texas at Austin.

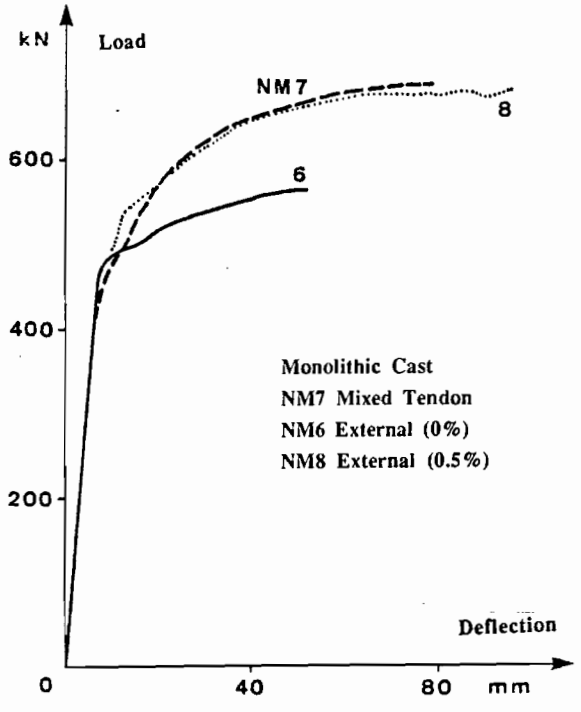

Figure 1.10 Load-deflection curve, cast-in-place beams [From REf. (4)] (comparison of mixted tendon with totally external).

1.3 Objectives of the Study

The objectives of this part of the study of strength and ductility of external tendon bridges were to:

a) determine whether external tendons bonded at intermediate diaphragms improve strength and ductility of segmentally precast bridges with external post-tensioning tendons.

b) determine the effect of using supplementary tendons on strength and ductility of this kind of construction.

c) recommend practical methods to enhance the strength and ductility of segmental box girder construction with external tendons.

d) recommend methods to predict the ultimate external tendon stress.

e) develop, implement, test, and use a finite element computer program to analyze this kind of construction. The program should take into consideration the influence of joint opening, slip of external tendons at deviators, slip of internal tendons near the opened joint, and second order effects caused by the interaction between axial load and flexural deformations.

f) make recommendations for design and construction regulations to reflect the improved behavior.

This part of the overall study was restricted to the behavior of multi-span segmental box girder bridges with external tendons, and focused on the results of a reduced-scale model test.

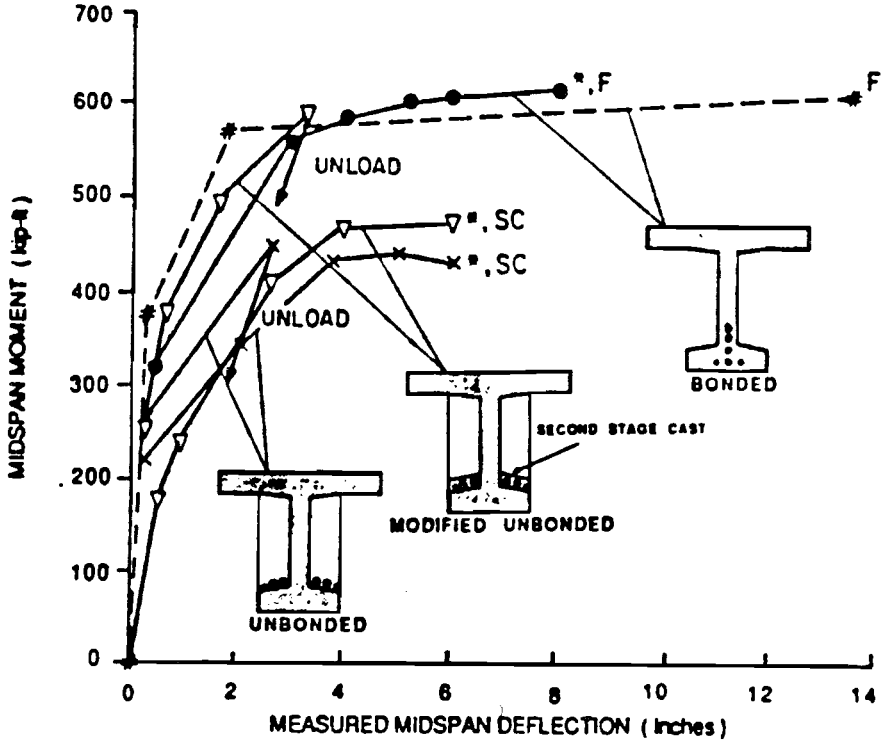

Notes:

Midspan Moment = dead load moment + applied load moment

Measured midspan deflection = deflection due to applied load only

- -- # -- Monolithic with bonded tendons (theoretical)
- —●— Segmental with bonded tendons and dry joints
- —×— Segmental with unbonded tendons and dry joints
- —▽— Segmental with modified unbonded tendons and dry joints

Failure modes: *F* = Flexural failure

SC = Shear compression failure

* Some anchorages burned before reloading.

Figure 1.11 Load-deflection responses for CTL tests [From Ref. (1)].

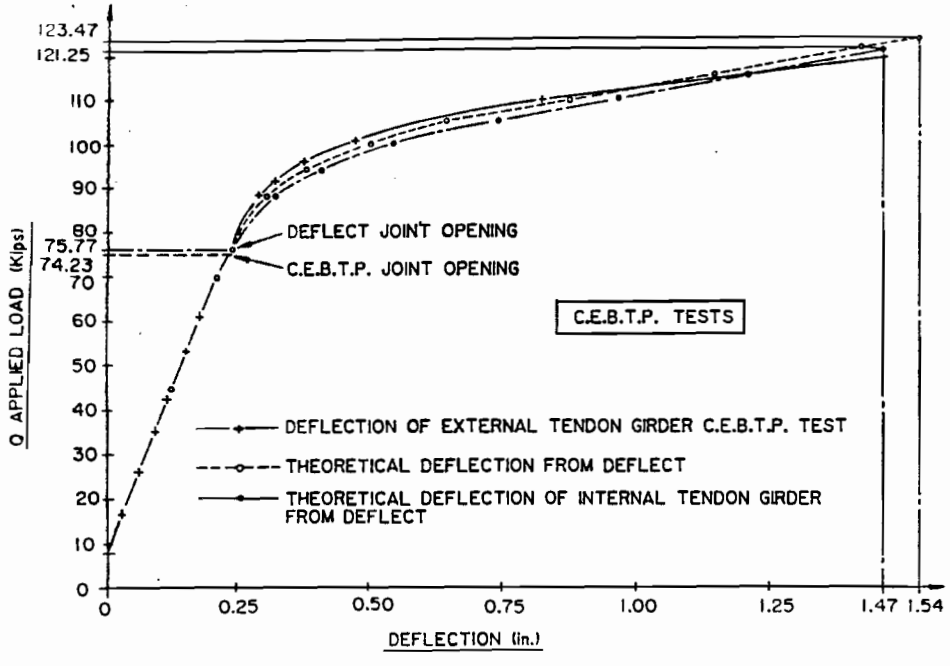

Figure 1.12 Load-deflection response predictions by deflect for CEBTP test specimen [From Ref. (6)].

1.4 Summary

The body of this study is organized as follows:

Chapter 2 contains details of the model and the experimental program. Chapter 3 gives the test results, while Chapter 4 discusses the test data. Chapter 5 presents the analytical model used in the finite element program, while Chapter 6 presents a verification of the computer program by comparing analytical predictions and experimental results. Chapter 7 contains an analytical study of critical variables and recommendations, and Chapter 8 gives the conclusions and final design recommendations.

CHAPTER TWO

EXPERIMENTAL PROGRAM

2.1 Description of the Model

The model was constructed in the first phase of this study by MacGregor(1) in the Ferguson Structural Engineering Laboratory at the Balcones Research Center of the University of Texas at Austin. The three-span continuous model was geometrically symmetrical about the center of the interior span as shown in Figure 2.1. The only exception was in jointing material. The north span had dry joints while the south and center span had epoxy joints. The model was erected using a span-by-span procedure. Each span consisted of ten typical segments plus a pier segment at each support. Post-tensioning tendons were anchored at the pier segments, with some tendons continuous over two spans. Cast-in-place closure strips were provided between the pier segments and the typical segments.

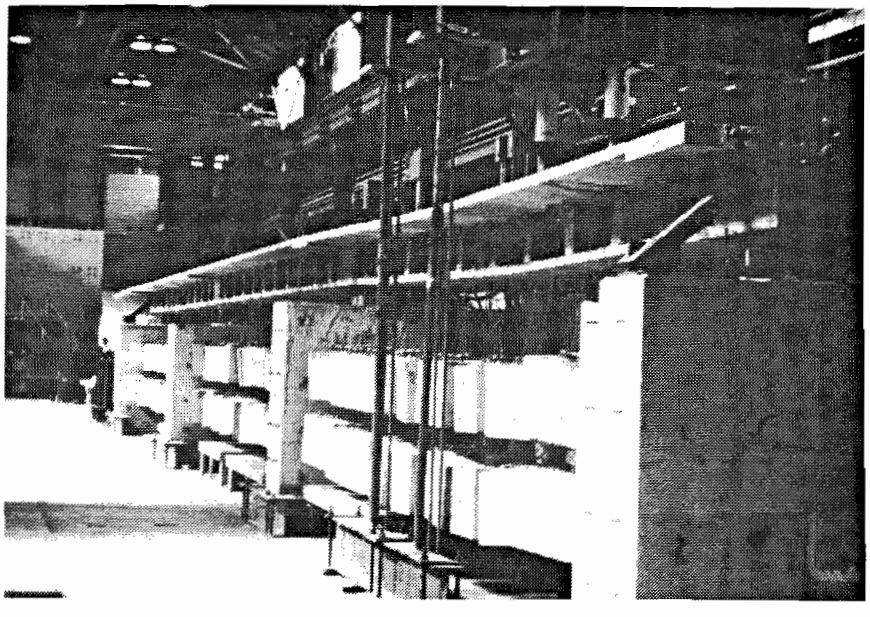

Figure 1. Model of externally post-tensioned bridge.

The typical segment cross section is shown in Fig 2.2(a). At the middle of each typical segment, a full depth diaphragm was used to deviate the external tendons and to serve as discrete bonding points for the external tendons at later stages. Span-to-depth ratio, transformed area, and moment of inertia are shown in Fig 2.2(a). Figure 2.2(b) shows the cross section of the pier segment with its transformed area and moment of inertia. The external tendon anchorages were contained in the portion outside of the web. More details can be obtained from MacGregor(1).

Figure 2.3 shows the external tendon layout. External tendons were draped from low points near the midspan to high points near the supports. Exterior support, midspan, and interior support sections are illustrated in Fig 2.3 to show the tendon locations. The

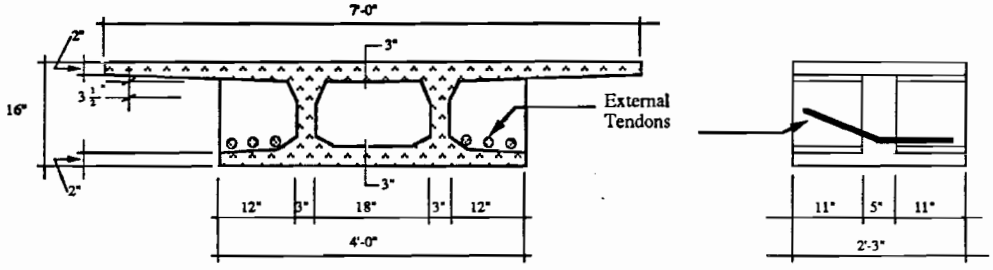

Section Side View

Notes:
Span to Depth Ratio = 18.75
$A^* = 450 \text{ in}^2$
$I^* = 16540 \text{ in}^4$

a) Typical Span Segment

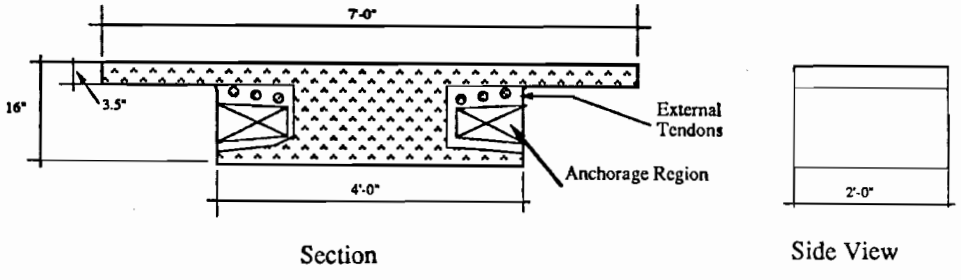

Section Side View

$A^* = 894$

$I^* = 20741$

b) Pier Segment

* Transformed Section Properties

Figure 2.2 Cross sections [from Ref. (1)].

external tendons were bonded at diaphragm locations where the tendons were deviated, and at all pier segments. At all other diaphragm locations, tendons were simply passed through the diaphragms. Provisions were also made to allow bonding of external tendons at all pass-through locations in diaphragms. Flexible electrical conduit was used as a duct at pass-through locations to allow bonding of the external tendons to the diaphragms. Provisions were made for the addition of internal tendons in the bottom flange of the box girder. Grout ports were provided in the internal tendon ducts to allow bonding of the continuous internal tendons.

Single-span tendons and continuity tendons were used in the model. Tendons 1A, 1B, 2, 4A, and 4B were composed of 10-3/8 in. diameter strands (five on each side of the model) and were stressed as single span tendons. Tendons 3 and 5 contained 4-3/8"

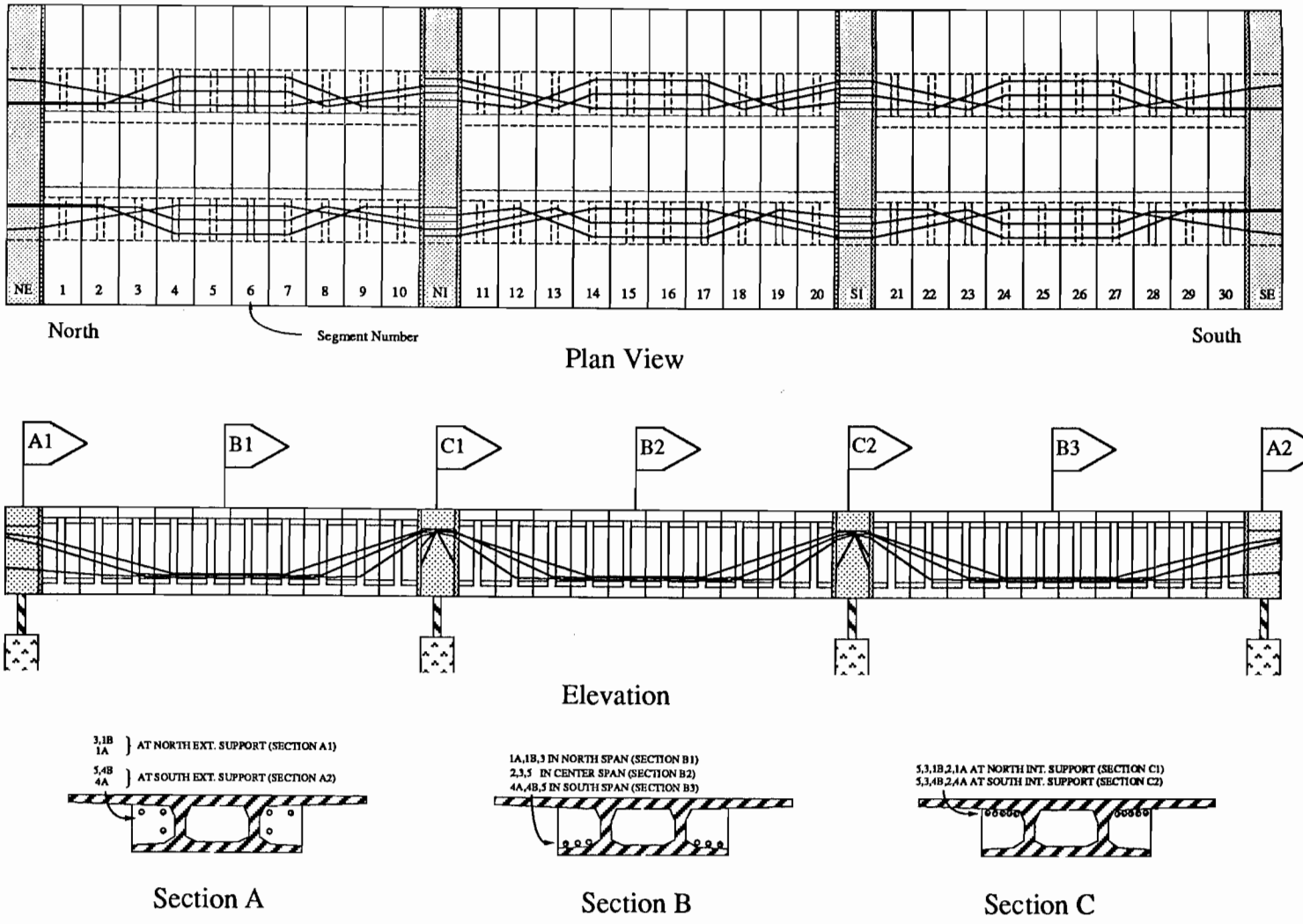

Figure 2.3 Schematic post-tensioning layout [from Ref. (1)].

diameter strands (2 on each side) which were the continuity tendons. Tendons 3 were stressed after erecting span one and two while Tendons 5 were stressed after erecting all three spans. Tendons 5 were continuous through spans two and three. Figure 2.4 shows the position of the external tendons along the model.

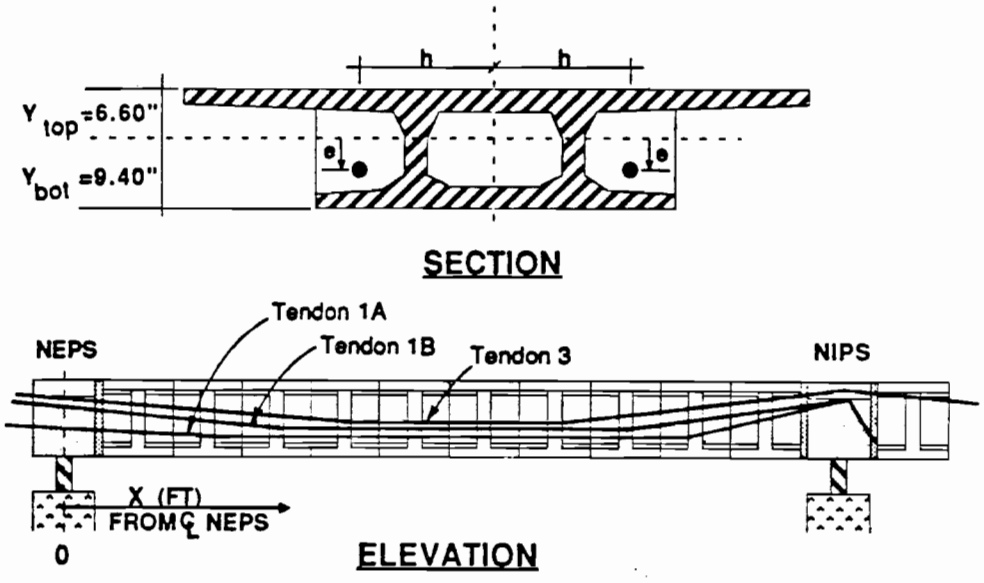

TENDON 1A : 2 x (5-3/8" dia. Grade 270 Strands)

x (ft)	-1	0	4.625	9.125	15.875	20.375	25	26
e (in)	2.9	3.4	5.65	6.23	6.23	5.65	-2.67	3.15
h (in)	15	15	15	22	22	15	14	15.25

TENDON 1B : 2 x (5-3/8" dia. Grade 270 Strands)

x (ft)	-1	0	6.875	9.125	15.875	18.125	25	26
e (in)	-2.48	-2.1	5.65	5.94	5.94	5.65	-2.81	3.15
h (in)	15	15	15	18.5	18.5	15	18.25	20.75

TENDON 3 : 2 x (2-3/8"dia. Grade 270 Strands)

x (ft)	-1	0	9.125	15.875	25	31.875	Continues
e (in)	-2.6	-2.1	5.65	5.65	-2.88	5.65	in Center Span
h (in)	21.5	21.5	15	15	20.38	15	

NORTH EXTERIOR SPAN

Figure 2.4a Tendon layout [from Ref. (1)].

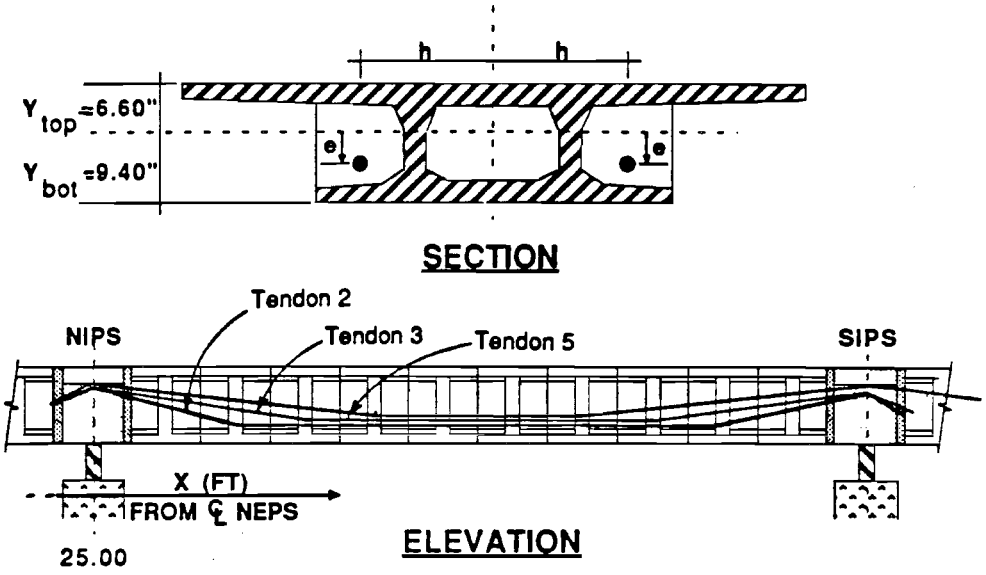

TENDON 2 : 2 x (5-3/8" dia. Grade 270 Strands)

x (ft)	24	25	29.625	34.125	40.875	45.375	50	51
e (in)	2.65	-2.74	5.65	6.23	6.23	5.65	-2.74	2.65
h (in)	16	16.13	15	22	22	15	16.13	16

TENDON 3 : 2 x (2-3/8" dia Grade 270 Strands)

x (ft)*	15.875	25	31.875	34.125	40.875	43.125	50	51
e (in)	5.65	-2.88	5.65	5.94	5.94	5.65	-2.88	2.4
h (in)	15	20.38	15	18.5	18.5	15	20.38	22

*continues in North Span

TENDON 5 : 2 x (2-3/8" dia. Grade 270 Strands)

x (ft)	24	25	34.125	40.875	50	59.125	Continues
e (in)	1.4	-2.95	5.65	5.65	-2.95	5.65	In South Span
h (in)	22	22.5	15	15	22.5	15	

INTERIOR SPAN

Figure 2.4b Tendon layout [from Ref. (1)].

Figure 2.5 shows the distribution of internal tendons and the four auxiliary tendons. The internal and the auxiliary tendons had a straight profile. Eight 3/8" diameter strands were provided in the top flange. These tendons were stressed in the first part of the project but they were ungrouted. Four unstressed 3/8" diameter strands were provided in the bottom flange. They were stressed in this part of the study. Four unstressed auxiliary 3/8" diameter strands were added within the box void. These tendons provided the ability to add

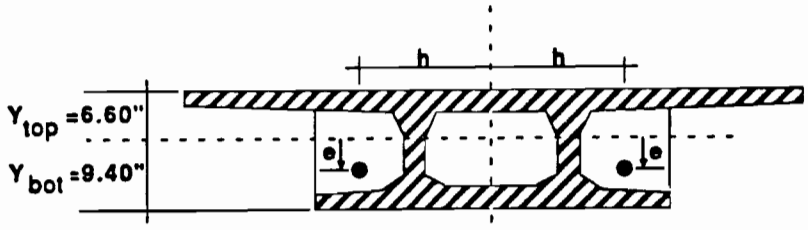

SECTION

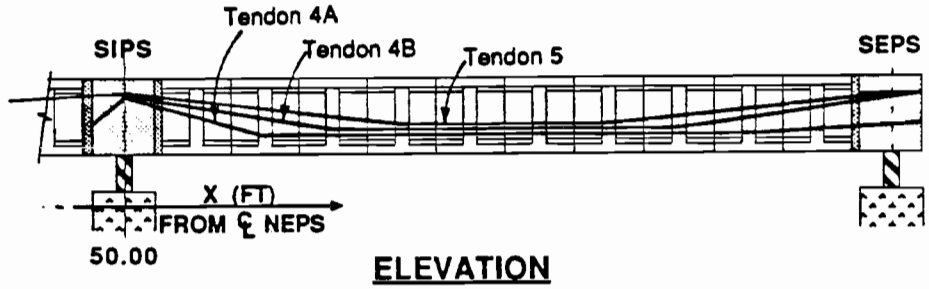

ELEVATION

TENDON 4A : 2 x (5-3/8" dia. Grade 270 Strands)

x (ft)	49	50	54.625	59.125	65.875	70.375	75	76
e (in)	3.15	-2.67	5.65	6.23	6.23	5.65	3.4	2.9
h (in)	15.25	14	15	22	22	15	15	15

TENDON 4B : 2 x (5-3/8" dia Grade 270 Strands)

x (ft)	49	50	56.875	59.125	65.875	68.125	75	76
e (in)	3.15	-2.81	5.65	5.94	5.94	5.65	-2.1	-2.48
h (in)	20.75	18.25	15	18.5	18.5	15	15	15

TENDON 5 : 2 x (2-3/8" dia. Grade 270 Strands)

x (ft)	Continues	40.875	50	59.125	65.875	75	76
e (in)	In Center Span	5.65	-2.95	5.65	5.65	-2.1	-2.6
h (in)		15	22.5	15	15	21.5	21.5

SOUTH EXTERIOR SPAN

Figure 2.4c Tendon layout [from Ref. (1)].

additional prestress to the model to compensate for unexpected prestress losses or for serviceability considerations. The four auxiliary tendons were unstressed during all tests carried out in this program. The internal and auxiliary tendons were anchored only at the exterior pier segments.

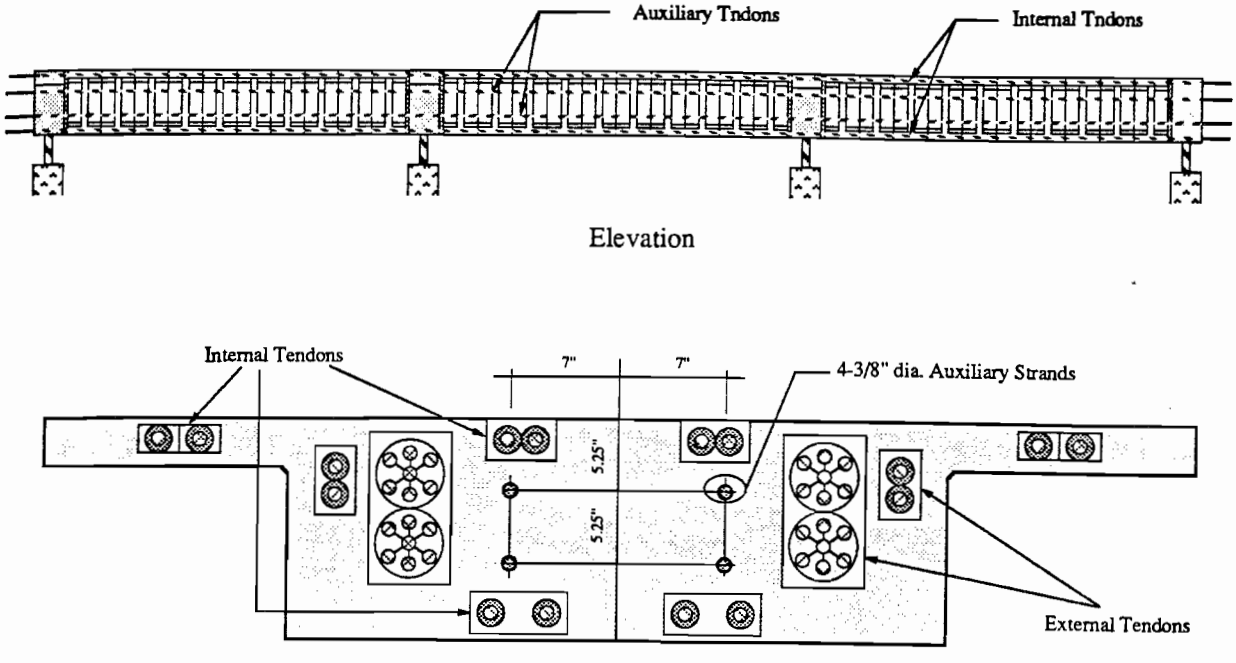

Figure 2.5 Internal and auxiliary tendons.

2.2 Material Properties

2.2.1 Concrete. A minimum 28 day compressive strength of 6000 psi was chosen to match the prototype construction. Maximum aggregate size of 3/8 in. was required for 1/2" minimum concrete cover due to the reduced scale. High strength concrete was used in the pier segments to increase the bearing stress capacity as required for the post-tensioning anchorages. Table 2.1 shows the concrete strength and the elastic modulus for the segments.

2.2.2 Steel Reinforcement. Welded wire fabric was used in the skeleton of the typical segment cages. The welded wire fabric had high yield and ultimate strength and limited ductility as shown in Table 2.2. Small diameter micro-reinforcing bars were used in the typical segment diaphragms. The yield and ultimate strength of the micro-reinforcing bars are shown in Table 2.2. Grade 60 normal size reinforcement was also used in typical and pier segments. Bar sizes ranged from #3 to #5. The strength characteristics are shown in Table 2.2.

2.2.3 Prestressing Strands. Grade 270 low relaxation strands were used for all prestressing steel. The stress-strain relationship furnished by the supplier is shown in Fig 2.6. The ultimate strength of the strands is 279 ksi at 5.47 percent elongation with an elastic modulus of 28,400 ksi. All the prestressing strands were 3/8" diameter with an area of 0.085 square inches. Figure 2.6 also shows the stress strain relationship of the strands obtained by testing a 3/8" diameter strand and measuring the strain with electronic strain gauges. This test gave an apparent elastic modulus of 30,300 ksi.

Table 2.1 Segment Concrete Properties Segment Information

Segment No.	Mix No.	Date Cast	f'_{c28} (psi)	$f'_{c\,use}$ Cylinder (psi)	$f'_{c\,use}$ Calc. (psi)	$E'_{c\,use}$ Cylinder (ksi)	$E'_{c\,use}$ Calc. (ksi)
NEPS	4	05/26/87	12746[1]		13383		6594
1	2	07/31/86	5855		6558		3986
2	2	07/28/86	5094		5705		3718
3	1	06/30/86	4343		4864		3592
4	1	06/12/86	5355	6022		3997	
5	1	05/28/86	6006	6839			4260
6	1	06/12/86	5355	6022		3997	
7	1	06/30/86	4343		4864		3592
8	1	07/14/86	4744		5313		3755
9	2	07/28/86	5094		5705		3718
10	2	07/31/86	5855		6558		3986
NIPS	4	07/26/87	9652[2]		10135		5738
11	2	09/10/86	6707		7512		4266
12	2	08/27/86	5930		6642		4012
13	2	08/21/86	5630		6306		3909
14	2	08/18/86	6429	7187			4173
15	2	08/14/86	6948	7777		4341	
16	2	08/18/86	6429	7187			4173
17	2	08/21/86	5630		6306		3909
18	2	08/27/86	5930		6642		4012
19	2	09/10/86	6707		7512		4266
20	2	09/16/86	6954		7788		4342
SIPS	4	03/12/87	12805[3]		13445		6609
21	3	10/16/86	6498		7148		4495
22	3	10/10/86	6780		7458		4591
23	3	10/08/86	6709	7348			4557
24	3	10/06/86	7351	7409		4576	
25	2	08/25/86	7744	8769			4610
26	3	10/06/86	7351	7409			4576
27	3	10/08/86	6709	7348			4557
28	3	10/10/86	6780		7458		4591
29	3	10/16/86	6498		7148		4495
30	3	10/24/86	7848		8633		4940
SEPS	4	06/08/87	13270[4]		13934		6728

[1] 94-day strength

[2] 31-day strength

[3] 35-day strength

[4] 81-day strength

Table 2.2 Reinforcement Properties [from Ref. (1)]		
	f_y	f_{ult}
Welded Wire Fabric (W5.5)		
Non-heat treated	82	88
Heat treated	75	79
Micro Reinforcing Bars		
#1.25 (non-heat treated)	83.0	92.5
#1.5 (heat treated)	42.5	61.3
#2 (heat treated)	44.5	65.7
#3	67.3	110
#4	85.3	128
#5	78.7	117

2.3 Typical Segment

Figure 2.7 shows typical segment reinforcement while Figure 2.8 shows welded wire fabric details. Figure 2.9 shows the special reinforcement used in the deviator. Reinforcement was designed to carry longitudinal bending stresses, shear flow in the webs and flanges, transverse bending stresses, local forces in the segments, and deviation forces. Details of the design process are given by MacGregor(1).

The segments were match-cast on a long, smooth casting bed using formwork shown in Fig 2.10. The model had neither horizontal nor vertical curvature. Shear keys were provided in the web and in the top and bottom flanges as shown in Fig 2.11. The web shear keys were provided to transfer shear across the joints between the segments. The keys used in the flange were provided to align the segment during erection and to transfer torsional shear.

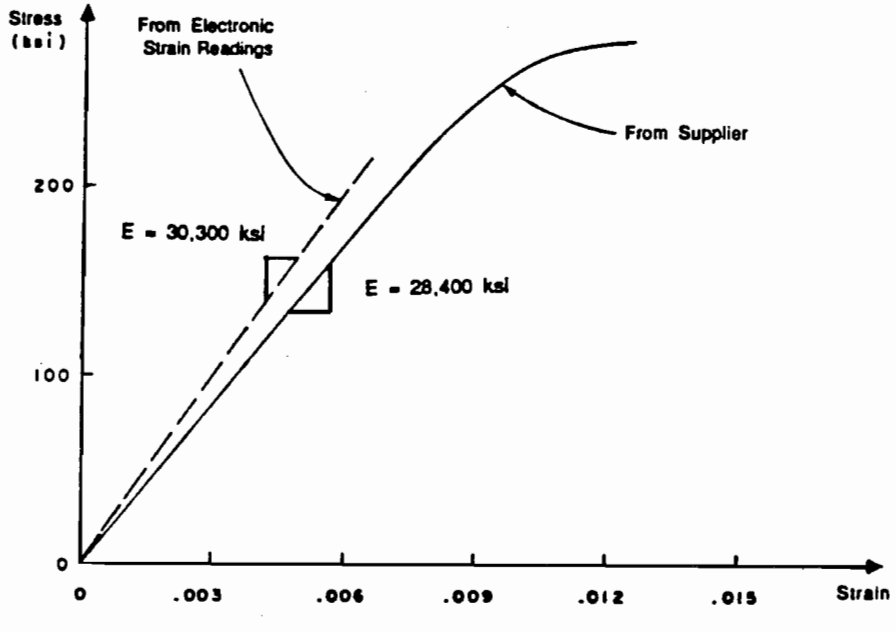

Figure 2.6 Prestressing strand stress-strain relationship [from Ref. (1)].

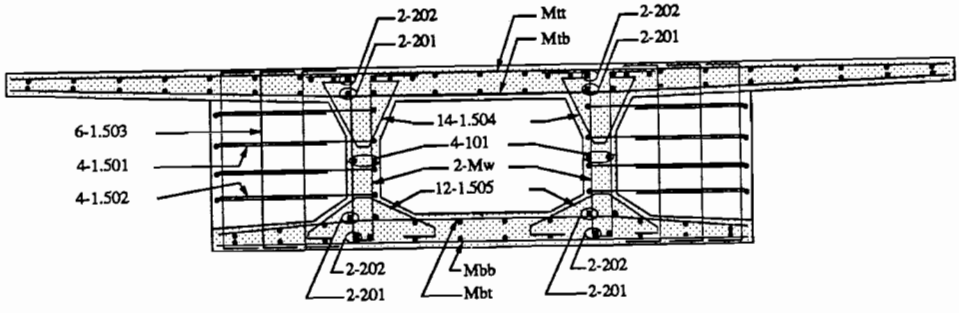

Section

Figure 2.7 Typical segment reinforcement [from Ref. (1)].

2.4 Pier Segment

The pier segments contained all anchorages for the post-tensioning tendons. Figures 2.12 and 2.13 and Table 2.3 show the reinforcement provided in pier segments to transfer the forces. The pier segments were cast separately from typical segments. Cast-in-place closure strips were used in the model between each pier segment and adjacent span segments.

2.5 Erection Procedures

The span-by-span erection method, which was similar to the method used in the prototype construction, was used to erect the model. Figure 2.14 shows the sequence of erection. The erection process started with the north span, progressed to the interior span, and then finished with the south span. Falsework was used to support all segments of the north span while pier segments were erected and closure strips were cast between the pier segments and span segments. The prestressing strands were stressed after the compensating dead load blocks were suspended. The falsework was moved to the interior span to support the typical segments. Closure joints were cast, dead load blocks were suspended, and finally the tendons were stressed. Subsequently, in the same manner, the south span was erected.

2.6 Evaluation and Repair of the Model

Flexural and shear strength tests were carried out on the three-span bridge model in the first part of the project (1). MacGregor stopped all strength tests as the specimen approached a target stiffness of 4 percent its initial stiffness but before severe concrete crushing was apparent. At conclusion of the first part of the project the structure was highly cracked and locally severely damaged but appeared to be basically structurally intact. A complete evaluation and repair was carried out to determine the model condition and to restore it to a good condition before beginning testing in the second part of the project. The evaluation of the model concentrated on two items: careful estimation of insitu forces, and damage inspection and repair.

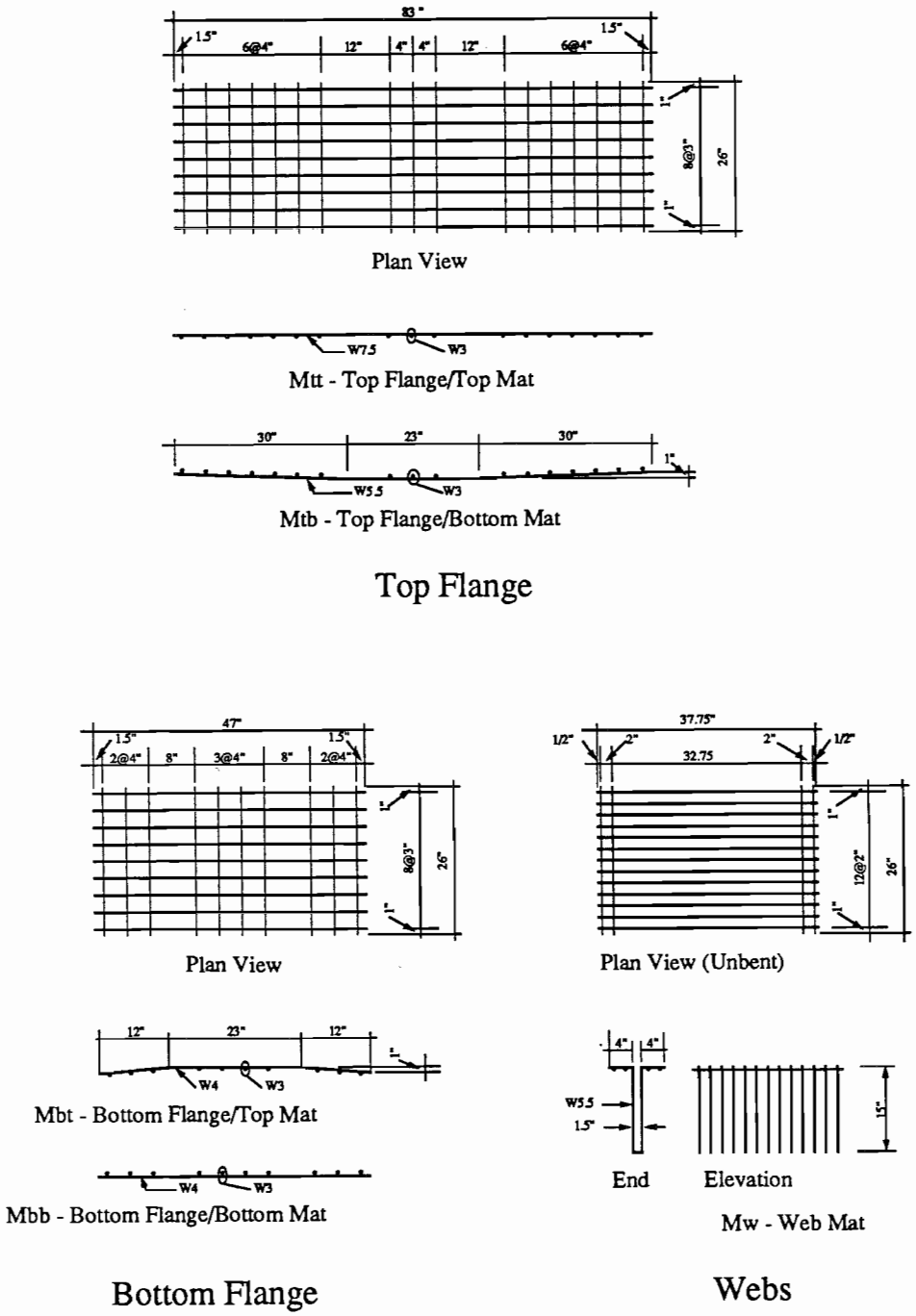

Figure 2.8 Welded wire fabric details [from Ref. (1)].

Table 2.3 Anchorage Zone Reinforcement Details

Bar No.	Type	Bar Size	Dimensions (inches)		
			A	B	C
201	Straight	2	23		
202	B1	2	2	4	2
203	B1	2	2	5.5	2
204	B1	2	2	6	2
301	Straight	3	83		
302	B2	3	47	4	
303	Straight	3	47		
304	B3	3	14	14.5	4
305	B4	3	14.5	2.5	4
306	Straight	3	23		
307	B1	3	5.5	11	4
305	B5	3	1.75	10	
309	B5	3	2.25	9	
310	B5	3	1.75	9	
311	B1	3	5.5	5.5	4
312	B1	3	6	9	4
313	B1	3	10	11	4
314	B5	3	1.75	14	
315	B1	3	6.5	14.5	5
401	Straight	4	83		
402	B2	4	47	4.5	
403	Straight	4	47		
501	B2	5	47	12	
SP1	SP	1/4″	5	11	1
SP1	SP	1/4″	3	6	1
SP3	SDP	1/4″	1.5	4.5	.75
SP4	SP	1/4″	4	4	.75
SP5	SP	1/4″	2.5	18	1
SP6	SP	1/4″	4	6	.75
SP7	SP	1/4″	2.5	20	1

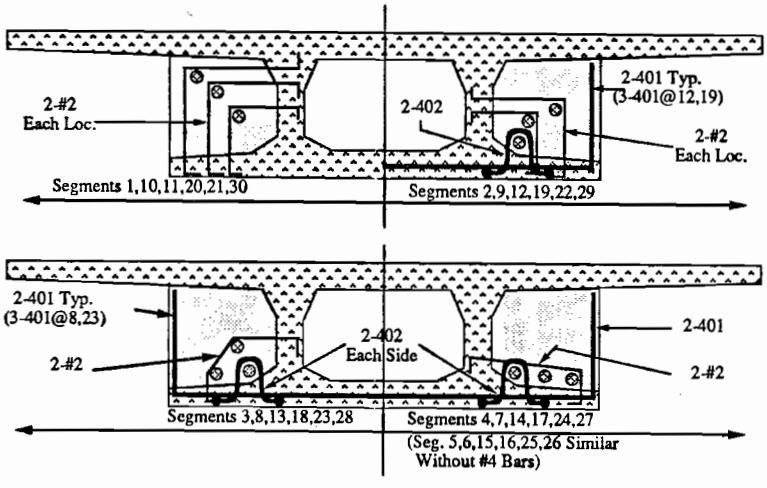

Tendon Deviation and Diaphragm Reinforcement

Bar Type 401

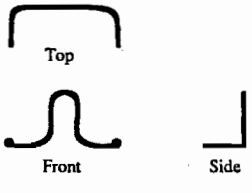

Bar Type 402

Figure 2.9 Deviator reinforcement [from Ref. (1)].

2.6.1 Estimation of Insitu Forces. In order for proper conclusions to be drawn from the test data collected during the second testing program, it was necessary to estimate the internal forces in the structure before the start of testing. This is particularly important in the case of prestressed structures. The stresses in the structure at the start of the second testing program were functions of dead load and the effective prestress forces.

2.6.1.1 Measuring and Resetting the Exterior Reactions. The reactions were measured and modified by hydraulically lifting the exterior pier segments and inserting shims at the supports. Lifting of the pier segment was done to equalize and measure the reactions under each web at a particular exterior support.

Determination of the force at which the structure lifted off the bearings provided the measured reaction at the exterior support. The measured exterior reactions were required to calculate the moment at any section in the exterior spans. The exterior reactions were determined. As lifting force was applied by a hydraulic ram to the underside of an exterior

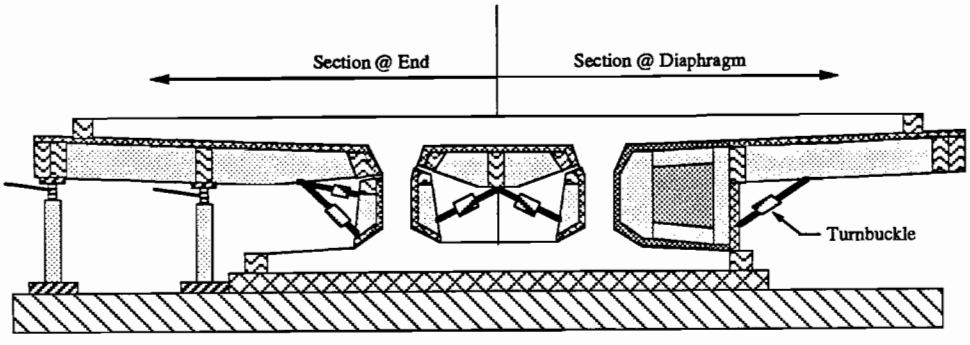

Cross Section

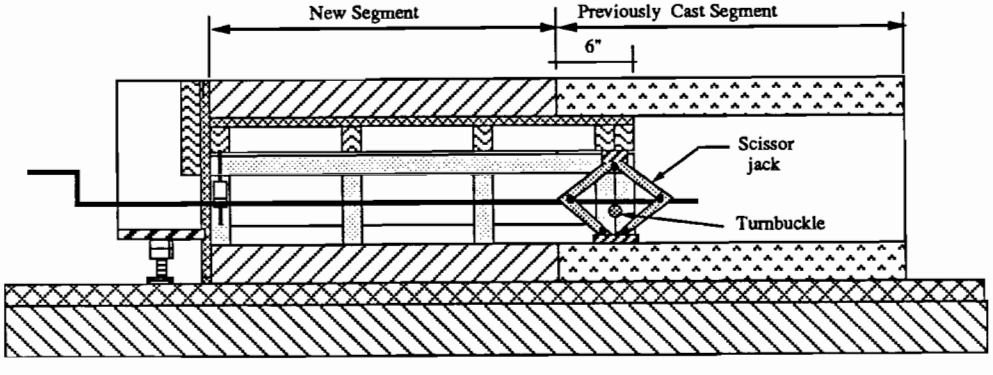

Longitudinal Section

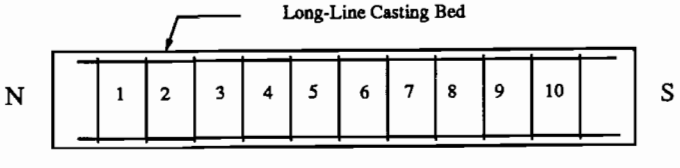

North Span:	6	4,5	3	2	1	2	3	4	5	6
Center Span:	5	4	3	2	1	2	3	4	5	6
South Span:	5	4	3	2	1	2	3	4	5	6

Casting Sequence

Figure 2.10 Typical segment formwork [from Ref. (1)].

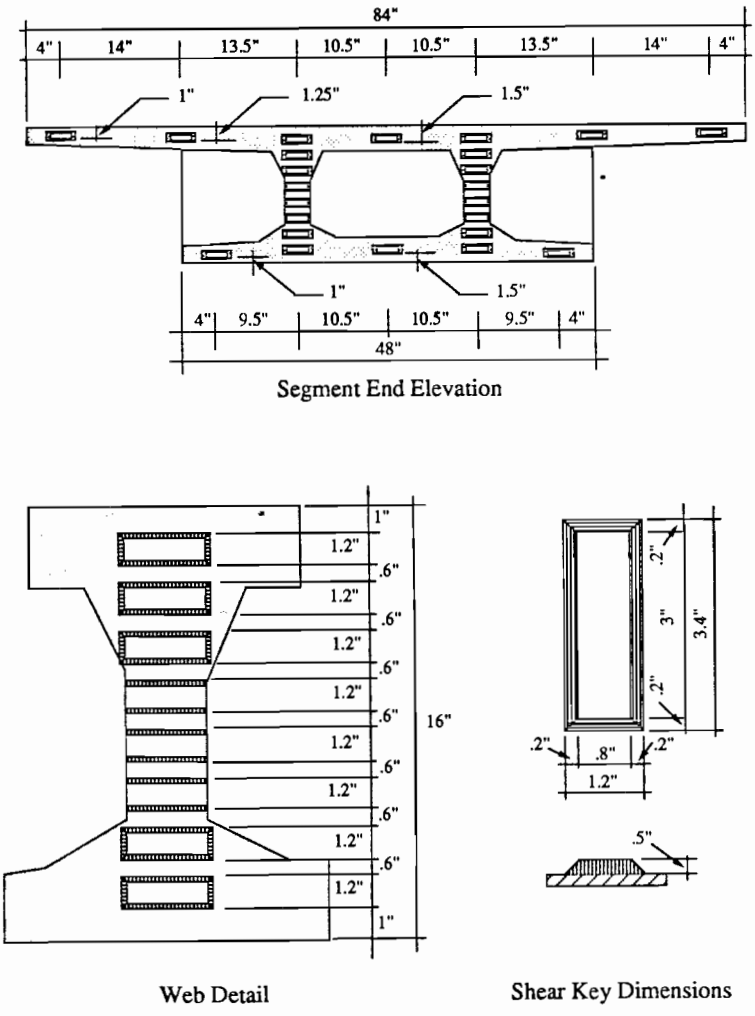

Figure 2.11 Shear key details [from Ref. (1)].

pier segment, the reaction force shifted from the bearing to the hydraulic system. Upward movement during this stage was limited to the rebound deformation of the bearing assembly under the changing reaction force. When the actual reaction force was finally exceeded, the load displacement response at the end of the span changed dramatically. The additional ram force then acted on the end of a long cantilever with a length equal to the span length. With a very small increase in lifting force, the pier segment moved up a relatively large distance. The dramatic change in load-displacement response is clearly seen in Fig. 2.15 for lift-off at the north exterior support and Fig. 2.16 for the south exterior support. The reaction under each web was measured by lifting the structure from the bearing, intializing the load cells, and then setting the structure back on the bearings. The load cell readings gave the reaction under each web. Measured reactions under each web were equalized by lifting the pier segment and inserting shims under the web over the bearings.

2.6.1.2 Effective Prestress Forces. A primary variable for estimating the strength capacity of unbonded prestressing systems is the stress that exists in the tendons prior to reloading of the structure. The effective prestress forces can be best estimated from

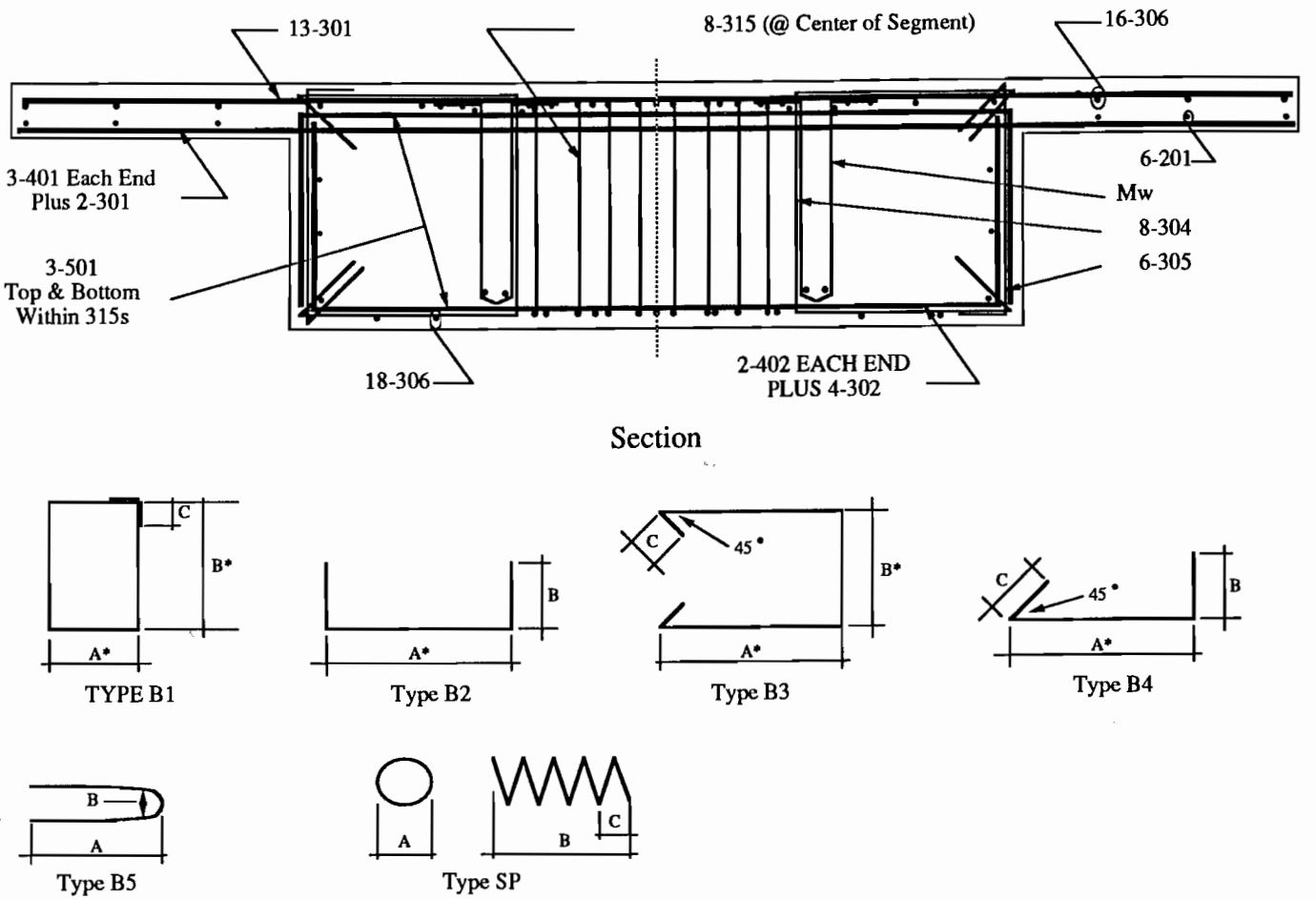

Figure 2.12 Pier segment reinforcement [from Ref. (1)].

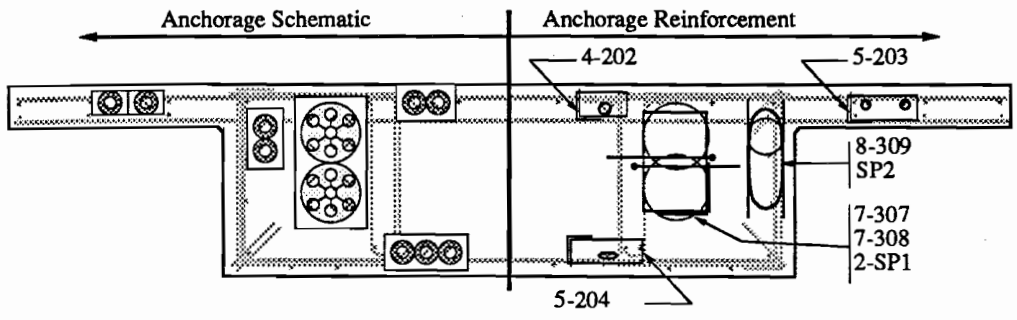

Exterior Face of Exterior Pier Segment

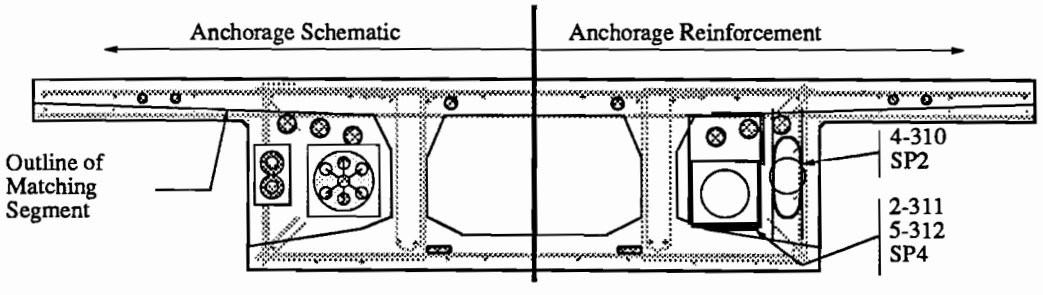

Exterior Face of Interior Pier Segment

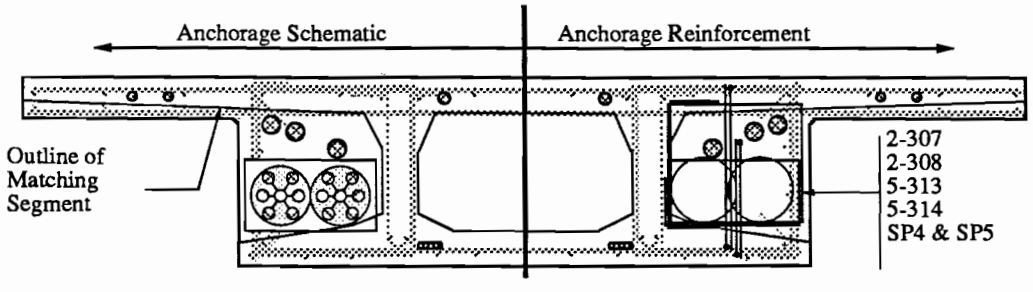

Interior Face of Interior Pier Segment

Figure 2.13 Anchorage zone reinforcement [from Ref. (1)].

the applied moment that causes decompression of the critical joint section. At the decompression moment, stress in the extreme tension fiber at the critical joint becomes zero. From the properties of the uncracked cross section and the experimentally determined decompression moment, stress in the prestress tendons (f_{pd}) can be calculated. Knowing the measured stress changes in the prestress due to the applied decompression loads (f_{pd}-f_{pe}), the effective prestress forces can be calculated.

Three loading cycles were carried out on each exterior span to determine the decompression moment. Changes in prestress forces were measured using strain gauges.

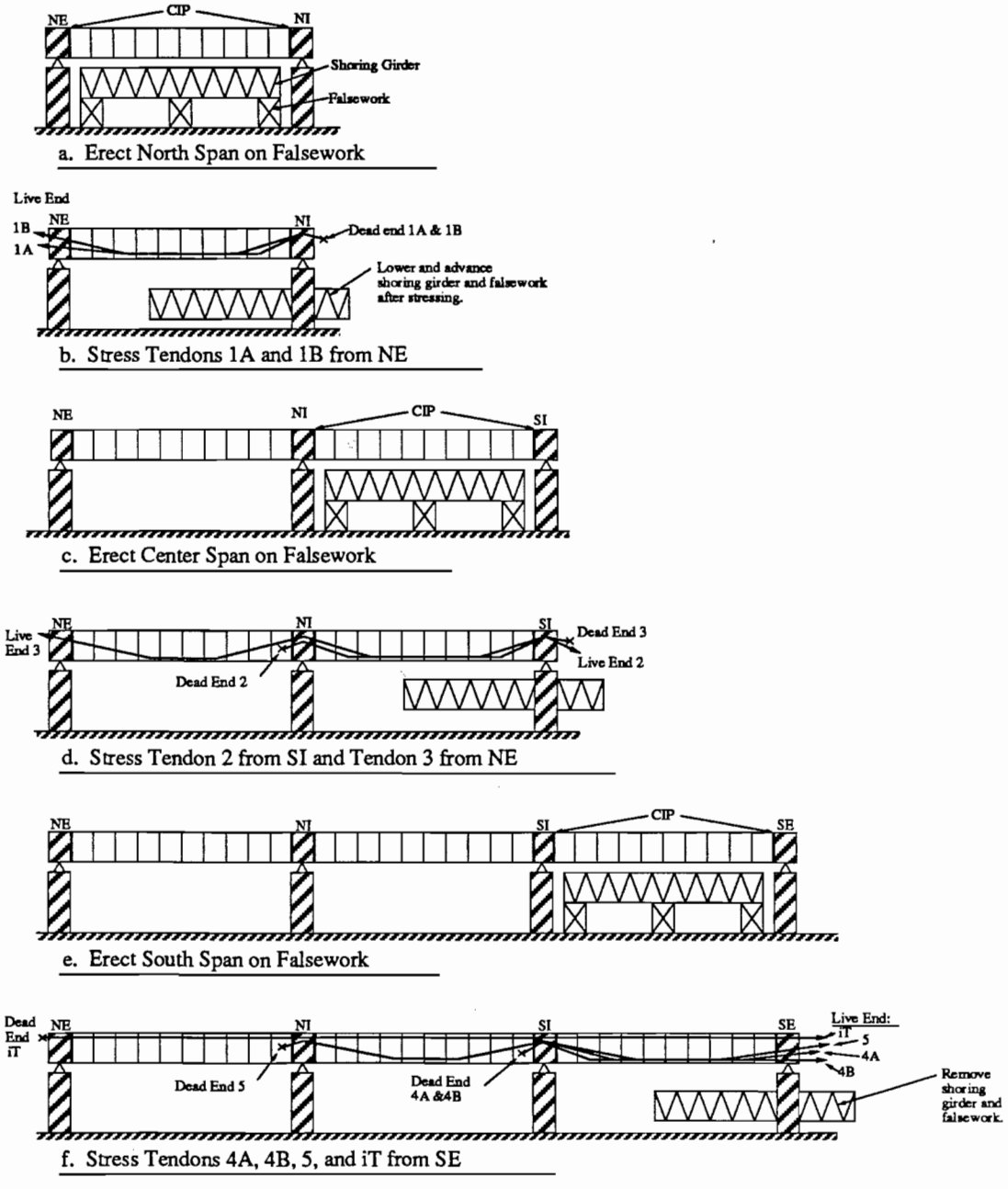

Steps:

a. Erect North Span on Falsework
b. Stress Tendons 1A and 1B from NE
c. Erect Center Span on Falsework
d. Stress Tendon 2 from SI and Tendon 3 from NE
e. Erect South Span on Falsework
f. Stress Tendons 4A, 4B, 5, and iT from SE

Figure 2.14 Span-by-span erection system [from Ref. (1)].

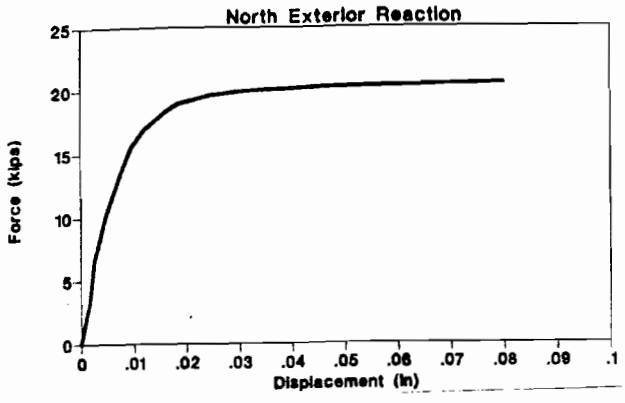

Figure 2.15 North exterior reaction.

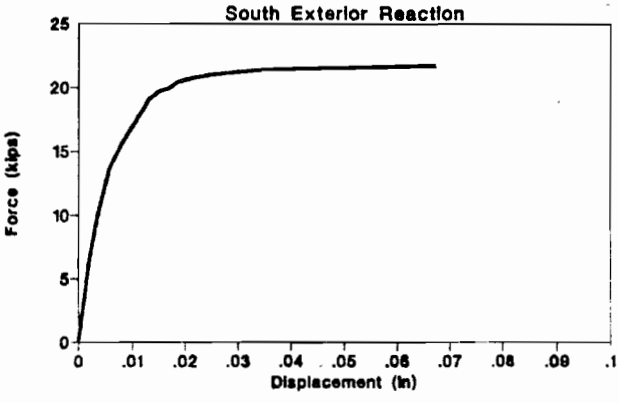

Figure 2.16 South exterior reaction.

The dead load moment was known from the measured reactions as described in Section 2.6.1.1.

Table 2.4 shows the calculation procedure of the effective prestress forces at the critical joint of each exterior span and at the interior supports of the model.

The top and bottom fiber stresses for dead load plus prestress along the bridge model were calculated using a finite element program. Top and bottom fiber stresses are shown in Fig. 2.17. These stresses were within the specified limits shown in Table 2.5. Maximum compressive stresses were well below the limiting stress, and no tension stresses were present in the joints.

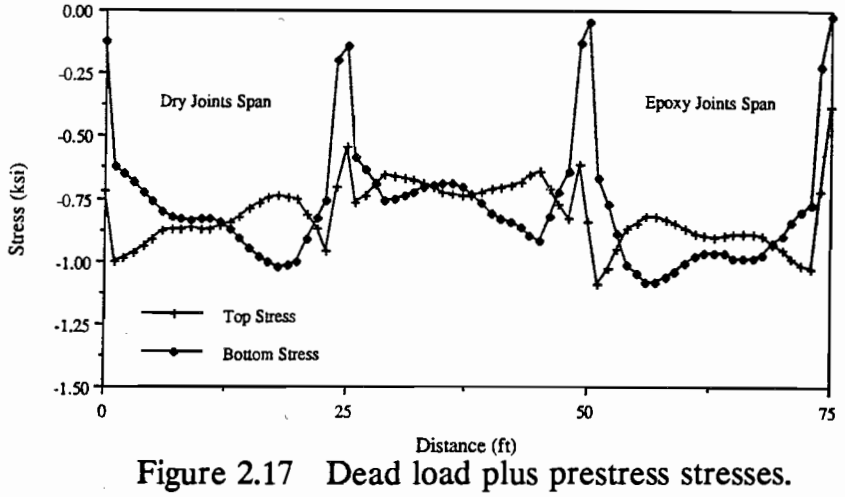

Figure 2.17 Dead load plus prestress stresses.

2.6.2 Damage Inspection and Repair. Damage evaluation and repair of the structure were concentrated in top flanges, webs and bottom flanges, and grout of external tendons. Repairs were needed for the cracks in the webs and bottom flanges of a few segments.

2.6.2.1 Top Flanges. The joints between segments 25-26 and 5-6 were the critical joints for the tests performed in the first part of the program by MacGregor(1). The top flange in the positive moment region carried high compressive stress during flexural strength tests. The strength tests in the first part of the overall program were stopped before the model reached widespread crushing in the top flange but after very low stiffness was observed. This left the top flange essentially undamaged. To further ensure that the tests carried out in the first part by MacGregor(1) would have no effect on the results of the tests which were to be carried out in this part of the study, the load positions were moved away from their previous positions in order to change the position of the critical joints.

2.6.2.2 Webs and Bottom Flanges. Many cracks were found in the bottom flanges and webs of several segments located on both sides of the critical joints of tests carried out in the first part of the project. In the dry joints span many cracks were found in the webs of segments 5 and 6, as shown in Fig 2.18. Also, cracks were found in the bottom flanges and webs of segments 25 and 26 of the epoxy joints span, as shown in Fig 2.19. The web crack widths were of 0.3 mm and less. The bottom flange crack in segment 25 near the joints between segments 25 and 26 was approximately 0.5 mm width. The crack width in segment 26 near the joint between segments 26 and 27 was 0.4 mm. These relatively large crack widths were due to large joint openings during the flexural strength tests carried out in the first part of the project. A fine crack of 0.15 mm width was found in the middle of the bottom flange of segment 26. This crack occurred during the shear strength test.

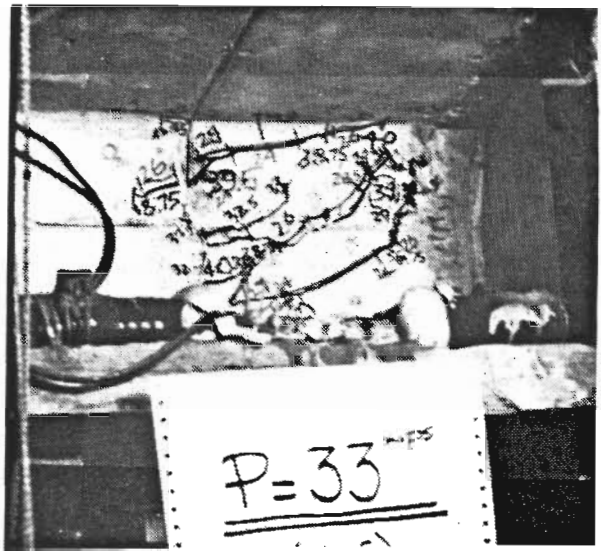

Figure 2.18 North span cracks.

2.6.2.3 Epoxy Injection. Epoxy injection was used to repair the cracked segments of the model. This method of repair was chosen because crack widths were generally small. The HILTI (EP-IS 650) crack injection system was used to repair the cracked segments. The crack injection process was carried out according to recommendations furnished by the manufacturer of the injection system. The crack injection steps were as follows:

a) Sealing Cracks Inside the Box Section

Cracks were sealed from the inside of the box cross section using HILTI (EP-CA) sealing agent to prevent leaking of epoxy into the box section during injection. Two six-inch diameter holes were drilled in the top flange of segments 5 and 26 of the model as shown in Fig. 2.20. These holes were used for access to seal the cracks from the inside of the box section. A coring machine was used to drill the two holes. The holes were drilled in the middle of segment 5 and 26 away from the joints because the top-flange joint carries high compressive stresses at ultimate.

b) Injection Ports

Injection ports were installed on the cracks on the outside face of the box cross section. Spacing between the ports ranged from 3 to 5 inches. Short port spacings were used on fine crack widths to ease the injection process and to make sure that cracks were filled with epoxy. Ports were installed, as shown in Fig. 2.21, using the EP-CA Trowel Compound.

c) Sealing of the Cracks on Exterior of Section

Sealing of the cracks from the outside face of the box cross section between the injection ports was carried out by using Ep-CA Trowel Compound. The sealing process, as shown in Fig. 2.22, was carried out twenty four hours after installing the injection ports.

d) Injection of Cracks

Mixing of resin with the hardener, and the injection process were carried out using the HILTI (EP-IS 650) crack injection system. The injection process is shown in Fig. 2.23. No loads were applied to the model while injecting the web and the wide, bottom-flange cracks. Service loads were applied to the model while injecting the fine crack in the bottom flange of segment 26 (0.15 mm width) to ease injection by reducing the compressive stress in the crack. Loads were removed as soon as the injection process was completed and before the epoxy was hardened to insure that no additional prestress was added once the epoxy material injected in the crack hardened.

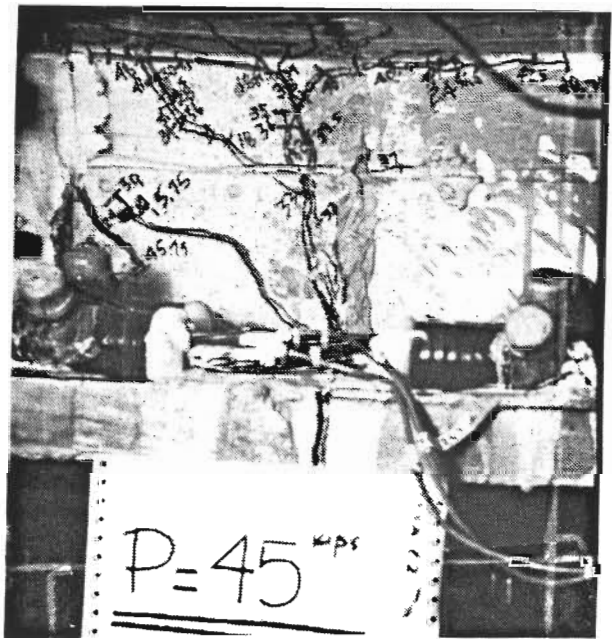

Figure 2.19 South span cracks.

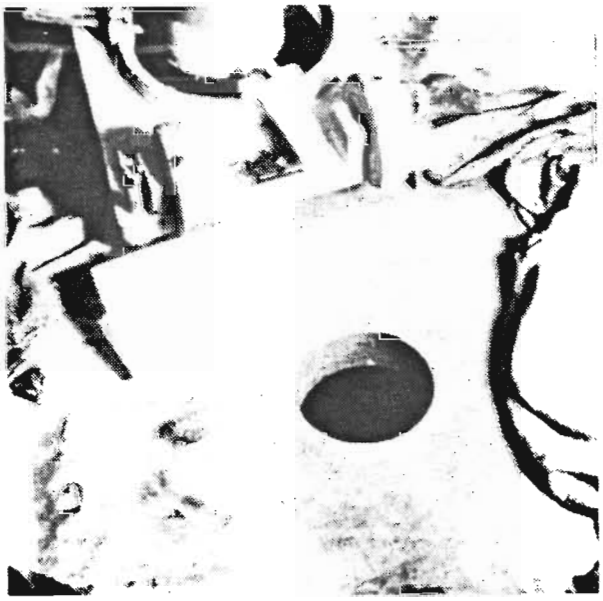

Figure 2.20 Access holes.

2.6.2.4 Grout of External Tendons. The external tendons were to be bonded to the diaphragms at pass through locations in this part of the program. The external tendons were grouted inside 1.5" diameter ducts in the first part of the study by MacGregor(1). The grouted ducts would be bonded to the diaphragms at pass through locations in this part of the program. The limiting bond strength between the tendons and the concrete diaphragms is the lesser of two bond values: The bond strength of the grout between the tendons and the duct, and the bond strength between the duct and concrete diaphragms. The bond between the tendons

Table 2.4 Calculation of Effective Prestress Forces

Location	4:5	N1:11	20:S1	26:27
Joint Type	Dry	Epoxied	Epoxied	Epoxied
x (ft.)	10.25	26	49	64.75
Ac: ($in.^2$)	450	450	450	450
S. top: ($in.^3$)	2512	2512	2512	2512
S. bot:	1757	1757	1757	1757
(Ap) ext. ($in.^2$)	2.04	1.53	1.53	2.04
(Ap) int	.68	.68	.68	.68
(Ap)	2.72	2.21	2.21	2.72
(3) ext (in.)	6.01	-1.4	-1.4	6.01
Corrected (e) ext	5.76	-1.4	-1.4	5.76
(e) int	-5.35	-5.35	-5.35	-5.35
(e) eff	2.983	-2.62	-2.62	2.983
$(A) = \left(\left(\frac{1}{A_c}\right) + \left(\frac{e}{S}\right)\right)$	.0039	.0033	.0033	.0039
Dead Load Moments (M_{d1}) Measured Moments (from reaction data)	110.0	-64	-23	127.0
Decompression Load Moments (M_d) Measured Moments	100	-200	-250	135
$(B) = \frac{(M_{d1} + M_d)}{S}$ Data	1.43	-1.26	-1.30	1.790
Tendon Force and Tresses $T_{pd} = \frac{(B)}{(A)}$ Data	360.0	381.8	394.0	458.0
$fpd = \frac{Tpd}{Ap}$ (ksi) Data	134.0	172.5	178.0	168.0
$fpd - fpe$ (Measured in Tests) (ksi)	2.5	1	1	3.0
fpe (ksi) Data	131.5	171.5	177.0	165.0

Figure 2.21 Injection ports.

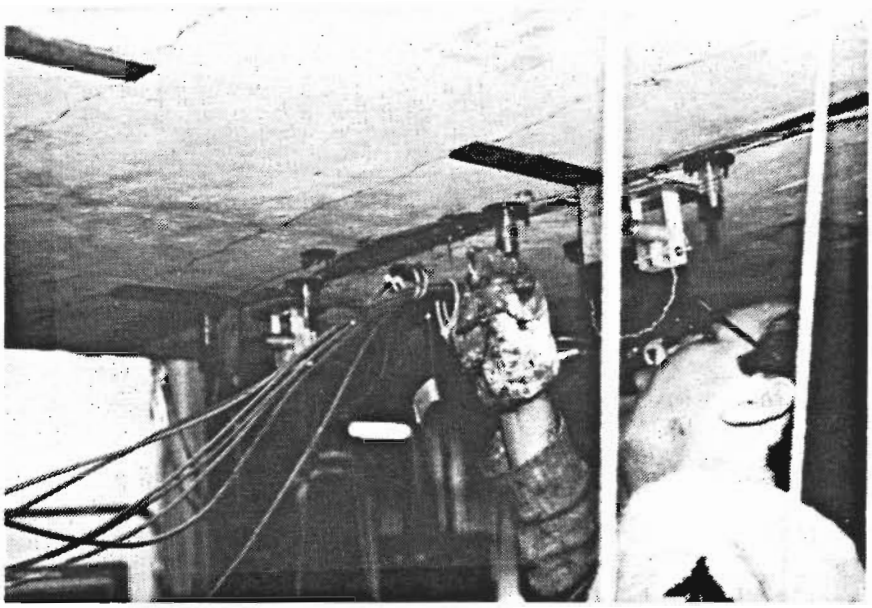

Figure 2.22 Sealing the cracks.

and the duct was studied by Radloff(10) as part of this project. The bond between the duct and the concrete diaphragms was studied in this portion of the project and will be reported later in this chapter. The bond material inside the duct (the grout) was inspected at pass-through locations. The inspection process was done at randomly selected places. An opening was made in the duct on the two sides of the diaphragm to inspect the grout. The inspection process showed the grout to be in good condition; and no cracks were found in the grout.

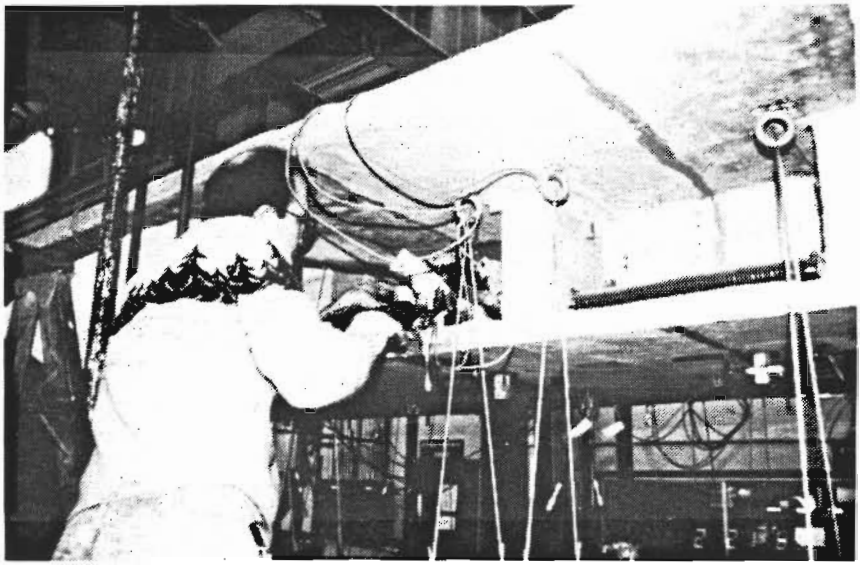

Figure 2.23 Injection of epoxy.

2.7 Bonding of External Tendons

External tendons were bonded, during construction, at diaphragm locations where tendons were deviated, and at all pier segments. At all other diaphragm locations, tendons were simply passed through the diaphragms. Provisions were made to allow bonding of external tendons at all pass-through locations in diaphragms. Flexible electrical conduit was used for the duct at pass-through locations to allow bonding of the external tendons to the diaphragms. One of the objectives of this study was to examine the behavior of segmental bridges with bonded external tendons. In the test program, external tendons were bonded in three stages at various pass-through locations as shown in Table 2.6. Load tests were executed between the stages of tendon bonding. Bonding of the external tendons at pass-through locations was done by bonding the 1.5" thin-walled electrical conduit to the diaphragms. The electrical duct contained the previously grouted external tendon and had passed through an oversize 2" diameter hole preformed in each diaphragm. The electrical ducts were bonded to the diaphragm at the 2" diameter hole as shown in Fig. 2.24. Before bonding the duct to the concrete diaphragms, different materials and procedures were tested to find the best bonding procedure and material.

2.7.1 Tests of Different Materials for Tendon Bonding. Concrete blocks with 2" diameter holes were cast to test the bond strength of the materials expected to be used with the bridge model. The concrete blocks had the same thickness (5") and hole dimensions (2") as the diaphragms in the model. The variables used in the bonding tests were the sealing agent and the bonding material. The sealing agent was used to seal the outer edges of the space between the duct and the concrete holes in the diaphragms in order to contain the injected bonding material. Two different sealing agents (silicone and epoxy) were tried. The second variable was the bonding material injected in the space between the duct and the concrete hole. Three different injection materials were used in this study (Cement grout, A103 epoxy adhesive, and the Hilti crack injection epoxy system). Cement grout was

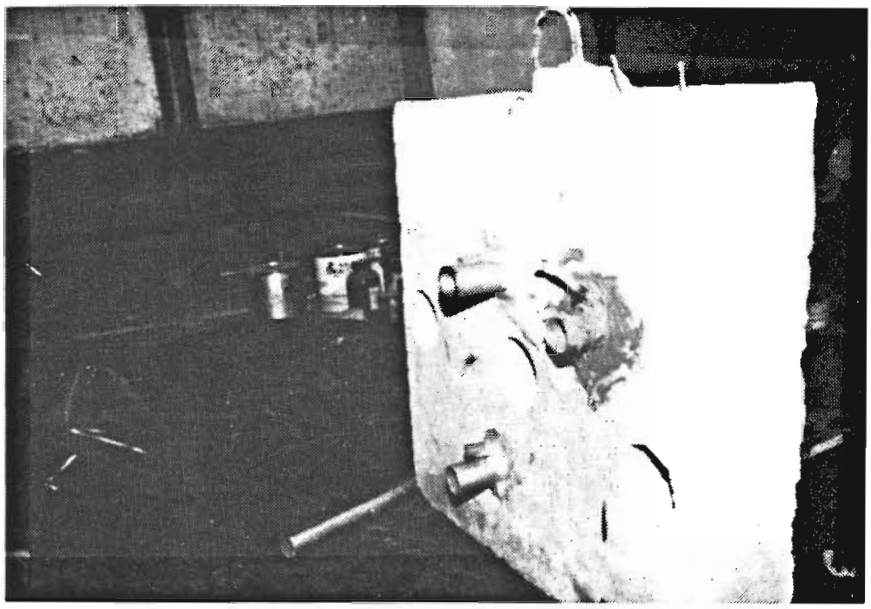

Figure 2.24 Bonding specimen.

used with two different water cement ratios (0.4 and 0.5). A103 epoxy adhesive was used with two different fillers (magnesium and sand). The filler was used to increase the modulus of elasticity of the epoxy and to reduce the amount of epoxy used in the bonding process. The Hilti crack injection system (EP-IS 650) was used as the third injection material.

Three specimens were tested for each combination of sealing agent and bonding material. A seven day curing period was given for the injected epoxy to cure before testing was carried out. Specimens were tested by pushing the grouted duct through the concrete blocks using a 600 kip testing machine. All specimens failed in bond between the duct and the bonding material.

A103 epoxy adhesive with 50% sand as filler was selected for bonding the external tendons to the diaphragms because of its high strength compared to the other materials. Test results are shown in Fig. 2.25. Epoxy sealing agent was selected because of its high strength and workability. The A103 epoxy was obtained from the Texas State Department of Highways and Public Transportation. A103 epoxy is usually used to bond steel to fresh or hardened concrete, or bond concrete to concrete. Mixing of the epoxy was done according to the recommendations obtained from the material supplier.

2.7.2 Bonding Procedure. Due to its simplicity and efficiency, the following procedure was used for bonding the external tendons to the intermediate diaphragms. The bonding procedure was as follows:

a) Install two injection ports between the duct and the concrete hole, one on each side of the diaphragm. The ports consisted of 1/2" diameter flexible plastic pipe (because the flexible pipe can be bent to fit in the space between the duct and the concrete diaphragm). The first port (inlet) was installed in the lowest part of the space between the duct and the concrete hole. This port was used for injection of the

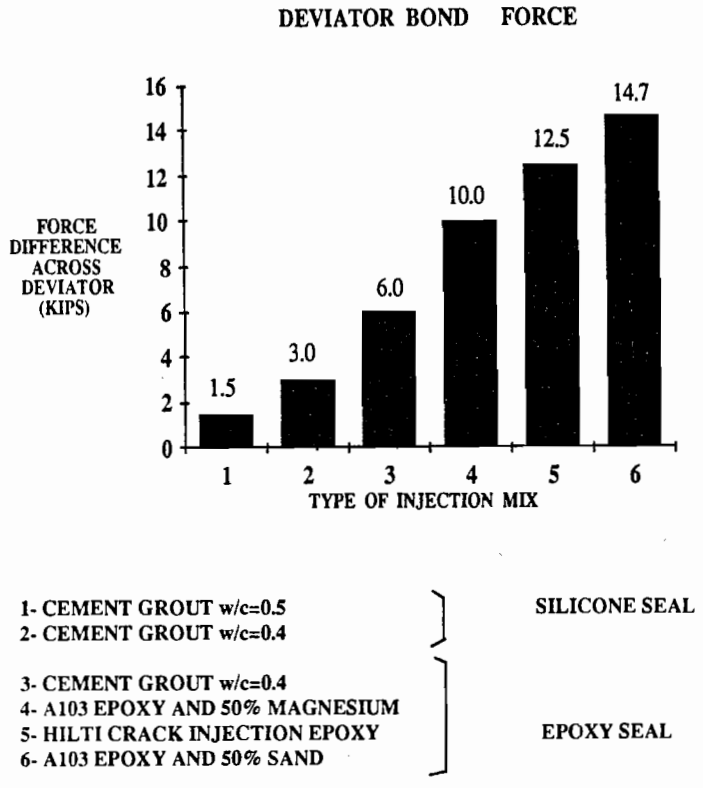

Figure 2.25 Bond tests.

bonding material. The second port (outlet) was installed on the opposite side of the diaphragm at the highest part of the space between the duct and the concrete diaphragm, as shown in Fig 2.26. This port was used to get the trapped air out of the space and to make sure that the space was full. Injection was continued until the epoxy material flowed out through the upper port (outlet).

b) Seal the outer edges of the space between the duct and the concrete on the outer sides of the diaphragm after installing the two ports. Sealing was done using mid-range epoxy A103 obtained from the Texas State Department of Highways and Public Transportation. The sealing agent was allowed to cure for 24 hours before injection. Mixing and handling of the epoxy material was done according to the recommendations obtained from the supplier.

c) Inject the epoxy with a plastic tube and a caulking gun. The tubes were filled with the mixed epoxy and the material was injected using the caulking gun. A seven day curing period for the injected epoxy was observed before loading the model.

2.8 Strengthening of the Model

Strengthening of the three-span bridge model was done by prestressing and grouting four 3/8" diameter internal tendons in the bottom flange of the model. Tests were carried out after stressing the internal tendons but before grouting them. After the first series of

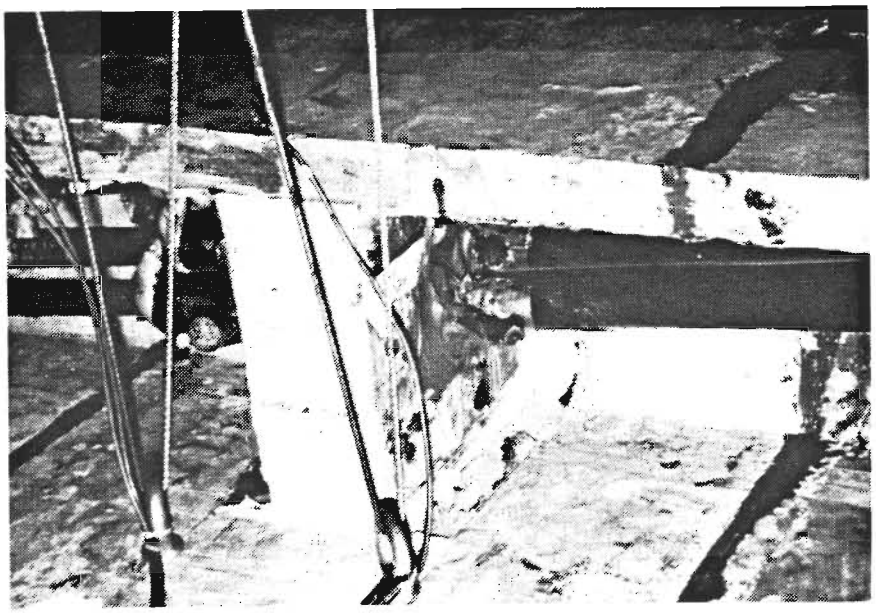

Figure 2.26 External tendons bonding.

tests, the bottom internal tendons were grouted and a second series of tests were carried out.

2.8.1 Stressing of Internal Tendons. Stressing of the four 3/8" diameter strands in the bottom flange of the bridge model was done using a monostrand ram with an internal seating device. During the seating process, the internal seating cone extends forward until the ram force bears against the wedges. This forces the wedges into the anchor barrel and reduces the subsequent loss.

The jacking force was controlled with the use of a by using a pressure dial gauge and an electrical pressure transducer. Approximate forces were controlled visually by reading the pressure gauge while the exact jacking forces were measured with the pressure transducer connected to a strain indicator box. Each hydraulic setup used (rams, hoses, pressure gauges, and transducers) was calibrated prior to the stressing process.

The four single-strand tendons were stressed alternately beginning with one of the outside two tendons and ending with one of the inside two tendons. Strands were stressed in one operation to the full jacking force of 80% of the nominal tendon capacity.

2.8.2 Grouting of Internal Tendons. The grout mixture used was the standard Texas State Department of Highways and Public Transportation grout mixture used for post-tensioning ducts. It consists of 1 part cement to 1/2 part water with 1 oz. expansive admixture per hundred pounds of cement. The grout was mixed in a grout mixer and then dispensed into a 10 gallon pressure canister which forced the grout into the internal tendon ducts. A compressed air system was used for the injection so that excessive pressures would not build up within the tendon ducts. Grout ports for the internal tendons were provided at cast-in-place closure strips at the end of each span.

2.9 Instrumentation

The three-span bridge model was instrumented to measure the response of the structure to the applied loads. The applied loads and reactions were measured to calculate moments and to monitor the load distribution in the model. Deflections were measured along the three-span model and were used to obtain the load-deflection response of the structure. External tendon stresses were measured along the model to get the load vs external tendon stress response and to monitor bond stresses between of the external tendons and the diaphragms. Joint openings along the loaded span were measured at different load levels.

Due to the large number of measurements an electronic data acquisition system was used to record the model response to the loads. Electronic and manual gauge readings were used to record deflections and joint openings.

2.9.1 Support Reactions. Reactions were measured for the exterior supports and the south interior support as shown in Fig. 2.27. Two load cells (one under each web) were used for each reaction. Two 100-kip capacity load cells were used for the exterior reaction, and two 200-kip capacity load cells were used for the south interior support. The full bearing assembly was calibrated in the testing machine and the overall compressive deformations were measured.

2.9.2 Deflections. The locations of potentiometers used to measure vertical deflections during testing of the bridge are shown in Fig. 2.27 and Fig 2.28. Figure 2.27 shows the position of potentiometers for any unloaded span during all tests performed in this study. Figure 2.28 shows the potentiometer locations in a loaded span. The vertical deflections are measured under the bottom flange either at two points at equal distance from the center line or along the center line. Dial gauges were used to measure vertical deflections at maximum displacement locations to verify the electronic data.

2.9.3 Joint Opening. Distortions along the height of the critical opening joint or crack and the two adjacent joints (one on each side of the critical joint) were measured during testing. The critical joint position was determined from elastic and plastic analysis. The critical joint position moved as the load position moved. Behavior of the joints was measured in two ways. Linear voltage displacement transducers were mounted on the tension flange of the section using plexiglass brackets as shown in Fig. 2.29. Distortion at various depths of the joint was measured by grid-type crack monitors shown in Fig. 2.30. The device consists of overlapping planes of plexiglass. The joint opening at that level is measured by the relative displacement of the matching grid on the two planes of plexiglass. Relative movement of the grid was read using a theodolite. Joint rotations were calculated from joint opening measurements at different levels. Fig. 2.31 shows the positions of the joint opening transducers.

2.9.4 Load. Two 60-kip capacity hydraulic rams were used to apply the load to the structure. Two pressure transducers and a pressure gauge were used to measure and control the hydraulic pressure while testing.

2.9.5 Strand Strain. External tendon strains were measured along the three-span model at locations shown in Fig. 2.32. Two strain gages were attached to each strand at each location. The strains were measured using 0.16 in. by 0.24 in. resistance type strain gauges. The gauges were attached to single wires of a 3/8 in. diameter, 7-wire strand.

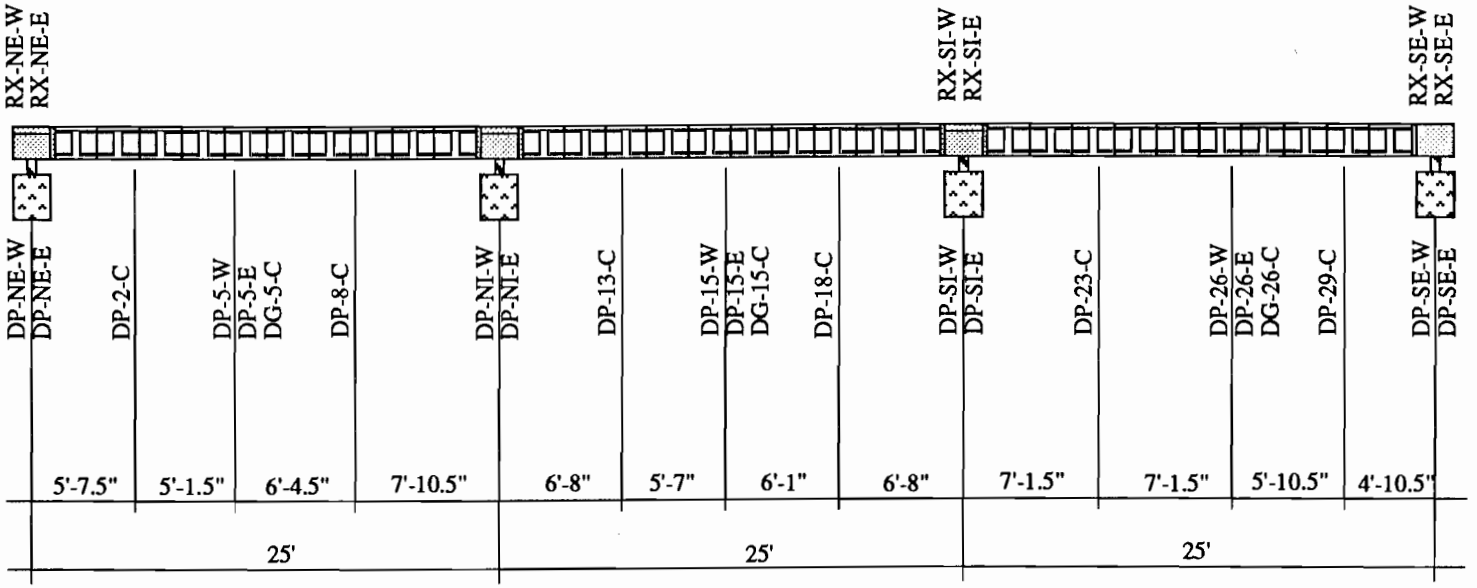

RX-NE-W: Reaction-North Exterior End-West Side

DP-SI-E: Deflection Potentiometer-South Interior- East Side

Figure 2.27 Instrumentation layout for reactions and deflection (deflection of unloaded span).

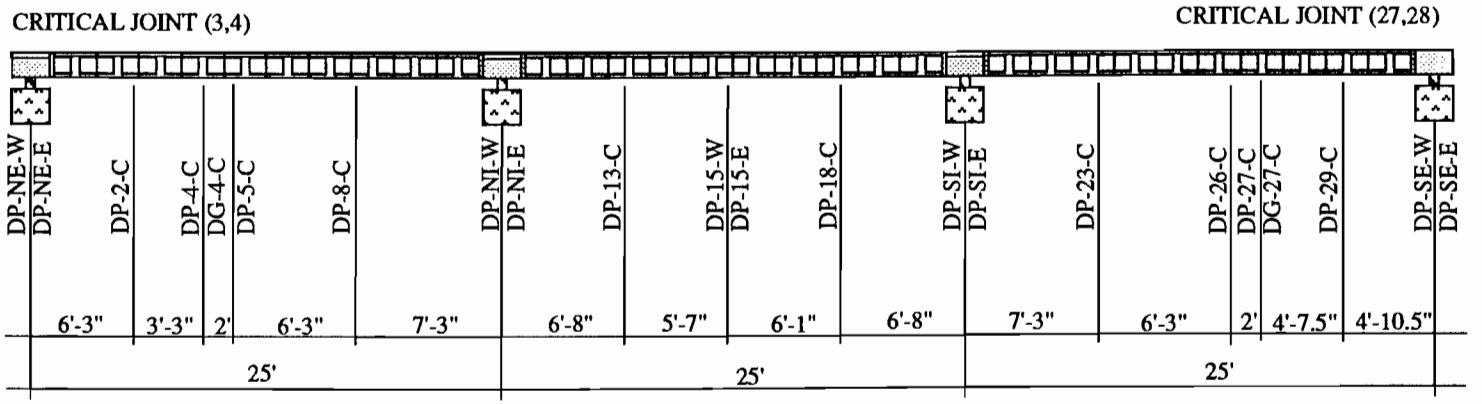

a) Phase One and Two

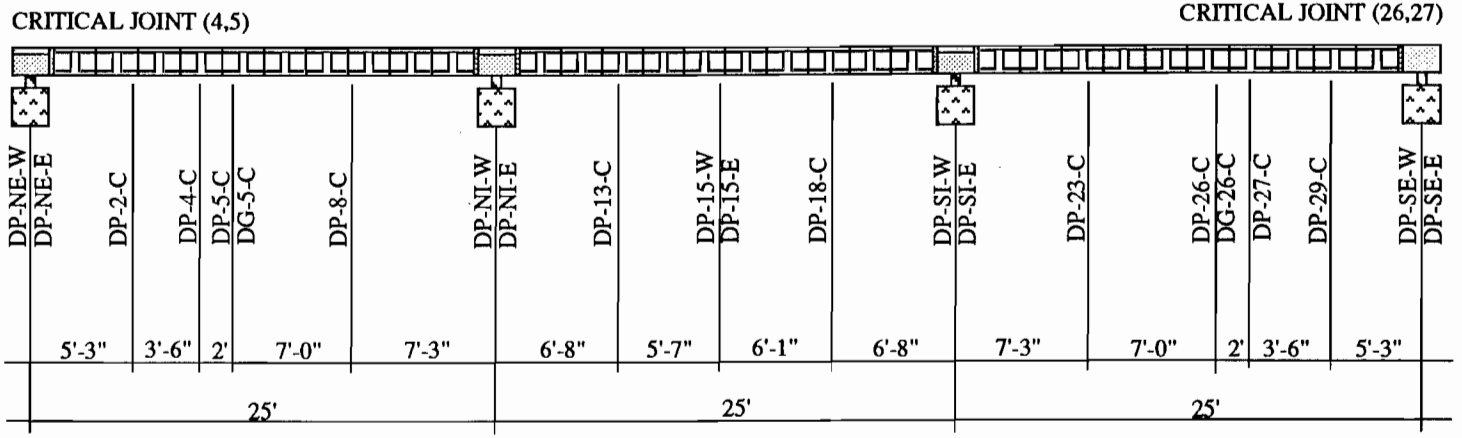

b) Phase Three

Figure 2.28 Instrumentation layout for deflection of loaded span.

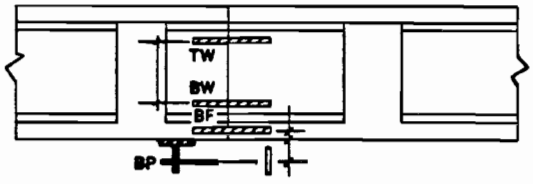

Distance
from Top (inches) *

	JOINT				
LOCATION	(3,4)	* (4,5)	(5,6)	(25,26)	(26,27)
Top Web	6.95	7.00	7.05	7.11	7.12
Bottom of Web	11.01	11.06	11.11	11.17	11.18
Bottom of Flange	15.12	15.18	15.19	15.10	15.15
Bottom Potentiometer	17.65	17.71	17.72	17.63	17.68

*Calculated from measured segment dimensions

Figure 2.29 Web distortion and joint opening instrumentation [Ref. (1)].

2.10 Demolition of the Model. The three-span bridge model was demolished soon after all tests were carried out. A finite element program was used to calculate the top and bottom fiber stresses of the bridge cross section at different stages of the demolition process. Fig. 2.33 shows the calculated top and bottom fiber stresses with full dead load blocks suspended from the model before starting the demolition process.

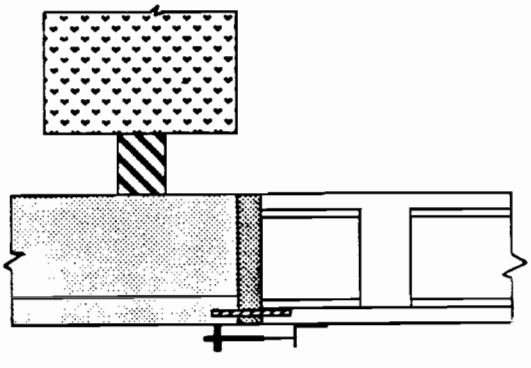

Figure 2.30 Joint opening instrumentation [Ref. (1)].

2.10.1 Demolition Procedures. A demolition procedure was decided on after studying many possible alternatives. The first of the two main alternatives studied in detail was to disassemble the bridge into the original segments by supporting each span on falsework, detention the prestressed tendons, then, finally, break the epoxy joints. The second alternative was to disassemble the model into three pieces by supporting only the middle span, and then break out the sections at the two ends of the middle span after cutting the prestressed tendons at these sections. The bridge could then be removed by picking up each span as a unit. The two alternatives were judged based on applicability, safety, difficulty, and demolition time. The second alternative was chosen for its safety, simplicity, and speed. Top and bottom fiber stresses were checked at all stages of the proposed demolition processes for the two alternatives using a finite element program. The procedure selected for use in demolishing the model was as follows:

Figure 2.28 Instrumentation layout for deflection of loaded span.

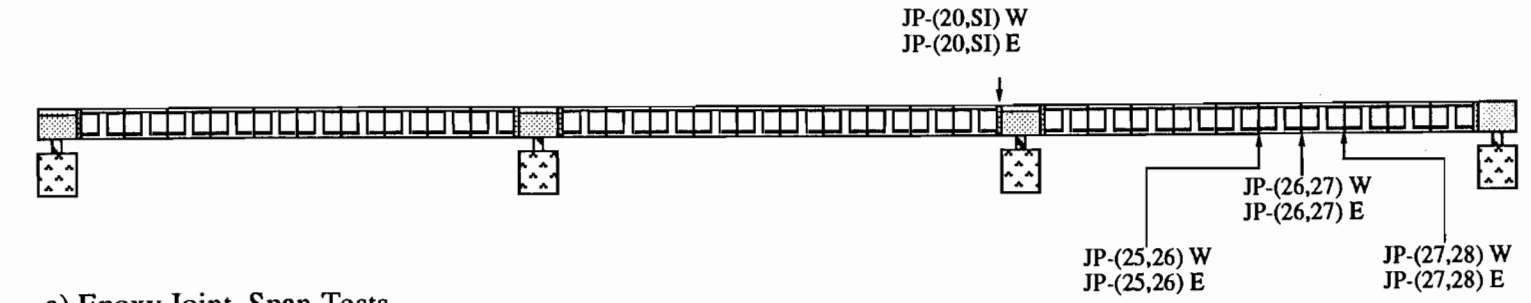

a) Epoxy Joint Span Tests

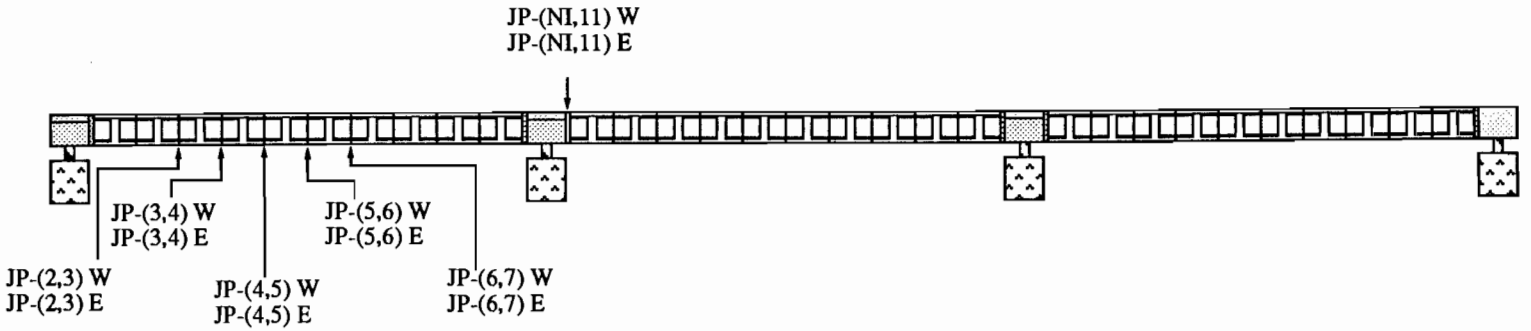

b) Dry Joint Span Tests

JP-(6,7) W: Joint Potentiometer- Joint (6,7)- West

Figure 2.31 Joint opening instrumentation layout during testing.

Figure 2.31 Joint opening instrumentation layout during testing.

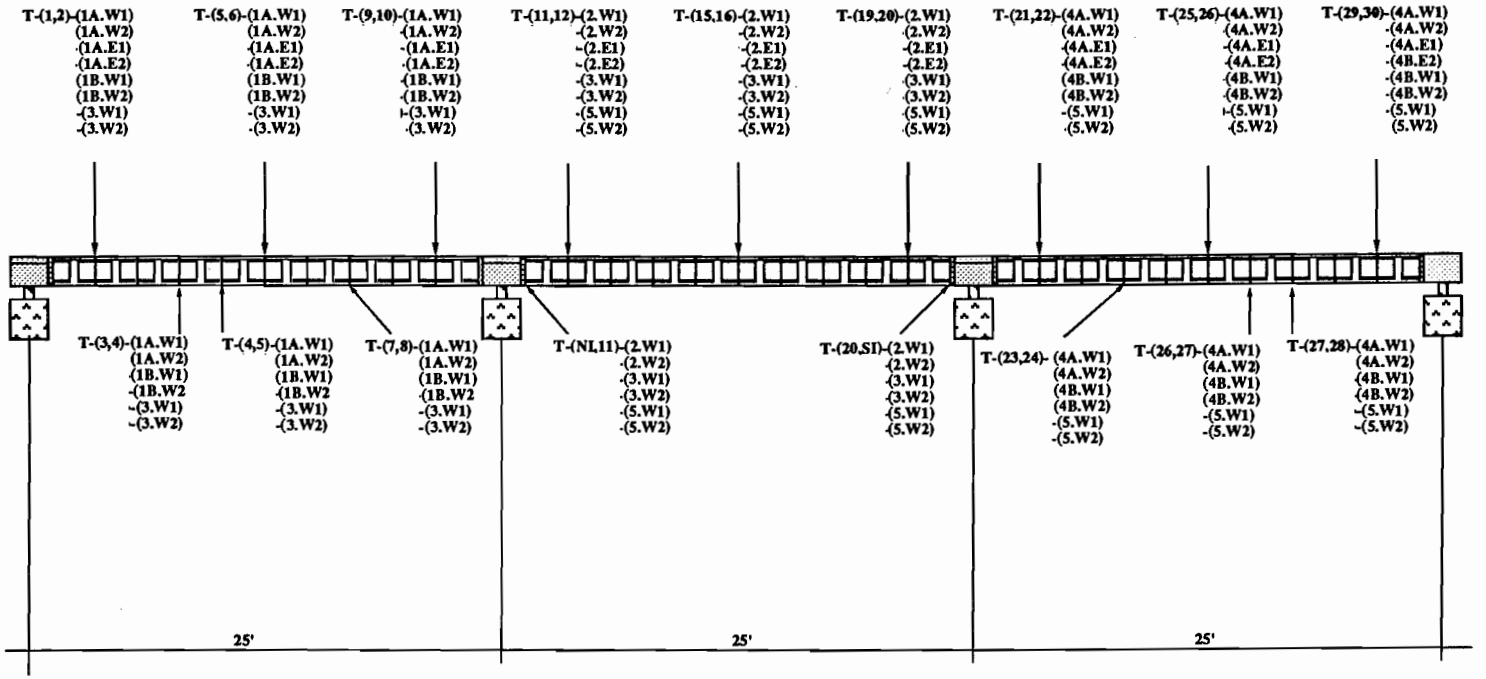

T-(9,10)-1A.W1: Tendon Strain-Joint (9,10)-Tendon 1A.West 1

Figure 2.32 Instrumentation layout for strain gauges.

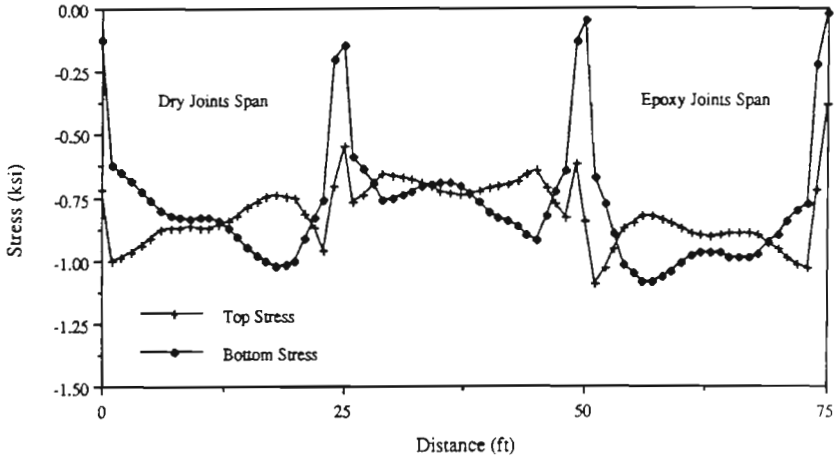

Figure 2.33 Flexural Stresses due to dead load plus prestress.

a) Remove Dead Load Blocks

The dead load blocks were removed from the middle span of the three span bridge model as shown in Fig. 2.34. The calculated top and bottom fiber stresses after their removal were obtained by using a finite element program and are shown in Fig. 2.35. Compressive stresses at this stage were within the allowable limits shown in Table 2.5. The finite element program showed that there could be a small tension stress of 0.15 ksi in the bottom flange of the interior pier segment. The predicted tension stress was well below the tension capacity of the concrete, so no cracks were expected to occur by removing the dead load blocks from the interior span.

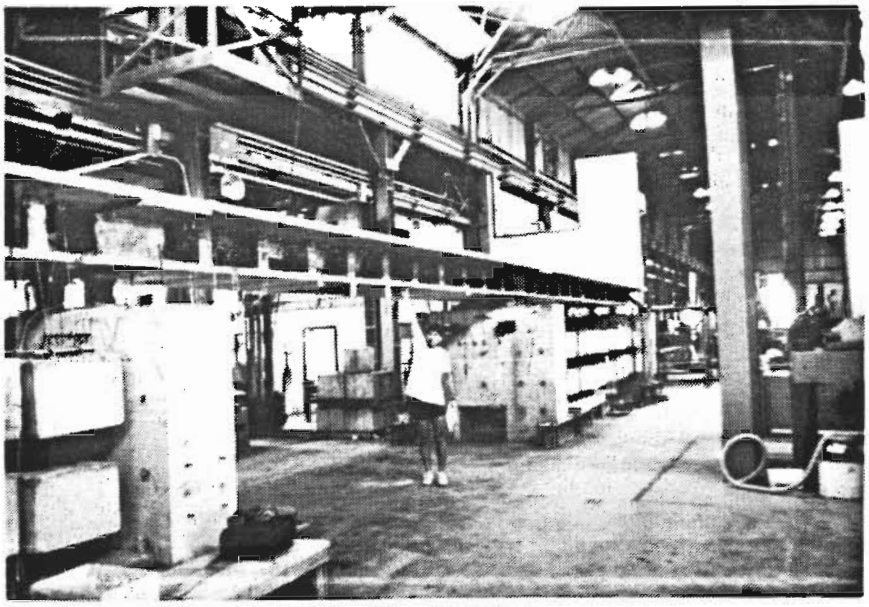

Figure 2.34 Middle span dead load blocks removed.

Table 2.5 Concrete Stress Limits for Model Structure

Condition:

- Segmental construction
- Stresses at service loads after losses have occurred
- Less than 50% bonded prestressed reinforcement
- Without bonded mild reinforcement crossing joints
- Design specified concrete strength (f_c') of 6000 psi

	February 1988 Final Report[16] Limit:	AASHTO Interim Specification[15] Limit:
Compression All Members	$0.40f_c'$	f_c'
Tension Precompressed Tensile Zones:		
Dry Joints:	200 psi (comp.)	200 psi compression
Epoxied joints:	0 psi	0 psi tension

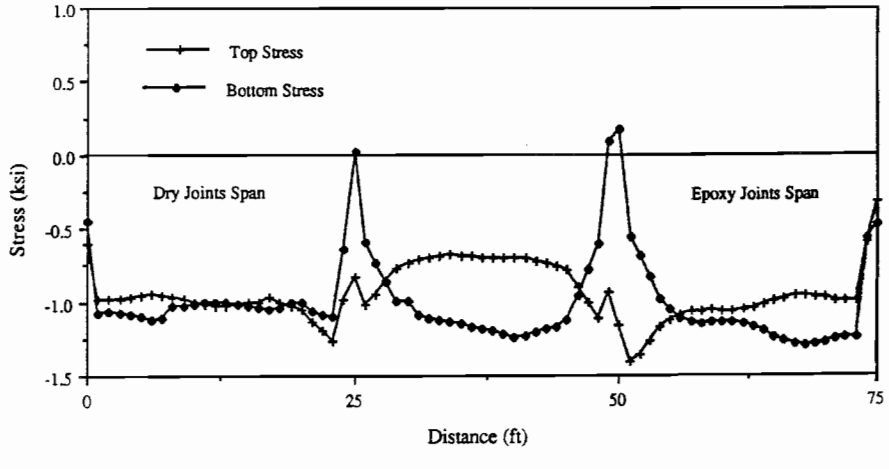

Figure 2.35 Flexural stresses without center span dead load blocks.

b) Support the Middle Span

The middle span was then supported by a steel beam as shown in Fig. 2.36. Two I-section beams were inserted between the supporting beam and the bridge at the two ends of the interior span. A 1" gap was left between the I-section beams and the bridge bottom flange. The interior span rested on the two I-sections after the interior span was separated

Table 2.6 Segments Bonded to External Tendons			
Tendon	Stage One	Stage Two	Stage Three
1A	2,4,7,9	2,4,6,7,9	1,2,3,4,5,6,7,8,9,10
1B	3,4,7,8	2,3,4,6,7,8,9	1,2,3,4,5,6,7,8,9,10
2	12,14,17,19	12,14,17,19	11,12,13,14,15,16,17, 18,19,20
3	4,7,13,14,17,18	2,4,6,7,9,12,13,14,17, 18,19	1,2,3,4,5,6,7,8,9,10,1 1,12,13,14,15,16,17,1 8,19,20
4A	22,24,27,29	22,24,25,27,28	21,22,23,24,25,26,27, 28,29,30
4B	23,24,27,28	22,23,24,25,27,28,29	21,22,23,24,25,26,27, 28,29,30
5	14,17,24,27	12,14,17,19,22,24,25, 27,29	11,12,13,14,15,16,17, 18,19,20,21,22,23,24, 25,26,27,28,29,30

from the two exterior spans by cutting the tendons and demolishing the concrete at the two ends of the interior span.

c) Cut the Tendons

The prestress tendons were cut at the ends of the interior span to separate the middle span from the two exterior spans. External tendons were cut first using a cutting torch, then the internal tendons were cut using a grinder. Figure 2.37 shows the tendons after they have been cut.

d) Separate the Three Spans.

Separation between the interior span and the two exterior spans (at each end) was accomplished by demolishing the concrete at the two ends of the interior span. A jack hammer was used to remove the concrete. A gap of about 2" was created at the two ends of the center span, as shown in Fig. 2.38. The interior span was completely supported by the two I-sections as soon as the separations were formed.

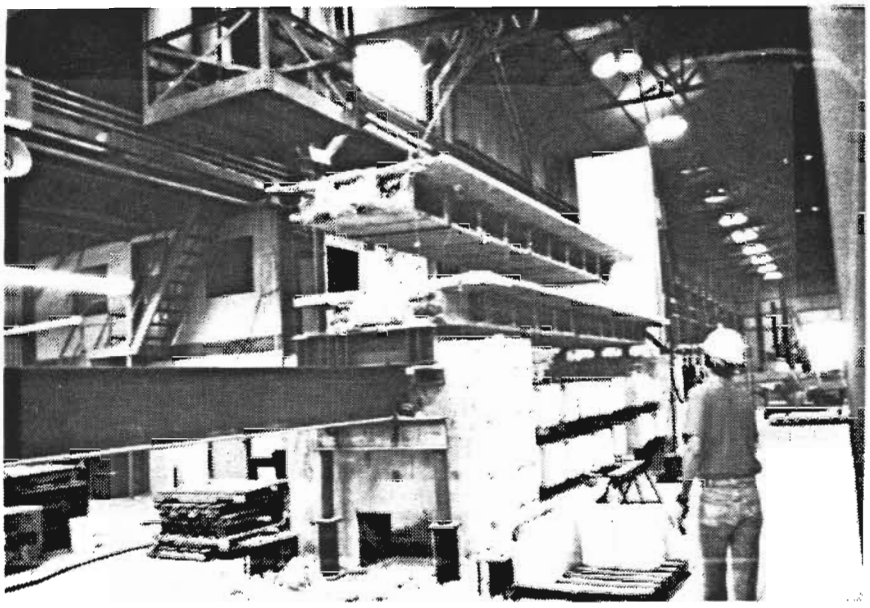

Figure 2.36 Supporting beams.

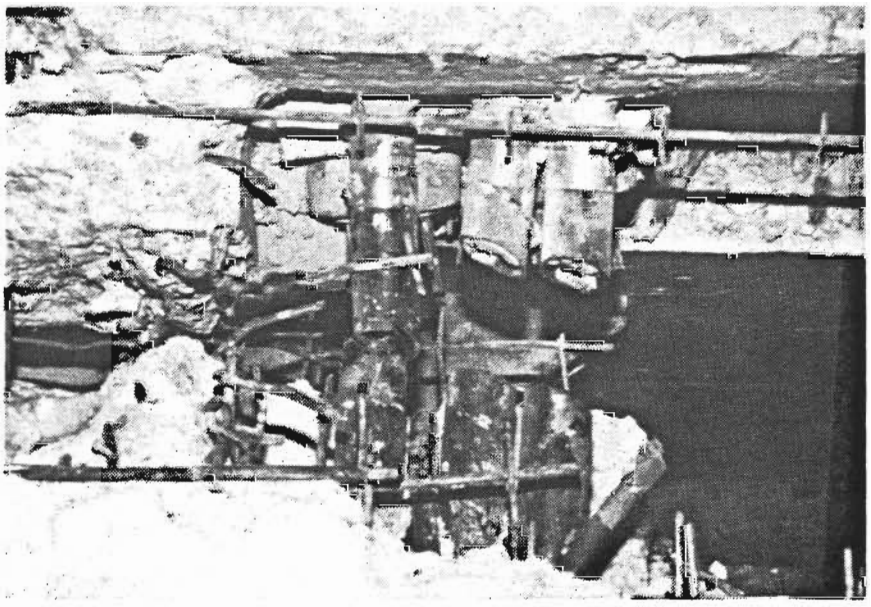

Figure 2.37 Cutting of tendons.

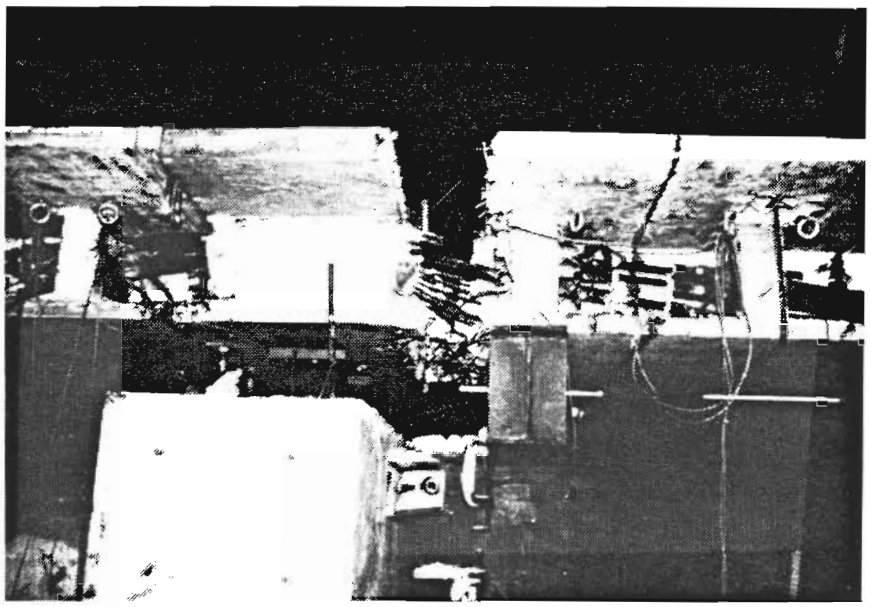

Figure 2.38 Separation at ends of interior span.

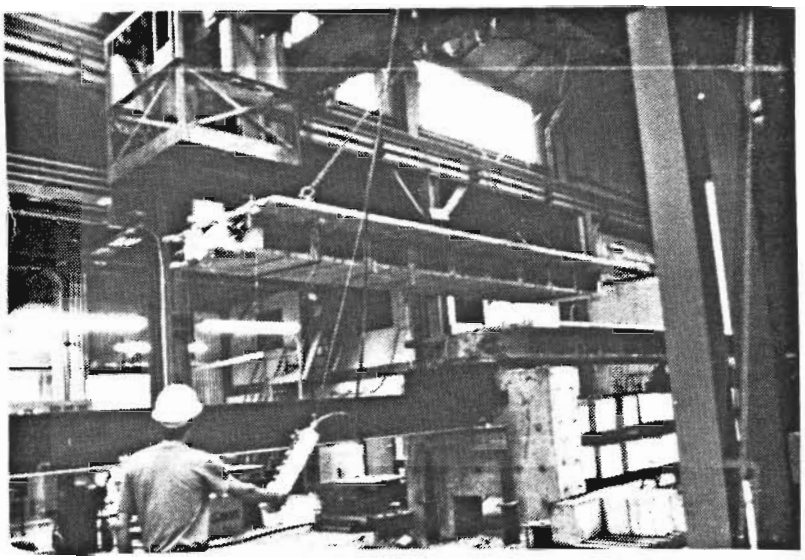

Figure 2.39 Hauling of interior span.

e) Transporting the Three Spans

The interior span was removed first from the testing location using a 25 ton capacity crane as shown in Fig. 2.39. The span was then moved outside the laboratory and placed in a storage area. Dead load blocks were then removed from the exterior spans, and spans were then transported outside the laboratory. Figures 2.40 through 2.43 show the stresses

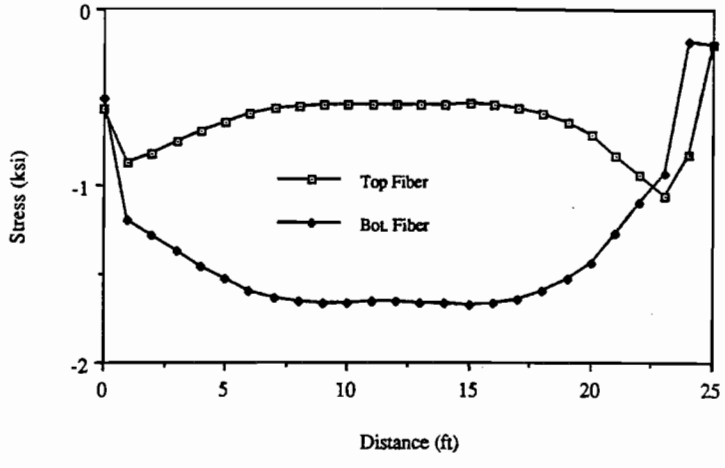

Figure 2.40 Stresses before removing dead load blocks (dry joints span).

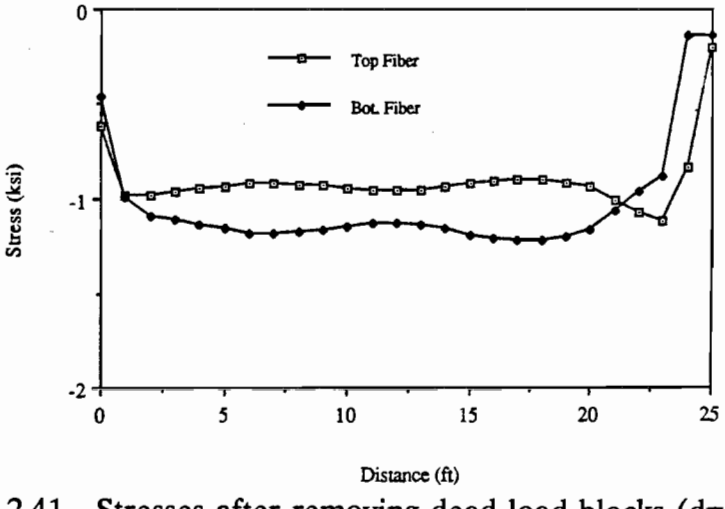

Figure 2.41 Stresses after removing dead load blocks (dry joints span).

before and after removing the dead load blocks. Finally, the piers were transported outside the laboratory using a fork lift.

2.10.2 Tendon Release Tests. After the spans were moved outside the laboratory, the external tendon stresses were released. The two objectives of releasing the external tendon stresses were to (1) reduce the potential danger created by the prestress force when the spans were trucked to a burial site, and (2) to measure the bond stress between the external tendons and each of the bonded diaphragms. Bond stress at each diaphragm was calculated by measuring the tendon stress on the two sides of the diaphragm before and after cutting a tendon. In this way, differences in measured stress measured before and after cutting a tendon yielded the bond stress developed through the diaphragm. A schematic of the procedure is shown in Fig. 2.44.

The process of measuring the bond strength by cutting external tendons along the span was carried out as follows:

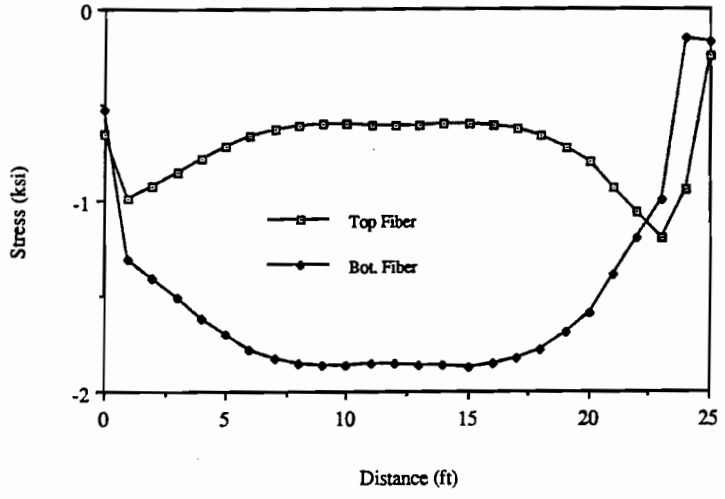

Figure 2.42 Stresses before removing dead load blocks (epoxy joints span).

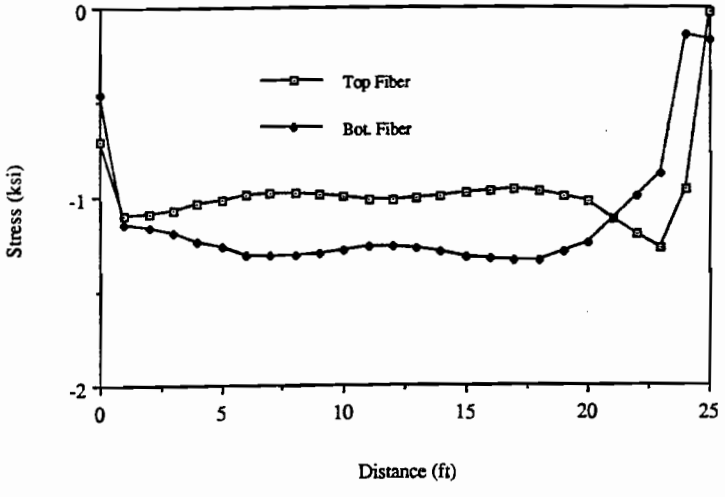

Figure 2.43 Stresses after removing dead load blocks (epoxy joints span).

a) Measure the relative stresses along the specified tendon to be cut. The stresses were measured by the strain gauges installed and used during testing of the bridge model as shown in Fig. 2.32.

b) Cut the specified tendon in the middle of the span and measure the relative stresses along the tendon. Corresponding tendons were cut simultaneously from the two sides of the bridge in order to reduce the flexure stresses on the concrete section and to reduce the effect of horizontal flexural displacements on the measured tendon stresses.

c) Calculate the bond strength in the diaphragm adjacent to the cut as shown in Fig. 2.44. Repeat the same process for the adjacent diaphragm with the same tendon. After completing one tendon, repeat the process for the other tendons one tendon at a time. More details and the test results are presented by Radloff(10).

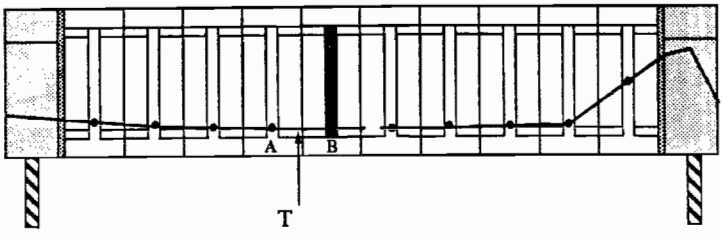

a) Before Cutting the Tendon (A-B)

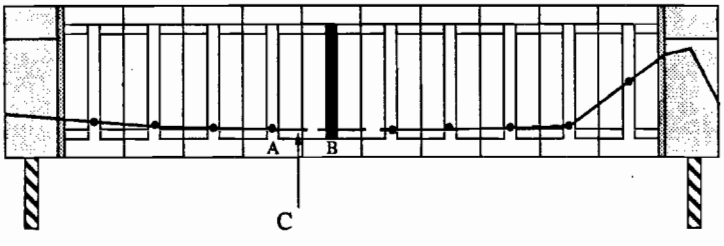

b) After Cutting the Tendon (A-B)

T and C are the stress measured by strain gauges
T-C is the bond developed through the blackened diaphragm

Figure 2.44 Bond stress determination by cutting of tendons.

CHAPTER THREE

LOAD TESTS

3.1 Loading Program

The three-span model was tested to investigate the effect on flexural behavior of improved bonding of the external tendons and the use of supplemental internal tendons. The test program consisted of three phases:

Phase one - epoxy injection and structural characterization tests

Phase two - bonded external tendon load tests

Phase three - supplemental tendon load tests

The first phase of testing involved loading the model to a load higher than the decompression load of the critical joints to establish the effect of epoxy injection in previously formed cracks, and to characterize the model with external tendons bonded at pier segments and at a maximum of four of the interior diaphragms in each span. The structural characterization of the model was carried out to define the in-situ condition of the model before any improvement in tendon bonding was carried out. Each of the exterior spans was loaded in the same manner through five cycles to a load higher than the measured decompression load. Three of the cycles were applied before injecting the cracks with epoxy to determine the decompression load for each of the exterior spans. The decompression load is defined as the load which reduces the stress in the extreme tension fiber to zero. The measured decompression load was used to calculate the effective prestress in each span. Two of the cycles were applied after the crack injection to determine the effect of the epoxy injection.

The second phase of testing followed completion of the first phase. In this phase of testing, the model was loaded in four stages. In each of three stages the external tendons were bonded at varied numbers of internal diaphragms in each span. In the first three stages, each exterior span was subjected to two cycles of load higher than the observed joint opening load. In the first load stage, the two load cycles were applied to the model in its original condition. The external tendons were bonded at diaphragm locations where the tendons were deviated, and at all pier segments. As discussed in Section 2.7 and shown in Fig. 2.3 and Table 2.6, some tendons were deviated at four locations in each span while the others were deviated at two locations only. In this case, the external tendons were bonded to only the pier segments and a maximum of four interior diaphragms in each span. In the second stage, two of the load cycles were applied after bonding the external tendons locally to a maximum of three additional interior diaphragms. In the third stage of tests, two load cycles were applied after bonding the external tendons to all remaining diaphragms (A total

of 10 diaphragms in each span). After finishing the six cycles of loading in the first three test stages, in the fourth stage, each of the exterior spans was loaded monotonically until the flexural strength was essentially reached. Loading was discontinued when the top flange at the critical joint/crack location exhibited concrete crushing.

In the third and final testing phase, the structure was loaded during two series of tests after supplemental internal tendons were added. In the first series, the exterior spans were loaded simultaneously to the flexural capacity after supplemental ungrouted internal tendons were added and stressed in the bottom flange of the model. In the second series, one load cycle to failure was applied to each exterior span after grouting the supplemental internal tendons in the bottom flange only. In both series of tests, loading was discontinued when the compression flange of the critical joints crushed. Different load locations were used so that the critical joints of the phase three load tests were different than the critical joints of the phase one and two load tests.

All testing was conducted on the exterior spans individually. Comparisons were made between the dry joints and epoxy joints exterior spans at all load levels.

3.2 Description of Loading System

3.2.1 Location of loads. Loads were applied at locations coinciding with the rod-cluster anchorages in the test floor. The loads were applied using two identical rams operated with the same hydraulic system. These requirements led to the use of two equal loads spaced at 4-ft. on center. The rams were attached to a steel frame which was tied to the test floor with eight, 1-inch diameter rods.

The position of the loads for the phase one and phase two tests is shown in Fig. 3.1. Figure 3.2 shows the load location for the phase three tests.

The position of the critical joints was determined by elastic and plastic analysis. For phase one and phase two tests, the elastic analysis indicated that joint (4,5) had a higher moment than joint (3,4). However, the plastic analysis for the same load position showed that joint (3,4) would fail before joint (4,5) due to reduced flexural capacity at joint (3,4) because the external tendon eccentricity was smaller at joint (3,4) than at joint (4,5). In the same way, the critical joint for the epoxy joint span was determined to be joint (27,28). For the phase three tests, joint (4,5) was the critical joint for the dry joint span and joint (26,27) was the critical joint for the epoxy joint span. In this case, the elastic analysis showed that the critical joint had the highest elastic moment, while the plastic analysis confirmed that the critical joint failed first. The load positions were moved after ultimate strength test in order to relocate the critical joints and to reduce the effect of damage due to previous tests.

3.2.2 Load Application Equipment. The loading frame consisted of two braced cross-beams tied to the test floor with eight 1-inch diameter steel rods, as shown in Fig. 3.3.

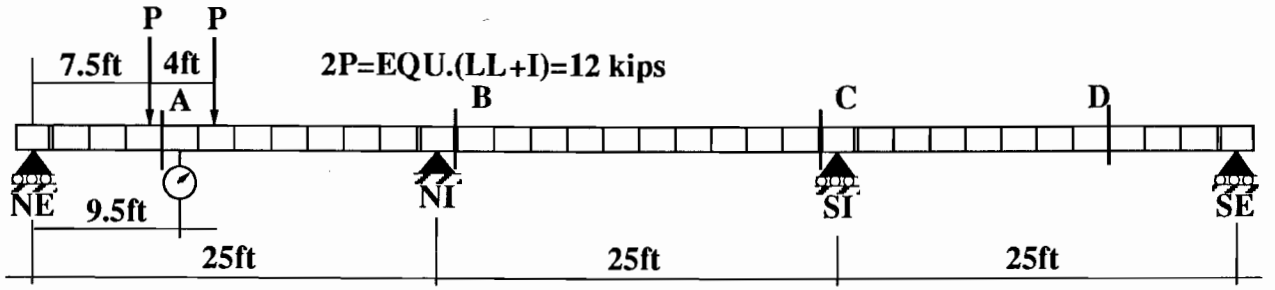

a) Dry-Joint Span

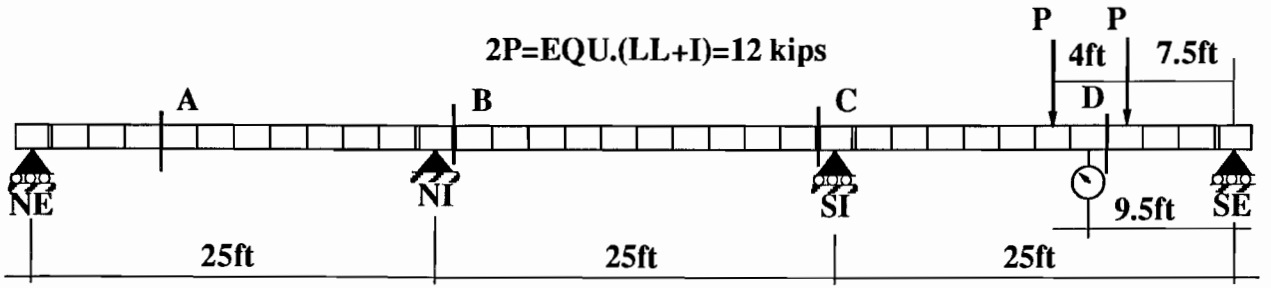

b) Epoxy-Joint Span

Figure 3.1 Load positions - Phase One and Phase Two tests.

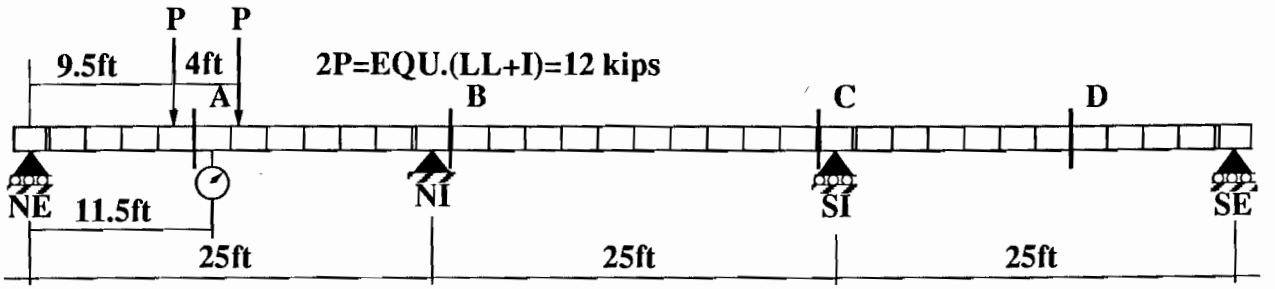

a) Dry-Joint Span

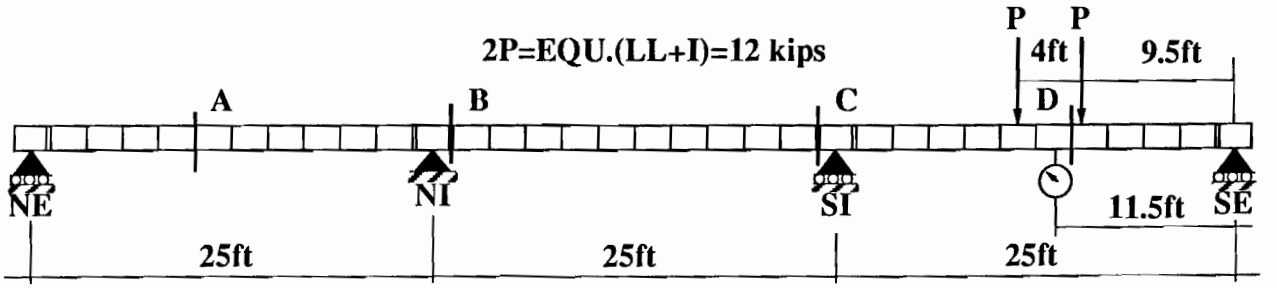

b) Epoxy-Joint Span

Figure 3.2 Load positions - Phase Three tests.

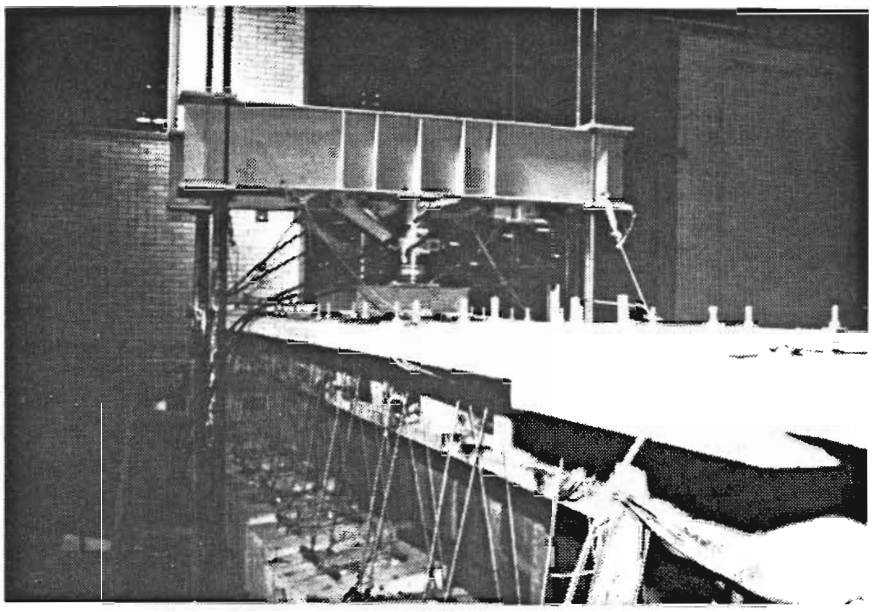

Figure 3.3 Load frame.

The load frame was supported by four adjustable post-shores when no load was being applied. The two rams were placed between the two cross-beams and the model. Each ram was positioned over a spherical bearing which was supported by a spreader beam. The spreader beams were used to apply the loads directly over the webs of the box girder. Load was transmitted from each end of the spreader beams to the top of the box girder through 1/2-inch thick neoprene pads.

For the phase one and phase two tests, two double-action 30 ton rams were operated with a single pump, while two double action 60 ton rams were used for phase three tests. The loads were monitored by two pressure transducers. One transducer was connected to a strain indicator box and was used to control loading while the other was connected to the electronic data acquisition system.

3.3 Equivalent Live Load and Impact

The equivalent live load plus impact EQU.(LL+I), is defined as the ram load which produces the same maximum moment at the critical joint as the reduced-scale AASHTO HS20 truck load applied in two lanes would produce. The reduced-scale loading for two lanes of AASHTO HS20 truck load is shown in Fig. 3.4. The maximum moments at any joint resulting from the reduced-scale truck load were obtained using the moment influence line for that joint. The maximum moment for all joint moments was used to determine the necessary equivalent live load plus impact (LL+I). The influence line for moment at the critical joint was also used to obtain the equivalent live load plus impact.

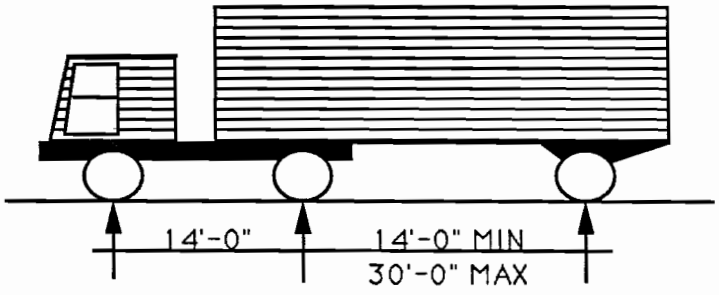

HS20 TRUCK	8 KIPS	32 KIPS	32 KIPS
IMPACT (22%)	1.8 KIPS	7.0 KIPS	7.0 KIPS
HS20 W/ IMPACT	9.8 KIPS	39 KIPS	39 KIPS
2 LANES OF HS20 W/ IMPACT	20 KIPS	78 KIPS	78 KIPS

a. AASHTO HS20 TRUCK LOAD

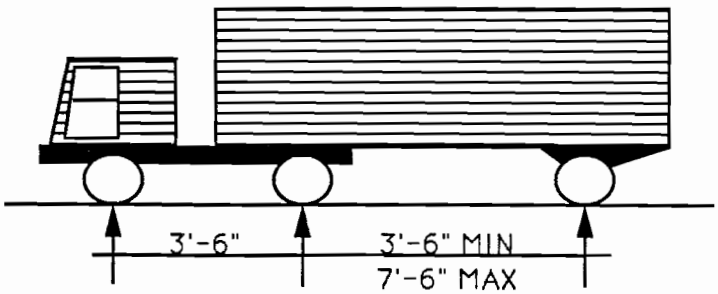

1/4 SCALE

HS20 TRUCK	0.5 KIPS	2.0 KIPS	2.0 KIPS
IMPACT (22%)	0.11 KIPS	0.44 KIPS	0.44 KIPS
HS20 W/ IMPACT	0.61 KIPS	2.44 KIPS	2.44 KIPS
2 LANES OF HS20 W/ IMPACT	1.25 KIPS	4.88 KIPS	4.88 KIPS

b. REDUCED SCALE HS20 TRUCK LOAD

Figure 3.4 1/4-scale truck load.

3.4 Presentation of Test Data

All test data is presented as a function of the applied load. The applied load is expressed as equivalent (LL+I). The test data presented are deflections, reactions, joint moments, changes in tendon stress, and joint openings.

3.4.1 Epoxy Joints Span. Three phases of tests were carried out on this span as discussed in Section 3.1.

3.4.1.1 Decompression Load Cycles. Five loading cycles to a maximum load of 4.0(LL+I), which was higher than the measured decompression load by 50 percent, were applied to the epoxy joints span. Three cycles of loading were applied before injecting the cracks and two cycles were applied after injecting the cracks with epoxy. The applied load was increased from zero to 2.0(LL+I) in 0.25(LL+I) increments. Then the load was increased in 0.16(LL+I) for the remainder of the loading cycle. Each of the three cycles indicated the same response of the model to the applied loads. Figures 3.5 through 3.10 show the response of the structure.

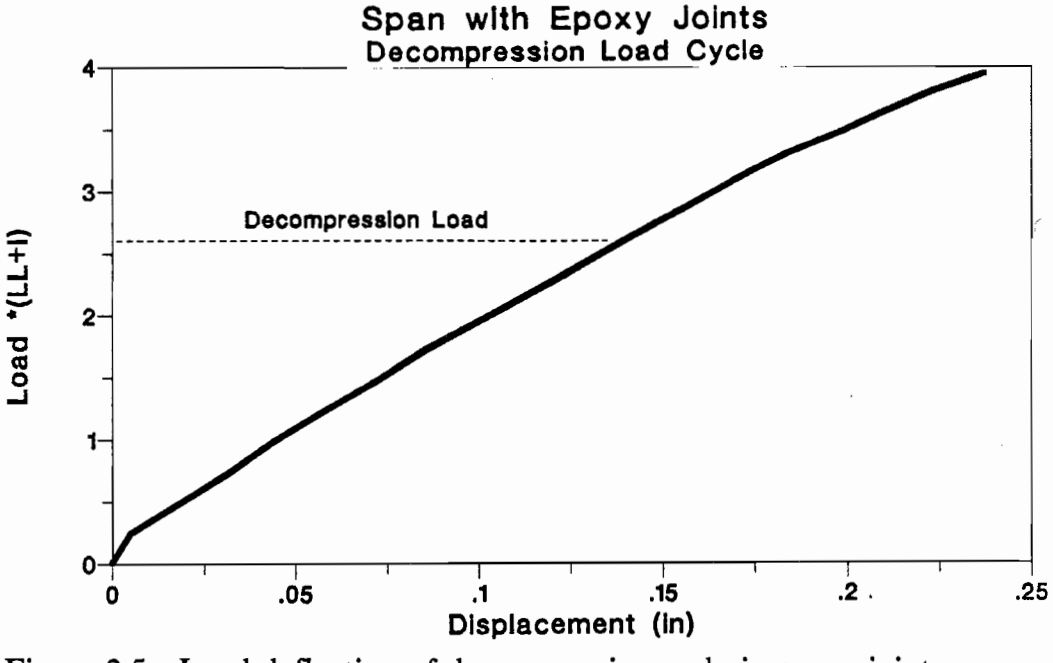

Figure 3.5 Load-deflection of decompression cycle in epoxy joints span.

The measured decompression load was approximately 2.6(LL+I), and resulted in only slight changes in the behavior of the structure. The decompression load was obtained from a large-scale plot for the applied load-deflection response of the model. Figure 3.5 shows the load-deflection response of the structure. The joint moments and reactions also show slight changes at the decompression load as illustrated in Fig. 3.7 for joint moments and Fig. 3.6 for reactions. The stress changes in the external tendons appeared to be linear up to a load higher than the decompression load, as shown in Fig. 3.8 through Fig. 3.10.

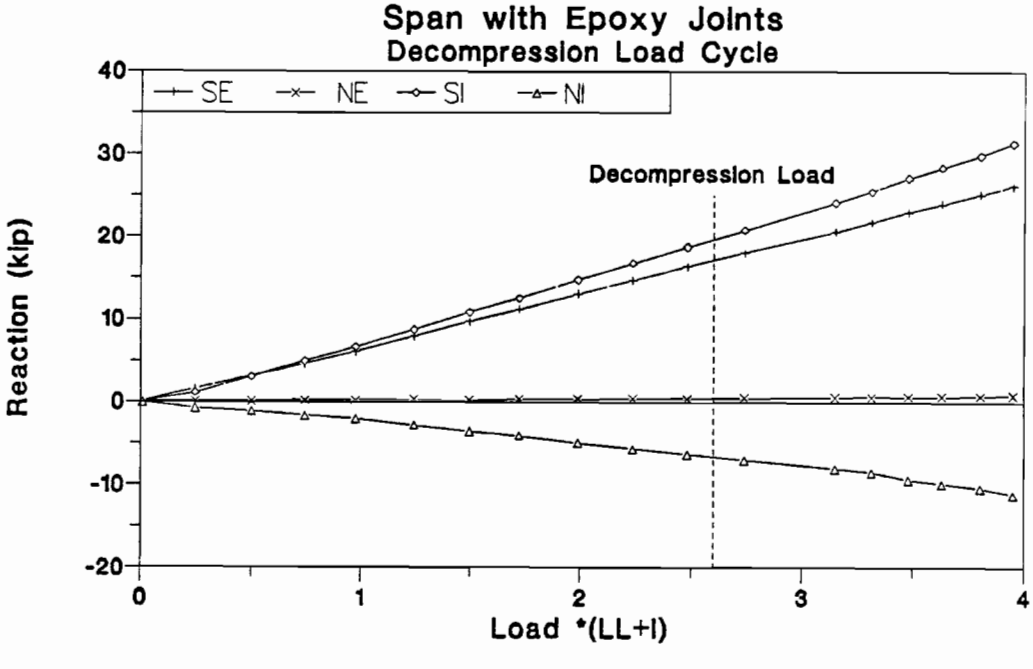

Figure 3.6 Reaction-load of decompression cycle in epoxy joints span.

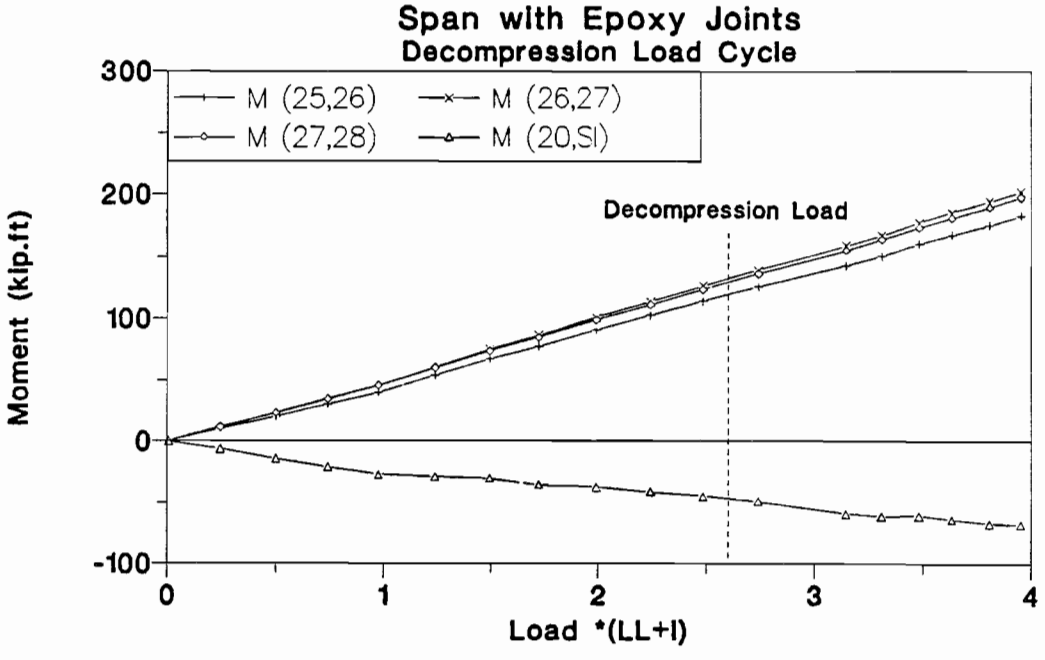

Figure 3.7 Moment-load of decompression cycle in epoxy joints span.

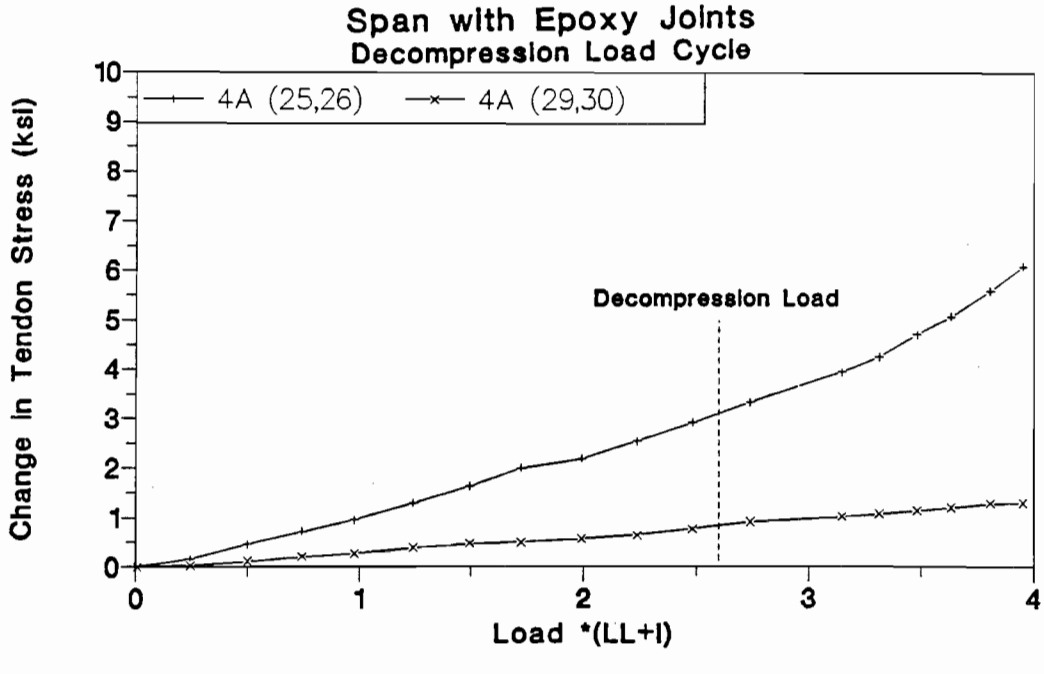

Figure 3.8 Tendon 4A stress-load of decompression cycle in epoxy joints span.

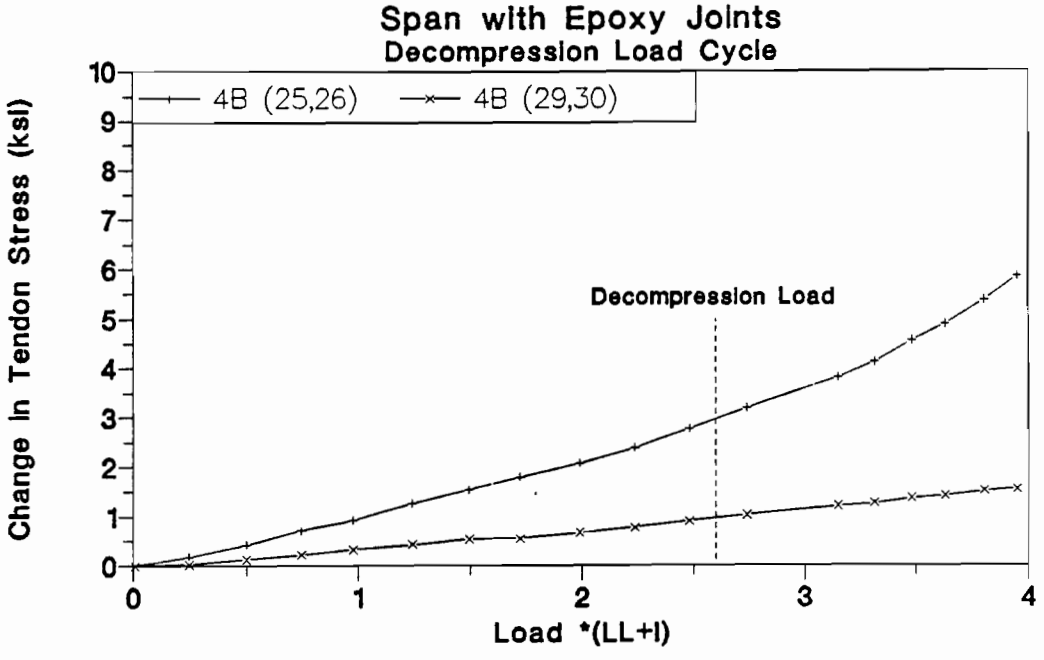

Figure 3.9 Tendon 4B stress-load of decompression cycle in epoxy joints span.

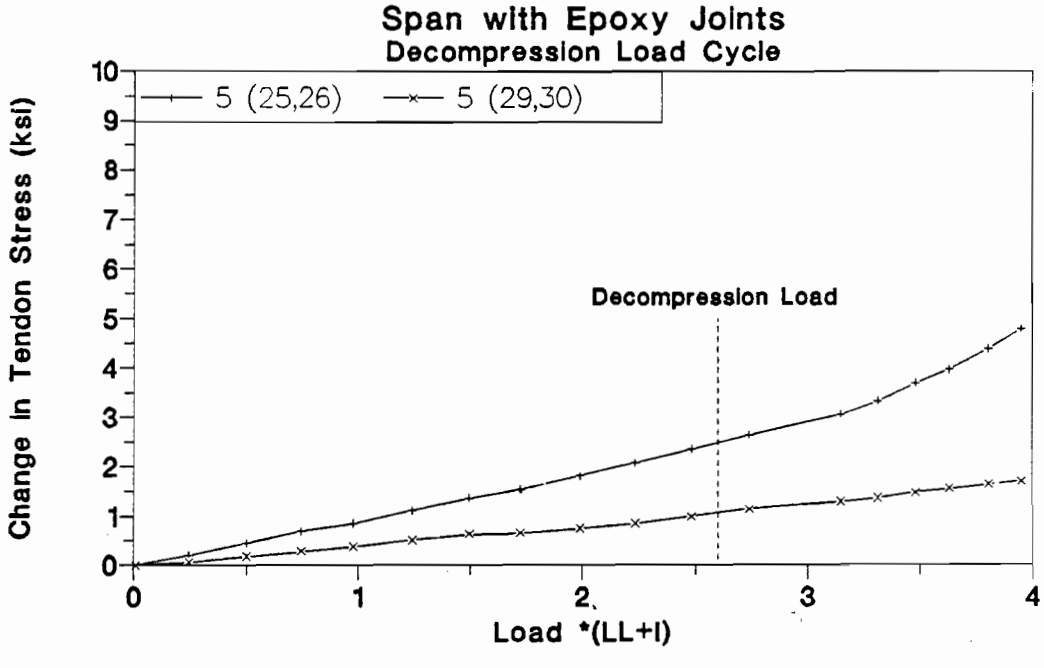

Figure 3.10 Tendon 5 stress-load of decompression cycle in epoxy joints span.

The maximum measured deflection of the epoxy joint span at service load 1.0(LL+I) was 0.049 inches which corresponds to a span to deflection ratio of (6122) as shown in Table 3.1. The maximum stress change noted in the external tendons at service load 1(LL+I) was 1.1 ksi while the maximum change in tendon stress at the end of the load tests at 4.0(LL+I) was 6 ksi.

Two load cycles were applied after the crack injection process was completed. The cracks in the webs and bottom flanges of few segments in this span were injected with epoxy (see Chapter two). The response of the structure after crack injection is shown in Figures 3.11 through 3.16. A maximum load of 4.0(LL+I) was applied in all the first-phase loading tests of this span.

Table 3.1 Service Load (Epoxy Joints Span)

Deflection	0.049 in. (Span/6122)
Change in Tendon Stress	1.1 ksi

Figure 3.17 shows the effect of epoxy injection of cracks on the load-deflection behavior of the model. The injection effects become apparent at a load of 2(LL+I) which is lower than the decompression load. Crack injection had a very small effect on the flexural behavior of the fully compressed section. The stiffness of the structure below the decompression load was slightly higher because the epoxy injection filled the spaces between the cracks and increased the contact area of the previously cracked section. The effect of epoxy injection was clear at a load higher than the decompression load when the previously cracked section began to resist tension.

3.4.1.2 Cracking Cycle. It was necessary to crack the epoxy joints span after the cracks were injected with epoxy resin to measure the cracking load and the joint opening load. The applied load was increased from zero to 3(LL+I) in 0.5(LL+I) increments, and from 3(LL+I) to a maximum of 5.6(LL+I) at 0.2(LL+I) increments. The response of the structure is shown in Figures 3.18 through 3.24. The epoxy joints span cracked in segment 26 adjacent to joint (26,27) at a load of 4.8(LL+I).

The applied load-deflection response for the cracking cycle is shown in Fig. 3.18, while Fig. 3.19 and Fig. 3.20 show the measured reactions and the calculated joint moments. The changes in external tendon stress are shown in Figures 3.21 through 3.23. Joint openings are shown in Fig. 3.24.

At a load of approximately 4.8(LL+I), segment 26 cracked through the concrete adjacent to joint (26,27). After cracking, the loads redistributed towards the interior support as illustrated in Fig. 3.19 for the reactions and Fig. 3.20 for joint moments.

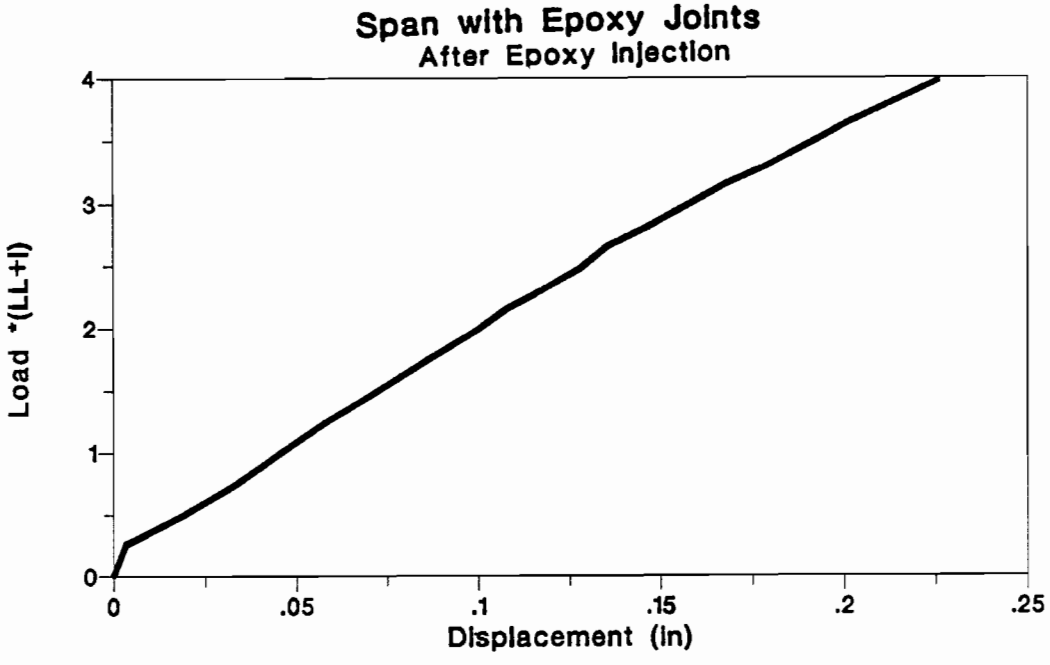

Figure 3.11 Load-deflection of injection cycle in epoxy joints span.

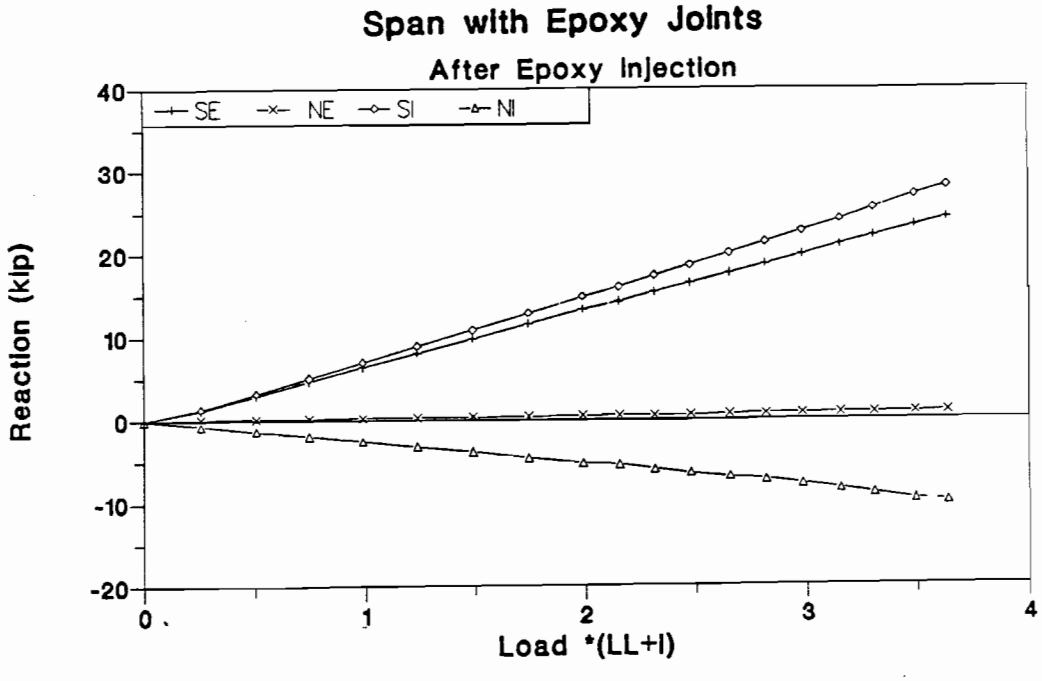

Figure 3.12 Reaction-load of injection cycle in epoxy joints span.

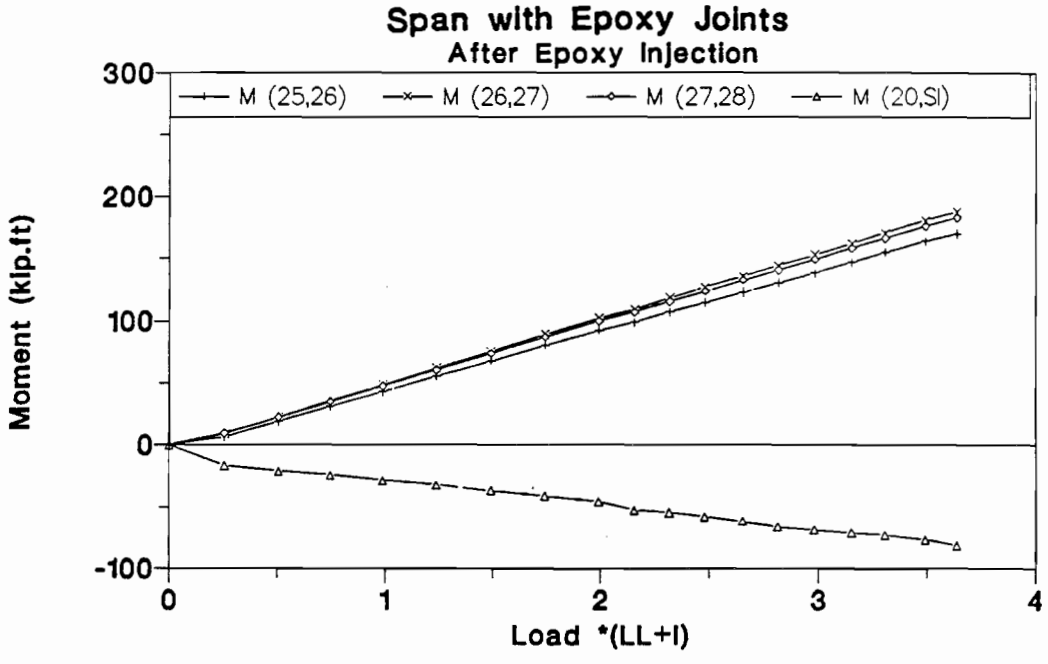

Figure 3.13 Moment-load of injection cycle in epoxy joints span.

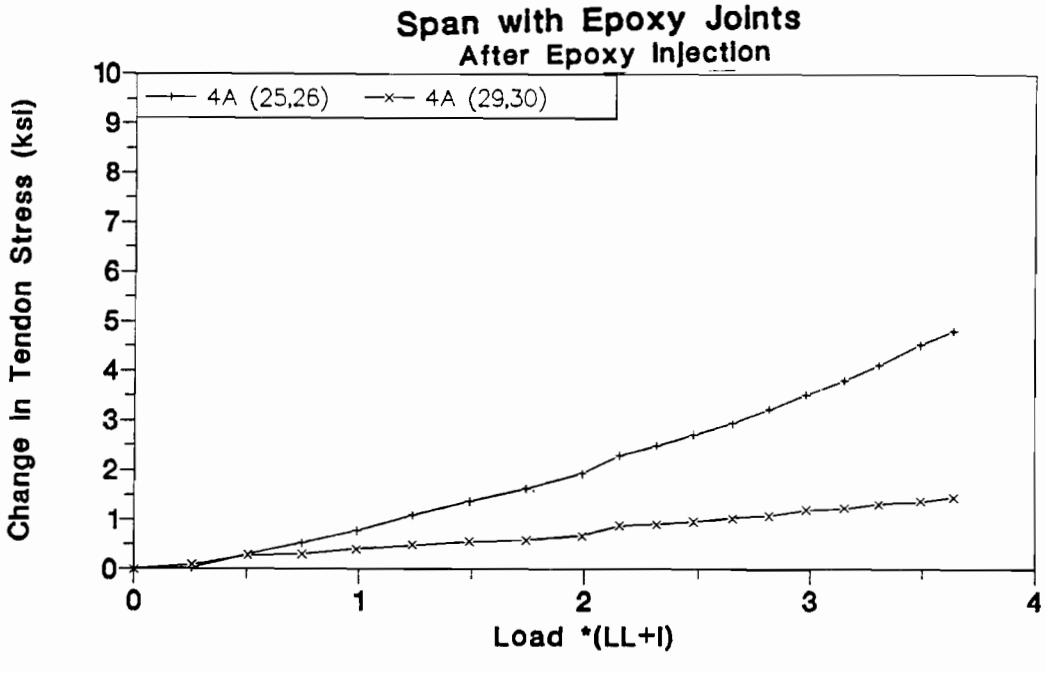

Figure 3.14 Tendon 4A stress-load of injection cycle in epoxy joints span.

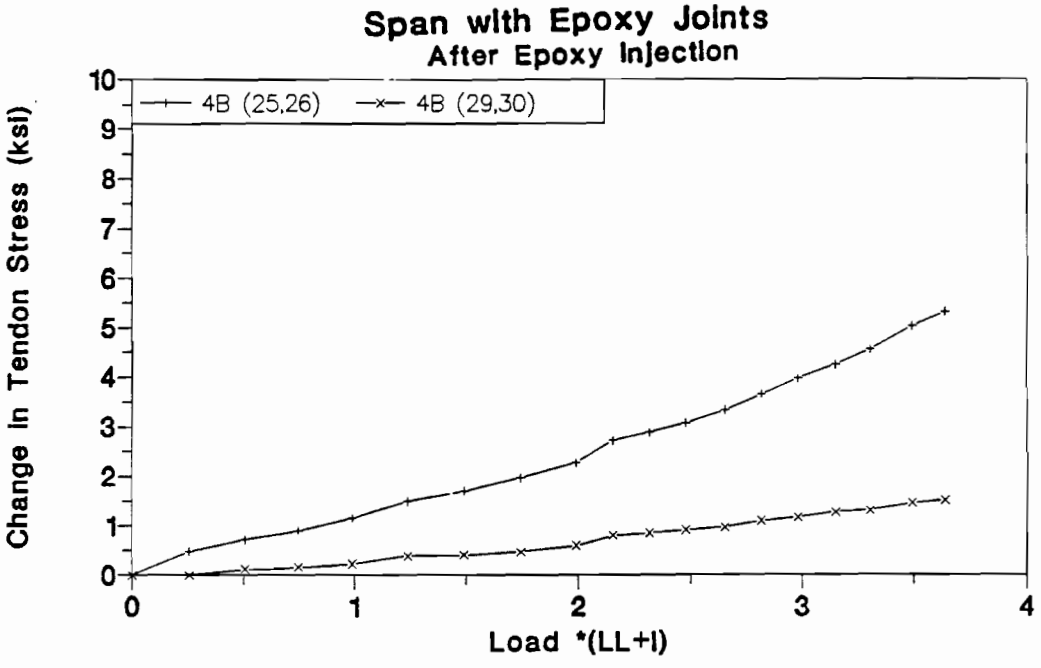

Figure 3.15 Tendon 4B stress-load of injection cycle in epoxy joints span.

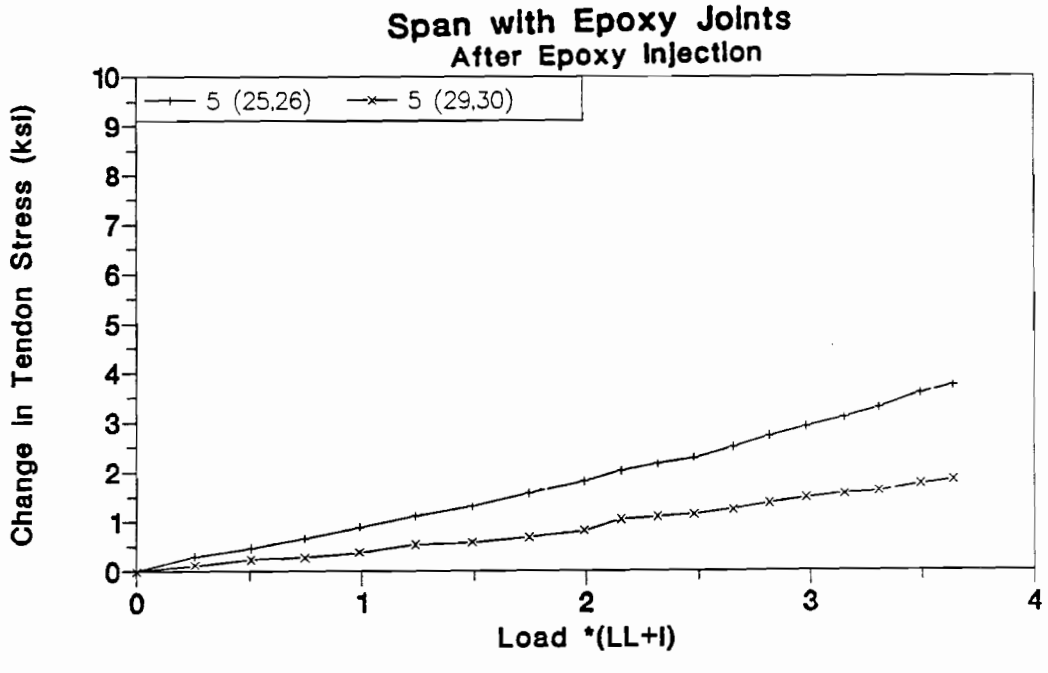

Figure 3.16 Tendon 5 stress-load of injection cycle in epoxy joints span.

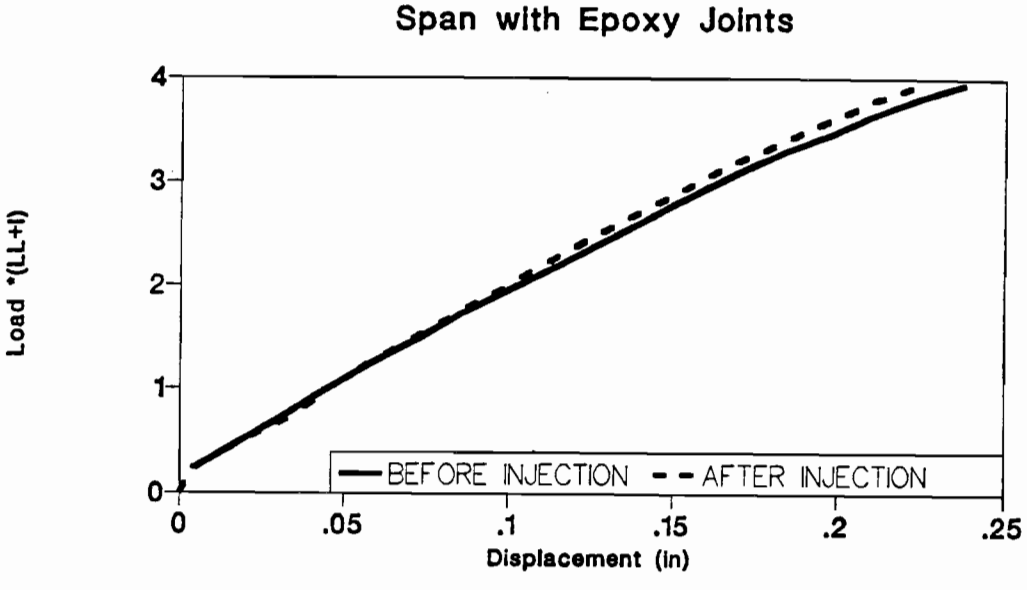

Figure 3.17 Effect of epoxy injection in epoxy joints span.

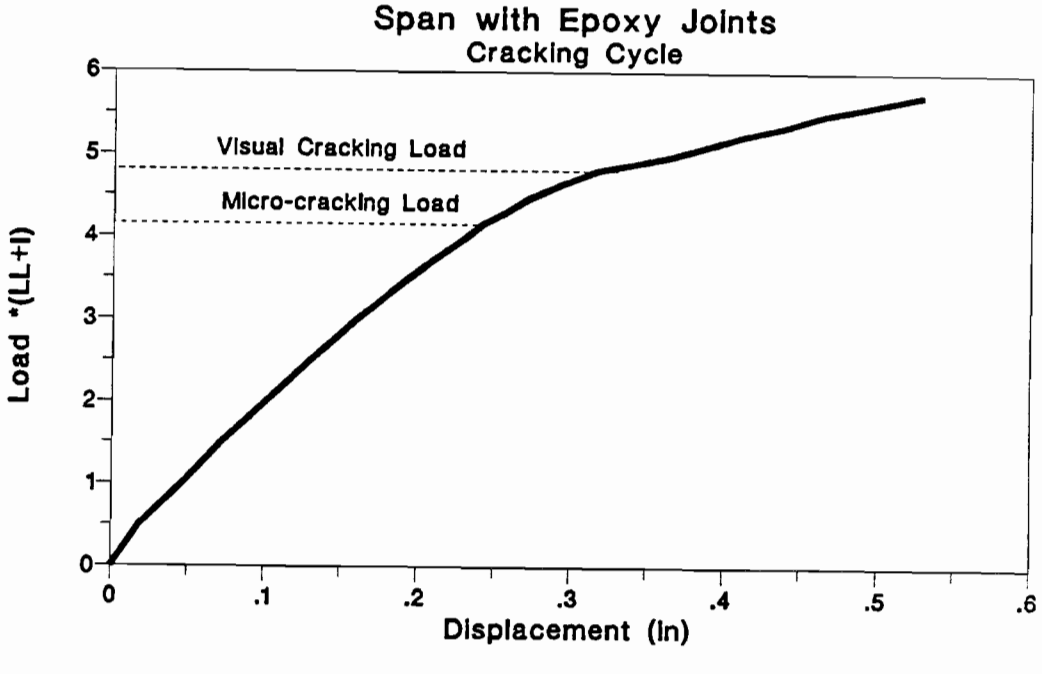

Figure 3.18 Load-deflection of cracking cycle in epoxy joints span.

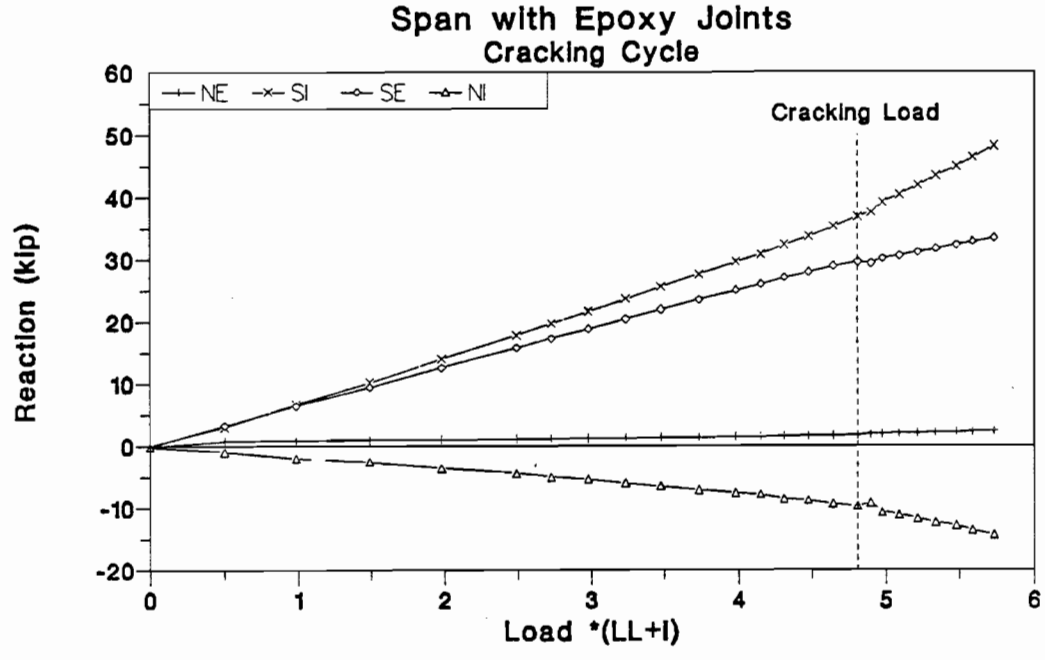

Figure 3.19 Reaction-load of cracking cycle in epoxy joints span.

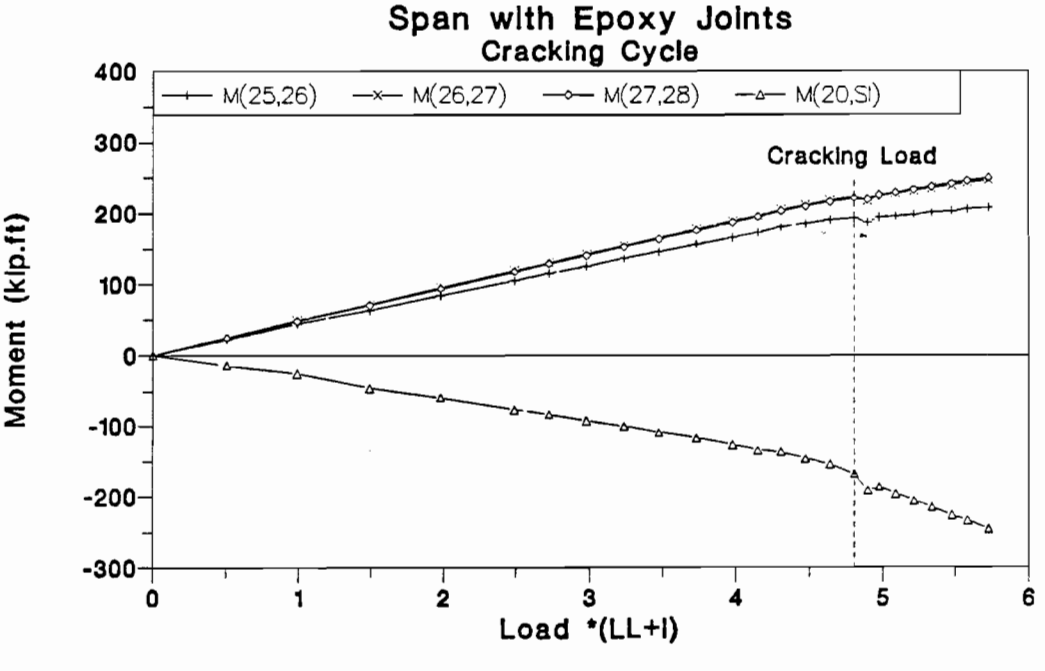

Figure 3.20 Moment-load of cracking cycle in epoxy joints span.

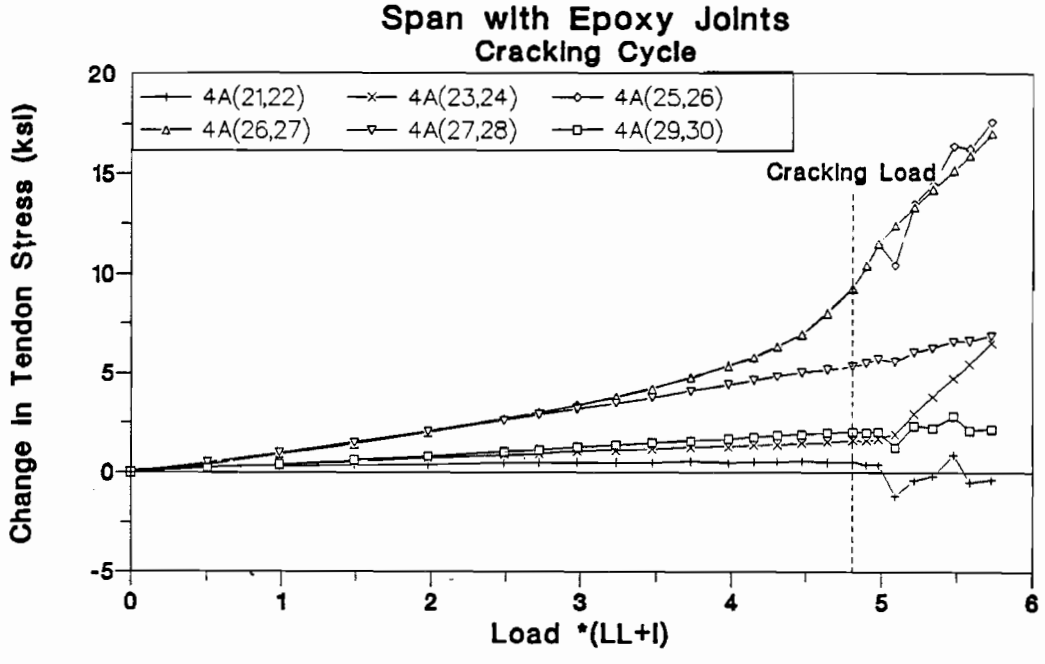

Figure 3.21 Tendon 4A stress-load of cracking cycle in epoxy joints span.

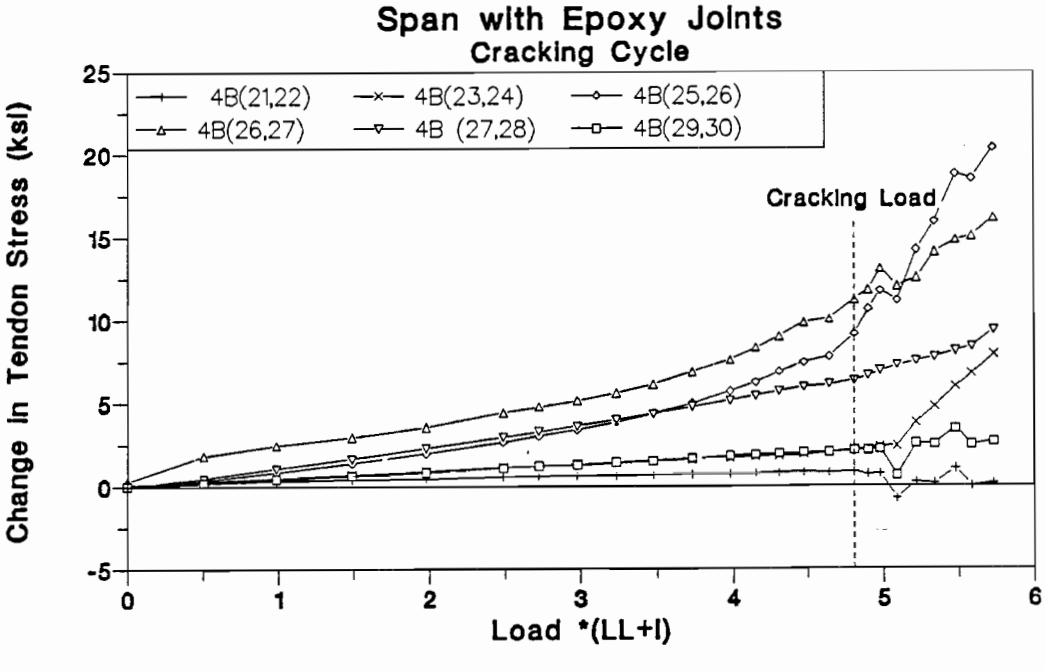

Figure 3.22 Tendon 4B stress-load of cracking cycle in epoxy joints span.

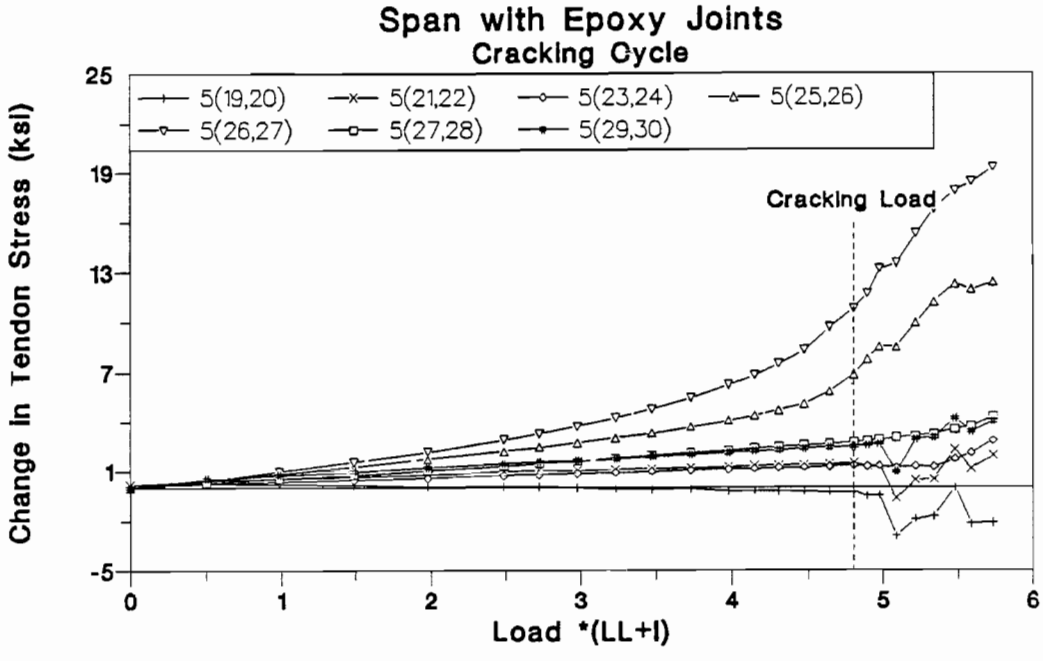

Figure 3.23 Tendon 5 stress-load of cracking cycle in epoxy joints span.

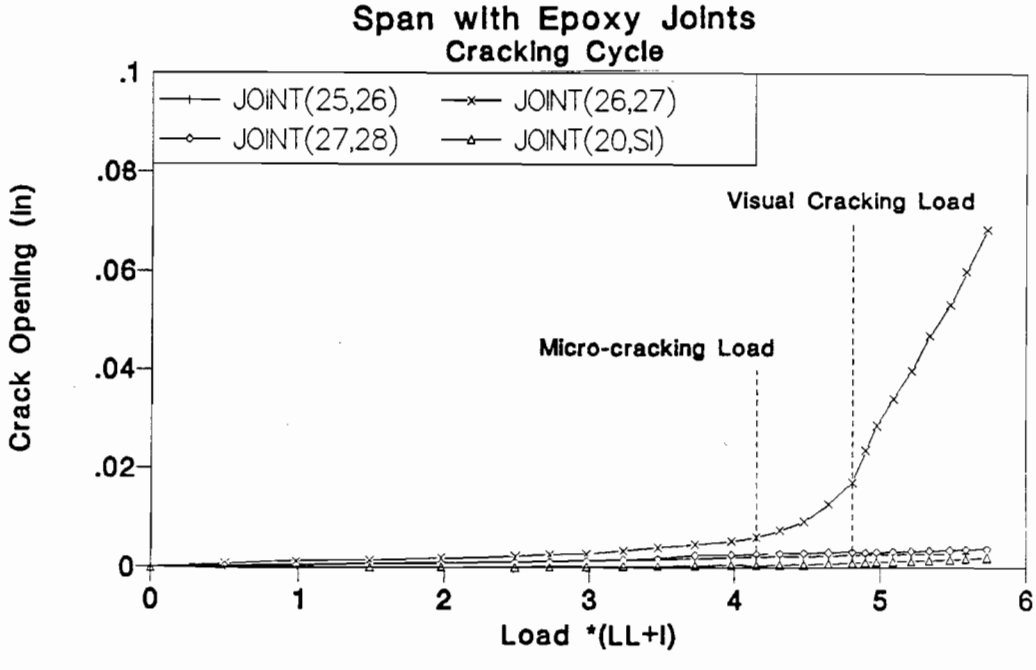

Figure 3.24 Crack opening-load of cracking cycle in epoxy joints span.

From Figures 3.18 and 3.24 it appears that cracking at joint (26,27) initiated at a load of approximately 4.0(LL+I), but a sudden increase in crack opening and a cracking sound emitted by the model occurred at a load of 4.8(LL+I). As the concrete cracked, the tension force transferred from the concrete to the steel and the crack opening increased sharply causing a higher Xdeflectionand slip of the external tendons 4A and 4B at joint 24 and 27.

3.4.1.3 Bonded External Tendon Load Tests. Six cycles of load higher than the crack opening load were applied during three testing stages to the epoxy-joints span. The load applied was increased from zero to 3(LL+I) in 0.5(LL+I) increments, from 3(LL+I) to 4(LL+I) in 0.25(LL+I) increments, and from 4(LL+I) to 5.7(LL+I) in 0.16(LL+I) increments. Two load cycles were applied during each of the three testing stages:

Stage One - External tendons bonded to the pier segments and to a maximum of four internal diaphragms along any tendon in each span as shown in Figure 3.25(a).

Stage Two - External tendons bonded to the pier segments and a maximum of seven internal diaphragms along any tendon in each span as shown in Figure 3.25(b).

Stage Three - External tendons bonded to the pier segments and at all ten internal diaphragms as shown in Figure 3.25(c).

As mentioned earlier in Section 3.1, bonding of the external tendons to the internal diaphragms was done in increments so that each loading stage was carried out for different bonding conditions. As discussed in Section 3.2.1, joint (27,28) was the critical joint as determined by plastic analysis, while joint (26,27) had a higher elastic moment. Joint (26,27) was the only joint cracked during the cracking load cycle. In the three testing stages, joint (27,28) was never cracked which made joint (26,27) as the critical joint in these three tests. The first loading stage was carried out on the model in its original bonding condition. The external tendons were bonded to the pier segments and at diaphragm locations where the tendons were deviated. Four external tendons were bonded to four internal diaphragms, while the other two external tendons were bonded to two internal diaphragms. External tendons were bonded to a maximum of four internal diaphragms in each span, as shown in Fig. 3.25(a) and Table 2.6. At the critical joint (26,27), all external tendons had unbonded length of three segment length.

The second loading stage was executed after the external tendons were bonded to a maximum of three additional interior diaphragms in each span as shown in Fig. 3.25(b) and Table 2.6. Bonding locations was chosen so that all external tendons at the critical joint location had unbonded length of two segment length and this will be different than stage

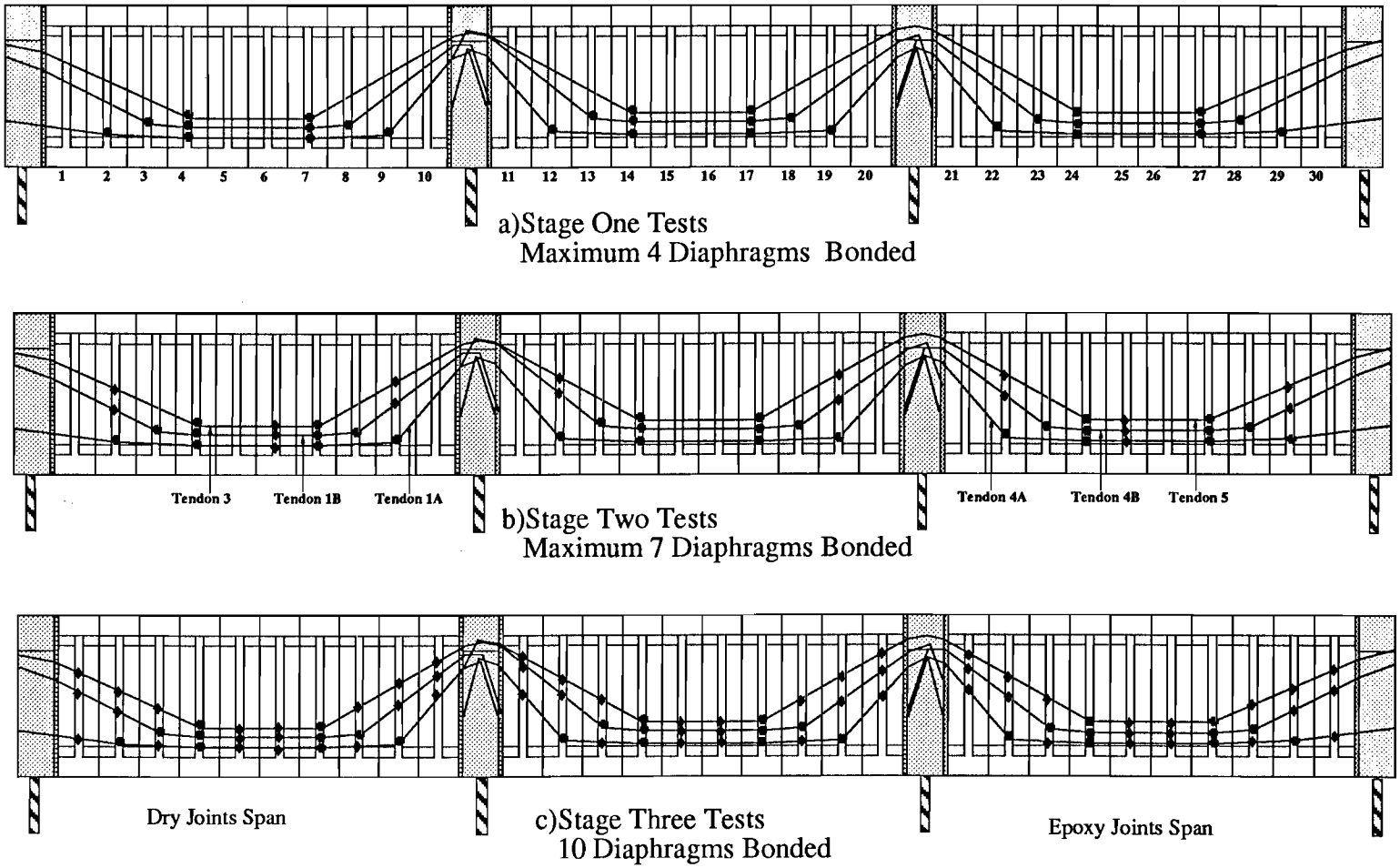

● : Interior Diaphragm Originally Bonded

♦ : Interior Diaphragm Bonded

Figure 3.25 Bonding stages of external tendons.

one tests. The last loading stage was carried out on the model after the external tendons were bonded to all remaining diaphragms as shown in Figure 3.25(c) and Table 2.6. In this case, all tendons had one segment length as unbonded length.

Stage One Tests (4 tendons bonded at four diaphragms and 2 tendons bonded at 2 internal diaphragms in this span)

Two loading cycles were applied during this stage of testing. A maximum load of 5.7(LL+I) was applied in each of the two loading cycles. The bonding of the tendons is shown in Fig. 3.25(a). The response of the structure is shown in Figures 3.26 through 3.32.

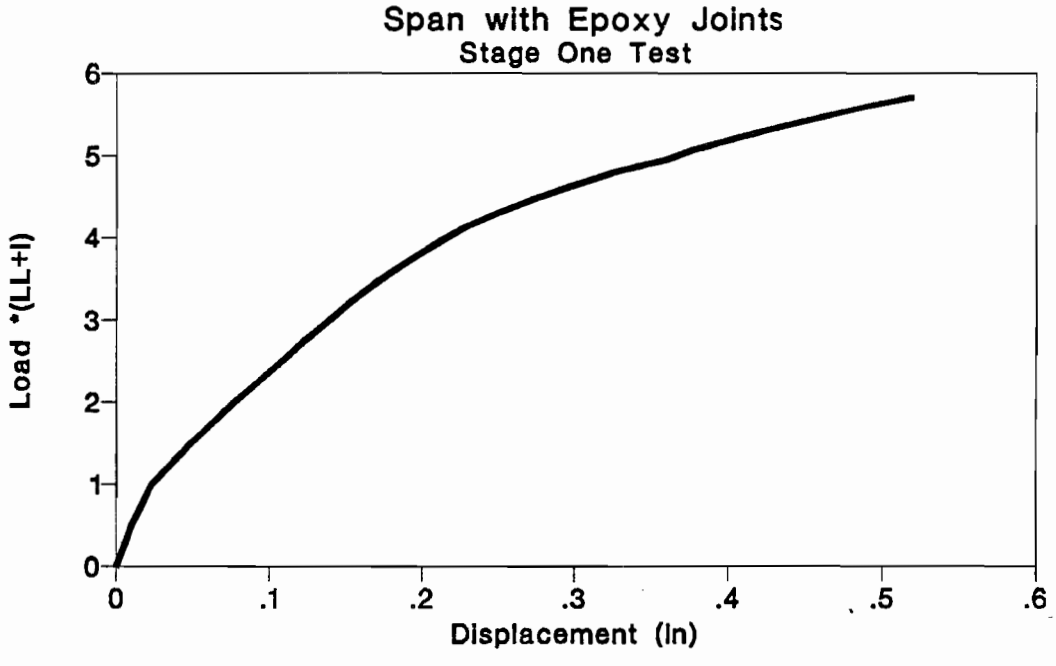

Figure 3.26 Load-deflection of Stage One test in epoxy joints span.

The applied load-deflection response of the model is shown in Fig. 3.26. The measured reactions and the calculated joint moments are shown in Fig. 3.27 and Fig. 3.28. Figures 3.29 through 3.31 show the changes in external tendon stress, while Fig. 3.32 shows the measured crack openings for the model.

At a load of 4(LL+I) the crack adjacent to joint (26,27) started opening as shown in Fig. 3.32. The changes in external tendon stress in the mid-span region started to increase at a higher rate after crack opening began (Fig. 3.29 through Fig. 3.31). At this load level the internal forces were redistributed to the interior support due to reduction in

the positive section stiffness as indicated in Fig. 3.27 for reactions and Fig. 3.28 for joint moments.

Stress of tendons 4A was the same at joint (25,26) and (26,27) because the tendons were unbonded at segment 26 as indicated in Figure 3.29. For the same reason, tendons 4B stress at the two joints were the same as shown in Fig. 3.30.

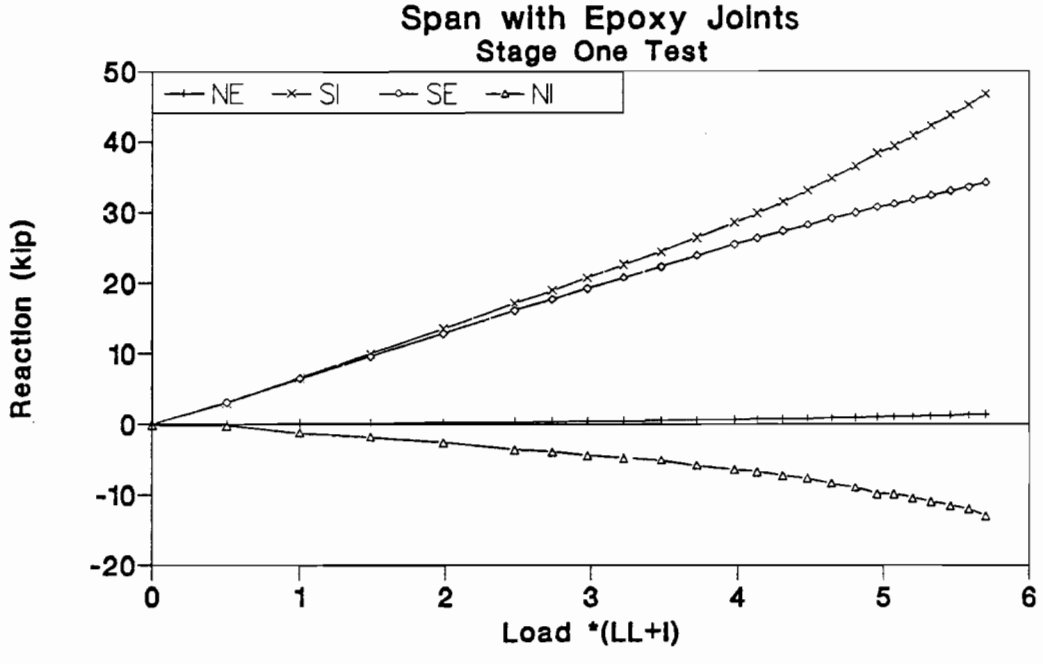

Figure 3.27 Reaction-load of Stage One test in epoxy joints span.

At a load of 4.8(LL+I) the external tendons 4A and 4B started slipping at segment 24 as shown in Fig. 3.29 and Fig. 3.30, while tendons 5 started slipping at a load of 5.2(LL+I) as shown in Fig. 3.31.

At a load of 5.6(LL+I) tendons 4A and 4B started slipping at segment 27 as shown in Fig. 3.29 and Fig. 3.30, while tendons 5 started slipping at segment 26 when joint (26,27) started opening as shown in Fig. 3.31.

The maximum change in tendons 4A stress at the end of the test at 5.7(LL+I) was 18 ksi. The maximum applied load of 5.7(LL+I) was 15 percent higher than the load at which most of the external tendons slipped.

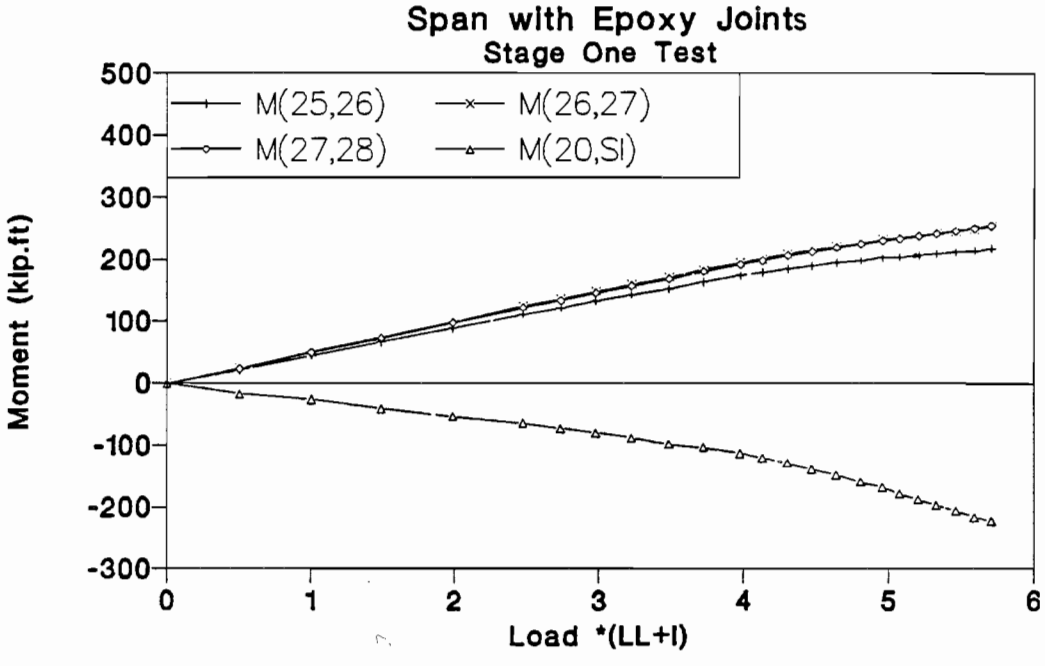

Figure 3.28 Moment-load of Stage One test in epoxy joints span.

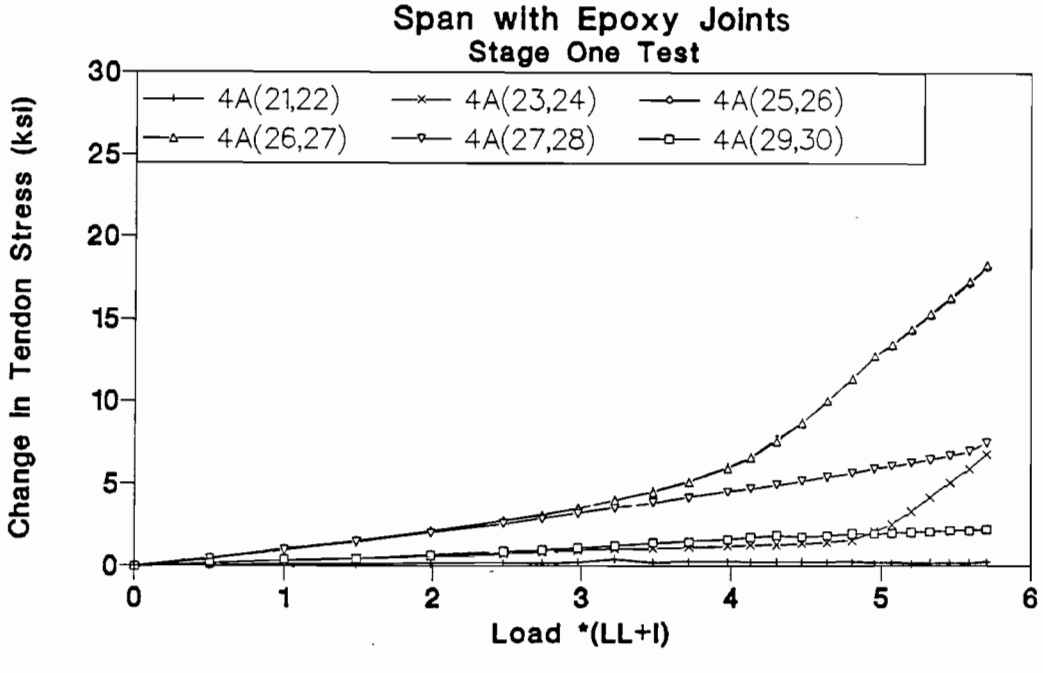

Figure 3.29 Tendon 4A stress-load of Stage One test in epoxy joints span.

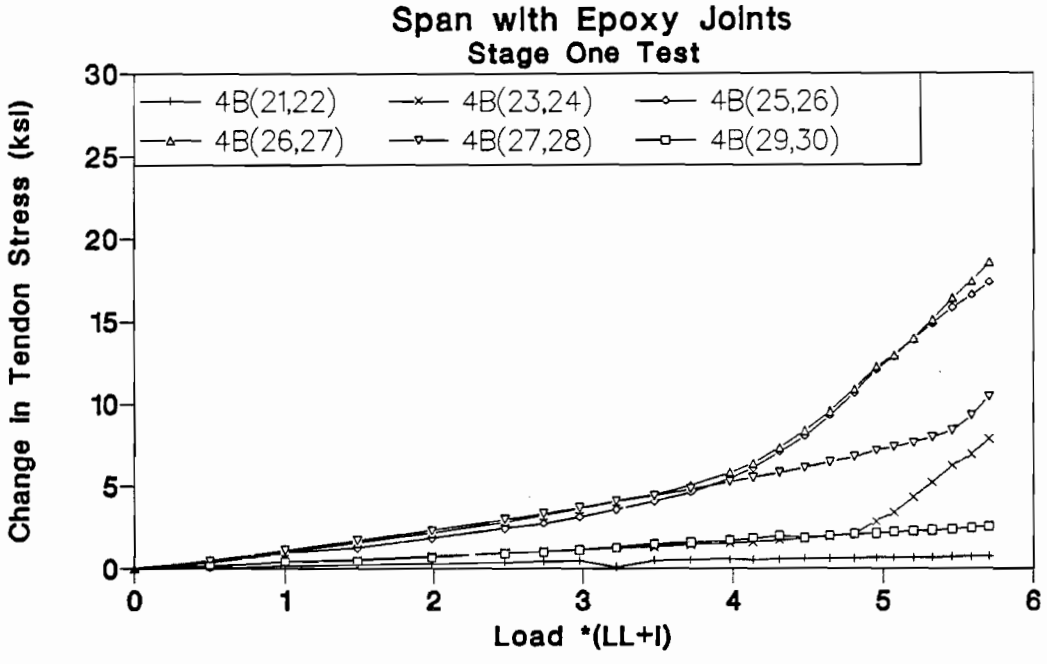

Figure 3.30 Tendon 4B stress-load of Stage One test in epoxy joints span.

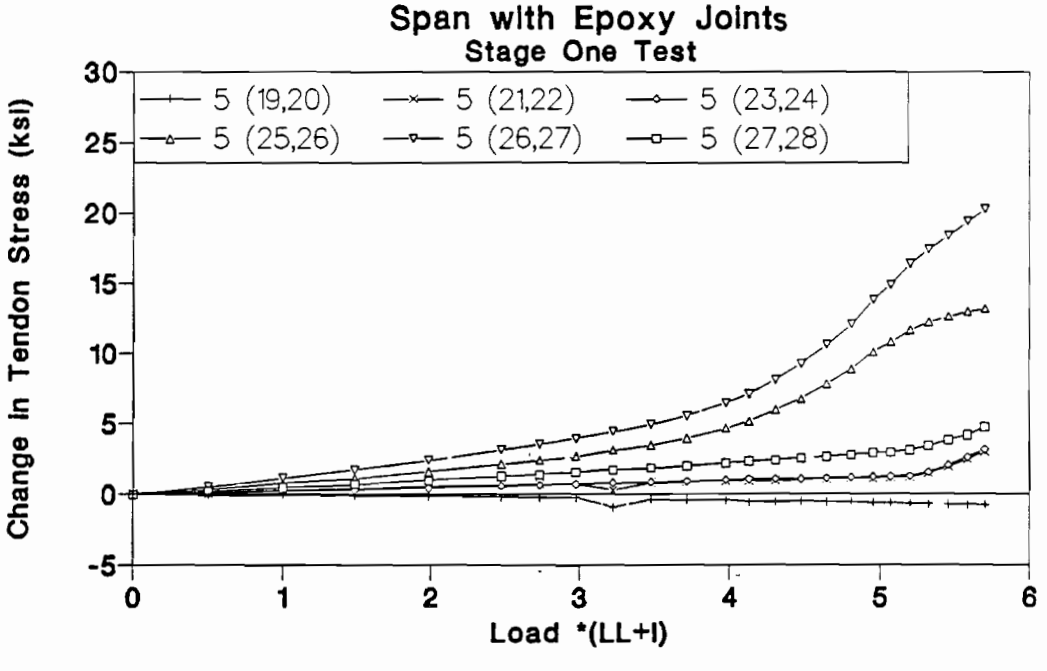

Figure 3.31 Tendon 5 stress-load of Stage One test in epoxy joints span.

Stage Two Tests (2 Tendons bonded at 7 internal diaphragms and 4 tendons bonded at 5 internal diaphragms)

Two load cycles with a maximum of 5.7(LL+I) were applied to the structure. The bonding of the external tendons to a maximum of seven diaphragms in each span is shown in Fig. 3.25(b). Figures 3.33 through 3.39 show the response of the structure to the loads.

Figure 3.33 shows the applied load-deflection response of the structure, while the measured reactions and the calculated moments are shown in Fig. 3.34 and Fig. 3.35. The changes in external tendon stress are shown in Figures 3.36 through 3.38. Crack opening responses are shown in Fig. 3.39.

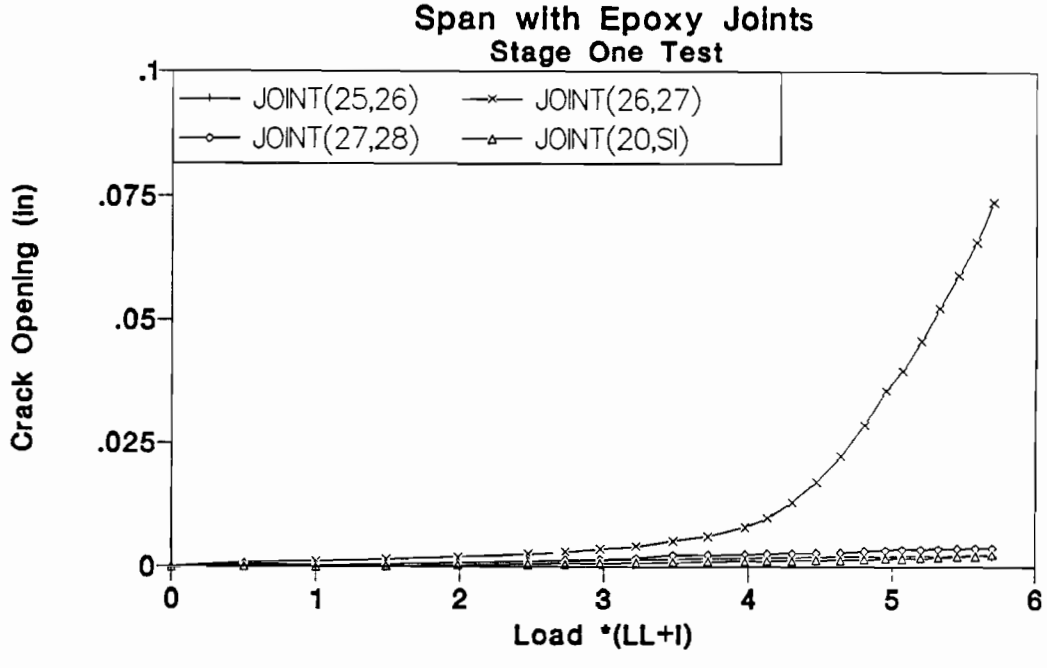

Figure 3.32 Crack opening-load of Stage One test in epoxy joints span.

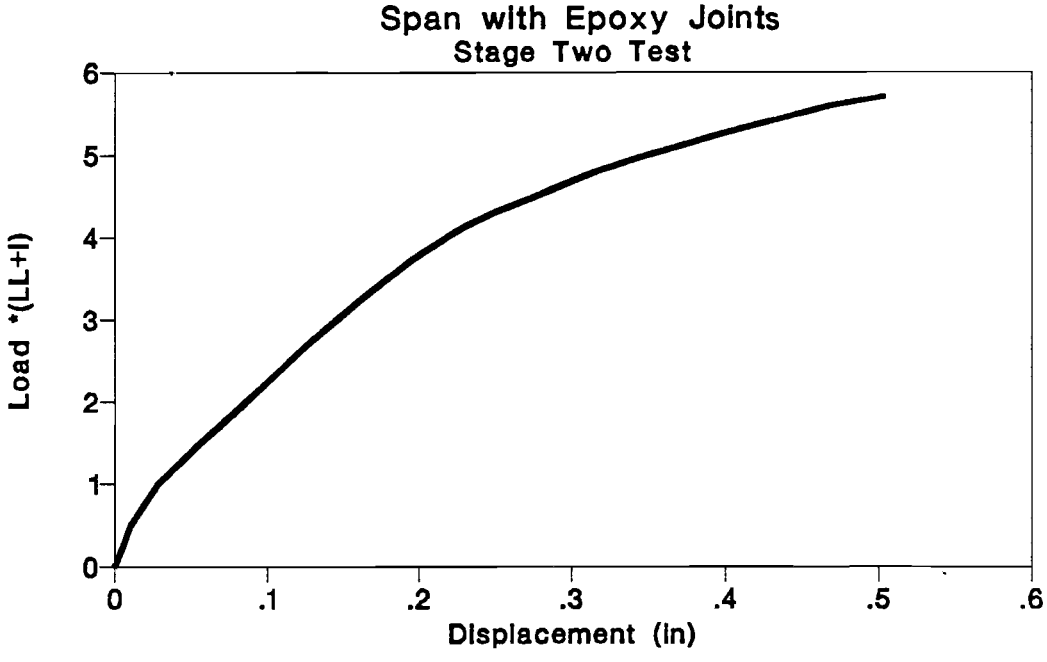

Figure 3.33 Load-deflection of Stage Two test in epoxy joints span.

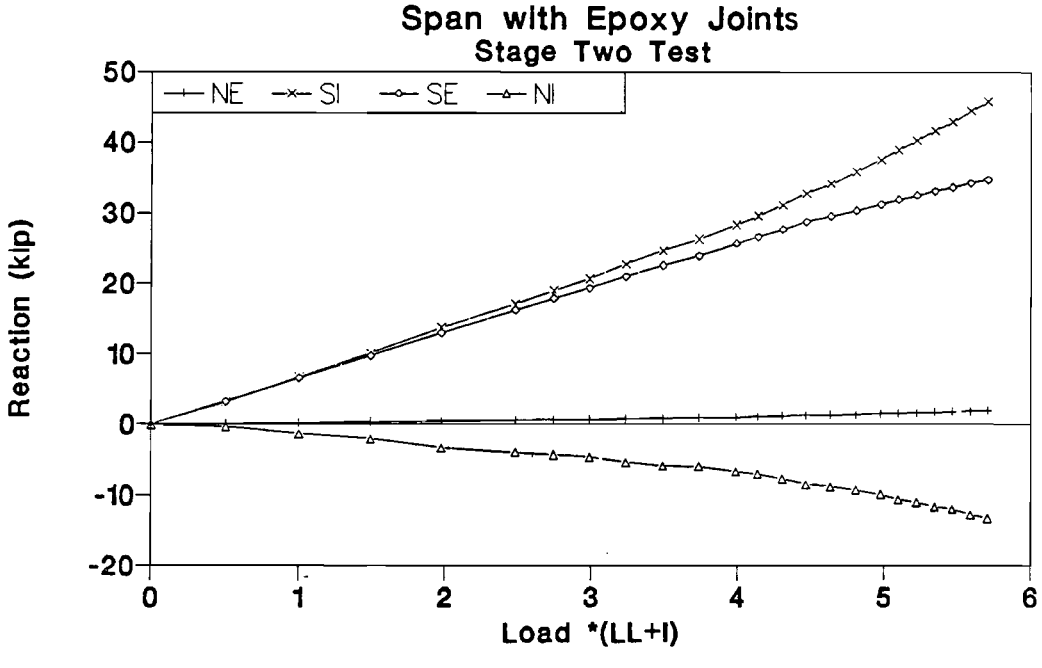

Figure 3.34 Reaction-load of Stage Two test in epoxy joints span.

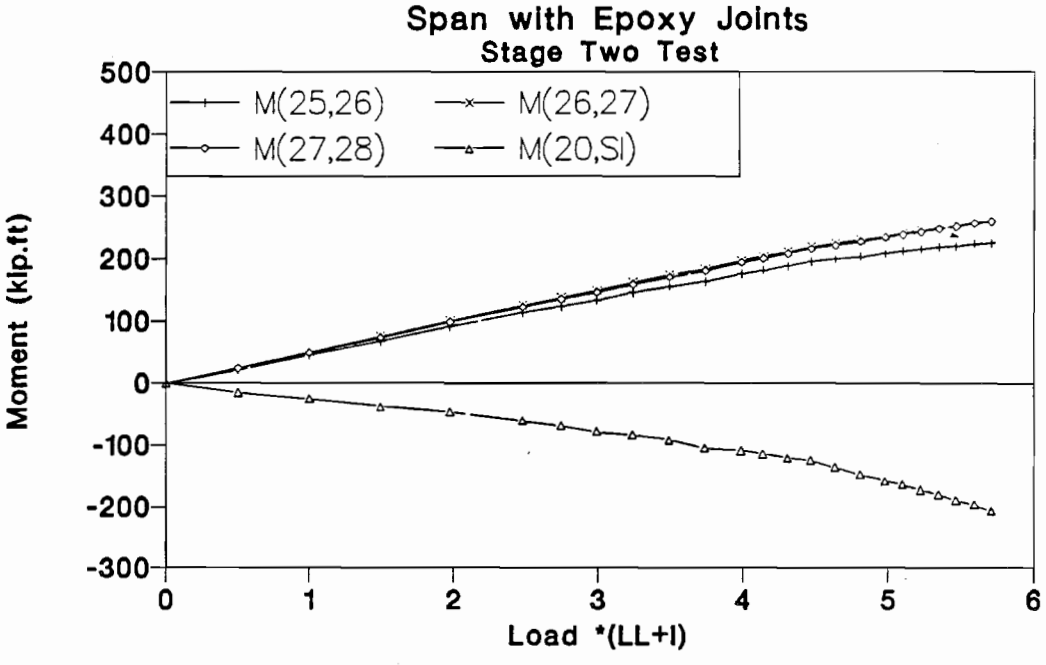

Figure 3.35 Moment-load of Stage Two test in epoxy joints span.

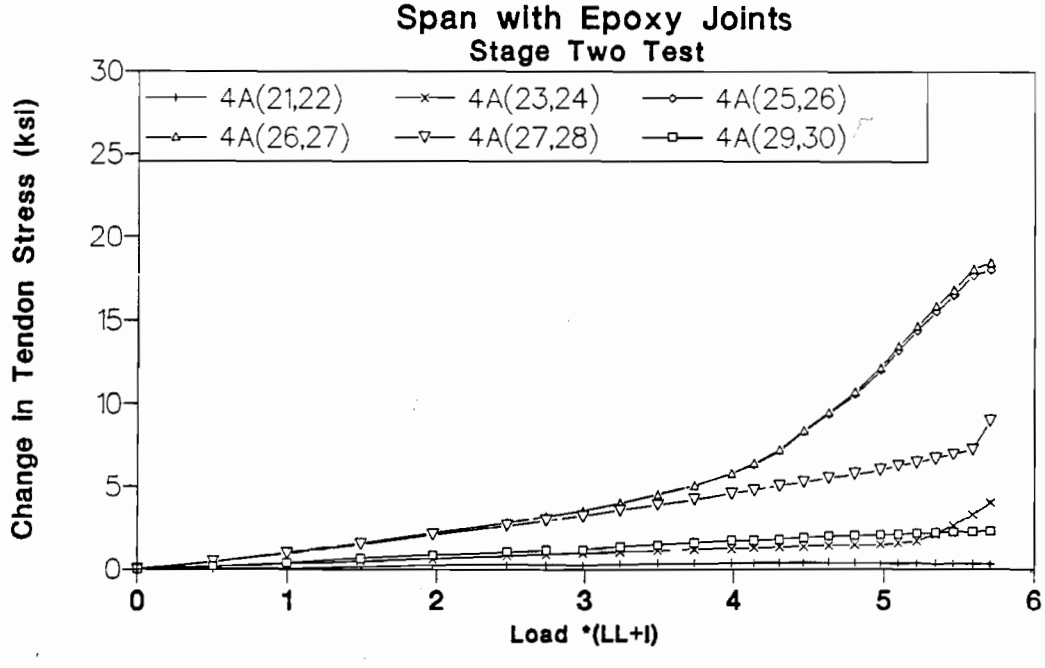

Figure 3.36 Tendon 4A stress-load of Stage Two test in epoxy joints span.

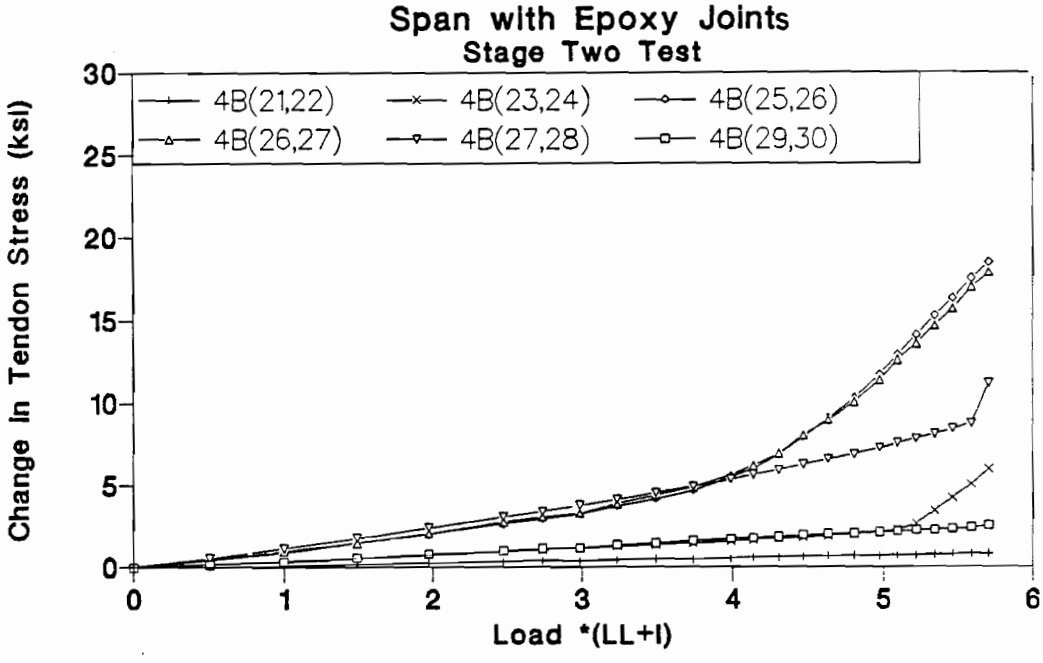

Figure 3.37 Tendon 4B stress-load of Stage Two test in epoxy joints span.

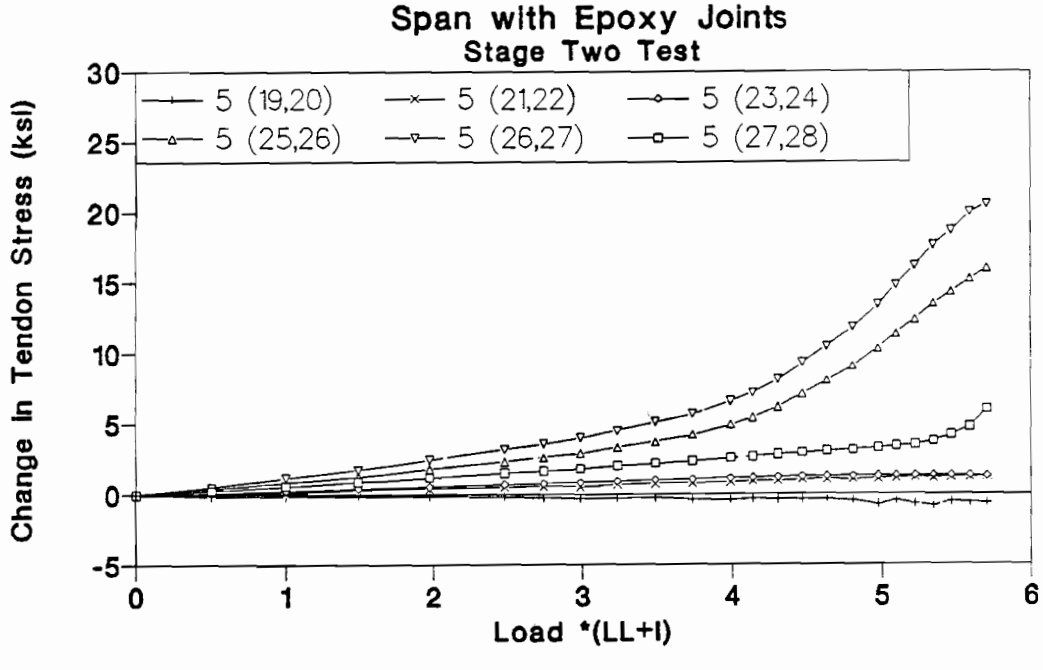

Figure 3.38 Tendon 5 stress-load of Stage Two test in epoxy joints span.

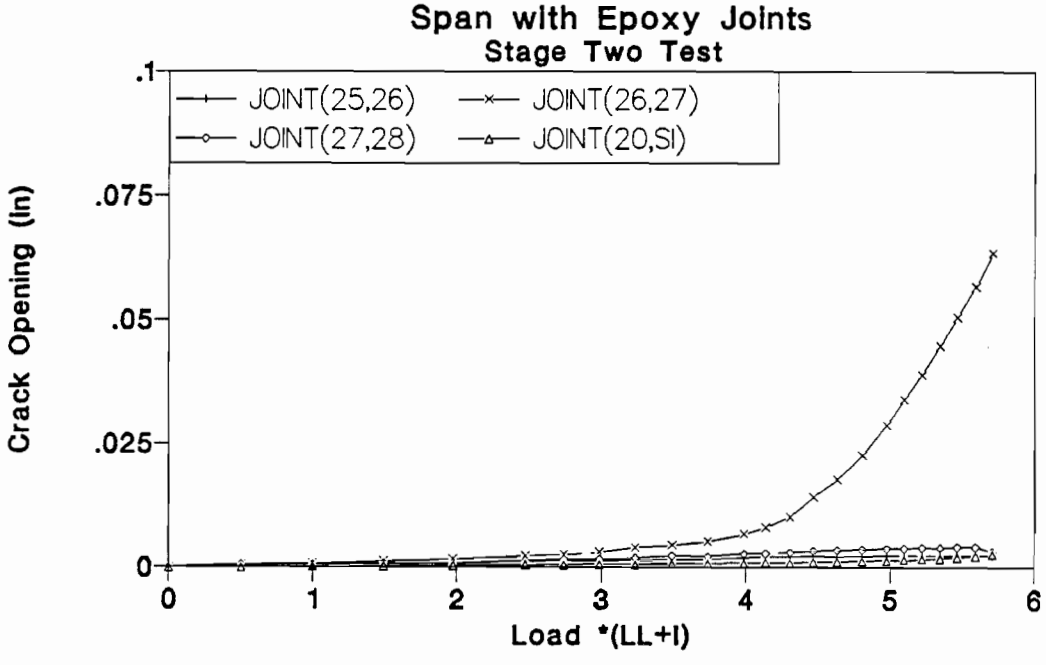

Figure 3.39 Crack opening-load of Stage Two test in epoxy joints span.

At a load of 4.0(LL+I), the same load as for the stage one test, the crack adjacent to joint (26,27) started opening as shown in Fig. 3.39. The joint opening reduced the flexural stiffness of the mid-span region which led to redistribution of the internal forces to the internal support as shown in Fig. 3.34 for reactions and Fig. 3.35 for joint moments.

At a load of 5.3(LL+I) the external tendons 4A and 4B started slipping at segment 24 as shown in Fig. 3.36 and Fig. 3.37 while tendons 5 began slipping at segment 27 at a load of 5.5(LL+I) as indicated in Fig. 3.38. The maximum change in tendon 4A stress at the end of the test was 19 ksi. By bonding the external tendons to an additional one or three internal diaphragms, the slip was reduced and delayed to a higher load.

Stage Three Tests (All tendons bonded to all 10 internal diaphragms)

External tendons were bonded to all diaphragms before executing the stage three tests as shown in Fig. 3.25(c). The response of the structure to one of the two cycles of loading is shown in Figures 3.40 through 3.46. Figure 3.40 shows the applied load-deflection response of the structure, while the measured reactions and the calculated moments are shown in Fig. 3.41 and Fig. 3.42. The changes in external tendon stress are shown in Figures 3.43 through 3.45. Crack opening response is shown in Fig. 3.46.

At a load of 4.0(LL+I), the same load as for the stage one and two tests, the crack adjacent to joint (26,27) started opening, as indicated in Fig. 3.46.

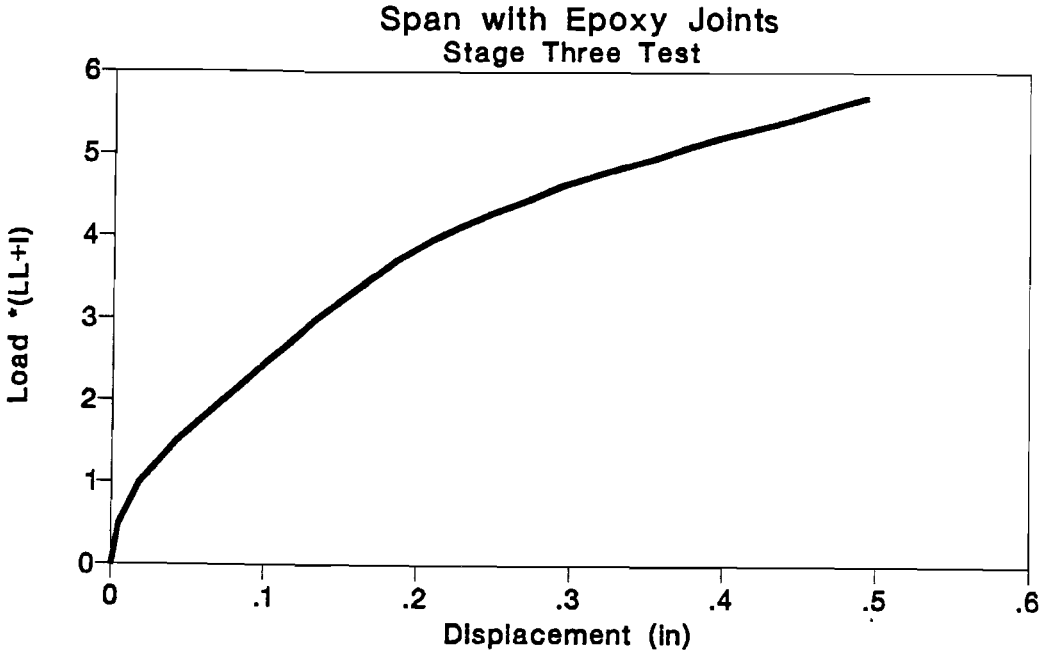

Figure 3.40 Load-deflection of Stage Three test in epoxy joints span.

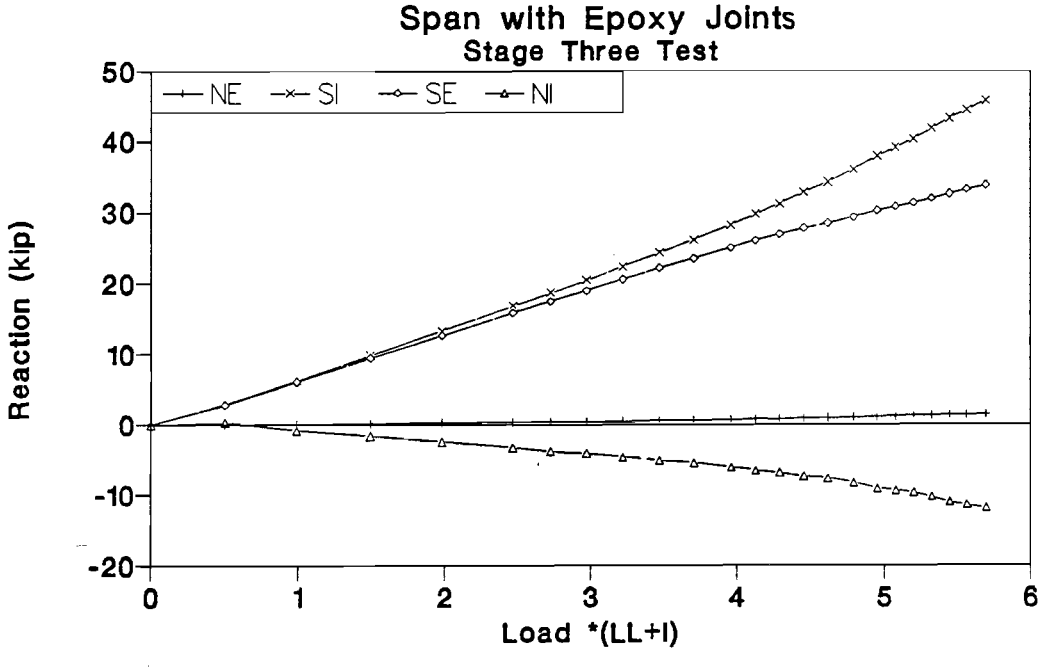

Figure 3.41 Reaction-load of Stage Three test in epoxy joints span.

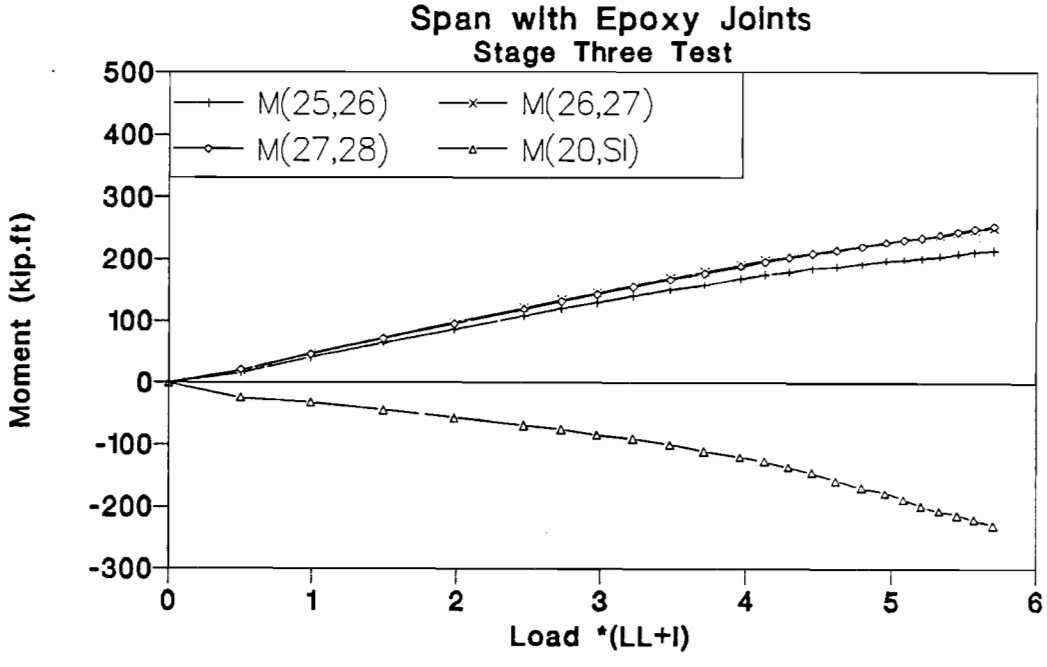

Figure 3.42 Moment-load of Stage Three test in epoxy joints span.

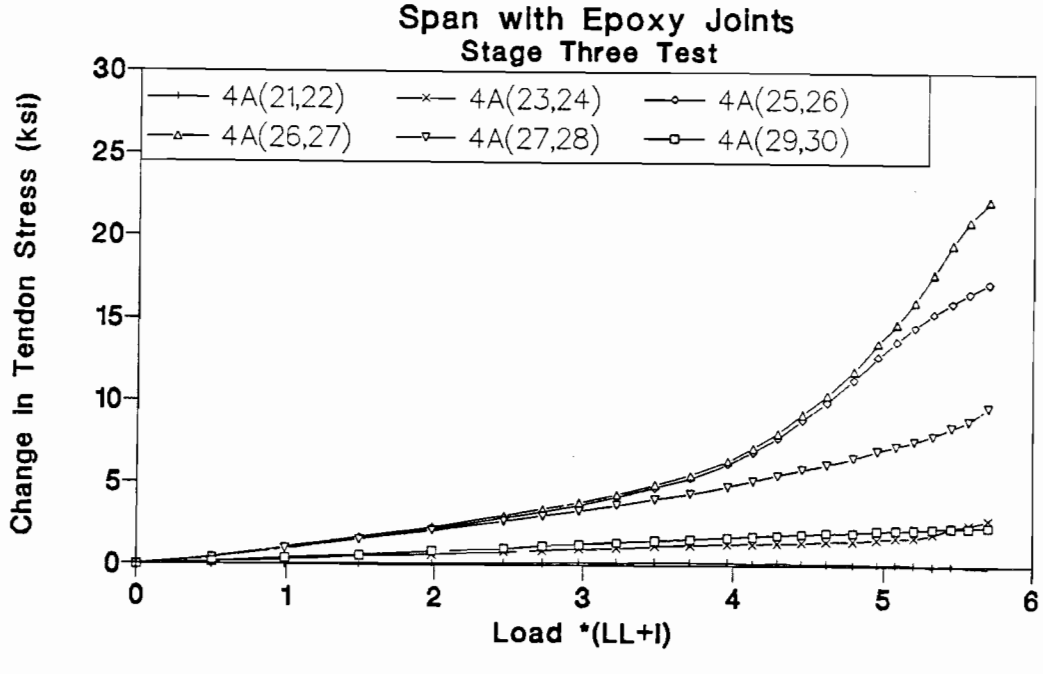

Figure 3.43 Tendon 4A stress-load of Stage Three test in epoxy joints span.

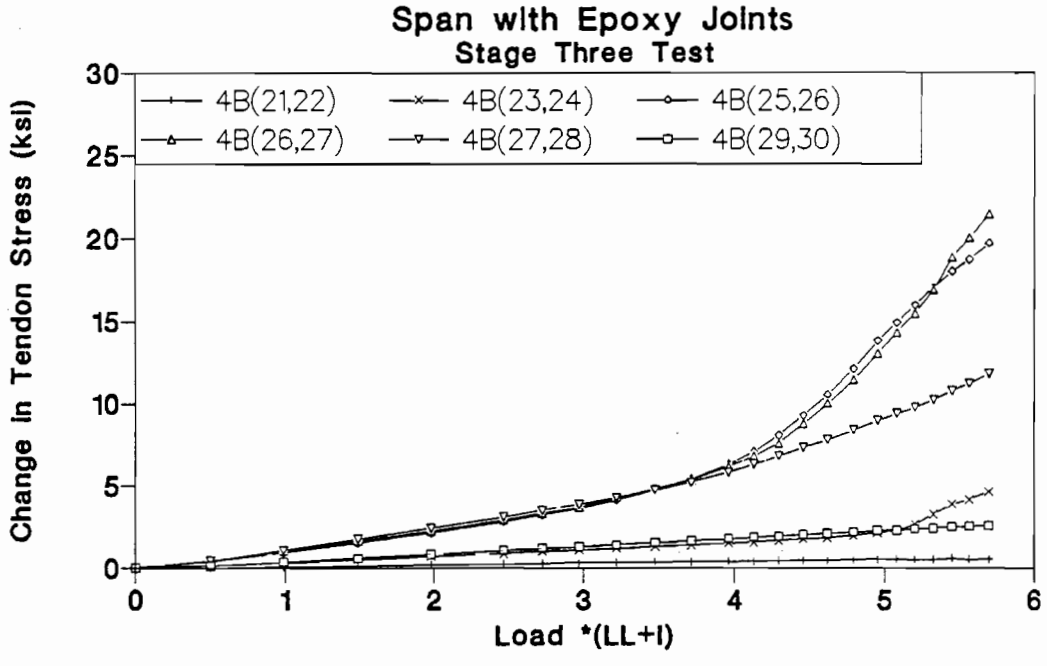

Figure 3.44 Tendon 4B stress-load of Stage Three test in epoxy joints span.

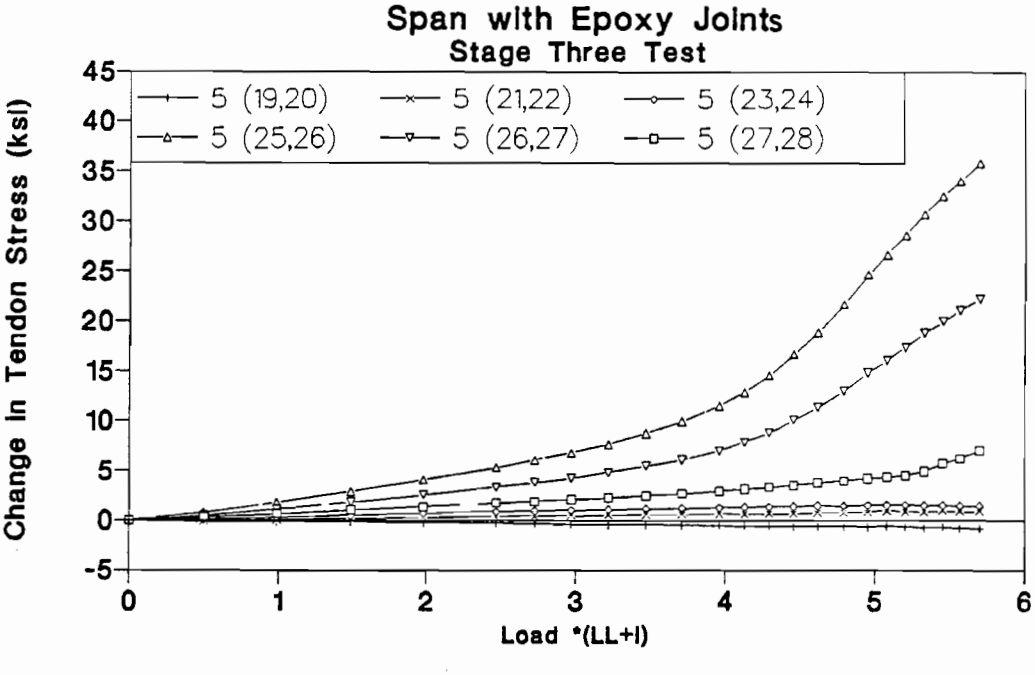

Figure 3.45 Tendon 5 stress-load of Stage Three test in epoxy joints span.

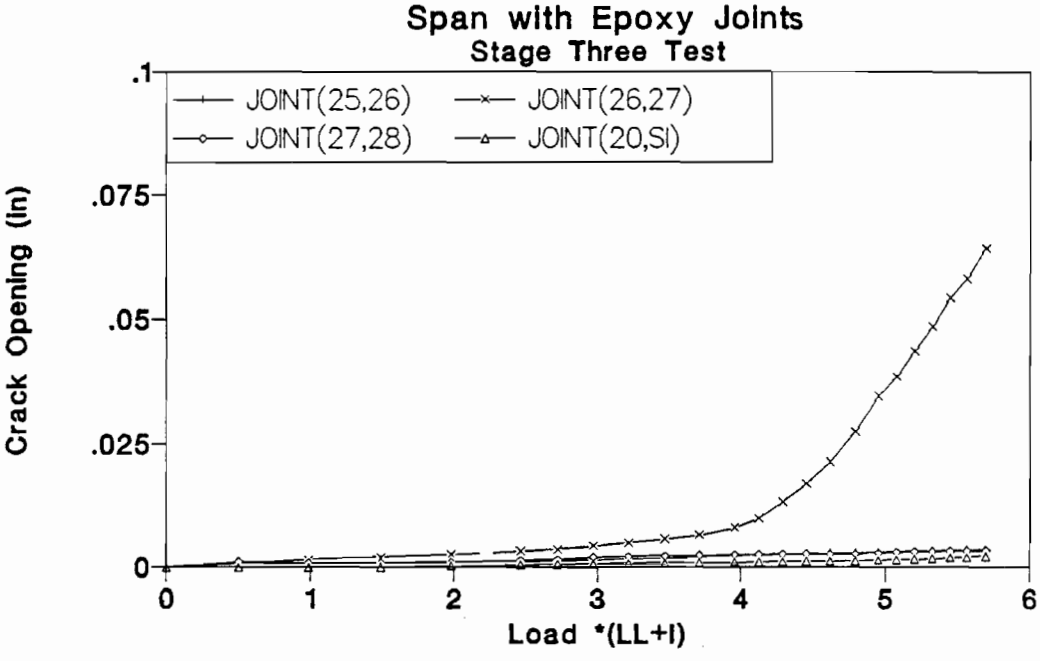

Figure 3.46 Crack opening-load of Stage Three test in epoxy joints span.

As indicated in Figure 3.43, the stress of tendons 4A at joint (25,26) and (26,27) was the same until joint (26,27) started opening and the stress difference across the diaphragm in segment 26 started increasing. A slip must occur between the tendon and the deviator to develop the bond stress as will be discussed in Chapter Five.

At a load of 5.4(LL+I), external tendons 4A started slipping at segment 24, as indicated in Fig. 3.43 while tendons 4B started slipping at approximately 5.2(LL+I) (Fig. 3.44). Tendons 5 began slipping at segment 27 at a load of 5.4(LL+I) as indicated in Fig. 3.45. The maximum change in tendons 4A stress at the end of the test at 5.7(LL+I) was 24 ksi.

The maximum load experienced during the three stages of testing (5.7(LL+I)) is only 15 percent higher than the load at which external tendons slipped. This load was not high enough to demonstrate dramatic differences in the response of the structure during the different testing stages. The critical crack started opening at the same load in all three test stages. However, tendon slip was apparently reduced and slip was delayed by the supplementary bonding of the tendons which resulted in higher change in tendon stresses.

Flexural Strength Test (All tendons bonded at 10 internal diaphragms)

The model was subjected to two cycles of loading during this portion of the testing program. The epoxy joints span was initially loaded until the flexural strength was assumed to be reached when the model stiffness was approximately 6 percent of its original stiffness

in the first load cycle or the top flange started crushing in the second load cycle. The load was increased in increments which decreased from 1(LL+I) at initial load levels to 0.1(LL+I) as failure became imminent.

In the first load cycle, the loading was stopped at 1DL+9.1(LL+I) with a maximum deflection of 2.75 inches (equivalent to L/109).

The load-deflection response of the model is shown in Fig. 3.47. The measured reactions are plotted in Fig. 3.48 while the calculated joint moments are plotted in Fig. 3.49. The changes in external tendon stresses are shown in Figures 3.50 through 3.52. The measured crack opening is plotted in Fig. 3.53.

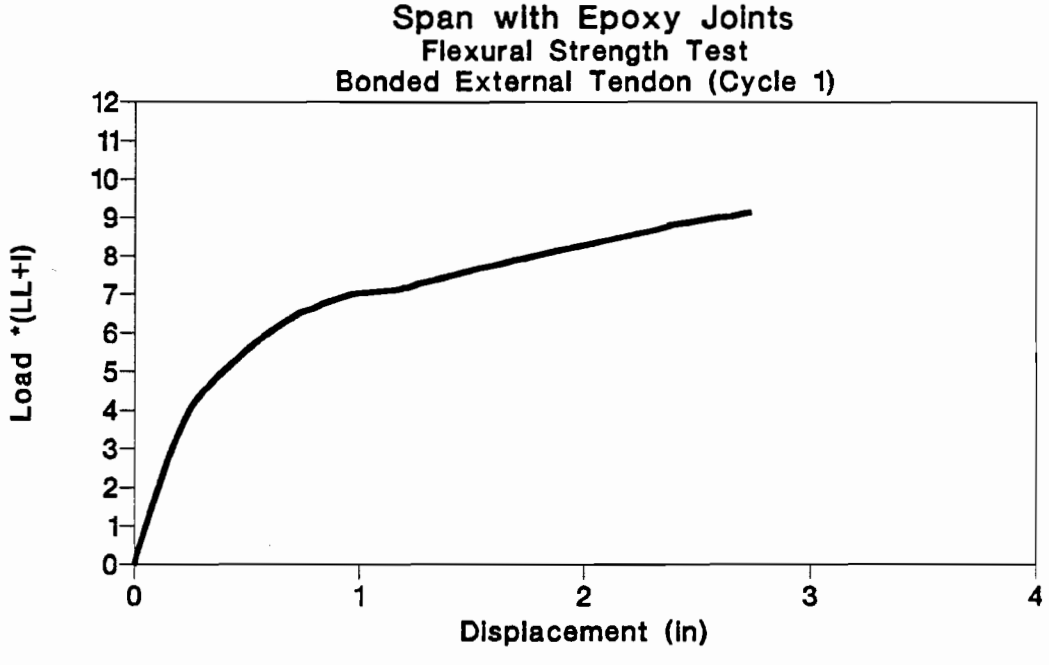

Figure 3.47 Load-deflection of flexural strength test (cycle 1) in epoxy joints span.

At a load of 4.0(LL+I), the crack adjacent to joint (26,27) started opening as shown in Fig. 3.53 causing external tendon stresses to increase at a higher rate as shown in Figures 3.50 through 3.52.

At a load of 5.4(LL+I) external tendons 4A and 4B started slipping at segment 24 toward the critical joint as shown in Fig. 3.50 and Fig. 3.51, while tendons 5 started slipping at a load of 5.5(LL+I) at segment 27. Tendons 5 also started slipping at a load of 6.2(LL+I) at segments 24 and 22 toward the critical joint as shown in Fig. 3.52.

At a load of 5.8(LL+I) external tendons 4A and 4B started slipping at segment 27 toward joint (26,27) as shown in Fig. 3.50 and Fig. 3.51, while tendon 5 started slipping when joint (26,27) started opening as shown in Fig. 3.52.

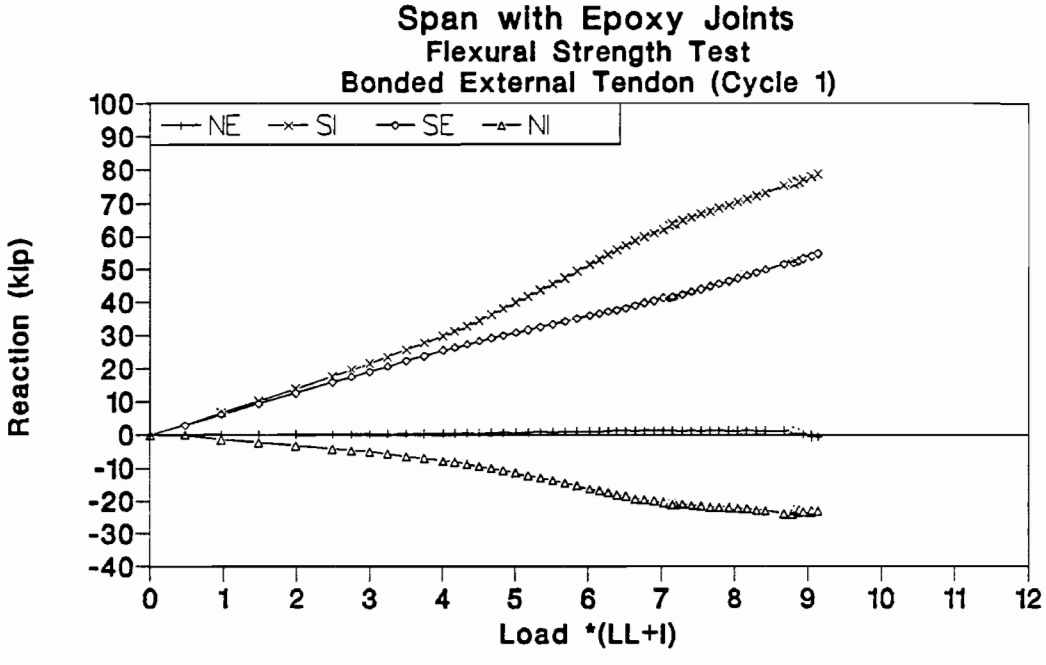

Figure 3.48 Reaction-load of flexural strength test (cycle 1) in epoxy joints span.

At a load of 7(LL+I) cracks formed adjacent to joints (27,28) and (20,SI) as indicated in Fig. 3.53. As the joint cracked the tension force carried by the concrete was transferred to the steel, which caused external tendon stresses to increase suddenly as shown in Fig. 3.50 through Fig. 3.52.

At a load of 7(LL+I) external tendons 4A and 4B started slipping at segment 29 as shown in Fig. 3.50 and Fig. 3.51.

At a load of 8.4(LL+I) a crack adjacent to joint (25,26) was formed as shown in Fig 3.53.

The test was stopped at a load of 9.1(LL+I) when the stiffness was approximately 6 percent of the initial stiffness.

During the second loading cycle, the epoxy joints span was loaded until the flexural strength was assumed reached when the positive moment compression flange started crushing. The ultimate strength measured was 1DL+9.6(LL+I) with a maximum deflection of 3.05 inches (equivalent to L/98).

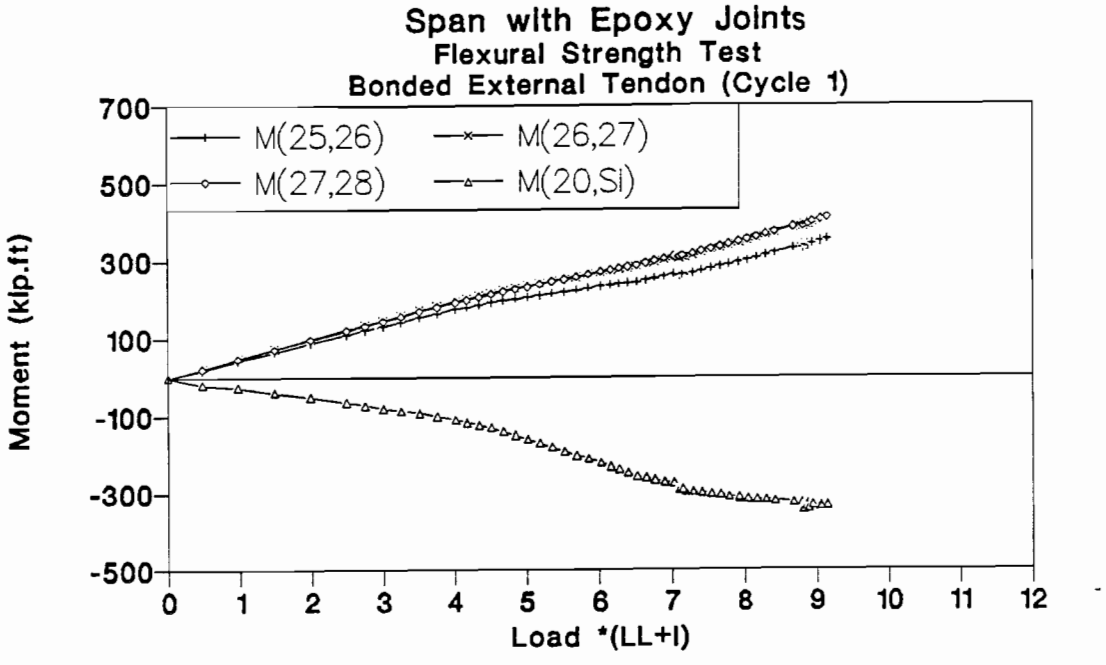

Figure 3.49 Moment-load of flexural strength test (cycle 1) in epoxy joints span.

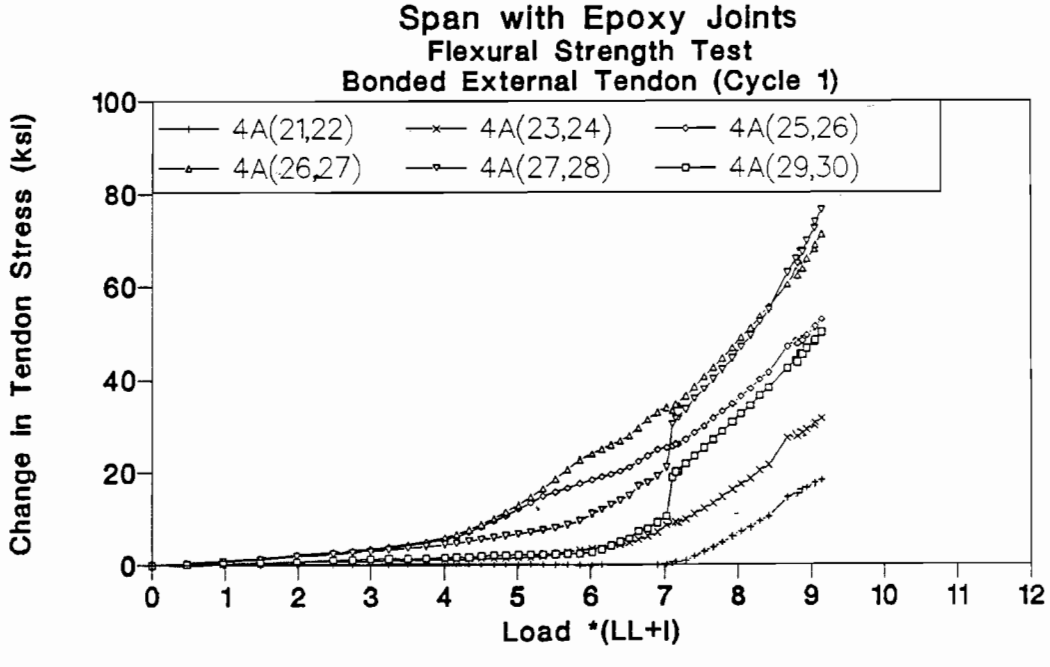

Figure 3.50 Tendon 4A stress-load of flexural strength test (cycle 1) in epoxy joints span.

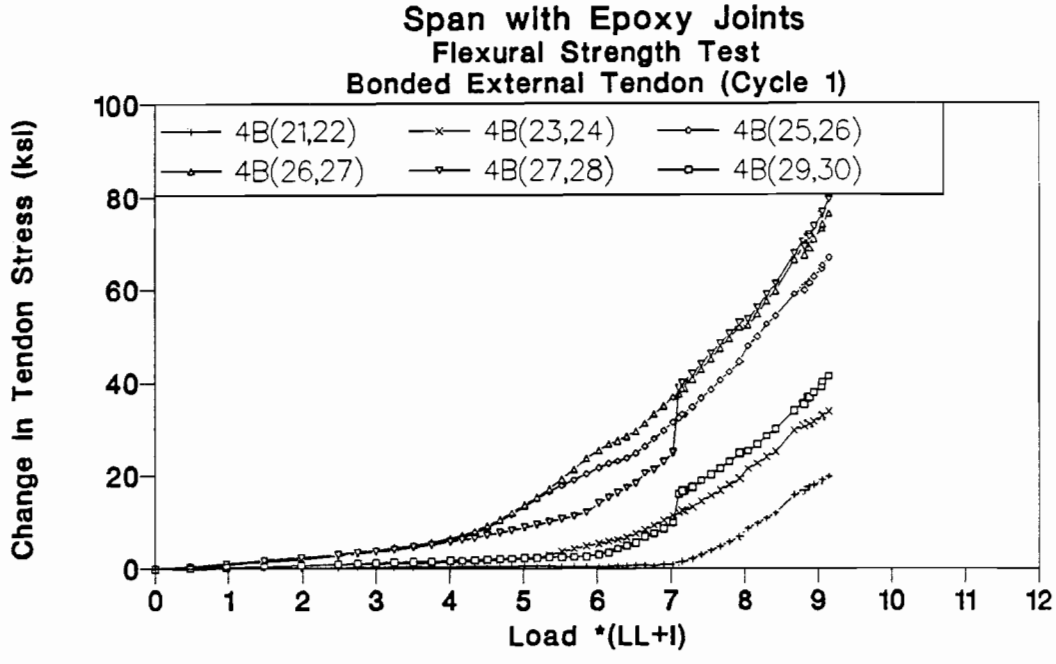

Figure 3.51 Tendon 4B stress-load of flexural strength test (cycle 1) in epoxy joints span.

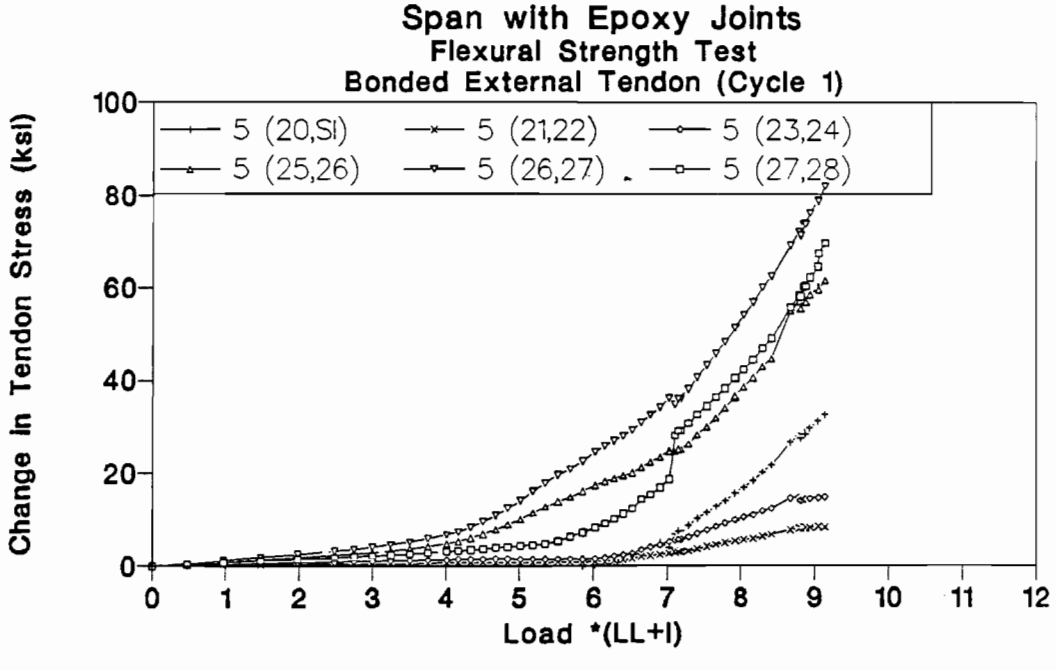

Figure 3.52 Tendon 5 stress-load of flexural strength test (cycle 1) in epoxy joints span.

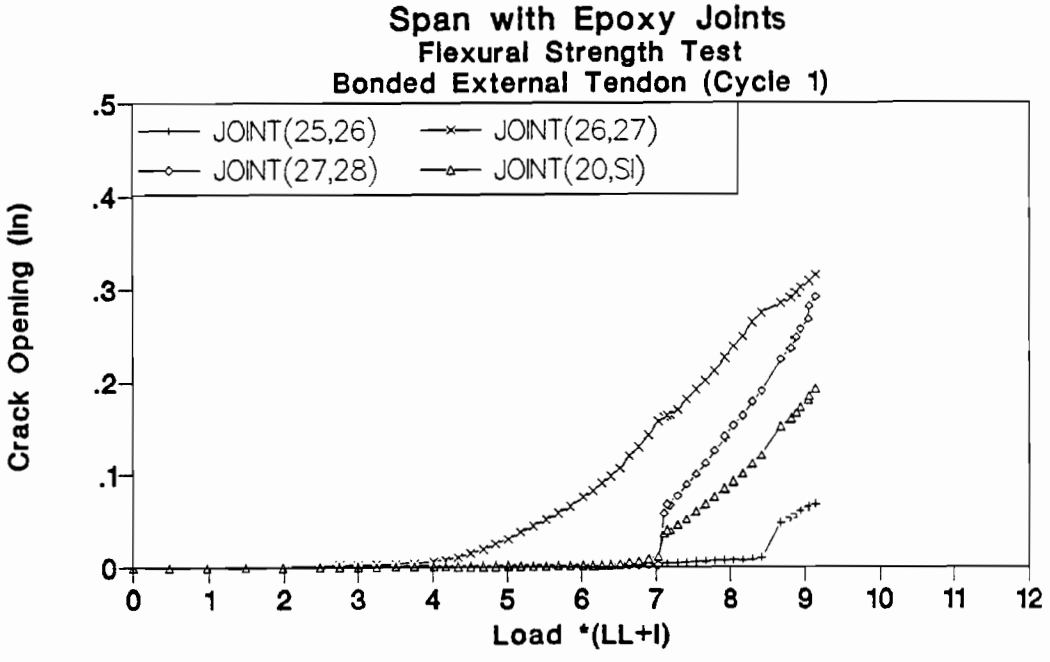

Figure 3.53 Crack opening-load of flexural strength test (cycle 1) in epoxy joints span.

The load-deflection response of the model is shown in Fig. 3.54. The measured reactions are plotted in Fig. 3.55, while the calculated joint moments are plotted in Fig. 3.56. Changes in tendon stress are shown in Fig. 3.57 through Fig. 3.59. Measured Crack openings are plotted in Fig. 3.60.

At a load of 4.0(LL+I), the crack adjacent to joint (26,27) started opening as shown in Fig. 3.60 causing external tendon stresses to increase at a higher rate as shown in Fig. 3.57 through Fig. 3.59.

At a load of 4.8(LL+I), the crack adjacent to joint (27,28) started opening as shown in Fig. 3.60 causing the external tendon stresses to increase at a higher rate as shown in Fig. 3.57 through Fig. 3.59.

At a load of 5.5(LL+I) external tendons 4A and 4B started slipping at segments 24 and 29 toward the critical joint as shown in Fig. 3.57 and Fig. 3.58, while tendons 5 started slipping at a load of 6.2(LL+I) at segments 24 and 22 toward the critical joint as shown in Fig. 3.59.

At a load of 6.2(LL+I) joint (20,SI) adjacent to the interior support started opening as shown in Fig. 3.60, causing additional changes in the redistribution of the load as shown in Fig. 3.55 and Fig. 3.56.

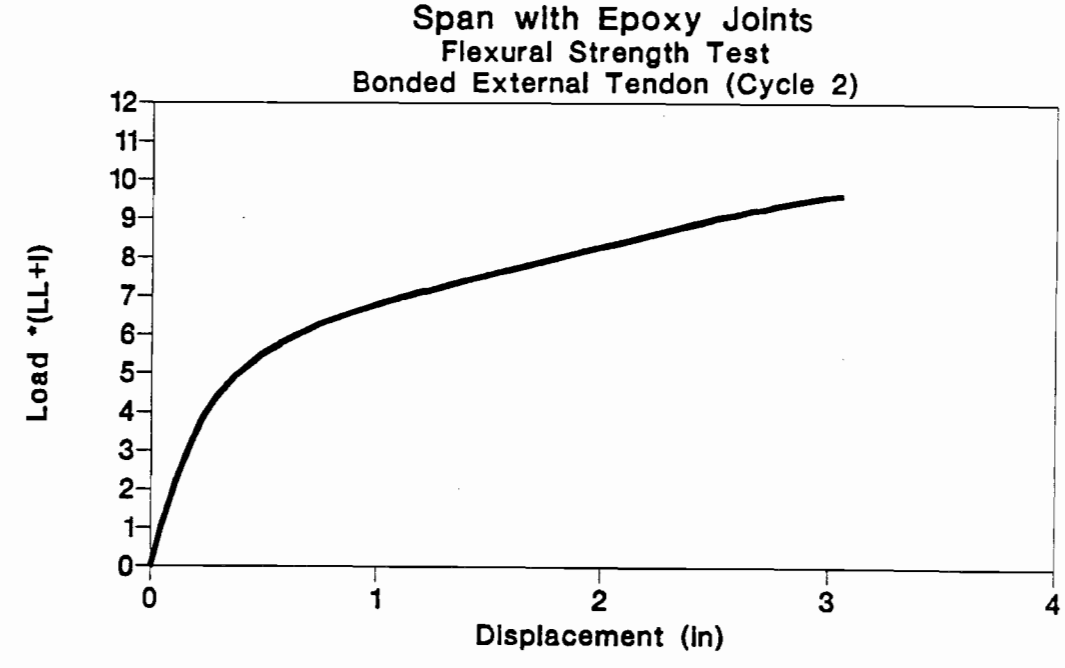

Figure 3.54 Load-deflection of flexural strength test (cycle 2) in epoxy joints span.

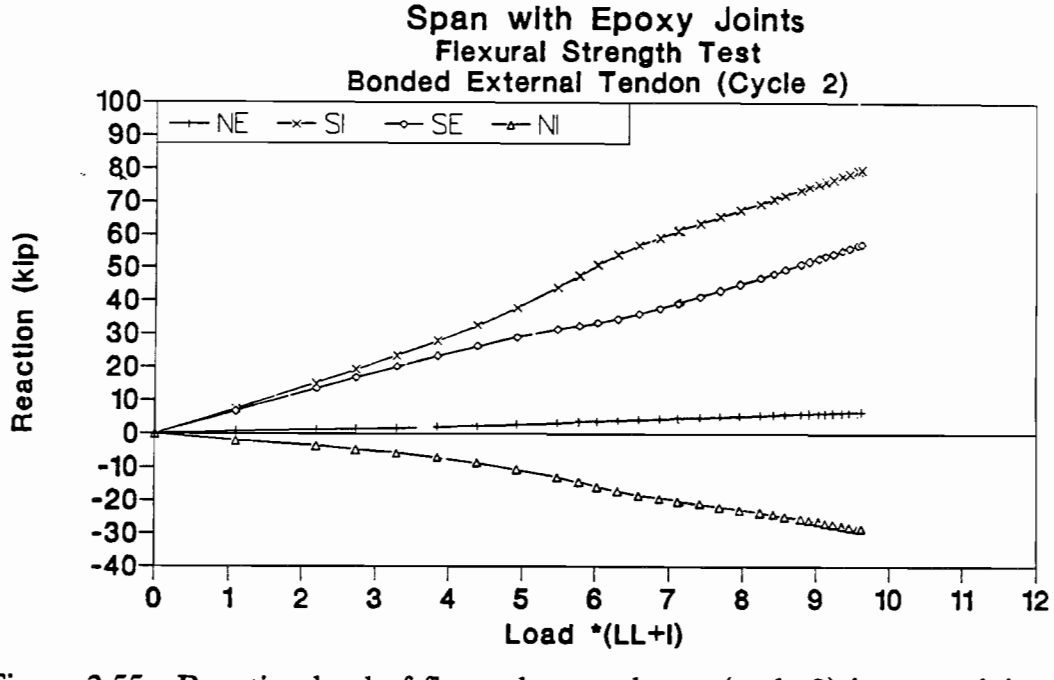

Figure 3.55 Reaction-load of flexural strength test (cycle 2) in epoxy joints span.

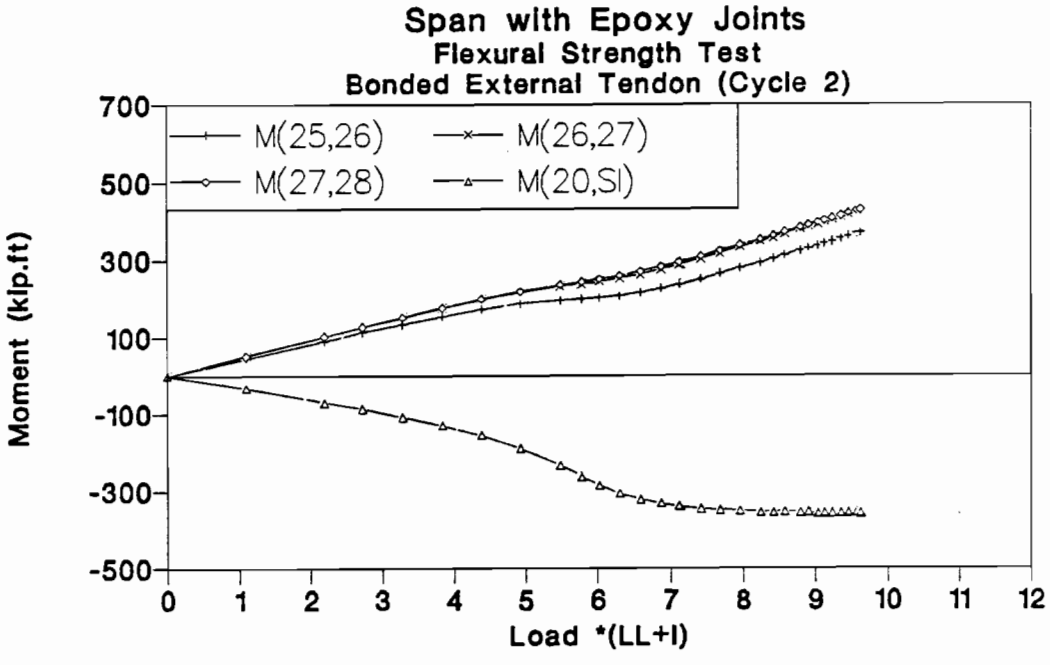

Figure 3.56 Moment-load of flexural strength test (cycle 2) in epoxy joints span.

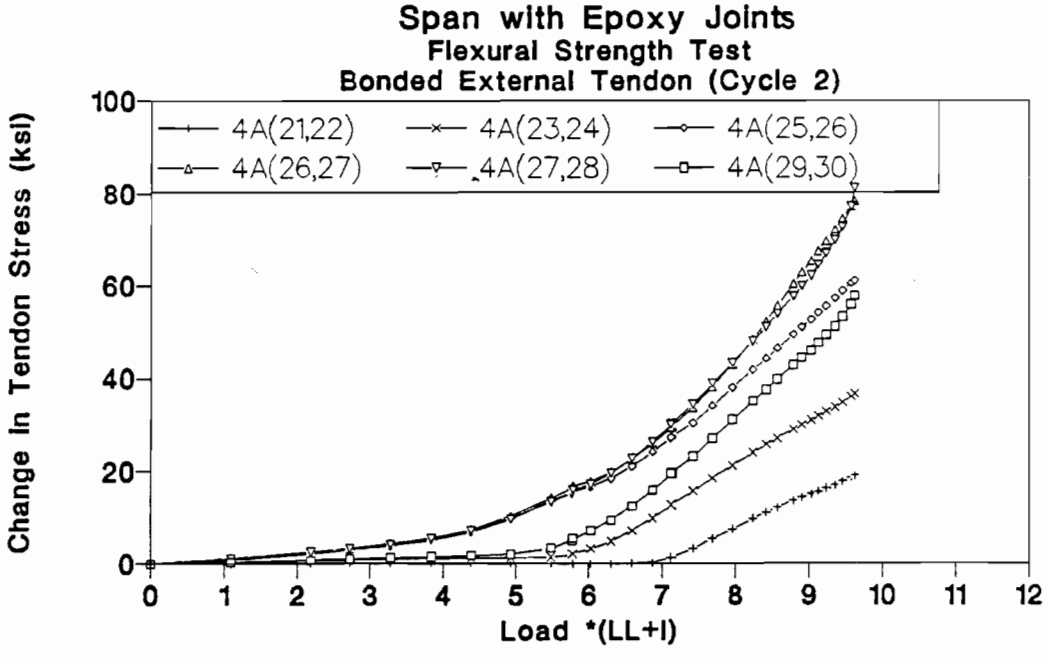

Figure 3.57 Tendon 4A stress-load of flexural strength test (cycle 2) in epoxy joints span.

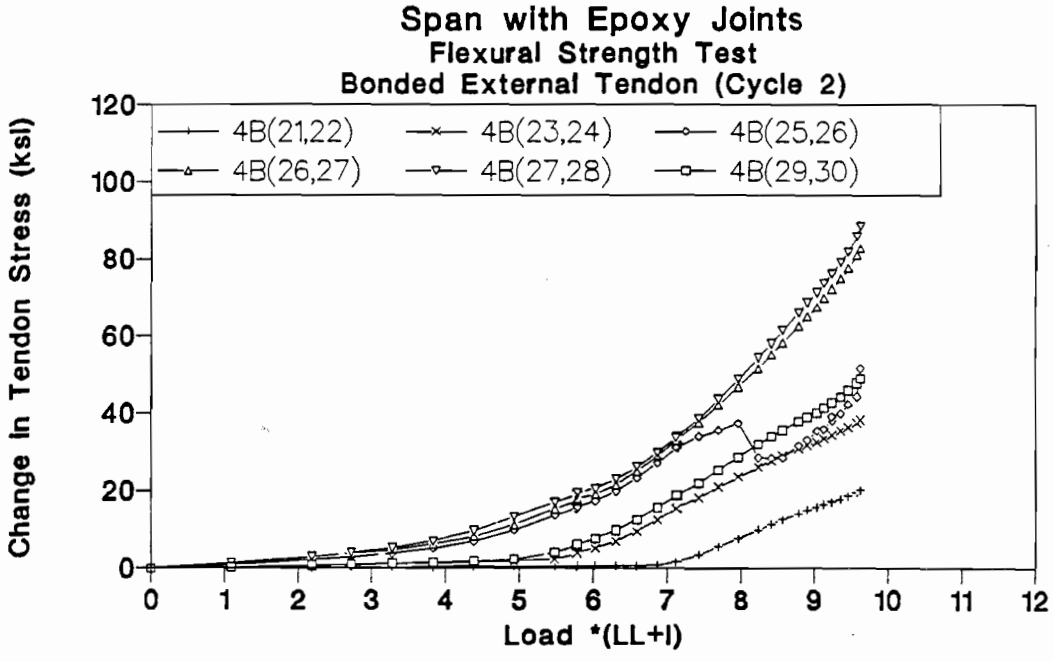

Figure 3.58 Tendon 4B stress-load of flexural strength test (cycle 2) in epoxy joints span.

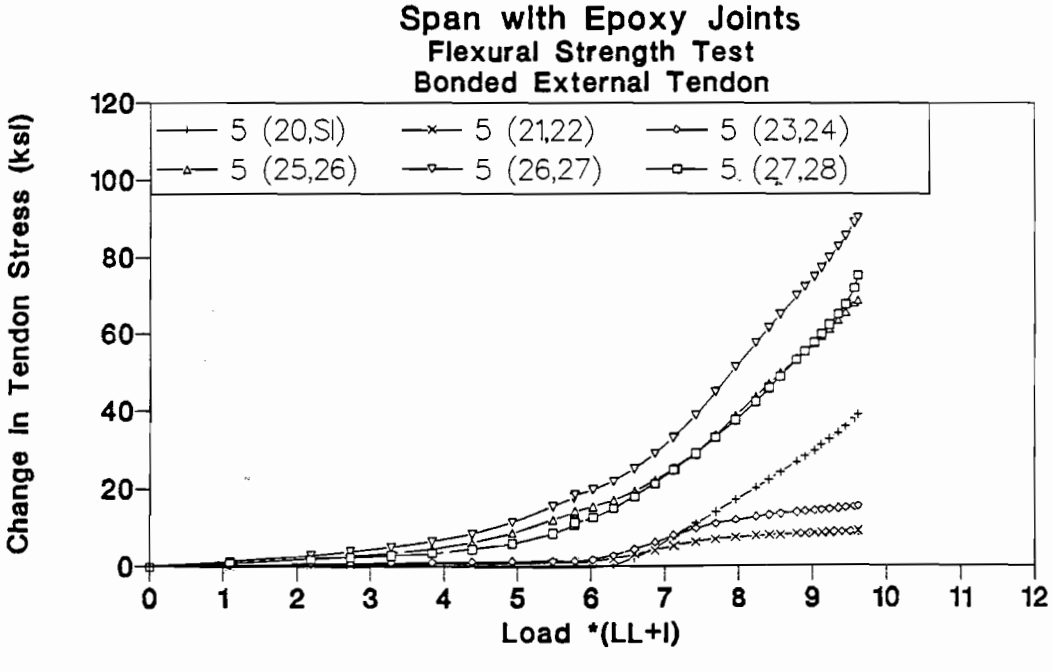

Figure 3.59 Tendon 5 stress-load of flexural strength test (cycle 2) in epoxy joints span.

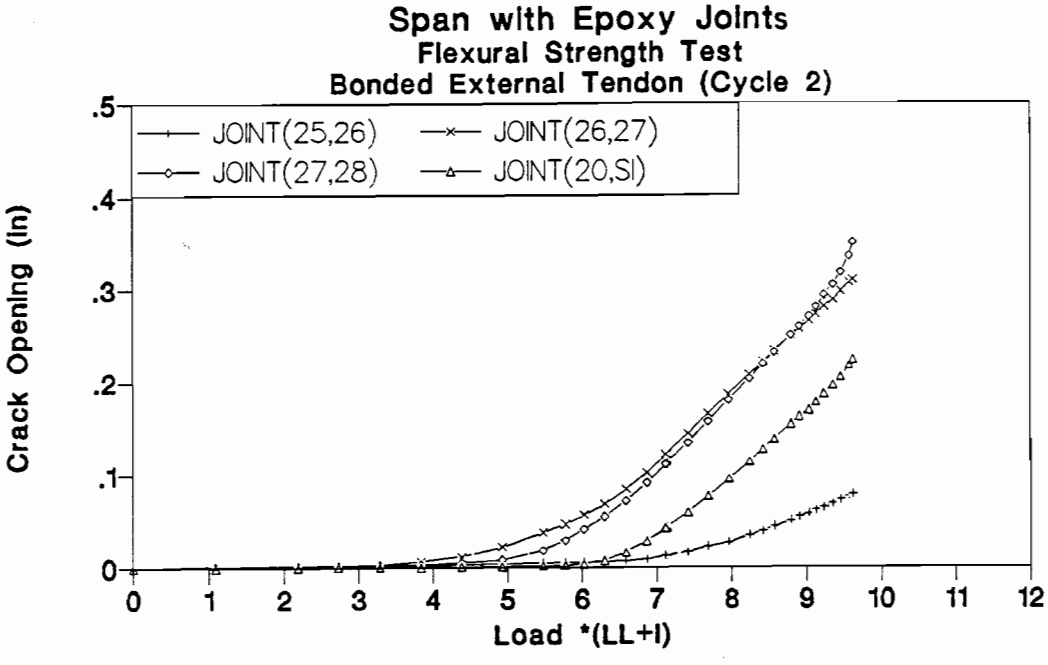

Figure 3.60 Crack opening-load of flexural strength test (cycle 2) in epoxy joints span.

At a load of 6.7(LL+I), a crack adjacent to joint (25,26) started opening as shown in Fig. 3.60 causing external tendon stresses to increase at a higher rate as shown in Fig. 3.57 through 3.59.

At a load of 9.6(LL+I), initiation of crushing of the top flange occurred at joint (27,28), and the test was stopped.

As shown in Fig. 3.55 the reaction curves exhibited double curvature. As the positive moment critical joint opened, the mid-span stiffness reduced and the internal forces redistributed toward the interior support. Since the support stiffness reduced when joint (20,SI) opened, this caused a redistribution of the internal forces back towards the positive moment region. The double curvature behavior was also exhibited in the moment curves shown in Fig. 3.56 due to the same reasons.

Figure 3.60 shows that cracks located adjacent to joint (27,28) and joint (26,27) exhibited large openings as required to increase the tendon stresses in the positive moment region. Web cracks occurred at joint (26,27) at a load of 6.3(LL+I). The cracks extended into the top flange as the span reached its ultimate flexural strength, which was an indication that the neutral axis had shifted into the top flange.

3.4.1.4 Supplemental Tendon Load Tests. Two additional flexural strength tests were carried out on the model to show its response after adding and stressing internal

tendons. Four 3/8" diameter internal tendons were added to the bottom flange of the bridge.

3.4.1.4.1 Ungrouted Internal Tendon Test. An ultimate flexural strength test was carried out on the model after adding and stressing the four internal tendons, but before grouting them. The epoxy joints span was loaded until the flexural strength was reached as evidenced by the initiation of crushing of the top flange at the critical joint. The test was stopped before serious damage occurred in the flange at joint (26,27), as shown in Fig. 3.61. The stiffness of the model at termination of the test was approximately 5% its initial stiffness.

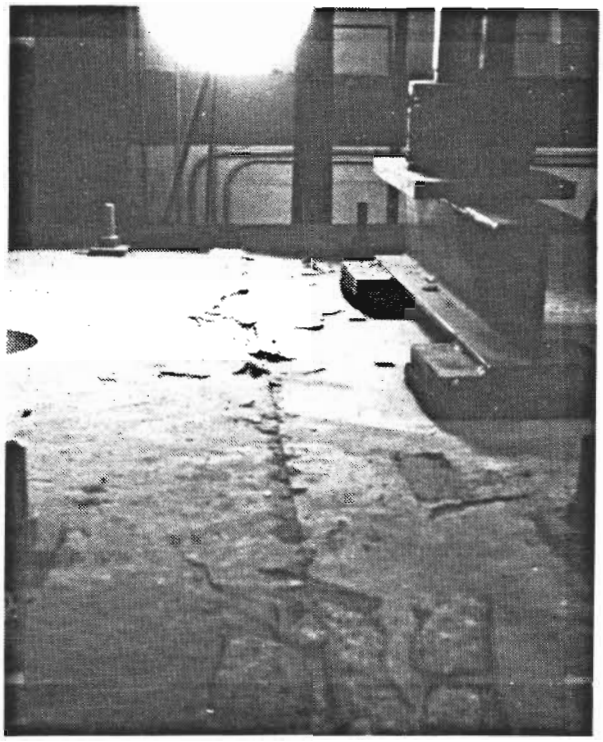

Figure 3.61 Crushing of top flange in epoxy joints span.

The load was increased from zero to 2(LL+I) in 1(LL+I) increments, from 2(LL+I) to 7.6(LL+I) in 0.5(LL+I) increments, and from 7.6(LL+I) to 10.4(LL+I) in 0.2(LL+I) increments. The test was carried out in one loading cycle, and the flexural strength measured was 1DL+10.4(LL+I) with a maximum deflection of 2.95 inches (equivalent to L/102).

The load deflection response of the model is shown in Fig. 3.62. The measured reactions are plotted in Fig. 3.63 while the calculated moments are plotted in Fig. 3.64. The measured stress changes in the external tendons are plotted in Fig. 3.65 through 3.67. The measured crack openings are plotted in Fig. 3.68. The change in the internal tendon stress at two segments are plotted in Fig. 3.69.

At a load of 5(LL+I) the crack adjacent to joint (26,27) started opening as shown in Fig. 3.68 causing the external tendon stresses to increase rapidly as shown in Fig. 3.65 through 3.67. The crack opening near joint (26,27) reduced the positive moment section stiffness and redistributed the internal forces to the support section as shown in Fig. 3.63 for reactions and Fig. 3.64 for moments.

As soon as joint (26,27) started opening, the stresses of the external tendons at joints (25,26), (26,27), and (27,28) started increasing at higher rate. The stresses in the three joints were more or less the same when the joint started opening and a stress difference was built as the slip required to develop bond stress was increased as shown in Fig. 3.65 and Fig. 3.66.

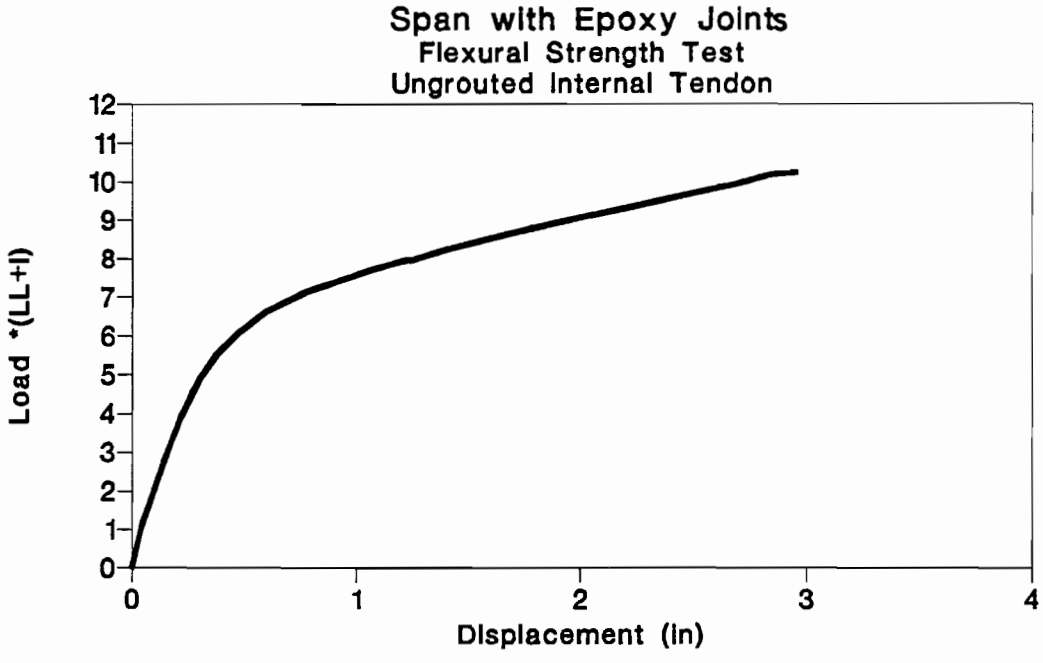

Figure 3.62 Load-deflection of ungrouted internal tendons test in epoxy joints span.

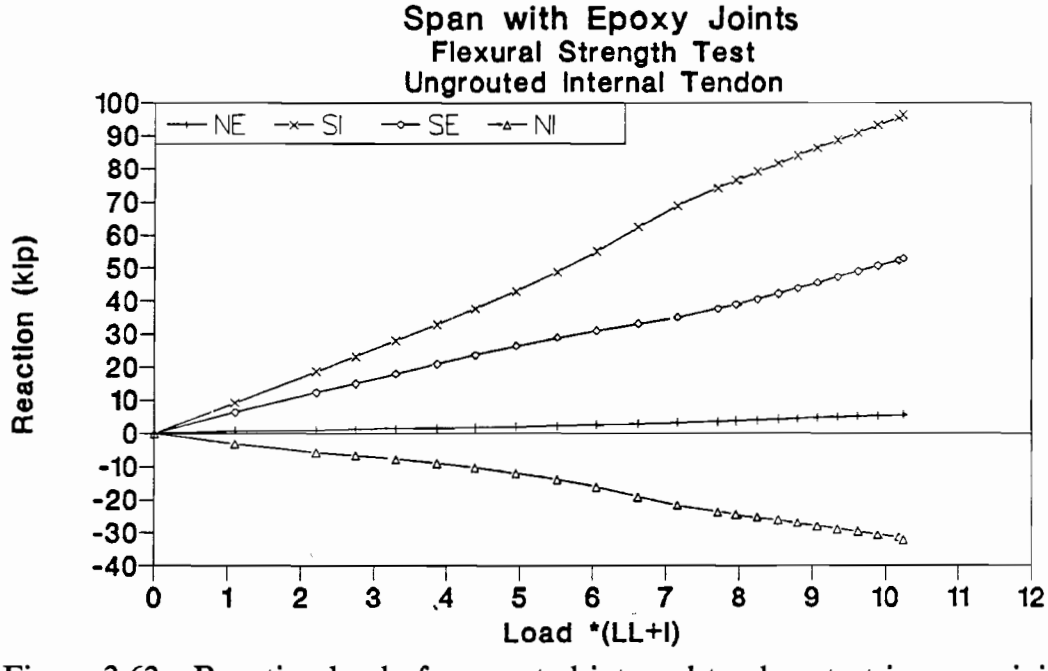

Figure 3.63 Reaction-load of ungrouted internal tendons test in epoxy joints span.

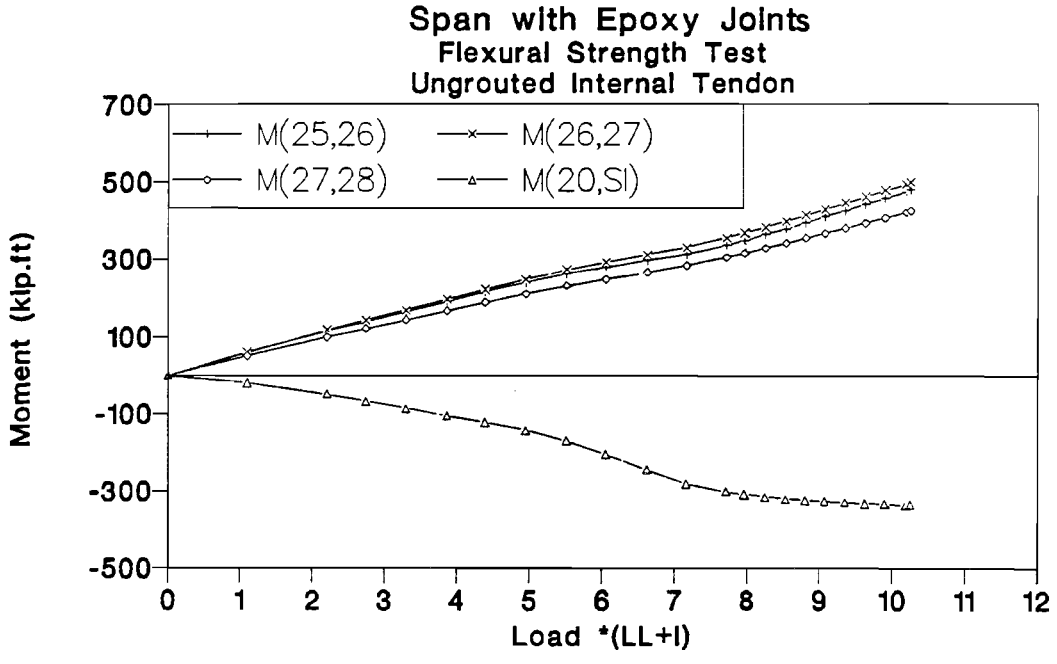

Figure 3.64 Moment-load of ungrouted internal tendons test in epoxy joints span.

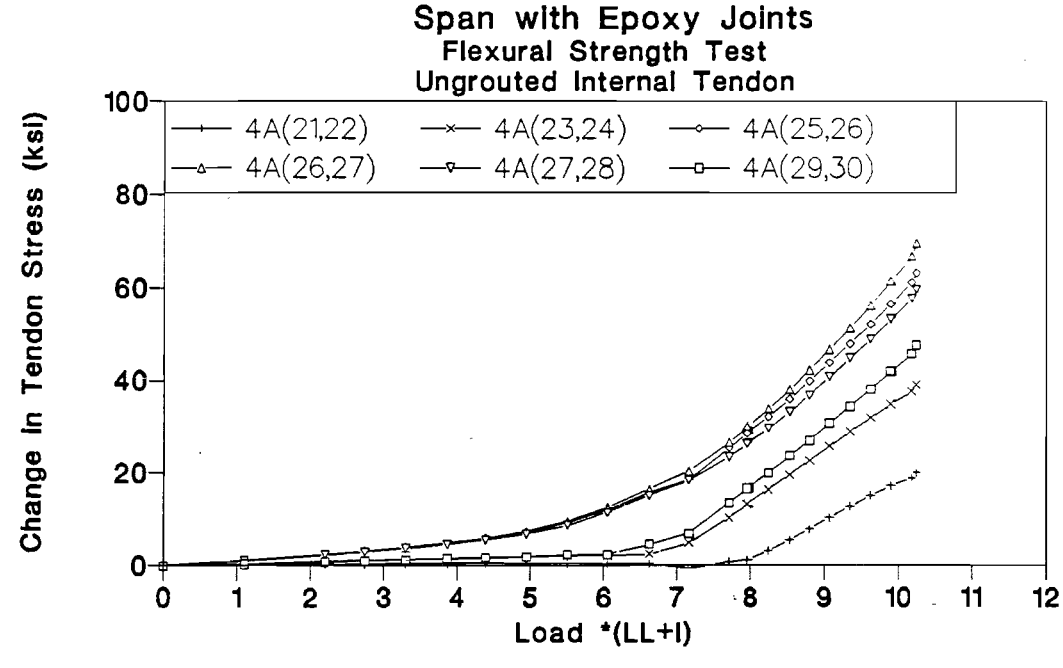

Figure 3.65 Tendon 4A stress-load of ungrouted internal tendons test in epoxy joints span.

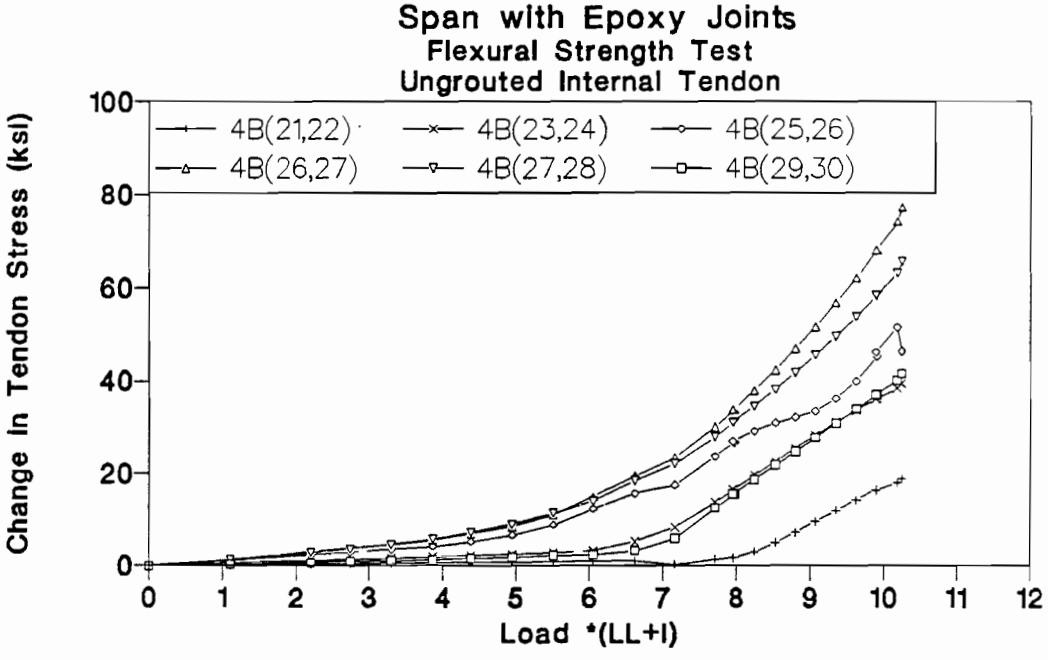

Figure 3.66 Tendon 4B stress-load of ungrouted internal tendons test in epoxy joints span.

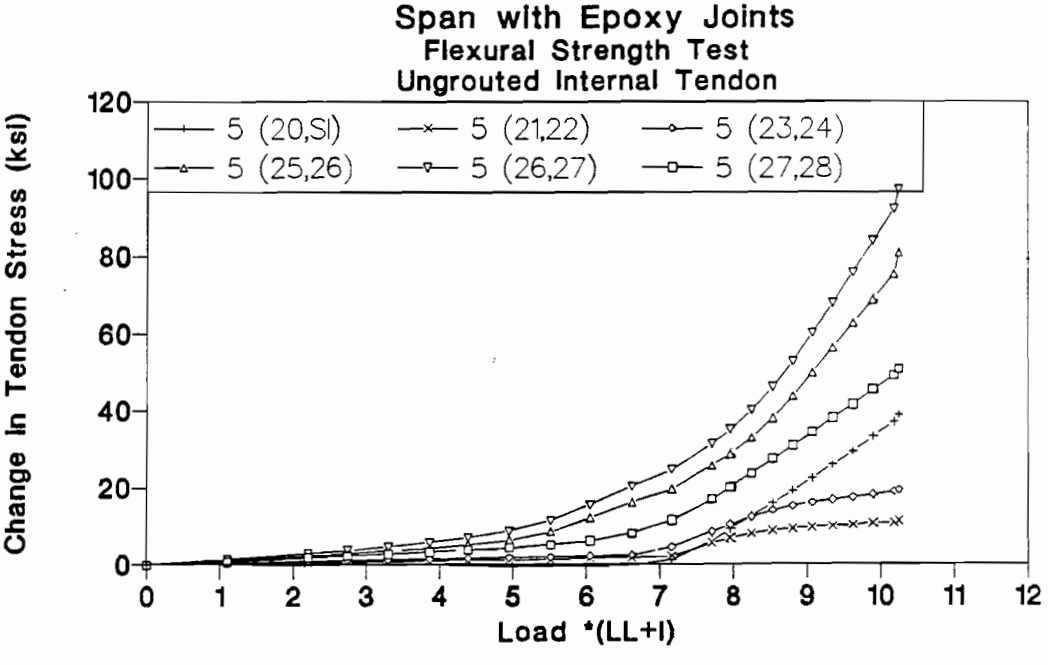

Figure 3.67 Tendon 5 stress-load ungrouted internal tendons test in epoxy joints span.

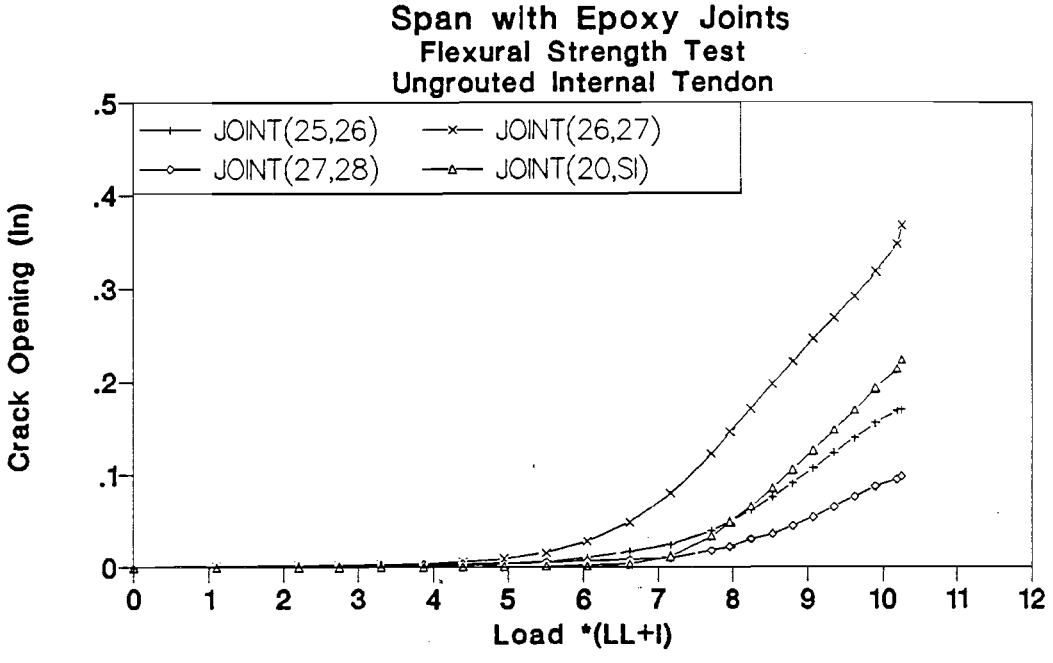

Figure 3.68 Crack opening-load of ungrouted internal tendons test in epoxy joints span.

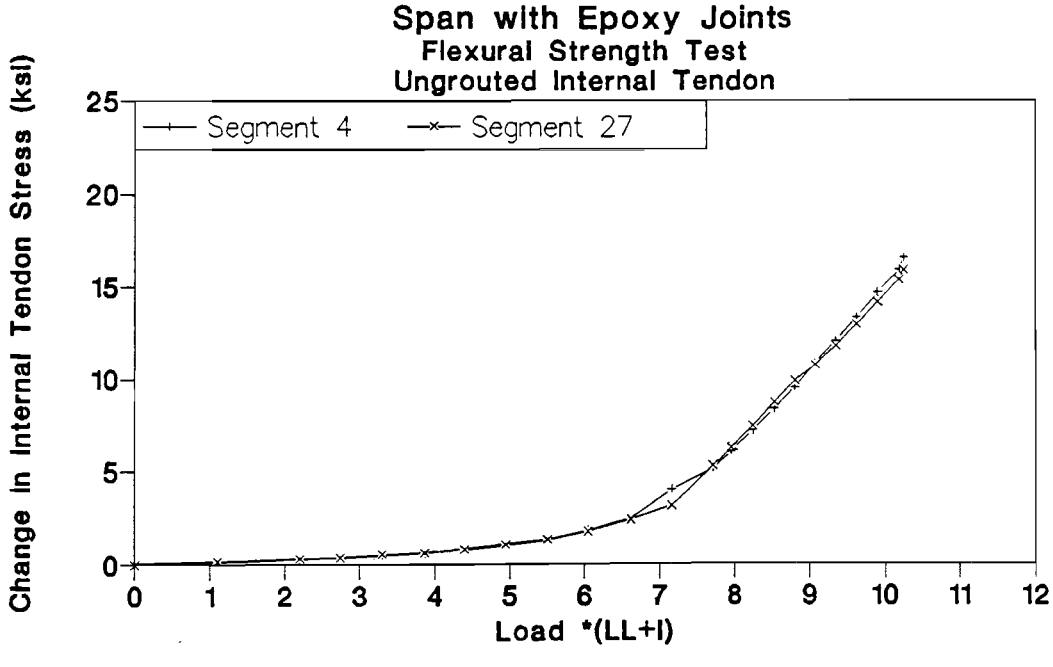

Figure 3.69 Internal tendon stress of upgrouted tendons test in epoxy joints span.

At a load of 6.5(LL+I) the external tendons started slipping in segments 24 and 29 toward joint (26,27) as shown in Figures 3.65 through 3.67.

At a load of 7(LL+I) a crack near joint (20,SI) (adjacent to the support) started opening as shown in Fig. 3.68 causing changes in the load distribution as shown by changes in the reactions (Fig. 3.63) and joint moments (Fig. 3.64).

At a load of 7.2(LL+I), tendons 5 started slipping in segment 22 and 24 toward the critical joint as shown in Fig. 3.67.

At a load of 8(LL+I), tendons 4A and 4B started slipping in segments 22 toward the critical joint as shown in Fig. 3.65 and Fig. 3.66.

At a load of 10.4(LL+I) the top flange at joint (26,27) started crushing as shown in Fig. 3.61. The test was stopped immediately because a second test was to be run on the same critical joint after grouting the bottom internal tendons. The stiffness of the structure at termination of the test was about 5% of its original stiffness.

Figure 3.69 indicates that the stress in the internal tendons was the same along the length. The friction between the internal tendon and the duct was very small because the tendons were straight over the entire length of the bridge model.

The reaction and moment curves exhibit double curvature as shown in Fig. 3.63 and Fig. 3.64 due to different distributions of internal forces when the positive moment cracks opened and when the support crack opened. The crack near joint (26,27) exhibited a wide opening required to increase the external tendon stresses in the positive moment region as shown in Fig. 3.68.

3.4.1.4.2 Grouted Internal Tendon Test. After grouting the four internal tendons in the bottom flange of the model cross section, a flexural strength test was conducted. The epoxy joints span was loaded until the top flange of joint (26,27) crushed as shown in Fig. 3.70. The load was increased from zero to 11(LL+I) in increments which varied from 1(LL+I) to 0.2(LL+I). The test was carried out in one loading cycle, and the maximum flexural strength measured was 1DL+11(LL+I) with a maximum deflection of 3.11 inches (equivalent to L/96).

The load deflection response of the model is shown in Fig. 3.71. The measured reactions and the calculated joint moments are plotted in Fig. 3.72 and Fig. 3.73. Measured changes in external tendon stresses are plotted in Fig. 3.74 through 3.76. Measured crack openings are plotted in Fig. 3.71. The stress changes in the grouted internal tendons are plotted in Fig. 3.78.

At a load of 5(LL+I) a crack near joint (26,27) started opening as shown in Fig. 3.77 which caused changes in tendon stresses and internal redistribution of forces.

Figure 3.70 Crushing of top flange in epoxy joints span.

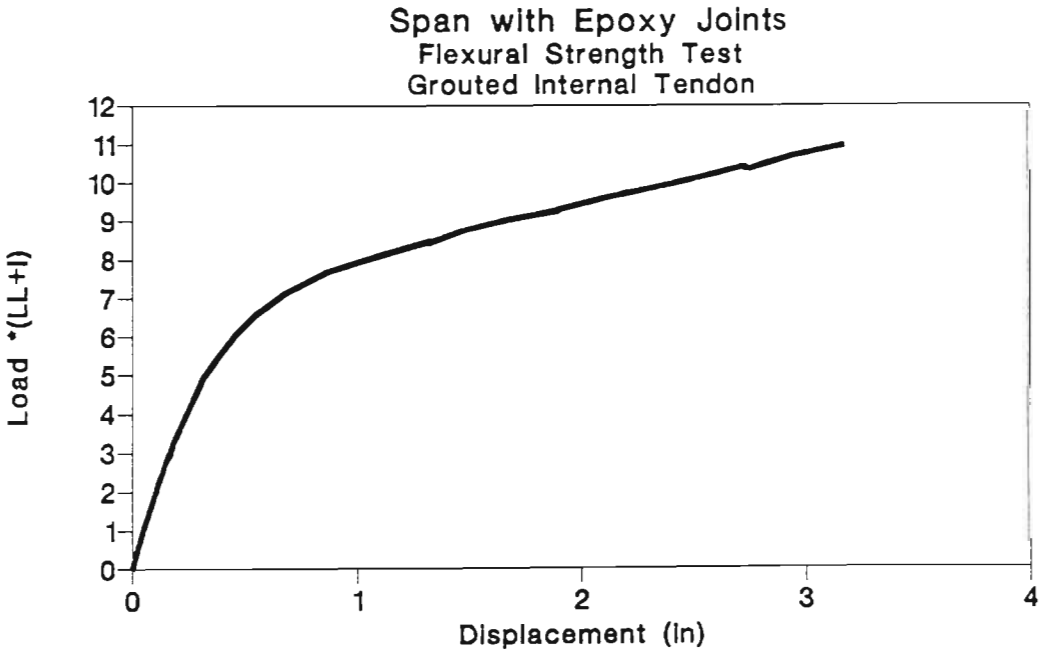

Figure 3.71 Load-deflection of grouted internal tendons test in epoxy joints span.

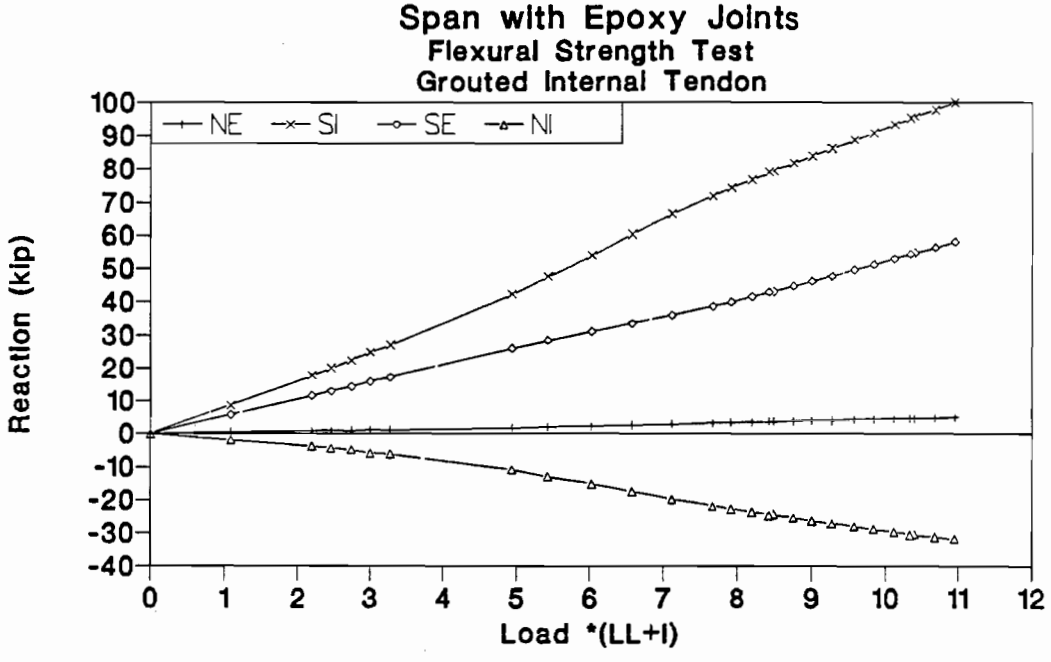

Figure 3.72 Reaction-load of grouted internal tendons test in epoxy joints span.

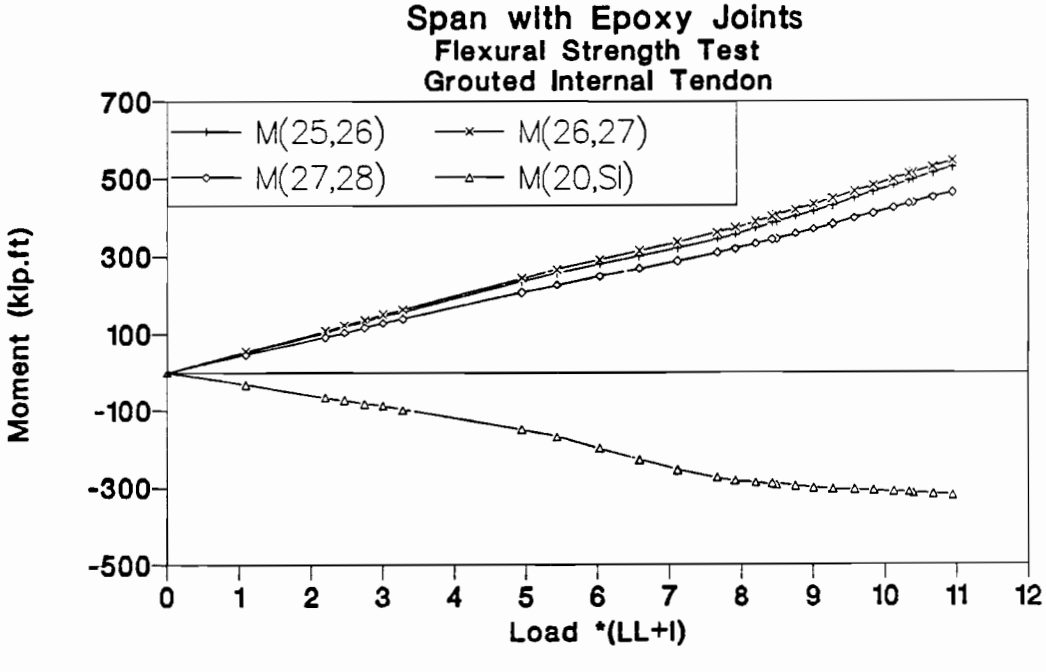

Figure 3.73 Moment-load of grouted internal tendons test in epoxy joints span.

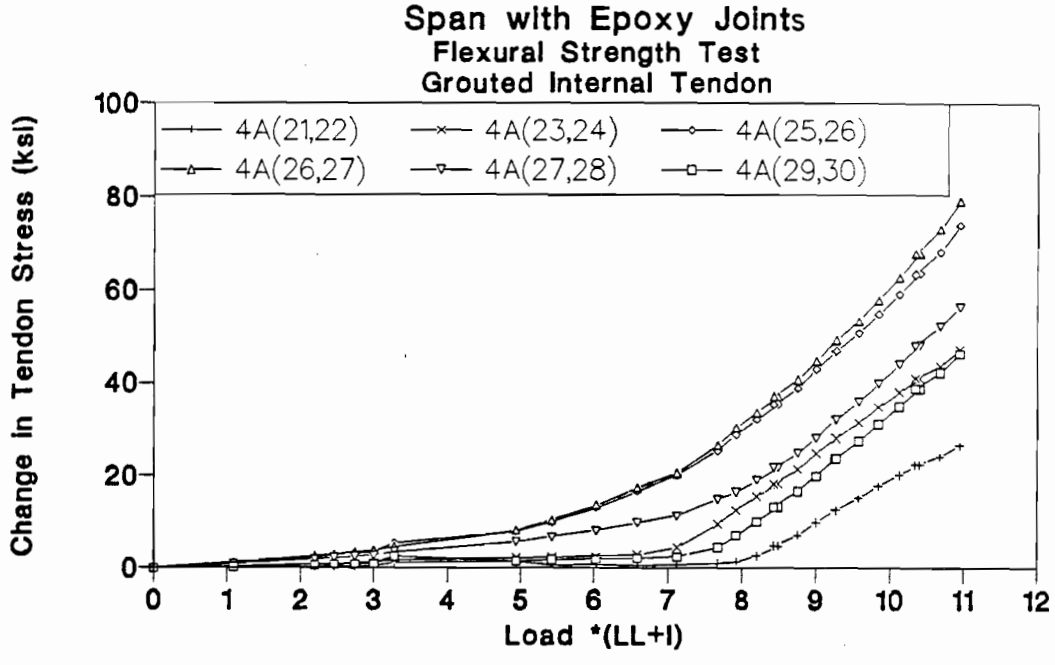

Figure 3.74 Tendon 4A stress-load of grouted internal tendons test in epoxy joints span.

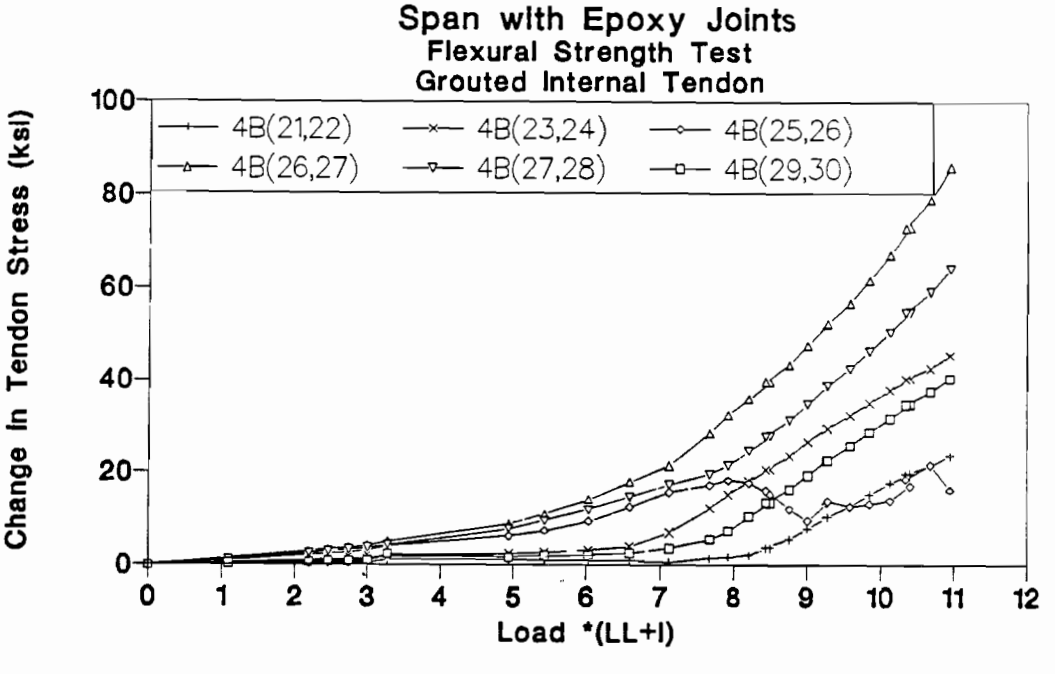

Figure 3.75 Tendon 4B stress-load of grouted internal tendons test in epoxy joints span.

At a load of 6.8(LL+I) tendons 4A and 4B started slipping in segment 24 toward the critical joint, as shown in Fig. 3.74 and Fig. 3.75.

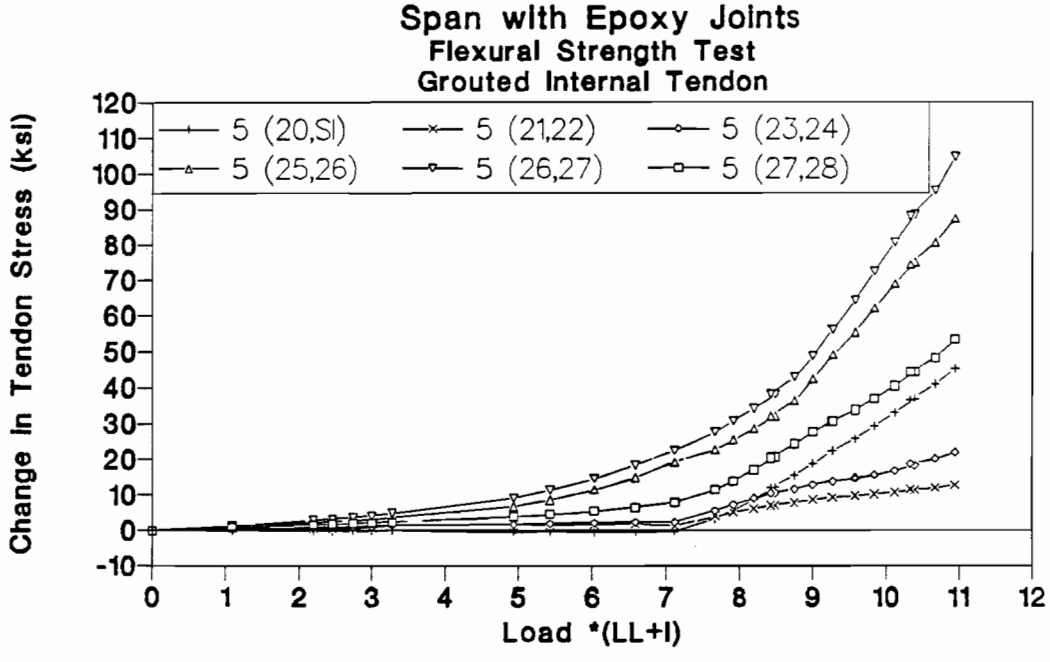

Figure 3.76 Tendon 5 stress-load grouted internal tendons test in epoxy joints span.

At a load of 7(LL+I) joint (20,SI) started opening as shown in Fig. 3.77 causing additional changes in the load distribution.

At a load of 7.6(LL+I) tendons 5 started slipping in segment 22 and 24 toward the critical joint as shown in Fig. 3.76.

At a load of 7.7(LL+I) tendons 4A and 4B started slipping in segment 29 toward the critical joint as shown in Fig. 3.74 and Fig. 3.75.

At a load of 8.0(LL+I) tendons 4A and 4B started slipping in segment 22 toward the critical joint as shown in Fig. 3.74 and Fig. 3.75.

The loading was stopped at a load of 11(LL+I) when the top flange of joint (26,27) crushed as shown in Fig. 3.70.

Figure 3.78 shows the stresses of the internal tendons at two locations along the model. The internal tendons yielded at the critical joint section, while small stress change was measured at the midspan section in unloaded span.

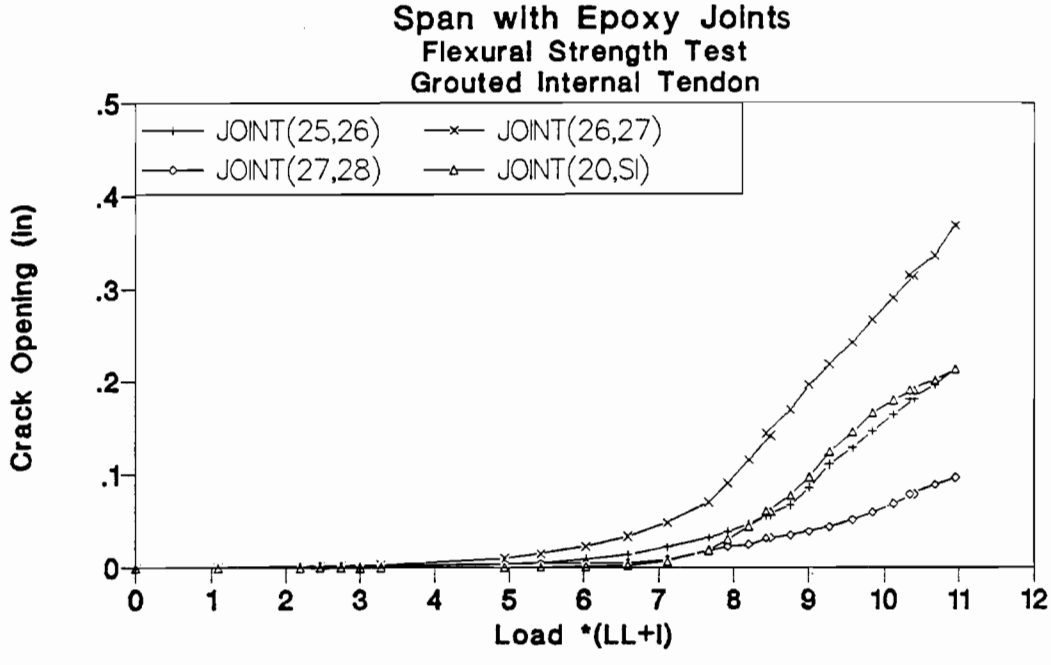

Figure 3.77 Crack opening-load of grouted internal tendons test in epoxy joints span.

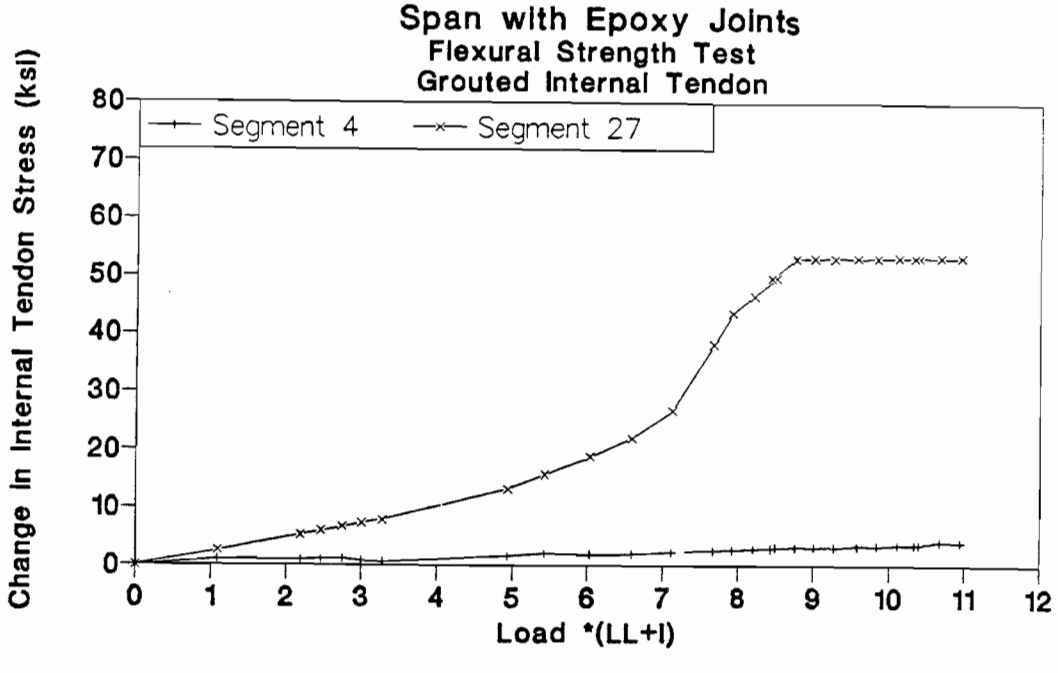

Figure 3.78 Internal tendon stress of grouted internal tendons test in epoxy joints span.

The reaction and moment curves exhibited double curvature as shown in Fig. 3.72 and Fig. 3.73 due to different distributions of internal forces as the critical joint and the support joint opened.

3.4.2 Dry Joints Span. Three phases of tests were carried out on this span as discussed in Section 3.1.

3.4.2.1 Decompression load cycles. Five cycles of loading to 3(LL+I), which was higher than the measured decompression load by 50 percent, were applied to the north span. Three cycles of loading were applied before injecting the cracks and two cycles were applied after injecting the cracks with epoxy. The applied load was increased from zero to 2.0(LL+I) in 0.25(LL+I) increments. Then the load was increased in 0.16(LL+I) for the remainder of the loading cycle. Each of the three cycles indicated the same response of the model to the applied loads. Figures 3.79 through 3.84 show the typical response of the structure.

The measured decompression load was approximately 2.0(LL+I). The decompression load was obtained from a large-scale plot of the applied load-deflection response of the model (Fig. 3.79). Beyond the decompression load, only slight changes in the behavior of the structure were observed. The joint moments and reactions show slight changes at the decompression load as shown in Fig. 3.80 for joint moments and Fig. 3.81 for reactions. The decompression load of dry joints span was 30 percent lower than the decompression load of the epoxy joints span due to different effective prestress as discussed in Chapter two.

Table 3.2 Service Load (Dry Joints Span)

Deflection	0.055 in. (Span/5455)
Change in Tendon Stress	1.4 ksi

The maximum measured deflection of the epoxy joints span at service load 1.0(LL+I) was 0.055 inches which corresponds to a span to deflection ratio of (5455) as shown in Table 3.2. The maximum stress change noted in the external tendons at service load 1(LL+I) was 1.4 ksi while the maximum change in tendon stress at the end of the load tests was 3.5 ksi.

Two cycles of loading were applied after the crack injection process was finished. The response of the structure after crack injection is shown in Fig. 3.85 through 3.90. A maximum load of 3(LL+I) was applied in all first phase tests. The measured decompression load after crack injection was the same as the one measured for the decompression load cycle before the crack injection.

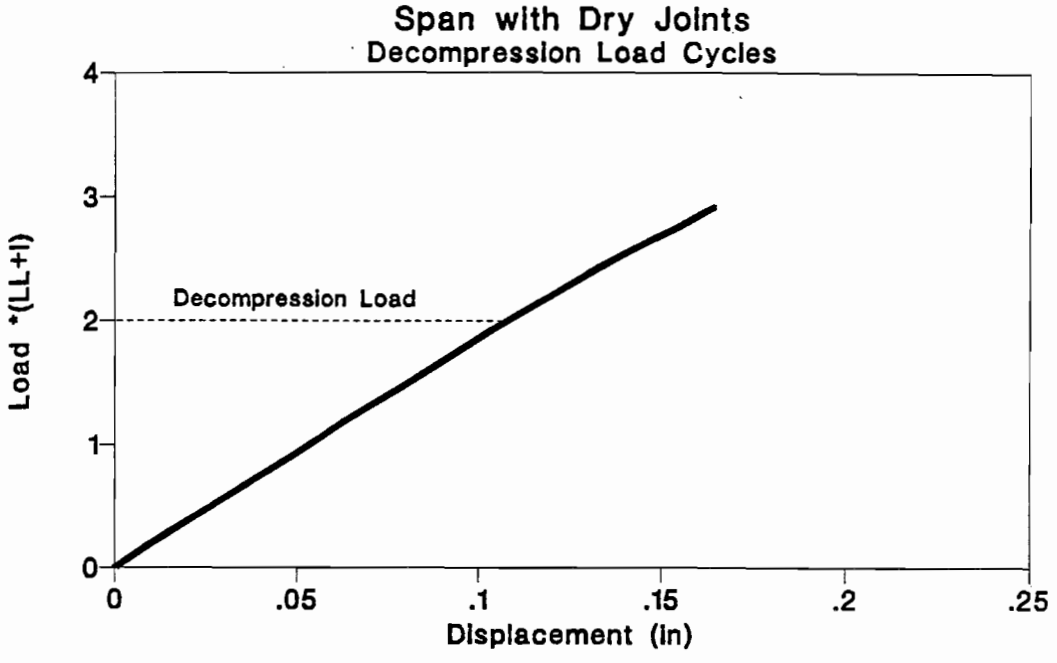

Figure 3.79 Load-deflection of decompression cycle in dry joints span.

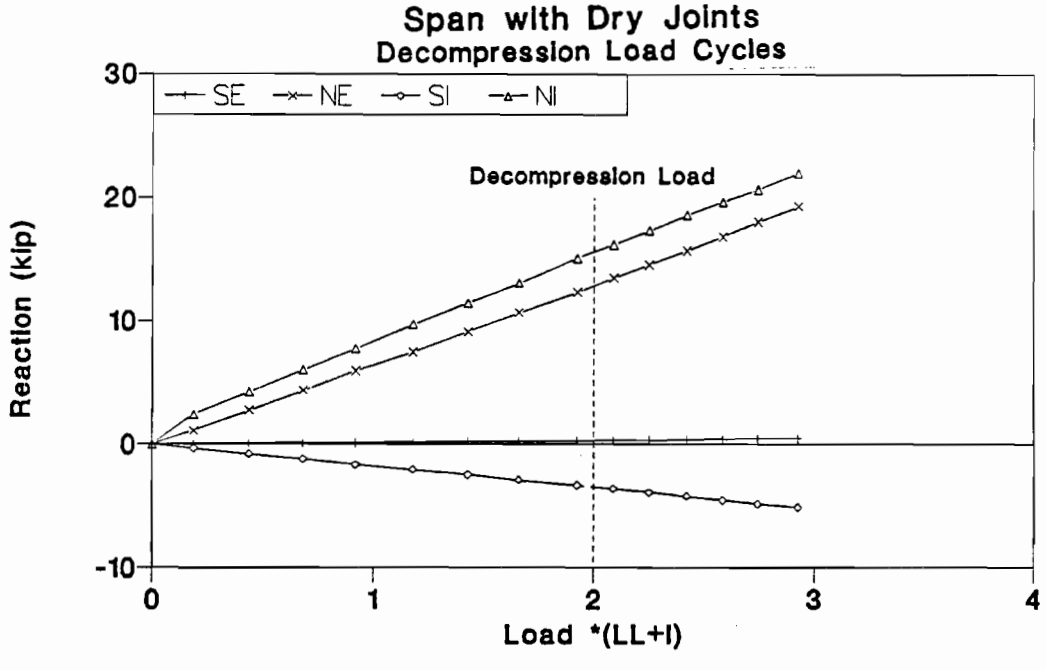

Figure 3.80 Reaction-load of decompression cycle in dry joints span.

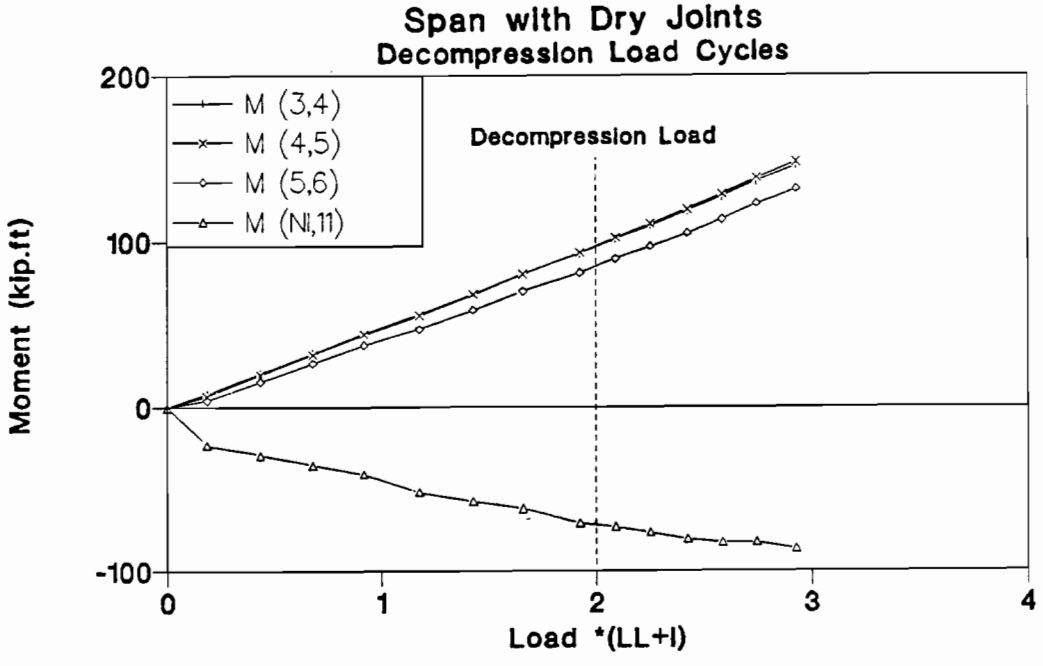

Figure 3.81 Moment-load of decompression cycle in dry joints span.

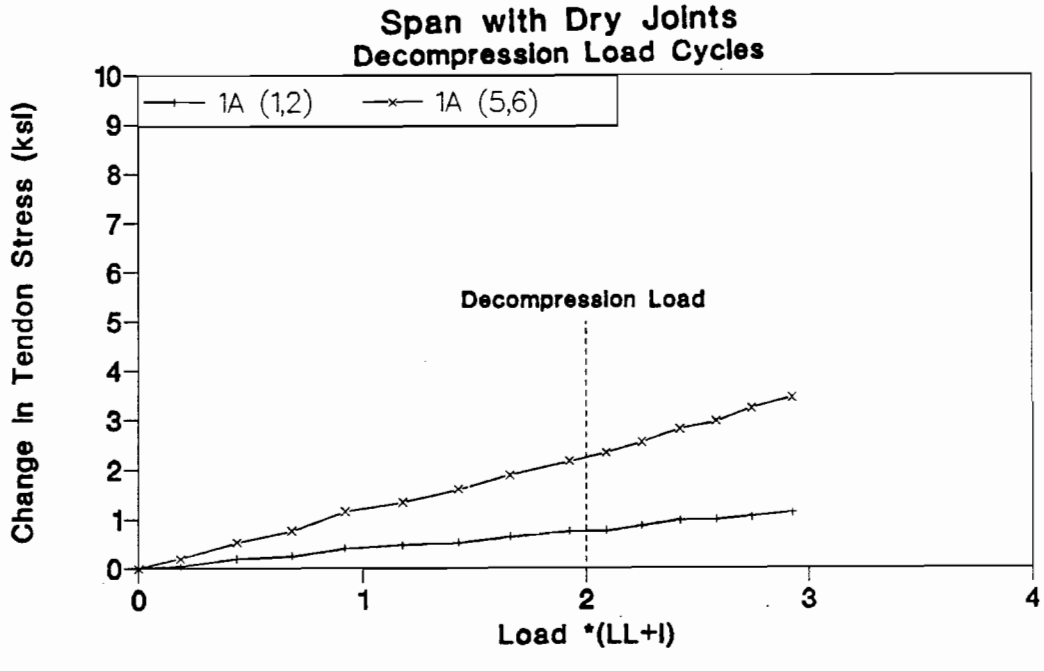

Figure 3.82 Tendon 1A stress-load of decompression cycle in dry joints span.

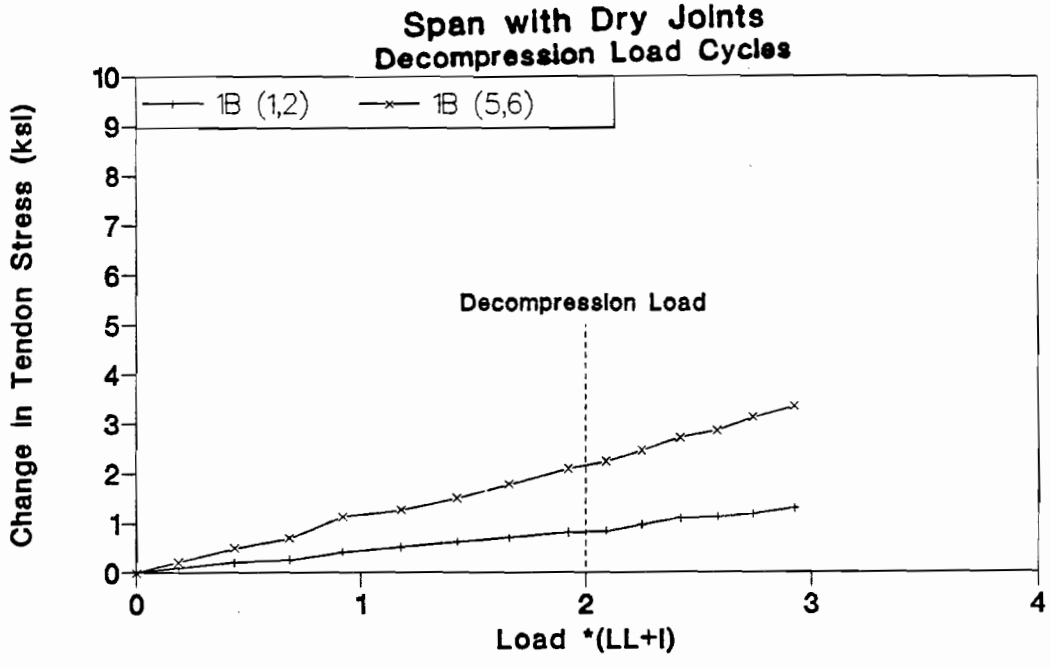

Figure 3.83 Tendon 1B stress-load of decompression cycle in dry joints span.

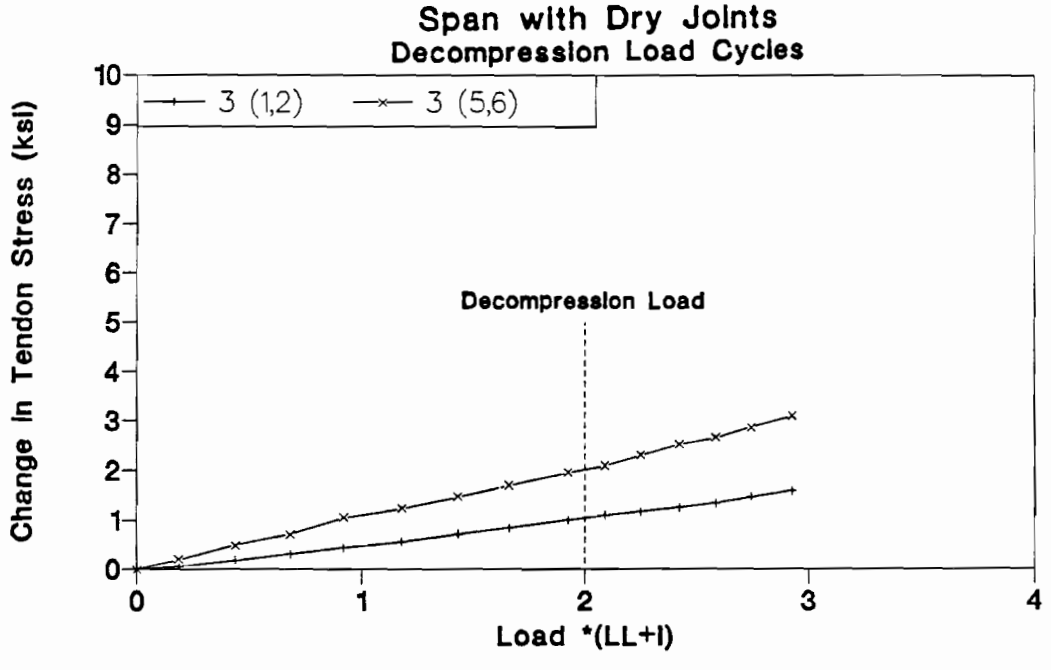

Figure 3.84 Tendon 3 stress-load of decompression cycle in dry joints span.

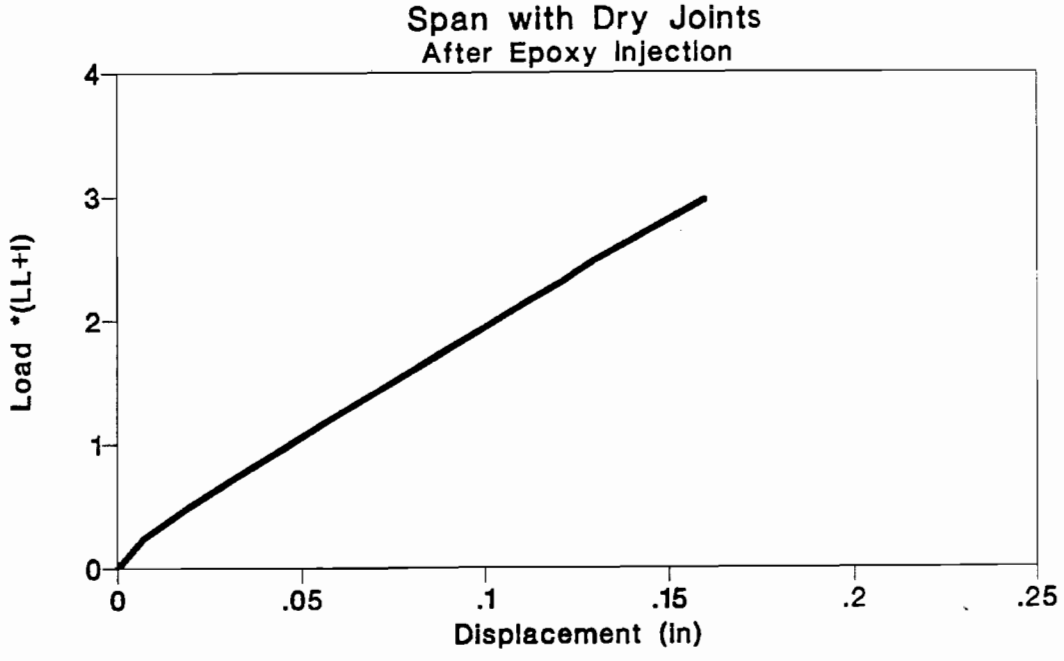

Figure 3.85 Load-deflection of injection cycle in dry joints span.

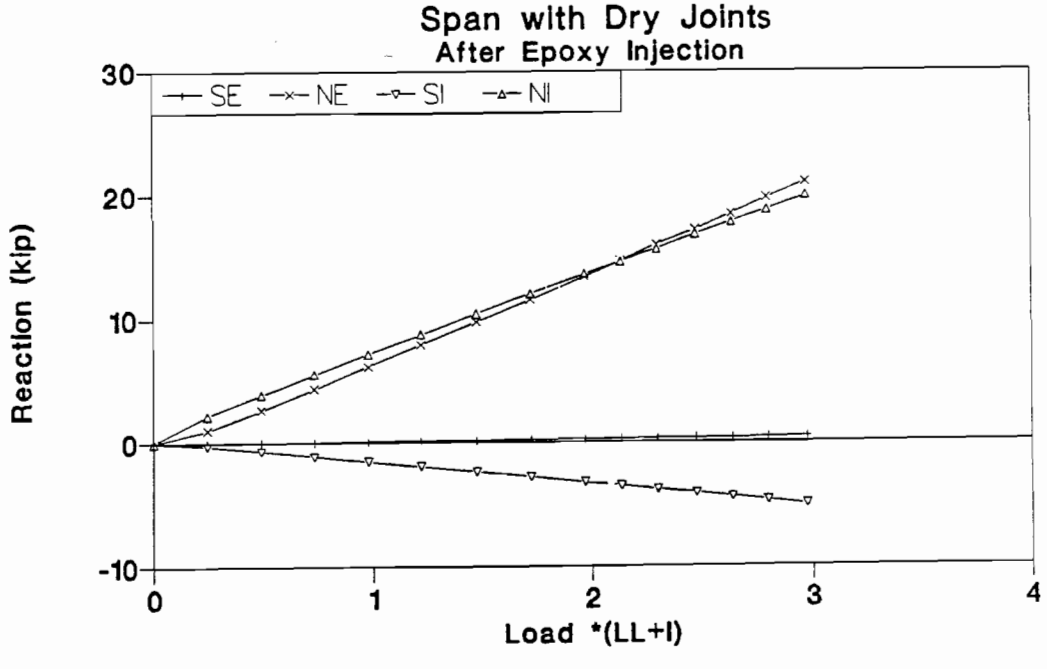

Figure 3.86 Reaction-load of injection cycle in dry joints span.

Figure 3.91 shows the effect of epoxy injection on the load-deflection behavior of the model. The crack injection effects were very small because only web cracks were injected while joints between segments were left dry. The stiffness of the structure below the decompression load was slightly higher because the epoxy injection filled the spaces between the cracks and increased the contact area of the previously cracked sections.

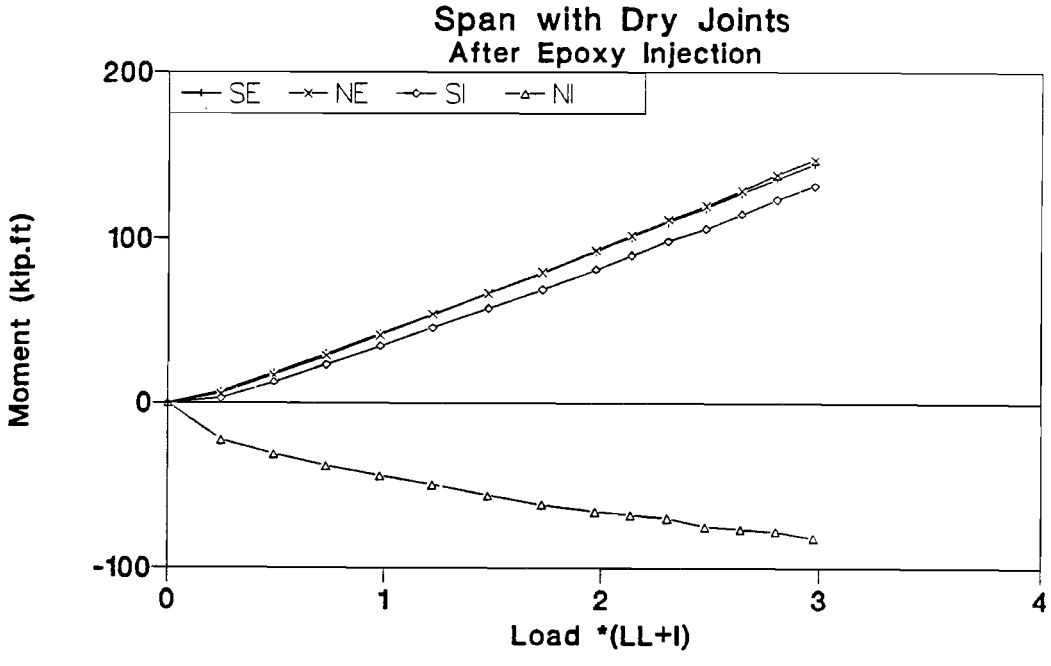

Figure 3.87 Moment-load of injection cycle in dry joints span.

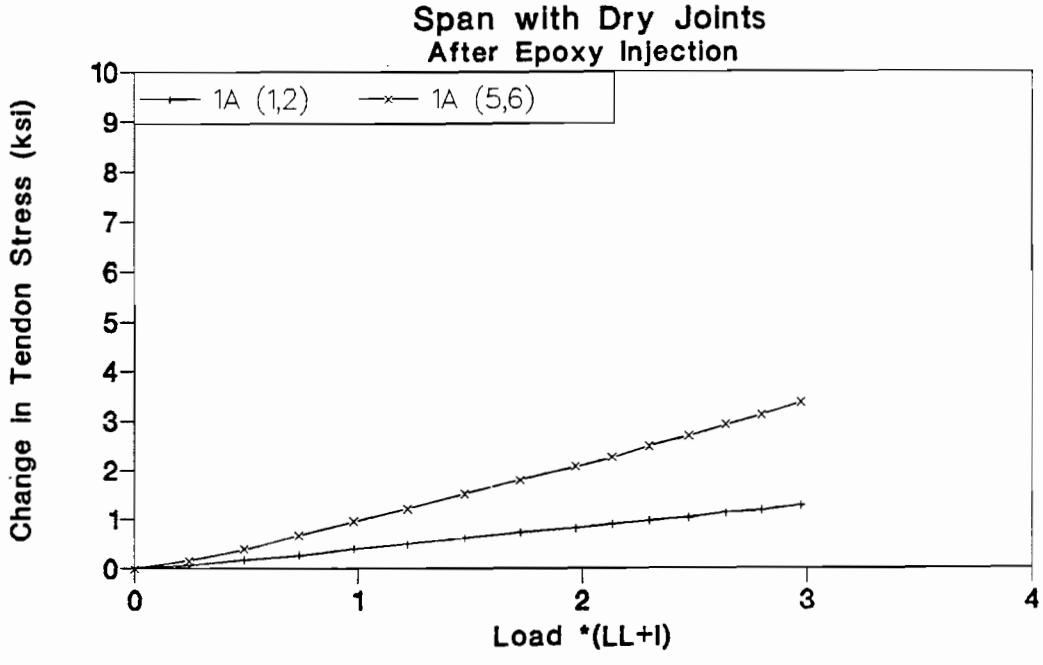

Figure 3.88 Tendon 1A stress-load of injection cycle in dry joints span.

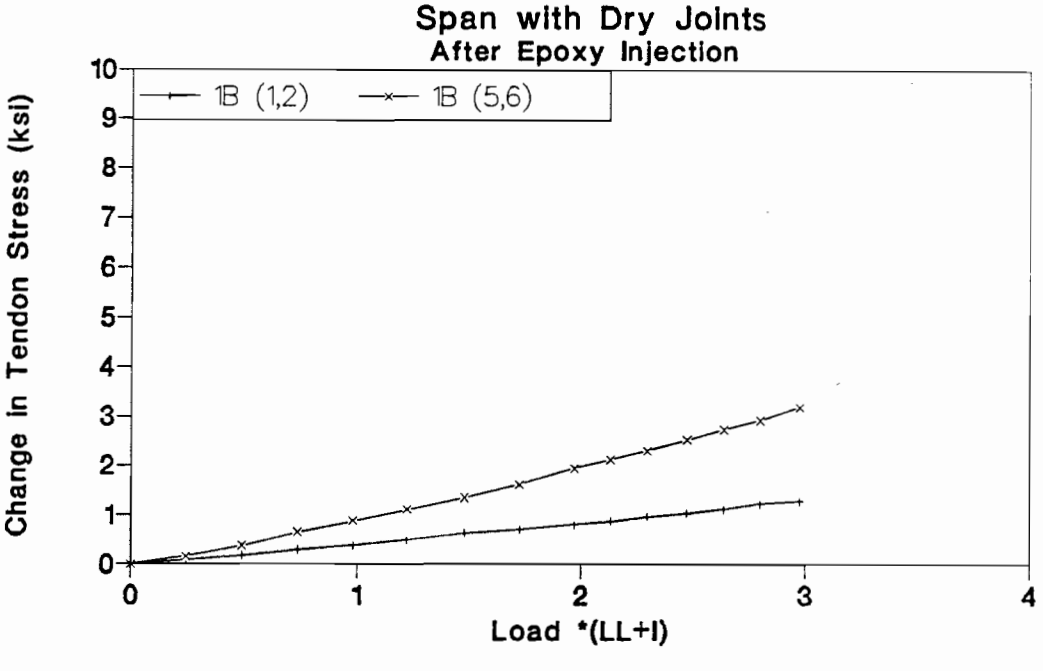

Figure 3.89 Tendon 1B stress-load of inject cycle in dry joints span.

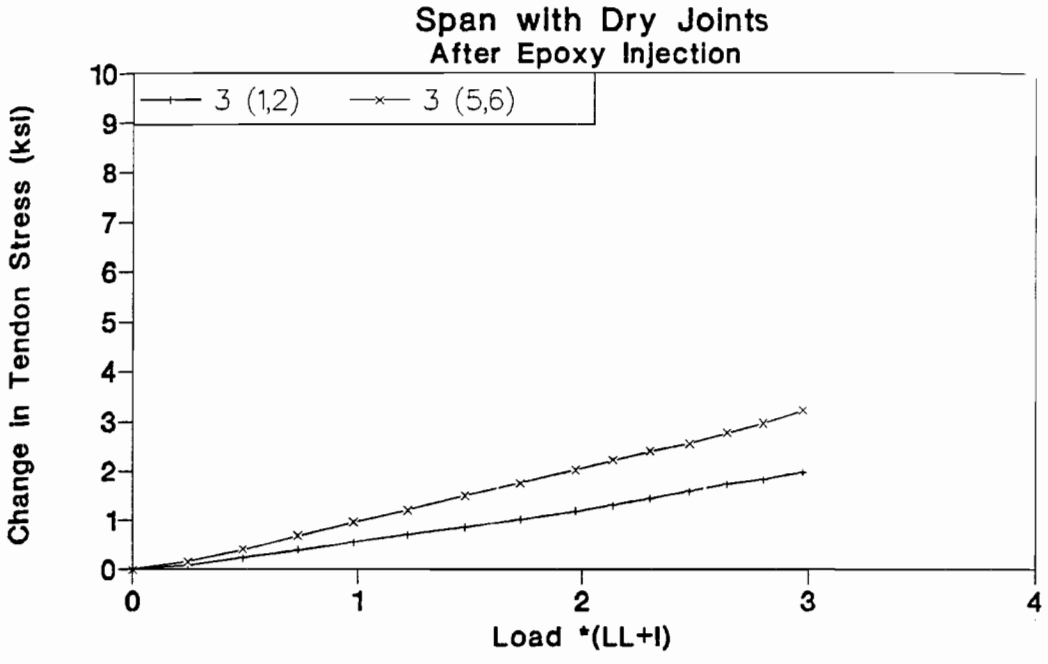

Figure 3.90 Tendon 3 stress-load of injection cycle in dry joints span.

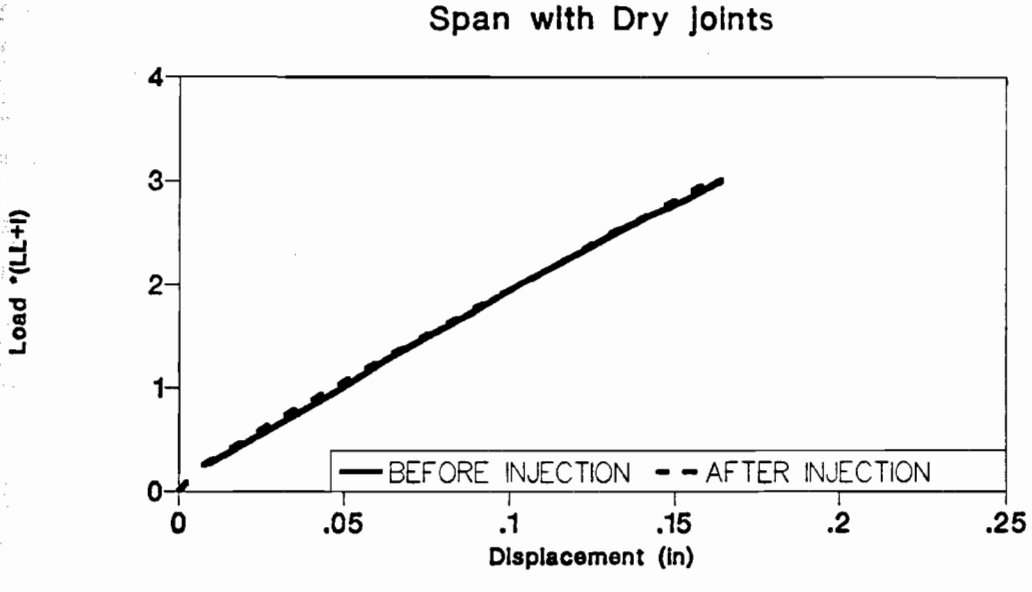

Figure 3.91 Effect of epoxy injection in dry joints span.

3.4.2.2 Bonded External Tendon Load Tests. Six cycles of load, 50 percent higher than the measured joint opening load, were applied to the span in three stages. The load applied was increased from zero to 3(LL+I) in 0.5(LL+I) increments, from 3(LL+I) to a 4(LL+I) in 0.25(LL+I) increments, and from 4(LL+I) to 5.7(LL+I) in 0.16(LL+I) increments. Two cycles of loading were applied during each of the three stages:

Stage One - External tendons bonded to the pier segments and to a maximum of four internal diaphragms along any tendon in each span as shown in Figure 3.25(a).

Stage Two - External tendons bonded to the pier segments and a maximum of seven internal diaphragms along any tendon in each span as shown in Figure 3.25(b).

Stage Three - External tendons bonded to the pier segments and at all ten internal diaphragms as shown in Figure 3.25(c).

As discussed earlier in Section 3.1, Bonding of external tendons to the diaphragms was done in increments so that each loading stage was carried out for different bonding conditions. As discussed in Section 3.2.1, joint (3,4) was the critical joint as determined by plastic analysis, while joint (4,5) had higher elastic moment. The first testing stage was carried out on the model in its original bonding condition. The external tendons were bonded to the pier segments and at diaphragm locations where the tendons were deviated. The external tendons were bonded to a maximum of four internal diaphragms in each span as shown in Fig. 3.25(a) and Table 2.6. In the first loading stage joint (4,5) opening was higher than joint (3,4) opening which made joint (4,5) as the critical joint in these three stages. At the critical joint (4,5), the external tendons had unbonded length of three segment length. The second loading stage was executed after the external tendons were bonded to a maximum of three additional interior diaphragms in each span as shown in Fig. 3.25(b) and Table 2.6. Bonding locations were chosen so that all external tendons had unbonded length of two segment length which was different than stage one tests. The last loading stage was carried out on the model after the external tendons were bonded to all remaining diaphragms as shown in Fig. 3.25(c) and Table 2.6. In this stage, all tendons had unbonded length of one segment length.

Stage One Tests (4 tendons bonded at four internal diaphragms and 2 tendons bonded at two internal diaphragms in this span)

Two loading cycles were applied to the structure during this stage of testing. The bonding condition of the tendons is shown in Fig. 3.25(a). A maximum load of 5.7(LL+I) was applied in each of two loading cycles of the stage one test. The response of the structure is shown in Figures 3.92 through 3.98.

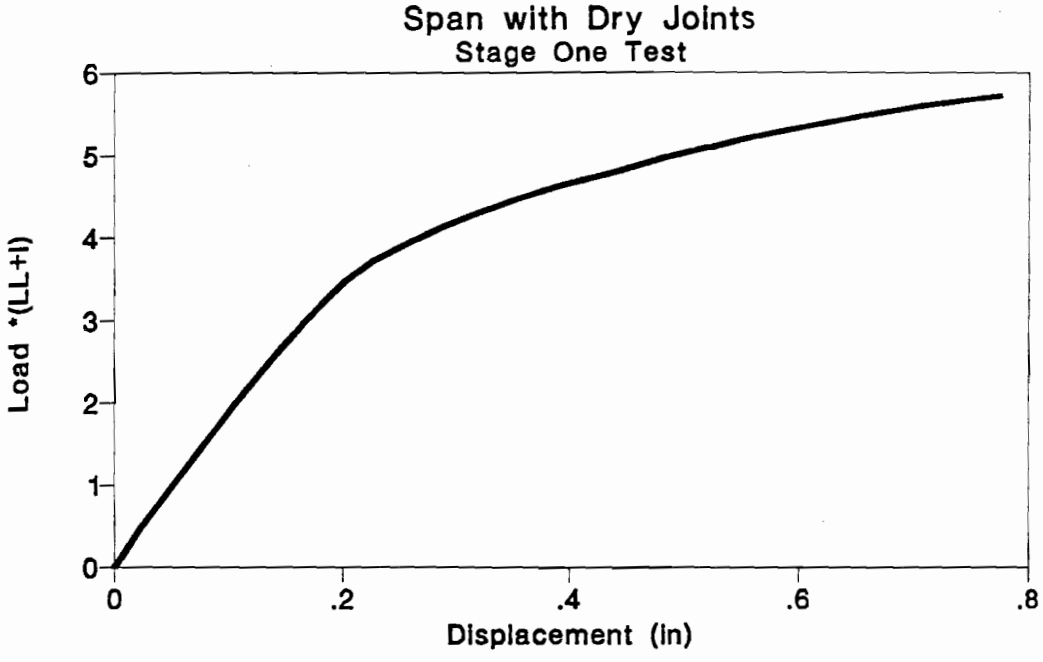

Figure 3.92 Load-deflection of Stage One test in dry joints span.

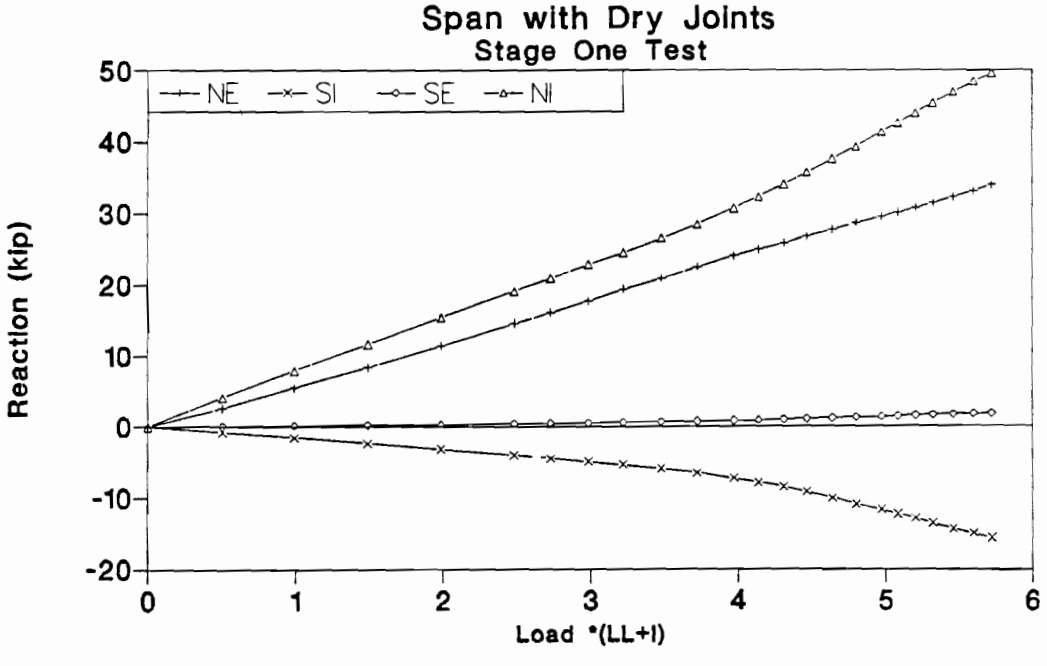

Figure 3.93 Reaction-load of Stage One test in dry joints span.

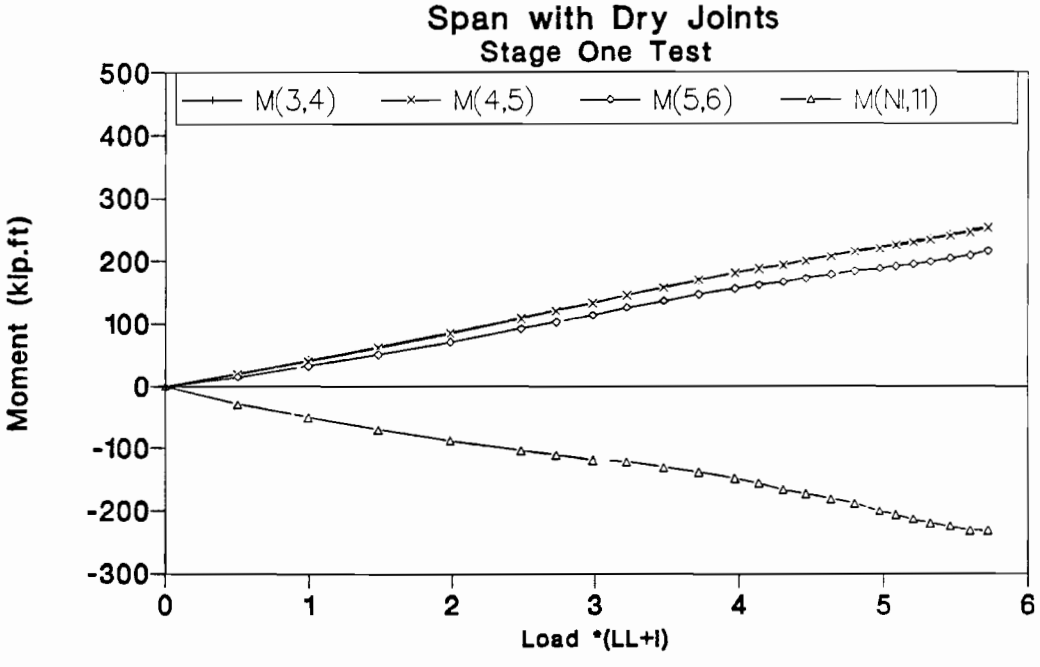

Figure 3.94 Moment-load of Stage One test in dry joints span.

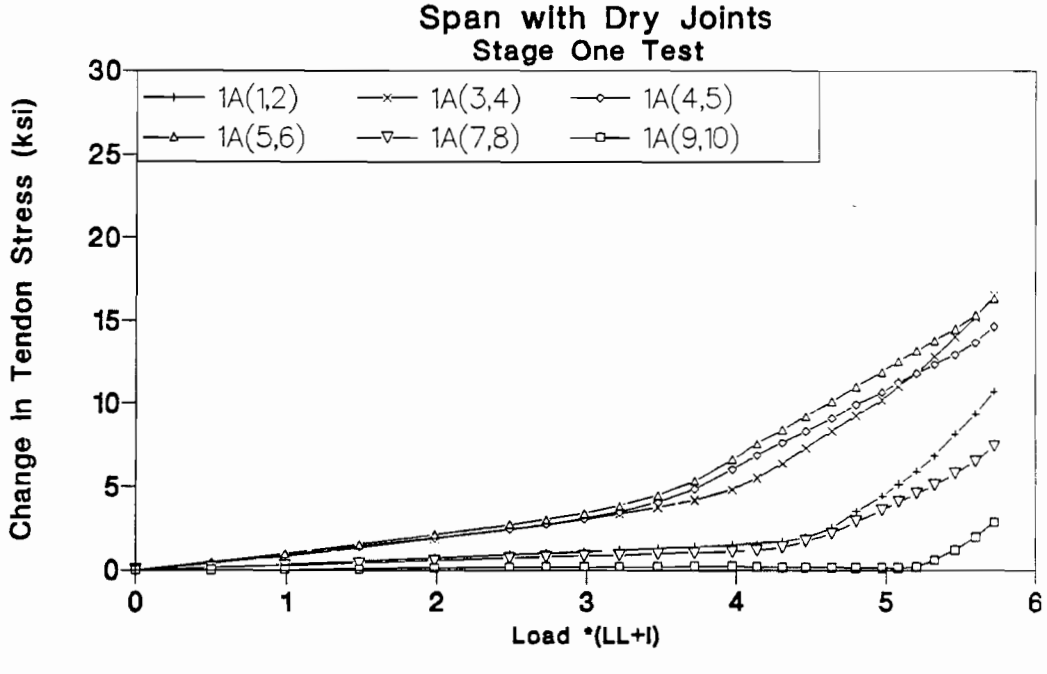

Figure 3.95 Tendon 1A stress-load of Stage One test in dry joints span.

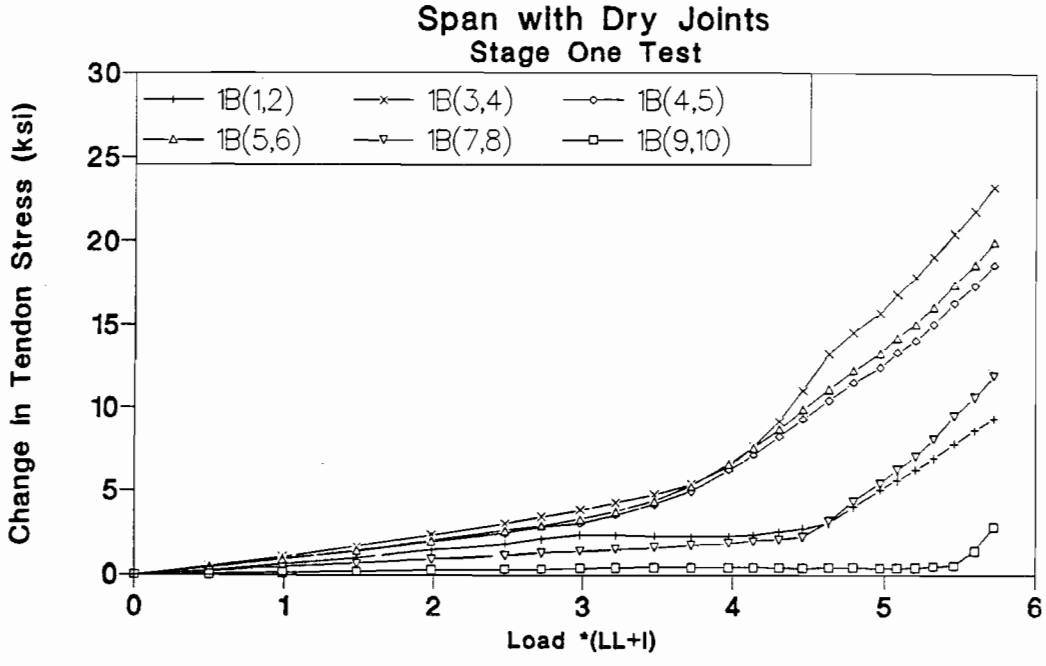

Figure 3.96 Tendon 1B stress-load of Stage One test in dry joints span.

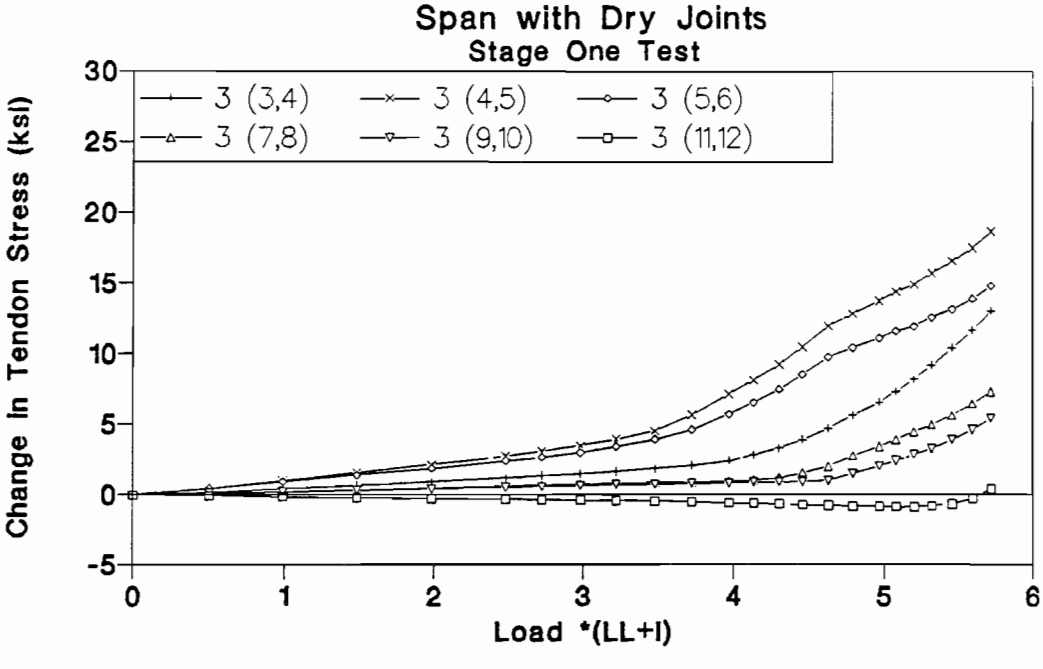

Figure 3.97 Tendon 3 stress-load of Stage One test in dry joints span.

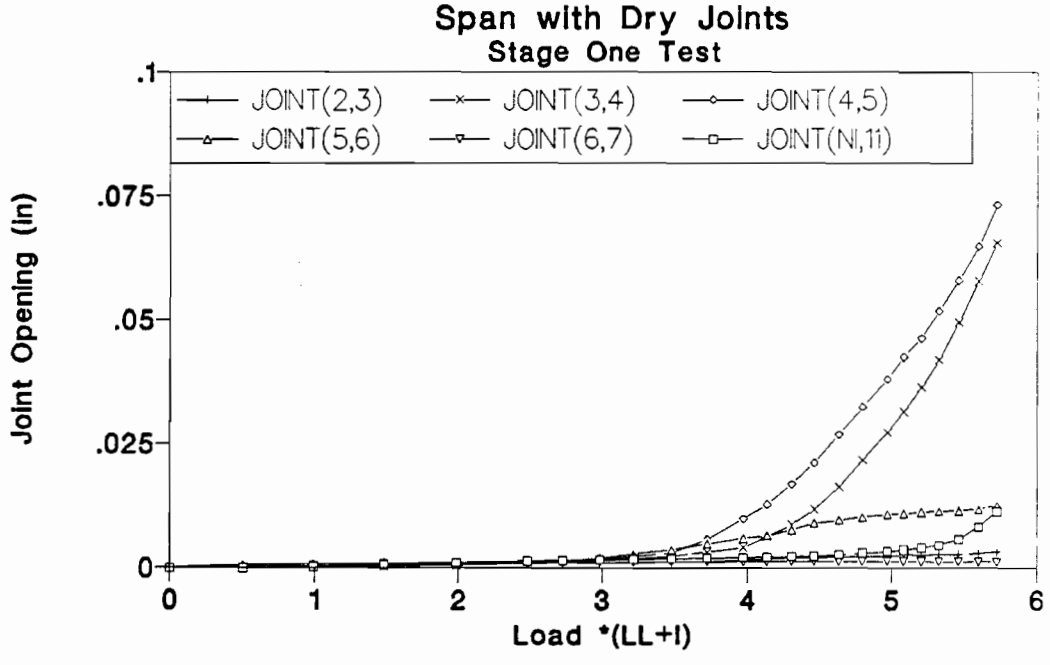

Figure 3.98 Joint opening-load of Stage One test in dry joints span.

The applied load-deflection response of the model is shown in Fig. 3.92. The measured reactions and calculated joint moments are shown in Fig. 3.93 and Fig. 3.94. Figures 3.95 to 3.97 show the changes in external tendon stress while Fig. 3.98 shows the joint openings for the model.

At a load of 3.5(LL+I) joints (4,5) and (5,6) started opening as shown in Fig. 3.98. The changes in external tendon stress in the mid-span region increased at a higher rate after joint opening initiated as shown in Figures 3.95 through 3.97. At this load level, internal forces redistributed toward the internal support due to reduction in the positive section stiffness as shown in Fig. 3.93 for reactions and Fig. 3.94 for joint moments.

At a load of 3.75(LL+I) joint (3,4) started opening as shown in Fig. 3.98. Joint opening led to rapid increases in the external tendon stress and additional changes in the internal force distribution.

At a load of 4.3(LL+I) the tendons 1A and 1B started slipping at segments 2 and 7 as shown in Fig. 3.95 and Fig. 3.96, while tendons 3 slipped at segments 7 and 9 as indicated in Fig. 3.97. The maximum change in tendons 1B stress at the end of the test at 5.7(LL+I) was 23 ksi. At all loads, joint (4,5) had higher joint opening than joint (3,4).

Stage Two Tests (2 tendons bonded at 7 internal diaphragms and 4 tendons bonded at 5 internal diaphragms)

Two cycles of loading with a maximum load of 5.7(LL+I) were applied to the structure. The external tendons were bonded to a maximum of seven diaphragms in each span as shown in Fig. 3.25(b) and Table 2.6. Figures 3.99 through 3.105 show the response of the structure to the loads.

Figure 3.99 shows the applied load-deflection response of the structure while the measured reaction and the calculated moments are shown in Fig. 3.100 and Fig. 3.101. The changes in external tendon stress are shown in Figures 3.102 through 3.104. Joint opening response is shown in Fig. 3.105.

At a load of 3.5(LL+I), the same load as for the stage one test, joints (4,5) and (5,6) started opening as shown in Fig. 3.105. The joint opening reduced the flexural stiffness of the mid-span region which led to redistribution of the internal forces to the internal support as shown in Fig. 3.100 for reactions and Fig. 3.101 for joint moments.

At a load of 3.75(LL+I) joint (3,4) started opening as shown in Fig. 3.105. Joint opening led to rapid increases in external tendon stresses and additional changes in internal forces distribution.

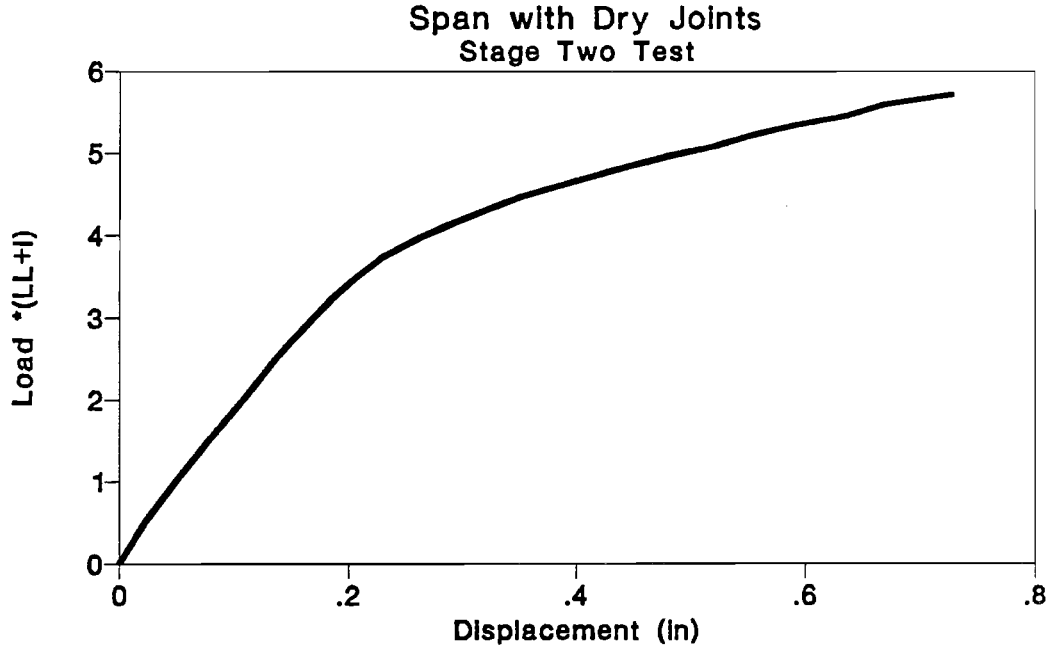

Figure 3.99 Load-deflection of Stage Two test in dry joints span.

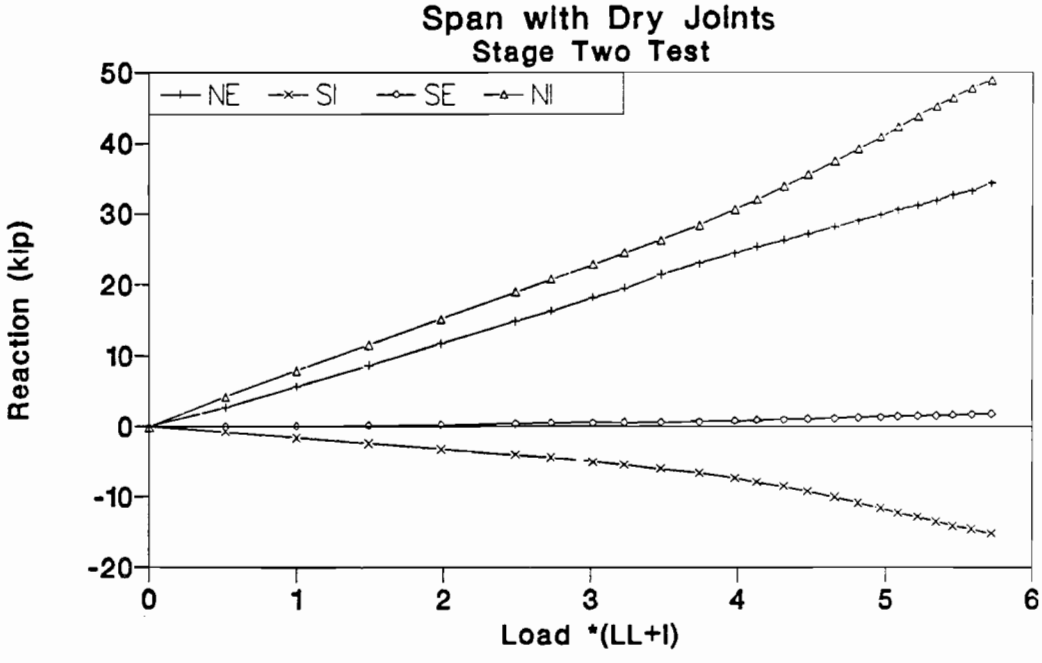

Figure 3.100 Reaction-load of Stage Two test in dry joints span.

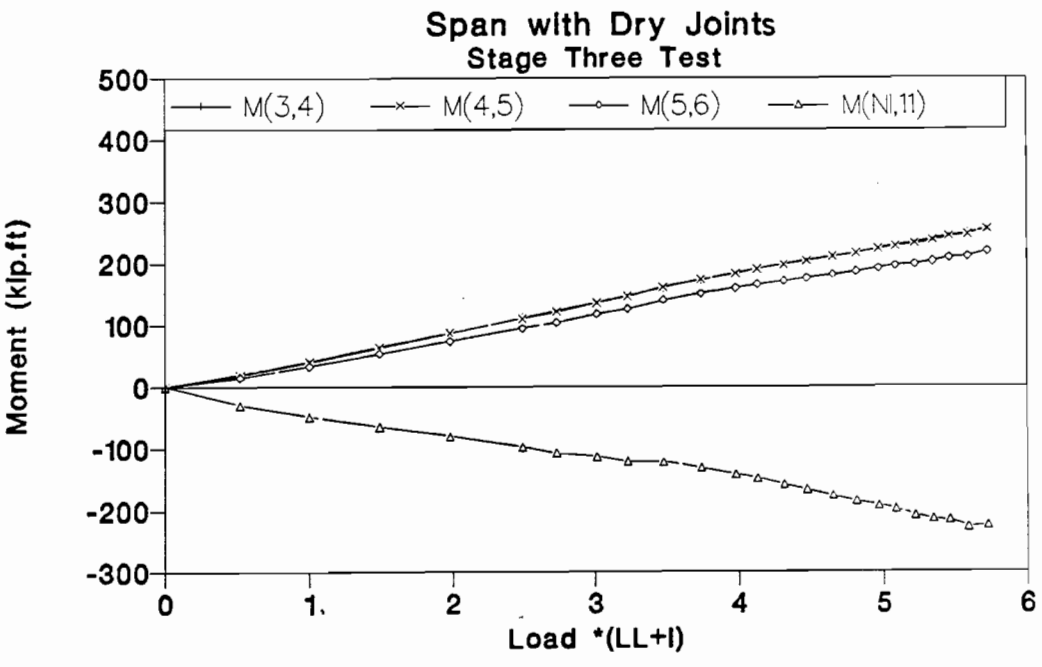

Figure 3.101 Moment-load of Stage Two test in dry joints span.

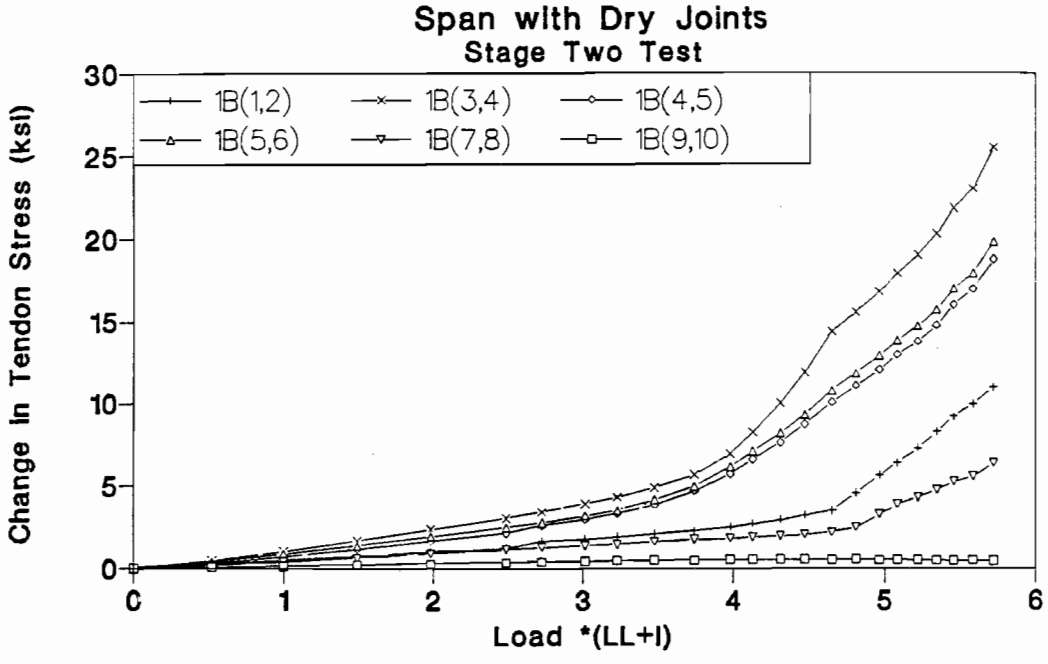

Figure 3.102 Tendon 1A stress-load of Stage Two test in dry joints span.

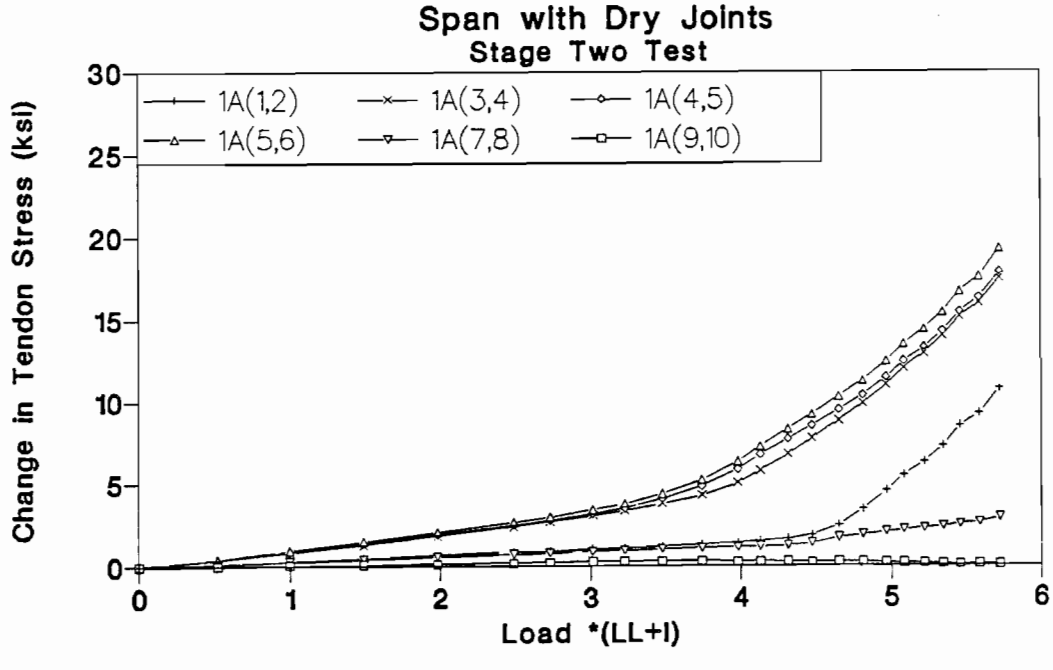

Figure 3.103 Tendon 1B stress-load of Stage Two test in dry joints span.

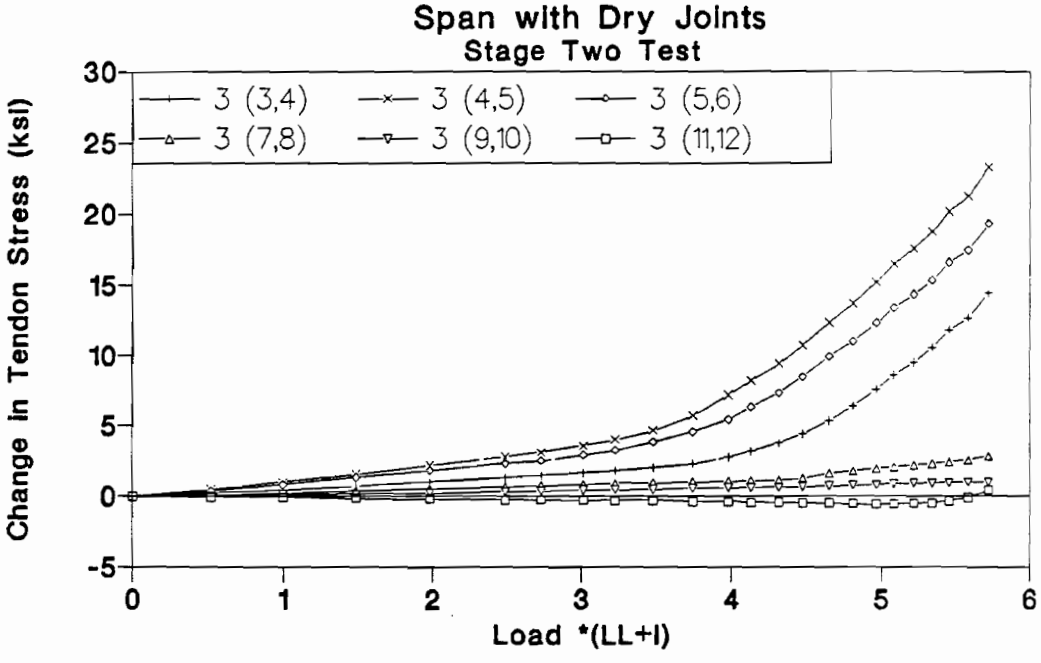

Figure 3.104 Tendon 3 stress-load of Stage Two in dry joints span.

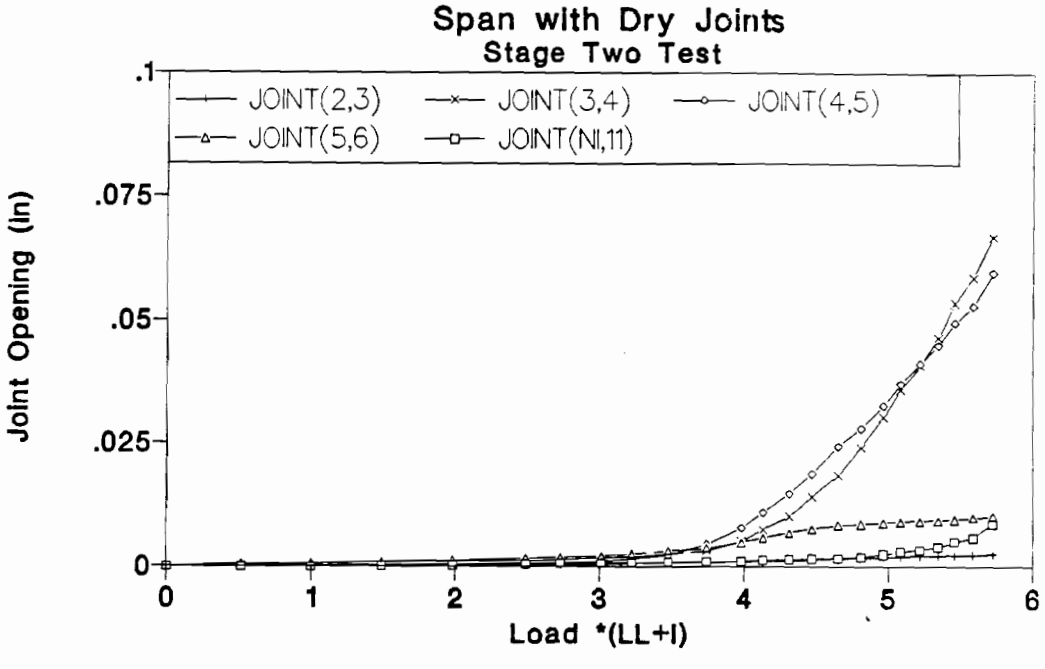

Figure 3.105 Joint opening-load of Stage Two in dry joints span.

At a load of 4.6(LL+I), external tendons 1A and 1B started slipping at segments 2 and 7 as shown in Fig. 3.102 and Fig. 3.103. The maximum change in tendons 1B stress at the end of the test at 5.7(LL+I) was 26 ksi. By bonding the external tendons to three additional diaphragms, tendon slip was reduced and delayed to a higher load.

Stage Three Tests (All tendons bonded to all 10 internal diaphragms)

The bonding of the external tendons to all diaphragms is illustrated by the schematic in Fig. 3.25(c). The response of the structure to one of the two cycles of loading is shown in Figures 3.106 through 3.112.

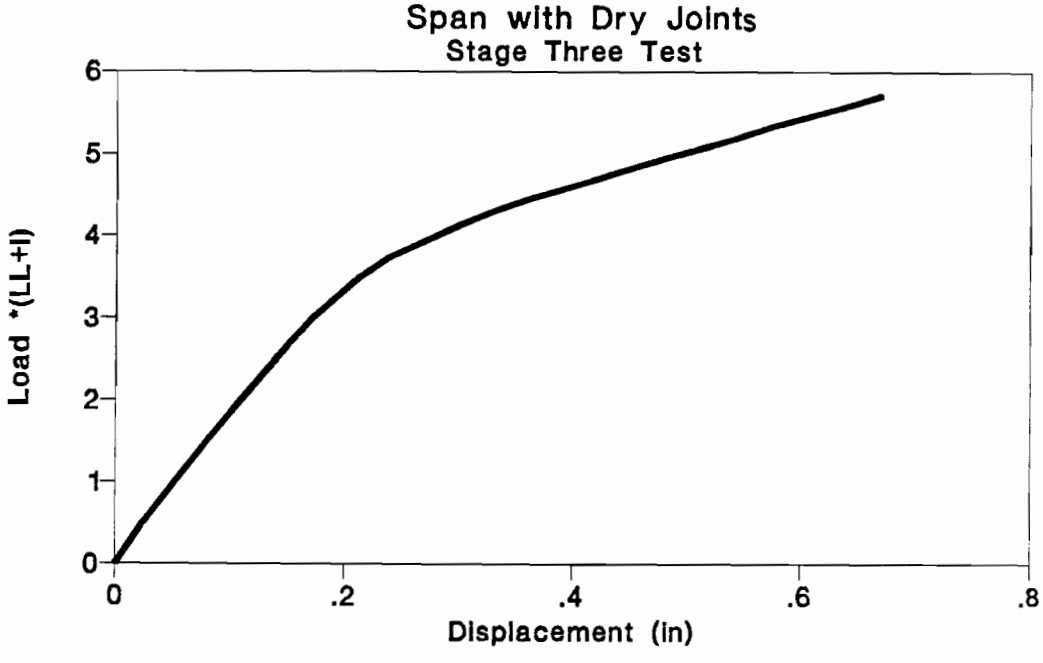

Figure 3.106 Load-deflection of Stage Three test in dry joints span.

Figure 3.106 shows the applied load-deflection response of the structure while the measured reactions and the calculated moments are shown in Fig. 3.107 and Fig. 3.108. Changes in external tendon stresses are shown in Figures 3.109 through 3.111. Joint opening response is shown in Fig. 3.106.

At a load of 3.5(LL+I), the same load as for the stage-one tests, joints (4,5) and (5,6) started opening as shown in Fig. 3.112.

At a load of 3.75(LL+I) joint (3,4) started opening as shown in Fig. 3.112. Joint opening led to rapid increases in external tendon stresses and additional changes in internal forces distribution.

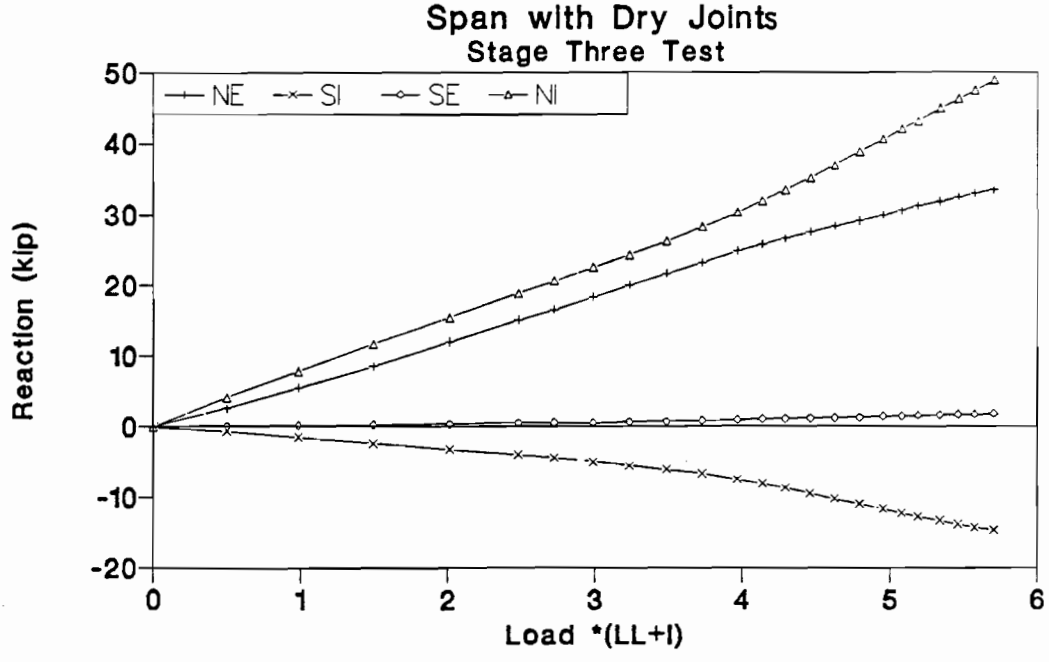

Figure 3.107 Reaction-load of Stage Three test in dry joints span.

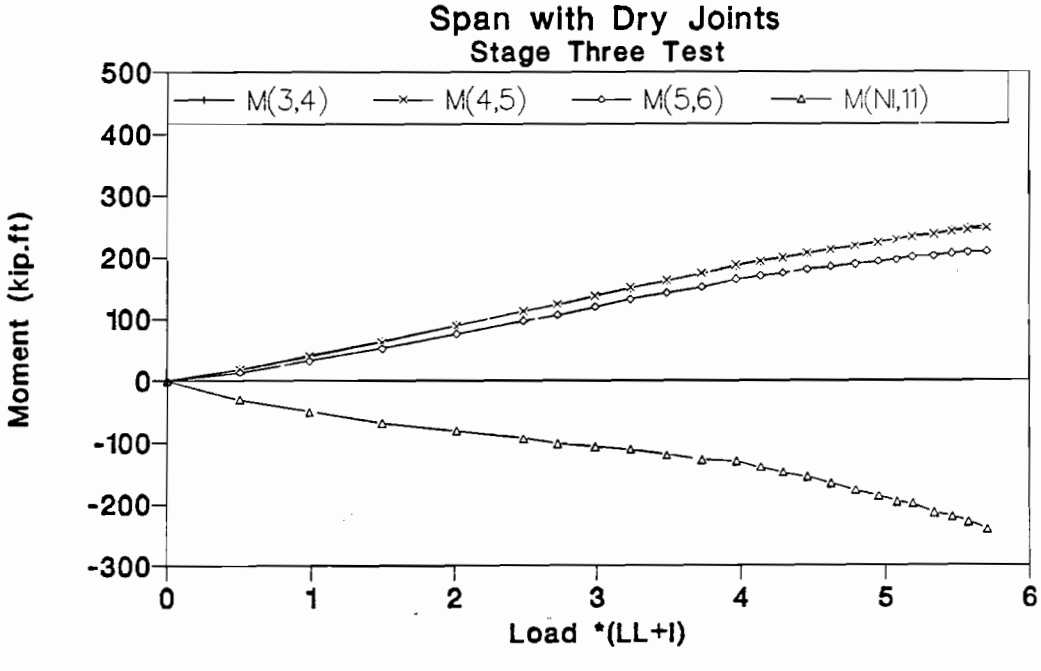

Figure 3.108 Moment-load of Stage Three in dry joints span.

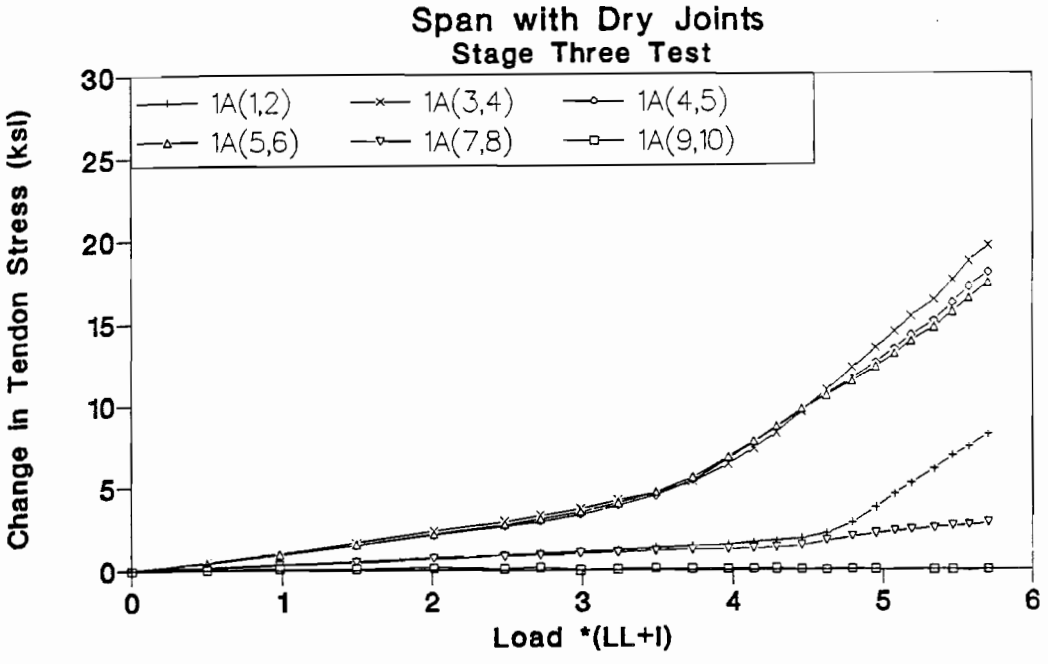

Figure 3.109 Tendon 1A stress load of Stage Three test in dry joints span.

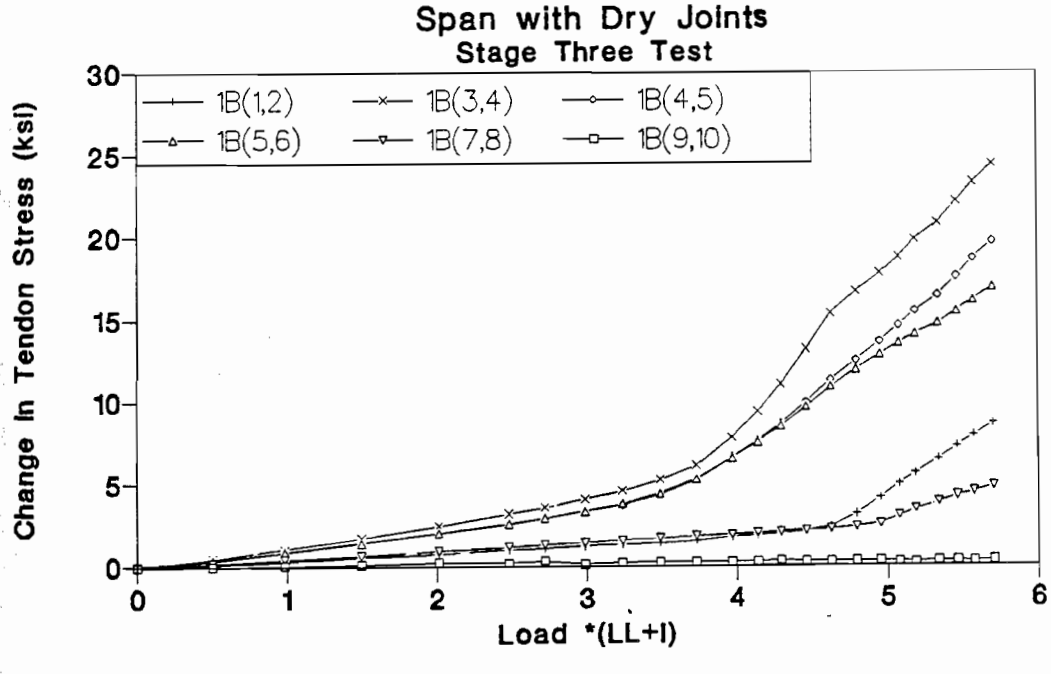

Figure 3.110 Tendon 1B stress-load of Stage Three in dry joints span.

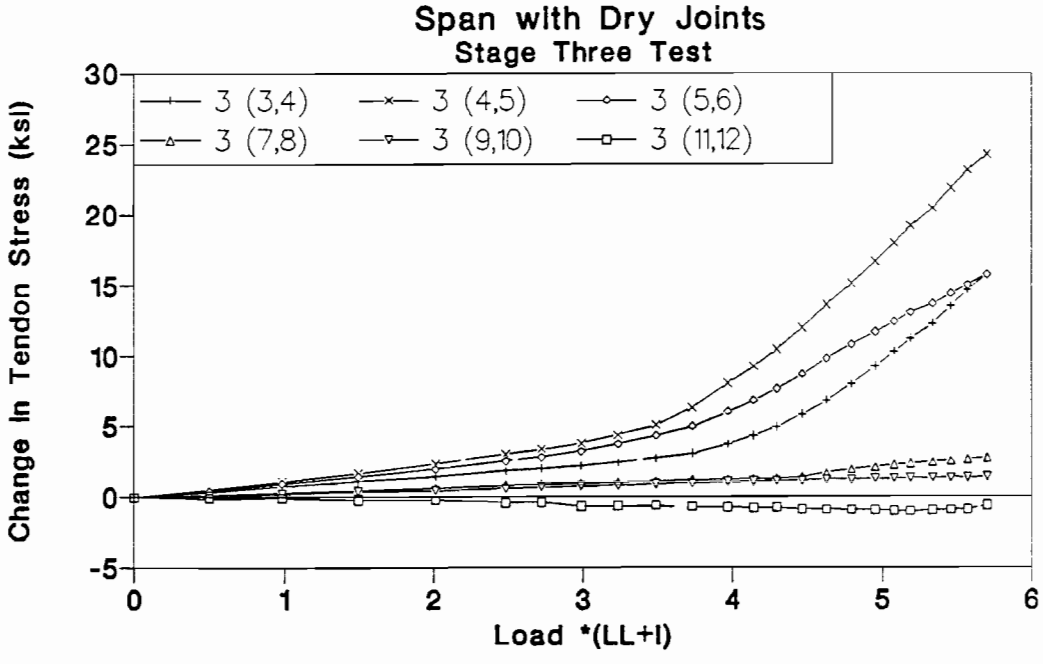

Figure 3.111 Tendon 3 stress-load of Stage Three test in dry joints span.

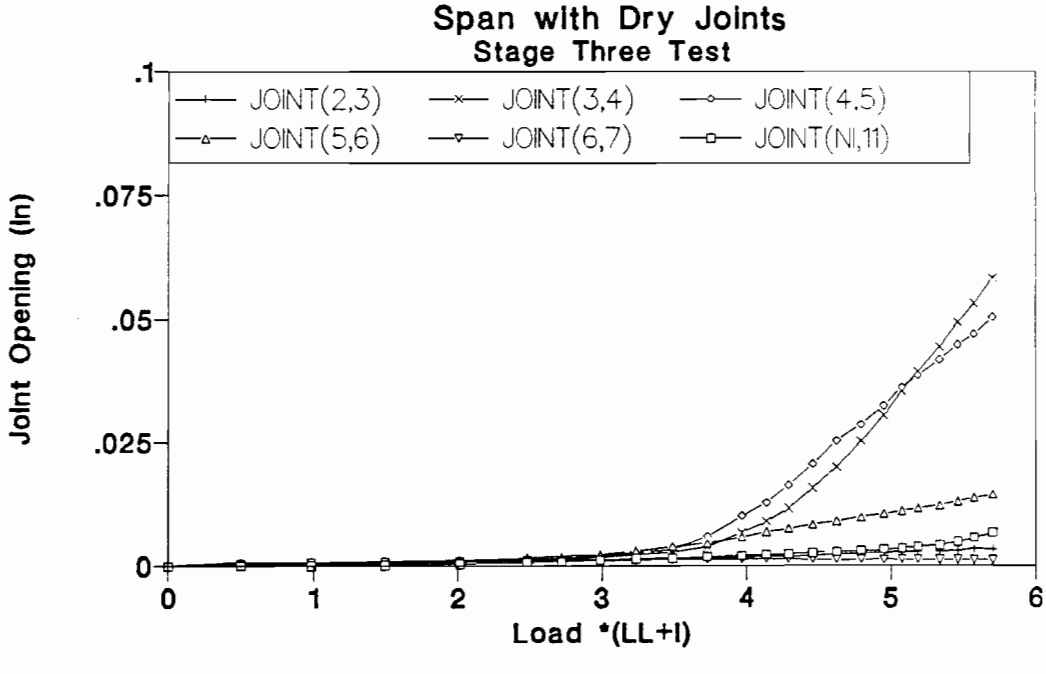

Figure 3.112 Joint opening-load of Stage Three test in dry joints span.

At a load of 4.7(LL+I), external tendons 1A and 1B started slipping at segments 2 and 7 as shown in Fig. 3.109 and Fig. 3.110, while tendon 3 slipped at segment 7 as indicated in Fig. 3.111.

The maximum load during the three stages of testing was 5.7(LL+I), which was 25 percent higher than the load at which external tendons started slipping. This load was not high enough to show dramatic changes in the response of the structure. Although the critical joint started opening at the same load in all three testing stages, tendon slip was reduced and delayed by supplementary bonding of external tendons which resulted in higher maximum change in external tendon stress.

Flexural Strength Test (All tendons bonded at 10 diaphragms)

The dry joints span was loaded until the flexural strength was assumed to be reached when the positive moment compression flange started crushing. The load was increased from zero to 8.0(LL+I) in increments which varied from 1(LL+I) to 0.1(LL+I). The flexural strength test was applied in one cycle. The Measured strength was 1DL+8.0(LL+I) with a maximum deflection of 2.4 inches (equivalent to L/125).

The load-deflection response of the model is shown in Fig. 3.113. The measured reactions are plotted in Fig. 3.114 while the calculated joint moments are plotted in Fig. 3.115. Changes in external tendon stress are shown in Figures 3.116 through 3.118. Measured joint openings are plotted in Fig. 3.119.

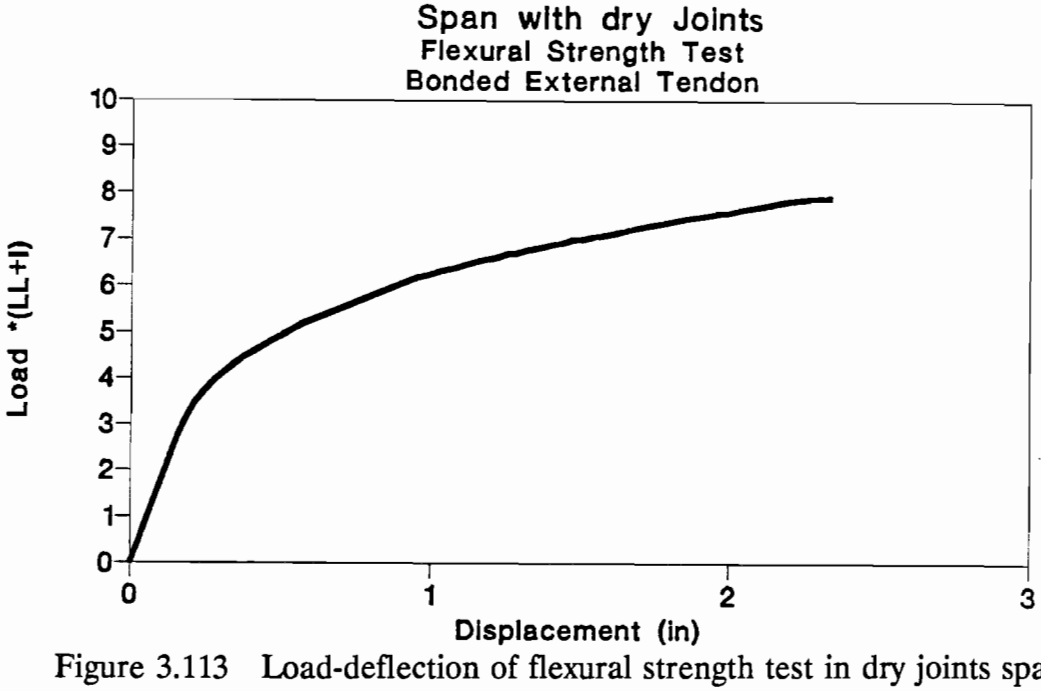

Figure 3.113 Load-deflection of flexural strength test in dry joints span.

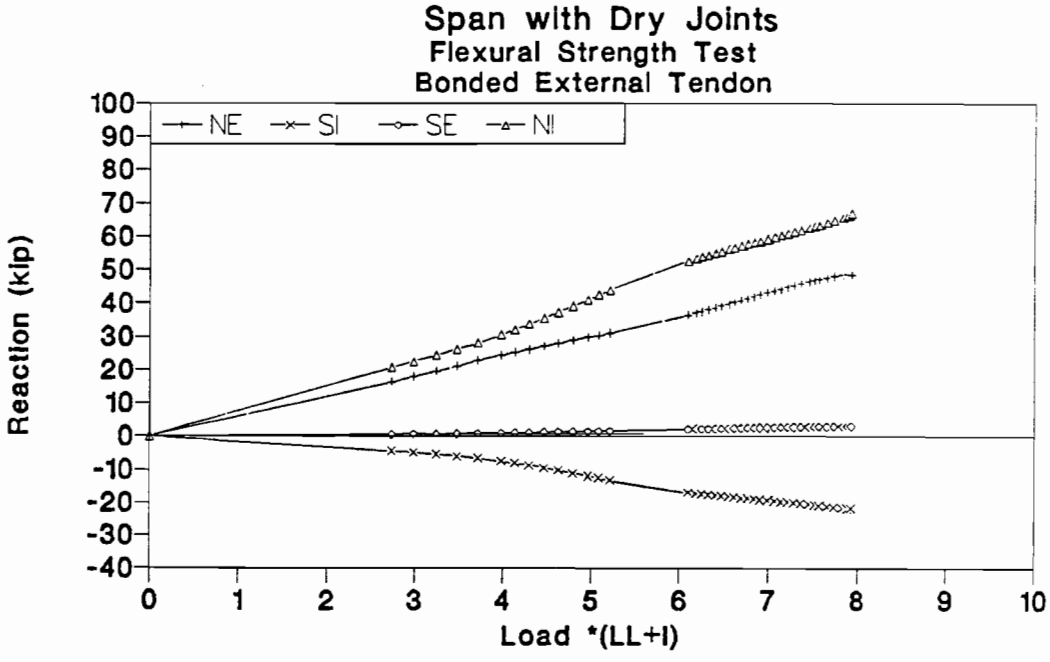

Figure 3.114 Reaction-load of flexural strength test in dry joints span.

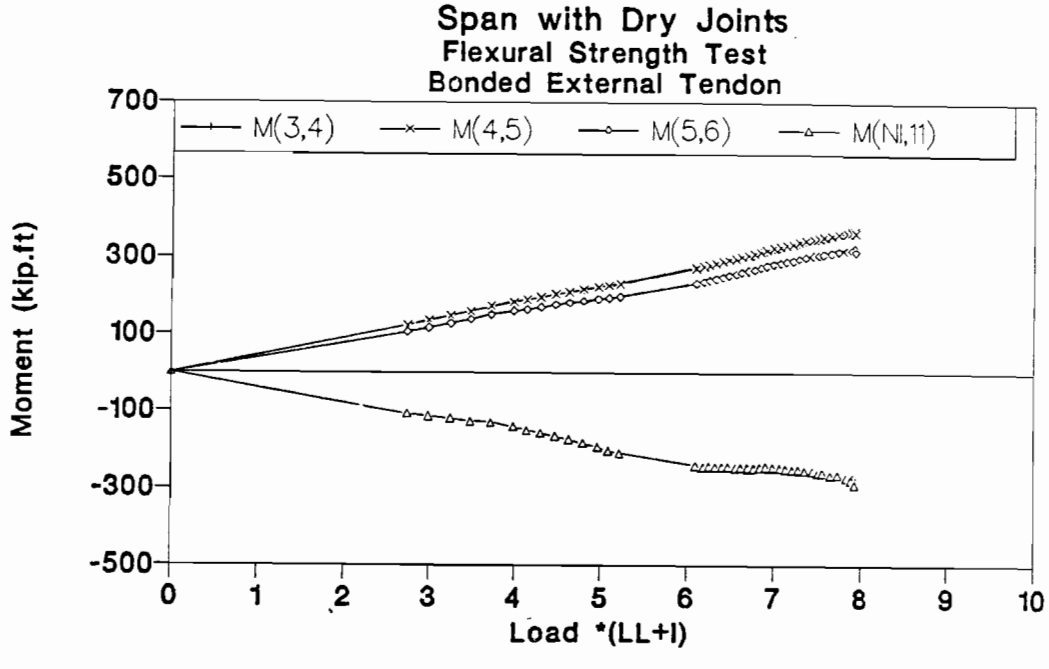

Figure 3.115 Moment-load of flexural strength test in dry joints span.

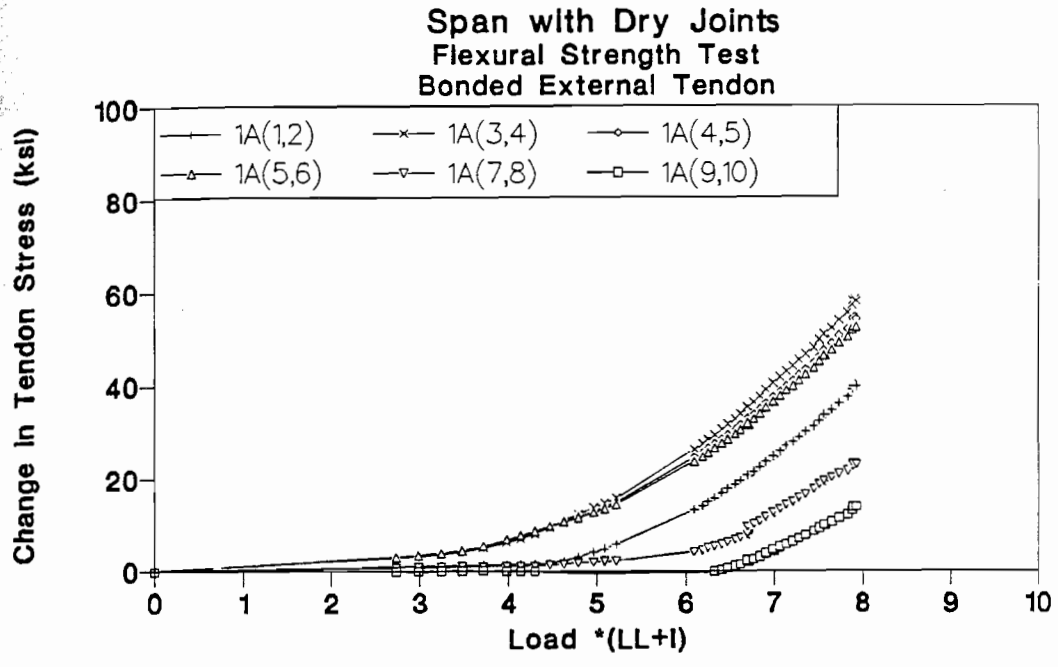

Figure 3.116 Tendon 1A stress-load of flexural strength test in dry joints span.

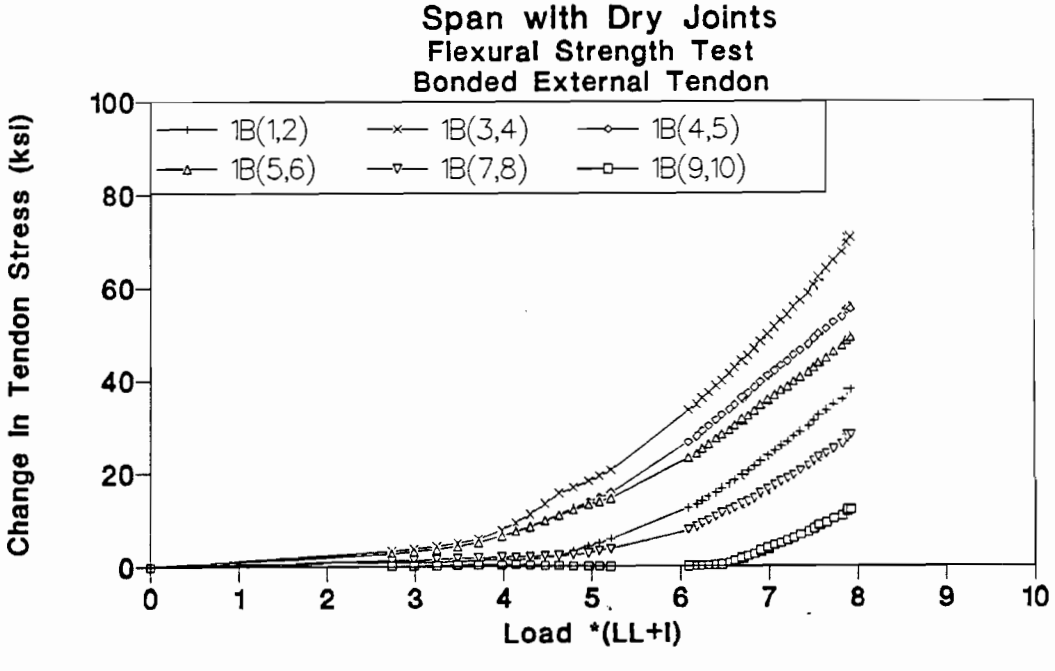

Figure 3.117 Tendon 1B stress-load of flexural strength test in dry joints span.

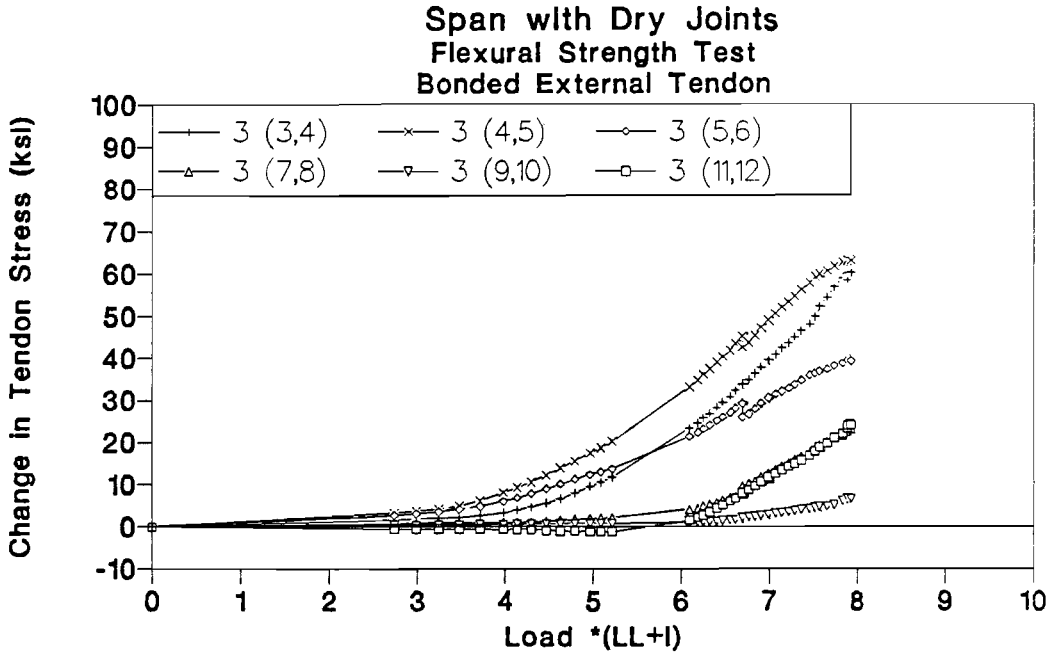

Figure 3.118 Tendon 3 stress-load of flexural strength test in dry joints span.

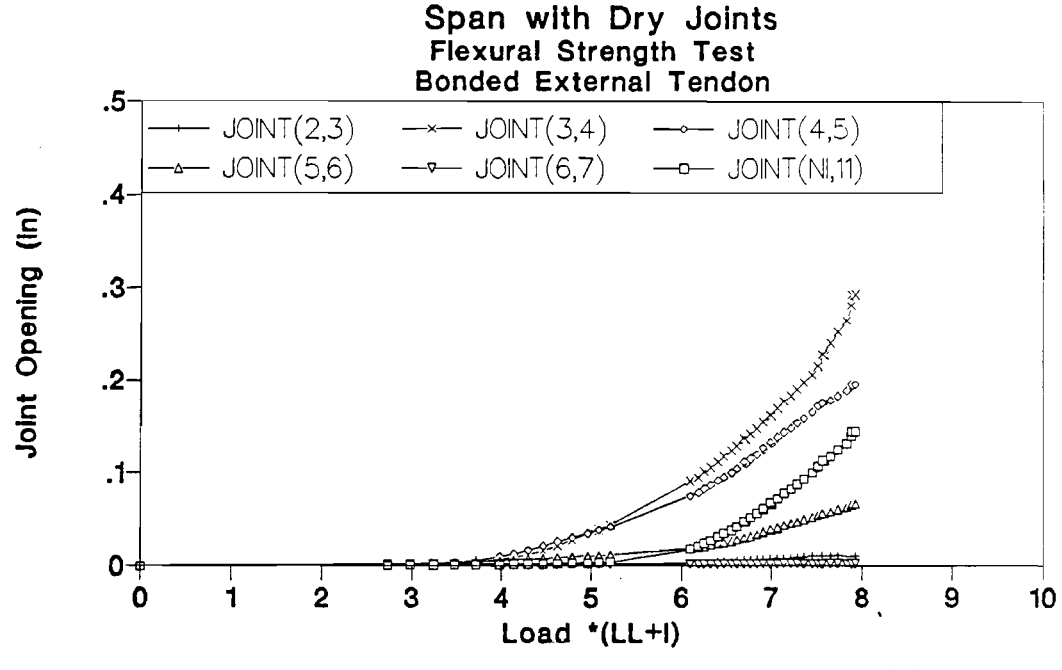

Figure 3.119 Joint opening-load of flexural strength test in dry joints span.

At a load of 3.5(LL+I), joints (4,5) and (5,6) started opening, as shown in Fig. 3.119, causing external tendons stresses to increase at a higher rate as shown in Figures 3.116 through 3.118.

At a load of 3.75(LL+I), joint (3,4) started opening, as shown in Fig. 3.119, resulting in external tendon stresses to increase at a higher rate as shown in Figures 3.116 through 3.118.

At a load of 4.6(LL+I) external tendons 1A and 1B started slipping at segments 2 and 7 toward the critical joint as shown in Fig. 3.116 and Fig. 3.118, while tendons 3 started slipping at a load of 6.0(LL+I) at segment 7, 9, and 11 toward the critical joint as shown in Fig. 3.119.

At a load of 5.5(LL+I) joint (NI,11) adjacent to the interior support started opening as shown in Fig. 3.119, causing additional changes in the redistribution of internal forces as shown in Fig. 3.114 and Fig. 3.115.

At a load of 8(LL+I) the test was stopped when crushing of the top flange at joint (3,4) was observed.

As shown in Fig. 3.114, the reaction curves exhibited double curvature. As the positive moment joints opened (at 3.5(LL+I)), the mid-span stiffness reduced and the internal forces redistributed toward the interior supports. Since the support stiffness reduced when joint (NI,11) opened, this caused a redistribution of the internal forces back towards the positive moment region. The double curvature behavior was exhibited in the moment curves shown in Fig. 3.115 for the same reasons.

Figure 3.119 demonstrates that joints (3,4), (4,5) and (5,6) exhibited large joint openings as required to increase tendon stresses in the positive moment region. Web cracks occurred at joint (3,4) at a load of 6.4(LL+I). The cracks extended into the top flange as the span reached its flexural strength, which was an indication that the neutral axis had shifted into the top flange.

3.4.2.3 Supplemental Tendon Load Tests. Two additional flexural tests were carried out on the model to investigate its response after adding internal tendons. Four 3/8" diameter internal tendons were added to the bottom flange of the bridge.

3.4.2.3.1 Ungrouted Internal Tendon Tests. A flexural strength test was carried out on the model after adding and stressing the four internal tendons but before grouting them. The dry joint span was loaded until the flexural strength was reached and the top flange of the critical joint showed signs of concrete crushing. The test was stopped when concrete crushing was first observed in the top flange at joint (4,5) (Fig. 3.120). The stiffness of the model when the test was stopped was about 5% its initial stiffness.

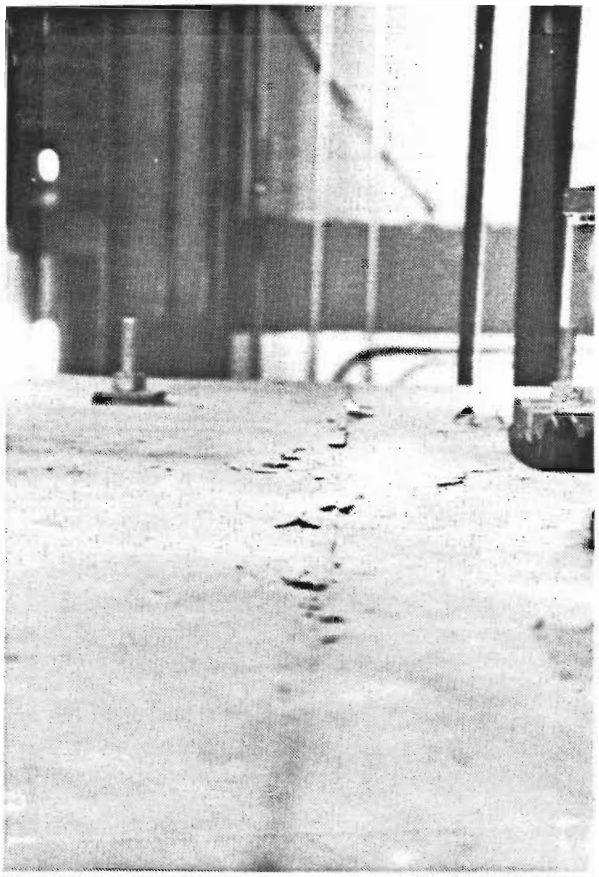

Figure 3.120 Crushed critical joint top flange.

The load was increased from zero to 2(LL+I) in 1(LL+I) increments, from 2(LL+I) to 6(LL+I) in 0.5(LL+I) increments, and from 6(LL+I) to 9(LL+I) in 0.2(LL+I) increments. The test was carried out in one loading cycle, and the flexural strength measured was 1DL+9(LL+I) with a maximum deflection of 2.45 inches (equivalent to L/122).

The load-deflection response of the model is shown in Fig. 3.121. Measured reactions are plotted in Fig. 3.122, while calculated moments are plotted in Fig. 3.123. Measured stress changes in the external tendons are plotted in Figures 3.124 through 3.126. Measured joint openings are plotted in Fig. 3.127. Changes in internal tendon stresses at two segments are plotted in Fig. 3.128.

At a load of 4.5(LL+I) joint (4,5) started opening as shown in Fig. 3.127 causing external tendon stresses to increase rapidly as shown in Figures 3.124 through 3.126. The opening of joint (4,5) reduced the positive moment section stiffness and distributed the internal forces to the support section as shown in Fig. 3.122 for reactions and Fig. 3.123 for moments.

At a load of 5.5(LL+I) the external tendons started slipping in segments 2 and 7 toward joint (4,5) as shown in Fig. 3.124 to Fig. 3.126.

At a load of 6(LL+I) joint (NI,11) adjacent to the support started opening as shown in Fig. 3.127 causing additional changes in the load distribution as indicated in Fig. 3.122 and Fig. 3.123.

At a load of 6.9(LL+I) external tendons 3 started slipping in segments 9 and 11 toward the critical joint as shown in Fig. 3.126.

At a load of 7.0(LL+I) external tendons 1A started slipping in segment 9 toward the critical joint as shown in Fig. 3.124, while tendons 1B started slipping at 7.4(LL+I) as indicated in Fig. 3.125.

At a load of 9(LL+I) the top flange of joint (4,5) started crushing, as shown in Fig. 3.120. The test was stopped immediately because a second test was to be run on the same critical joint after grouting the bottom internal tendons. The stiffness of the structure when the test was stopped was about 5% of its original stiffness.

Figure 3.128 shows that the stress in the internal tendons was different along the length due to friction between the internal tendon and the duct. The internal tendons started slipping at 7.7(LL+I).

The reaction and moment curves exhibit double curvature as shown in Fig. 3.122 and Fig. 3.123 due to redistribution of internal forces when the positive-moment joints open and when the interior support joint opens.

3.4.2.3.2 Grouted Internal Tendons. After grouting the four internal tendons in the bottom flange of the model, a flexural strength test was carried out on the model. The dry joints span was loaded until the top flange of joint (4,5) crushed as shown in Fig. 3.129. The load was increased from zero to 9(LL+I) in increments which varied from 1(LL+I) to 0.2(LL+I). The test was carried out in one loading cycle, and the maximum flexural strength measured was 1DL+9.4(LL+I) with a maximum deflection of 2.5 inches (equivalent L/120).

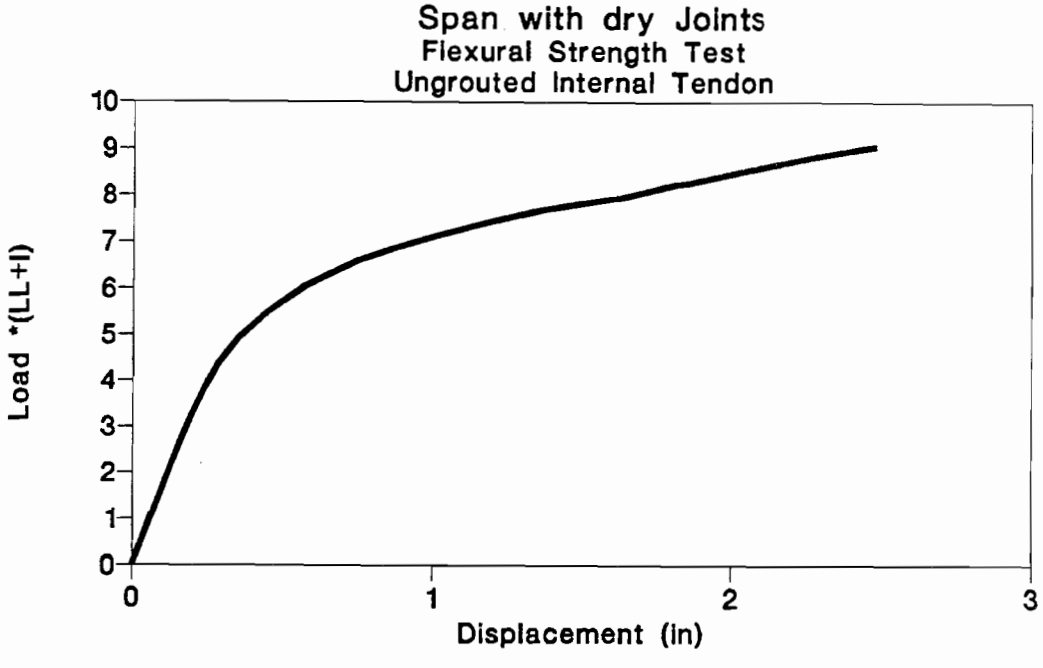

Figure 3.121 Load-deflection of ungrouted internal tendon test in dry joints span.

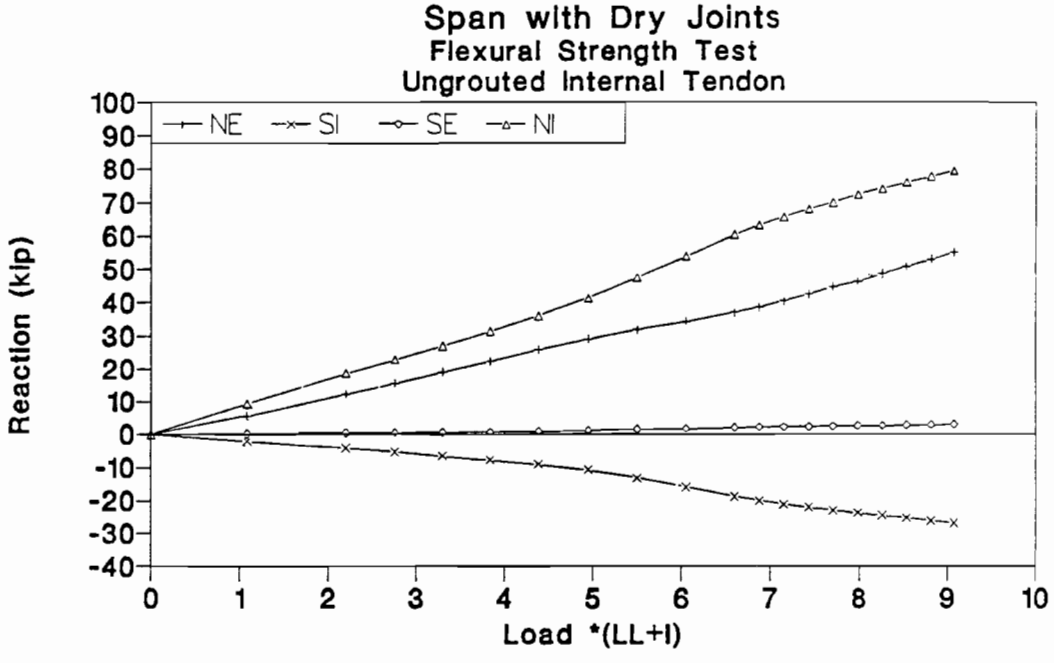

Figure 3.122 Reaction-load of ungrouted internal tendon test in dry joints span.

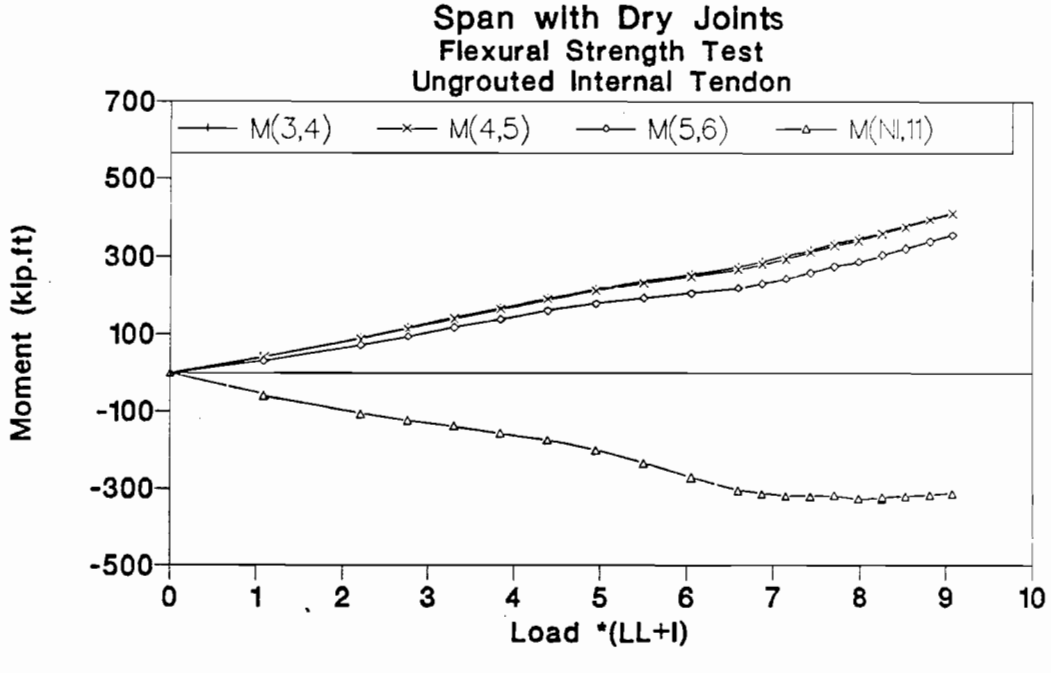

Figure 3.123 Moment-load of ungrouted internal tendon test in dry joints span.

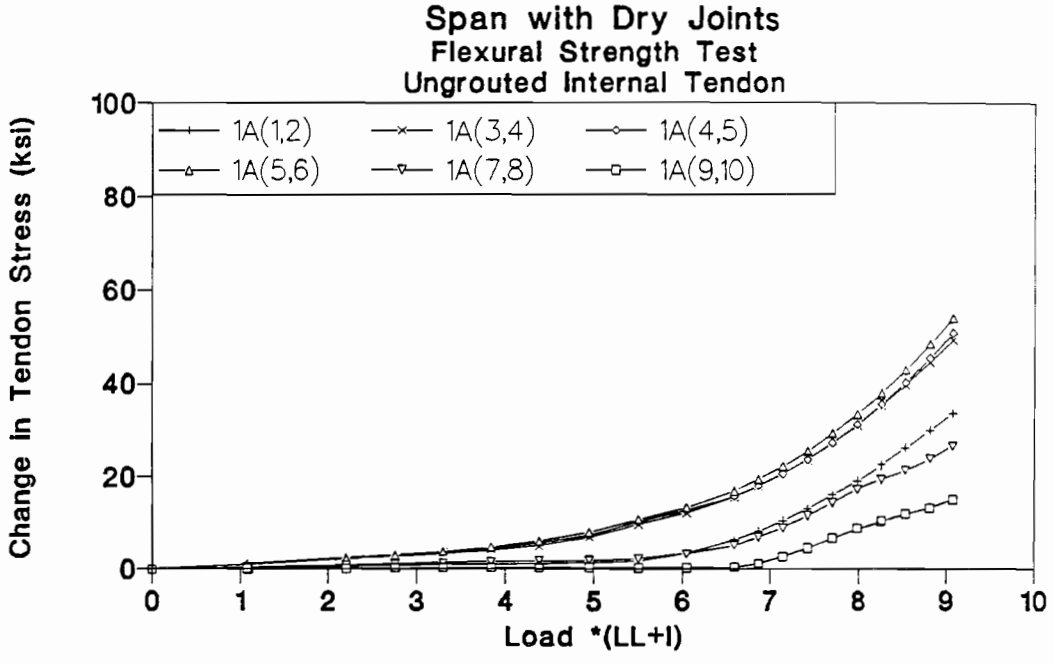

Figure 3.124 Tendon 1A stress-load of ungrouted internal tendon test in dry joints span.

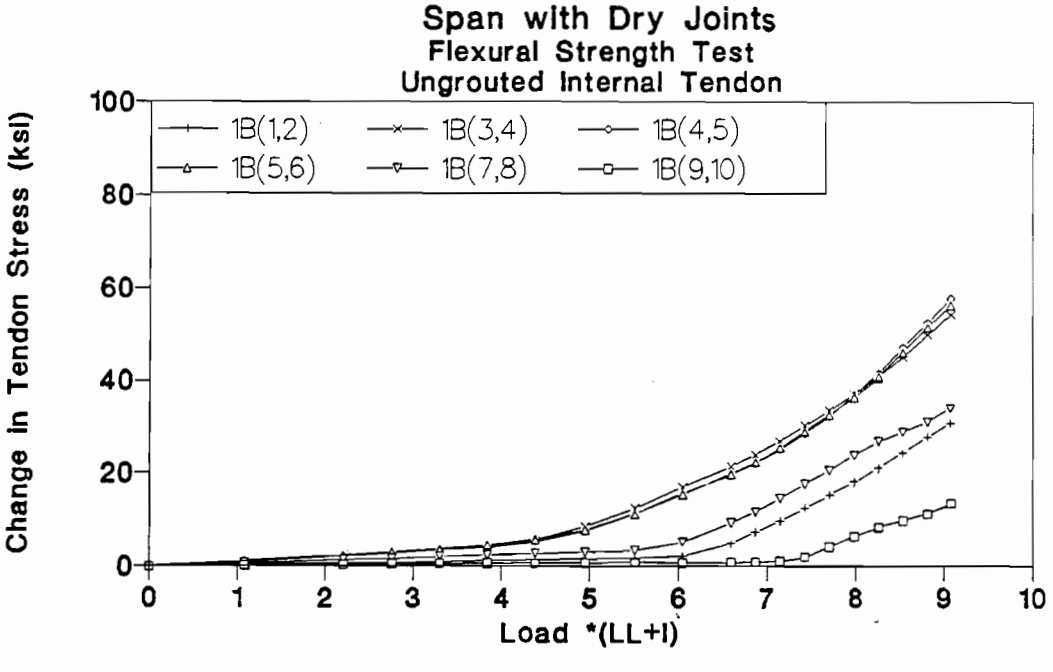

Figure 3.125 Tendon 1B stress-load of ungrouted internal tendon test in dry joints span.

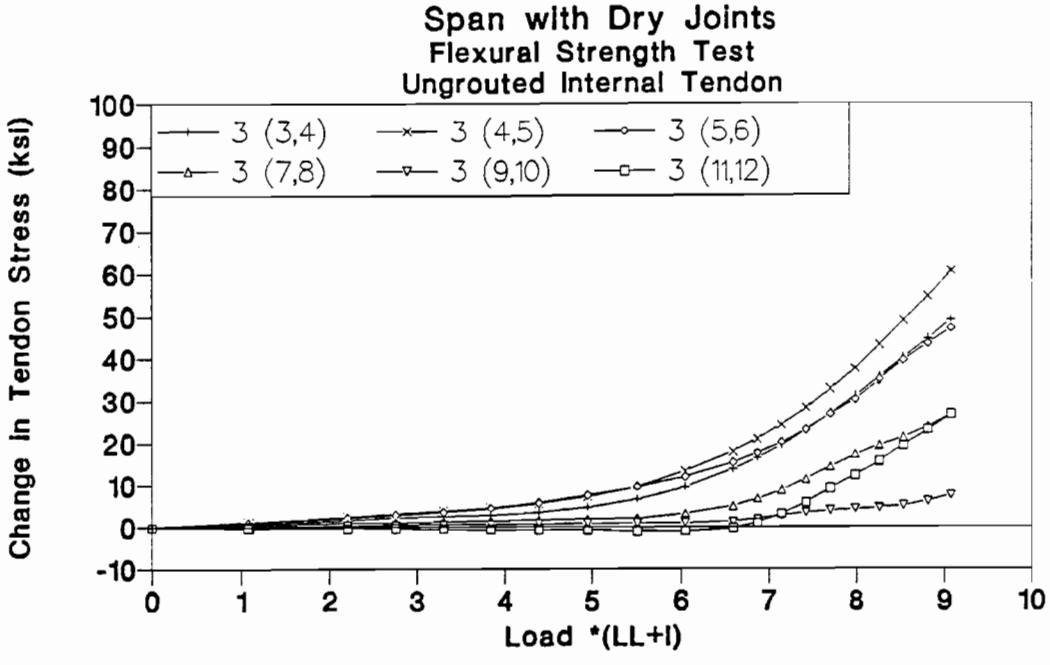

Figure 3.126 Tendon 3 stress-load of ungrouted internal tendon test in dry joints span.

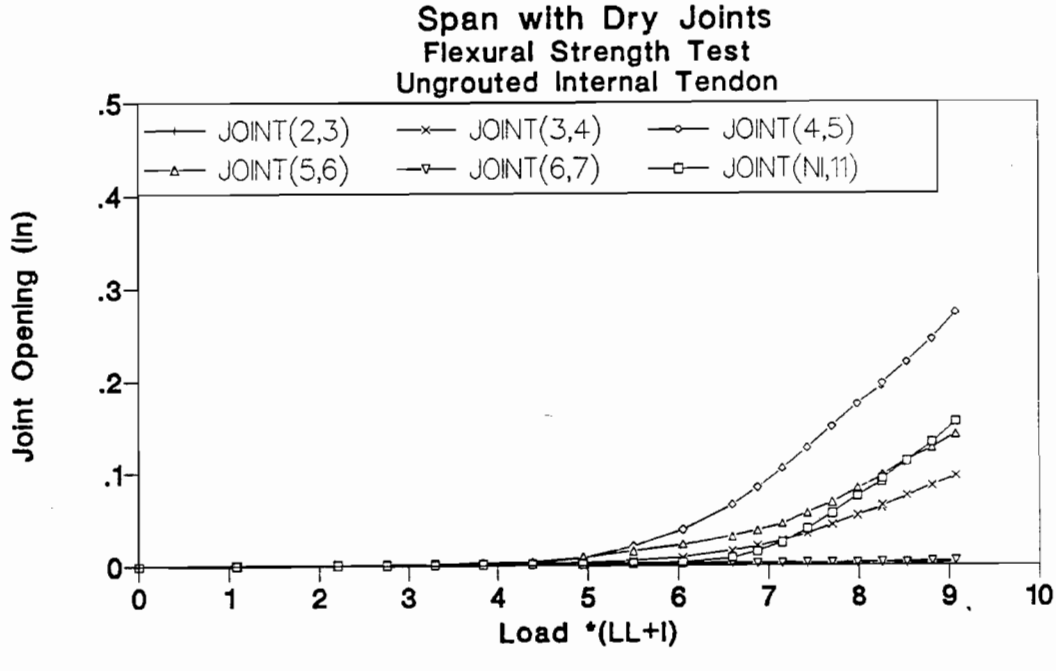

Figure 3.127 Joint opening-load of ungrouted internal tendon test in dry joints span.

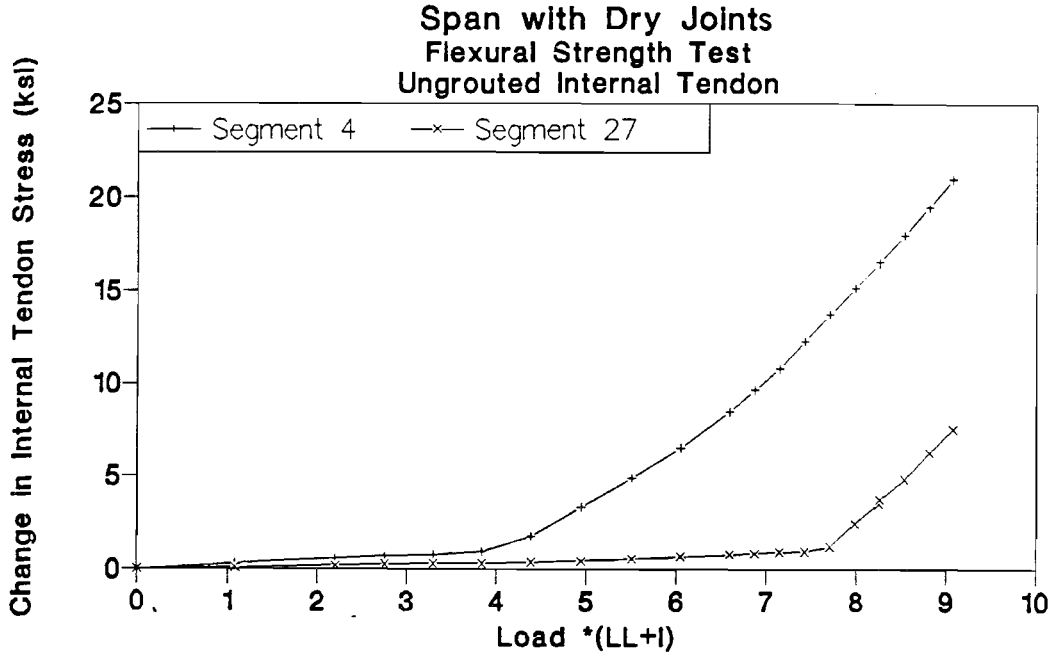

Figure 3.128 Internal tendon stress-load of ungrouted internal tendon test in dry joints span.

The load deflection response of the model is shown in Fig. 3.130. Measured reactions and calculated joint moments are plotted in Fig. 3.131 and Fig. 3.132. Measured changes in the external tendon stresses are plotted in Figures 3.133 through 3.135. Measured joint openings are plotted in Fig. 3.136. Stress changes in the grouted internal tendons are plotted in Fig. 3.137.

At a load of 4(LL+I) joint (4,5) started opening as shown in Fig. 3.136 causing changes in tendon stress and internal force distribution. At a load of 5.4(LL+I) external tendon 1A and 1B started slipping in segment 7 toward the critical joint as shown in Fig. 3.133 and Fig. 3.134.

At a load of 6.5(LL+I) joint (NI,11) started opening as shown in Fig. 3.136 causing additional changes in the load distribution.

At a load of 5.4(LL+I) tendons 3 started slipping in segment 7 toward the critical joint as shown in Fig. 3.135.

At a load of 6.8(LL+I) tendons 1A and 1B started slipping in segment 2 toward the critical joint as shown in Fig. 3.133 and Fig. 3.134.

At a load of 7.0(LL+I) tendons 1A and 1B started slipping in segment 9 toward the critical joint as shown in Fig. 3.133 and Fig. 3.134.

Loading was stopped at 9.4(LL+I) when the top flange of joint (4,5) crushed as shown in Fig. 3.129.

Figure 3.137 shows the stresses of the internal tendons at two locations along the model. The internal tendons yielded at the critical joint section, while small stress change was measured at the midspan section in unloaded span. The reaction and moment curves exhibited double curvature as shown in Fig. 3.131 and Fig. 3.132 due to different distributions of internal forces as the critical joint and the support joint opened.

Figure 3.129 Crushed critical joints top flange.

3.5 Bond Strength

External tendon stresses were measured at many joints along the model in each span. The stresses were used to determine the load at which tendons slipped and to calculate the bond stress between the tendons and the diaphragms. External tendon stresses were measured at six locations in each of the exterior spans and at five locations in the interior span as shown in Fig. 2.32 and Table 3.3.

Table 3.3 Joints with Strain Measurement Gages

Span	Joints
Dry Joints	(1,2),(3,4),(4,5),(5,6),(7,8),(9,10)
Interior	(NI,11),(11,12),(15,16),(19,20),(20,SI)
Epoxy Joints	(21,22),(23,24),(25,26),(26,27),(27,28),(29,30)

3.5.1 Epoxy Joints Span. Six tendons were used in this span as shown in Fig. 2.4(c) with two tendons of 4A, 4B, and 5. Tendons 4A and 4B were 5-3/8" diameter strands while tendon 5 was 2-3/8" diameter strands. The critical joint for phase three tests was joint (26,27) as discussed in Section 3.2.1.

During the flexural strength test with bonded external tendons at all interior diaphragms and with ungrouted internal tendons, three joints were opened as shown in Fig 3.68. Joints (25,26), (26,27), and (27,28) were the only three joints opened in the midspan region. These joint openings caused a large increase in tendon stress at these joints, and the tendons slipped toward these joints as shown in Fig. 3.138.

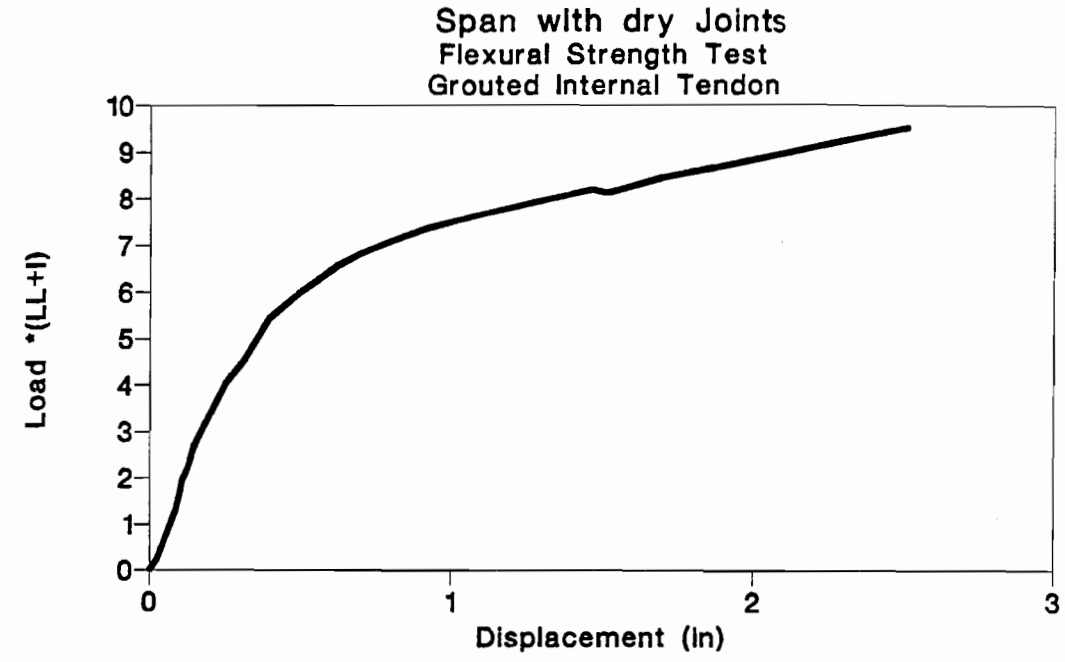

Figure 3.130 Load-deflection of grouted internal tendon test in dry joints span.

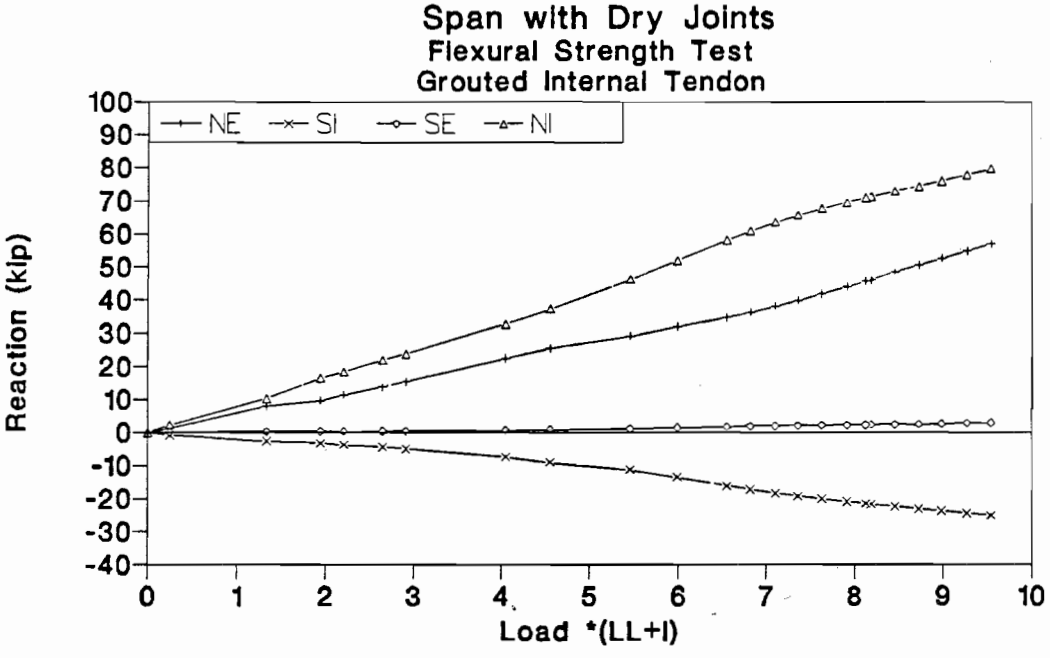

Figure 3.131 Reaction-load of grouted internal tendon test in dry joints span.

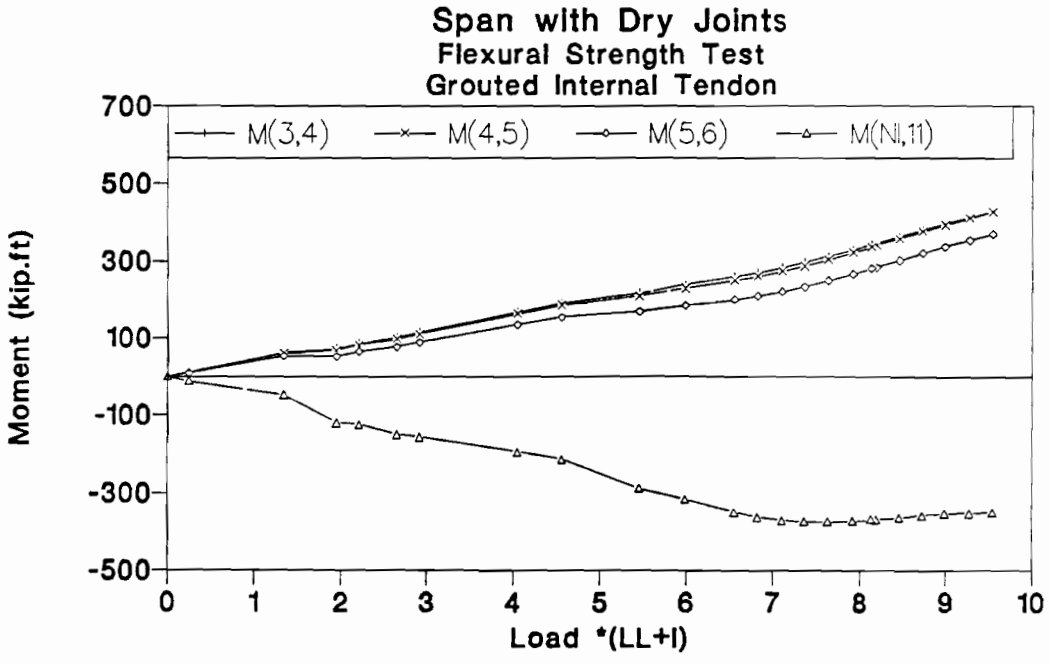

Figure 3.132 Moment-load of grouted internal tendon test in dry joints span.

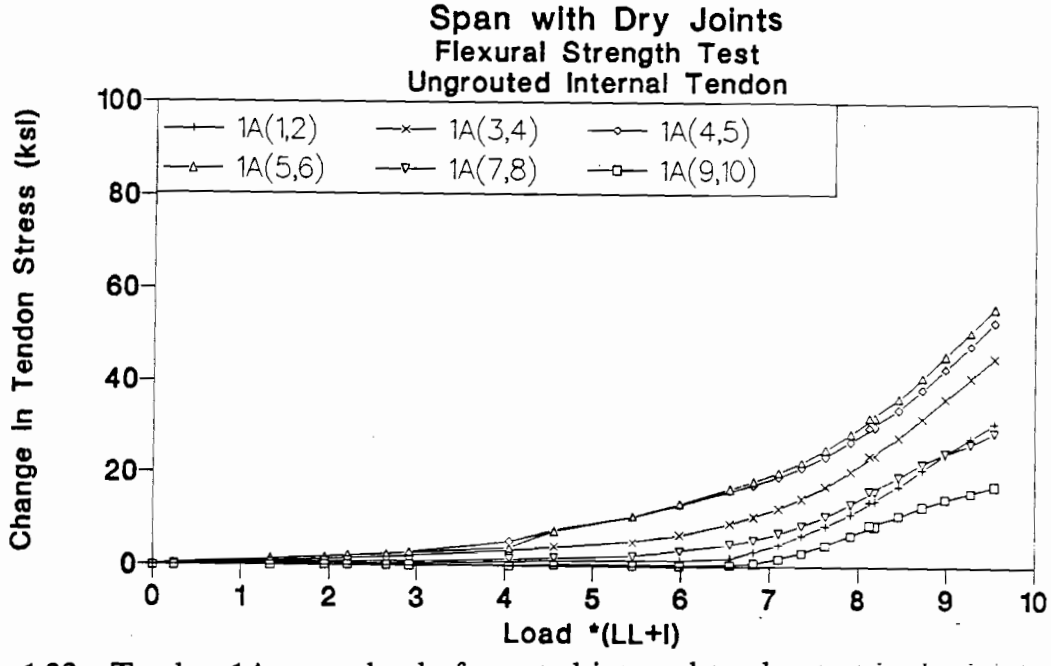

Figure 1.33 Tendon 1A stress-load of grouted internal tendon test in dry joints span.

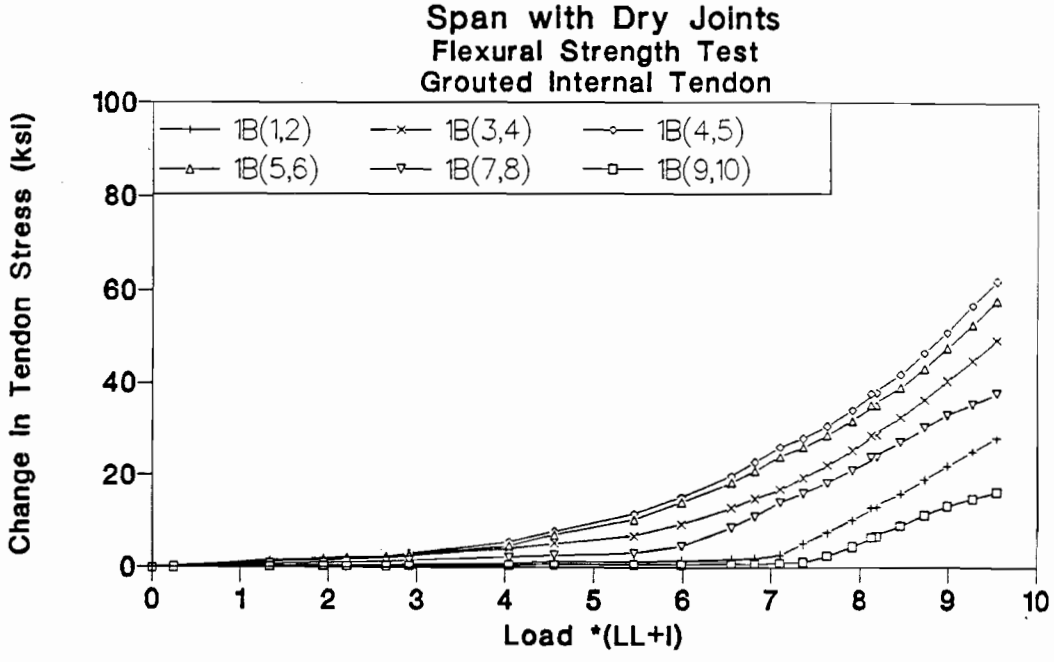

Figure 1.134 Tendon 1B stress-load of grouted internal tendon test in dry joints span.

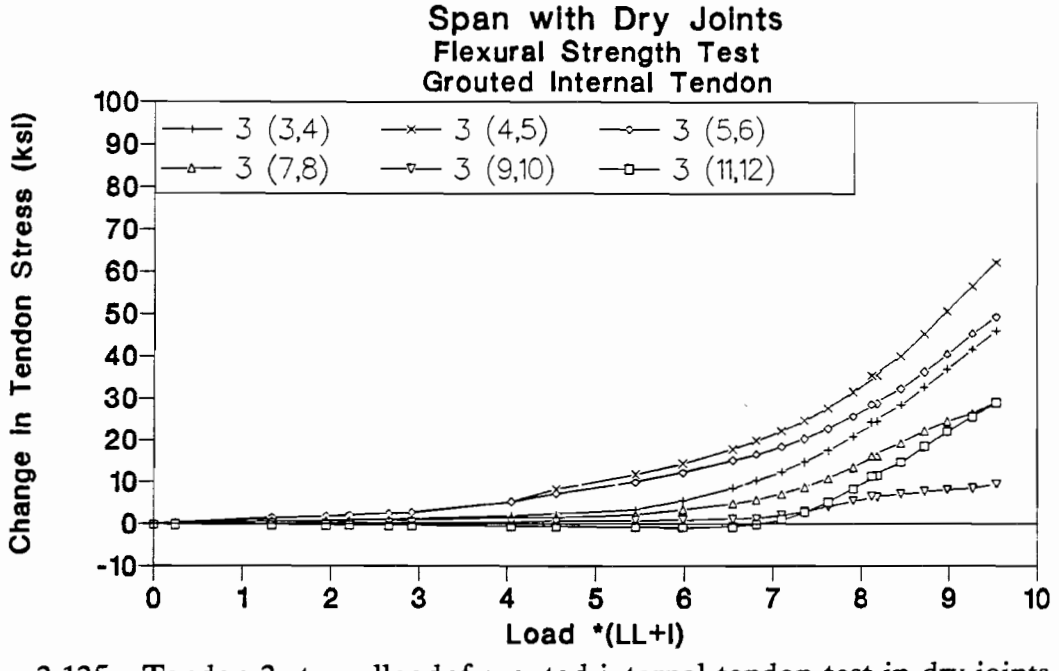

Figure 3.135 Tendon 3 stress-lloadof grouted internal tendon test in dry joints span.

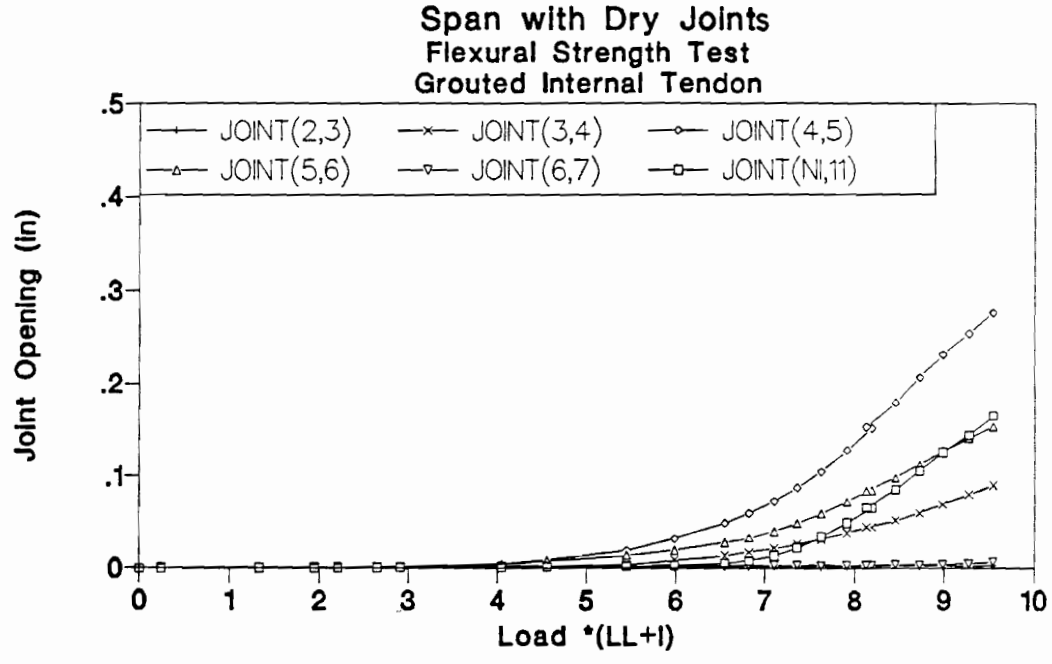

Figure 1.136 Joint opening-load of grouted internal tendon test in dry joints span.

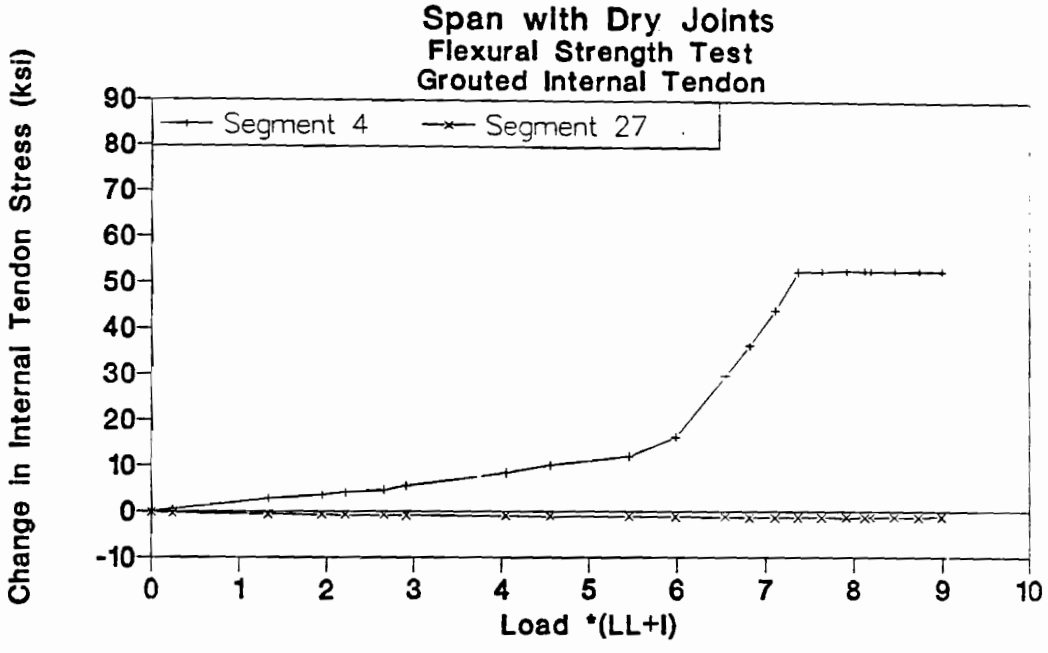

Figure 3.137 Internal tendon stress-load of grouted internal tendon test in dry joints span.

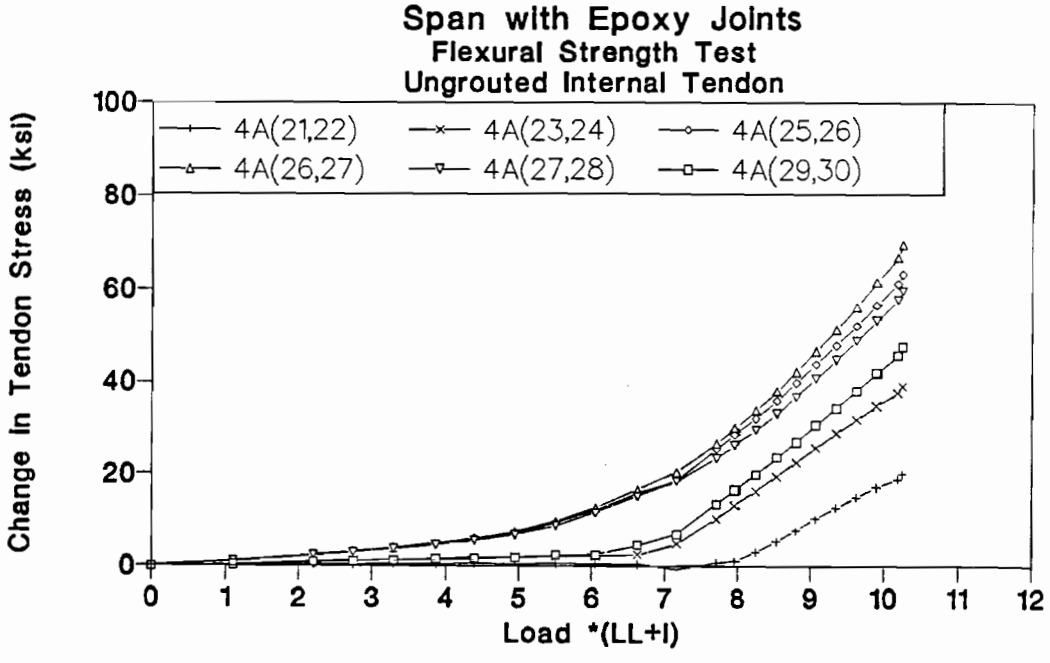

Figure 3.138 Change in Tendon 4A stress in epoxy joints span.

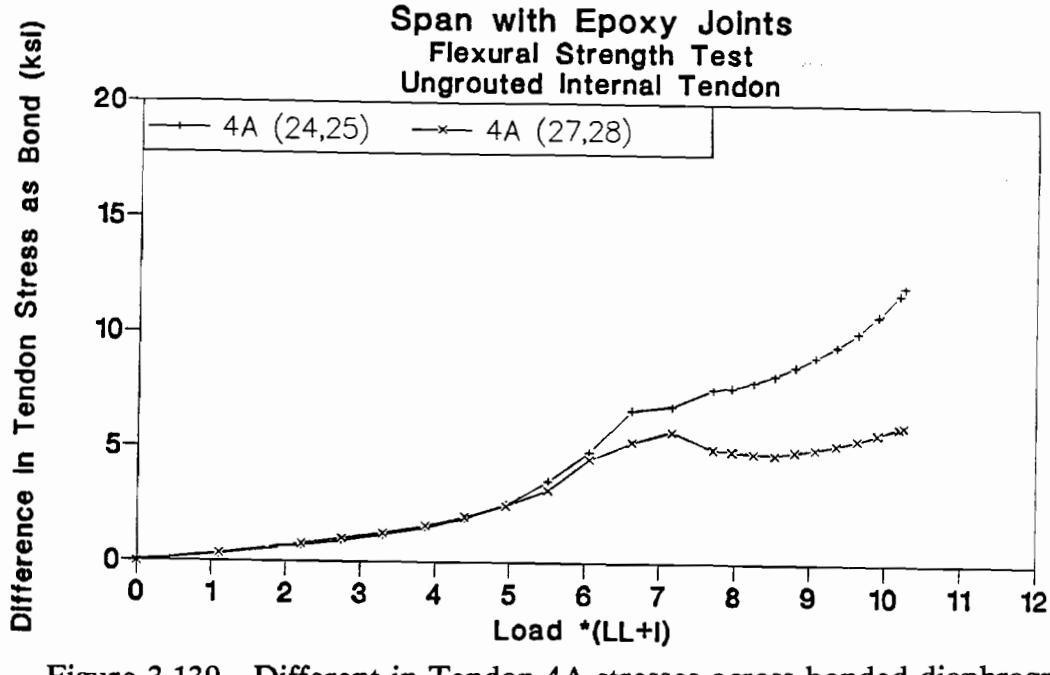

Figure 3.139 Different in Tendon 4A stresses across bonded diaphragms.

Figure 3.139 shows the difference in tendon stress across the diaphragm as measured during the flexural strength test. The average difference in stress at segments (24, and 25) was calculated from the difference in measured tendon stress at joints (25,26) and (23,24). While the average difference in tendon stress at segments (27, and 28) was calculated from the difference in tendon stress between joints (29,30) and (27,28). The difference in tendon stress across a diaphragm will be referred to as "bond", while the stress over the contact area between the tendon and the grout will be referred to as "bond stress".

Bond at segments 24 and 25 increased at a high rate with load up to a load of 6.5(LL+I) (Fig. 3.139) at which point the stress at joint (23,24) started increasing rapidly because tendons slipped toward joint (25,26) as shown in Fig. 3.138. After that, the bond increased at low rate with the load. The difference in tendon stress (bond) was about 7 ksi when the full slip was apparent (tendon stress increased rapidly at joint(23,24)), while the difference in tendon stress increased to about 12 ksi at the end of the test. When slip occurs over the full width of the diaphragm, it will be called "full" slip or "general" slip.

The difference in tendon stress across diaphragms 27 and 28 is shown in Fig. 3.139. The bond was increased up to a load of about 7(LL+I) (Fig. 3.138) at which time full slip was apparent by the increase in tendon stress at joint (29,30). After that, the bond slightly reduced and then increased with the load. The difference in tendon stress at full slip was about 6 ksi, while it was 7 ksi at the end of the test. This shows that the difference in tendon stress across a bonded diaphragm (bond) increased up to full slip, after which the bond stabilized or continued increasing slowly. The difference in bond at different diaphragms was due to different bond quality at these locations.

3.5.2 Dry Joints Span. Tendons 1A and 1B had 5-3/8" diameter strands, while tendon 3 had 2-3/8" diameter strands as shown in Fig. 2.32. The phase three test for the case with ungrouted internal tendons and bonded external tendons to all ten diaphragms was used to study the bond stress. Joint (4,5) was the critical joint for this test as discussed in Section 3.2.1. Joints (3,4), (4,5), and (5,6) opened widely in this test as shown in Fig. 3.127. Due to these joint openings, the external tendon stresses were increased substantially at these joints and the tendons slipped toward these joints as shown in Fig. 3.140.

The difference in the tendon 1B stress (bond) across diaphragms 6 and 7 is shown in Fig. 3.141. The bond increased with the load up to full slip at a load of 6(LL+I) when the tendon stress at joint (7,8) started increasing rapidly, as shown in Fig. 3.140. After that the bond increased slowly up to failure of the structure. The difference in tendon 1A stress across the diaphragm at full slip was about 8 ksi, while the maximum difference at the end of the test was 12 ksi.

Bond at segments 2 and 3 increased at high rate with the load up to full slip at a load of 6(LL+I) at which time the tendon stress at joint (1,2) increased rapidly. After that, the bond generally stabilized but increased sharply at the end of the test. The difference in tendon stress across the diaphragm at full slip was 5 ksi, while the maximum difference in tendon stress at the end of the test was 11 ksi.

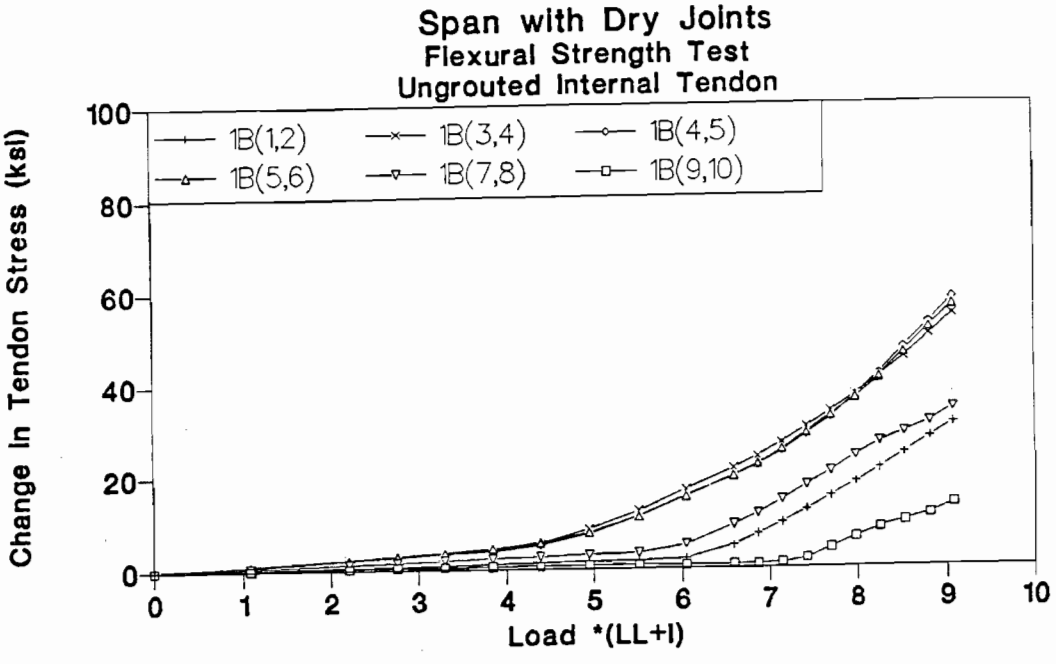

Figure 3.140 Change in Tendon 1B stress in dry joints span.

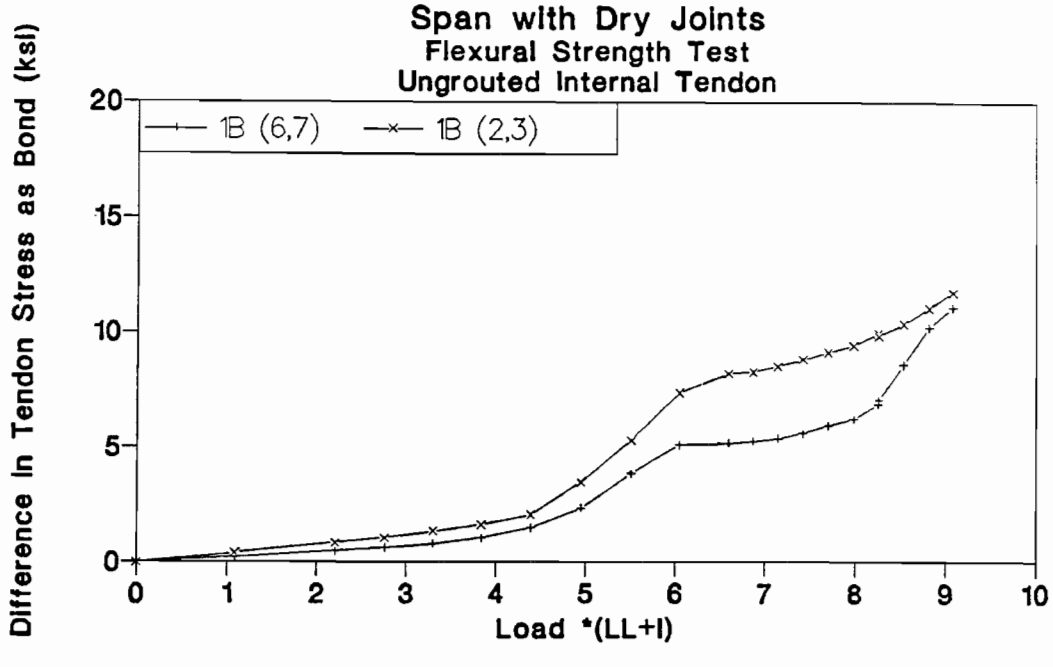

Figure 3.141 Difference in Tendon 1B stresses across bonded diaphragms.

Table 3.4 Difference in Tendon Stress (ksi) Across Diaphragm

Segment	Full Slip	Maximum	Average
(2,3)	5	11	8
(6,7)	8	12	10
(24,25)	7	12	9.5
(27,28)	6	7	6.5

Table 3.4 shows the differences in tendon stress across bonded diaphragms measured during the model tests. The value of 10 ksi difference that was used in Chapter Four to calculate the external tendon stress at flexural capacity was based on this study and the cut tests presented in Chapter Two. A stress difference of 10 ksi in tendon A and B corresponds to a bond stress of 0.38 ksi between the tendon and the grout. The tests show that the bond increased at a high rate with slip until full slip occurred, after which the bond increased slowly or stabilized. The relation between the bond stress and slip used in the analytical model assumes that the bond increases with slip until full slip of the tendon occurs. After that the bond stress remains constant (see Chapter Five).

3.6 Joint Profile

Distortions along the height of the critical joint were measured during testing. The critical joint distortion at various depths of the joint were measured by grid-type crack monitors as discussed in Chapter Two. Figure 3.142 (a) and (b) shows the joint opening profile for the ultimate tests carried out on the dry joints span and the epoxy joints span. The joint profile shows that the critical joint cross section remains plane section at ultimate load. The joint rotations can be calculated from the joint opening measurements at different levels. Joint (4,5) of the dry joints span had a maximum rotation of 0.02 radius before failure, while joint (26,27) of the epoxy joints span had a maximum rotation of 0.023 radius before failure. The epoxy joint maximum rotations were 15 percent higher than the dry joint maximum rotations.

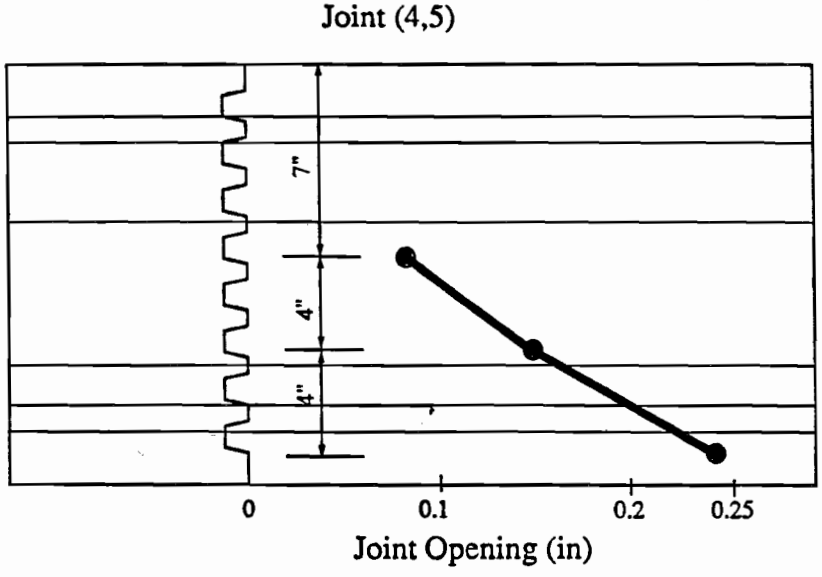

a) Dry Joints Span Ultimate Test

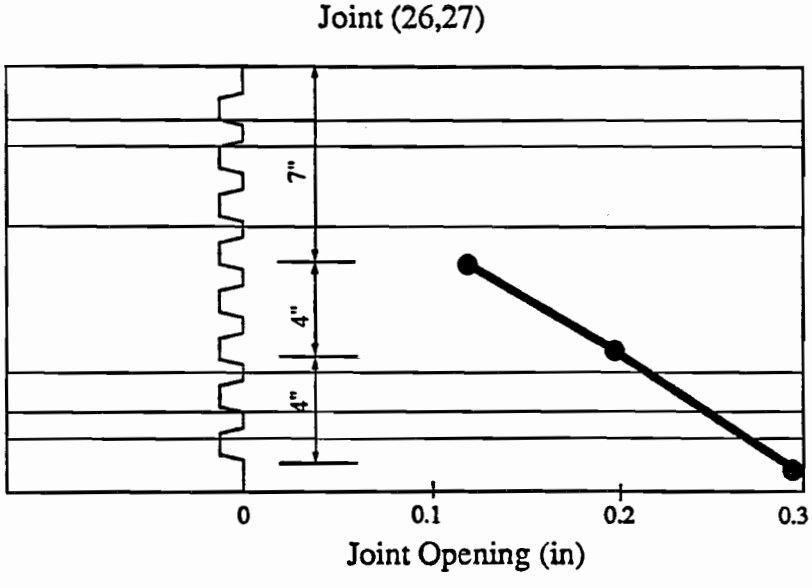

b) Epoxy Joints Span Ultimate Test

Figure 3.142 Joint opening profile.

CHAPTER FOUR

INTERPRETATION OF TEST DATA

4.1 Adequacy of Repair Procedures

The previously tested three span bridge model was evaluated and repaired as discussed in Chapter Two. Cracks in the webs and bottom flange of the epoxy joints exterior span were injected with epoxy while only cracks in the webs of the dry joints exterior span were injected. The model was tested before and after injection to show the effect of the epoxy injection.

4.1.1 Epoxy Joints Span. The cracks in the webs and bottom flange of this span resulting from the previous ultimate load tests were injected with epoxy resin. The response of the structure to loads is shown in Fig. 4.1. The stiffening effect of the crack injection was apparent at a load of 2.0(LL+I) which is 23 percent below the measured decompression load of the epoxy joints span. The epoxy injection affected the load deflection response in two ways. First, the epoxy filled space between the cracks and increased the area of contact between the segments. As a result, the stiffness of the structure was higher. Secondly, the epoxy bonded together the cracked concrete in the box sections which started behaving more like uncracked sections. This increased the stiffness of the structure at loads higher than the decompression load.

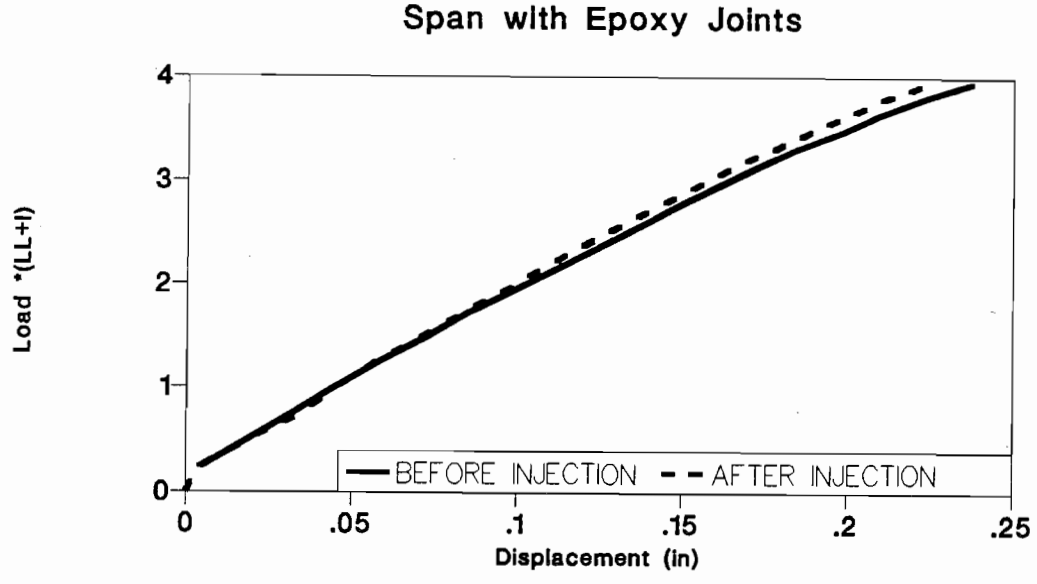

Figure 4.1 Effect of crack injection on epoxy joints span.

4.1.2 Dry Joints Span. Figure 4.2 shows the load deflection response of the dry joints span of the structure before and after injecting the web cracks with epoxy. No epoxy was injected into the original dry joints. In this span, the effect of the repair injection was very small because the web cracks were the only cracks injected with epoxy while joints between the segments were left dry. The injection had two effects. The first was observed below the decompression load and was due to the increase in contact area between the filled cracks. The second effect started at a load of 2.7(LL+I), which was 35 percent above the decompression load of the dry joints span. This small stiffening effect was due to the tensile stress carried by the injected web cracks as the neutral axis moved up higher in the section.

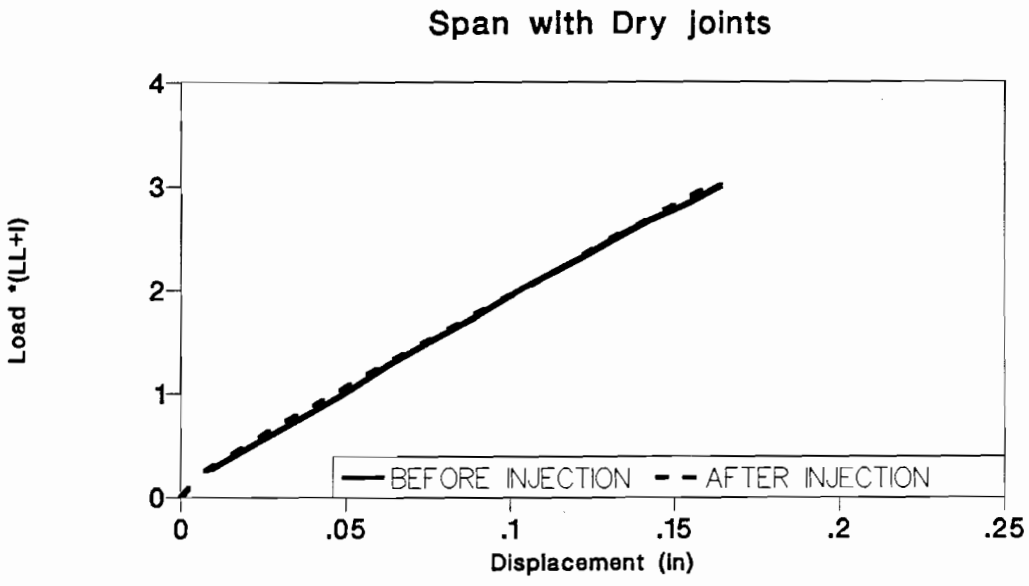

Figure 4.2 Effect of crack injecton on dry joints span.

4.1.3 Effect of Epoxy Injection.

4.1.3.1 Service Load Behavior. The effect of epoxy injection on the epoxy joints span was that it increased the reserve capacity against joint opening. Before injection, the crack opened at a load of 2.6(LL+I), while after epoxy injection of the cracks the critical joint cracked at a load of 4.8(LL+I). This provided a reserve capacity against joint opening of 2.2(LL+I). The load required to crack the joint after injection was about 80 percent higher than the joint opening load before epoxy injection.

The design criteria shown in Table 2.5 take the epoxy joint effect into consideration by requiring no residual compressive stress in the extreme tension fiber if segments are

epoxied together. However for dry joints bridges a residual compressive stress in the extreme tension fiber is needed to give a reserve capacity against joint opening.

4.1.3.2 Flexural Strength and Ductility. Two flexural strength tests were carried out on the epoxy joints span after all external tendons were bonded to all ten diaphragms as discussed in Chapter Two. At the beginning of the first test, joint (26,27) was the only joint cracked during the cracking load cycle. During the first strength test, joints (25,26) and (27,28) became cracked too. At the beginning of the second strength test, joints (25,26), (26,27), and (27,28) were cracked. It can be assumed that during the first strength test, the adjacent joints in the critical positive moment region were epoxy joints because they were uncracked and they initially carried tension during the test. It follows that, joints in the critical positive moment region in the second strength test were similar to dry joints because they were already cracked and carried zero tension. From this discussion, a comparison of test one (as an epoxy joints case) with test two (as an dry joints case) is valid.

The results of the two flexural strength tests carried out on the epoxy joints span with external tendons bonded to all interior diaphragms are shown in Figures 4.3 through 4.5. The first strength test was done after joint (26,27) was cracked while the second strength cycle was carried out after joints (25,26), (26,27), and (27,28) were cracked in the first strength loading cycle. The flexural strength test was controlled by crushing of the top flange at the critical joint.

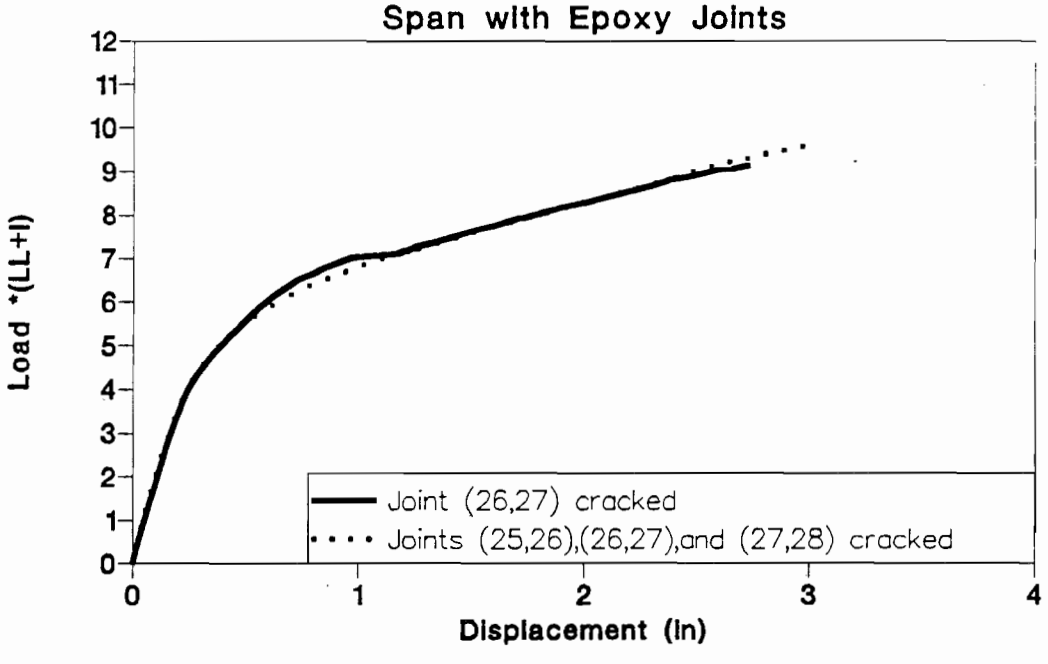

Figure 4.3 Effect of epoxy injection on load-deflection response.

Fig. 4.3 shows that the epoxy injection had a small negative effect on the strength and ductility of the segmental model with bonded external tendons. The small negative effect on the strength and ductility was due to concentration of joint opening in the critical joint as shown in Fig. 4.4. The critical joint in the first test reached its maximum opening at a lower load than in the second load test. The maximum critical joint opening was approximately the same in the two tests as shown in Fig. 4.4. The two joints (25,26) and (27,28) adjacent to the critical joint cracked at a load of 7(LL+I) in the first test as shown in Fig. 3.53, while joint (27,28) opened at 4.8(LL+I) and joint (25,26) opened at 6.7(LL+I) in the second test as shown in Fig. 3.60. The epoxy delayed the opening of the adjacent joints due to the fact that the cracking moment is higher than the crack opening moment.

Figure 4.5 shows that the maximum cumulative positive joint opening in the positive moment region was lower in the single cracked joint case. This difference was due to the higher moment required to crack the joint adjacent to the critical joint in the single cracked joint case test than the moment required to open the cracked adjacent joint in the second test. This caused an earlier opening of the adjacent joints in the second test than the single cracked joint test, and resulted in higher total joint opening in the critical region. Higher cumulative joint opening caused a greater increase in external tendon stresses and resulted in a higher strength and larger maximum deflection at failure.

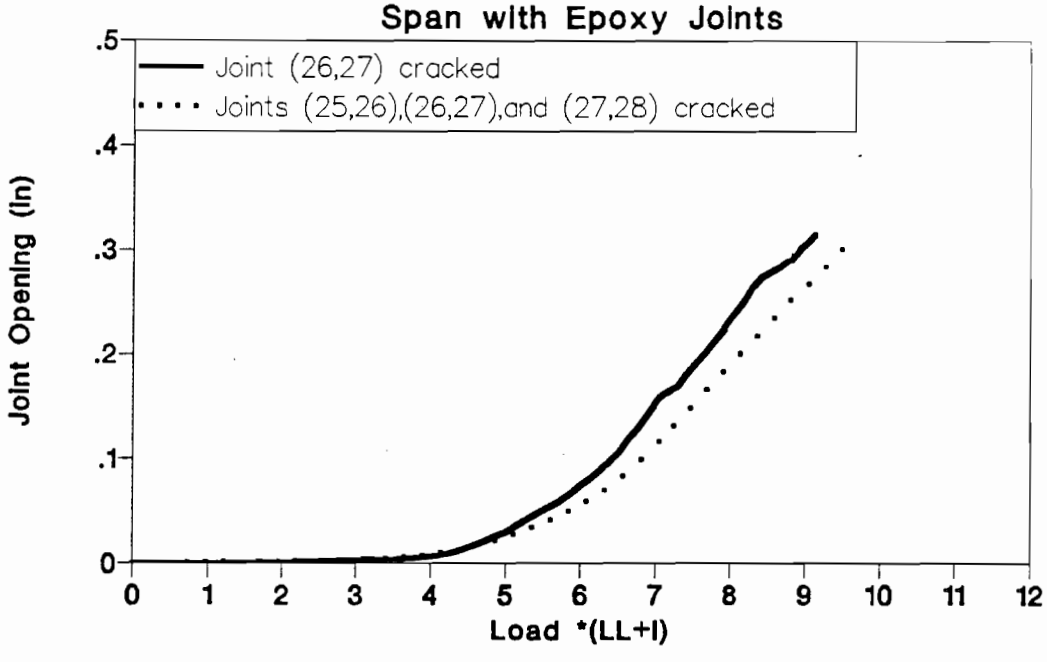

Figure 4.4 Effect of epoxy injection on critical joint opening response.

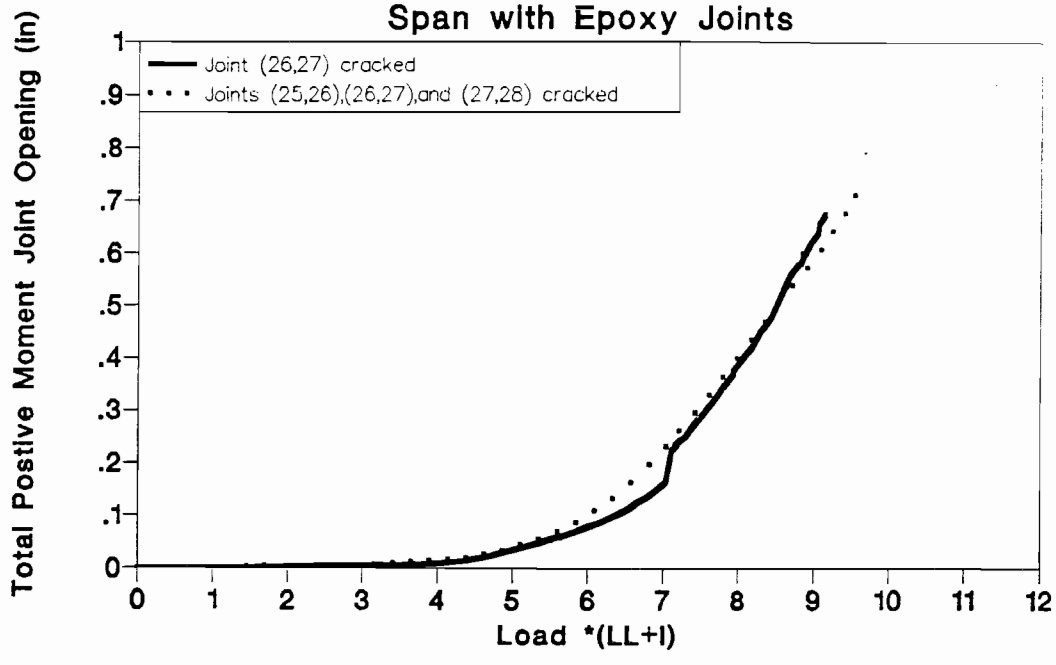

Figure 4.5 Effect of epoxy injection on total joint opening.

Three joints cracked during the first flexural strength test when external tendons were bonded at all diaphragms, while only one joint was cracked during the strength tests carried out by MacGregor (1) in the first part of this study when the external tendons were discretely bonded at fewer diaphragms. Bonding the external tendons at all diaphragms over short or discrete lengths (called discrete bonding) increased the stiffness and strength of the critical joint which attracted more moment to the critical region and caused the adjacent joints to crack before the critical joint crushed. Discrete bonding of the external tendons to all ten intermediate diaphragms reduced the adverse effects of the epoxy joints.

4.2 Effect of Incremental Bonding of External Tendons

Additional local bonding of external tendons to intermediate diaphragms was performed in two steps so that tests could be carried out for different bonding conditions. The first test (stage one test) was carried out on the model with the external tendons bonded to the pier segments and to a maximum of four internal deviators in each span, as shown in Fig. 4.6(a) and Table 4.1. The second test (stage two test) was conducted after the external tendons were bonded to a maximum of three additional interior deviators in each span as shown in Fig. 4.6(b) and Table 4.1. The last test (stage three test) was carried out on the model when the external tendons were locally bonded to all diaphragms as shown in Fig. 4.6(c) and Table 4.1. After finishing the three testing stages, each of the exterior

spans was loaded monotonically until the span flexural strength was essentially reached. Loading was discontinued when the top flange at the critical joint started crushing.

Table 4.1 Segments Bonded to External Tendons

Tendon	Stage One	Stage Two	Stage Three
1A	2,4,7,9	2,4,6,7,9	1,2,3,4,5,6,7,8,9,10
1B	3,4,7,8	2,3,4,6,7,8,9	1,2,3,4,5,6,7,8,9,10
2	12,14,17,19	12,14,17,19	11,12,13,14,15,16,17,18,19,20
3	4,7,13,14,17,18	2,4,6,7,9,12,13,14,17, 18,19	1,2,3,4,5,6,7,8,9,10,11,12,13,14,15, 16,17,18,19,20
4A	22,24,27,29	22,24,25,27,28	21,22,23,24,25,26,27,28,29,30
4B	23,24,27,28	22,23,24,25,27,28, 29	21,22,23,24,25,26,27,28,29, 30
5	14,17,24,27	12,14,17,19,22,24, 25, 27,29	11,12,13,14,15,16,17,18,19,20,21,22,23,24,25,26,27, 28,29,30

4.2.1 Observations from Tests at Different Stages of Bonding of External Tendons. The first three stages of testing were carried out on the model to show the effect of incremental bonding of external tendons. In each of these three stages the model was loaded up to 5.7(LL+I). This load was chosen since it was higher than the load at which the external tendon started slipping in the original tests. This was desirable since the effect of bonding can only be seen if the external tendon slips. Figure 4.7 shows that the external tendon initially slipped at a load of 4.8(LL+I) in the epoxy joints span, while Fig. 4.8 shows that the external tendon initially slipped at a load of 4.3(LL+I) in the dry joints span.

The maximum load applied for these three stages of tests was higher than the external tendon initial slipping load by 19 percent in the epoxy joints span and 30 percent in the dry joints span. This load limit was high enough to show some effect of incremental bonding of external tendons without causing any damage to the critical joints. The effect

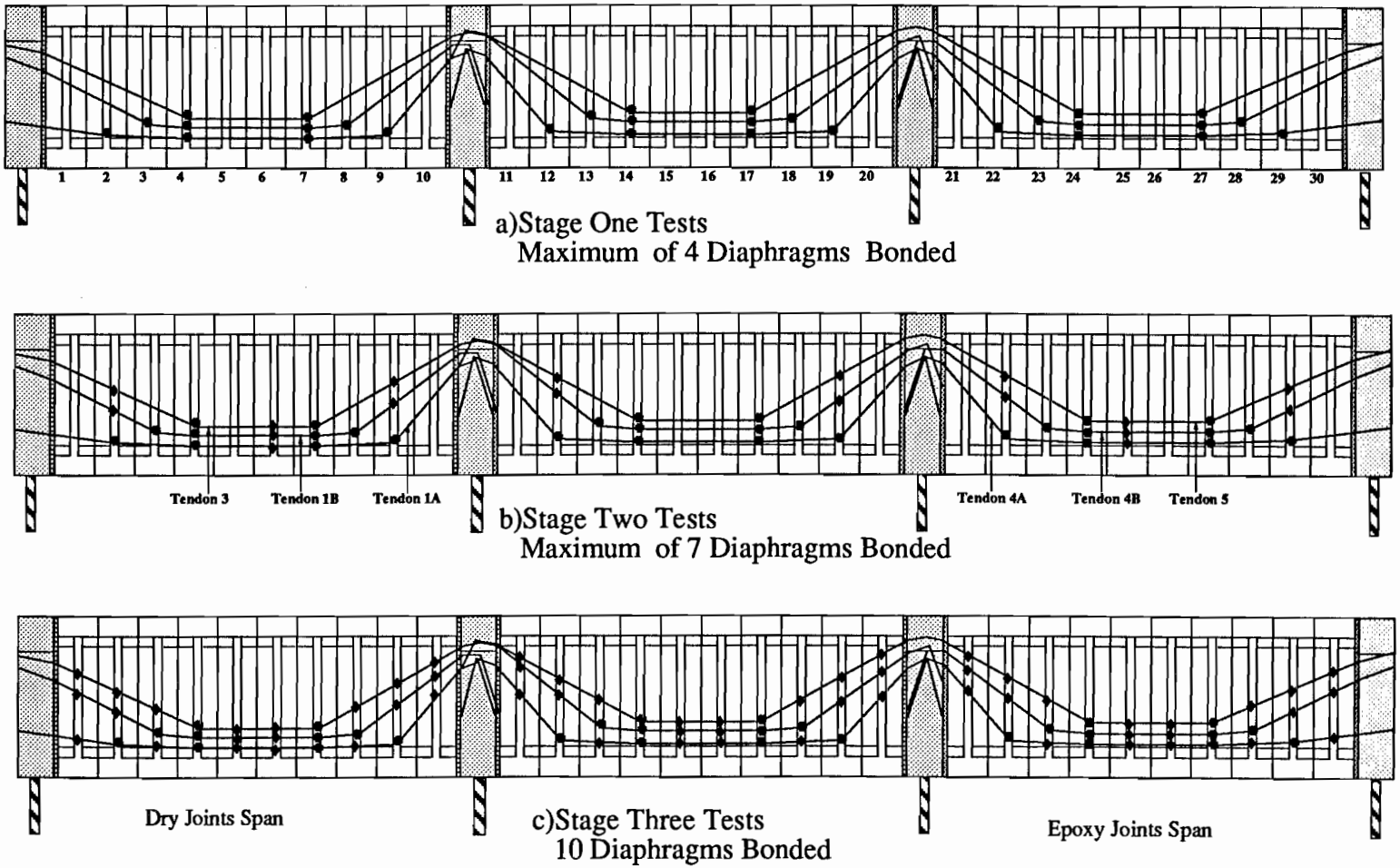

● : Diaphragm Originally Bonded

♦ : Diaphragm Bonded

Figure 4.6 Bonding stages for external tendons.

of discrete bonding of the external tendons to all diaphragms was demonstrated by carrying out ultimate load cycles on the exterior span after bonding of the external tendons at all diaphragms. Due to the low maximum load used in the first three stages of testing of each exterior span, trends were evident but the differences in behavior were small.

Figures 4.9 through 4.11 show the effect of incremental bonding of external tendons on load-deflection response, changes in external tendon stress, and joint opening in the epoxy joint span. Figures 4.12 through 4.14 show the effect of incremental bonding in the dry joint span.

At a load lower than the joint opening load, changes in external tendon stress were slightly increased with the increase in number of bonded diaphragms as shown in Fig. 4.10 for the epoxy joints span and Fig. 4.13 for the dry joints span. Due to this slight increase in tendon stress, joint opening loads were slightly different too as shown in Fig. 4.11 and Fig. 4.14.

Figure 4.7 and Fig. 4.8 show that by bonding the external tendons at more locations, the external tendon slip was reduced and delayed to a higher load. The reduction in slip caused a greater increase in the external tendon stress. The greater increase in external tendon stress resulted in higher strength as indicated in Fig. 4.9 and Fig. 4.12.

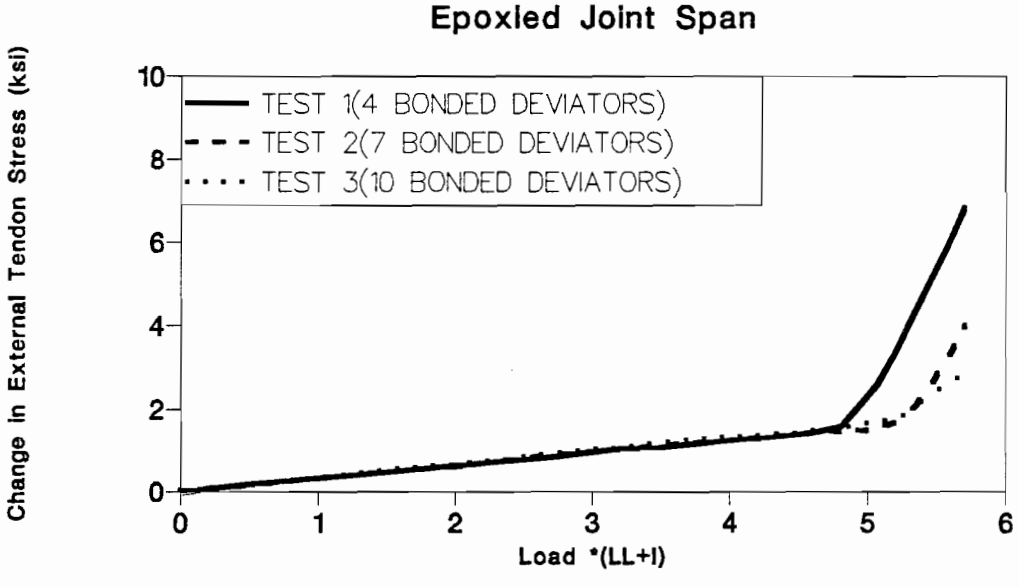

Figure 4.7 Effect of bonding on tendon slip in epoxy joints span.

4.2.2 Flexural Strength Tests. Bonding of external tendons increased the strength and ductility of the model. The deflection increased substantially to give more warning

before the model failed as shown in Fig 4.15. In the first part of the overall testing program, flexural strength tests were carried out by MacGregor (1) on the model when the external tendons were only bonded to the pier segments and at diaphragm locations where tendons were deviated. Four tendons were bonded to four internal diaphragms, while two tendons were bonded to two internal diaphragms in each span. Additional strength tests were carried out on the model as part of this study after external tendons were discretely bonded to all ten diaphragms.

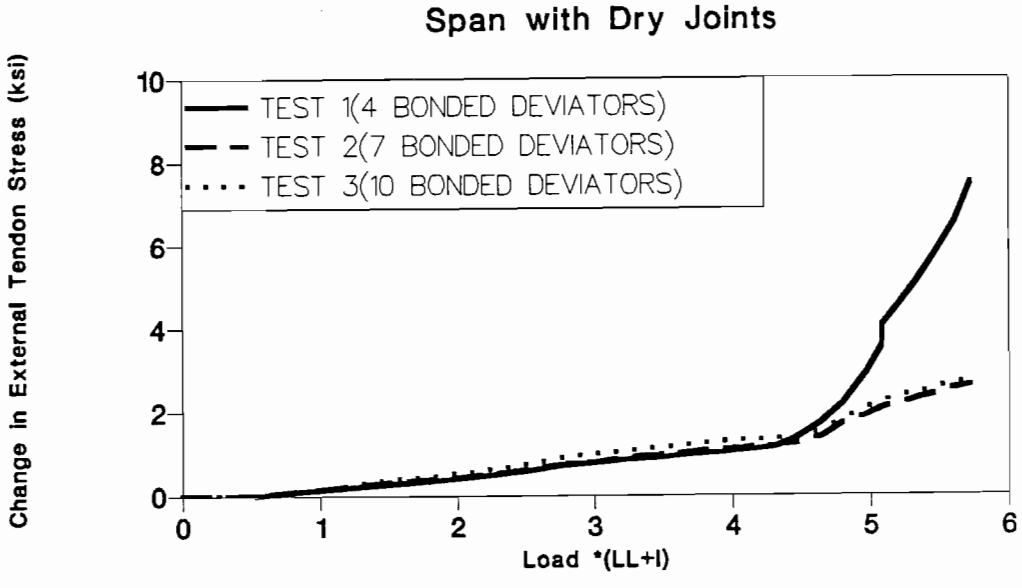

Figure 4.8 Effect of bonding on tendon slip in dry joints span.

4.2.2.1 Epoxy Joints Span. The structure was tested to ultimate for two conditions of bonding of external tendons to the diaphragms. The bonding conditions are shown in Fig. 4.16(a) and (b). The first bonding condition was the as-built model (1). The external tendons were locally bonded to the pier segments and to a maximum of four interior diaphragms in each span. This will be called the partially bonded case. In the second bonding case, the external tendons were locally-bonded to all ten interior diaphragms in each span. This will be called the fully-bonded case.

Strength and ductility were substantially higher in the model with external tendons discretely bonded in each segment (the fully-bonded case) than when bonded to only few segments (the partially-bonded case) as shown in Fig. 4.17. Stiffness of the model at a load higher than the load at which the joints opened was also higher in the fully-bonded case. Changes in the external tendon stress with load varied slightly with the tendon bonding conditions, but the maximum stress change was much higher for the fully-bonded case as shown in Fig. 4.18.

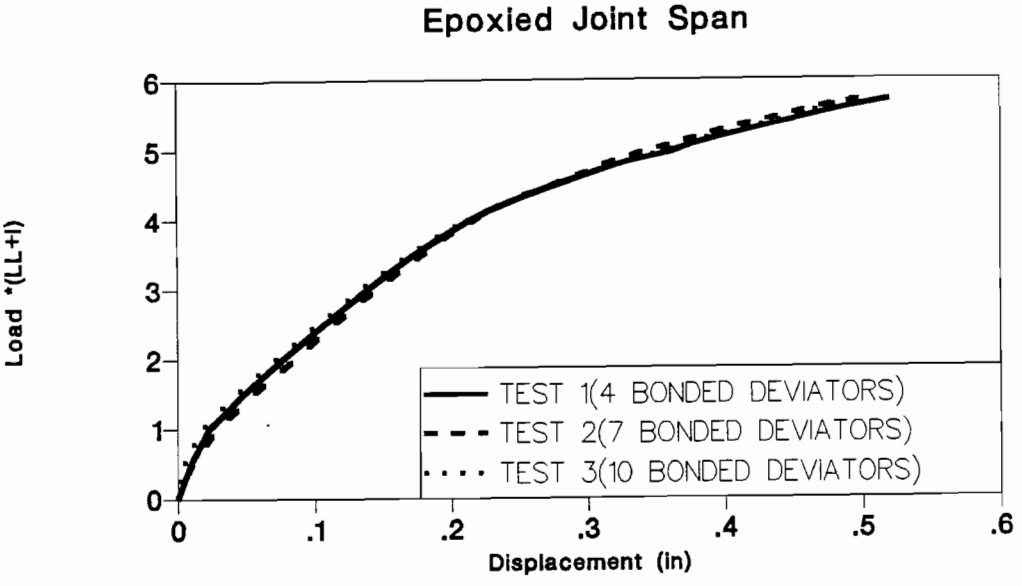

Figure 4.9 Effect of bonding on load-deflection response in epoxy joints span.

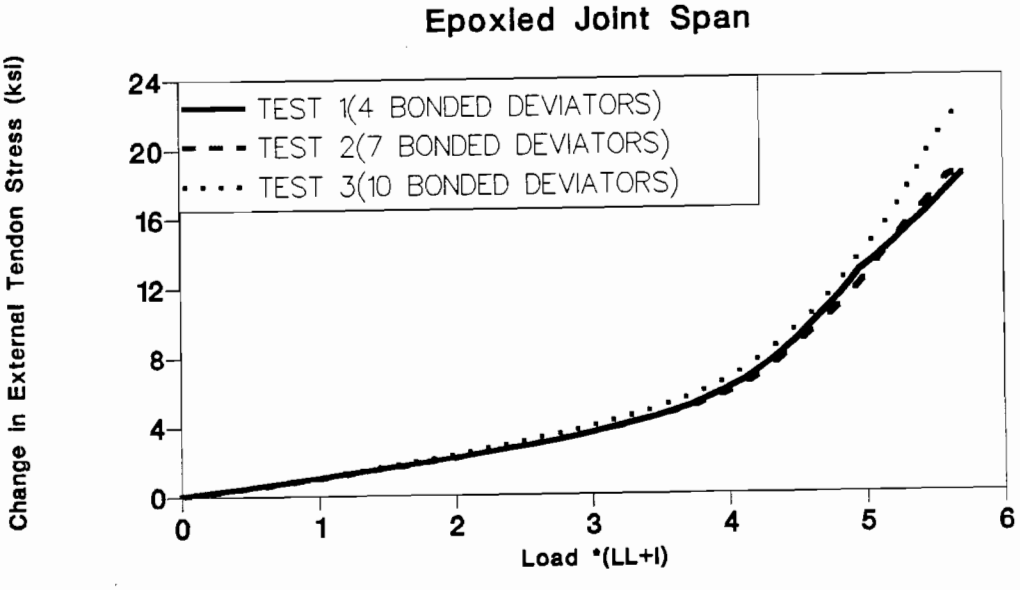

Figure 4.10 Effect of bonding on change in tendon stress in epoxy joints span.

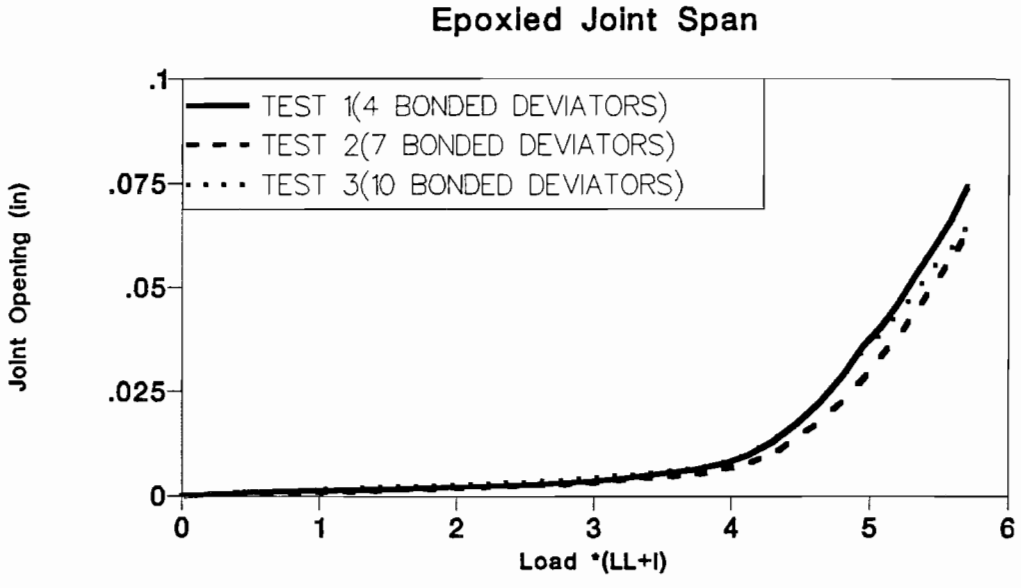

Figure 4.11 Effect of bonding on joint opening in epoxy joints span.

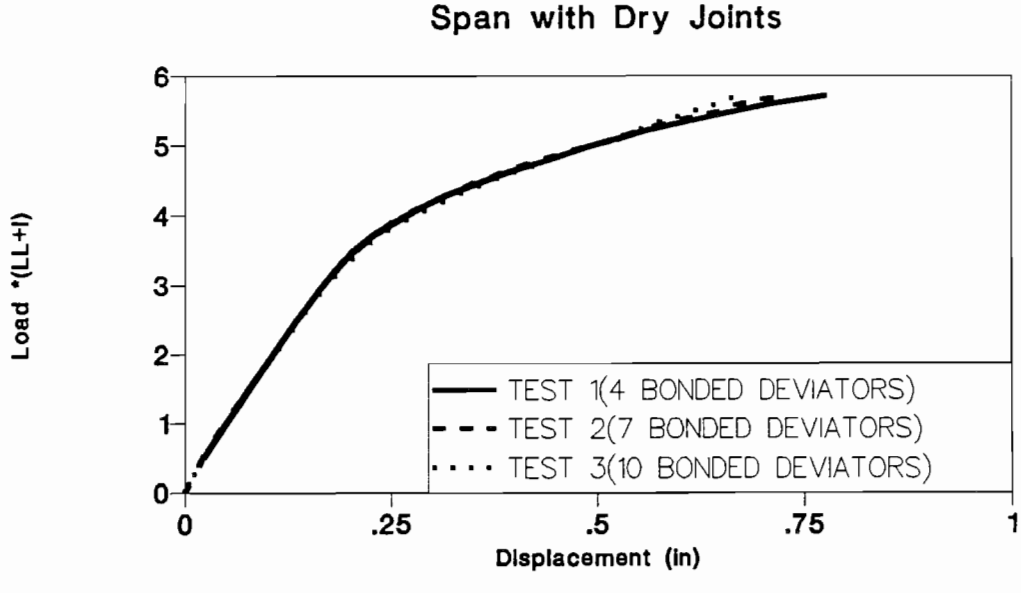

Figure 4.12 Effect of bonding on load-deflection response in dry joints span.

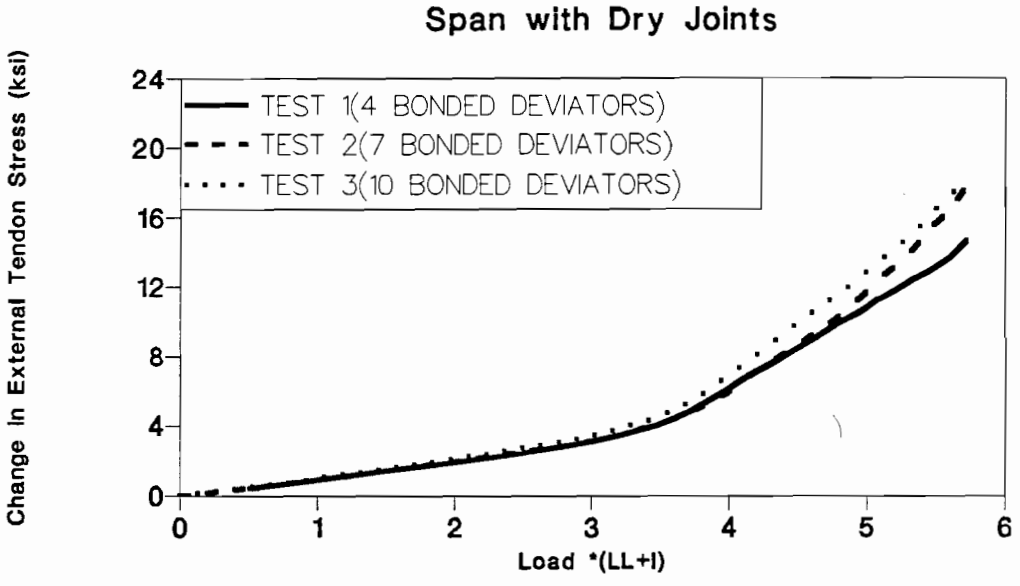

Figure 4.13 Effect of bonding on change in tendon stress in dry joints span.

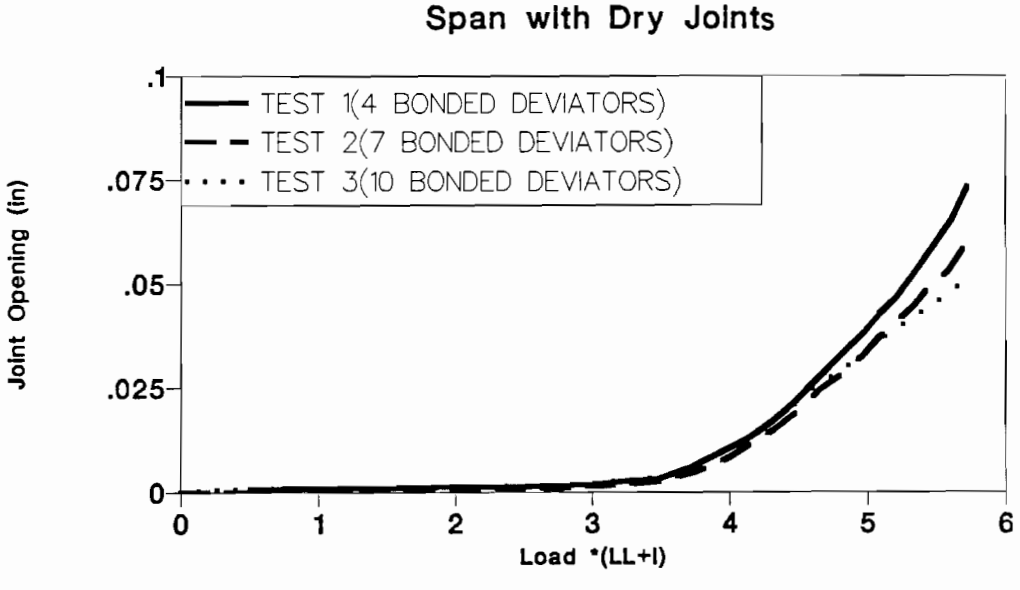

Figure 4.14 Effect of bonding on joint opening in dry joints span.

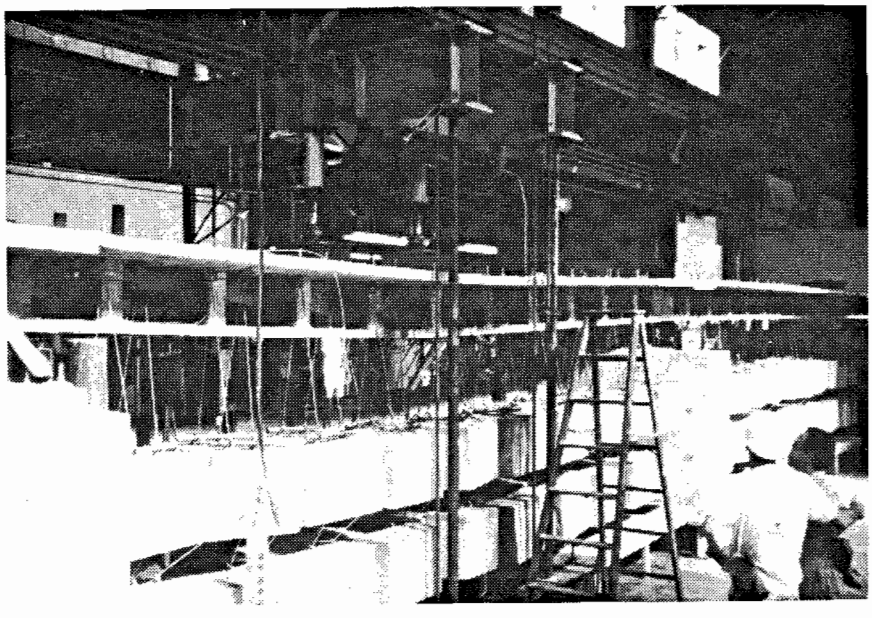

Figure 4.15 Deflected shape of the model for the fully bonded strength test.

Figure 4.19 shows that the critical positive moment joint had the same maximum joint opening, but it occurred at a substantially higher load for the fully-bonded case. The joint opening "rates" at the critical joint and support joint were higher in the partially-bonded case than the fully-bonded case, as shown in Fig. 4.19 and 4.20.

Changes in the external tendon stress increased at slightly different rates with mid-span displacement as shown in Fig. 4.21. The rate was slightly higher for the fully-bonded case than the partially-bonded case. The maximum increase in the external tendon stress was much higher and at a higher maximum displacement for the fully-bonded case than the partially-bonded case.

Joint openings at the critical positive moment joint and the support joint increased at a higher rate with displacement for the partially-bonded case than the fully-bonded case as shown in Fig. 4.22 and 4.23. Maximum cumulative joint opening in the positive moment region was higher and occurred at a higher load for the fully-bonded case as shown in Fig. 4.24.

The ultimate loading cycle for the partially-bonded case was controlled by stiffness of the structure, while the strength test of the fully-bonded case was controlled by concrete crushing at the critical joint. The test data in Fig. 4.19 show that the maximum critical joint opening was the same for the two loading cycles at ultimate. However, the maximum critical joint opening for the fully-bonded case occurred at a much higher load, as shown in Fig. 4.19, and much higher displacement, as shown in Fig. 4.22.

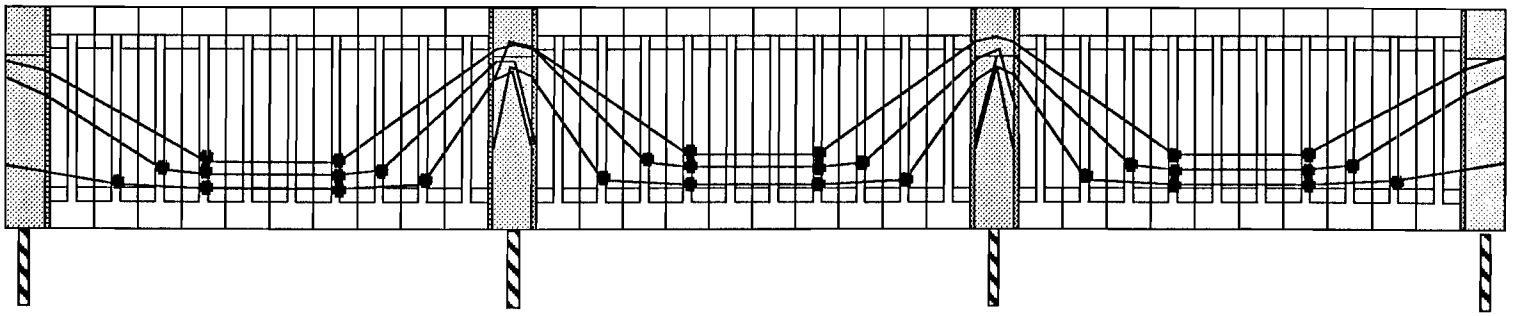

a) 2 or 4 diaphragms bonded in each span

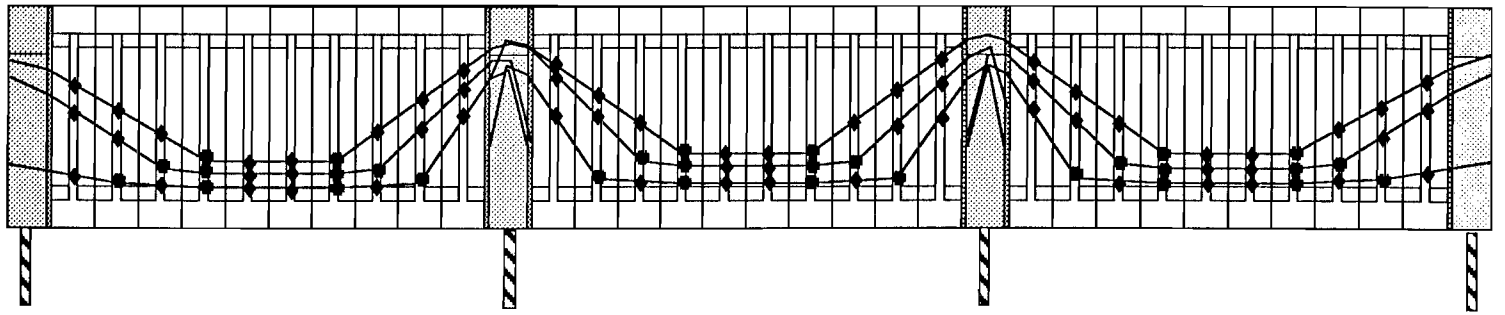

b) 10 diaphragms bonded in each span

● : Diaphragm Originally Bonded

♦ : Diaphragm Bonded Later

Figure 4.16 Bonding conditions of external tendons for flexural strength tests.

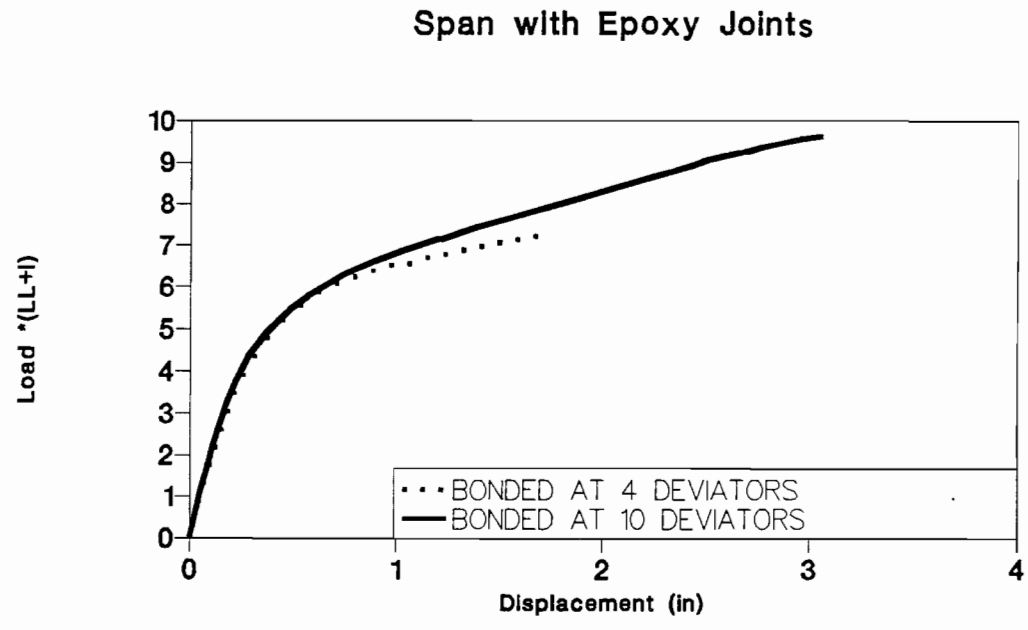

Figure 4.17 Effect of bonding on load-deflection response during flexureal strength tests on epoxy joints span.

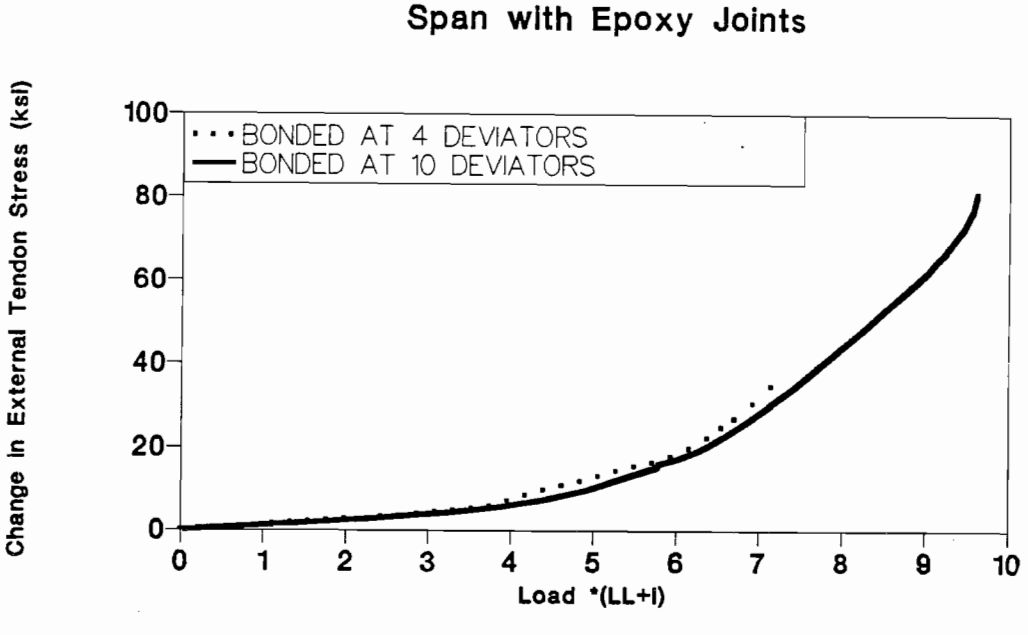

Figure 4.18 Effect of bonding on tendon stress-load response during flexural strength tests on epoxy joints span.

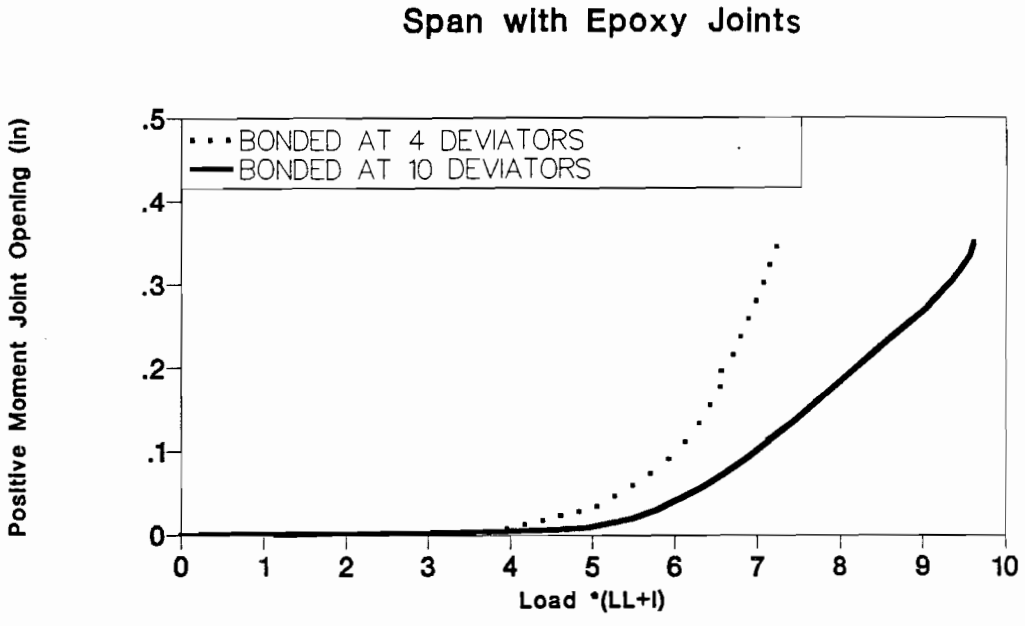

Figure 4.19 Effect of bonding on positive moment joint opening-load for flexural strength tests of epoxy joints span.

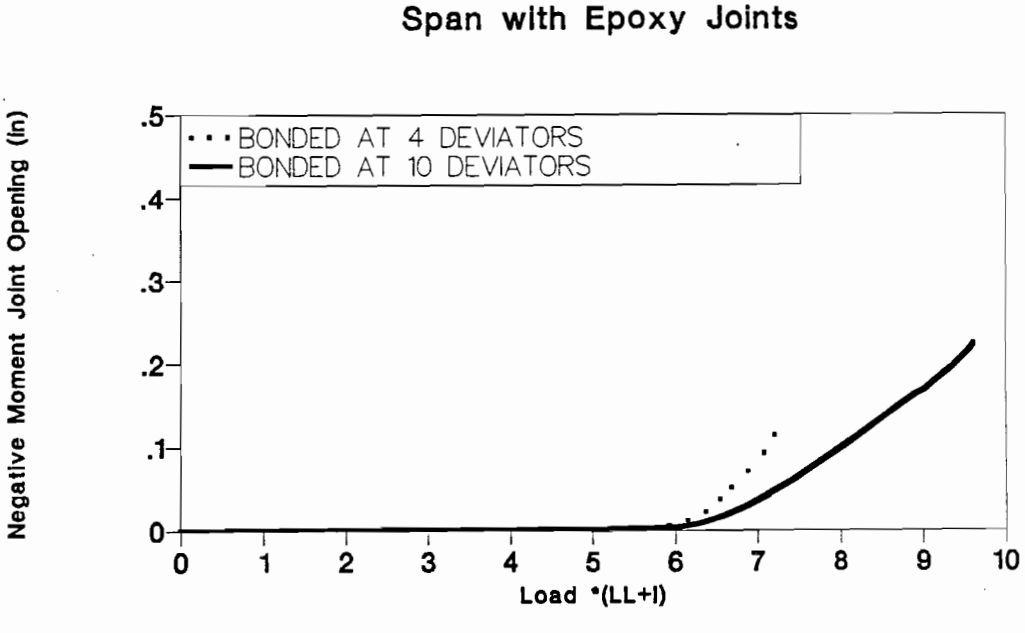

Figure 4.20 Effect of bonding on negative moment joint opening-load for flexural strength tests of epoxy joints span.

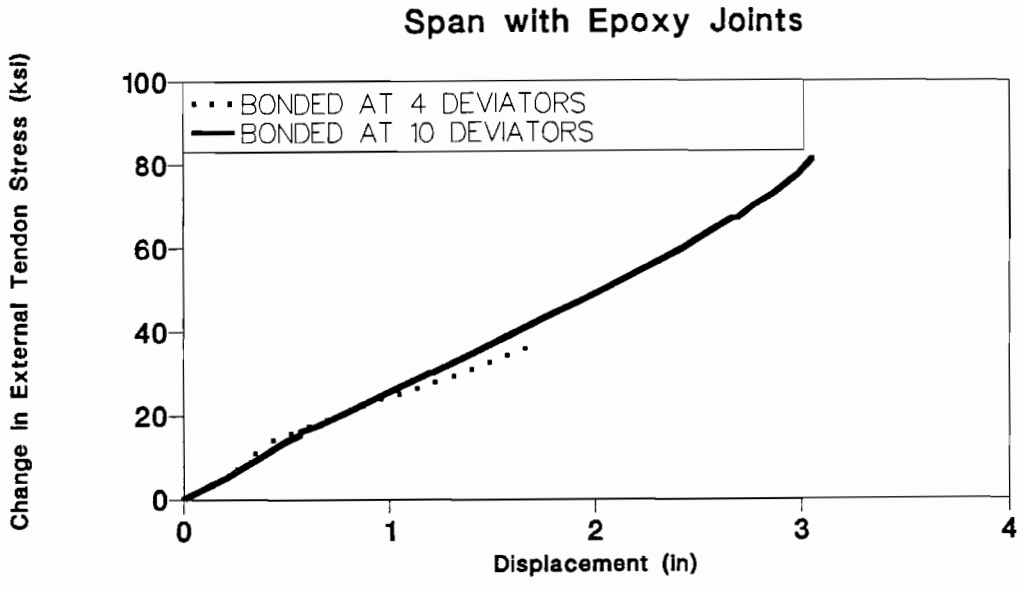

Figure 4.21 Effect of bonding on tendon stress-displacement for flexural strength tests of epoxy joints span.

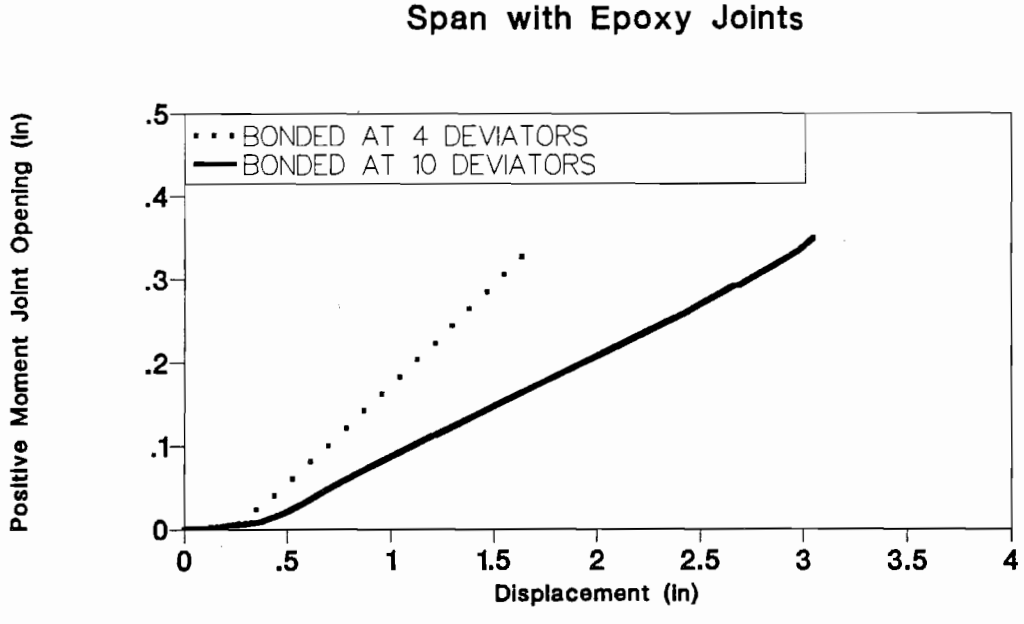

Figure 4.22 Effect of bonding on positive moment joint opening-displacement for flexural strength tests of epoxy joints span.

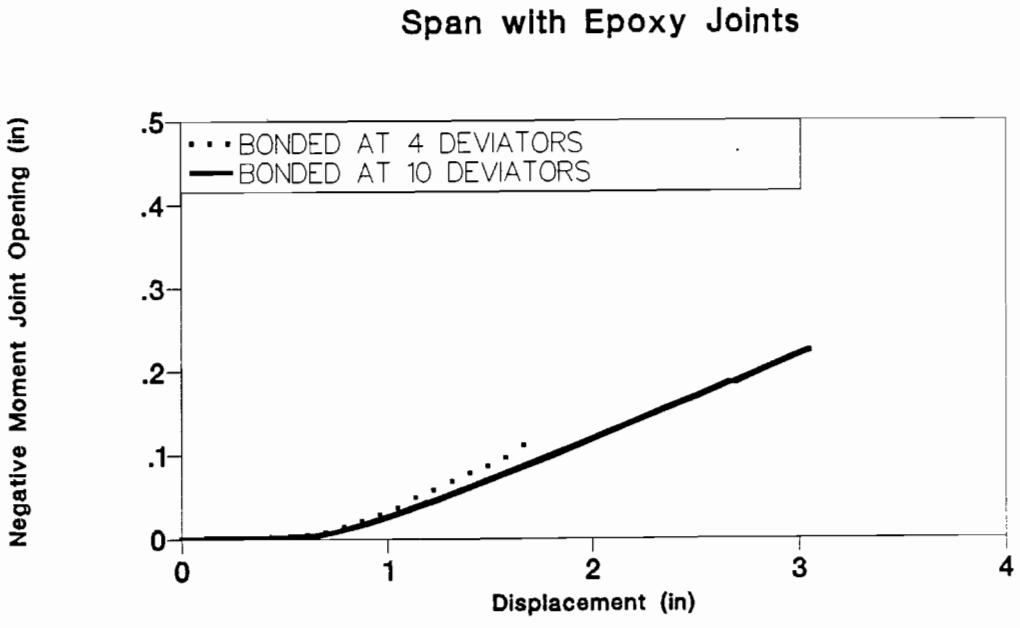

Figure 4.23 Effect of bonding on negative moment joint opening - displacement for flexural strength tests of epoxy joints span.

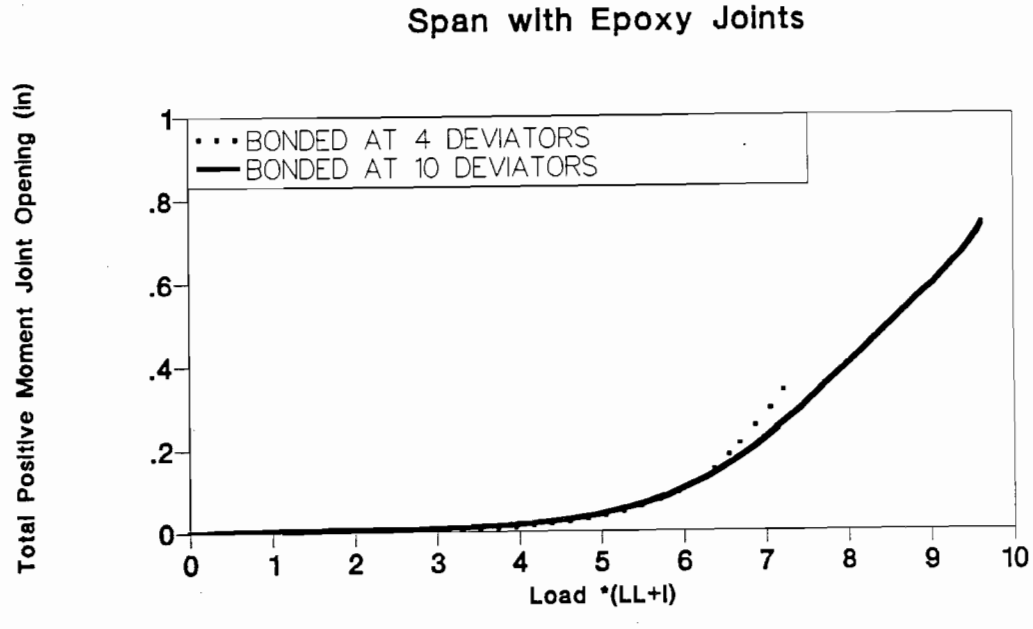

Figure 4.24 Effect of bonding on total positive moment joint opening for flexural strength tests of epoxy joints span.

Figure 4.24 shows that the maximum cumulative joint opening in the positive moment region was higher for the fully-bonded case. Higher cumulative joint opening in the positive moment region for the fully-bonded case was due to the greater number of joints which opened. Joints (25,26), (26,27), and (27,28) opened for the fully-bonded case while only joint (25,26) opened for the partially-bonded case.

A higher cumulative joint opening translates to greater changes in external tendon length. The effective external tendon unbonded length was reduced due to bonding of the tendon. Greater changes in tendon length with shorter unbonded lengths resulted in higher tendon stress and higher moment capacity at the critical joint. Critical-joint moment capacity was the key factor effecting strength so that any increase in moment capacity of the critical joint would result in higher strength of the model. Higher ductility in the fully-bonded case was due to higher cumulative joint opening which resulted in greater displacement of the structure at failure of the critical joint.

4.2.2.2 Dry Joints Span. The dry joints span was loaded to ultimate for two different conditions of bonding of external tendons to the diaphragms. The bonding conditions are shown in Fig. 4.16(a) and (b). The first bonding condition was the as-built model (1). The external tendons were locally bonded to the pier segments and to a maximum of four interior deviators in each span. This case will be called the partially-bonded case. In the second case, the external tendons were locally bonded to all ten diaphragms in each span. This will be called the fully-bonded case.

Strength and ductility were substantially higher in the dry joints span with fully-bonded external tendons than the partially-bonded case as shown in Fig. 4.25. Stiffness of the model after the critical positive moment joint opened was higher for the fully-bonded case. Changes in external tendon stress with load varied slightly with the external tendon bonding conditions, but the maximum change in tendon stress was higher and occurred at a higher load for the fully-bonded case as shown in Fig. 4.26.

The maximum critical joint opening for the fully bonded case was higher than for the partially-bonded case. The strength test for the partially-bonded case was controlled by the stiffness of the model, while the flexural test for the fully-bonded case was controlled by crushing of the top flange concrete at the critical joint. The joint opening rate at the critical joint and the support joint was higher for the partially-bonded case than the fully-bonded case, as shown in Fig. 4.27 and 4.28.

Changes in external tendon stresses increased at different rates with displacement, as shown in Fig. 4.29. The rate was higher for the fully-bonded case than the partially-bonded case. The maximum increase in external tendon stress was much higher for the fully-bonded case than the partially-bonded case.

Joint openings at the critical positive moment joint and support joint increased at a higher rate with displacement for the partially-bonded case than the fully-bonded case as shown in Fig. 4.30 and 4.31.

The ultimate strength loading cycle for the fully-bonded case was controlled by crushing of concrete at the critical positive moment joint. The test data in Fig. 4.27 show that the maximum critical joint opening was different for the two loading cycles primarily because the test for the partially-bonded case was discontinued before the crushing of the joint initiated.

Figure 4.32 shows that the maximum cumulative joint opening in the positive moment region was higher for the fully-bonded case. Higher cumulative joint opening in the positive moment region for the fully-bonded case was due to the greater number of joints that opened. Joints (3,4), (4,5), and (5,6) opened for the fully-bonded case, while only joints (4,5) and (5,6) opened for the partially-bonded case.

A higher cumulative joint opening means a greater change in external tendon length. Higher change in tendon length over shorter unbonded tendon length caused by more discrete bonding resulted in higher tendon stresses and higher moment capacity at the critical joint. Critical joint moment capacity has direct influence on the structure strength, so any increase in moment capacity of the critical joint would increase the strength of the model. Higher ductility for the fully-bonded case was due to the higher cumulative joint opening which resulted in greater displacement of the structure at failure of the critical joint.

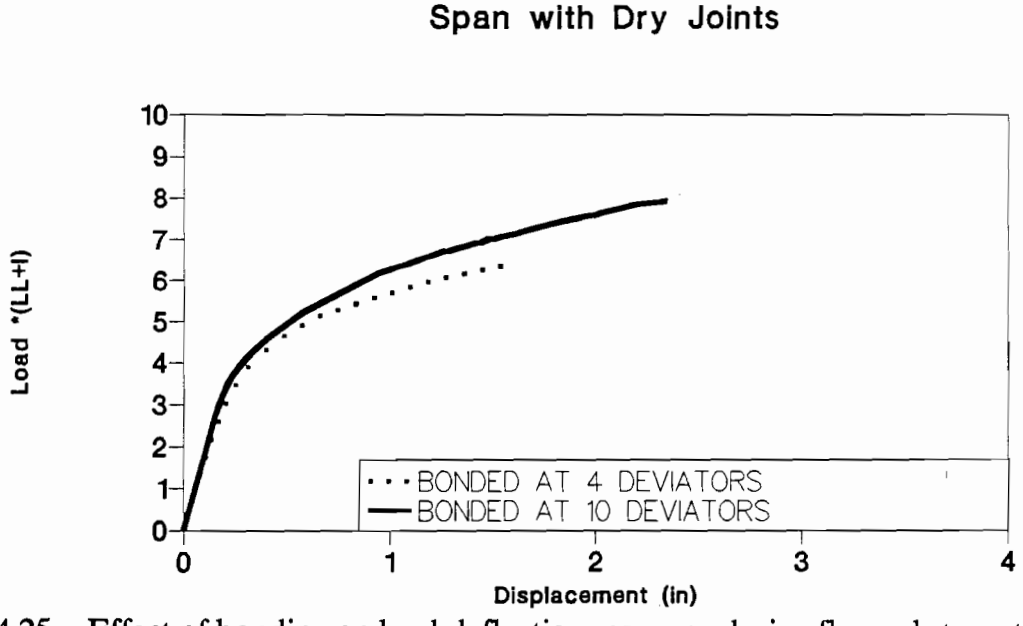

Figure 4.25 Effect of bonding on load-deflection response during flexural strength tests of dry joints span.

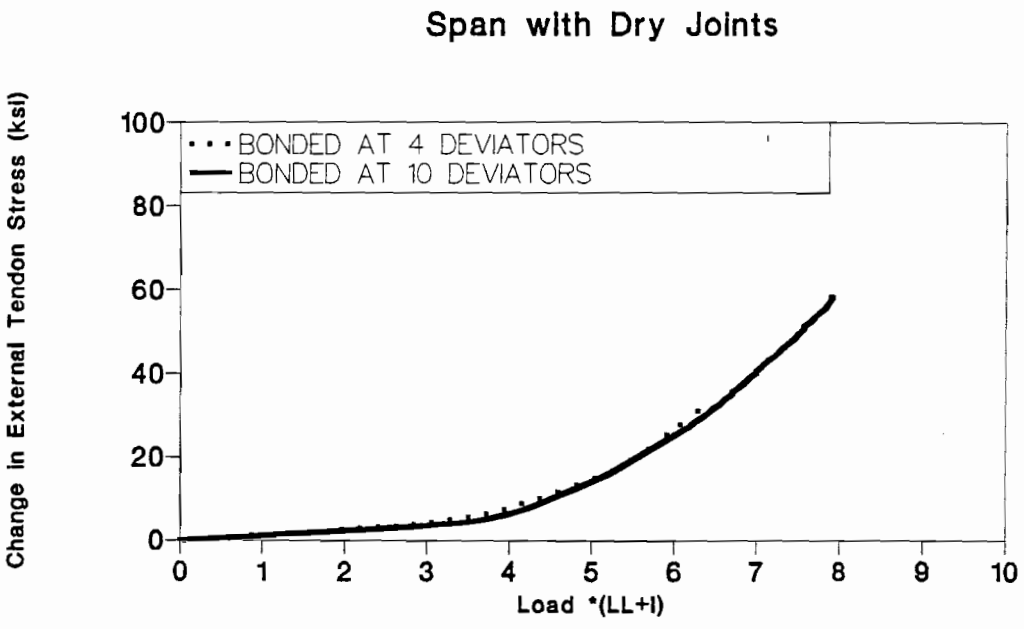

Figure 4.26 Effect of bonding on tendon stress-load during flexural strength tests of dry joints span.

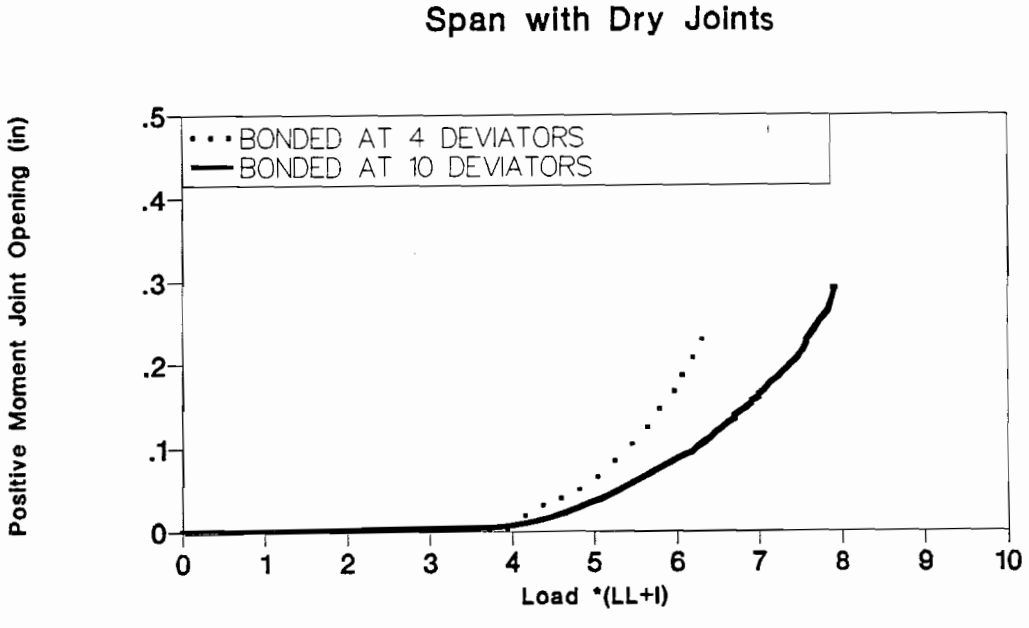

Figure 4.27 Effect of bonding on positive moment joint opening-load response for flexural strength tests of dry joints span.

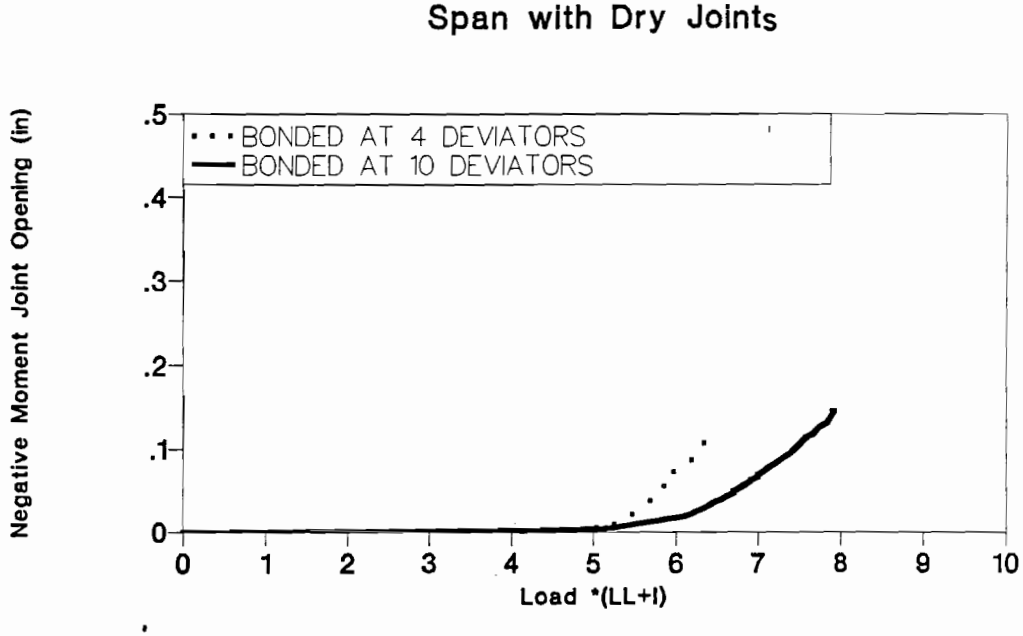

Figure 4.28 Effect of bonding on negative moment joint opening-load for flexural strength tests of dry joints span.

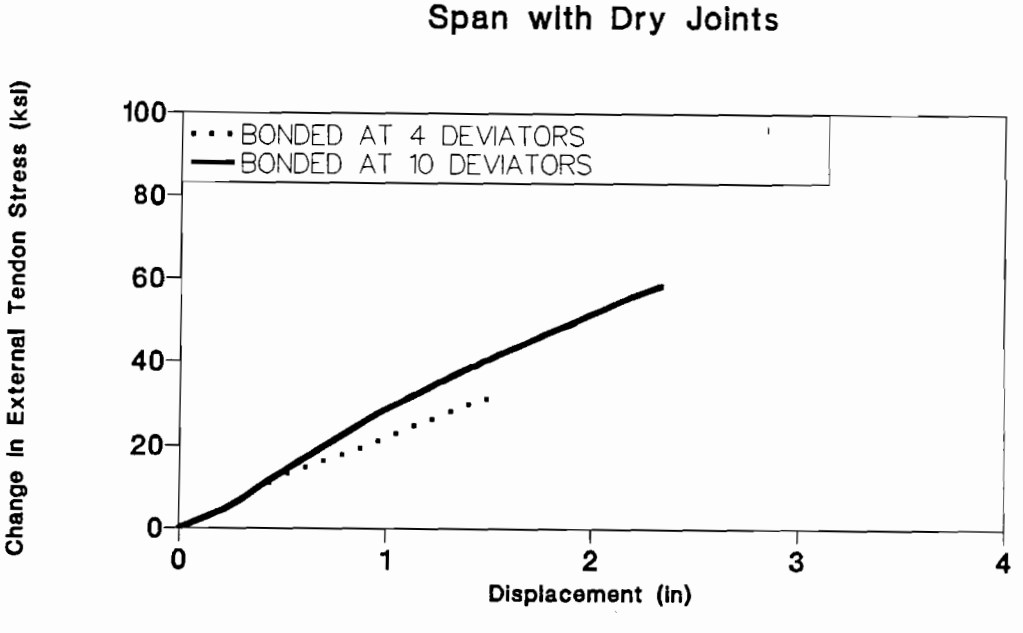

Figure 4.29 Effect of bonding on tendon stress-displacement for flexural strength tests of dry joints span.

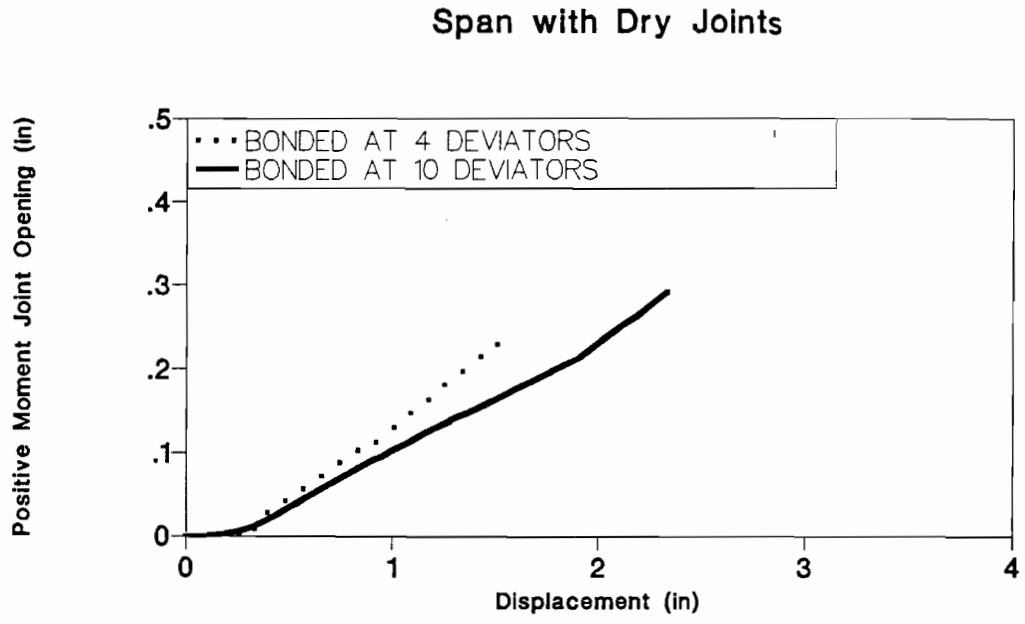

Figure 4.30 Effect of bonding on positive moment joint opening-displacement for flexural strength tests of dry joints span.

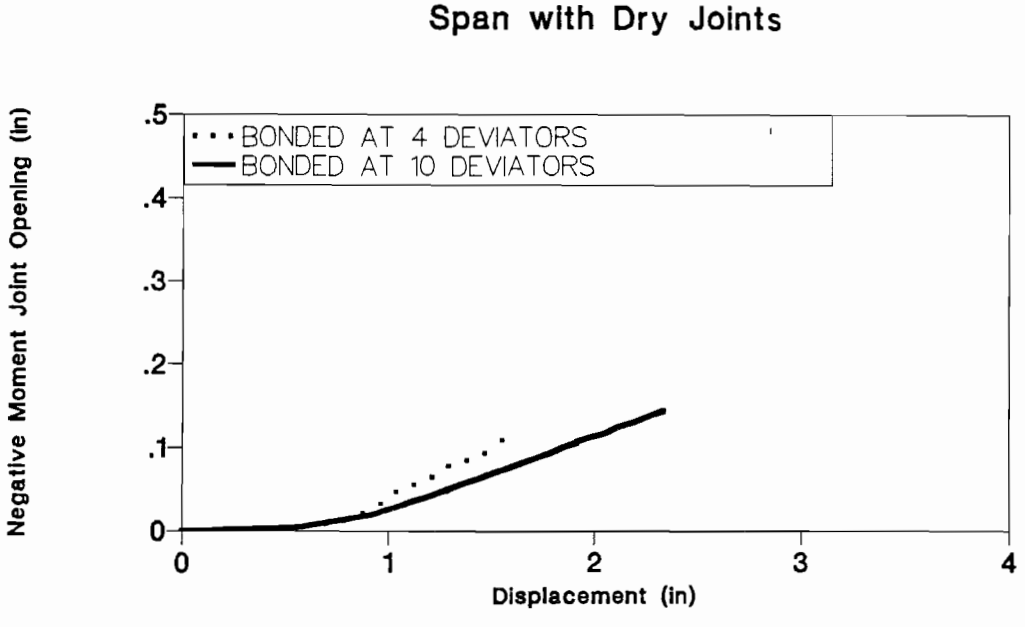

Figure 4.31 Effect of bonding on negative moment joint opening-displacement for flexural strength tests of dry joints span.

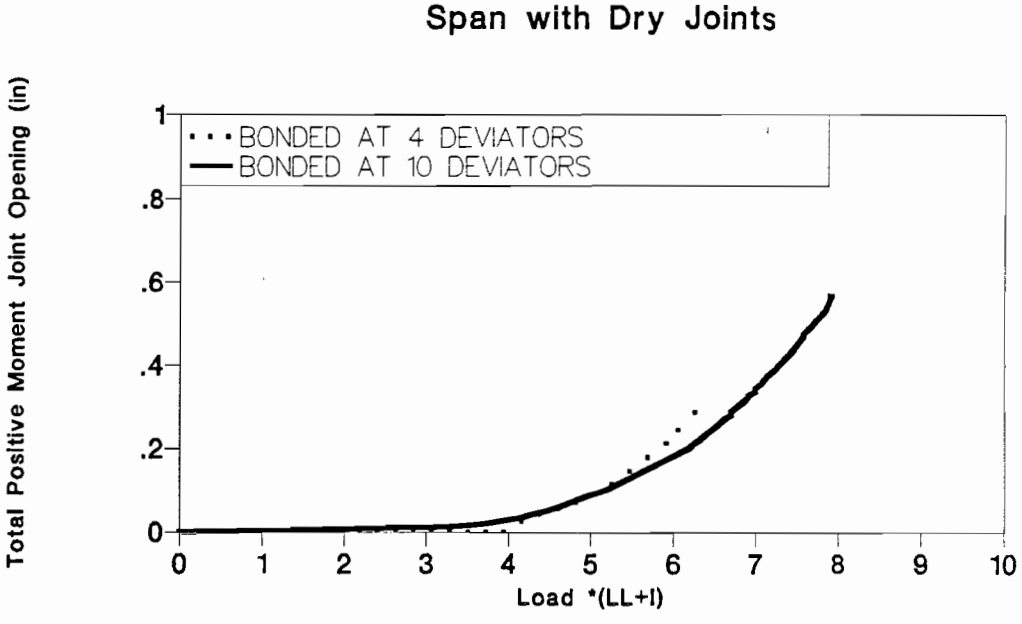

Figure 4.32 Effect of bonding on total positive moment joint opening for flexural strength tests of dry joints span.

4.2.2.3 Observations. Additional bonding of external tendons at all intermediate diaphragms increased the strength and ductility by increasing the number of joints/cracks opened during loading of the model. The epoxy joints span strength was increased by 35 percent while the ductility was increased by 75 percent. The dry joints span strength was increased by 23 percent while the ductility was increased by 47 percent. The number of opened joints increased due to two effects of bonding. The first effect, dividing the external tendons into shorter elements by locally bonding the tendons at the intermediate diaphragms caused a higher increase in tendon stresses at the critical joint and reduced the tendon stresses at the surrounding joints. This reduced the moment required to open the adjacent joints. The second effect, local bonding of the external tendons increased the critical joint stiffness and strength which resulted in higher moments at the critical positive moment region and in delaying the crushing of the critical joint. These two effects increased the number of opened joints and increased the adjacent joint openings. A greater number of opened joints resulted in higher total joint opening in the critical region.

Higher total joint opening increased the change in tendon length. In addition, the unbonded tendon length was reduced by bonding the tendon at the intermediate diaphragms. Higher change in tendon length over shorter unbonded length caused a larger increase in tendon stress which resulted in higher ultimate strength. Higher total joint opening increased the ultimate displacement of the structure.

Bonding of external tendons was more effective in the epoxy joints span than in the dry joints span. This difference was due to the fact that bonding increased the number of opened joints (in the positive moment region) in epoxy joints span from one in the partially-bonded case to three in the fully-bonded case. Bonding increased the number of opened joints in the dry joints span from two in the partially-bonded case to three in the fully-bonded case. The cracking moment for an epoxy joint is higher than the joint opening moment for a dry joint. This increased the need for full bonding of external tendons in the epoxy joint span to open the adjacent joints, while the partially bonded case was enough to open a second joint in the dry joints span.

4.3 Effect of Supplemental Internal Tendons

Four 3/8" diameter internal tendons were added to the bottom flange of the model after the supplemental bonding tests were completed. The additional prestress steel area provided about an 11 percent increase in the total prestress steel area. Two ultimate load cycles were carried out on each of the exterior spans after stressing the four internal tendons. One test cycle was carried out before grouting the internal tendons, and the second cycle was carried out after grouting the internal tendons in the bottom flange of the model.

4.3.1 Effect of Ungrouted Internal Tendons. Differences in model behavior after adding the four ungrouted internal tendons to the bottom flange of the model were very small due to the fact that the internal tendons added only 11 percent to the total prestress steel area.

4.3.1.1 Dry Joints Span. Figures 4.33 through 4.40 show the effect of adding the ungrouted internal tendons on the behavior of the model. Strength and moment were increased by adding the internal tendons as shown in Fig. 4.33 and Fig. 4.34 due to the higher effective prestress. The critical joint started opening at higher loads, as shown in Fig. 4.37 which delayed the increase in external tendon stress as shown in Fig. 4.35. Figure 4.36 shows that the increase in the ungrouted tendon stress was very small due to the long unbonded length of the internal tendons. The support joint started opening at a higher load, and the maximum opening was slightly higher, as shown in Fig. 4.39.

Maximum total joint opening in the positive moment region was reduced by using ungrouted internal tendons, as shown in Fig. 4.40. The reduction in total joint opening was due to the reduction in opening of the joints adjacent to the critical joint as shown in Fig. 4.38. The maximum critical joint opening was also slightly less due to the higher compressive force. This reduction in total joint opening in the critical region reduced the maximum change in the external tendon stress as shown in Fig. 4.35. The reduction in the opening of the adjacent joints was due to the internal tendon stress at these joints which increased the moment required to open the joints and to increase their openings.

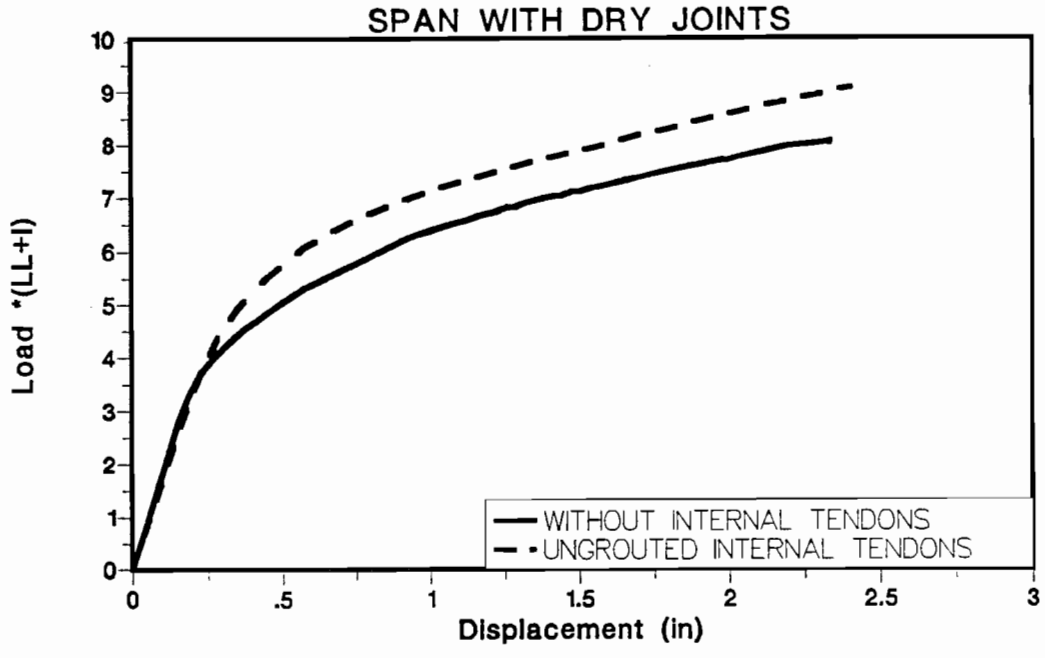

Figure 4.33 Ungrouted internal tendon effect on load-deflection response of dry joints span.

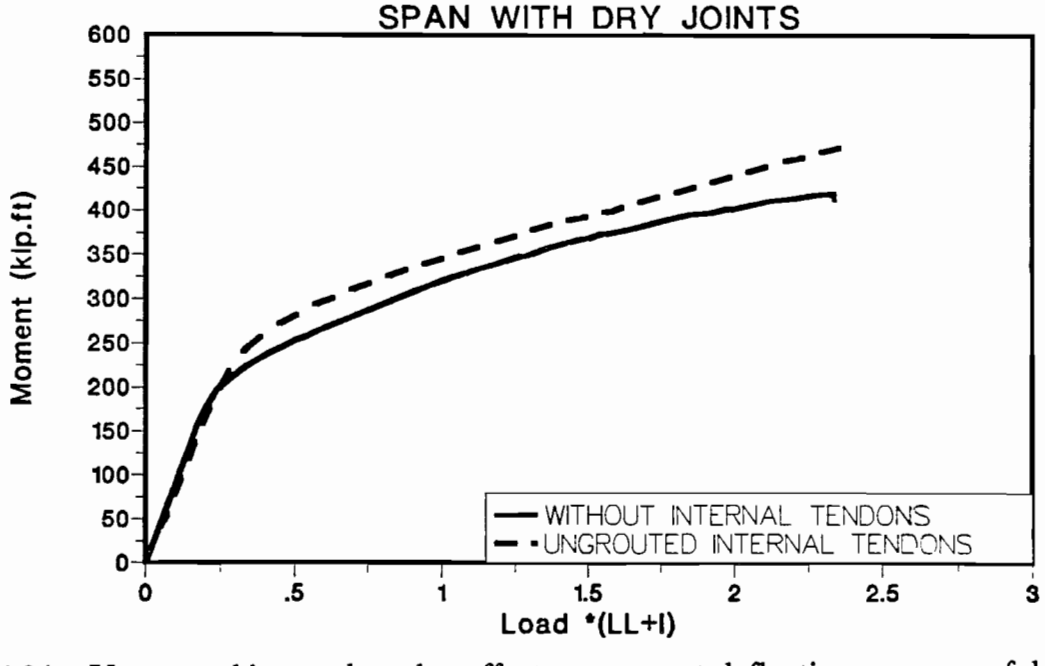

Figure 4.34 Ungrouted internal tendon effect on moment-deflection response of dry joints span.

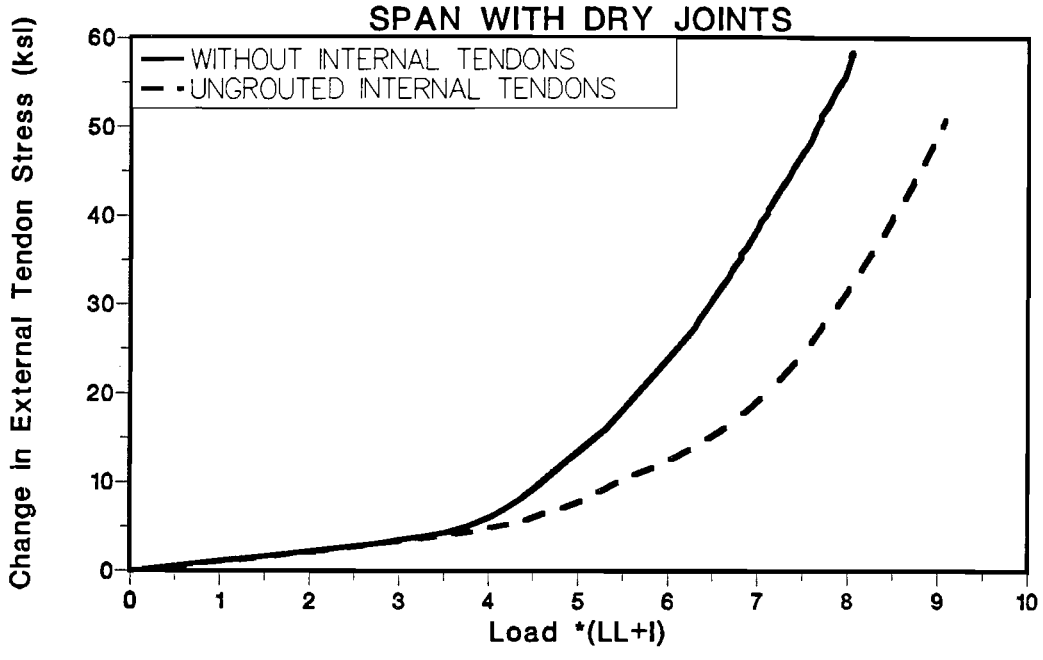

Figure 4.35 Ungrouted internal tendon effect on tendon stress-load for dry joints span.

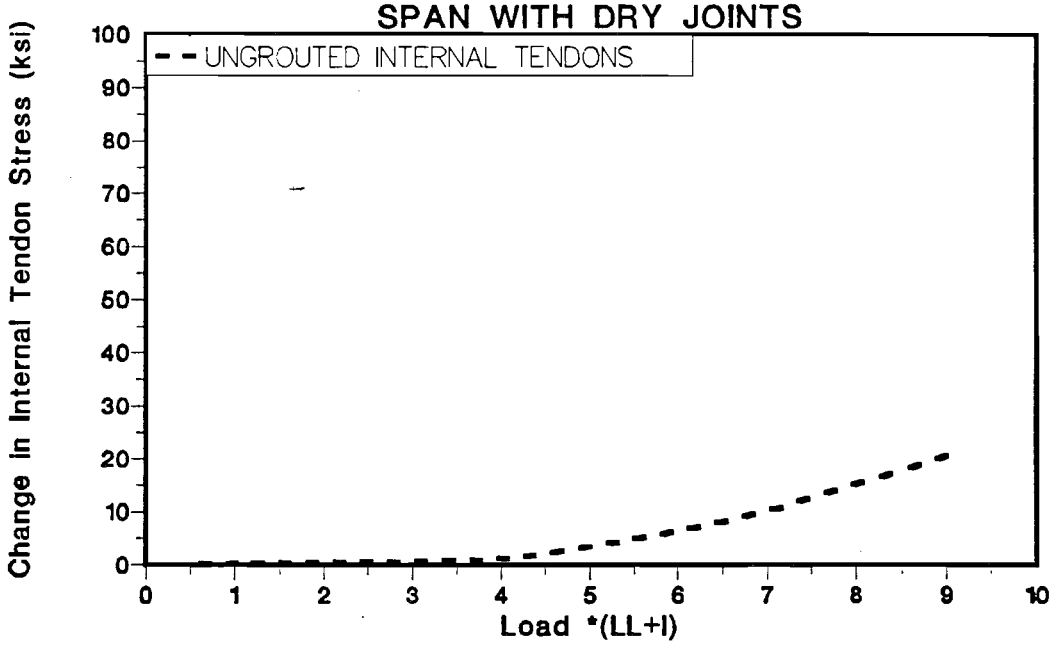

Figure 4.36 Ungrouted internal tendon effect on internal tendon stress-load for dry joints span.

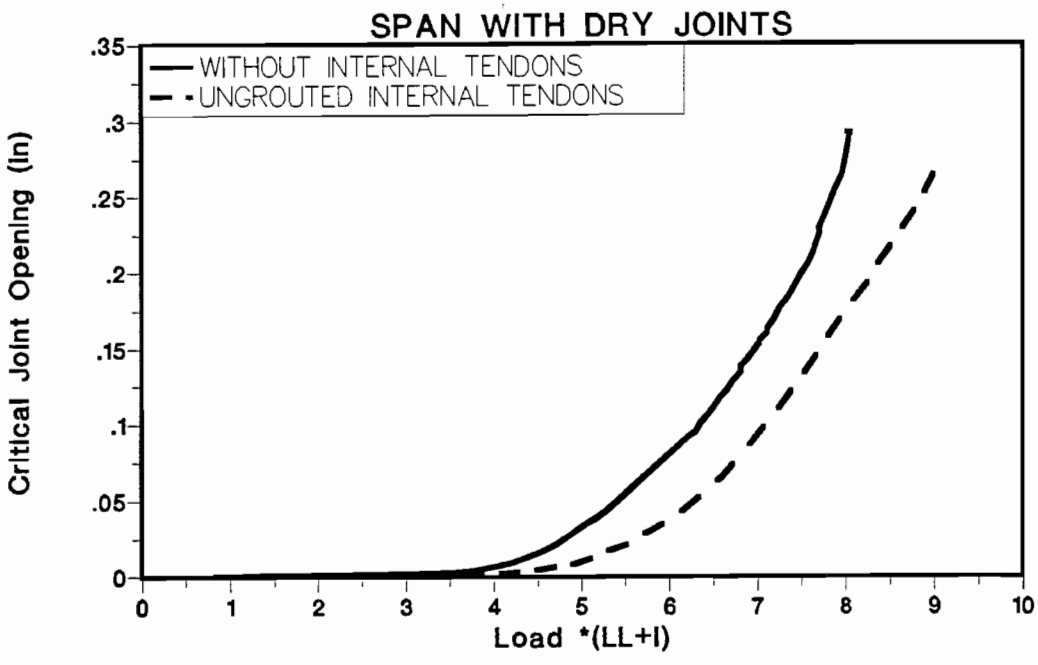

Figure 4.37 Ungrouted internal tendon effect on critical joint opening-load for dry joints span.

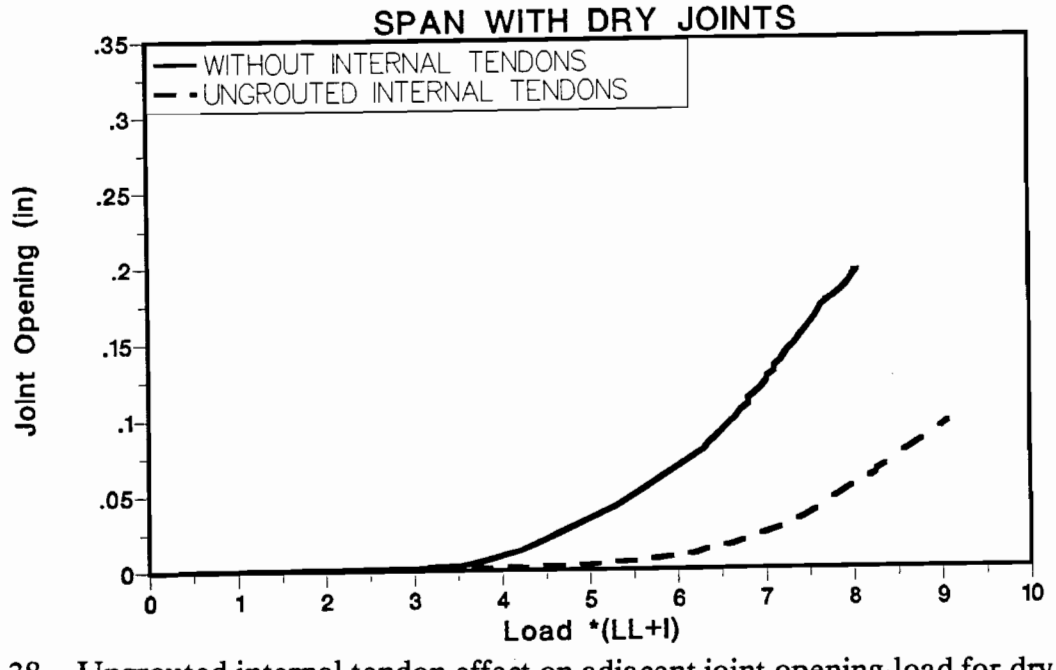

Figure 4.38 Ungrouted internal tendon effect on adjacent joint opening-load for dry joints span.

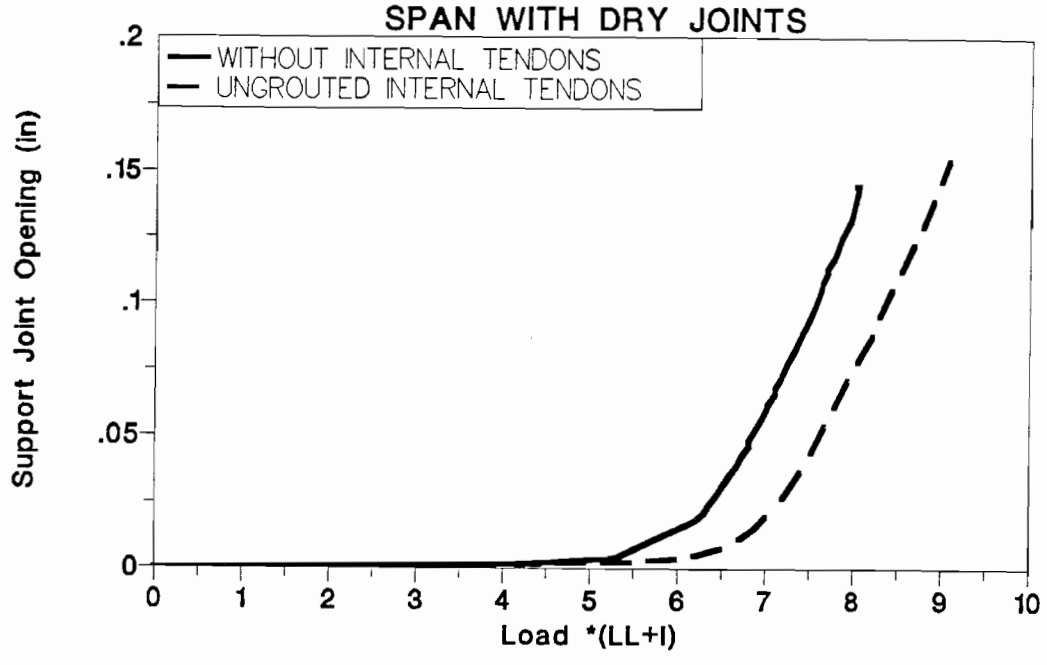

Figure 4.39 Ungrouted internal tendon effect on support joint opening-load for dry joints span.

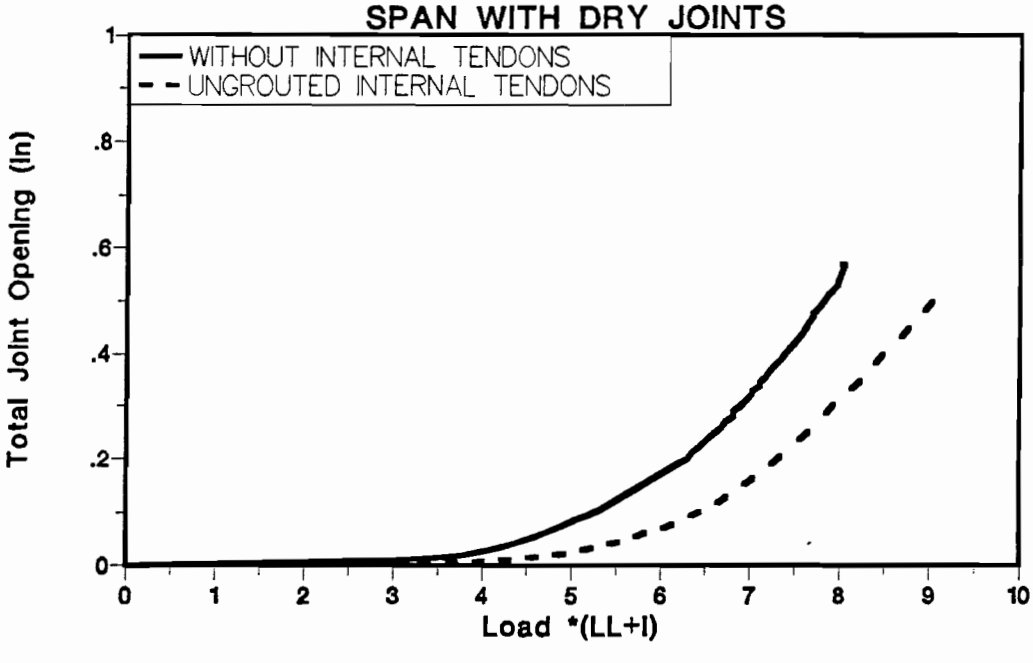

Figure 4.40 Ungrouted internal tendon effect on total joint opening-load for dry joints span.

The reduction in total joint opening in the critical region should result in lower ductility, however, the maximum deflection was slightly higher for the case with internal tendons. The increase in maximum deflection was due to loading of the structure to a greater crushing of the critical joint in the ungrouted internal tendons test than in the first test (without internal tendon test) where loading was stopped to prevent collapse.

4.3.1.2 Epoxy Joints Span. Figures 4.41 through 4.48 show the effect of adding the ungrouted internal tendons on the behavior of the epoxy joints exterior span of the model. Strength and moment were increased by adding the internal tendons, as shown in Fig. 4.41 and Fig. 4.42 due to higher effective prestress force. The critical positive moment joint started opening at a higher load, as shown in Fig. 4.45, which delayed the increase in external tendon stress as indicated in Fig. 4.43. The support joint started opening at a higher load, but the maximum opening was about the same, as shown in Fig. 4.47. Figure 4.44 shows that the increase in the ungrouted tendon stress was very small due to long unbonded length.

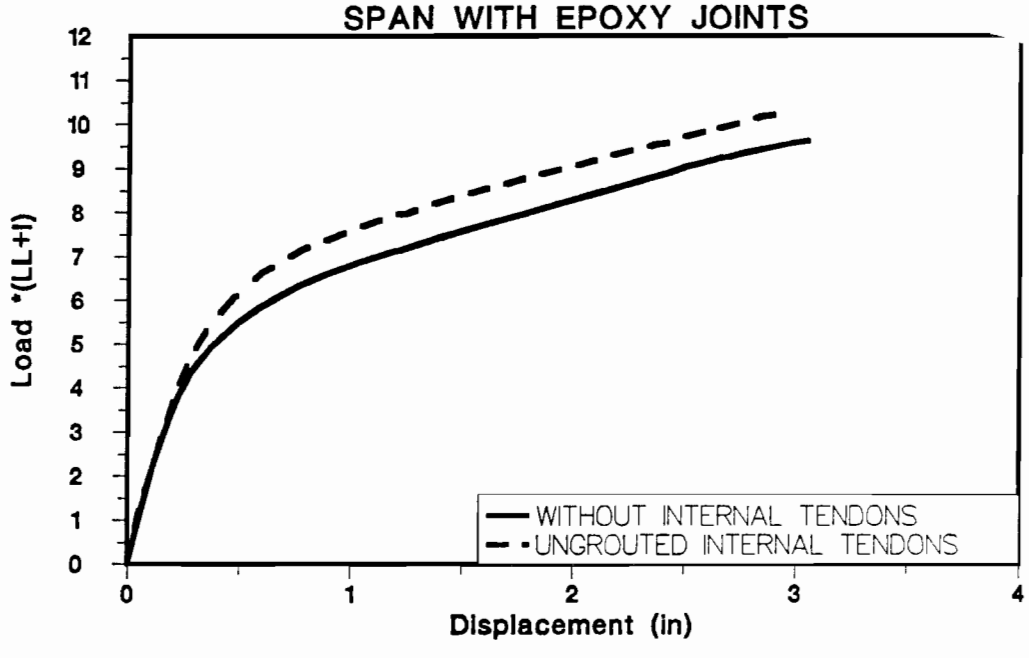

Figure 4.41 Ungrouted tendon effect on load-deflection response of epoxy joints span.

Maximum total joint opening in the positive moment region was reduced by adding ungrouted internal tendons, as shown in Fig. 4.48. The reduction in total joint opening was due to reduction in opening of the joints adjacent to the critical joint, as shown in Fig. 4.46. This reduced the maximum change in external tendon stress, as shown in Fig. 4.43. The reduction in the openings of the adjacent joints was due to the internal tendon stress at these joints, which increased the moment required to open the joints and to increase their openings. Maximum deflection was reduced due to the reduction in total joint opening.

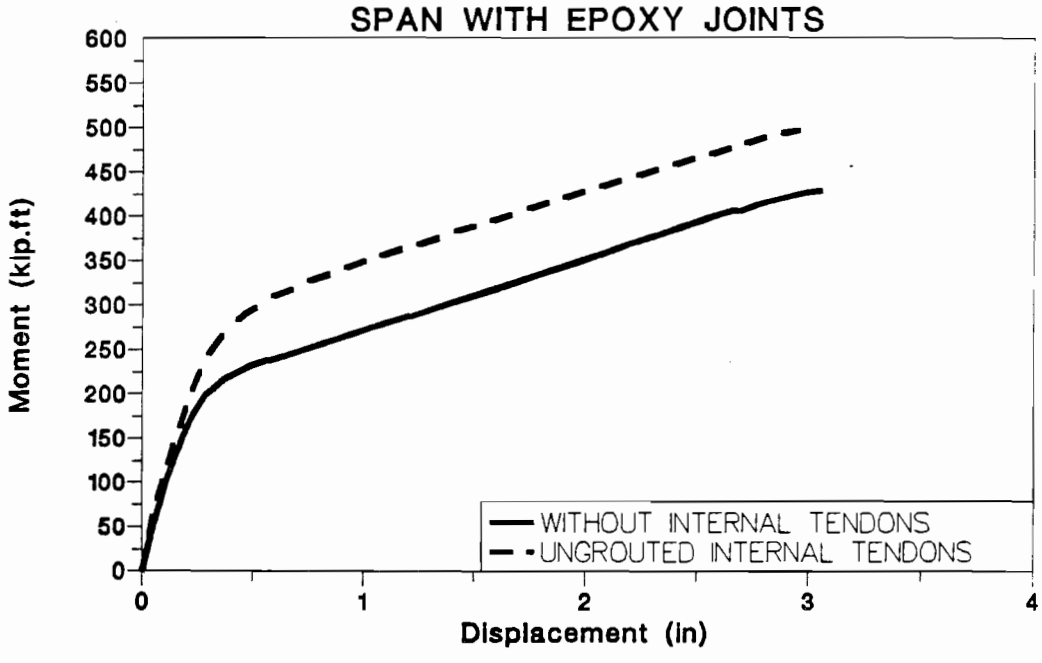

Figure 4.42 Ungrouted tendon effect on moment-deflection response of epoxy joints span.

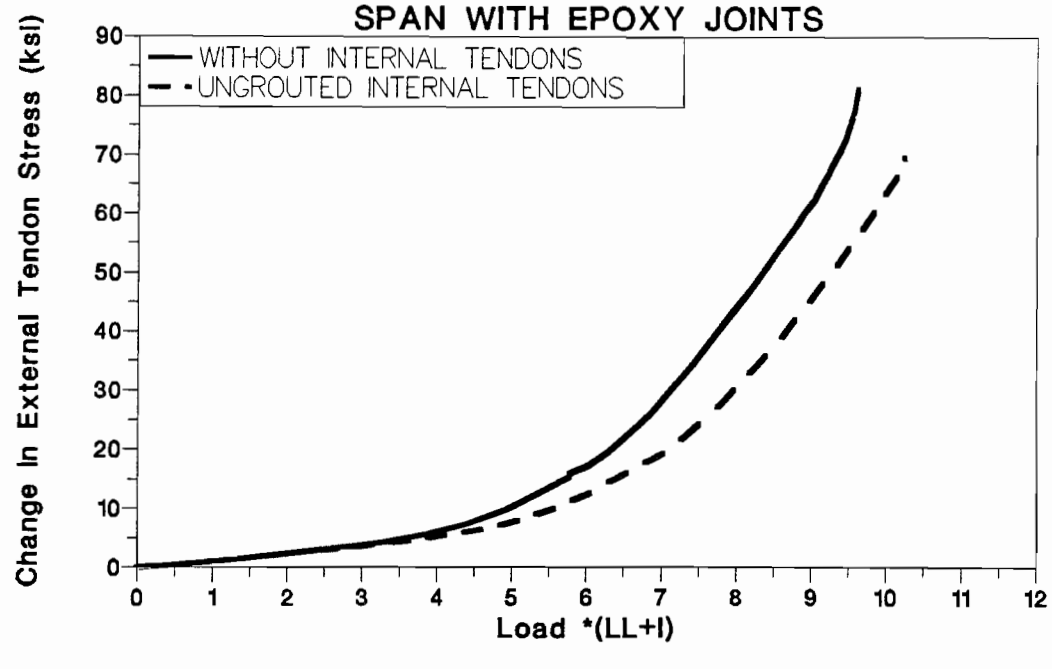

Figure 4.43 Ungrouted tendon effect on tendon stress-load for epoxy joints span.

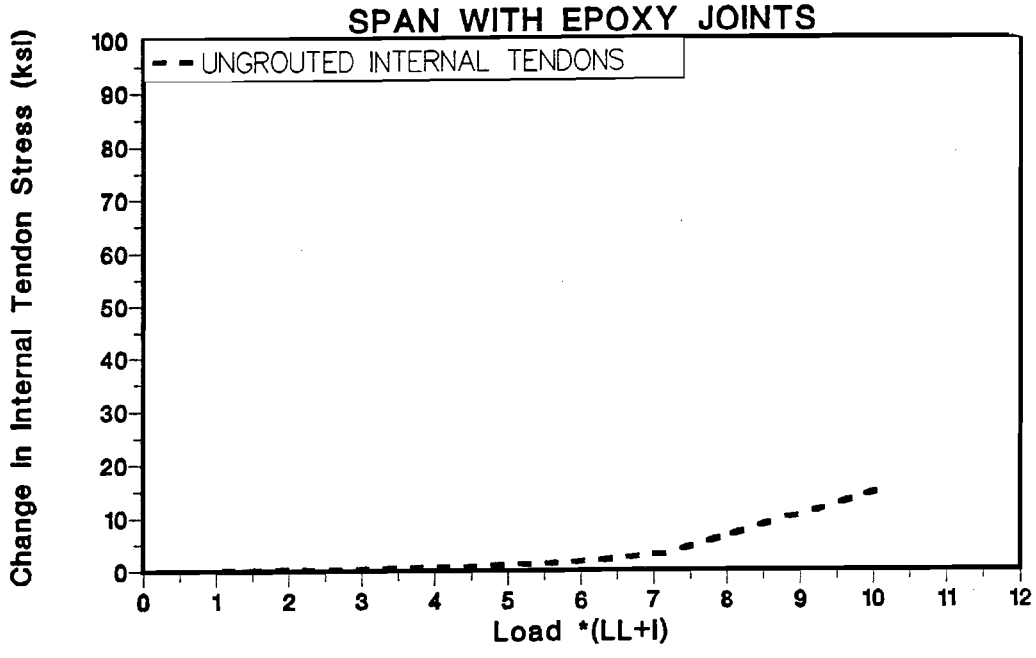

Figure 4.44 Ungrouted tendon effect on internal tendon stress-load for epoxy joints span.

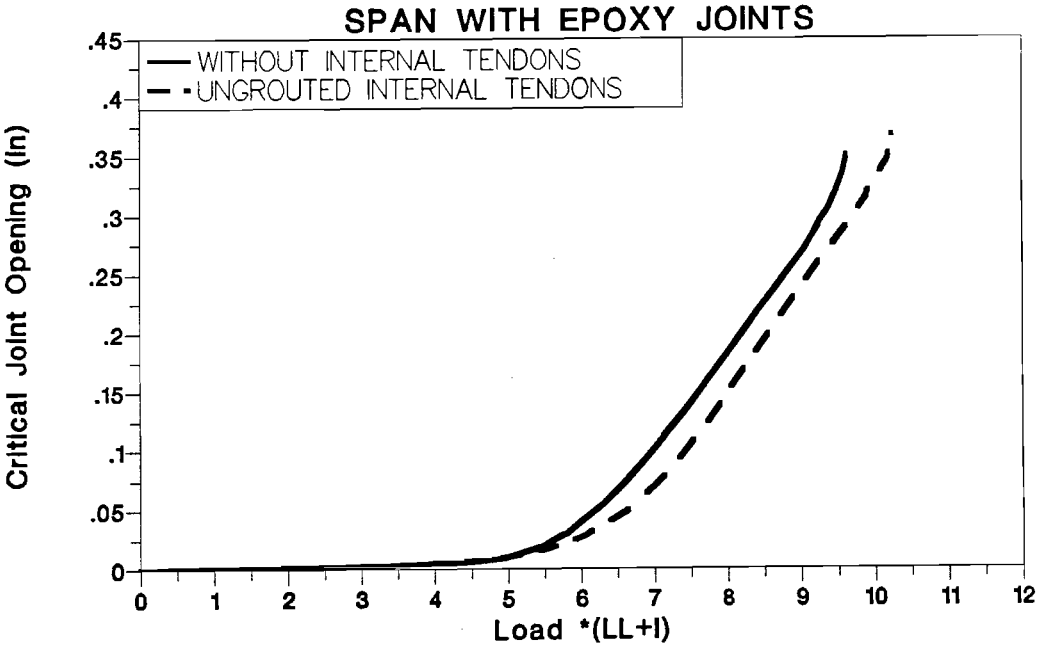

Figure 4.45 Ungrouted tendon effect on critical joint opening-load for epoxy joints span.

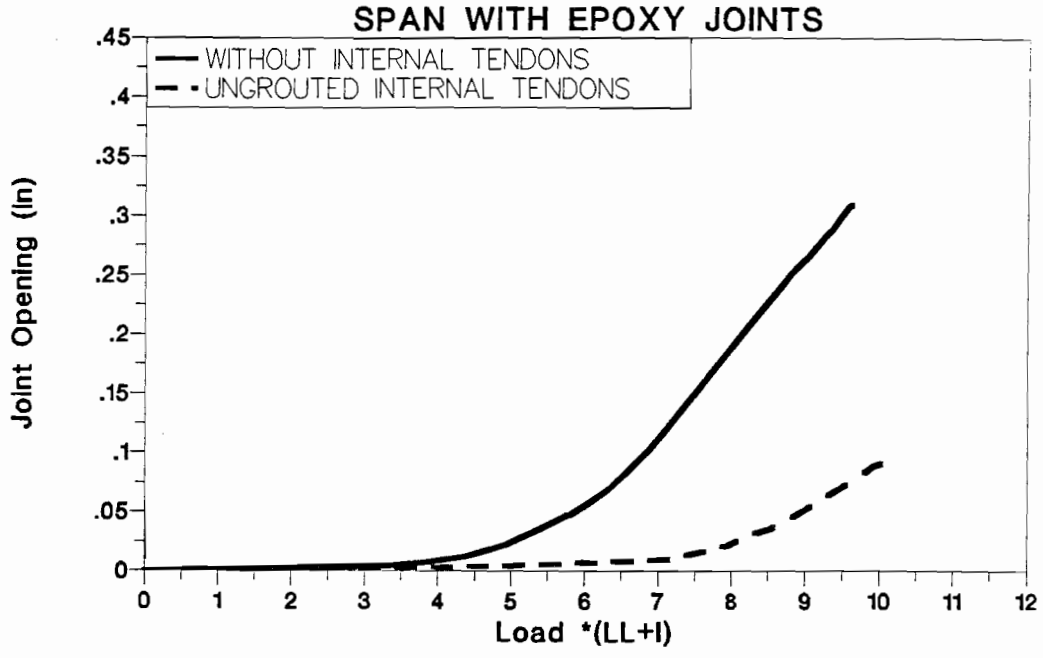

Figure 4.46 Ungrouted tendon effect on adjacent joint opening-load for epoxy joints span.

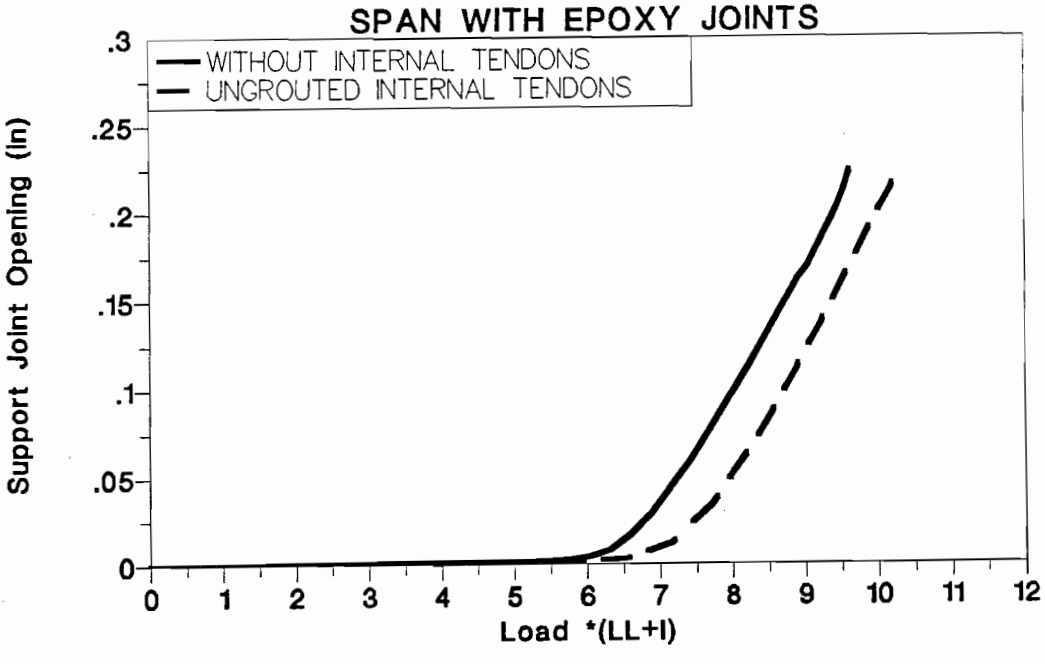

Figure 4.47 Ungrouted tendon effect on support joint opening-load for epoxy joints span.

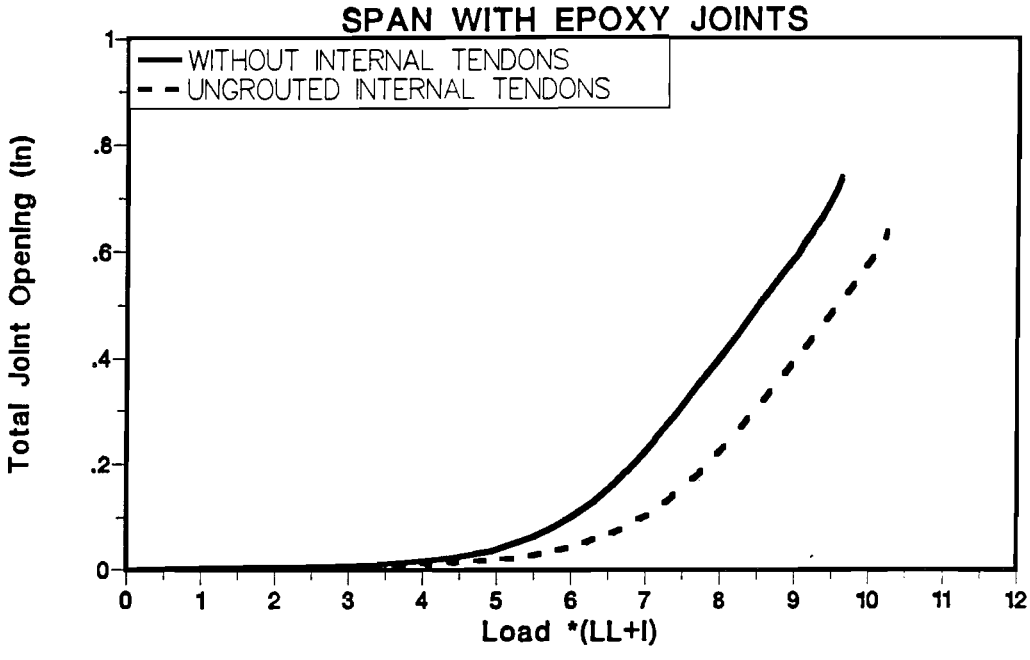

Figure 4.48 Ungrouted tendon effect on total joint opening-load for epoxy joints span.

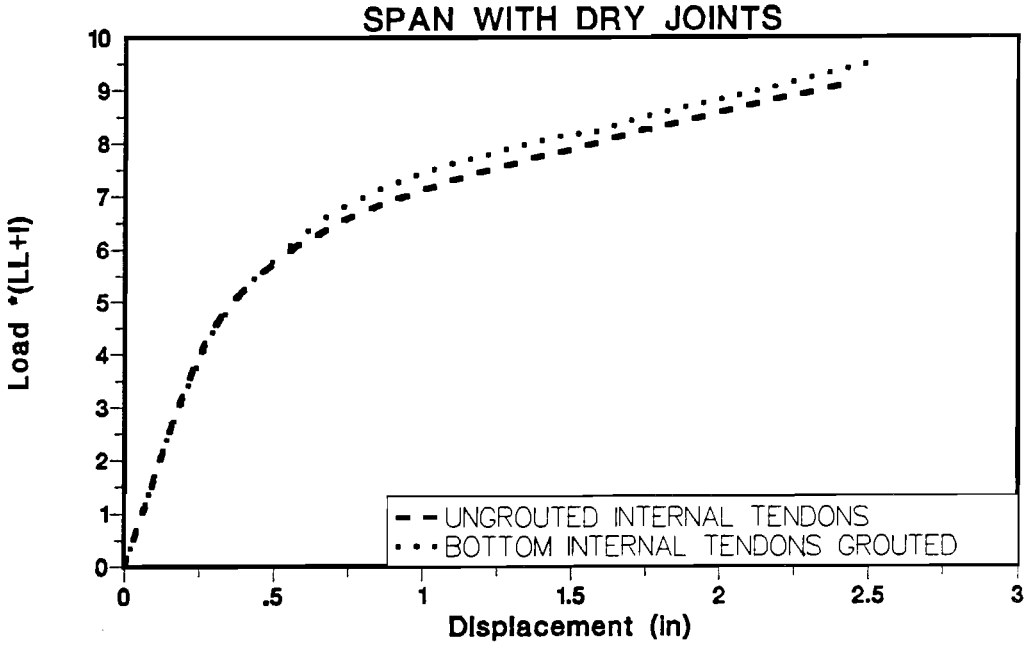

Figure 4.49 Grouted tendon effect on load-deflection response of dry joints span.

4.3.1.3 Observations. The addition of ungrouted internal tendons increased the strength of the model as a result of higher prestress, but reducedits ductility slightly. The ungrouted internal tendons behaved similar to unbonded external tendons. This means that the stress in the ungrouted internal tendons was approximately the same at the critical joint and at surrounding joints. As a result, the moment required to open a second joint was increased. This delayed the opening of adjacent joints and reduced their maximum opening at failure which resulted in lower total joint opening in the critical positive moment region. Lower total joint opening resulted in lower change in external tendon stress and lower maximum displacement at failure.

Adding ungrouted internal tendons increased strength by 14 percent in the dry joints span and by 6 percent in the epoxy joints span. This difference was due to the fact that the additional effective prestress in the dry joints span was higher due to its lower initial effective prestress (see Chapter Two).

4.3.2 Effect of Grouting Internal Tendons. One load cycle was carried out on each of the exterior spans after grouting the four internal tendons in the bottom flange.

4.3.2.1 Dry Joints Span. Figures 4.49 through 4.55 show the differences in the model behavior due to grouting of the internal tendons. Due to the small percentage (internal tendon made about 11 percent of the total prestress area) of grouted internal tendons as compared to the external tendons which were essentially fully bonded, differences in behavior were small. Strength and ductility were slightly higher in the grouted case as shown in Fig. 4.49 and Fig. 4.50. The maximum change in external tendon stress was a little higher in the grouted case as shown in Fig. 4.51. The change in the internal tendon stress was much higher in the grouted case as shown in Fig. 4.52 which shows that the internal tendon yielded before the critical joint crushed. The critical joint opening at failure was slightly less due to higher compression forces on the cross section, as shown in Fig. 4.53. The support joint opening was higher at the end of the test as shown in Fig. 4.54.

Although the maximum critical joint opening was slightly less in the grouted case, as shown in Fig. 4.53, the total joint opening in the positive moment region was slightly higher, as shown in Fig. 4.55 due to large opening in the joints adjacent to the critical joint. This increase in the total joint opening resulted in a greater increase in the external and internal tendon stresses which resulted in higher strength and higher deformation and ductility. Strength was higher due to higher internal and external tendon stresses at failure.

4.3.2.2 Epoxy Joints Span. Figures 4.56 through 4.62 show the differences in the model behavior due to grouting of the internal tendons. Strength and ductility were higher in the grouted case as shown in Fig. 4.56 and Fig. 4.57. The maximum change in external tendon stress was slightly higher in the grouted case as shown in Fig. 4.58. The change in the internal tendon stress was much higher in the grouted case as shown in Fig. 4.59, which shows that the internal tendon yielded before the joint crushed. The critical joint opening at failure was slightly less in the grouted case due to higher compression force,

as shown in Fig. 4.60. The support joint opening was about the same at the end of both tests, as shown in Fig. 4.61.

Although the maximum critical joint opening was less at the end of loading, as shown in Fig. 4.60, the total joint opening in the positive moment region was slightly higher, as shown in Fig. 4.62 due to large opening of the joints adjacent to the critical joint. This increase in total joint opening caused a greater increase in the external and internal tendon stresses which resulted in higher strength. Higher total joint opening translated to higher deformation and member ductility.

4.3.2.3 Observations. Grouted internal tendons behave in a similar manner to fully-bonded external tendons; they result in a different tendon stresses at the critical joint and the surrounding joints. This decreases the moment required to open the adjacent joints and to increase the opening of those joints which result in higher total joint opening in the critical region. Grouting the internal tendons increases the stiffness and strength of the critical joint especially after joint opening which attracts more external forces moment and delays failure of the critical joint. These effects increase the adjacent joint openings which increase the total joint opening in the critical region. Higher total joint opening results in higher tendon stresses. As a result, higher strength due to higher tendon stress, and improved ductility due to higher total joint opening is developed. Figure 4.63 shows the deflected shape of the structure.

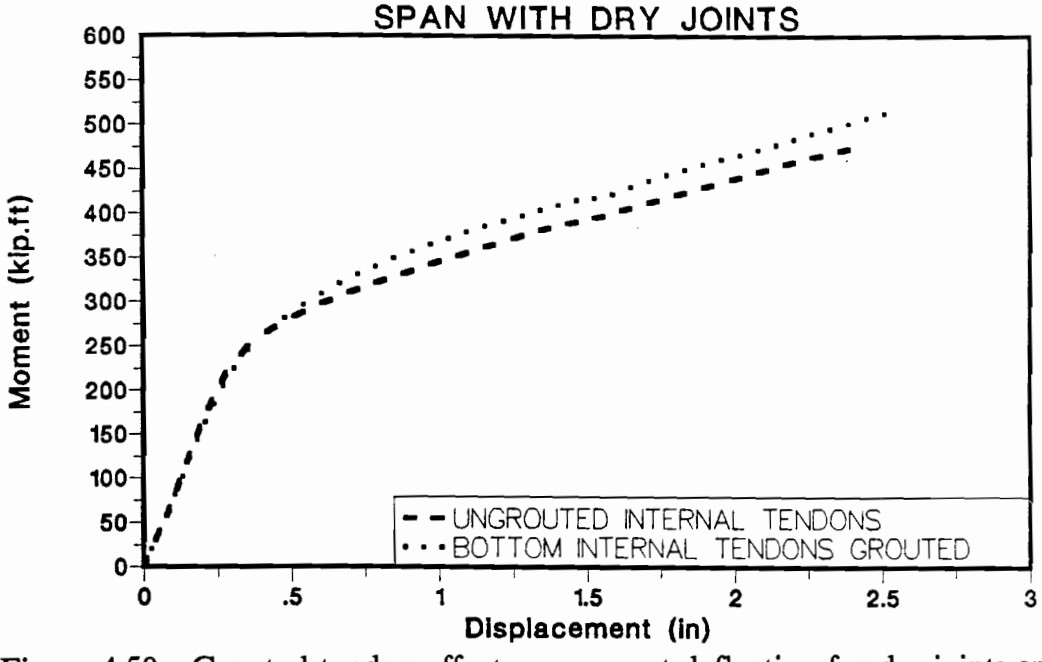

Figure 4.50 Grouted tendon effect on moment-deflection for dry joints span.

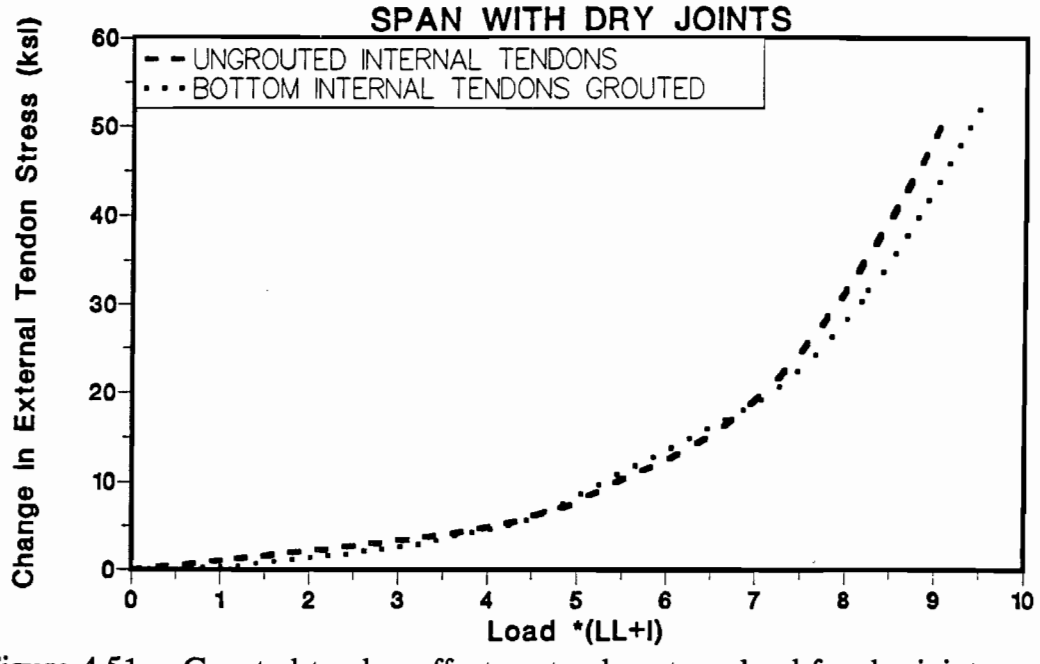

Figure 4.51 Grouted tendon effect on tendon stress-load for dry joints span.

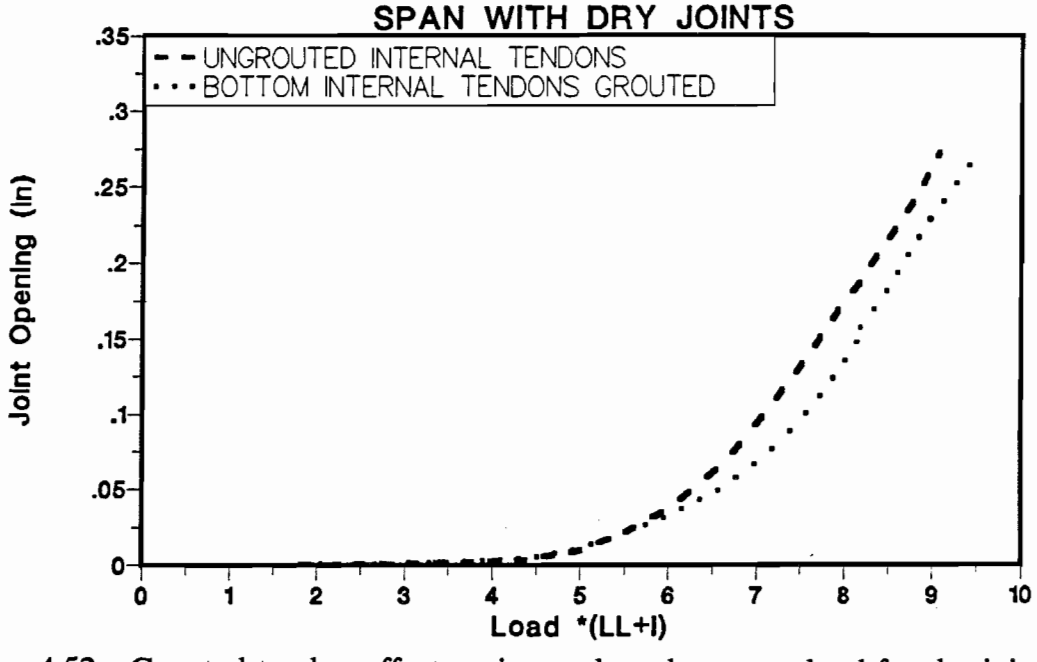

Figure 4.52 Grouted tendon effect on internal tendon stress-load for dry joints span.

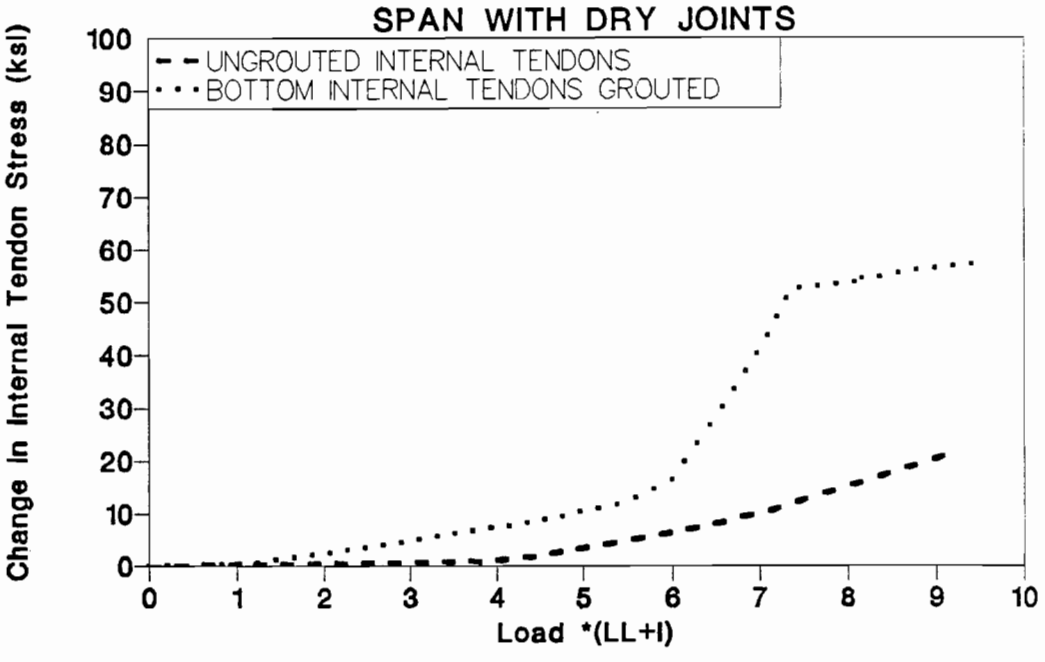

Figure 4.53 Grouted tendon effect on critical joint opening-load for dry joints span.

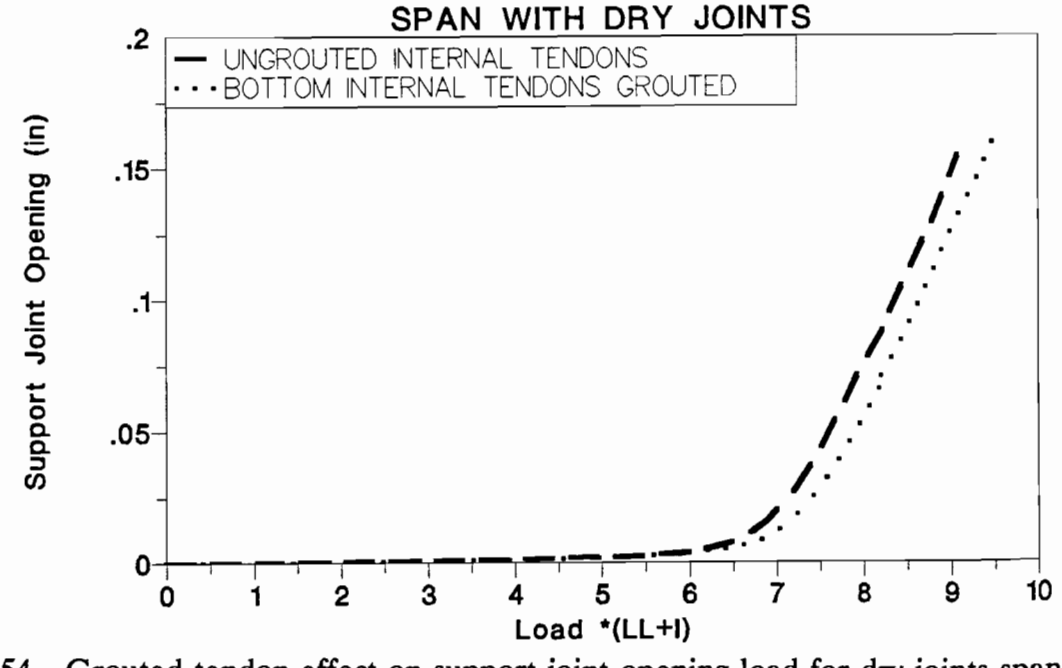

Figure 4.54 Grouted tendon effect on support joint opening-load for dry joints span.

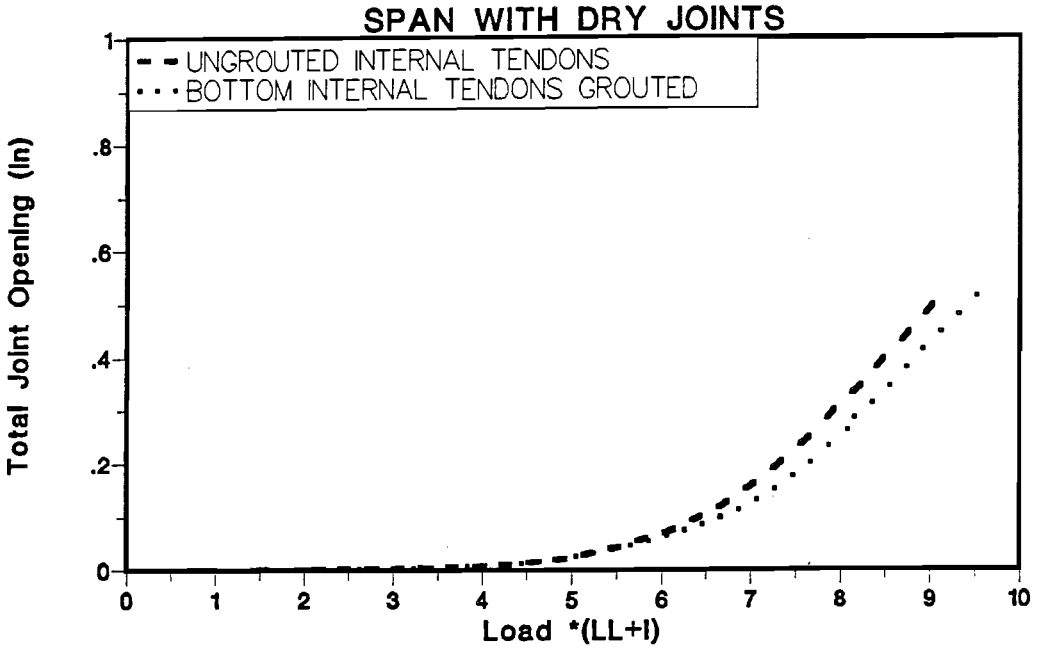

Figure 4.55 Grouted tendon effect on total joint opening-load for dry joints span.

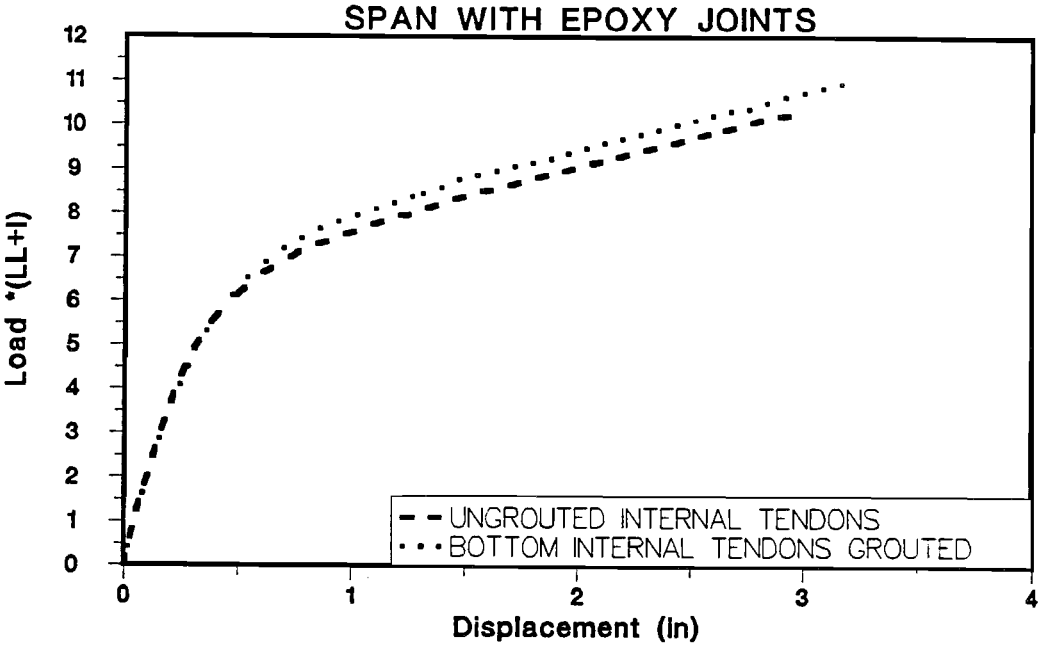

Figure 4.56 Grouted tendon effect on load-deflection response of epoxy joints span.

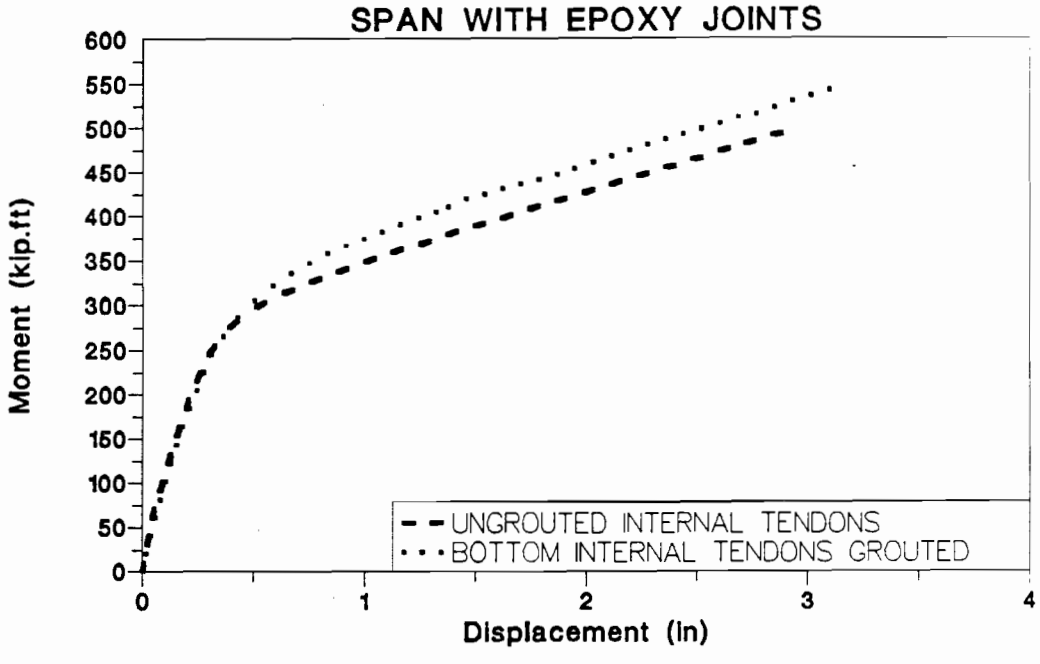

Figure 4.57 Grouted tendon effect on moment-deflection for epoxy joints span.

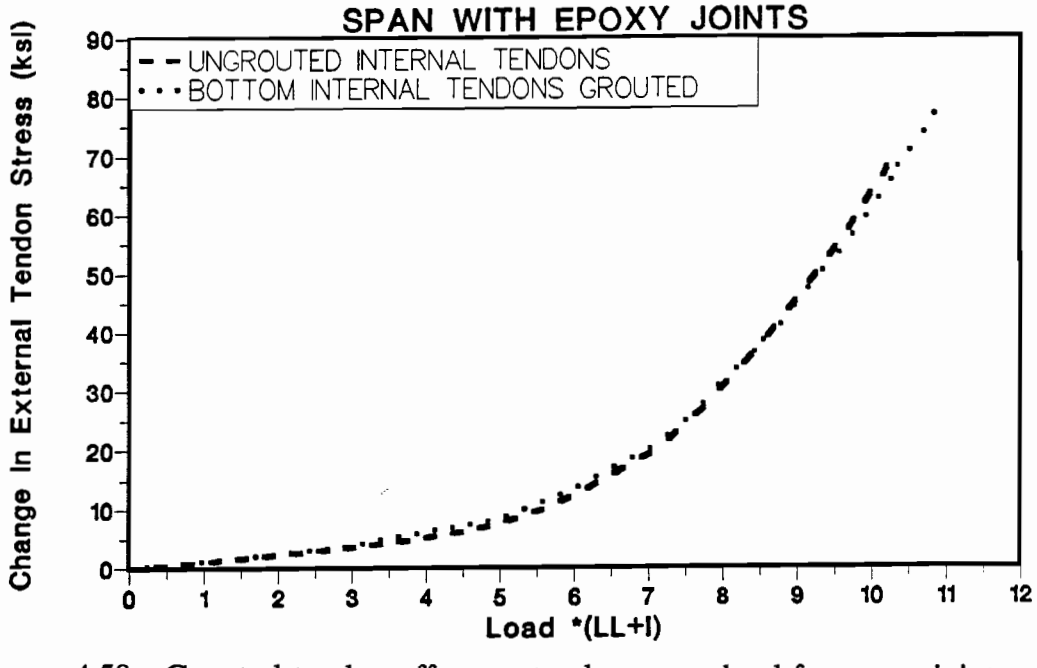

Figure 4.58 Grouted tendon effect on tendon stress-load for epoxy joints span.

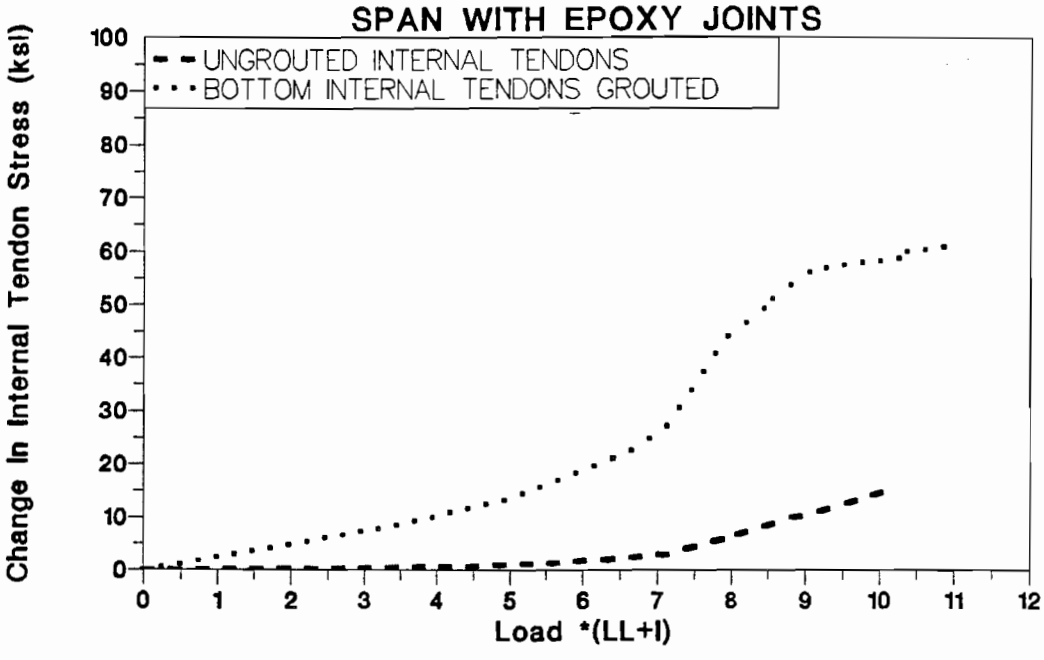

Figure 4.59 Grouted tendon effect on internal tendon stress-load for epoxy joints span.

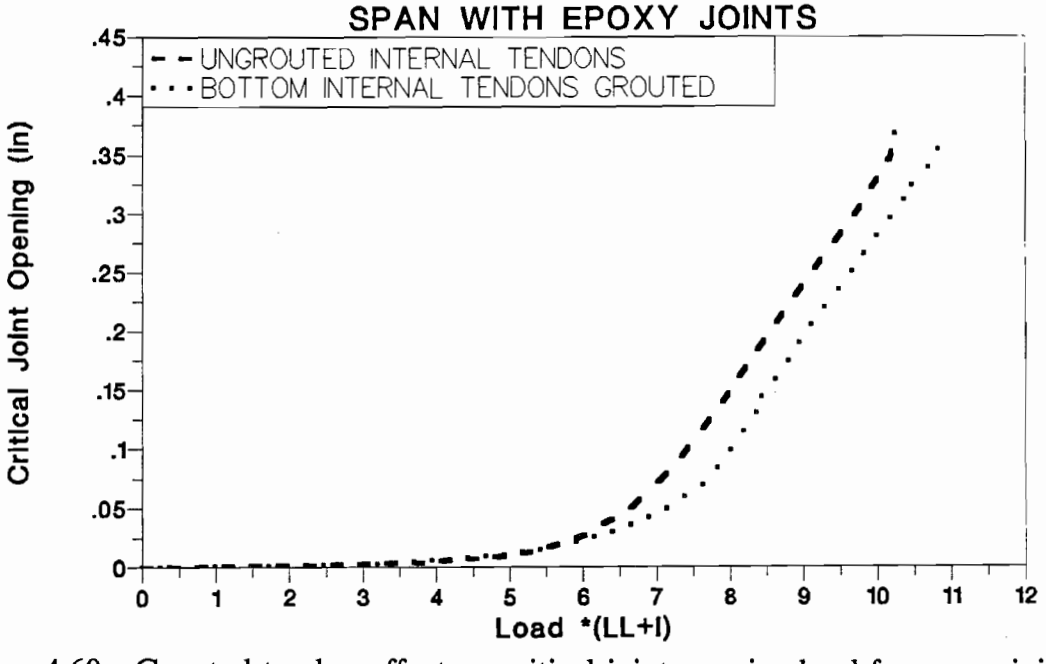

Figure 4.60 Grouted tendon effect on critical joint opening-load for epoxy joints span.

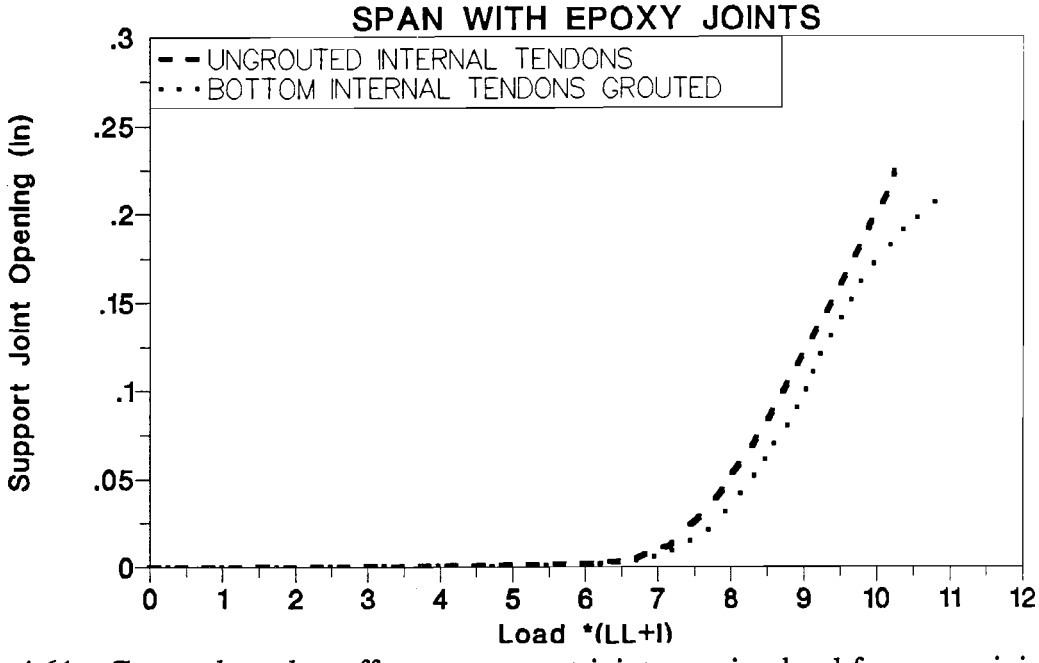

Figure 4.61 Grouted tendon effect on support joint opening-load for epoxy joints span.

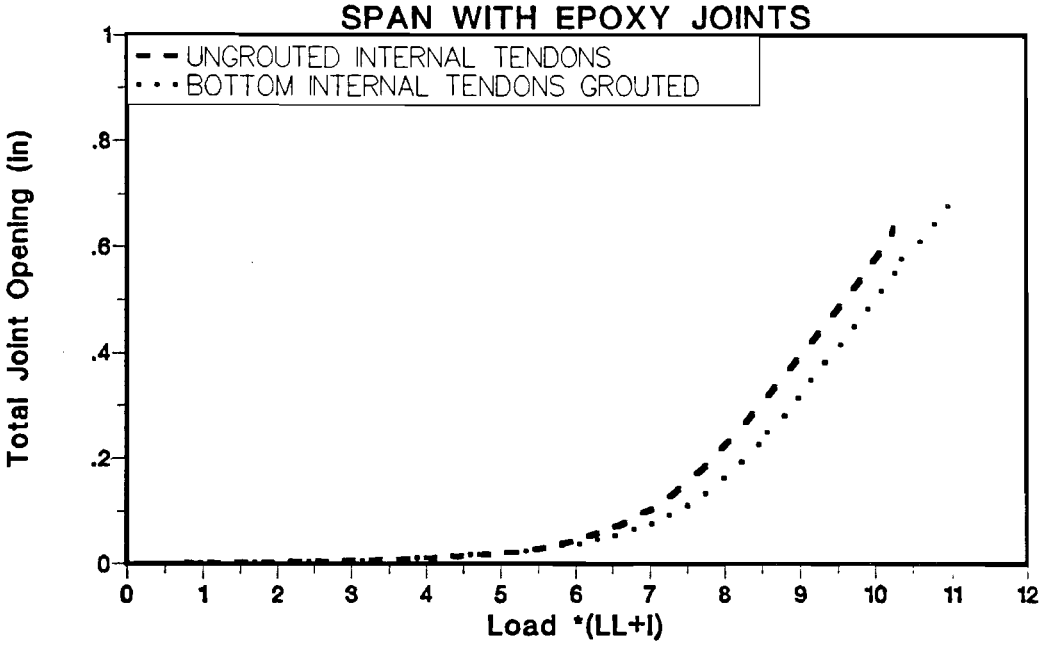

Figure 4.62 Grouted tendon effect on total joint opening-load for epoxy joints span.

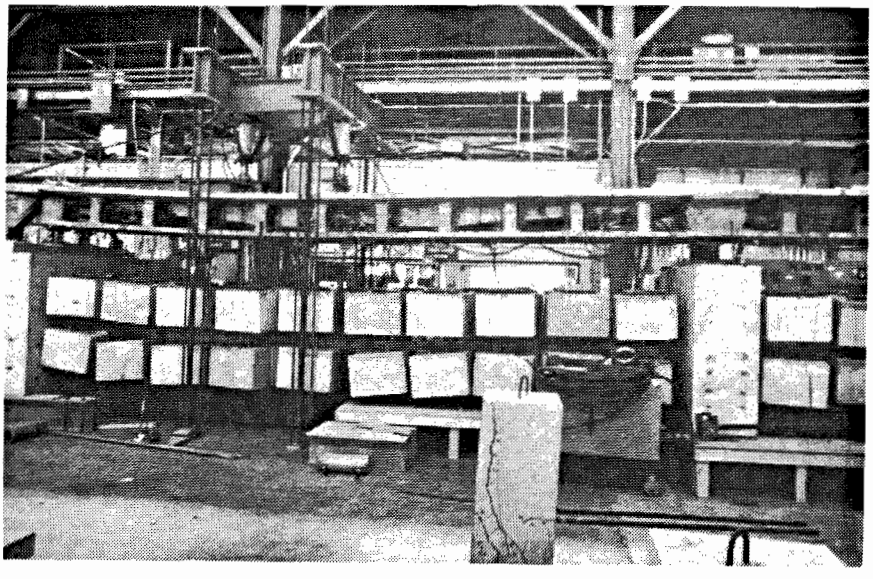

Figure 4.63 Deflection of the model at ultimate load.

4.4 Typical Load-Deflection

The load-deflection response of the epoxy joints span with external tendons locally bonded to all diaphragms is shown in Fig. 4.64. This is a typical load-deflection response for all flexural strength tests carried out in this study. The deflection increased in a linear manner up to the decompression load of the previously cracked epoxy joints span which was 2.6(LL+I). Between the decompression load and a load of 4.0(LL+I), which causes the mid-span critical joint to start opening, the structure behaved non-linearly with only a small reduction in stiffness. As the load increased beyond 4.0(LL+I) the stiffness reduced at a higher rate and displacement increased rapidly until the support joint started opening at a load of 6.2(LL+I). At loads higher than 6.2(LL+I), the stiffness remained relatively constant until the top flange of the critical joint started crushing. The structure stiffness after joints opened depended on the bonding condition of the tendons.

4.5 Comparisons between Dry Joints Span and Epoxy Joints Span

Two major differences existed between the two exterior spans of the model. One exterior span had epoxy joints, while the other exterior span had dry joints. In addition, the epoxy joints span had a substantially higher effective prestress than the dry joints span as illustrated in Table 4.2. These were design and construction conditions that was discussed by MacGregor (1).

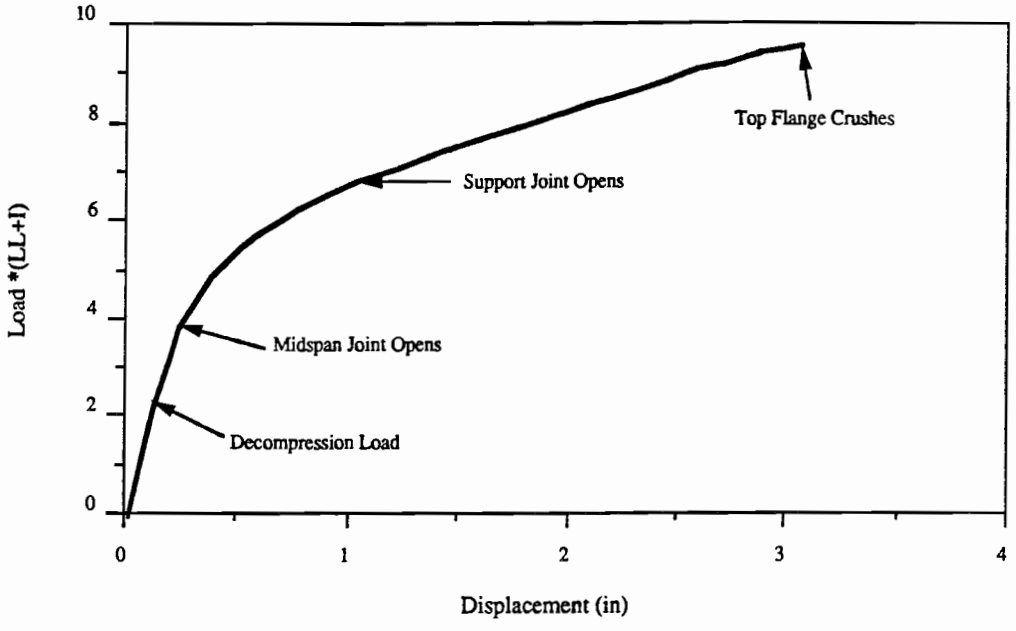

Figure 4.64 Stages of flexural behavior (epoxy joints span) for fully bonded external tendons.

Figures 4.65 through 4.69 show comparisons between the response of the two exterior spans. The comparisons are for the two strength tests that were carried out on the two exterior spans when the external tendons were bonded to all ten diaphragms. Figure 4.65 shows load-deflection response, while Fig. 3.66 shows the change in external tendon stress. Figures 4.67 and 4.68 show the critical joint and the support joint opening, while Fig. 4.69 shows the total joint opening.

Strength and ductility were substantially higher for the epoxy joints span than the dry joints span as shown in Fig. 4.65. The maximum change in external tendon stress was higher in the epoxy joints span as shown in Fig. 4.66. The maximum critical joint opening when the top flange of the critical joint started crushing was higher for the epoxy joints span as shown in Fig. 4.67. This effect is believed to be primarily due to the beneficial effect of epoxy joints on the cracking pattern, as will be discussed later in this chapter.

Although three joints opened in the positive moment region during the two tests, the maximum total joint openings in the positive moment region were higher in the epoxy joints span as shown in Fig. 4.69. This increase was due to the difference between the maximum critical joint opening.

As discussed in Chapter Three, the difference in the decompression load for the two exterior spans is 0.6(LL+I). Figure 4.65 shows that up to crushing of the dry joints span critical joint, the load-deflection response of the two spans is virtually identical except they

Table 4.2 Effective Prestress Force

Location:	4:5	N1:11	20:SI	26:27
Joint Type				
x: (ft)	10.25	26	49	64.75
Ac: ($in.^2$)	450	450	450	450
S. top: ($in.^3$)	2512	2512	2512	2512
S. bot.:	1757	1757	1757	1757
(Ap) ext ($in.^2$)	2.04	1.53	1.53	2.04
(Ap) int	.68	.68	.68	.68
(Ap)	2.72	2.21	2.21	2.72
(e) ext ($in.^2$)	6.01	-1.4	-1.4	6.01
Corrected (e) ext	5.76	-1.4	-1.4	5.76
(e) int	-5.35	-5.35	-5.35	-5.35
(e) eff	2.983	-2.62	-2.62	2.983
$(A) = \left(\left(\frac{1}{A_c}\right) + \left(\frac{e}{S}\right)\right)$	.0039	.0033	.0033	.0039
Dead Load Moments (M_{d1}) Measured Moments (from reaction data)	110.0	-64	-23	127.0
Decompression Load Moments (M_d) Measured Moments	100	-200	-250	135
$(B) = \frac{(M_{d1} + M_d)}{S}$ Data	1.43	-1.26	-1.30	1.790
Tendon Force and Stresses				
$T_{pd} = \frac{(B)}{(A)}$ Data	360.0	381.8	394.0	458.0
$fpd = \frac{Tpd}{Ap}$ (ksi) Data	134.0	172.5	178.0	168.0
fpd - fpe (ksi)	2.5	1	1	3.0
fpe (ksi) Data	131.5	171.5	177.0	165.0

are separated by the difference between the decompression loads. The critical joint for the dry joints span started crushing at a much lower load and displacement than the epoxy joints span due to its cracking pattern. Due to higher permissible joint opening, the epoxy joints span continued carrying load and displaced after the dry joints span failed.

In this study the difference in ultimate strength of the epoxy joints span and the dry joints span was due to two reasons. The first reason was the difference in decompression loads which is directly related to the difference in effective prestress force. The second reason is that the maximum obtainable joint opening was higher in the epoxy joint than in the dry joint due to different crack patterns. The epoxy joints seemed to develop somewhat greater compressive deformations which resulted in higher changes in tendon stress and in higher overall ductility.

4.6 Ductility

Ductility of a structural system is measured by the ability of the structure to sustain inelastic deformation (18). Ductile structures give warning to the occupants of possible distress and failure. Structures with bonded reinforcement have the ability to show greater warning when the steel yields.

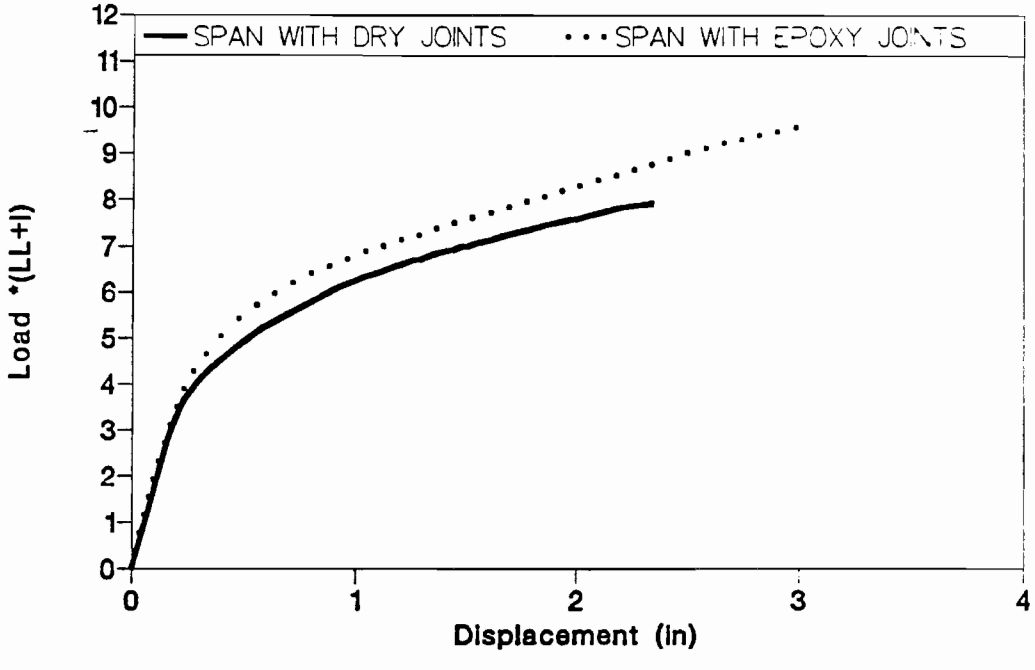

Figure 4.65 Effective prestress effect on load-deflection response.

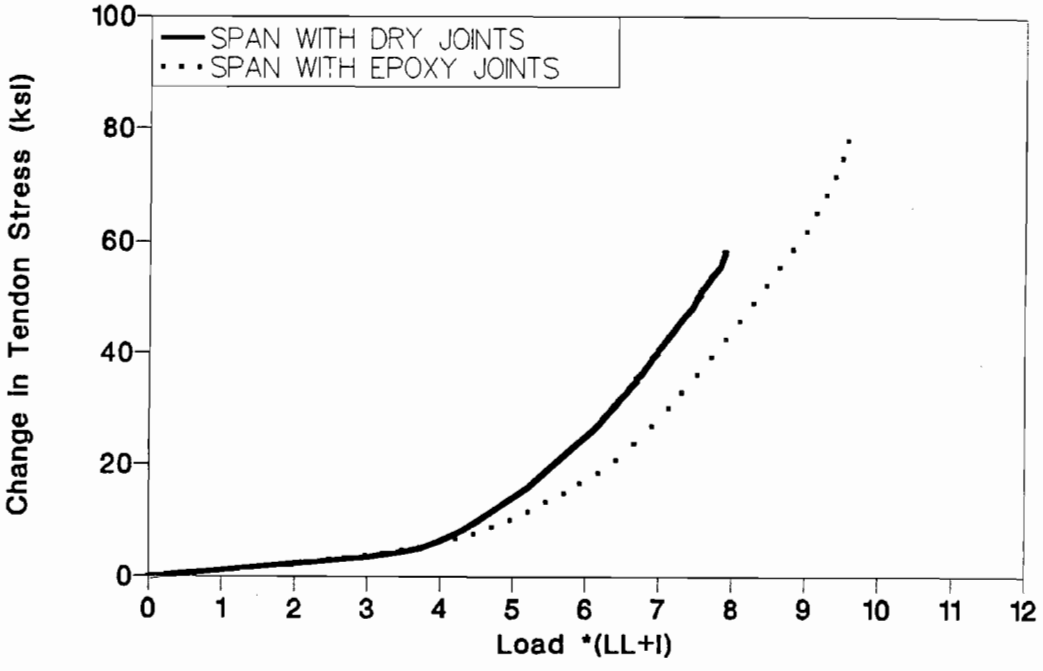

Figure 4.66 Effective prestress effect on change to tendon stress.

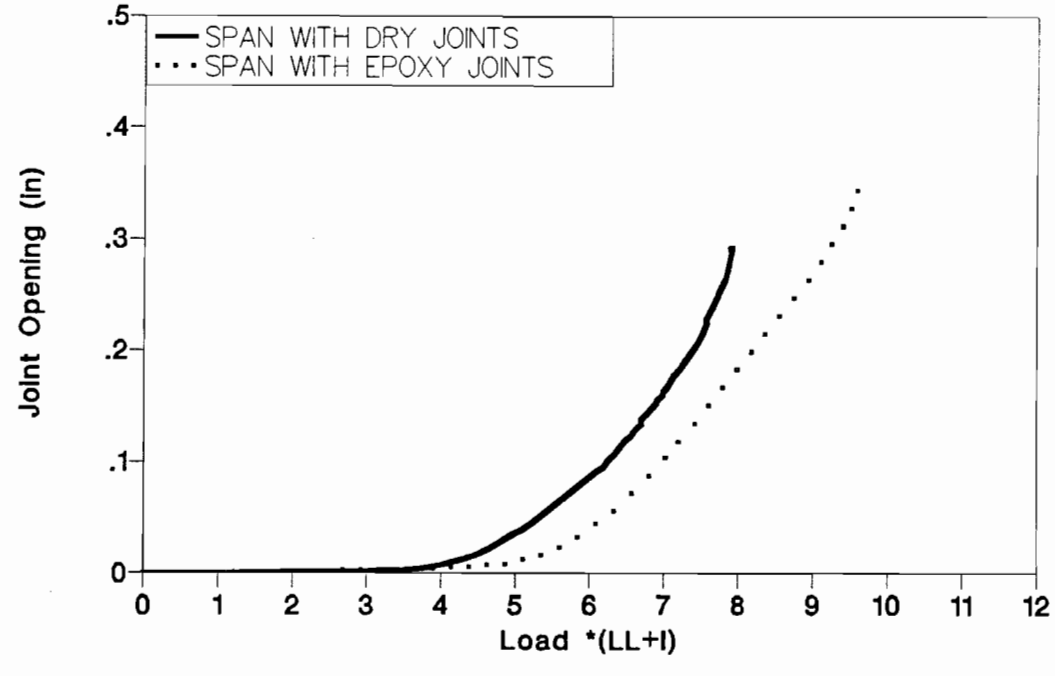

Figure 4.67 Effective prestress effect on critical joint openings.

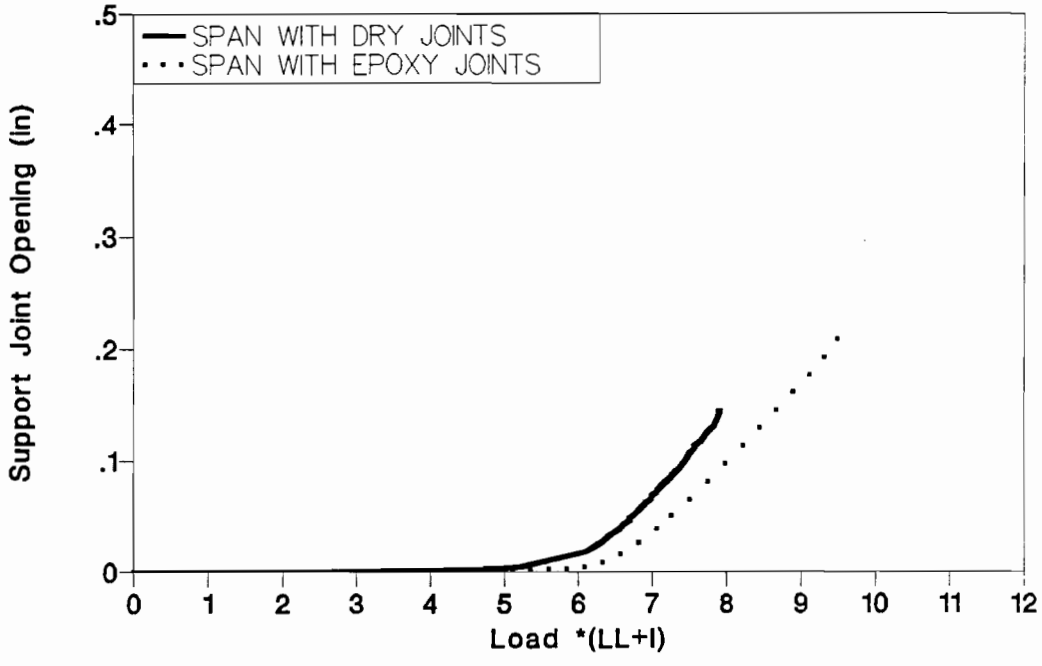

Figure 4.68 Effective prestress effect on support joint openings.

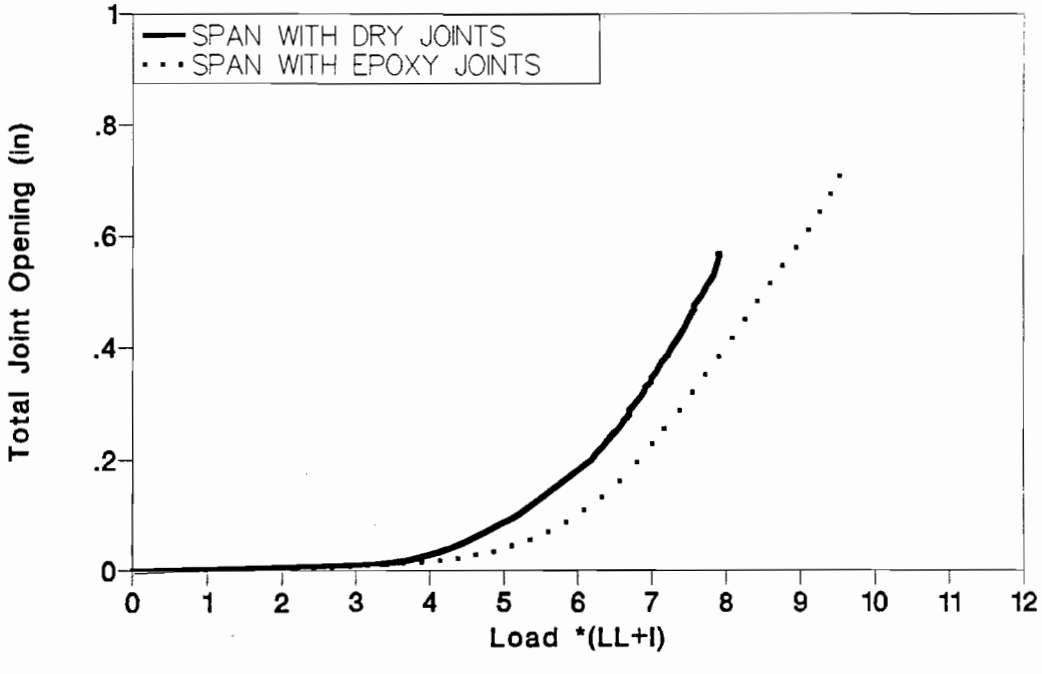

Figure 4.69 Effective prestress effect on total joint openings.

For proper warning and load redistribution, the structure must be able to withstand large deformations before failure. For unbonded post-tensioned structures, large joint rotations are required to increase the tendon stresses and to substantially deform the structure. For that reason good local ductile behavior of the joint is required which can be obtained by proper detailing of the segments to confine the concrete and sustain high strains and rotations. Epoxy joints seems to contribute to this local confinement and control of local crushing stresses.

4.6.1 Effect of Epoxy Joints on Maximum Joint Opening. The maximum opening in the joint is dependent on whether the joint is epoxy or dry. Figure 4.70 shows that the maximum joint opening at crushing was higher in the epoxy joints span than the dry joints span. This difference was due to the effect of using epoxy and is shown by the cracking pattern in Fig. 4.71.

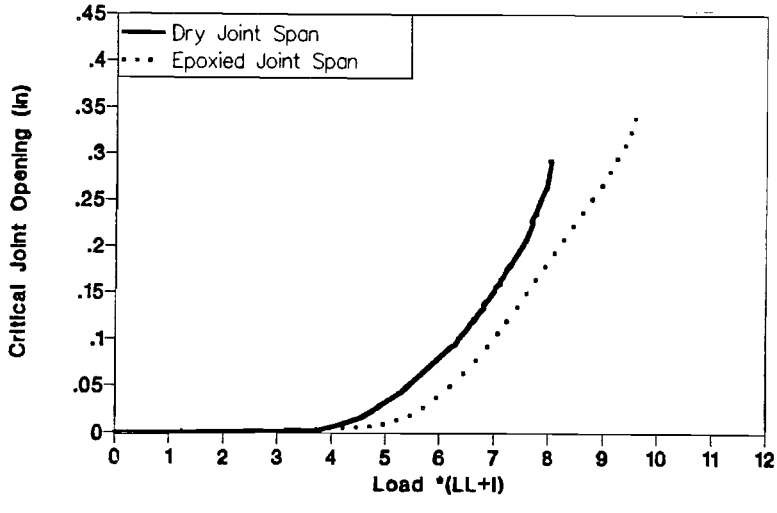

Figure 4.70 Effect of epoxy on maximum joint opening.

Figure 4.71 shows the difference in cracking pattern in epoxy and dry joints at crushing. The epoxy joint cracks were tree like and extended horizontally in the top flange at three locations. Three cracks were extended perpendicular to the webs in the top flange in the epoxy joint, while one crack extended in the top flange in the dry joint. The crack in top flange of the dry joint was predefined by the dry joint which prevented further cracking from occurring and this limited the maximum compressive zone to the dry joint area. The extension of a few cracks on both sides of the epoxy joint at a substantial distance away from the joint indicating that the maximum compression crushing zone is not limited to just the epoxy joint area but exists in the general concrete compressive zone. The increase in the volume of the highly stressed and strained concrete in the epoxy joint causes higher compressive deformation (before joint crushing) in the extreme fiber of the flange.

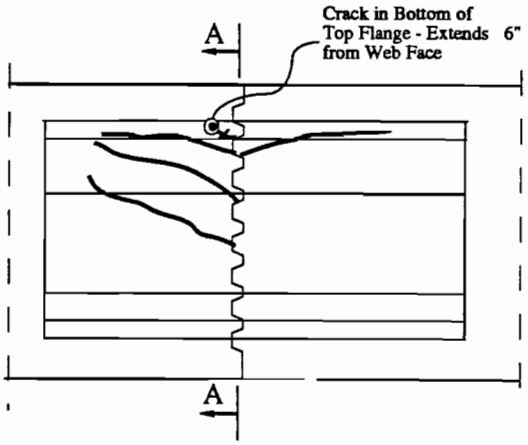

a) Crack in Dry Joints Span

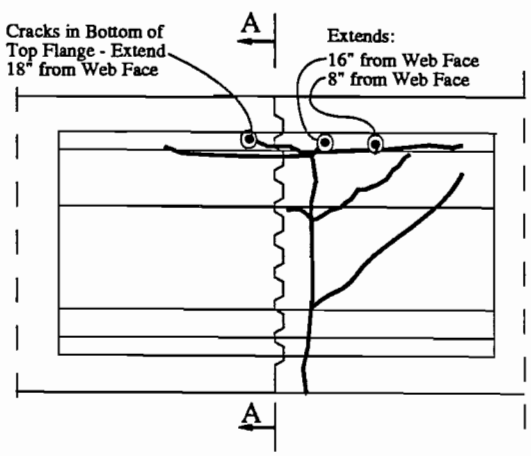

b) Crack in Epoxy Joints Span

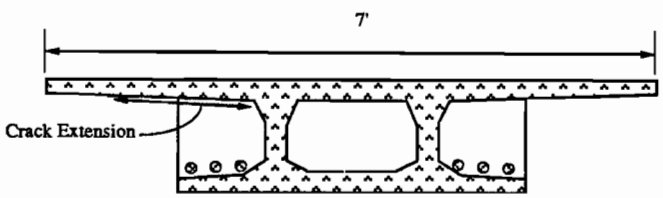

Section A-A

Figure 4.71 Crack pattern.

The joint opening depends mainly on the compressive deformation of the top fiber and the depth to the neutral axis. Increasing the compressive deformation increases the maximum joint opening.

4.6.2 Maximum Allowable Joint Opening. Two methods for prediction of maximum joint opening are presented in this section. One method is suggested by Virlogeux while the second method is suggested by the author.

4.6.2.1 Virlogeux Method. Figure 4.72 shows the method proposed by Virlogeux (13) for calculating the maximum joint opening. The plastic hinge length was assumed to be equal to twice the distance between the centroid of the compressive force and the center of the steel (Z). This corresponds to a force diffusion angle of 45 degrees. The method assumes that the strain varies linearly in the plastic zone. The maximum curvature in the plastic hinge is assumed to be dependent on the maximum concrete compressive strain and segment reinforcement strain. Virlogeux suggested that the maximum concrete crushing strain to be used in the maximum joint opening calculation is 0.002 while the steel strain is 0.01. Integrating the curvature in the plastic zone gives the joint rotation, while integrating the bottom fiber strain gives the joint opening.

In reinforced concrete structures, the plastic hinge length is assumed to be equal to the section depth with a constant curvature over the plastic length. The same hinge rotation can be obtained by assuming that the plastic zone length is equal to twice the depth while the curvature varies linearly over the plastic zone. These models are used for cast-in-situ beams and not for segmental beams but Virlogeux used this approach as a simplified method to calculate beam deflections and the tendon stresses for segmental beams. Conservatively, Virlogeux suggested using a maximum concrete crushing strain of 0.002 and a maximum steel strain of 0.01 which are well below the maximum possible strains.

4.6.2.2 Author's Method. The author recommends a second method to calculate the maximum joint opening. Figure 4.73 shows the author's procedure to predict the maximum joint opening.

For segment of a short length compared to the bridge span, the moment and axial force can be assumed constant. Before cracking, the position of the neutral axis is the same along the segment and the center of rotation of one section with respect to any other section lies on the neutral axis. However, as soon as the joint starts opening, the position of the neutral axis is disrupted near the joint and the position of zero displacement does not coincide with the neutral axis. In this model, the position of the neutral axis (zero strain) is assumed to have a 45 degrees angle and starts from the neutral axis position at section (B). This corresponds to a compressive force diffusion angle of 45 degree. Section (B) is assumed to remain plane based on the test results presented in Chapter Three. The displacement of the joint section (B) relative to section (A) can be found by integrating the concrete strain over half the segment length. The concrete strain variation between section (A) and (B) is assumed linear to simplify the integration. This assumption is based on the

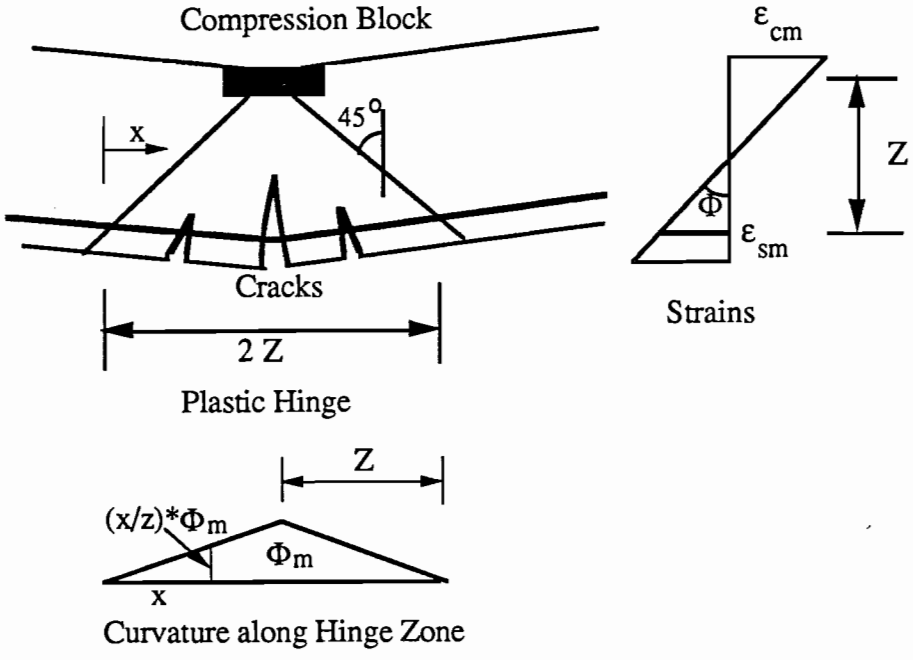

δ_h = Concrete Hinge Elongation (Joint Opening)

Φ_m = The Maximum Allowable Curvature = $\frac{\varepsilon_{cm}+\varepsilon_{sm}}{Z}$

ε_{cm}= The Maximum Allowable Concrete Strain

ε_{sm}= The Maximum Allowable Steel Strain

$$\delta_h = 2* \int_0^Z \Phi_m * Z * \left(\frac{X}{Z}\right) dx = Z^2 * \Phi_m$$

$$\delta_h = Z * (\varepsilon_{cm}+\varepsilon_{sm})$$

If $\varepsilon_{cm} \cong 0.002$, and $\varepsilon_{sm} \cong 0.01$

$$\delta_h = Z * 0.012$$

Figure 4.72 Prediction of joint opening (Virlogeux).

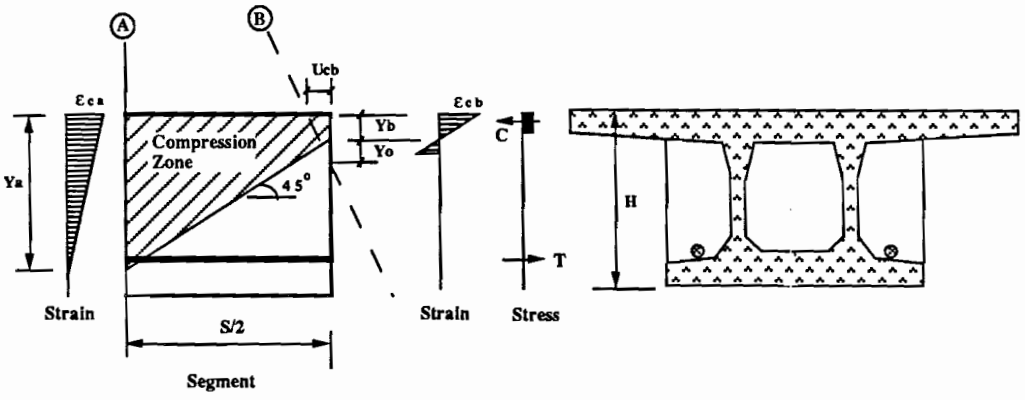

Section A : Segment Section

Section B : Deformed Joint Between Two Segments

S : Segment Length

H : Depth of Cross Section

ε_{cb} : Maximum Concrete Strain at the Joint

ε_{ca} : Top Fiber Concrete Strain at Section A

U_{cb} : Top Fiber Displacement at the Joint

Y_a : Neutral Axis Depth at Section A

Y_b : Neutral Axis Depth at Section B

Y_o : Depth from Neutral Axis to Center of Rotation

T : Tension Force assuming all Tendons Yielded

b_e : Effective Width (calculated according to AASHTO)

L_c : Length of Compression Zone between A @ B

$$L_c = \frac{S}{2} \qquad \text{if } H > \frac{S}{2}$$

$$L_c = H \qquad \text{if } H < \frac{S}{2}$$

$$U_{cb} = \int \varepsilon_c \, dx$$

$$U_{cb} = \frac{\varepsilon_{ca}+\varepsilon_{cb}}{2} * L_c$$

Assume $\varepsilon_{ca} << \varepsilon_{cb}$ Then

$$U_{cb} = \frac{\varepsilon_{cb}}{2} * L_c$$

$$Y_b = \frac{T}{\beta_1 * 0.85 * f'_c * b_e}$$

Find Y_a from geometry $\quad Y_a = Y_b + L_c$

$$Y_o = \frac{(Y_b)^2 * (Y_a - Y_b)}{((Y_a)^2 + (Y_b)^2)} \qquad \text{(see Eq. 5.28)}$$

$$\text{Maximum Joint Opening} = 2 * \frac{U_{cb} * (H - (Y_o + Y_b))}{(Y_o + Y_b)} = \varepsilon_{cb} * L_c * \frac{(H - (Y_o + Y_b))}{(Y_o + Y_b)}$$

a) Dry Joints

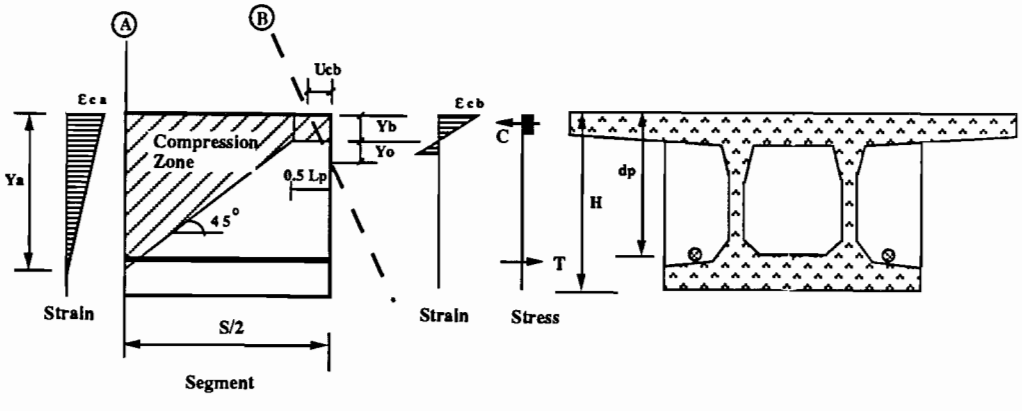

L_p : Length of Plastic Region Assume = $\frac{d_p}{2}$

d_p : Depth to Prestress Steel

$$U_{cb} = \frac{\varepsilon_{cb}}{2} * (L_c - 0.5 * L_p) + \varepsilon_{cb} * 0.5 * L_p$$

$$\text{Maximum Joint Opening} = 2 * \frac{U_{cb} * (H - (Y_o + Y_b))}{(Y_o + Y_b)}$$

b) Epoxy Joints

Figure 4.73 Prediction of joint opening.

CEBTP tests (24) which conclude that the concrete strain is much higher at the joint section than the segment sections. The center of rotation of section (A) is the point which has zero displacement. The full derivation and details are given in Chapter Five.

Figure 4.73(a) shows the method for dry joints while Fig 4.73(b) shows the method for epoxy joints. Increasing the compressive forces will increase the neutral axis depth in the joint section and reduce the maximum allowable joint rotation. To be conservative, the tension force was calculated assuming that all tendons yielded before the joint failed. From the tension force which is equal to the compression force, the position of the neutral axis at the plastic hinge section can be found according to the rectangular compressive stress distribution (stress block) procedure. As discussed in Section 4.6.1, the highly compressed region for the dry joint is concentrated at the joint section, while the length of the highly compressed region (along the span) for the epoxy joint is longer due to its cracking pattern. The length of the highly compressed region (L_p) at an epoxy joint is assumed to be equal to half the distance from the compressive force to the center of the steel. In ordinary reinforced concrete with bonded reinforcement, the plastic hinge length is assumed to be equal to the cross section depth. This is based on the assumption that when the concrete section cracks, the strain hardening of the bonded steel increases the internal moments and forces other adjacent sections to crack. Due to the probability of not having bonded steel across the flexural cracks, the length of the highly compressed region was assumed as half of that for structures with bonded steel.

The position of the neutral axis at sections in the segment can be found by assuming that the compressive force diffusion angle is 45 degrees. The top fiber maximum strain is assumed to vary linearly between the segment section and the end of the plastic hinge region. The deformation of the joint section top fiber can be found by integrating the compressive strain along the length. The center of rotation of the joint section, which has zero deformation, can be found as shown in the figure using an equation derived later in Chapter Five.

Figure 4.74 shows the calculation for maximum joint opening of the model. The predicted maximum joint opening according to the author's method was 0.28 inches for the dry joints span and 0.35 inches for the epoxy joints span while the joint opening predicted by Virlogeux method was 0.14 inches. The maximum joint opening experienced during the tests was 0.37 inches in the epoxy joints span and 0.30 inches in the dry joints span.

The method recommended by the author for prediction of the joint opening was much closer to the actual joint opening and was also conservative as shown in Table 4.3. This method is based on the displacement model of the segment which is close to the actual behavior of the segment during testing.

4.6.3 Global Ductility. The global ductility of a segmental post-tensioned bridge with external tendons is controlled by the maximum joint opening due to concentration of the deformation in a few joints. The concrete in critical joints must be detailed properly to

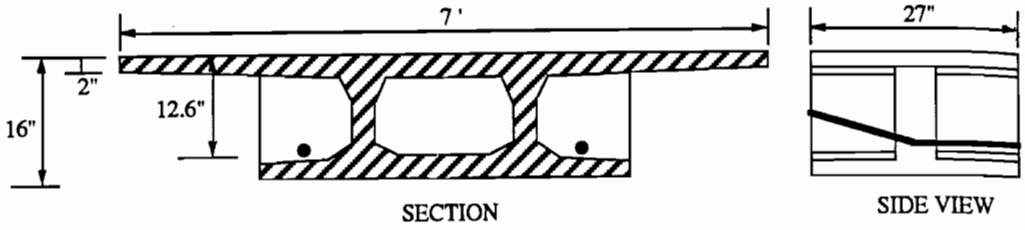

A_{ps} : Area of Prestress Steel = 2.05 in^2

f_c : Concrete Strength = 6 ksi

L_c : Length of Compression Zone = 13.5 in.

Dry Joint (Author's Method)

$$Y_b = \frac{2.05 * 245}{\beta_1 * 0.85 * 6 * 7 * 12} = 1.81 \text{ in.}$$

$$Y_a = 1.81 + \frac{27}{2} = 15.31 \text{ in.}$$

$$Y_o = \frac{(1.81)^2 * (15.31 - 1.81)}{((15.31)^2 + (1.81)^2)} = 0.186 \text{ in.}$$

$$\text{Maximum Joint Opening} = 2 * \frac{U_{cb} * (H - (Y_o + Y_b))}{(Y_o + Y_b)} = \varepsilon_{cb} * L_c * \frac{(H - (Y_o + Y_b))}{(Y_o + Y_b)}$$

$$\text{Maximum Joint Opening} = 0.003 * \frac{27}{2} * \frac{(16 - (0.186 + 1.81))}{(0.186 + 1.81)} = 0.28 \text{ in.}$$

Epoxied Joint (Author's Method) Assume $L_p = 12.6/2$

Maximum Joint Opening = 0.35 in.

Virlogeux's Model

Maximum Joint Opening = 0.012 * Z

$$\text{Maximum Joint Opening} = 0.012 * \left(12.6 - \frac{\beta_1 * 1.81}{2} \right) = 0.14 \text{ in.}$$

Figure 4.74 Calculations of maximum joint opening.

Table 4.3 Maximum Joint Opening

Case	Dry Joint	Epoxy Joint
Measured	0.30 in.	0.37 in.
Virlogeux	0.14 in.	0.14 in.
Author	0.28 in.	0.35 in.

ensure that large rotations can occur. Confinement of the concrete in the compressive zone at the critical joints will allow higher concrete strain and larger joint rotations. One method of increasing the concrete confinement is to increase the ratio of beam width to the shear span as proposed by Ford (12) and shown in Equation 4.1.

$$\epsilon_{cu} = 0.003 + 0.02 * \frac{b}{z} \tag{4.1}$$

where b is the beam width and z is the shear span. The maximum concrete strain calculated by Equation 4.1 for the model was 0.0035. As discussed in Section 4.6.1, using epoxy joints is another method for improving the concrete confinement and increasing the maximum allowable joint opening.

Another method for improving global ductility is to reduce the concentration of the deformation in the critical joint by increasing the number of opening joints. Bonding the external tendons to the diaphragms and using grouted internal tendons increased the number of opening joints and reduced the concentration of deformation at the critical joint.

Figure 4.75 shows the effect that bonding the external tendons has on the stiffness of the opened joint and the tendon stresses. Bonding the external tendons to the diaphragms has two effects. First, bonding makes the joints adjacent to the critical joint weaker by keeping the external tendon stresses in the adjacent joint sections lower than at the critical joint section. This reduces the moments required to open the adjacent joints. Second, bonding of the external tendons increases the critical joint stiffness and strength after the critical joint starts opening because the critical joint will carry higher moment for the same joint opening due to the higher tendon stress. This will attract more moment to that region and delay failure of the critical joint, and increase the chances of opening new joints. Opening new joints reduces the concentration of joint opening in the critical joint

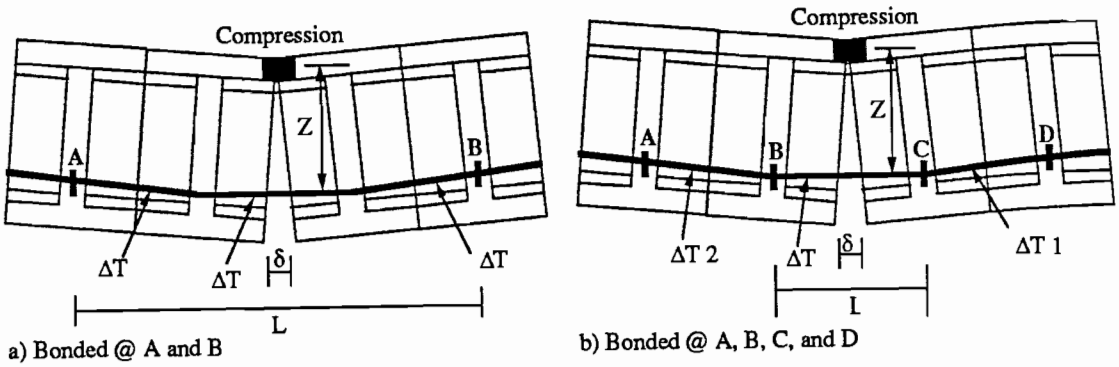

a) Bonded @ A and B

b) Bonded @ A, B, C, and D

L	: External Tendon Unbonded Length
Z	: Moment Lever Arm
E	: Modulus of Elasticity of Tendon
δ	: Joint Opening at Tendon Level
Δ_m	: Change in Moment
Δ_θ	: Change in Joint Angle
k_θ	: Rotational Stiffness
A_p	: Area of Prestress
S	: Segment Length
$\Delta_T, \Delta_{T1}, \Delta_{T2}$	: Change in External Tendon Stress

Assume no Slip at Bonded Diaphragm

$$\Delta_T = \frac{\delta * E * A_p}{L}$$

If no slip occurs $\Delta_{T2}, \Delta_{T1} \approx 0 << \Delta_T$

$$k_\theta = \frac{\Delta_m}{\Delta_\theta}$$

$$\Delta_m = Z * \Delta_T = Z * \frac{\delta * E * A_p}{L}$$

$$\Delta_\theta = \frac{\delta}{Z}$$

$$k_\theta = \frac{\Delta_m}{\Delta_\theta} = \frac{Z^2 * E * A_p}{L}$$

a) Unbonded External Tendons

$L = 3*S$

$$\Delta_T \text{ (Unbonded)} = \frac{\delta * E * A_p}{3 * S}$$

$$k_\theta \text{ (Unbonded)} = \frac{Z^2 * E * A_p}{3 * S}$$

b) Bonded External Tendons

$L = S$

$$\Delta_T \text{ (Bonded)} = \frac{\delta * E * A_p}{S}$$

$$k_\theta \text{ (Bonded)} = \frac{Z^2 * E * A_p}{S}$$

$$\Delta_T \text{ (Bonded)} = 3 * \Delta_T \text{ (Unbonded)}$$

$$k_\theta \text{ (Bonded)} = 3 * k_\theta \text{ (Unbonded)}$$

Figure 4.75 Stiffness of opened joint.

Figures 4.76 and 4.77 illustrate the effect of bonding the external tendons and using grouted internal tendons on the ductility of the model. Table 4.4 shows the increase in ductility with respect to the partially-bonded external tendon case.

Table 4.4 Ductility

Case	Epoxy Joints	Dry Joints
Bonded External Tendons	+75%	+47%
Bonding External +Ungrouted Internal Tendons	+67%	+51%
Bonded External + Grouted Internal Tendons	+80%	+57%
+: Increase with respect to the Partially-Bonded case		

The effect of bonding in the epoxy joints span was higher than in the dry joints span. In the partially-bonded tests, two joints opened in the dry joints span while one joint opened in the epoxy joints span. Three joints in both spans opened during the fully-bonded tests. Bonding was less effective in the dry joints span because the partially-bonded tendons had already improved its ductility (two joints opened) before bonding the tendons to all diaphragms.

4.7 Live Load Capacity

Figures 4.76 and 4.77 show the effect of bonding the external tendons and using internal tendons on the live load capacity of the model. Table 4.5 shows the increase in live load capacity (in %) relative to the capacity of the partially-bonded external tendon case. Ultimate live load capacity for the fully-bonded external tendons case was higher than the partially-bonded external tendons case by 33% for the epoxied joints span and 23% for the dry joints span. This large increase in ultimate live load capacity was due to the change in the external tendons maximum stress. Changes in the external tendon stress were much higher for the fully-bonded case, as shown in Fig. 4.78 and Fig. 4.79. The external tendon stress in the bonded case was much higher due to short tendon length in Equation 4.2 (obtained from Fig 4.75).

$$\Delta T = \frac{\delta * E * A_p}{L} \qquad \text{Eq. 4.2}$$

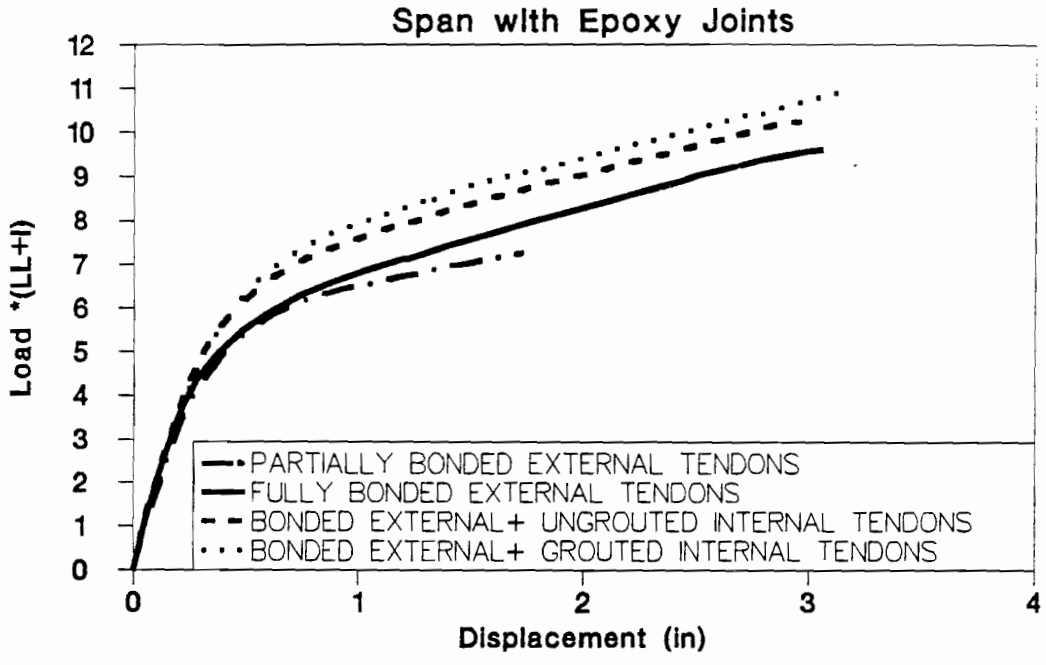

Figure 4.76 Effect of bonding and grouted internal tendons on strength and ductility of epoxy joints span.

The strength was increased to 39 percent in the epoxy joints span and 40 percent in the dry joints span higher than the partially-bonded case by using ungrouted internal tendon and bonded external tendons. The four internal tendons added to the bottom flange increased the prestress area by about 11 percent. After grouting the bottom flange internal tendons, the live load capacity exceeded that of the partially-bonded external tendon case by 48 percent in the epoxy joints span and 50 percent in the dry joints span.

Table 4.5 Live Load Capacity Increase

Case	Epoxy Joints	Dry Joints
Bonded External Tendons	+33%	+23%
Bonding External + Ungrouted Internal Tendons	+39%	+40%
Bonded External + Grouted Internal Tendons	+48%	+50%

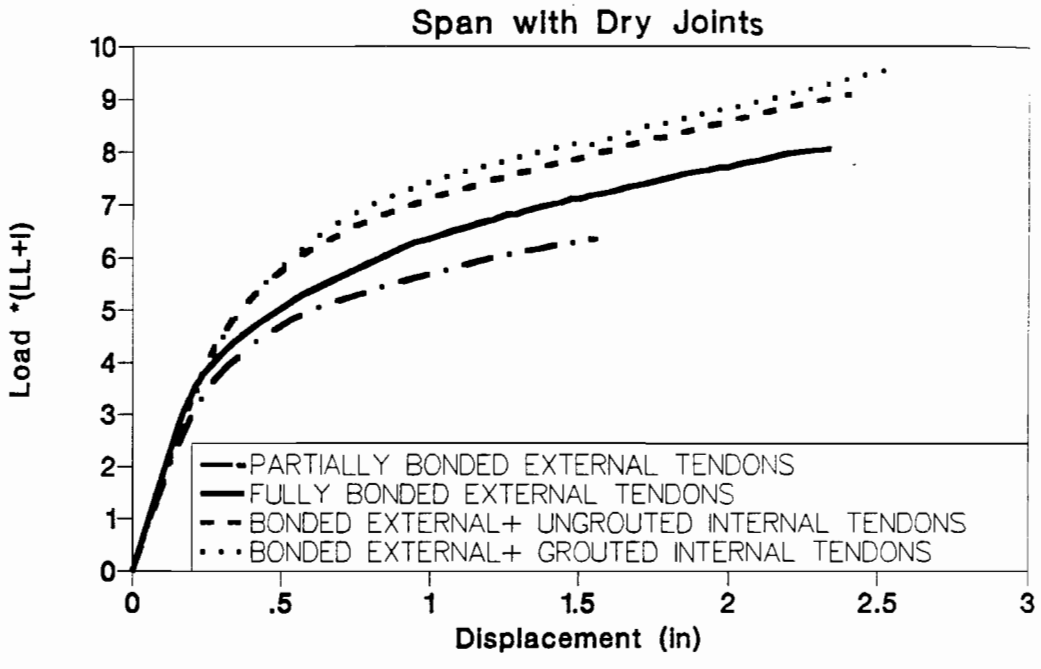

Figure 4.77 Effect of bonding and grouted internal tendons on strength and ducility of dry joints span.

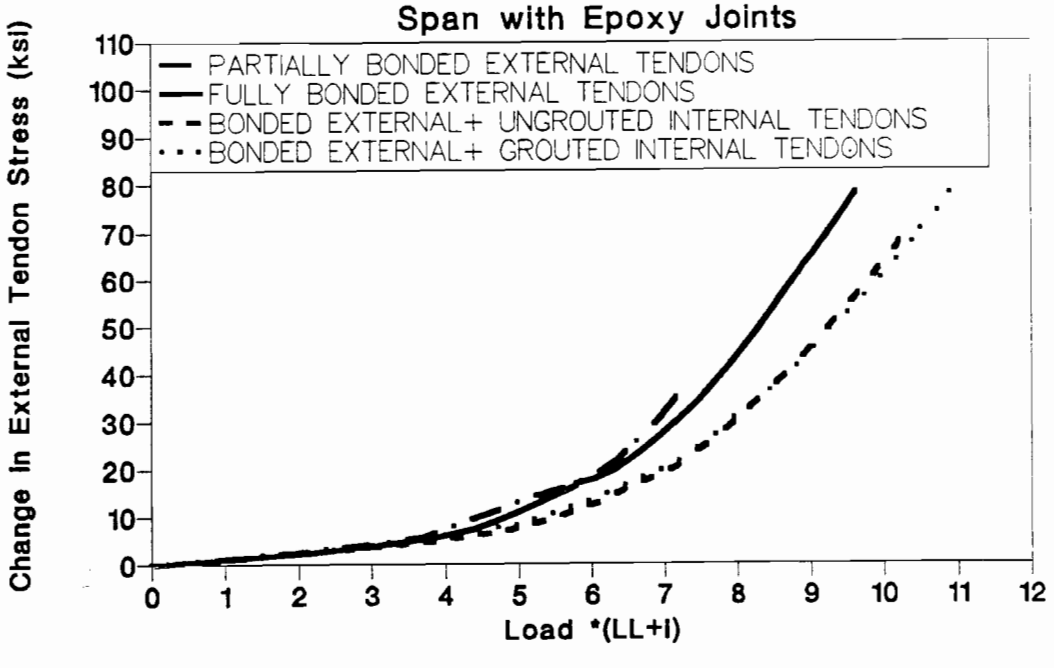

Figure 4.78 Effect of bonding and grouted internal tendons on external tendon stress in epoxy joints span.

4.8 Stiffness

As shown in Figure 4.75, the stiffness of any joint section after the joint starts opening is higher when the external tendons are bonded to the diaphragms because the section stiffness varies inversely with the unbonded length of the external tendons in that section according to Equation 4.3 from Fig 4.75. The short unbonded tendon length increases the structure stiffness especially at loads greater than the joint opening load.

$$k_\theta = \frac{Z^2 * E * A_p}{L} \qquad \text{Eq. 4.3}$$

The grouted internal tendons behave similar to the bonded external tendon since the internal tendon will slip from the segment sections toward the joint when the joint opens. The development length over which the tendon will slip depends on the joint opening, the tendon stresses at the joint section and inside the segment sections, and the bond strength between the internal tendon and the surrounding concrete. If the internal tendons are ungrouted, the length (L) used in Equation 4.3 is the total tendon length. However by grouting the internal tendon, the unbonded length becomes much smaller. The actual length needs to be obtained from a bond slip relationship such as that discussed in Chapter Five.

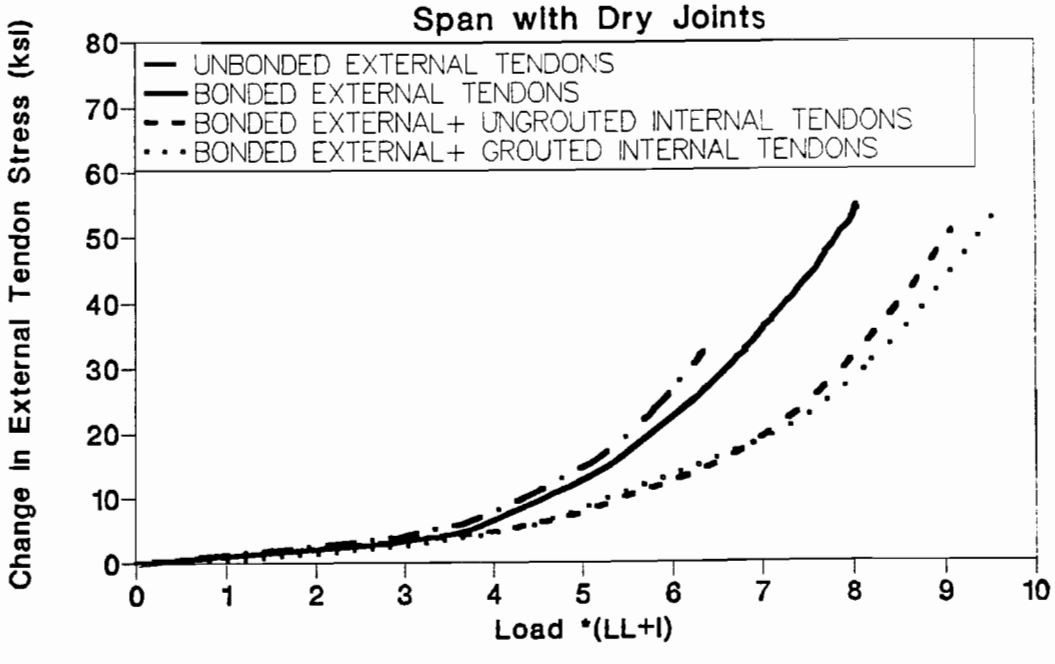

Figure 4.79 Effect of bonding and grouted internal tendons on tendon stress in dry joints span.

4.9 Moment Redistribution

Bonding of external tendons and/or using grouted internal tendons increased the number of joints which opened before the critical joint failed. As a result, the total joint opening in the critical regions increased substantially as discussed earlier in this chapter. This higher potential rotational capacity will allow greater redistribution of moment in continuous members.

4.10 External Tendon Stress

The external tendon strain is not compatible with the concrete adjacent to it but the strain is averaged over the length between two discrete points of bonding. The change in tendon length between the two discrete bonding points is the sum of the change in length of the concrete section along the tendon between the two points. Thus, the strain variation in the external tendon is a function of the overall structure deformations and not of the local concrete section as for grouted internal tendons.

The external tendon stress exhibited different stages as loads were increased as shown in Fig. 4.80. The tendon stress increased linearly up to the load level when the neutral axis at the critical joint reached the tendon elevation. This load was higher than the decompression load. After that the external tendon stress increased slowly as the additional applied moment was resisted primarily by the increase in moment lever arm due to concentration of the compression force in the top flange. When the critical joint opened, the additional moment was resisted primarily by an increase in tendon stress which increased at a higher rate. The tendon stress increased at a very high rate when the support joint started opening and the internal forces were redistributed back to the critical joint. The maximum opening capacity of the critical joint controlled the ultimate strength of the structure.

4.10.1 Before Cracking. The grouted tendon strain is assumed equal to the concrete strain at the level of the tendon in a fully bonded system. For external tendons or ungrouted internal tendons, the tendon strain is not compatible with the adjacent concrete strain; the tendon strain is constant over the length between the discrete bonded points. The tendon strain is calculated from the change in length between the two discrete bonded points. The change in length is equal to the integration of the concrete strain at the tendon level along the tendon length between the two discretely bonded points.

The linear portion of change in tendon stress can be calculated from moment curvature relationships because the sections are uncracked. Figure 4.81 shows the procedure for calculating the change in length of the unbonded tendon. The curvature diagram can be found from the moment diagram. The area between any two points under the curvature-eccentricity diagram (which is obtained by multiplying the curvature by the eccentricity along the tendon), is the change in tendon length between these points. The tendon strain change

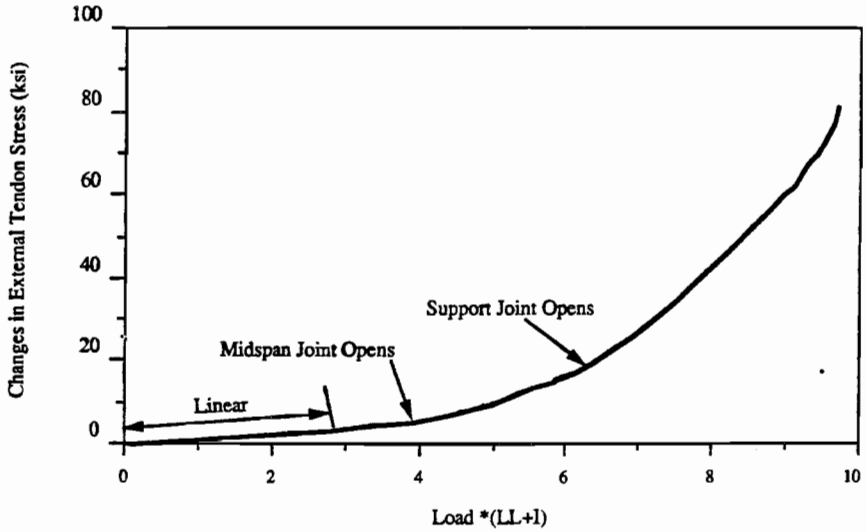

Figure 4.80 Typical tendon stress response (epoxy joints span).

between any two discretely bonded points is equal to the area under the curvature-eccentricity diagram between these two points divided by the length between the two points.

In this method of calculation, it is assumed that there is no friction between the tendon and surrounding concrete along the length between the discretely bonded points of the external tendon. An alternate assumption which is the basis for calculation for bonded tendons is that there is no slip at the bonded points and at the anchored points.

Calculation of the change in stress of unbonded internal tendons and the external tendons is shown in Fig. 4.82. The calculated stress change agrees with the measured values from the test. The measured change in external tendon stress at 2.7*(LL+I) was 3.71 ksi while the calculated change in stress was 3.84 ksi (a difference of 3 percent).

4.10.2 After Cracking. After the epoxy joint had cracked or the dry joint had opened, curvature increases over the hinge length as shown in Fig. 4.83. Finding the hinge length and hinge curvature is difficult. However, what is actually required is to find the maximum joint opening before failure. The maximum joint opening (which is the area under the curvature-eccentricity diagram in the hinge region) can be obtained as discussed in Section 4.6.2.

4.10.2.1 Rigid Body Mechanism. In segmental construction, the deformation is concentrated in the joint area and the structure can be modeled as rigid segments connected by hinges at the opened joints. In this model, the structure has no deformation

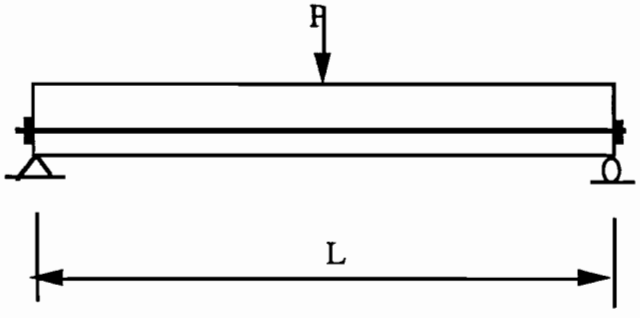

Simple span beam with unbonded tendon anchored at the end with eccentricity (e)

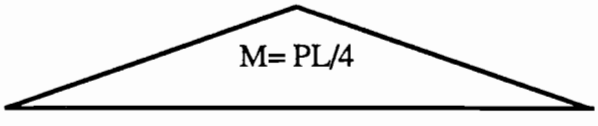

Moment Diagram

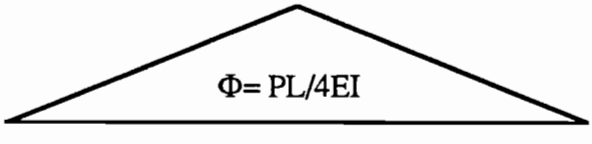

Curvature (M/EI)

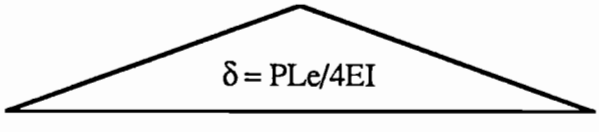

Deformation per unit length = Curvature * Eccentricity (e)

Elongation of Tendon= Δ= Area under $\delta = \frac{PL^2 e}{8EI}$

Stress Change in Tendon $= \frac{PL\ e\ E_p}{8EI}$

Figure 4.81 Calculation of unbonded tendon stress before cracking.

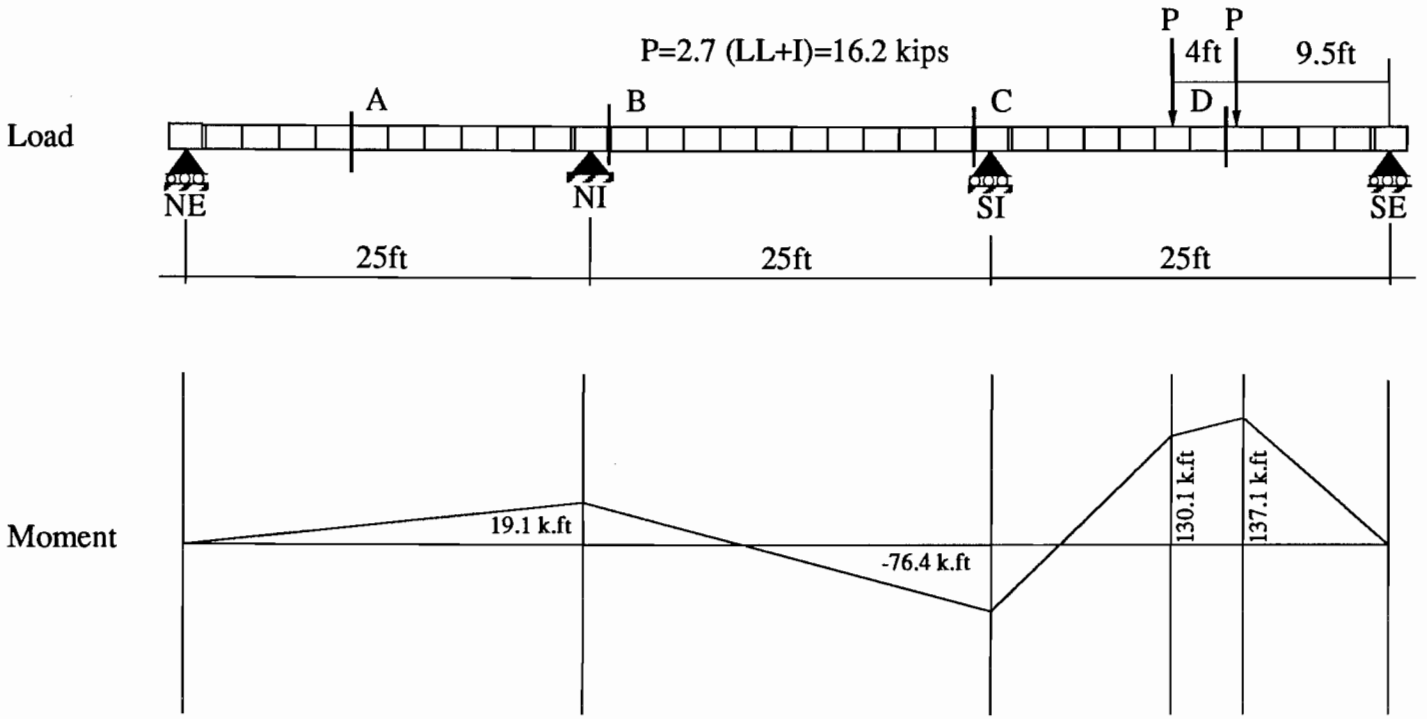

Internal Tendon Anchored at the Ends of the Model

Calculated Stress Change of Internal Tendon From Moment Curvature = 0.45 ksi

Measured Stress Change of Internal Tendon From Test Result = 0.40ksi

External Tendon Bonded at All Deviators

Calculated Stress Change of External Tendon at D From Moment Curvature = 3.84ksi

Measured Stress Change of External Tendon at D From Test Result = 3.71ksi

Figure 4.82 Calculated tendon stress before cracking.

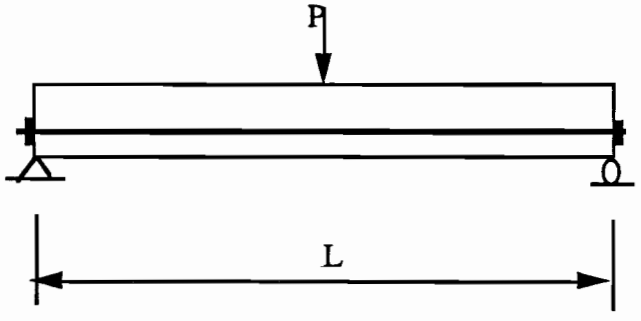

Simple Span Beam with Unbonded Tendon anchored at the end with eccentricity (e)

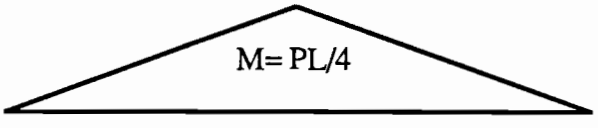

Moment Diagram

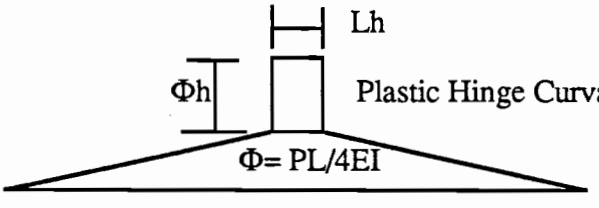

Curvature (M/EI)

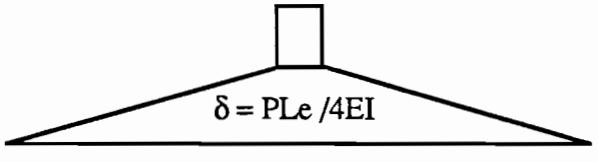

Deformation per unit length = Curvature * Eccentricity (e)

$$\text{Elongation of Tendon} = \Delta = \text{Area under } \delta = \frac{PL^2 e}{8EI} + \Phi_h \; L_h e$$

$$\text{Stress Change in Tendon} = \left[\frac{PL^2 e}{8EI} + \Phi_h \; L_h e\right] * \frac{E_p}{L}$$

Assume Rigid Body Mechanism $\quad \frac{PL^2 e}{8EI} << \Phi_h \; L_h e$

Then $\quad \Delta F_s = \Phi_h \; L_h e * \frac{E_p}{L}$

Figure 4.83 Calculation of unbonded tendon stress after cracking.

unless a joint is opened and a hinge is formed. As shown in Fig. 4.83, the elastic curvature is neglected so there is no change in tendon stress unless a joint starts opening. The joint opening is the only increase in the tendon length between any two points which is used to calculate the change in tendon stress. The joints start opening when the external moment exceeds the internal resistance moment of the joint assuming that the compression force has moved to the extreme compression fiber of the section and the moment lever arm is a maximum.

4.10.2.2 Multiple Joint Openings. In a rigid body mechanism, it is assumed that one joint opens in each of the plastic hinge locations. The tests showed that many joints opened in the positive moment region. The number of joints which open depends on the bonding condition of the external tendons and the amount of grouted internal tendons. The tests showed that the total joint opening in the positive moment region was higher than the maximum joint opening at the critical joint. Higher total joint opening means a larger change in tendon length and larger change in tendon stresses. To be conservative, only one joint is assumed to open in each hinge region in this model.

4.10.2.3 Calculation Procedure. Figure 4.84 shows the procedure for calculating the change in unbonded tendon stress assuming that a single joint will open in the critical positive moment region. In this calculation procedure, only one joint (critical joint) is assumed to reach its maximum joint opening (as calculated in Section 4.6), while the support joint has an opening lower than its maximum opening. This lower bound mechanism is the same as noticed in the tests since only the critical joint was crushed. This mechanism is different than the upper bound theory mechanism in which a full plastic mechanism is assumed and unlimited joint openings are assumed. Concrete structures have limited rotation capacity which should be taken into consideration otherwise the calculated strength is an upper bound to the actual strength. In this procedure, lower bound theory is assumed and the calculated strength is a lower bound of the actual strength.

A rigid body mechanism is assumed which means that the joint openings cause the only change in tendon length. The change in tendon length is calculated from the deflected shape of the structure. The change in tendon stress is calculated from the change in tendon length assuming that no slip occurs at the bonded diaphragms or the anchored points. After that, corrections are applied if the tendon has slipped at the bonded diaphragms. The bond-slip relationship is assumed as shown in Figure 4.84 to simplify the calculation.

Figures 4.85 and 4.86 show the calculation of change in external tendon stress for the flexural strength tests. The maximum calculated change in external tendon stress was 45.5 ksi for the dry joints span and 52 ksi for the epoxy joints span. The actual change in external tendon stress measured in the dry joints span was at least 50 ksi and in the epoxied joints span was at least 70 ksi. These measured values are higher than the calculated values by about 10 percent for the dry joints span and 25 percent for the epoxy joints span. This difference was due to two reasons. First, the model assumes that there is no increase in stress unless the critical joint starts opening (rigid body mechanism). In the actual

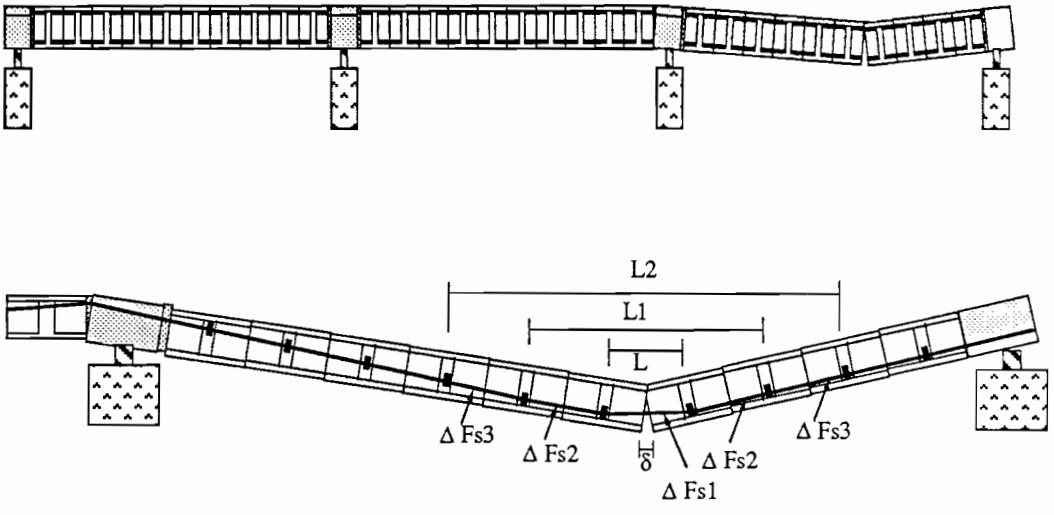

δ : Maximum Joint Opening at Prestress Level

Δ Fs1 :Change in Stress of Tendon Segment above Adjacent Tendon Segments

L, L1, L2 : Length of Tendon Segment

B : Bond Strength of One Deviator

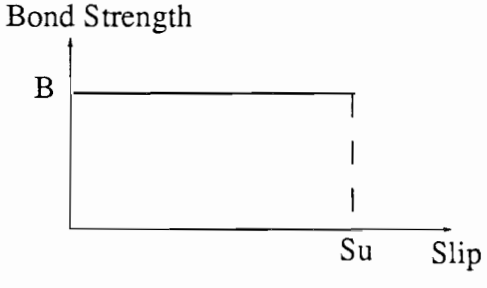

Assumed Bond- Slip Relation

$\Delta Fs1 = \delta * E / L$

If $\Delta Fs1 > B$ Tendon will slip

Then $\Delta Fs1 = B$

$\delta 1 = B * L / E$

$\Delta Fs2 = (\delta - \delta 1) * E / L1$

If $\Delta Fs2 > B$ Tendon will slip at the second deviator $\Delta Fs2 = B$

Then $\Delta Fs2 = B$

$\delta 2 = B * L1 / E$

$\Delta Fs3 = (\delta - \delta 1 - \delta 2) * E / L2$

Continues Till $\Delta Fsi = B$ Or No slip is possible

If slip at any deviator > Su, recalculate by neglecting bond on that deviator

Total $\Delta Fs = \Delta Fs1 + \Delta Fs2 + \Delta Fs3 + \ldots\ldots\ldots + \Delta Fsi$

Figure 4.84 Calculation procedure for tendon stress after cracking - single joint opening in positive moment region.

structure, there would be some elastic effects. Second, the test showed that multiple joints opened during the actual loading of the structure, not a single joint as assumed in the calculation model. The calculation model is hence simple and conservative.

4.11 Conclusions

a) Bonded external tendons or grouted internal tendons increased the number of opening joints in the critical positive moment region. Bonding of tendons increases the stiffness and strength of the critical joint which attracts more external moment to the critical region and delays crushing of the critical joint. Bonding creates a difference in tendon stresses between the critical joint and surrounding joints which results in lower cracking or joint opening moment in the surrounding joints. These two effects increase the number of opening joints which result in higher total joint opening in the critical region.

b) Ductility is increased with the amount of grouted internal tendons and/or bonded external tendons. Bonding or grouting tendons increased the total joint opening. Higher total joint openings resulted in larger deflection.

c) Strength is increased by bonding the external tendons to the intermediate diaphragms. Bonding increases the total joint opening in the critical region which increases the change in tendon length. Bonding reduces the external tendon unbonded lengths. Higher change in tendon length with shorter unbonded length causes a larger increase in tendon stress. A higher increase in tendon stress results in higher moment capacity at the critical joint and higher strength.

d) Strength is increased by grouting the internal tendons. Grouting the internal tendons increases the total joint opening and increase the change in tendon lengths. Higher change in tendon length increases the change in tendon stress, which results in higher strength.

e) Maximum allowable joint opening is larger for epoxy joints than for dry joints due to the more favorable crack patterns in the compression zone of the critical section. The crack pattern in epoxy joints increases the volume of the highly compressed region and reduces the concentration of the compressive strain in that region. At maximum allowable strain, the flange compressive deformation is increased and this leads to larger joint opening.

f) Maximum allowable joint opening reduced with higher compression forces. Higher compression forces means a greater depth to the neutral axis. An increase in neutral axis depth reduces the maximum joint opening.

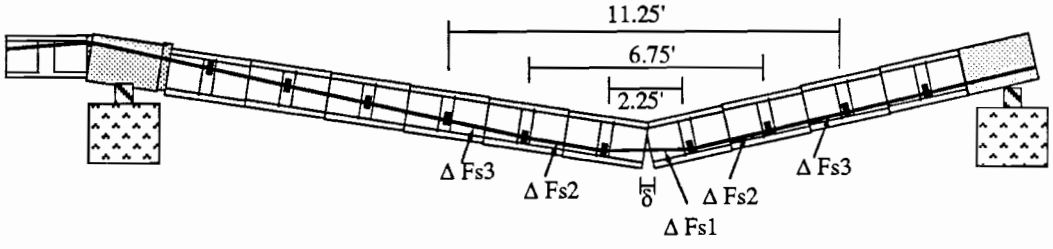

δ : Maximum Joint Opening Calculated =0.28 in. (see Figure 4.74)

δ : Maximum Joint Opening Calculated at Tendon Level =0.21 in.

Δ Fs1 : Change in Stress of Tendon Segment above Adjacent Tendon Segments

B : Bond Strength of One Deviator, Measured B=10 ksi (Chapter Three)

Δ Fs1= 0.21 *27000 / 2.25*12=210 ksi > 10 ksi Tendon will slip

Then Δ Fs1 = 10 ksi

δ1= 10*2.25*12 / 27000= 0.01 in.

Δ Fs2 = (0.21 – 0.01)*27000 / 6.75*12 =66 ksi > 10 Tendon will slip

Δ Fs2 = 10 ksi

δ2= 10*6.75 *12 / 27000 = 0.03 in.

Δ Fs3 = (0.21 – 0.04)*27000 / 11.25*12 =34 ksi > 10 ksi Tendon will slip

δ3= 10*11.25*12 / 27000 = 0.05 in.

Δ Fs4 = (0.21 – 0.09)*27000 / 15.75*12 =17 ksi > 10 ksi Tendon will slip

δ4= 10*15.75*12 / 27000 = 0.07 in.

Δ Fs5 = (0.21 – 0.16)*27000 / 20.25*12 =5.5 ksi < 10 ksi O.K No slip

Total ΔFs = 5.5+10+10 +10+10 = 45.5 ksi

Figure 4.85 Calculation of tendon stress after cracking single joint opened in positive moment region - dry joints span.

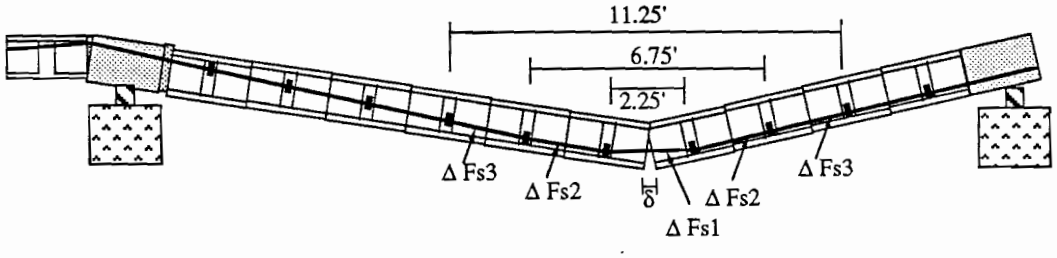

δ : Maximum Joint Opening Calculated =0.35 in. (see Figure 4.74)

δ : Maximum Joint Opening Calculated at Tendon Level =0.27 in.

Δ Fs1 : Change in Stress of Tendon Segment above Adjacent Tendon Segments

B : Bond Strength of One Deviator, Measured B=10 ksi (Chapter Three)

Δ Fs1= 0.27 *27000 / 2.25*12=270 ksi > 10 ksi Tendon will slip

Then Δ Fs1 = 10 ksi

δ1= 10*2.25*12 / 27000= 0.01 in

Δ Fs2 = (0.27 – 0.01)*27000 / 6.75*12 =86 ksi > 10 Tendon will slip

Δ Fs2 = 10 ksi

δ2= 10*6.75 *12 / 27000 = 0.03 in

Δ Fs3 = (0.27 – 0.04)*27000 / 11.25*12 =46 ksi > 10 ksi Tendon will slip

δ3= 10*11.25*12 / 27000 = 0.05 in

Δ Fs4 = (0.27 – 0.09)*27000 / 15.75*12 =26 ksi > 10 ksi Tendon will slip

δ4= 10*15.75*12 / 27000 = 0.07 in

Δ Fs5 = (0.27 – 0.16)*27000 / 20.25*12 =12.22 ksi < 10 ksi Tendon will slip

δ5= 10*20.25*12 / 27000 = 0.09 in

Δ Fs6 = (0.27 – 0.25)*27000 / 22.5*12 =2 ksi < 10 ksi No slip

Total ΔFs = 2+10+10+10 +10+10 = 52ksi

Figure 4.86 Calculation of tendon stress after cracking single joint opened in positive moment region - epoxy joints span.

g) Cracks at epoxy joints span always occur in the joint region and not in the segments. Segment sections are stronger than the joint sections due to the presence of passive reinforcement in the segment. Due to the discontinuity of the reinforcement in the joint region, the flexural cracks occur in the concrete section adjacent to the epoxy joint.

h) Ductility increases to a certain limit with the amount of grouted internal tendons and/or bonded external tendons. After this, ductility does not increase further since it is limited by the hinge region rotation capacity. The increase in maximum deflection is due to the increase in the number of opening joints during loading. An increase in the amount of bonded tendons higher than the amount required to open all possible opening joints does not increase the ductility further. Since all possible joints were already opened, the increase in number of bonded tendons would not increase the number of opening joints but might slightly increase the amount of the joint openings. In fact, the increase in the amount of bonded or grouted tendons increases the ultimate compressive force (bonded or grouted tendons reach a much higher stress at ultimate than unbonded tendons) in the joint section and reduces the maximum joint rotation which resulted in some reduction in ductility.

i) Crushing of the concrete in compression was always in the joint section. This gives an indication that the strain in the joint section is higher than the compressive strain in the segment.

j) Epoxy joints effect the ductility and strength of segmental beams. Epoxy has two effects on strength and ductility. First, epoxy joints have better confinement than dry joints which increases the maximum joint opening, and in turn, results in higher strength and ductility. Second, epoxy joints increase the moment required to open new joints because the cracking moment is higher than the joint opening moment.

This part will concentrate the rotations at few joints and reduce the strength and ductility. Bonding of external tendons or using grouted internal tendons reduces the adverse effect of epoxy joints by increasing the external moment on these joints which forces them to crack.

k) Bonding of external tendons and/or using grouted internal tendons increases the load redistribution. Bonded external tendons and/or grouted internal tendons increase the total joint opening in the critical regions which allows higher moment redistribution.

l) Lower bound plastic mechanisms were observed in all flexural strength tests. The critical joint reached its ultimate rotation and failed by crushing of the compression flange, while the support joint opened at a later stage during the tests but did not fail.

CHAPTER FIVE

ANALYTICAL MODEL

5.1 Introduction

The important questions posed by this study can be separated into two groups. The first group includes questions related to segment behavior before and after cracking. The second group concerns possible slipping of the external and internal tendons.

For load levels above normal design values, segmental post-tensioned bridges can open at dry joints between segments or crack immediately adjacent to the epoxy joints between segments. Dry joints are an obvious weak plane. Although the epoxy joints have higher tensile strength than unreinforced concrete, the concrete zone immediately adjacent to each epoxy joint is weaker than the remainder of the adjacent segments because the internal non-prestressed segment reinforcement is discontinuous in the joint zone for a distance equal to the clear cover from the joint face. The relation between the strain at any point in the beam and the deformation of nodes of a beam element that comprises part of a finite element model described in this chapter is dependent on whether the segment is cracked or uncracked. The finite element model for beam segments has to take into consideration changes due to cracking or joint opening.

External tendons are connected to diaphragms or deviation saddles by chemical bonding and/or friction due to the deviation of tendons at diaphragms. Slip of external tendons through these connections can have a substantial effect on the behavior of the structure, especially at large deformations. Due to wide joint or crack openings, internal tendons must also slip from the segment sections towards the opened joints. These two slip effects will be modeled in the analytical study.

5.2 Material Models

Non-linear stress-strain relationships for material are assumed in this study to allow prediction of the complete range of behavior for the structure. Due to concentration of rotations at the critical joints, externally post-tensioned segmental structures have the possibility of premature failure at these joints. The assumed concrete stress-strain relationship plays a major role in predicting the capacity of the structure when crushing occurs at critical joints.

5.2.1 Concrete. The stress-strain relationship assumed for concrete is very similar to that originally suggested by Hognestad (8), and is shown in Fig. 5.1. As shown, compression stress is assumed to vary with strain in a parabolic manner up to the specified compressive strength. A linear relationship is assumed for the descending branch of the

diagram shown in Fig. 5.1. The concrete stress-strain relationship is defined by two points. The first point is $(f_{cc},\varepsilon_{cc})$ while the second point is $(f_{cu},\varepsilon_{cu})$. The modulus of elasticity of the concrete at any point on the ascending branch is calculated as shown in Fig. 5.1 by differentiating the stress with respect to the strain. To simplify the analysis, the modulus of elasticity of the descending branch is assumed zero. The tension part of the concrete stress-strain curve is assumed to be a straight line up to the concrete fracture limit f_{ct}. The modulus of elasticity of the concrete in tension is assumed to be equal to the secant modulus of elasticity specified by the ACI code(9). The tension limit of the concrete f_{ct} can be calculated or obtained from a tension test.

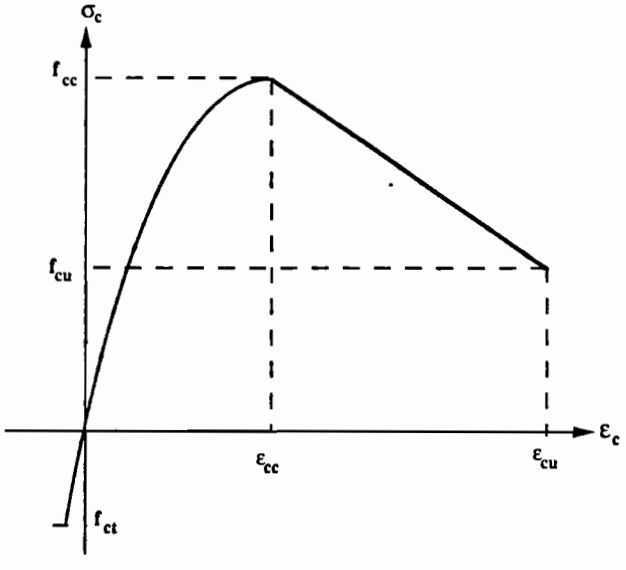

$$\sigma_c = \frac{\varepsilon_c}{\varepsilon_{cc}} * f_{cc} * \left(2 - \frac{\varepsilon_c}{\varepsilon_{cc}}\right) \qquad \text{for} \quad 0 < \varepsilon_c < \varepsilon_{cc}$$

$$E_c = \frac{2}{\varepsilon_{cc}} * f_{cc} * \left(1 - \frac{\varepsilon_c}{\varepsilon_{cc}}\right)$$

$$\sigma_c = f_{cc} - \frac{(\varepsilon_c - \varepsilon_{cc})}{(\varepsilon_{cu} - \varepsilon_{cc})} * (f_{cc} - f_{cu}) \qquad \text{for} \quad \varepsilon_{cc} < \varepsilon_c < \varepsilon_{cu}$$

$$E_c = 57{,}400 \ \text{sqrt}\,(f_{cc}) \qquad \text{for} \quad \varepsilon_c < 0$$

Figure 5.1 Concrete stress-strain relationship.

The maximum concrete strain is an important factor in predicating the capacity of segmental structures. Segmental structures prestressed with external tendons have the possibility of premature failure in the critical joints. A critical joint fails when strains exceeding the ultimate concrete strain develop in either flange. The ultimate concrete strain depends on the confinement condition of the flanges.

5.2.2 Steel. The stress-strain relationship for steel is shown in Fig. 5.2. Two points are required to define the stress-strain relationship for any reinforcement. The first point is (f_{sy},ϵ_{sy}), and the second point is (f_{su},ϵ_{su}). A linear relationship with constant slope is assumed up to yielding of the steel. Strain hardening is assumed between yielding and fracture of the steel. The steel is assumed to have the same stress-strain relationship in compression and tension. The modulus of elasticity at any point of the relationship can be obtained as shown in Fig. 5.2. The same bi-linear type of relation is assumed for the ordinary reinforcement and prestress steel.

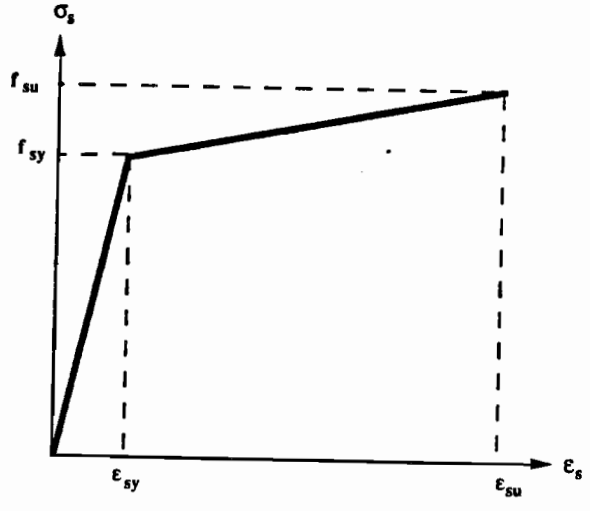

$$\sigma_S = \frac{\epsilon_S}{\epsilon_{sy}} * f_{sy} \qquad \text{for} \quad \epsilon_S < \epsilon_{sy}$$

$$E_S = \frac{f_{sy}}{\epsilon_{sy}}$$

$$\sigma_S = f_{sy} + \frac{(\epsilon_S - \epsilon_{sy})}{(\epsilon_{su} - \epsilon_{sy})} * (f_{su} - f_{sy}) \qquad \text{for} \quad \epsilon_{sy} < \epsilon_S < \epsilon_{su}$$

$$E_S = \frac{(f_{su} - f_{sy})}{(\epsilon_{su} - \epsilon_{sy})}$$

Figure 5.2 Steel stress-strain relationship.

5.2.3 Bond Stress versus Slip Relationship. Bond-slip relationships depend on many factors such as type of steel, duct, and injection. The bond-slip relationships used in this study are shown in Fig. 5.3. Figure 5.3(a) shows the bond slip relationship for the external tendon, while Fig. 5.3(b) shows the bond-slip relationship assumed for the internal tendon. Bond stress is the stress over the contact area between the tendon and the grout. The conventional reinforcement is assumed not to slip.

Higher stress changes in the external and internal tendons occur when the dry joints open or epoxy joints crack. As shown in Chapter Three, the change in external tendon stress was less than 4 ksi at loads lower than the joint-opening or cracking load. The stress change in the grouted internal tendon was less than 10 ksi at the joint-opening load. In an actual bridge, the bond stress between the tendon and the grout is subjected to change in direction as live loads move from one side of the diaphragm to the other (reversals in bond stress direction). The bond reversals occur at loads lower than the joint opening or cracking load.. Joint opening or cracking usually occurs at loads substantially higher than the service load. This limits the high tension variation in the tendons to special and unusual overload cases. Thus, a bond-slip relationship for monotonic loading was assumed in this study.

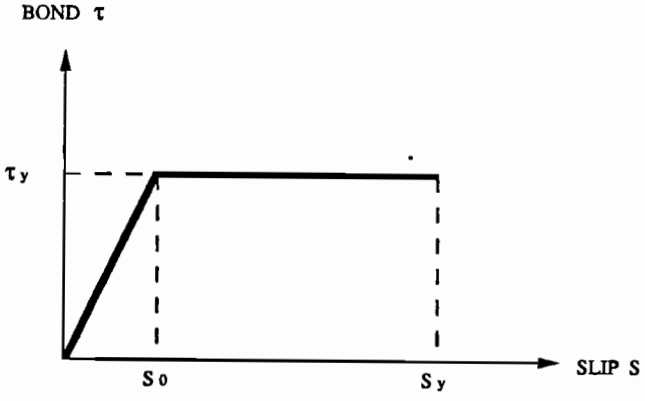

a) External Tendon Bond-Slip Relationship

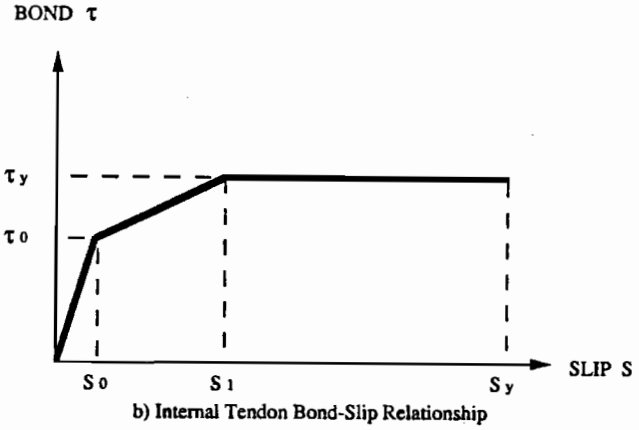

b) Internal Tendon Bond-Slip Relationship

Figure 5.3 Bond-slip relationships.

As discussed in Chapter Three, external tendon stresses were measured at six locations in each span during testing. The bond-load relationship obtained from the tests is shown in Figures 3.139 and 3.141. Bond increases at a high rate until full slip occurs at a diaphragm. After initial (general) slip, bond increases at a lower rate or stabilizes. The ordered pairs for points required to define the bond-slip relations for the external tendons were obtained from test data obtained by Radloff(10) in tests conducted as part of this

study, and from the test results discussed in Section 3.5. The points required to define the bond-slip relation for internal tendons were obtained from test data reported by Trost(11).

5.3 Analytical Formulation

The segmental bridge with external tendons is modeled with a one-dimensional beam element. As shown in Fig. 5.4, the beam element of length, L, consists of two halves of the adjacent segments with the dry or epoxy joint between them. In this model, the external tendon forces are applied as external forces.

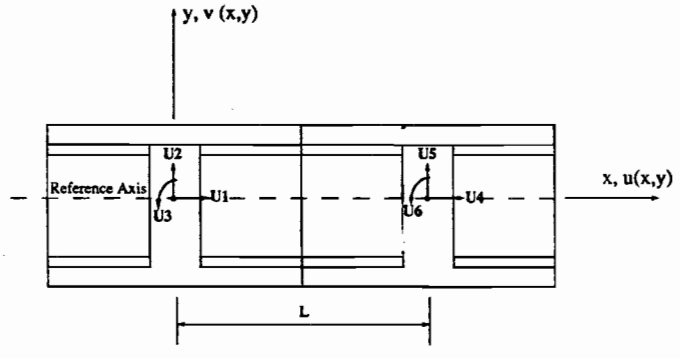

Figure 5.4 Beam element model.

5.3.1 Beam Element. The beam element, of length L, starts from the middle of one segment and extends to the middle of the next segment. It includes the dry or epoxy joint between the segments as shown in Fig. 5.4. A one dimensional beam element with axial and flexural deformations is used in this study. The beam element has a vertical axis of symmetry for properties and loads so that no torsional deformations are considered. Nonlinear material properties are included in the beam element modeling. The beam element formulation before cracking is based on small deflections, and no time-dependent effects are included at any stage.

5.3.1.1 Uncracked Beam Element. Before cracking or joint opening, the joints between segments have no effect on the flexural behavior of the beam elements. The beam elements are assumed to be continuous along their length and across the joints. The segment non-prestressed reinforcement is discontinuous in the joint zone, so the analysis neglects the non-prestressed reinforcement in the joint sections.

The beam element is shown in Fig. 5.4. The vertical displacement $v(x,y)$ and the horizontal displacement $u(x,y)$ are:

$$\begin{aligned} u(x,y) &= u_o(x,y) + \Delta u(x,y) \\ v(x,y) &= v_o(x,y) + \Delta v(x,y) \end{aligned} \tag{5.1}$$

in which $v_o(x,y)$ and $u_o(x,y)$ are the current displacements and $\Delta v(x,y)$ and $\Delta u(x,y)$ are the displacement increments which are given as follows:

$$\begin{aligned} \Delta u(x,y) &= \Delta u_r(x) + y \frac{d[\Delta v(x)]}{dx} \\ \Delta v(x,y) &= \Delta v(x) \end{aligned} \tag{5.2}$$

where $\Delta v(x)$ and $\Delta u_r(x)$ are the displacement increments along the reference line of the beam element.

The three degrees of freedom at each node of the beam element are two translations and one rotation as shown in Fig. 5.4. The displacements along the reference line are obtained from the nodal degrees of freedom as follows:

$$\begin{bmatrix} \Delta u_r(x) \\ \Delta v(x) \end{bmatrix} = \overline{N}.\Delta \underline{U} \tag{5.3}$$

where

$$\overline{N} = \begin{bmatrix} N_{1u}(x) & 0 & 0 & N_{2u}(x) & 0 & 0 \\ 0 & N_{1v} & N_{2v}(x) & 0 & N_{3v}(x) & N_{4v}(x) \end{bmatrix} \tag{5.4}$$

in which $N_{iu}(x)$ are the standard axial shape functions and $N_{iv}(x)$ are standard flexural cubic shape functions, and

$$\Delta \underline{U} = \begin{bmatrix} \Delta u_1 \\ \Delta u_2 \\ \Delta u_3 \\ \Delta u_4 \\ \Delta u_5 \\ \Delta u_6 \end{bmatrix} \tag{5.5}$$

Assuming plane sections remain plane, the longitudinal strain and curvature are :

$$\begin{aligned} \epsilon(x,y) &= \epsilon_o(x,y) + \Delta\epsilon(x,y) \\ \phi(x,y) &= \phi_o(x,y) + \Delta\phi(x,y) \end{aligned} \tag{5.6}$$

where

$$\begin{aligned} \Delta\epsilon(x,y) &= \Delta\epsilon_r(x) + y.\Delta\phi(x) \\ \Delta\phi(x,y) &= \frac{d^2[\Delta v(x)]}{dx^2} = \Delta\phi(x) \end{aligned} \tag{5.7}$$

Therefore

$$\begin{bmatrix} \Delta\epsilon_r(x) \\ \Delta\phi(x) \end{bmatrix} = \overline{B}.\Delta\underline{U} \tag{5.8}$$

where

$$\overline{B} = \begin{bmatrix} \frac{dN_{1u}(x)}{dx} & 0 & 0 & \frac{dN_{2u}(x)}{dx} & 0 & 0 \\ 0 & \frac{d^2N_{1v}(x)}{dx^2} & \frac{d^2N_{2v}(x)}{dx^2} & 0 & \frac{d^2N_{3v}(x)}{dx^2} & \frac{d^2N_{4v}(x)}{dx^2} \end{bmatrix} \tag{5.9}$$

Stress corresponding to a known strain at any location in the beam element can be found using the stress-strain relationship of the material as discussed in Section 5.2.

The beam cross section is divided into fibers, as shown in Fig. 5.5, to simplify the calculation. The strain and stress is assumed constant in each fiber. The stress in a fiber j is:

$$\sigma_j(x,y) = \sigma_{jo}(x,y) + \Delta\sigma_j(x,y) \tag{5.10}$$

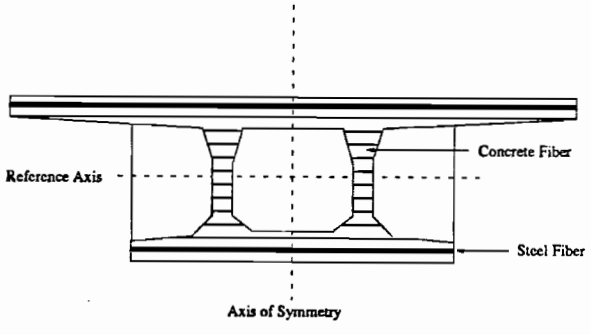

Figure 5.5 Reinforced-concrete fiber cross section.

where

$$\Delta\sigma_j(x,y) = \frac{d\sigma_j(x,y)}{d\epsilon}.\Delta\epsilon(x,y) \tag{5.11}$$

Forces on any section of the element are obtained by summing the forces over all the fibers of that section as follows:

$$
\begin{aligned}
P_o(x) &= \sum_{j=1}^{N} \sigma_{oj}(x,y_j).A_j \\
\Delta P(x) &= \sum_{j=1}^{N} \frac{d\sigma_j(x,y_j)}{d\epsilon}.\Delta\epsilon(x,y_j).A_j \\
M_o(x) &= \sum_{j=1}^{N} \sigma_{oj}(x,y_j).y_j.A_j \\
\Delta M(x) &= \sum_{j=1}^{N} \frac{d\sigma_j(x,y_j)}{d\epsilon}.\Delta\epsilon(x,y_j).y_j.A_j
\end{aligned}
\tag{5.12}
$$

The initial stresses $\sigma_{oj}(x,y_j)$ and the tangent modulus $\frac{d\sigma_j(x,y_j)}{d\epsilon}$ are evaluated at each fiber from the stress-strain relationship of the corresponding material.

Substituting Equations (5.7) into Equations (5.12) gives:

$$
\begin{bmatrix} \Delta P(x) \\ \Delta M(x) \end{bmatrix} = \underline{D}.\begin{bmatrix} \Delta\epsilon_r(x) \\ \Delta\phi(x) \end{bmatrix} \tag{5.13}
$$

where

$$
\underline{D} = \begin{bmatrix} \sum_{j=1}^{N} \frac{d\sigma_j(x,y_j)}{d\epsilon}.A_j & \sum_{j=1}^{N} \frac{d\sigma_j(x,y_j)}{d\epsilon}.y_j.A_j \\ \sum_{j=1}^{N} \frac{d\sigma_j(x,y_j)}{d\epsilon}.y_j.A_j & \sum_{j=1}^{N} \frac{d\sigma_j(x,y_j)}{d\epsilon}.y^2{}_j.A_j \end{bmatrix} \tag{5.14}
$$

Using the strain- displacement relationships in Equation (5.8), Equation (5.13) gives:

$$
\begin{bmatrix} \Delta P(x) \\ \Delta M(x) \end{bmatrix} = \underline{D}.\overline{B}.\Delta\underline{U} \tag{5.15}
$$

Using the virtual work principles to relate the internal forces with the external forces, gives:

$$\int_0^L \left(\delta\epsilon_r(x) \quad \delta\phi(x) \right) \begin{bmatrix} P(x) \\ M(x) \end{bmatrix} dx = \int_0^L \delta v(x).q(x).dx \tag{5.16}$$

where L is length of the beam element, q(x) is the external load applied, and

$$\delta v(x) = \overline{N}.\delta \underline{U} \tag{5.17a}$$

$$\begin{bmatrix} \delta\epsilon_r(x) \\ \delta\phi(x) \end{bmatrix} = \overline{B}.\delta \underline{U} \tag{5.17b}$$

and

$$\begin{bmatrix} P(x) \\ M(x) \end{bmatrix} = \begin{bmatrix} P_o(x) \\ M_o(x) \end{bmatrix} + \begin{bmatrix} \Delta P(x) \\ \Delta M(x) \end{bmatrix} \tag{5.18}$$

Substituting Equations (5.18), (5.17), and (5.15) into Equation (5.16) gives:

$$\overline{K_t}.\Delta \underline{U} = \overline{P_e} - \overline{P_r} \tag{5.19}$$

where

$$\overline{K_t} = \int_0^L (\overline{B})^T.\underline{D}.\overline{B}.dx \tag{5.20}$$

is the tangent stiffness matrix for the beam element,

$$\overline{P_r} = \int_0^L (\overline{B})^T.\begin{bmatrix} P(x) \\ M(x) \end{bmatrix} dx \tag{5.21}$$

is the internal resisting nodal force vector, and

$$\overline{P_e} = \int_0^{\frac{L}{2}} (\overline{N_v})^T . q(x) . dx \tag{5.22}$$

is the external applied nodal force vector.

The integrals are evaluated numerically using Gaussian quadrature. Three integration points are used in the beam element to provide sufficient accuracy.

5.3.1.2 Cracked Beam Element. For a beam element of short length in comparison to the beam span, the moment and axial force can be assumed constant. In this case, the position of the neutral axis is the same along the beam element. The center of rotation of one section with respect to any other section lies on the neutral axis. However, as soon as joint opening initiates, the position of the neutral axis is disrupted near the joint and the position of zero displacement does not coincide with the neutral axis, as shown in Fig. 5.6. This model is based on the work done by Giuriani (7). The displacement of the joint section B relative to the middle section A can be found by integrating the concrete strain over half the segment length as follows:

$$u_B(y) = \int_0^{\frac{L}{2}} \epsilon_c(x,y) dx \tag{5.23}$$

The position of the center of rotation of the joint is obtained by setting:

$$u(y_o) = 0 \tag{5.24}$$

The concrete strain variation between section B and section A is assumed linear which simplifies the integration required to find the joint displacement as follows:

$$u_{CB}(y) = \frac{\epsilon_{CB}(y) + \epsilon_{CA}(y)}{2} * \frac{L}{2} \tag{5.25}$$

Knowing the maximum concrete strain and the depth of the compression block at sections A and B, the position of the center of rotation and rotation angle can be found. The strain is assumed to vary linearly over the sections as follows:

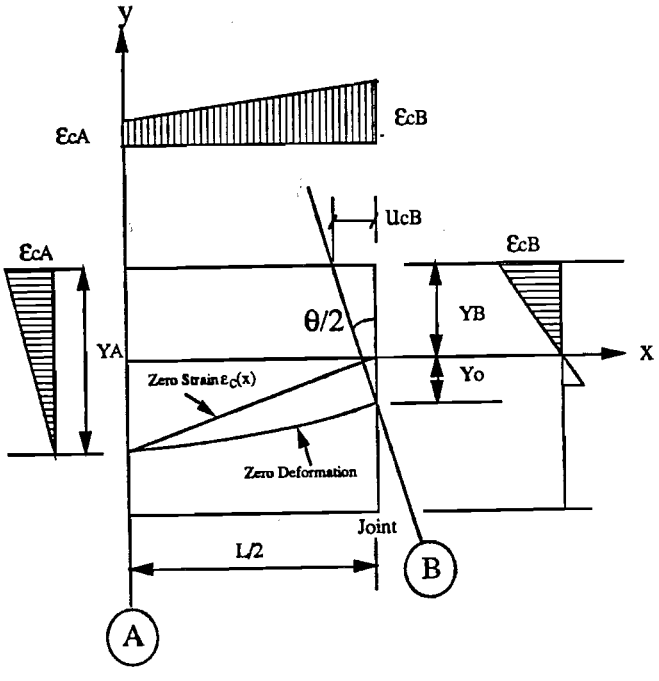

L: Segment length

u_{cB} : Deformation of the joint section

ε_{cA} : Concrete strain at section A

ε_{cB} : Concrete strain at the joint section

Y_A: Neutral axis depth at A

Y_B : Neutral axis depth at B

Y_o: Depth to the center of rotation

θ : Angle of rotation

Figure 5.6 Beam element model after cracking or joint opening.

$$\varepsilon_{CB}(y)=\frac{\varepsilon_{CB}}{y_B}*y$$

$$\varepsilon_{CA}(y)=\frac{\varepsilon_{CA}}{y_A}*(y_A-y_B+y) \qquad (5.26)$$

The relation between the maximum strain in sections A and B is obtained by assuming that the area under the strain diagram at section B is equal to that at section A. This assumption is based on the previous assumption that the moment and axial force are equal along the beam element. The relation is:

$$\frac{\varepsilon_{CA}*y_A}{2} = \frac{\varepsilon_{CB}*y_B}{2} \qquad (5.27)$$

From Equations (5.24), (5.25), (5.26), and (5.27) the position of the center of rotation can be found as follows:

$$y_o = \frac{y_B^2 * (y_A - y_B)}{(y_A^2 + y_B^2)} \tag{5.28}$$

and the angle of rotation of the joint section with respect to the middle section can be found as follows:

$$\theta = 2 * \frac{u_{CB}}{(y_B + y_o)} \tag{5.29}$$

Substituting Equations (5.25), (5.26), and (5.27) into Equation (5.29), gives:

$$\theta = \epsilon_{CB} * \frac{L}{y_B * FY} \tag{5.30}$$

where

$$FY = 2 * \frac{y_A^2}{(y_A^2 + y_B^2)} \tag{5.31}$$

A different algorithm must be applied after the beam element is cracked or the dry joint opened. The technique is based on partial continuity of the element after the joints are cracked or opened. Figure 5.7 shows the calculation algorithm for internal forces in a beam element with a cracked or opened joint. The calculation steps are as follows:

i) Find the strain ϵ_{CB} and compression depth y_B at the joint section B of Fig. 5.6 using Equations (5.6), (5.7), and (5.8). In this calculation, the beam element is assumed continuous and no discontinuity is created by the cracked or opened joint. The nodal displacements are the independent variables.

ii) Tests carried out in this study and presented in Chapter Three showed that cracking always occurred in the section immediately adjacent to the epoxy joint. Based on this observation, the depth to the neutral axis at section A (y_A) is assumed to be constant after the joint has opened . The depth, y_A, is calculated one time at the cracking or decompression load of the joint in the beam element. The depth is calculated using Equations (5.6), (5.7), and (5.8).

iii) Calculate the depth to the center of rotation y_o from Equation (5.28), and calculate FY from Equation (5.31).

iv) Calculate the joint rotation angle, θ, from Equation (5.30). The rotation angle calculation presented above is based on complete continuity of the beam element. The strain at any point of the beam is obtained from Equations (5.7) and (5.8), which are based on complete continuity of the beam element across the opened joint. In reality, the element is only partially continuous across the opened joint. This partial continuity is assumed to vary linearly from complete continuity at the cracking load to complete hinging when the extreme compression fiber of the joint section reaches the ultimate allowable concrete strain. The rotation of the joint element, if complete hinging is assumed, can be calculated from:

$$\theta = u_6 - u_3 \qquad (5.32)$$

where u_6 and u_3 are the nodal rotation of the beam element shown in Fig. 5.4. The final angle of rotation of the joint section is obtained as a combination of Equation (5.30) and Equation (5.32) according to the state of strain of the extreme compression fiber. The joint opening is obtained from the final angle of rotation.

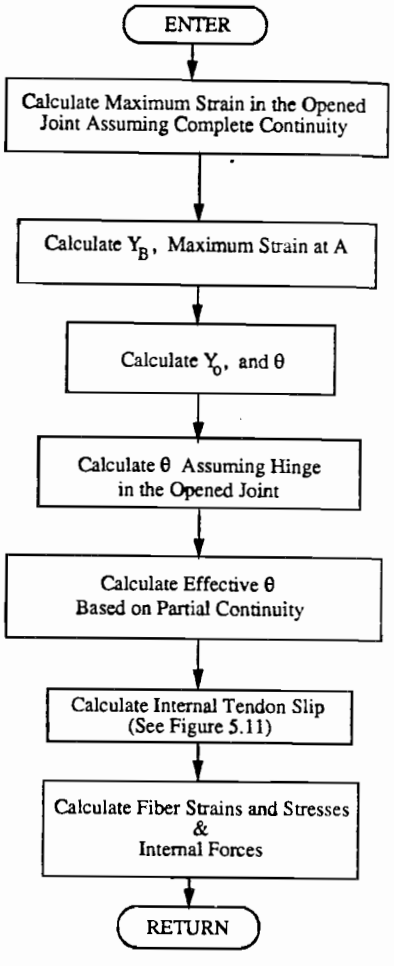

Figure 5.7 Internal forces for cracked or opened joint element.

As discussed in Chapter Four, the strain in the joint section near ultimate was higher than the strain inside the segment. CEBTP tests (4) showed that the concrete strain in the joint was much higher than that in the segment after the joint opened. The concrete strain at section B (ε_{CB}) calculated using the above procedure is based on complete continuity in the beam element. A new concrete strain is calculated according to Equation (5.30) by using the new calculated angle of rotation.

5.3.2 External Tendon Slip. The external tendon forces are applied as external forces on the beam. These external nodal forces are calculated in the same way as the external load in Equation (5.22). Possible slip of external tendons at deviators is increased with larger joint openings. The behavior associated with external tendon slip is not reversible. The solution has to be a step-by-step sequential loading process.

The solution for slip begins after computing the structure deformation at each iteration. The tension force variations in the external tendons are first calculated by assuming that no slip occurs at the deviators. The tension force variations are calculated from the variation in the tendon segment length due to the variation in nodal displacements. Then a check at each deviator is carried out to determine whether slip is possible or not. Figure 5.8(a) shows a typical external tendon layout in each span and the notation used in this derivation. Points g, h, i, and j are the deviation points of the external tendon. The external tendon segment immediately to the left of deviation point i has parameters with subscript i. The slip is assumed positive from left to right.

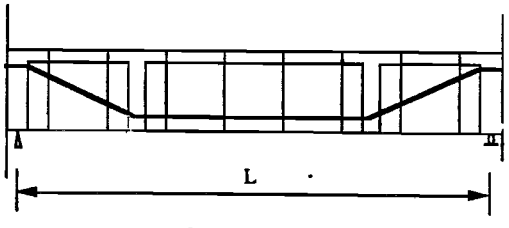

Span Elevation

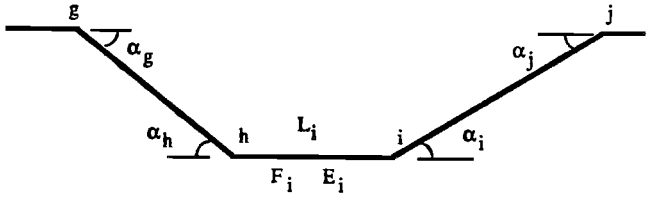

External Tendon Elevation

L_i:	Length of tendon piece i	A:	Area of tendon
g_i:	Slip at deviator i	F_i:	Force in tendon piece i
f_i:	Coefficient of friction at i		
b_i:	Coefficient of bond at i		
E_i:	Modulus of elasticity for tendon piece i		
α_g , α_h , α_i , α_j:	Deviation angle at g, h, i, and j		
a_i:	Coefficient for direction of slip at i (+1 to the right, -1 to the left)		

a) Notation for External Tendon Slip

Figure 5.8 Notation for external tendon slip.

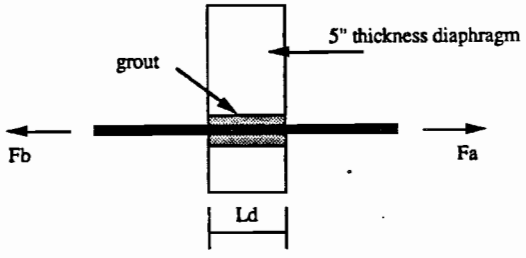

Elevation of Strand & Intermediate Diaphragm

L_d: Development Length A: Area of Tendon

D_e: Effective Diameter of Tendon = Sqrt (4 * A / π)

A_b: Area of Bond = π * D_e * L_d

u: Bond Strength

b: Bond Coefficient used in Program "Bridge"

F_a & F_b: Forces in External Tendon

Calculate $\frac{F_a}{F_b}$ from

$F_a - F_b = u * A_b$

The Program Bridge Uses $F_a = F_b * e^b$ (1)

Taking Ln of two the sides of Equation (1) gives:

$\text{Ln}\left(\frac{F_a}{F_b}\right) = b$ (2)

b is obtained from Equation (2)

b) Procedure for Calculating b Coefficient

Figure 5.8 (cont).

Figure 5.8(b) shows the procedure for calculating the coefficient of bond, b, from the bond-slip relationship shown in Fig 5.3(a). The forces on the two sides of any deviator (i) have to comply with:

$$F_i \cdot e^{-(f_i \alpha_i + b_i)} \le F_j \le F_i \cdot e^{(f_i \alpha_i + b_i)} \tag{5.33}$$

If the initial forces F_i and F_j do not comply with this relation, the external tendon slips and the final forces F_i^f and F_j^f have to comply with the relationship given in Equation (5.33).

After the external tendon slips at deviator i, Equation (5.33) can be written as:

$$\begin{aligned} e^{a_i(f_i\alpha_i+b_i)}.F_i^f &= F_j^f \\ F_i^f &= F_i+\Delta F_i \\ F_j^f &= F_j+\Delta F_j \\ e^{a_i(f_i\alpha_i+b_i)}.(F_i+\Delta F_i) &= (F_j+\Delta F_j) \end{aligned} \tag{5.34}$$

where ΔF_i and ΔF_j are the force increments due to slipping of the external tendon and can be calculated from:

$$\begin{aligned} \Delta F_i &= E_i.A.\frac{(a_i.g_i-a_h.g_h)}{L_i} \\ \Delta F_j &= E_j.A.\frac{(a_j.g_j-a_i.g_i)}{L_j} \end{aligned} \tag{5.35}$$

Substituting Equation (5.35) into Equation (5.34), gives:

$$\begin{aligned} &e^{a_i(f_i.\alpha_i+b_i)}.E_i.A.\frac{(a_i.g_i-a_h.g_h)}{L_i}- \\ &E_j.A.\frac{(a_j.g_j-a_i.g_j)}{L_j}=F_j-e^{a_i(f_i.\alpha_i+b_i)}.F_i \end{aligned} \tag{5.36}$$

Substituting

$$\begin{aligned} u_i &= e^{a_i(f_i\alpha_i+b_i)} \\ \sigma_i &= \frac{F_i}{A} \\ D_i &= \sigma_j-u_i\sigma_i \end{aligned} \tag{5.37}$$

into Equation (5.36), gives:

$$(-a_h.u_i.\frac{E_i}{L_i}).g_h+(a_i.u_i.\frac{E_i}{L_i}+a_i.\frac{E_j}{L_j}).g_i-(a_j.\frac{E_j}{L_j}).g_j=D_i \tag{5.38}$$

Equation (5.38) can be formed for each element of the external tendon to form the slip stiffness matrix:

$$\begin{bmatrix} S_{11} & S_{12} & . & . & . \\ . & . & . & . & . \\ . & S_{ih} & S_{ii} & S_{ij} & . \\ . & . & . & . & . \\ . & . & . & S_{nn-1} & S_{nn} \end{bmatrix} \cdot \begin{Bmatrix} . \\ . \\ g_i \\ . \\ . \end{Bmatrix} = \begin{Bmatrix} . \\ . \\ D_i \\ . \\ . \end{Bmatrix} \tag{5.39}$$

where

$$\begin{aligned} S_{ii} &= (a_i.u_i.\frac{E_i}{L_i} + a_i.\frac{E_i}{L_i}) \\ S_{ih} &= -a_h.u_i.\frac{E_i}{L_i} \\ S_{ij} &= -a_j.\frac{E_j}{L_j} \end{aligned} \tag{5.40}$$

Figure 5.9 shows the flow chart for calculating the external tendon slip . After calculating the external tendon forces based on the assumption of no slip at the deviators, the slip stiffness matrix for the external tendon is formed according to Equations (5.38), (5.39), and (5.40). After the slip stiffness matrix is modified for the deviators with no possible slip according to Equation (5.33), the slip stiffness matrix is used to calculate the slip at each deviator. From the new final slip at each deviator, the new modified external tendon forces are obtained according to Equation (5.35). Convergence of the external tendon slip is checked by the dot product of the slip increment vector

$$\begin{Bmatrix} . \\ . \\ g_i \\ . \\ . \end{Bmatrix}$$

and the load vector

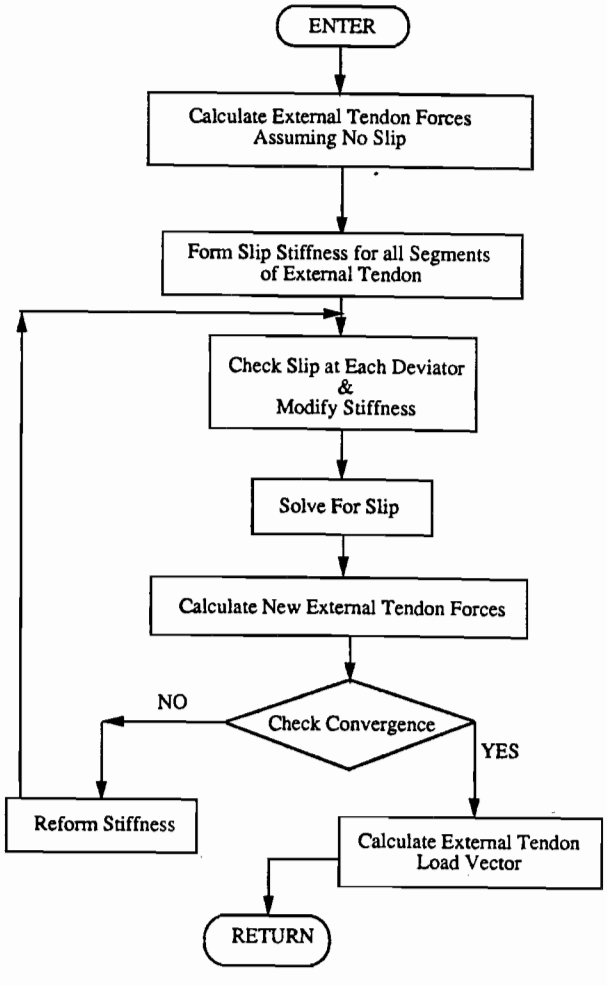

Figure 5.9 Calculation of external tendon slip.

$$\begin{Bmatrix} \cdot \\ \cdot \\ D_i \\ \cdot \\ \cdot \end{Bmatrix}$$

5.3.3 Internal Tendon Slip. As a dry joint or cracked epoxy joint starts to open, internal tendons start slipping from the segment sections toward the joint. As joint opening increases, the slip increases too. The slip between the internal tendon and grout must be considered after cracking or joint opening. The bond-slip relationship assumed in Section 5.2.3 and Fig 5.3(b) is used for the internal tendons. Equilibrium requirements for the internal tendon yields:

$$\tau(x)=\frac{1}{\pi D}.\frac{dT(x)}{dx} \tag{5.41}$$

where (T) is the tension force. While for a linear tendon Equation (5.41) becomes:

$$\frac{dT(x)}{dx} = E.\frac{\pi D^2}{4}\frac{d\epsilon(x)}{dx} \tag{5.42}$$

Combining Equations (5.41) and (5.42) yields:

$$\tau(x)=E.\frac{D}{4}.\frac{d\epsilon(x)}{dx} \tag{5.43}$$

The slip between the tendon and grout is the difference between the steel movement and the grout movement as follows:

$$S(x)=u_s(x)-u_c(x) \tag{5.44}$$

and consequently

$$\begin{aligned}\frac{dS}{dx} &= \frac{du_s}{dx} - \frac{du_c}{dx}\\ \frac{d^2S}{dx} &= \frac{d^2u_S}{dx^2}-\frac{d^2u_c}{d^2x}\end{aligned} \tag{5.45}$$

The strain in the steel and concrete can be expressed as:

$$\begin{aligned}\epsilon_s &= \frac{du_s}{dx} \rightarrow \frac{d\epsilon_s}{dx} = \frac{d^2u_s}{d^2x}\\ \epsilon_c &= \frac{du_c}{dx} \rightarrow \frac{d\epsilon_c}{dx} = \frac{d^2u_c}{d^2x}\end{aligned} \tag{5.46}$$

and Equation (5.45) can be given as:

$$\frac{d^2S}{dx^2} = \frac{d\epsilon_s}{dx} - \frac{d\epsilon_c}{dx} \tag{5.47}$$

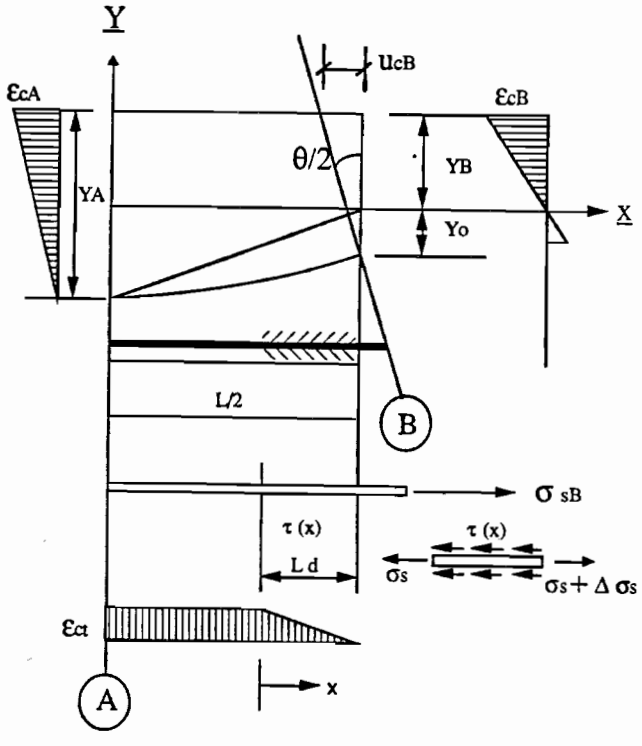

L_d : Development length σ_{sB} : Steel Stress at B

τ (x): Bond Stress for Steel

Figure 5.10 Internal tendon slip.

The distribution of strains in the concrete in tension at the level of the internal tendons shown in Fig. 5.10 is as follows:

$$\epsilon_c(x) = \frac{\epsilon_{ct}}{L_d}.(L_d - x)$$
$$\frac{d\epsilon_c}{dx} = -\frac{\epsilon_{ct}}{L_d} \tag{5.48}$$

Combining Equations (5.43), (5.47), and (5.48) gives:

$$\frac{d^2S(x)}{dx^2} - \frac{4}{E.D}.\tau(x) = \frac{\epsilon_{ct}}{L_d} \quad (5.49)$$

which is the fundamental differential equation to be solved to obtain the internal tendon strain and stress.

The bond-slip relationship assumed in Section 5.2.3 for an internal tendon has three zones. The solution of the differential equation obtained from Martins (4) for each of the three slip zones is as follows:

Zone one: $0 \le S(x) \le S_o$

$$\tau(x) = \frac{\tau_o}{S_o}.S(x)$$

$$S(x) = \frac{\epsilon_{ct}}{\alpha_o^2.L_d}.(\cosh(\alpha_o x) - 1) \quad (5.50)$$

$$\epsilon(x) = \frac{\epsilon_{ct}}{L_d}.(\frac{\sinh(\alpha_o x)}{\alpha_o} + L_d - x)$$

The adhesion length can be obtained from:

$$\cosh(\alpha_o.L_d) = 1 + (\alpha_o^2.\frac{L_d}{\epsilon_{ct}}).(u_{sB} - \epsilon_{ct}.(\frac{L}{2} - \frac{L_d}{2}) \quad (5.51)$$

and the length L_o, corresponding to the slip S_o is given by:

$$\epsilon_{ct}.\cosh(\alpha_o) - \epsilon_{ct} - \alpha_o^2.S_o.L_o = 0 \quad (5.52)$$

Zone Two: $S_o \le S(x) \le S_1$

$$\tau(x) = C_o + \frac{(\tau_y - \tau_o)}{(S_1 - S_o)}.S(x)$$

$$C_o = \frac{(\tau_o.S_1 - \tau_y.S_o)}{(S_1 - S_o)} \quad (5.53)$$

$$C_1 = \frac{\tau_1 - \tau_o}{S_1 - S_o}$$

The slip and strain are as follows:

$$S(x)=(S_o+\frac{C_o}{C_1}+\frac{\epsilon ct}{(\alpha_1^2.L_d)}).\cosh(\alpha_1.x)$$
$$+\frac{\epsilon_{ct}.\sinh(\alpha_o.L_o)}{\alpha_1.\alpha_o.L_o}.\sinh(\alpha_1.x)-\frac{C_o}{C_1}-\frac{\epsilon_{ct}}{\alpha_1^2.L_d} \quad (5.54)$$

$$\epsilon_s(x)=\alpha_1.(S_o+\frac{C_o}{C_1}+\frac{\epsilon ct}{\alpha_1^2.L_d}).\sinh(\alpha_1.x)$$
$$+\frac{\epsilon_{ct}.\sinh(\alpha_o.L_o)}{\alpha_o.L_o}.\cosh(\alpha_1.x)+\frac{\epsilon_{ct}}{L_d}.(L_d-x) \quad (5.55)$$

where

$$\alpha_1^2=\frac{4.C_1}{E.D} \quad (5.56)$$

The development length $\Delta L_1=L_d-L_o$ can be found from:

$$u_{sB}-\epsilon_{ct}.(\frac{L}{2}-\frac{L_d}{2})=(S_o+\frac{C_o}{C_1}+\frac{\epsilon_{ct}}{\alpha_1^2.L_d}).\cosh(\alpha_1.\Delta L_1)$$
$$+\frac{\epsilon_{ct}.\sinh(\alpha_o.L_o)}{\alpha_1.\alpha_o.L_o}.\sinh(\alpha_1.\Delta L_1)-(\frac{C_o}{C_1}+\frac{\epsilon_{ct}}{\alpha_1^2.L_d}) \quad (5.57)$$

The length L_1 corresponding to S_1 can be found from:

$$S_1=[\Gamma+\frac{\epsilon ct}{\alpha_1^2.(L_1+L_o)}].\cosh(\alpha_1.L_1)+\epsilon_{ct}.B.\sinh(\alpha_1.L_1)-\frac{C_o}{C_1}-\frac{\epsilon_{ct}}{\alpha_1^2.(L_1+L_o)} \quad (5.58)$$

where

$$\Gamma=S_o+\frac{C_o}{C_1}$$
$$B=\frac{\sinh(\alpha_o.L_o)}{(\alpha_1.\alpha_o.L_o)} \quad (5.59)$$

Zone Three: $S_1 \le S(x) \le S_y$

$$\tau(x) = \tau_y \tag{5.60}$$

The slip at any point can be obtained with:

$$\begin{aligned} L_{o1} &= L_1 + L_o \\ S(x) &= \left(\frac{4.\tau_y}{E.\phi} + \frac{\epsilon ct}{L_d}\right).\frac{x_2}{2} + \left[\alpha_1.\left(S_o + \frac{C_o}{C_1}\right).\sinh(\alpha_1.L_1)\right. \\ &\left. + \left(\frac{\sinh(\alpha_1.L_1)}{\alpha_1^2.L_{o1}} + \frac{\sinh(\alpha_o.L_o).\cosh(\alpha_1.L_1)}{\alpha_o.L_o}\right).\epsilon_{ct}\right].x + S_1 \end{aligned} \tag{5.61}$$

The strain in the steel at any point is as follows:

$$\begin{aligned} \epsilon_s(x) &= \left(\frac{4.\tau_y}{E.\phi} + \frac{\epsilon_{ct}}{L_d}\right).x + \alpha_1.\left(S_o + \frac{C_o}{C_1}\right).\sin(\alpha_1.L_1) \\ &+ \left(\frac{\sinh(\alpha_1.L_1)}{\alpha_1^2.L_{o1}} + \frac{\sinh(\alpha_o.L_o).\cosh(\alpha_1.L_1)}{\alpha_o.L_o}\right).\epsilon_{ct} + \epsilon_{ct}.(L_d - x) \end{aligned} \tag{5.62}$$

The length $\Delta L_2 = L_d - L_{o1}$ can be found from:

$$u_{sB} - \epsilon_{ct}.\left(\frac{L}{2} - \frac{L_d}{2}\right) = \left(\frac{4.\tau_y}{E.D} + \frac{\epsilon_{ct}}{L_d}\right).\frac{\Delta L_2^2}{2} + \alpha_2.\Delta L_2 + S_1 \tag{5.63}$$

where

$$\begin{aligned} \alpha_2 &= \alpha_1.\left(S_o + \frac{C_o}{S_1}\right).\sinh(\alpha_1.L_1) + \left[\frac{\sinh(\alpha_1.L_1)}{\alpha_1.L_{o1}}\right. \\ &\left. + \frac{\sinh(\alpha_o.L_o).\cosh(\alpha_1.L_1)}{\alpha_o.L_o}\right].\epsilon_{ct} \end{aligned} \tag{5.64}$$

The length L_2 corresponding to slip S_y can be obtained from:

$$\alpha_y^2.L_2^3+(\alpha_y^2.L_{o1}+\frac{\epsilon ct}{2}+\alpha^2).L_2^2 \\ +(S_1-S_2+\alpha_2.L_{o1}).L_2+(S_1-S_2).L_{o1}=0 \tag{5.65}$$

Figure 5.11 shows the flow chart for calculating the internal tendon stress taking into consideration tendon slip. The slip of the internal tendon at the joint section is equal to the crack or joint opening at the level of the tendon. Knowing the slip of the internal tendon, the slip zone can be obtained from the bond-slip relationship. Knowing the slip zone, the development length and the stress can be obtained according to the equations given in this section.

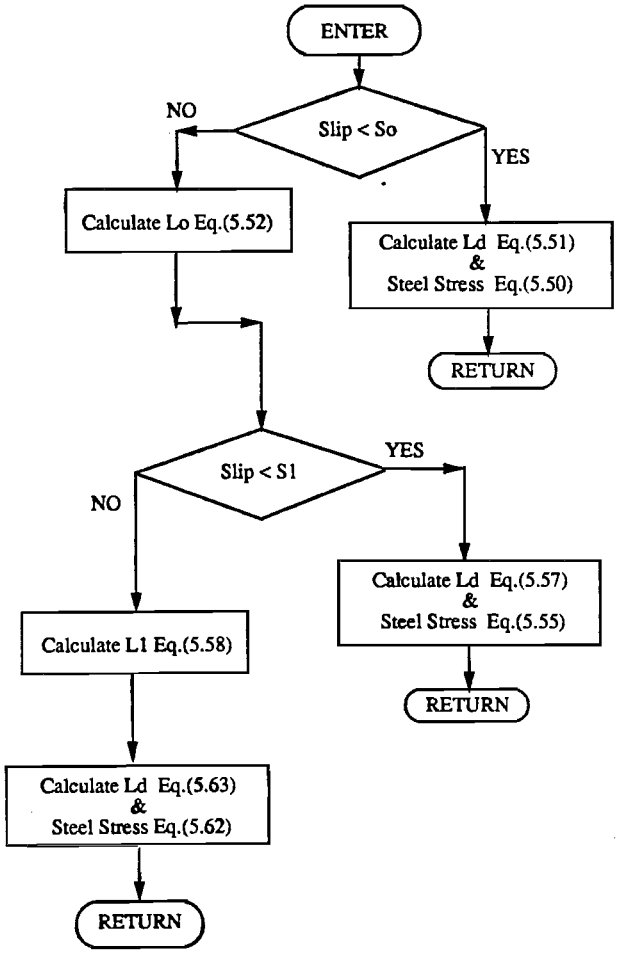

Figure 5.11 Flow chart for internal tendon slip.

5.4 Method of Calculation

The nonlinear solution procedure for the analysis of external prestressed segmental bridges is carried out by dividing the applied load into small load increments. The use of small load increments is necessary for convergence. A Modified Newton-Raphson method is used for the iteration procedure to obtain equilibrium convergence for each load increment.

The tangent stiffness matrix is reformed after several iterations in the Modified Newton-Raphson approach as shown in Fig. 5.12. In the Newton-Raphson method, the tangent stiffness matrix is reformed at every step. The Modified Newton-Raphson procedure is more economical but the convergence is slower. In this study, the Modified Newton-Raphson method was used.

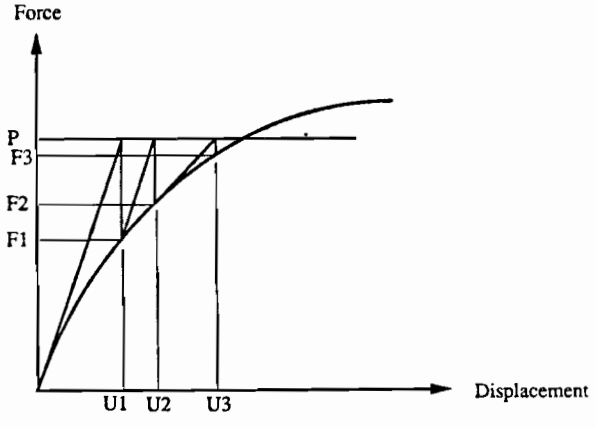

Figure 5.12 Modified Newton-Raphson iteration [from Ref. (5)].

The nonlinear equilibrium equations are:

$$\overline{P}_r(\underline{U}) = \overline{P}_e(\underline{U}) \quad (5.66)$$

where $\overline{P}_r$ and $\overline{P}_e$ are the internal and external nodal forces. These two vectors should be equal for convergence. The linearized forms of the equilibrium equations are:

$$\overline{K}_t(\underline{U})_n \cdot (\Delta \underline{U})_n = \overline{P}_e(\underline{U})_n - \overline{P}_r(\underline{U})_n \quad (5.67)$$

where

$$(\underline{U})_{n+1}=(\underline{U})_n+(\Delta\underline{U})_n \tag{5.68}$$

n is referred to as the iteration number. Convergence is based on the dot product between the unbalanced load vector on the right hand-side of Equation (5.67) and the nodal displacement increment.

The three computational steps involved in the solution for beam displacement are described in the following.

(1) The first step is the linearization of Equation (5.66) which results in Equation (5.67). The tangent stiffness matrix and the external nodal force vector are assembled as discussed in Section 5.3. (2) The second step is the solution of the linearized equilibrium Equation (5.67). (3) The third step requires the determination of the unbalanced nodal force vector, which is the right-hand side of Equation (5.67).

The internal force vector is determined from Equation (5.21), after obtaining the total nodal displacement and the total strain at any fiber of the cross section. Path independent state determination is used in this study. The stresses are computed from the accumulated strain at any iteration using the material stress-strain diagrams shown in Fig 5.1 and Fig 5.2. In this way, concrete stresses corresponding with the descending branch of the stress-strain model can be obtained. The summation of the moment and axial force required in Equation (5.21) can be obtained using Equations (5.12) and (5.18) as discussed in Section 5.3. If the strain of any fiber of the cross section is higher than the ultimate material strain, the program assumes that the structure has failed.

5.5 Second-Order Effects

The change in stress of external tendons with deformation of the tendons, taking into consideration slip at the deviators, is discussed in Section 5.2. A second problem associated with the tendons is the second-order moment due to change in position of the external tendons with respect to the deformed concrete member. Figure 5.13(a) shows the second-order effect in a simply supported beam without intermediate deviators, while Fig 5.13(b) shows the beam with intermediate deviators. The intermediate deviators reduce the second-order effect. The secondary effect is taken into consideration in the analytical model by assuming that the external tendon segments between deviators remain straight.

5.6 Computer Program "Bridge"

In this chapter, the techniques required for the analysis of segmental bridges were discussed. To carry out the analysis, computer program "Bridge" was developed. The computer program has the option to include external tendons only, internal tendons only,

or a mixture of external and internal tendons. Because of the nonlinear behavior, the program flow shown in Fig. 5.14 is used to converge to the correct solution.

Program "Bridge" was written in Fortran for use on a personal computer. It can be executed on an IBM compatible machine with a math co-processor chip. A User's guide and a listing of Program "Bridge" are included in Appendices A and B of Ref. 42.

Solution of the model tested in this study required approximately thirty minutes on a Dell Computer System 200 using 20 load increments and 33 beam elements.

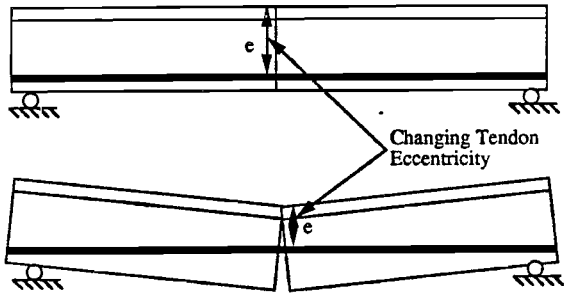

a) Without Intermediate Deviators

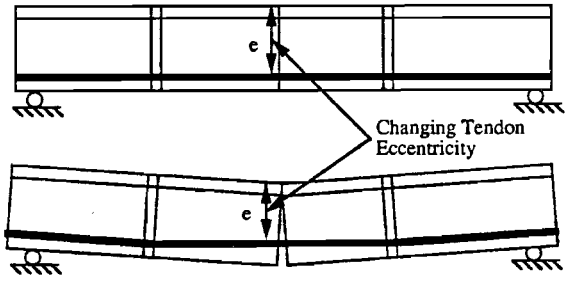

b) With Intermediate Deviators

Figure 5.13 Second-order effect.

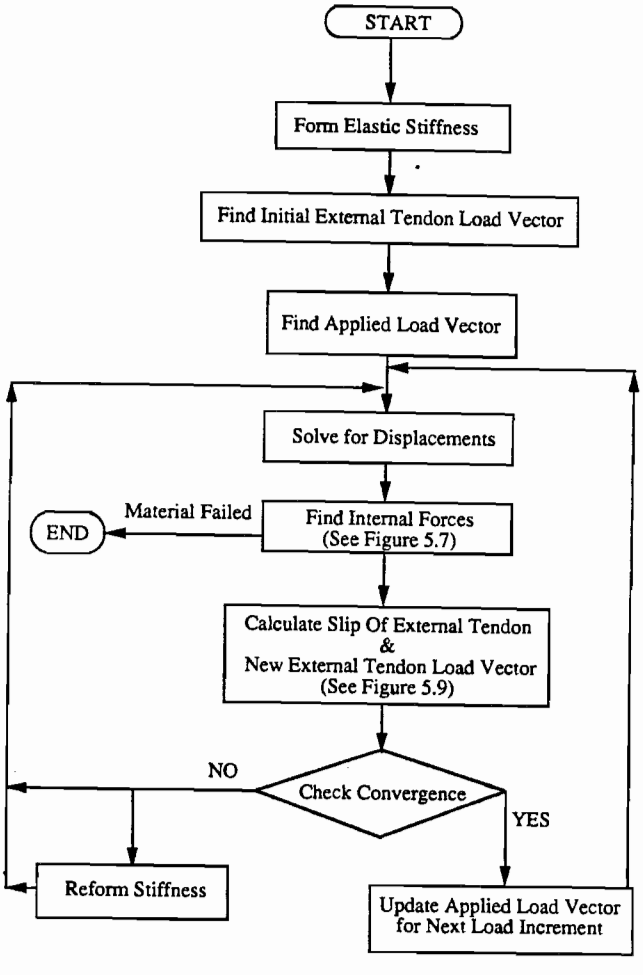

Figure 5.14 Program "Bridge" flow chart.

CHAPTER SIX

COMPARISON OF PREDICTIONS WITH EXPERIMENTAL RESULTS

6.1 General

The results obtained from the analytical model developed in this study (see Chapter 5) are compared with results of tests performed at the University of Texas, as well as CEBTP test results reported in France(4). The objective of this comparison is to verify the performance of the analytical model. The comparisons were performed for load-deflection, critical joint opening, change in external tendon stress, and change in internal tendon stress, if internal tendons were used.

6.2 Current Tests

Test results measured in the experimental part of this study are compared with Program Bridge predictions. The dimensions and material properties for the box-girder bridge model are described in Chapter 2. Thirty-three beam elements were used to model the bridge along its three-span length. Incremental loads were applied until the program indicated that the steel or concrete had failed by exceeding its strain capacity. The dead load of the model bridge and the prestress forces were applied as the first load increment. After that, the concentrated live loads were applied incrementally at two locations on the model similar to the physical test procedure (see Chapter Three). The load increments for the concentrated live loads on the exterior span were 0.5(LL+I). Since the convergence and accuracy of the analysis depend on the load increments used, the live load increments were the same for all computer runs to allow comparison between results of different runs.

6.2.1 Data for Modeling. Data values related to steel and concrete properties, the internal tendon bond-slip relation, and external tendon bond-slip relation are discussed in this Section. The prestressing steel properties required for use in Fig. 5.2 are shown in Table 6.1. The conventional steel properties are shown in Table 6.2. Steel properties were supplied by the material manufacturer.

The concrete stress-strain diagram shown in Fig. 5.1 is defined by the data given in Table 6.3. The values for the maximum concrete strength were obtained from cylinder tests conducted during construction of the model, while the concrete strain corresponding to the maximum concrete strength was assumed constant (0.002). The ultimate concrete

Table 6.1 Prestressing Reinforcement

F_{sy} = 245 ksi	F_{su} = 279 ksi
ϵ_{sy} = 0.00838	ϵ_{su} = 0.0623

strain value was obtained using Equation (6.1) from Reference (12) which takes into consideration the confinement of the concrete fibers. The width (b) used in Equation 6.1 was the flange thickness, while z was the shear span. The ultimate concrete strength was calculated according to the slope of the descending portion of the stress-strain relation given by Hognestad (8).

$$\epsilon_{cu} = 0.003 + 0.02 * \frac{b}{z} \tag{6.1}$$

The ordered pairs describing the internal tendon bond-slip relation shown in Fig. 5.3(b) were obtained from Trost (11). The values are shown in Table 6.4. These values are for equivalent bond area which is obtained from the equivalent tendon diameter calculated from the area of the cross section of the tendon.

Table 6.2 Conventional Reinforcement

F_{sy} = 60 ksi	F_{su} = 70 ksi
ϵ_{sy} = 0.0019	ϵ_{su} = 0.21

Values used to define the external tendon bond-slip relation were obtained from tests performed by Radloff (10) as part of the overall study and from tests conducted on the bridge model as discussed in Section 3.5. The values required in Fig. 5.3(a) for a bond-slip relationship are shown in Table 6.5.

Table 6.3 Concrete

F_{cc} = 6.0 ksi	F_{cu} = 4.65 ksi
ϵ_{cc} = 0.002	ϵ_{cu} = 0.0035

Table 6.4 Internal Tendon Bond-Slip Parameters

τ_o = 0.37 ksi	τ_y = 1.0 ksi	
S_o = 0.0007 inch	S_1 = .004 inch	S_y = 0.2 inch

Converting these values to the bond Coefficient (b) used in Section 5.4 according to the procedure shown in Fig. 5.8 gives the values listed in Table 6.6. Figure 6.1 illustrates the calculation of the bond coefficient (b). The values in Table 6.6 are used as input data for the external tendons in Program Bridge.

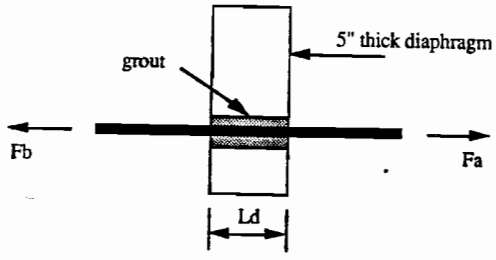

Elevation of Strand & Intermediate Diaphragm

L_d=5"

Area of Tendon = 0.425 in^2

D_e (Effective Diameter) = 0.735 in.

A_b (Area of Bond)=11.5 in^2

Assumed Effective Prestress =160 ksi

F_b(Tendon Force) =160 * 0.425 = 68 kips

Maximum Stress Difference across Deviator (Bond)=10 ksi (See Chapter Three)

F_a =68 + 10*0.425= 72.25 kips

b: Bond Coefficient used in Program Bridge

$\text{Ln}\left(\frac{F_a}{F_b}\right) = b$ (See Fig. 5.8)

b= 0.06

Figure 6.1 External tendon slip coefficient (b).

6.2.2 Initial Strength Tests. Two flexural strength tests carried out by MacGregor (1) in the initial part of this comprehensive testing program are compared to the program predictions. One analysis was carried out for the incremental live loading on each of the two exterior spans. One of the exterior spans had epoxy joints while the other exterior span had dry joints. The external tendons were bonded at the pier segments and at diaphragm locations where tendons were deviated. Four external tendons were bonded to four internal diaphragms, while two tendons were bonded to two internal diaphragms. The external tendons were bonded to a maximum of four intermediate diaphragms in each span as shown in Fig. 6.2(a) and Table 2.6. The tendon bonding condition at the initiation of the testing program described here was similar to that of the model when it was originally tested by

Table 6.5 External Tendon Bond-Slip.

τ_v = 0.37 ksi	
S_o = 0.004 inch	S_y = 0.4 inch

MacGregor (1). Dimensions and material properties for the box-girder bridge and its tendon layout are as described in Chapter Two.

Table 6.6 External Tendon Bond-Slip.

b_i = 0.06	
S_o = 0.004 inch	S_y = 0.4 inch

6.2.2.1 Epoxy Joints Span. Figures 6.3 through 6.5 show comparisons of the measured and computed load-deflection response, critical joint opening response, and change in external tendon stress in the epoxy joints span. Program Bridge predicted the capacity of the epoxy joints span within 3 percent of the measured load capacity, as shown in Fig. 6.3. The predicted ultimate displacement is 2.5 inches, while the test was stopped at a displacement of 1.75 inches before crushing of the critical joint flange. The reason for the difference in the predicted and the measured ultimate displacement is that the test was stopped before a material failure occurred. The maximum critical joint opening predicted by the program is 15 percent lower than the test value, as shown in Fig. 6.4. Program Bridge predicted that the maximum change in external tendon stress is 47 ksi while the measured value was 37 ksi as shown in Fig. 6.5. This difference is again believed to be due to stopping of the test before a material failure occurred.

6.2.2.2 Dry Joints Span. Figures 6.6 through 6.8 show the comparison between the predicted and measured response of the dry joints span. Program Bridge prediction of the load capacity is 1 percent higher than the measured capacity as shown in Fig. 6.6. The predicted ultimate displacement is 1.8 inches while the measured value was 1.6 inches (the test was stopped before material failure occurred). As shown in Fig. 6.7, the predicted maximum joint opening is 8 percent higher than the measured maximum joint opening because the test was stopped before material failure occurred. For the same reason, the predicted change in external tendon stress is 40 ksi while the measured change in tendon stress was only 35 ksi as shown in Fig. 6.8.

6.2.3 Exterior Spans without Internal Tendons. Two cases of external tendon bonding conditions were examined for each of the exterior spans. In the first analysis (unbonded case), the external tendons were assumed to have only friction at the deviators. Due to the deviation angle at each deviator, friction is developed between the tendon and deviator. Four external tendons were deviated at four deviators in each span, while two tendons were deviated at two deviators in each span. The deviation locations were the same as the bonding locations in the initial strength tests as shown in Fig. 6.2(a) and Table 2.6. The second analysis (bonded case) was for the external tendons bonded to all ten diaphragms in each span. This configuration is shown in Fig. 6.2(b) and Table 2.6.

6.2.3.1 Epoxy Joints Span. Figures 6.9 through 6.11 show the comparison of critical parameters such as deflection, critical joint opening, and change in external tendon stress between the test results and the program predictions for the "bonded" and "unbonded"

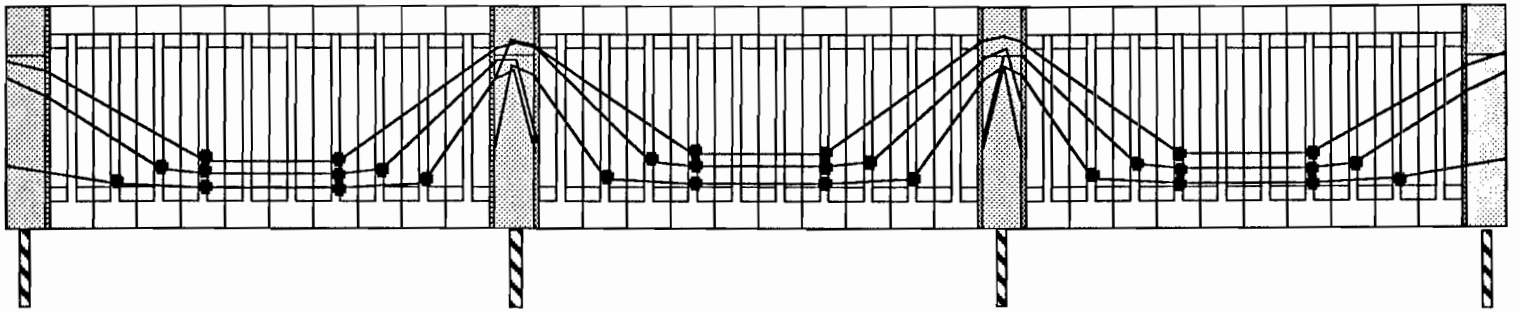

a) 2 or 4 diaphragms bonded in each span

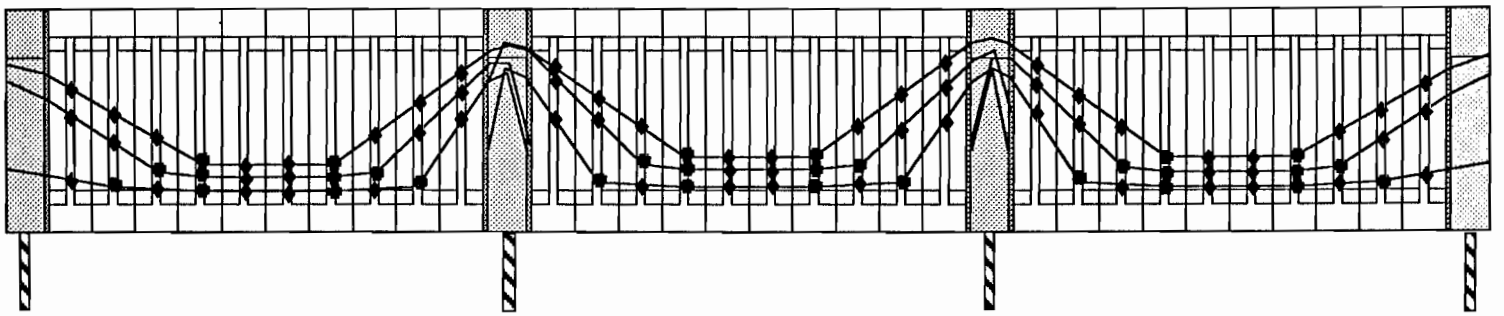

b) 10 diaphragms bonded in each span

● : Diaphragm Originally Bonded

♦ : Diaphragm Bonded Later

Figure 6.2 Bonding conditions of external tendons for flexural strength tests.

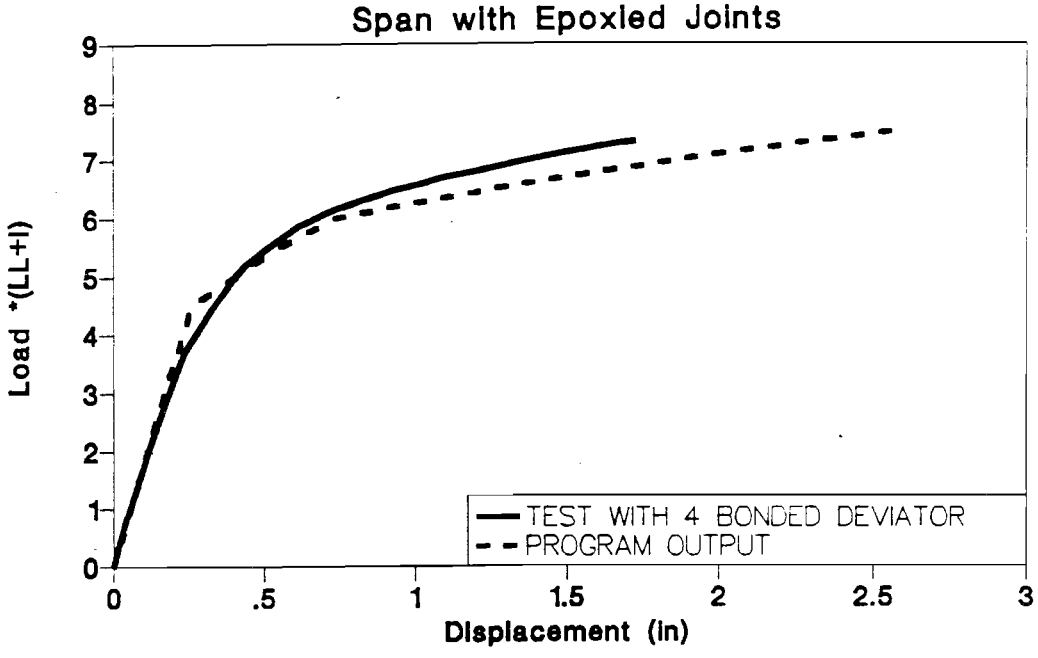

Figure 6.3 Load-deflection response (epoxy joints span - initial strength test).

cases of the epoxy joints span. The predicted capacity for the bonded case is 5 percent lower than the measured capacity, as shown in Fig. 6.9, while the predicted capacity for the unbonded case is 18 percent lower than the measured capacity. The ultimate deflection predicted by the program is 10 percent higher for the bonded case and 13 percent lower for the unbonded case than the measured ultimate deflection. The maximum critical joint opening predicted by Program Bridge for the bonded case is 13 percent higher than the measured value as shown in Fig. 6.10. The difference in the maximum joint opening between the program prediction and the test is due to lower predicted load capacity and external tendon stress. Figure 6.11 shows that the predicted external tendon stress is 5 ksi lower for the bonded case and 17 ksi lower for the unbonded case than the measured value.

6.2.3.2 Dry Joints Span. Figures 6.12 through 6.14 show the comparison for the critical parameters in the dry joints span. The program prediction of the load capacity for the bonded case is 2 percent lower than the measured value as shown in Fig. 6.12. However, the predicted capacity for the unbonded case is 16 percent lower than the measured ultimate strength. The predicted ultimate displacement is 8 percent higher for the bonded case and 3 percent lower for the unbonded case than the measured ultimate displacement. The predicted maximum joint opening is 2 percent higher than the measured value as shown in Fig. 6.13. The maximum change in external tendon stress predicted by the program is 6 ksi higher for the bonded case and 8 ksi lower for the unbonded case than the measured value as shown in Fig. 6.14.

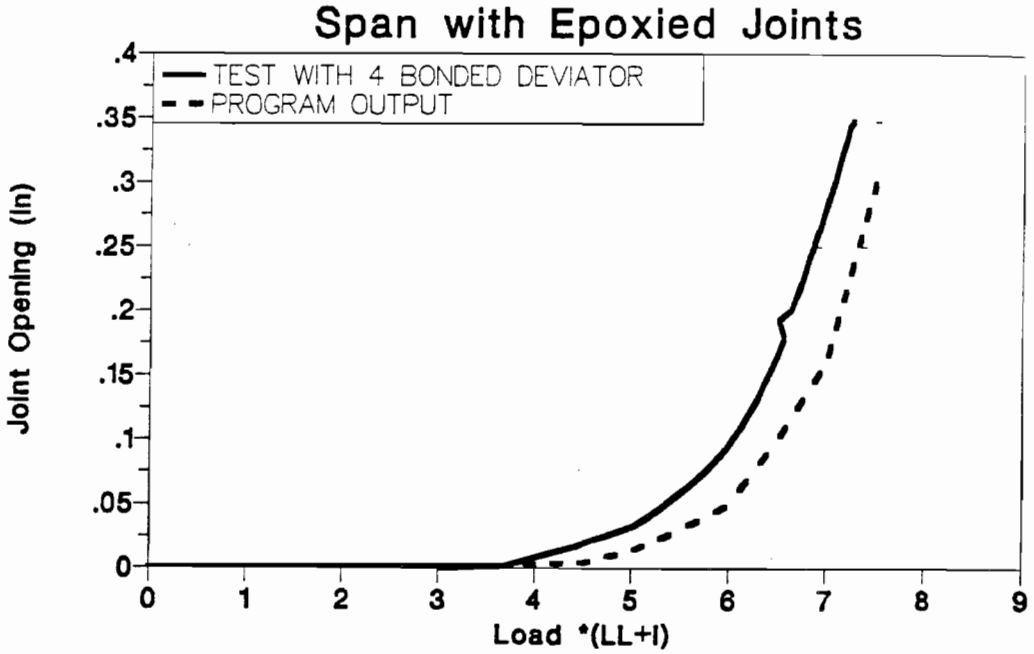

Figure 6.4 Joint opening response (epoxy joints span - initial strength test).

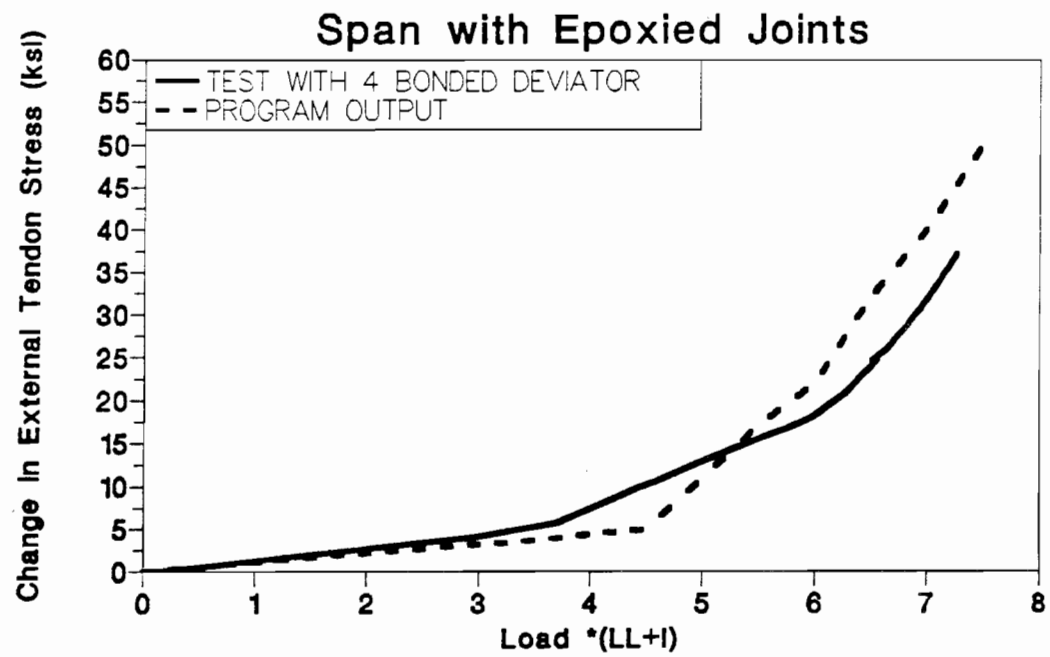

Figure 6.5 Change in external tendon stress (epoxy joints span - initial strength test).

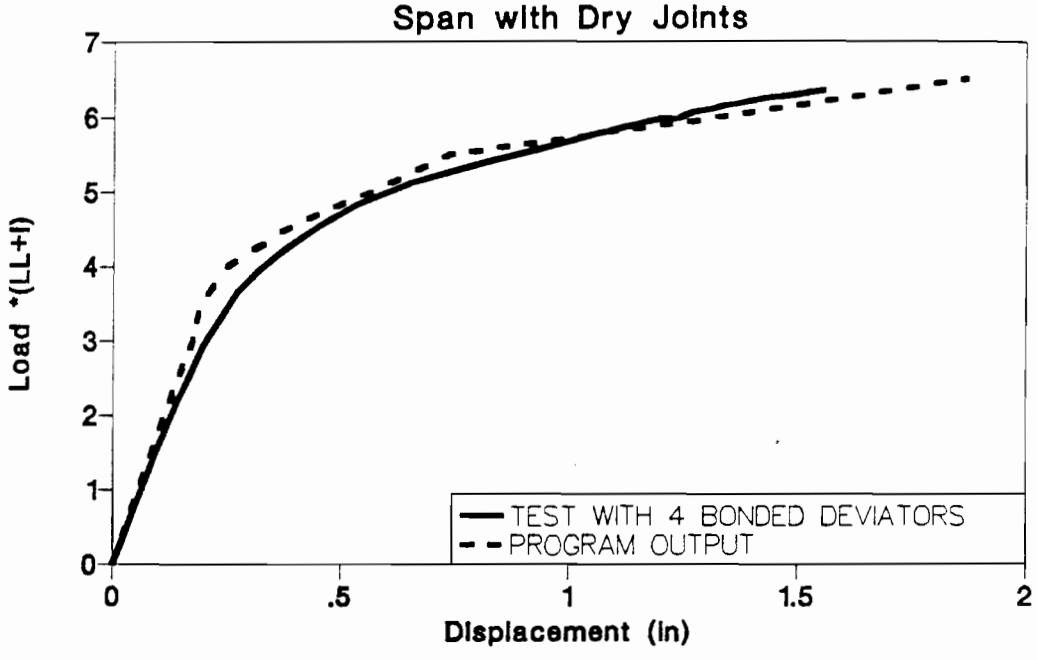

Figure 6.6 Load-deflection response (dry joints span - initial strength test).

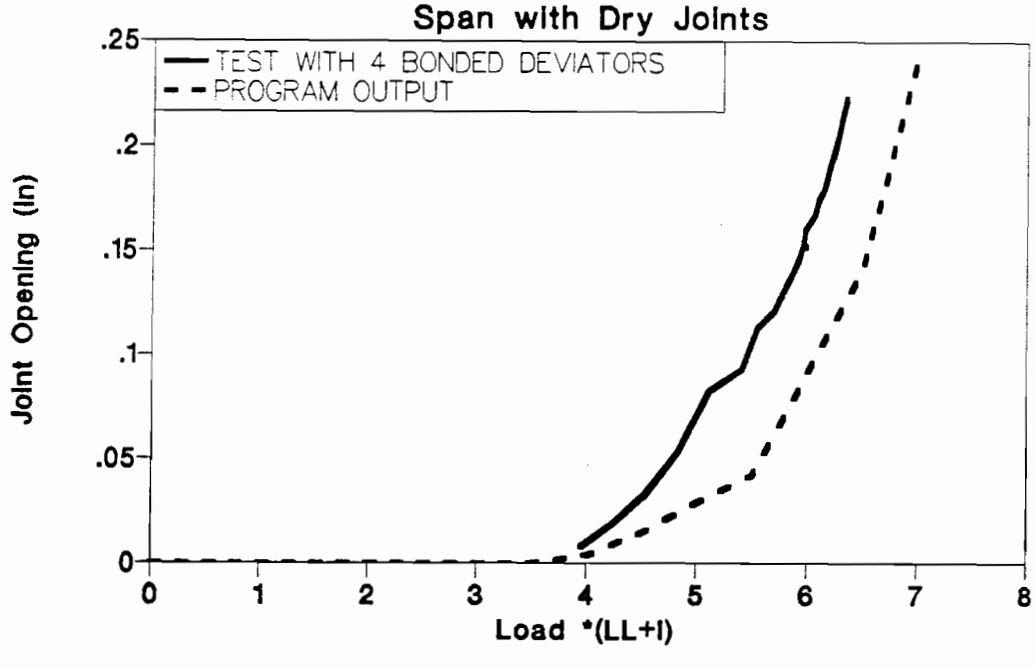

Figure 6.7 Joint opening response (dry joints span - initial strength test).

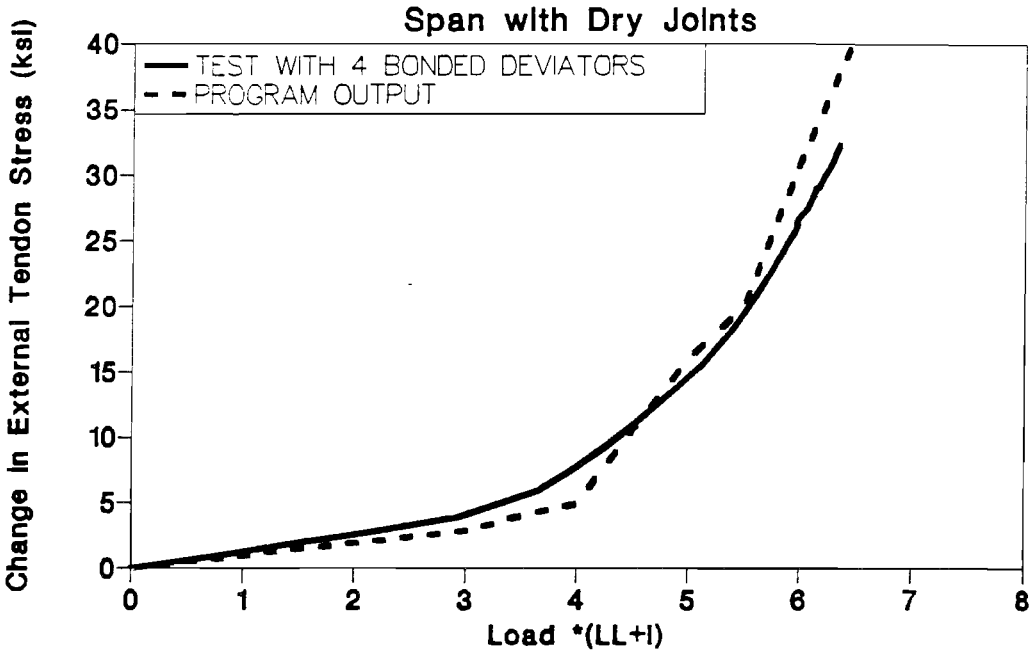

Figure 6.8 Change in external tendon stress (dry joints span - initial strength test).

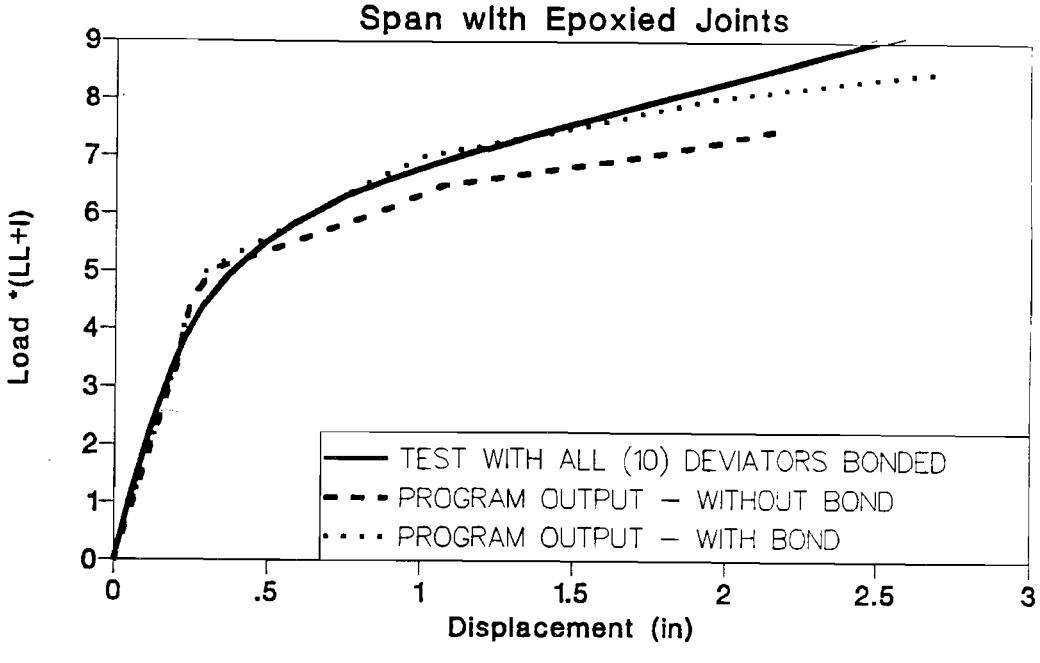

Figure 6.9 Load-deflection response (epoxy joints span without internal tendons).

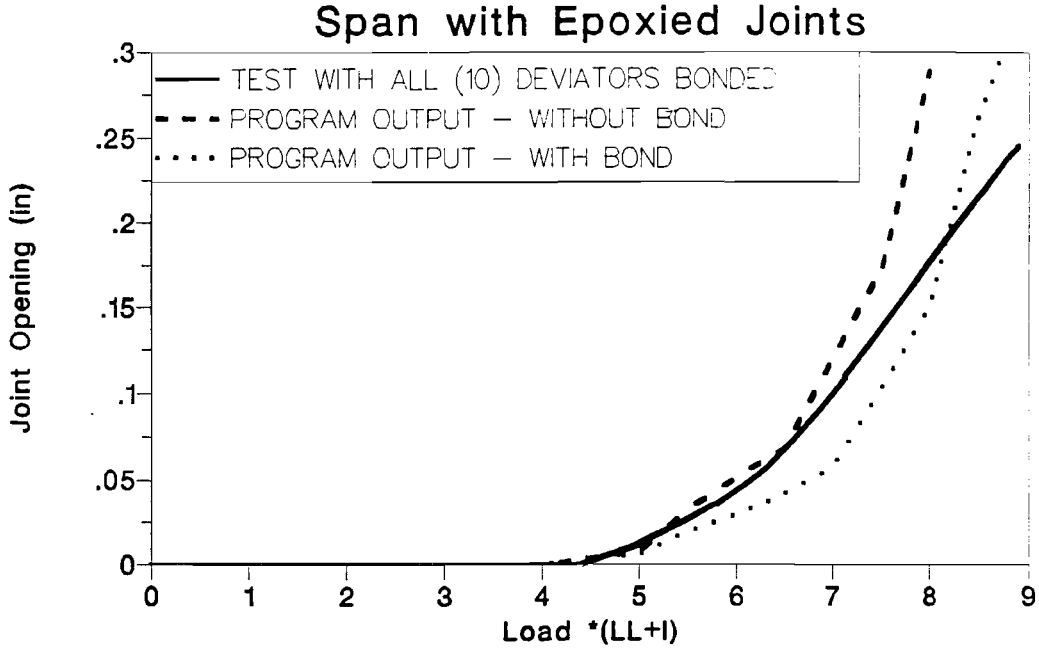

Figure 6.10 Joint opening response (epoxy joints span without internal tendons).

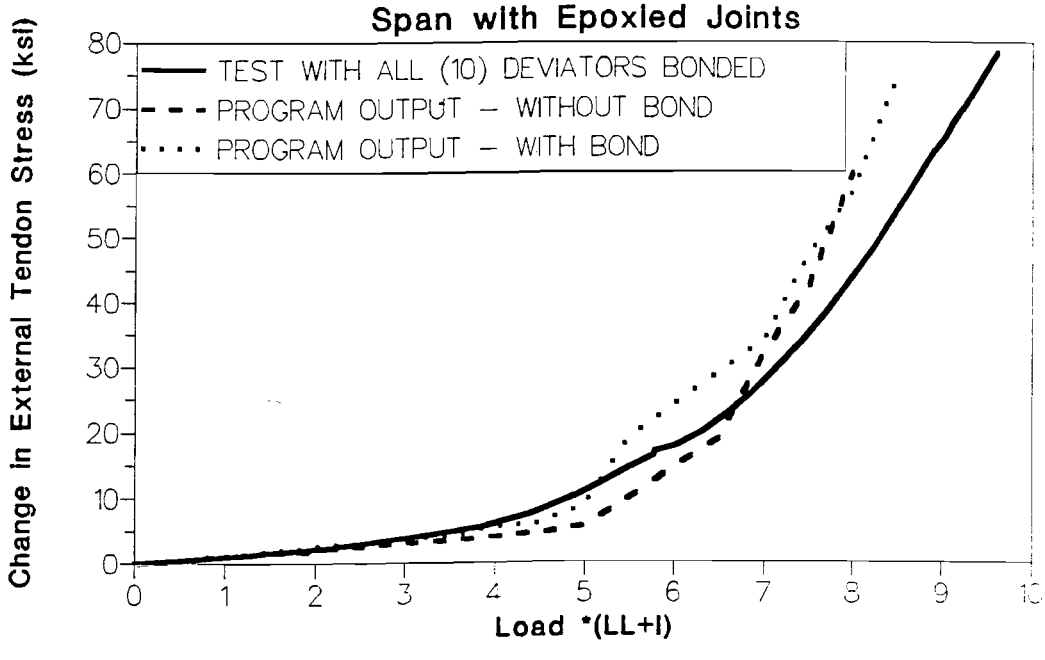

Figure 6.11 Change in external tendon stress (epoxy joints span without internal tendons).

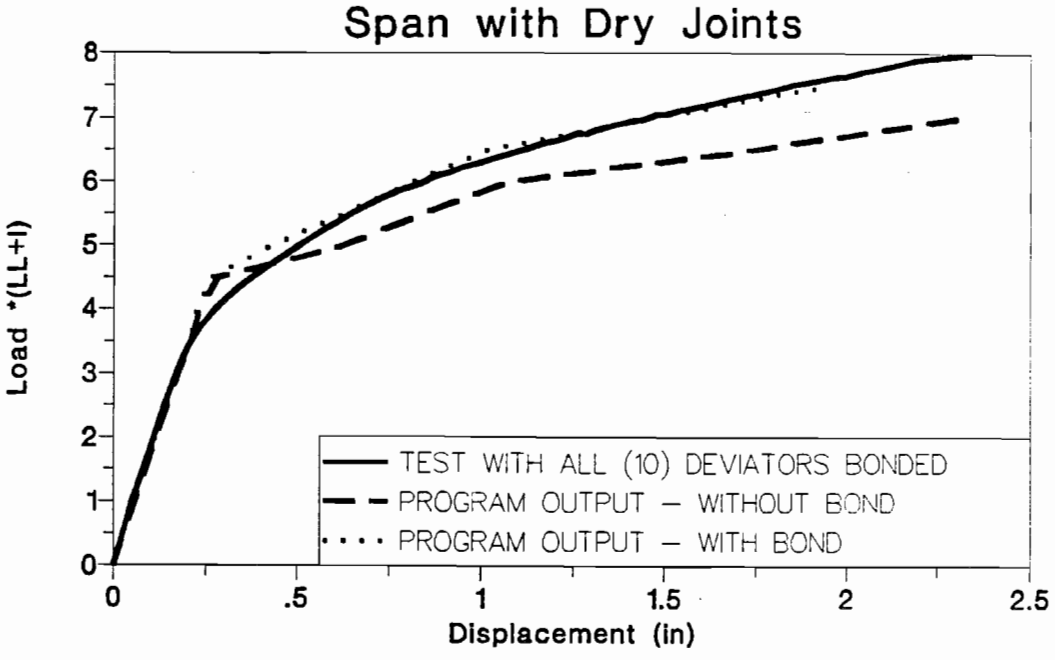

Figure 6.12 Load-deflection response (dry joints span without internal tendons).

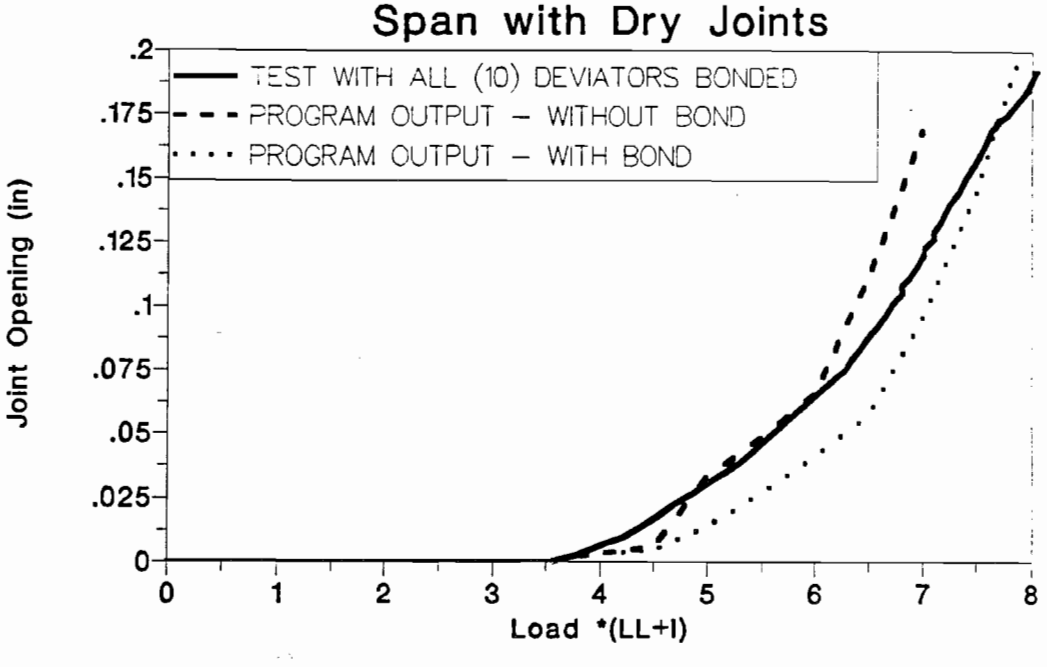

Figure 6.13 Joint opening response (dry joints span without internal tendons).

Table 6.7 shows the differences in the program prediction for the two cases (bonded and unbonded) as compared to the tests. The bonded case prediction is more representative of the measured behavior of the model because the external tendons were bonded to the ten diaphragms during the physical tests.

Table 6.7 Accuracy of Bonded and Unbonded Models

	Epoxy Joints Span		Dry Joints Span	
Parameters	Bonded Case	Unbonded Case	Bonded Case	Unbonded Case
Ultimate Load	-5%	-18%	-2%	-16%
Ultimate Displacement	+10%	-13%	+8%	-3%
Joint Opening	+13%	+10%	+2%	-10%
Change in External Tendon Stress	-5 ksi	-17 ksi	+6 ksi	-8 ksi
- : Lower than test +: Higher than test				

Figures 6.9 through 6.14 and Table 6.7 show the effect of bonding on the predicted behavior. The program predicted that bonding would increase the ductility and strength of the bridge, as shown in Fig. 6.9 for the epoxy joints span and Fig. 6.12 for the dry joints span. The program predicted that the critical joint openings were the same for the bonded and unbonded case for the epoxy joints span as shown in Fig. 6.10. A 10 percent difference between the maximum joint openings for the bonded and unbonded cases for the dry joints span was predicted by the program as shown in Fig. 6.13. The reason behind this difference is that a relatively large load increment (0.5(LL+I)) was used in analyzing these cases. The critical joint failed just before the applied load reached 7.5(LL+I) (confirmed by a special run with smaller load increments) while the last output obtained was for an applied load of 7.0(LL+I). The program predicted that the change in external tendon stress would be higher for the bonded case, as shown in Fig. 6.11 for the epoxy joints span and Fig. 6.14 for the dry joints span.

6.2.4 Exterior spans with Ungrouted Internal Tendons. One analysis run was carried out for each of the exterior spans to model the case where the external tendons were bonded to all intermediate diaphragms while the internal tendons were ungrouted.

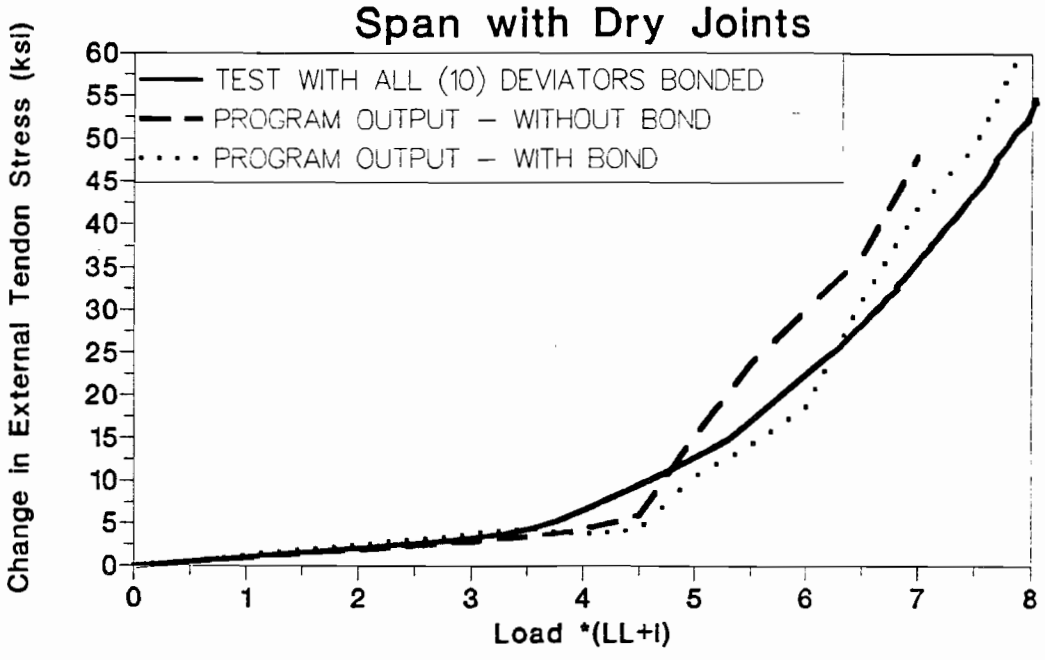

Figure 6.14 Change in external tendon stress (dry joints span without internal tendons).

6.2.4.1 Epoxy Joints Span. Figures 6.15 through 6.17 show the comparisons of critical parameters such as deflection, critical joint opening, and change in external tendon stress between the test results and Program Bridge predictions for the epoxy joints span. Program Bridge's prediction of the load capacity is 4 percent lower than the test result as shown in Fig. 6.15. The ultimate displacement prediction is 5 percent higher than the test ultimate displacement. Program Bridge predicted a maximum critical joint opening 10 percent lower than the test result, as shown in Fig. 6.16. The maximum change in external tendon stress predicted by the program is 2 ksi higher than the test data as shown in Fig. 6.17.

6.2.4.2 Dry Joints Span. Figures 6.18 to 6.20 show the comparison of the critical parameters for the dry joints span. The predicted load capacity is 2 percent lower than the test data as shown in Fig. 6.18. The ultimate deflection predicted by the program is 11 percent higher than the test result. The program prediction of the maximum critical joint opening is 3 percent lower than the test result as shown in Fig. 6.19. The prediction of the external tendon stress is 8 ksi higher than the data obtained from the test, as shown in Fig. 6.20.

6.2.5 Exterior spans with Grouted Internal Tendons. One analysis run was carried out for each of the exterior spans to mathematically model the case where the external tendons were bonded to all intermediate diaphragms while the bottom internal tendons were fully grouted.

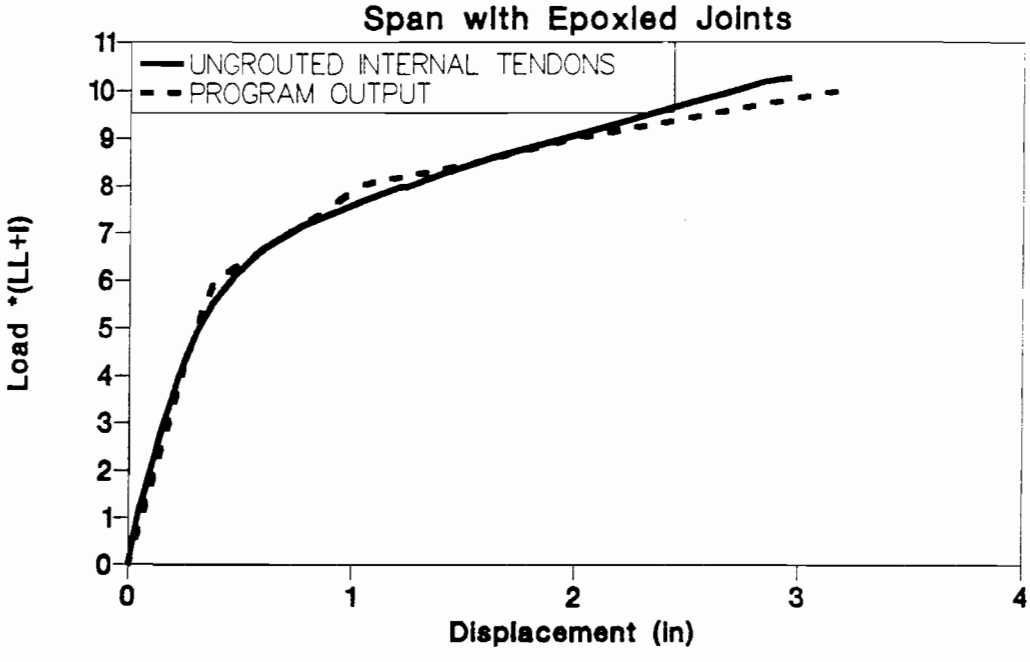

Figure 6.15 Load-deflection response (epoxy joints span - ungrouted internal tendons).

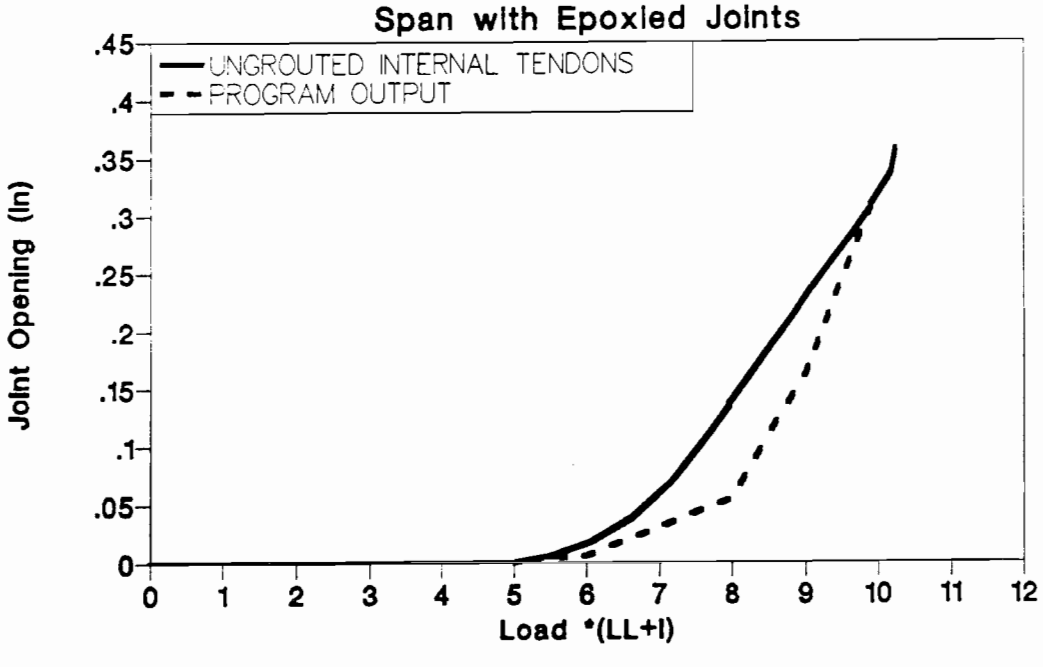

Figure 6.16 Joint opening response (epoxy joints span - ungrouted internal tendons).

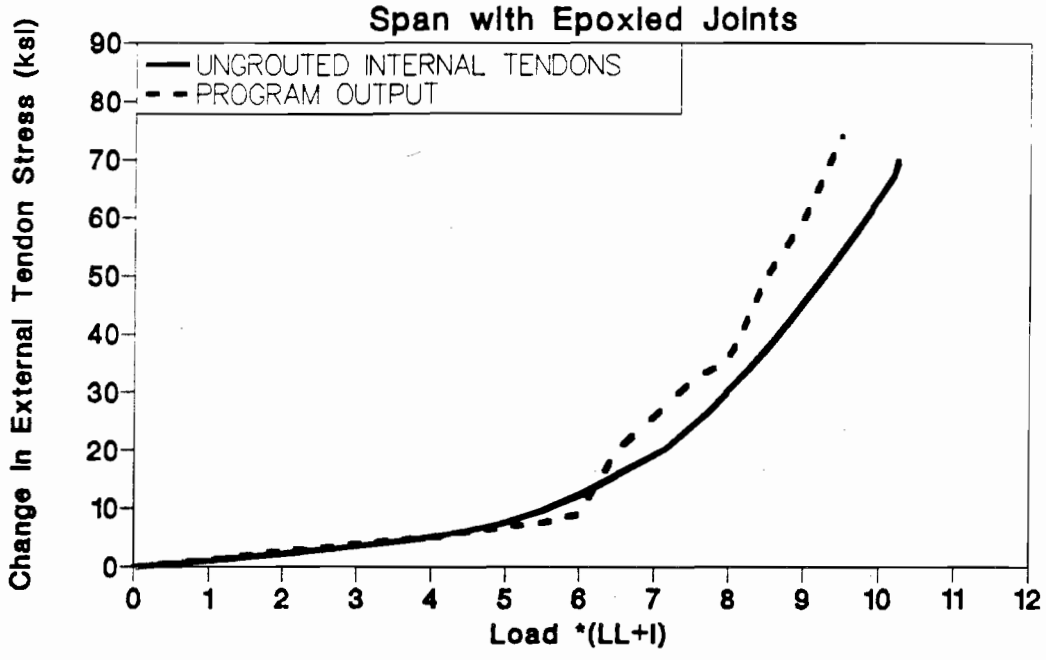

Figure 6.17 Change in external tendon stress (epoxy joints span - ungrouted internal tendons).

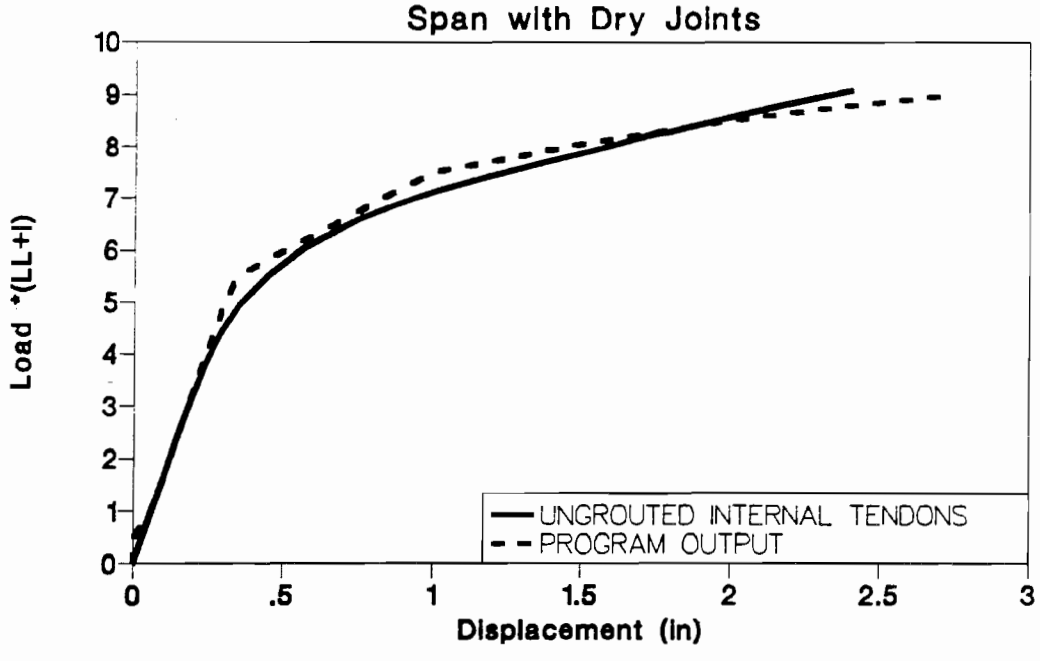

Figure 6.18 Load-deflection response (dry joints span - ungrouted internal tendons).

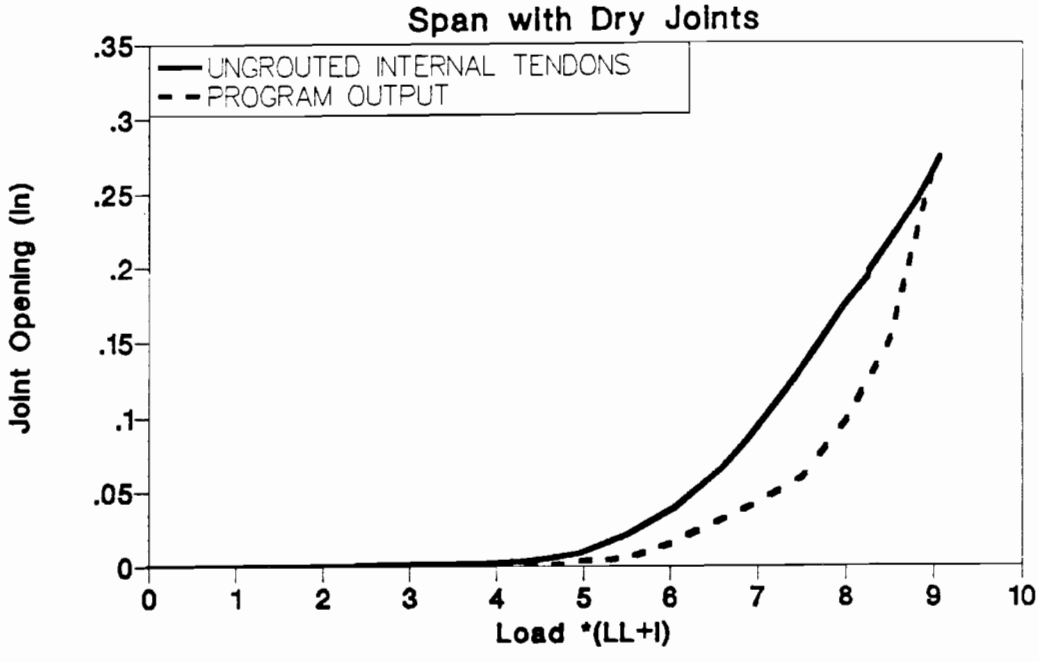

Figure 6.19 Joint opening response (dry joints span - ungrouted internal tendons).

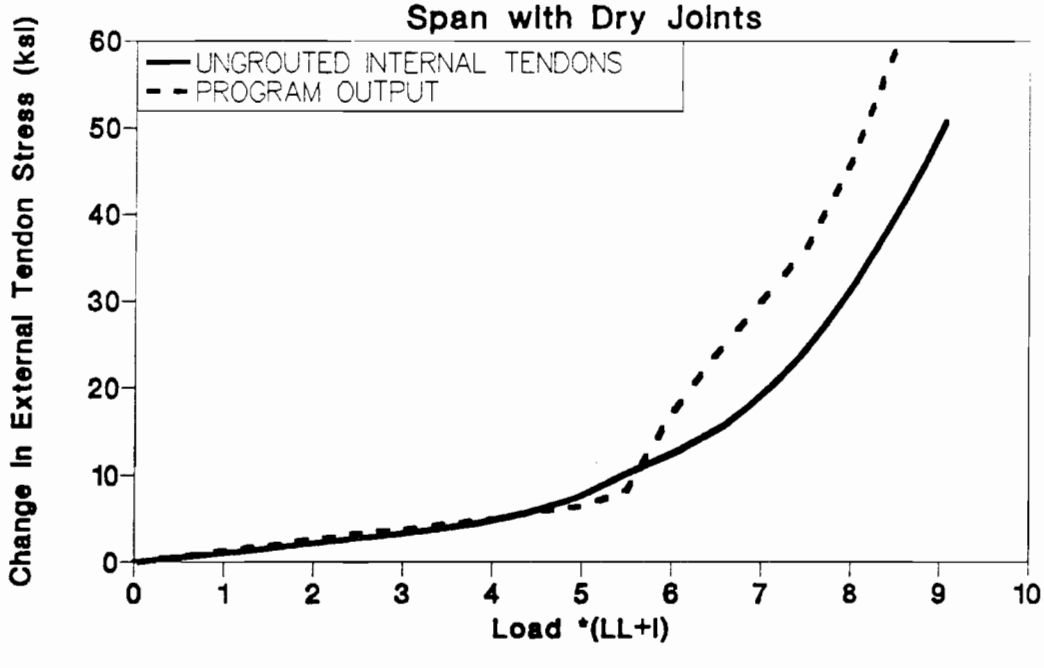

Figure 6.20 Change in external tendon stress (dry joints span - ungrouted internal tendons).

6.2.5.1 Epoxy Joints Span. Figures 6.21 through 6.24 show comparisons of critical parameters such as deflection, critical joint opening, change in external tendon stress, and change in internal tendon stress between the test results and the program output for the epoxy joints span. The load capacity predicted by the program is 4 percent lower than the test data as shown in Fig. 6.21. The prediction of the ultimate deflection is 6 percent higher than the test result. The maximum joint opening predicted by the program is 8 percent lower than the test data as shown in Fig. 6.22. The program prediction for the maximum change in external tendon stress is 6 ksi higher than the test value as shown in Fig. 6.23. The program prediction of the maximum change in internal tendon stress was the same as the test value because the internal tendon yielded in the two cases as shown in Fig. 6.24.

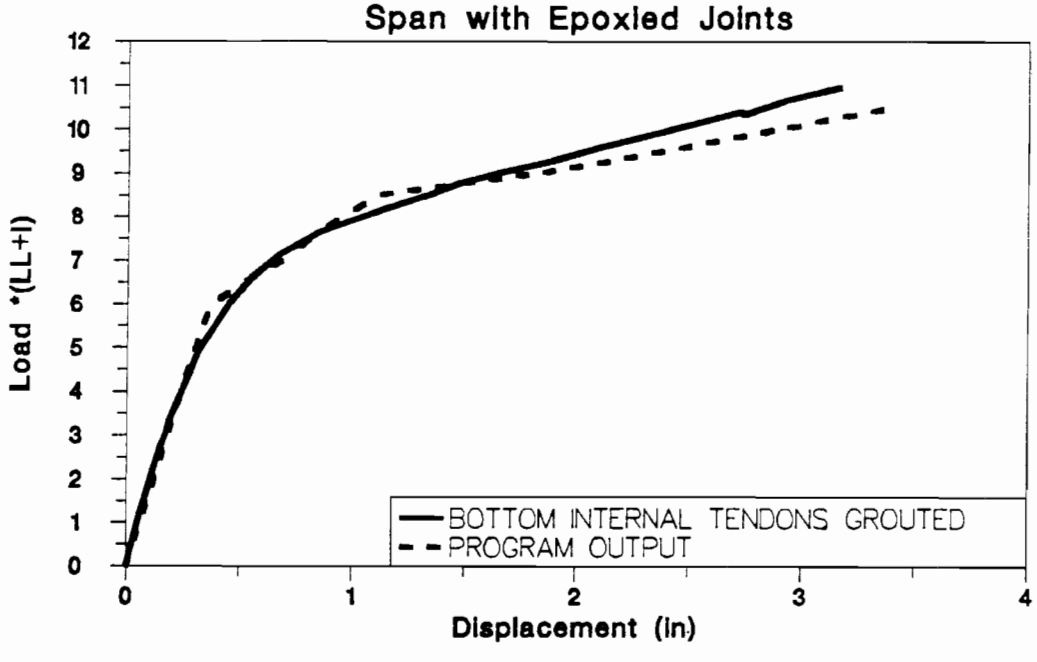

Figure 6.21 Load-deflection response (epoxy joints span - grouted internal tendons).

6.2.5.2 Dry Joints span. Figures 6.25 through 6.28 show comparisons of the critical parameters in the dry joints span. The program prediction for the load capacity is 7 percent higher than the test data as shown in Fig. 6.25. The ultimate displacement prediction is 8 percent higher than the test value. The maximum critical joint opening predicted by the program is 11 percent lower than the test value as shown in Fig. 6.26. The predicted maximum change in external tendon stress is 12 ksi higher than the measured value as shown in Fig. 6.27.

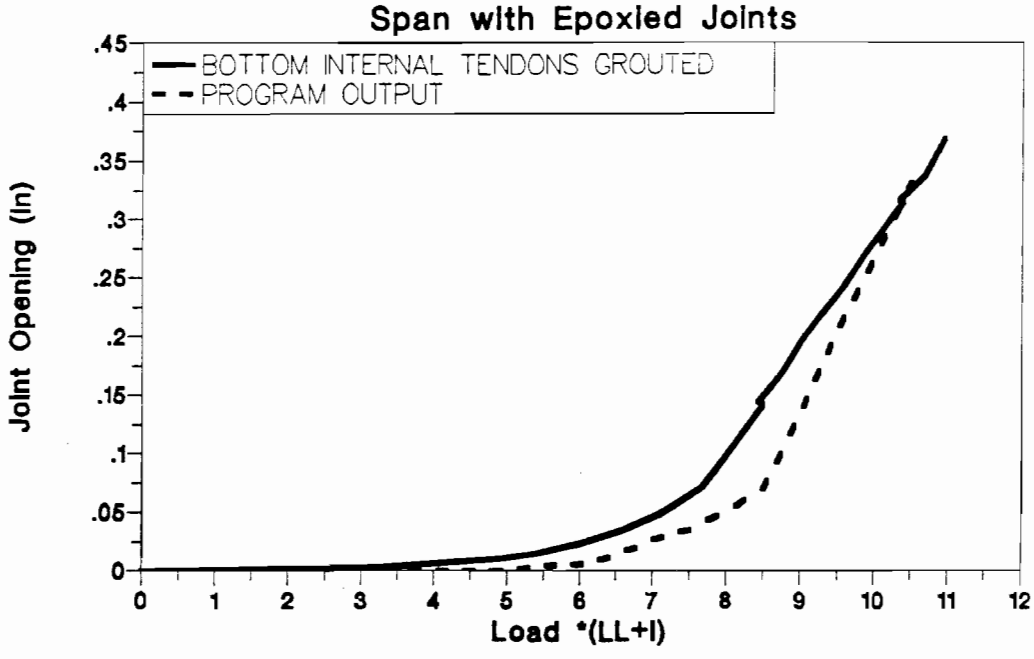

Figure 6.22 Joint opening response (epoxy joints span - grouted internal tendons).

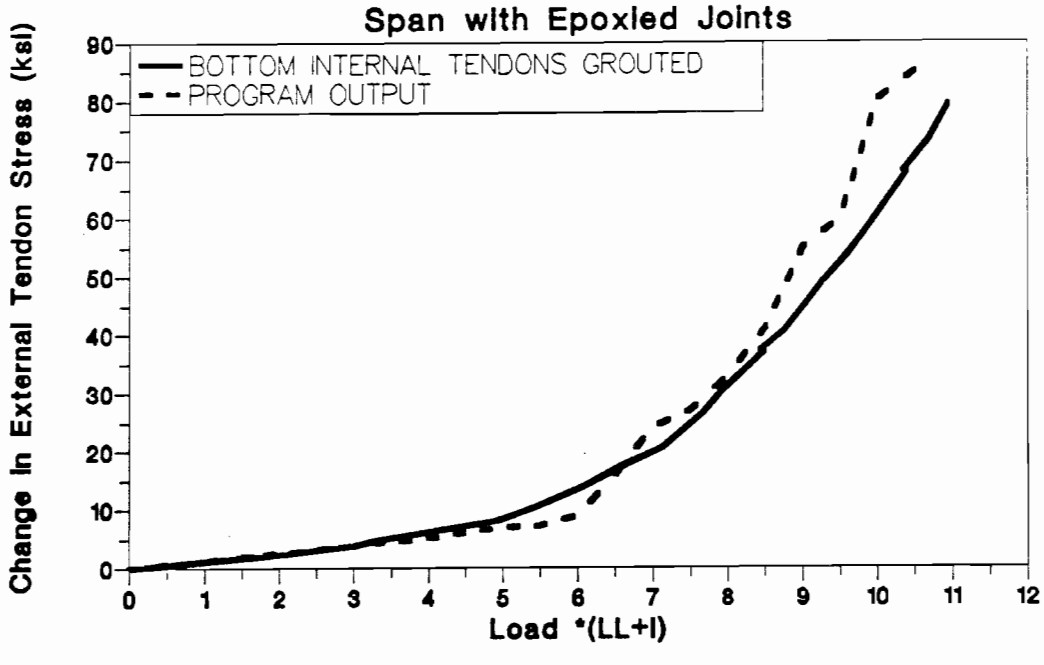

Figure 6.23 Change in external tendon stress (epoxy joints span - grouted internal tendons).

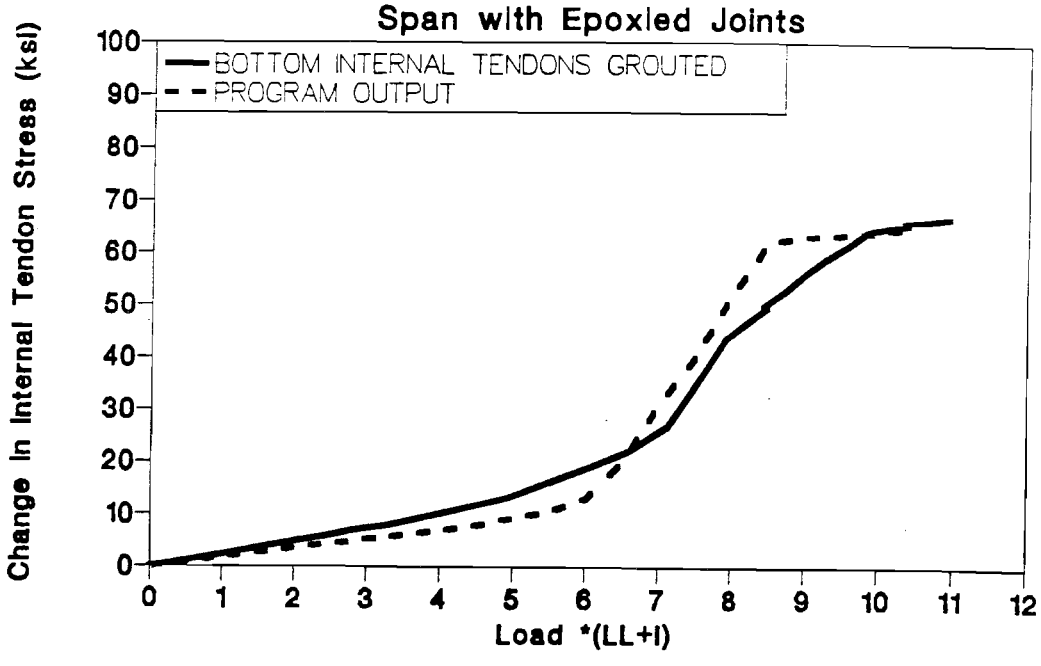

Figure 6.24 Internal tendon stress (epoxy joints span - grouted internal tendons).

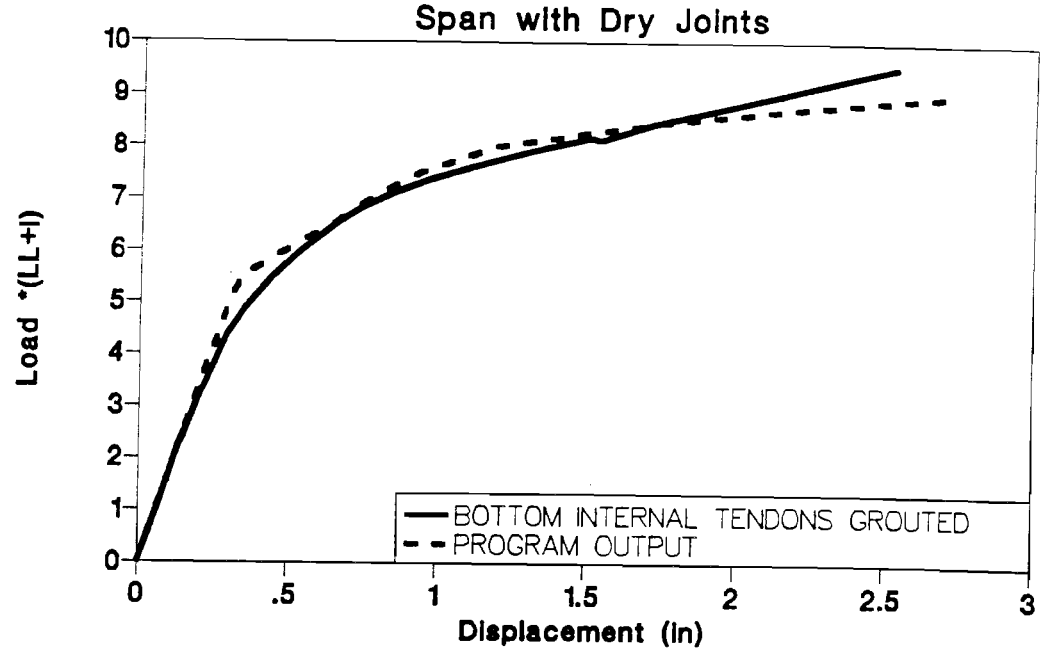

Figure 6.25 Load-deflection response (dry joints span - grouted internal tendons).

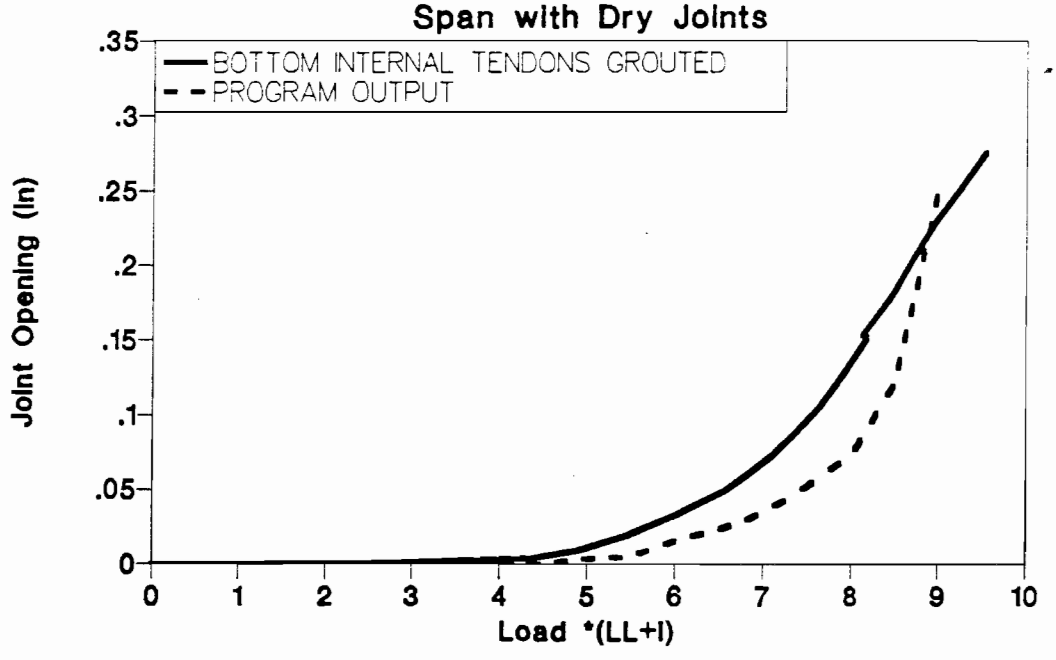

Figure 6.26 Joint opening response (dry joints span - grouted internal tendons).

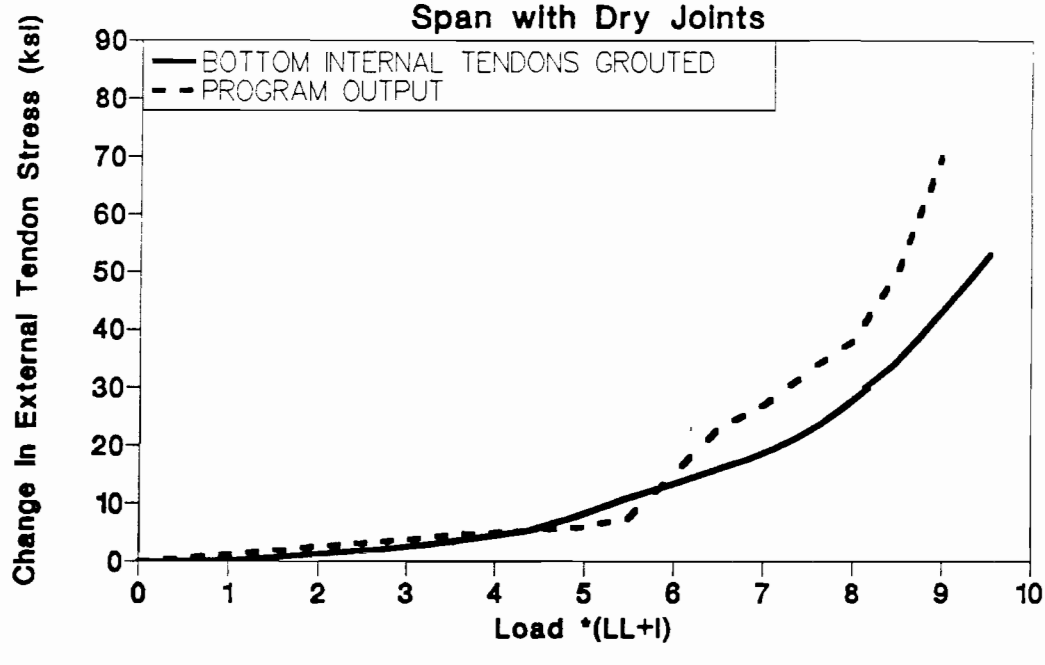

Figure 6.27 Change in external tendon stress (dry joints span - grouted internal tendons).

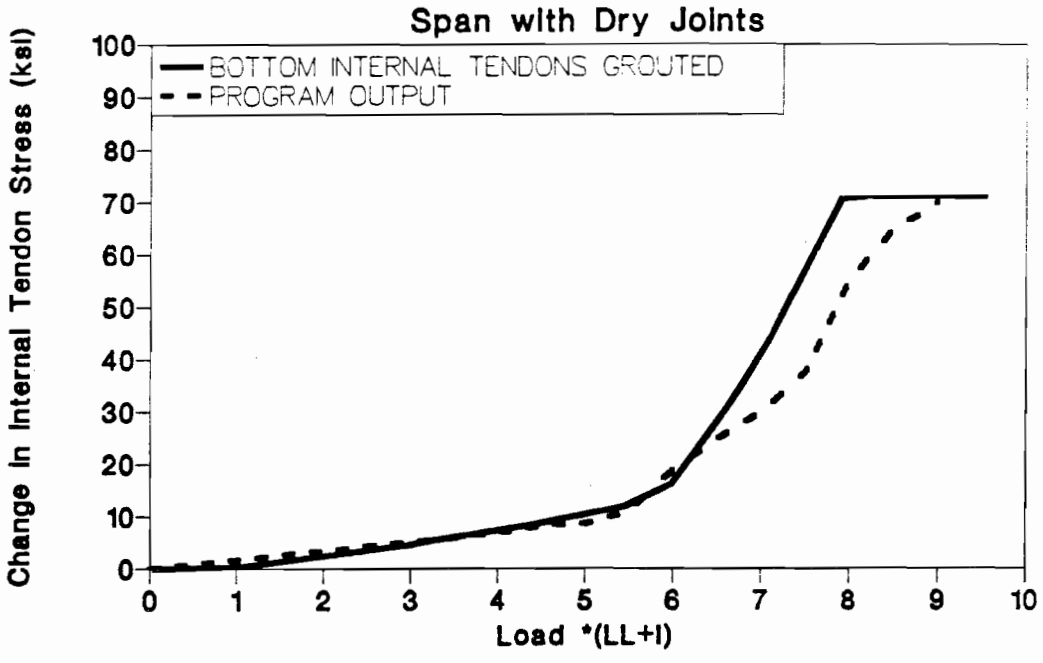

Figure 6.28 Internal tendon stress (dry joints span - grouted internal tendons).

6.3 C.E.B.T.P. Tests

Two of the tests reported by Martin (4) were used to extend the verification of the analysis program developed in this study. One beam had external tendons, while the second beam had a mix of external and internal tendons. The dimensions and material properties for the box girders are given in detail in Reference (4). A brief summary is presented in Fig. 6.29 and Fig. 6.30 and Tables 6.8, 6.9, and 6.10. The concrete strains were measured at the joints and in the segments during testing of the beams. The ultimate concrete strains were measured by Martin (4) at the end of the tests when the concrete failed.

Table 6.8 Prestressing Reinforcement

F_{sy} = 245 ksi	F_{su} = 279 ksi
ϵ_{sy} = 0.00838	ϵ_{su} = 0.0623

Eight beam elements were used to model each girder. The program applied the dead load and prestress load as one increment, then the concentrated live loads were applied in increments until the steel or concrete material failed by exceeding the strain limits. Each beam was simply supported and had nine segments.

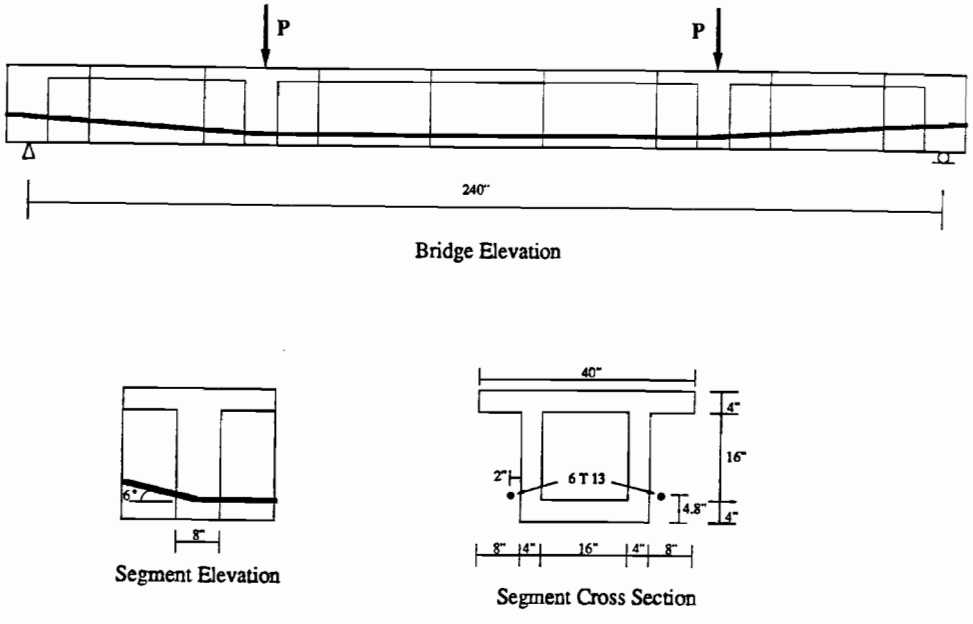

Figure 6.29 Beam NM3 details.

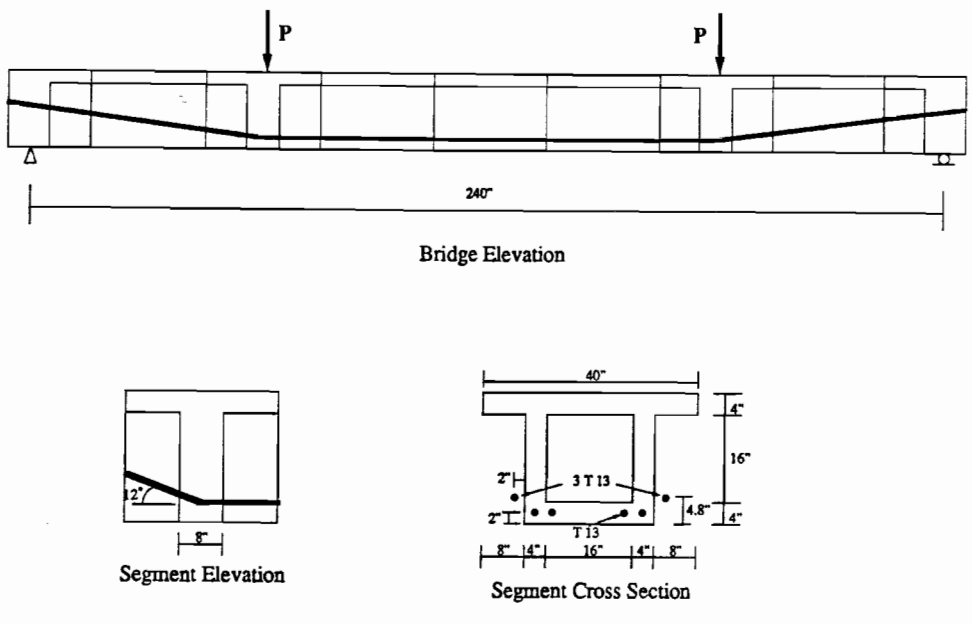

Figure 6.30 Beam NM4 details.

6.3.1 Beam NM3. The first beam modeled was beam NM3 (4). The external tendon ducts were filled with wax. The friction coefficient in this case is lower than for cement grouted tendons. A friction coefficient value of 0.15 was used in this analysis, while a friction coefficient of 0.25 was used for the cement-grouted tendons of beam NM4. Figures 6.31 through 6.33 show the comparison of critical parameters such as deflection, joint opening, and change in external tendon stress between the test results and the computer program predictions. Figure 6.31 shows the load capacity predicted by the program is 10 percent higher than the measured strength. The predicted maximum displacement is 15 percent higher than the maximum displacement measured during the test. Figure 6.32 shows that the joint opening prediction is 1 percent lower than the measured value. Figure 6.33 shows the change in external tendon stress predicted by the program is 6 ksi higher than the measured value.

Table 6.9 Conventional Reinforcement

F_{sy} = 69 ksi	F_{su} = 106 ksi
ϵ_{sy} = 0.0023	ϵ_{su} = 0.21

6.3.2 Beam NM4. The second beam modeled was beam NM4 which had a mixture of external and internal tendons as shown in Fig. 6.30. Figures 6.34 and 6.35 show the comparison of critical parameters such as deflection and joint opening. Figure 6.34 shows that the ultimate load predicted by the program is 1 percent higher than the measured strength. The ultimate displacement predicted by the program is 8 percent higher than the measured displacement. Figure 6.35 shows that the predicted maximum joint opening is 15 percent lower than the measured value. No comparison of the change in external tendon stress was carried out because the external tendon stress in the center of the girder was not reported in Reference (4).

Table 6.10 Concrete

F_{cc} = 6.25 ksi	F_{cu} = 5.0 ksi
ϵ_{cc} = 0.002	ϵ_{cu} = 0.045

6.4 Summary

The computer program predicted the behavior of the beams in a precise manner up to the load at which the joint opening started. This part of the analytical modeling was done using classical non-linear finite element analysis. It includes slipping of the external tendons and excludes consideration of the joints between the segments and slipping of the internal tendons.

The analysis after the joint opening started takes into consideration joint opening, slip of external tendons, and slip of internal tendons as discussed in Chapter Five.

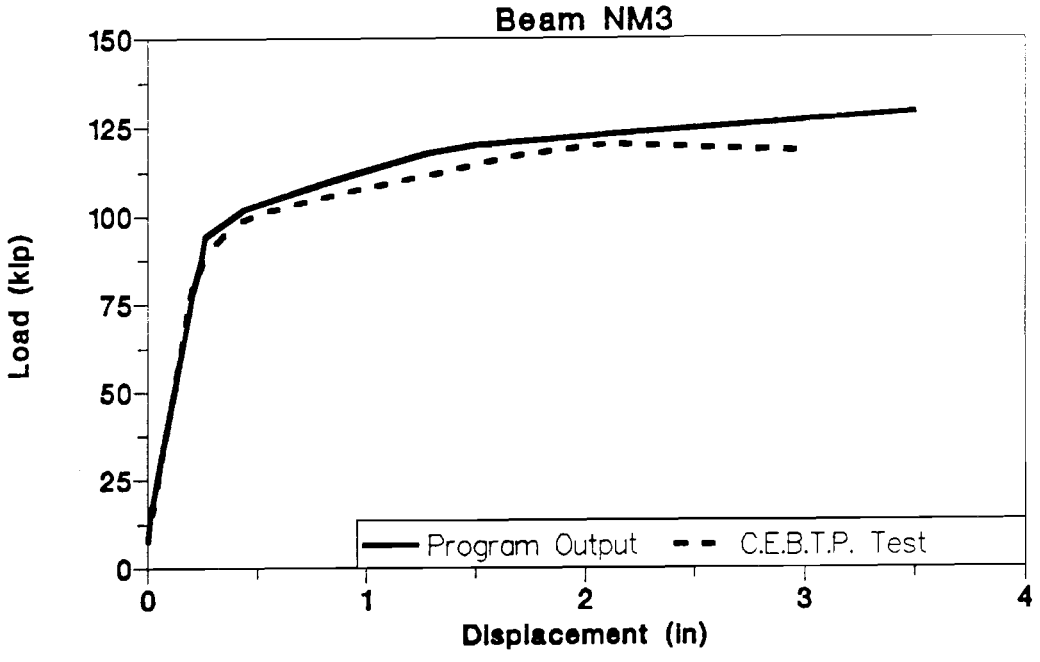

Figure 6.31 Load-deflection response (Beam NM3).

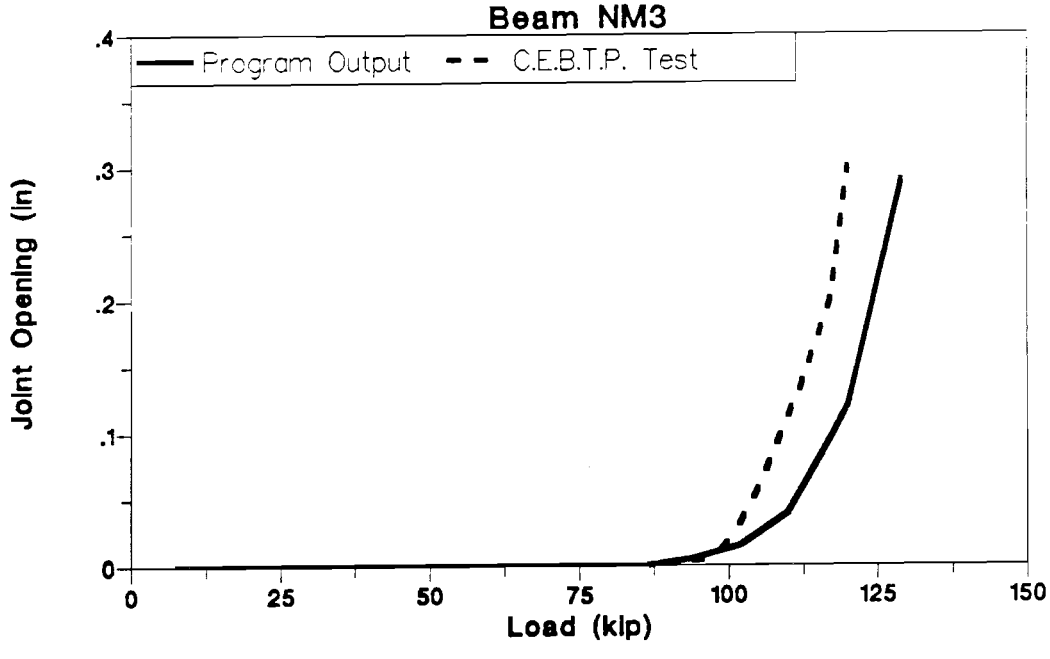

Figure 6.32 Joint opening response (beam NM3).

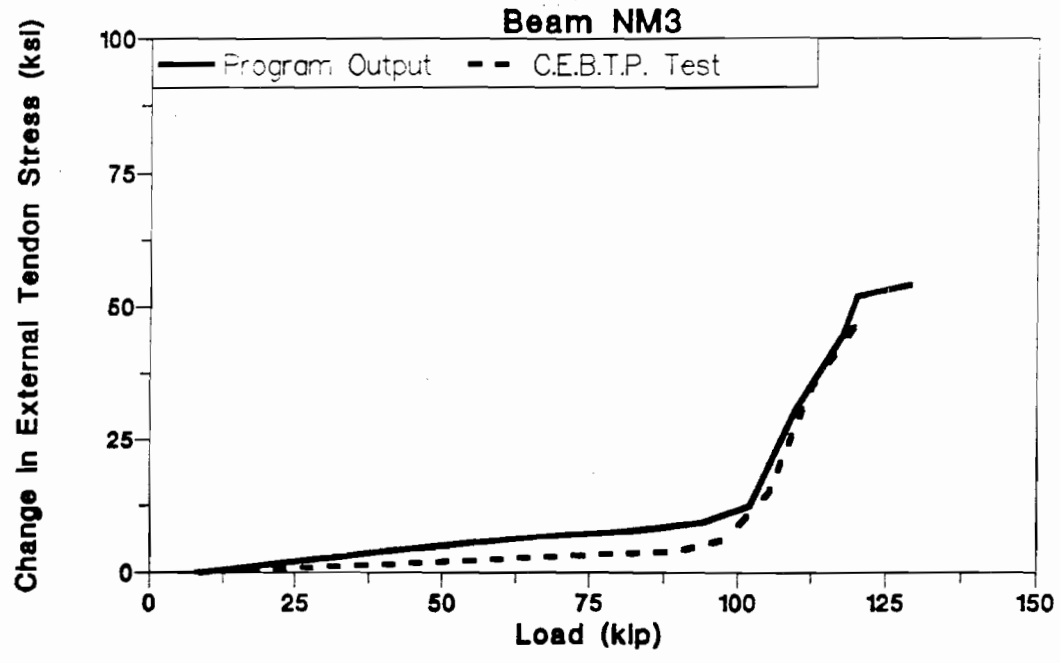

Figure 6.33 Change in external tendon stress (Beam NM3).

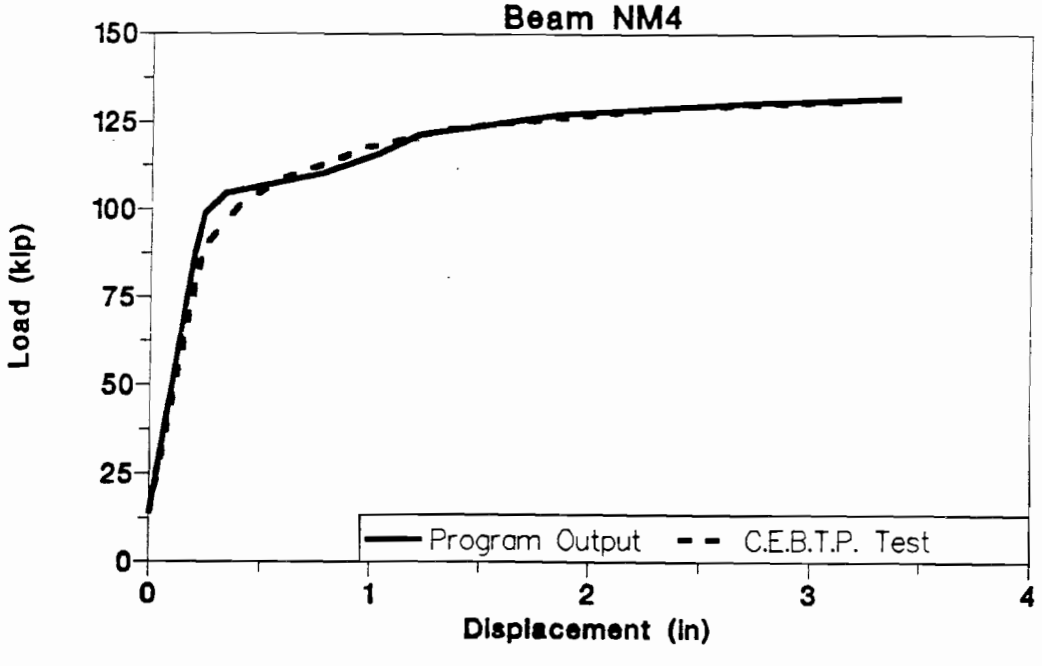

Figure 6.34 Load-deflection response (Beam NM4).

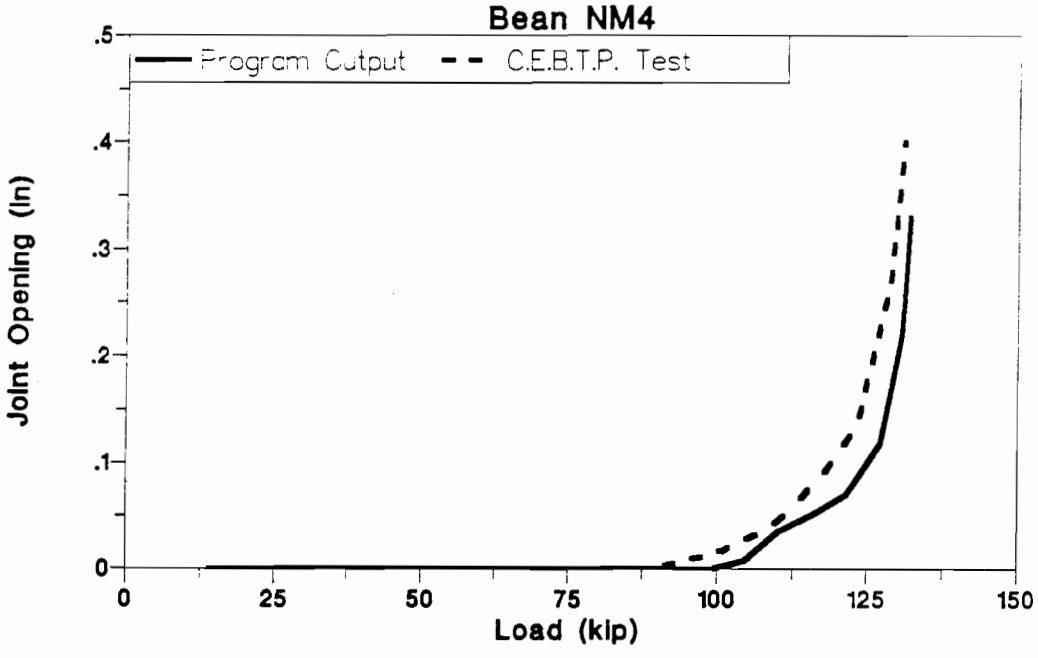

Figure 6.35 Joint opening response (Beam NM4).

Table 6.11 shows the program predictions for strength, ultimate displacement, joint opening, and change of external tendon stress. The program predictions for strength are within 5 percent of the measured strength of the epoxy joints structures, and within 10 percent of the measured values for dry joints structures. The ultimate displacement predictions by the program are within 11 percent of the measured values when the initial flexural strength tests of the three-span model are excluded. The tests were purposely stopped before the material completely failed to allow further studies on the model. The predicted maximum joint opening is within 15 percent of measured values for the dry joints structures and 10 percent for the epoxy joints structures (again, with the initial flexural strength tests excluded). The difference between predicted and measured change in external tendon stress is within 6 ksi for the epoxy joints structures and within 12 ksi for the dry joints structures.

Table 6.11 Accuracy of Program Bridge Predictions

Case	Epoxy Joints Span				Dry Joints Span			
	Ultimate Load	Ultimate Displacement	Joint Opening	External Tendon Stress	Ultimate Load	Ultimate Displacement	Joint Opening	External Tendon Stress
Initial Strength Tests **	+3%	+30%	+15%	+10 ksi	+1%	+12%	+8%	+5 ksi
Bonded External Tendons	-5%	+10%	+13%	-5 ksi	-2%	+8%	+2%	+6 ksi
Ungrouted Internal Tendons	-4%	+5%	-10%	+2 ksi	-2%	+11%	-3%	+8 ksi
Grouted Internal Tendons	-4%	+6%	-8%	+6 ksi	+7%	+8%	-11%	+12 ksi
CEBTP Tests Beam NM3					+10%	+15%	-1%	+6 ksi
CEBTP Tests Beam NM4					+1%	+8%	-15%	

**: Tests stopped before material failed +: Higher than test -: Lower than test

CHAPTER SEVEN

ANALYTICAL EXAMINATION OF VARIABLES

7.1 Introduction

Analytical examinations of critical variables such as percentage of discretely bonded external tendons at intermediate diaphragms, percentage of grouted internal tendons, the effect of various values for maximum concrete strain, and incremental bonding of external tendons are presented in this chapter. The computer program Bridge, which was discussed in Chapter Five and verified in Chapter Six was used to analyze the effects of a range of the critical variables. A full-scale three-span girder from the San Antonio "Y" project was used for the prototype structure in this analysis. The bridge details are shown in Fig 7.1. HS20-44 truck loads used in this analysis are shown in Fig 7.2. Steel and concrete properties used in this analysis are shown in Tables 7.1, 7.2, and 7.3. The maximum concrete strain and strength were calculated as discussed in Chapter Six.

The values to be used with the bond-slip relation for the internal tendons shown in Fig 5.3(b) are shown in Table 7.4. These values were obtained from test results reported by Trost (11). The values used to describe the external tendon bond-slip relation shown in Fig. 5.3(a) were obtained from tests performed by Radloff (10) as part of this study and from the model test results presented in Chapter Three (Section 3.5). These ordinate values are shown in Table 7.5. The friction coefficient used in the analysis was 0.25.

The critical variables examined in this chapter are the percentage of bonded external tendons, percentage of grouted internal tendons, maximum allowable concrete strain, and incremental bonding of external tendons.

7.2 Bonded External Tendons

Discretely Bonded external tendon effects were studied for three cases, each with a different amount of external tendons expressed as a percentage of total prestress, as shown in Table 7.6 and Table 7.7. To simplify the input data, the tendons shown in parentheses were assumed as a single tendon. The number of 0.6" diameter strands in each tendon is shown in Table 7.8. The bridge is symmetric about the cross-section center line with the same distribution of tendons in each half of the cross section. The bridge has two of each of the tendons. For all three cases, the total area of the prestressed tendons and the effective prestress are kept constant.

Two analyses were carried out for each case. One analysis assumed the external tendons were bonded at the end diaphragms and at two intermediate diaphragms in each span. The second analysis assumed that the external tendons were completely unbonded

Table 7.1 Prestressing Reinforcement

$F_y^* = 245\ ksi$	$F_s' = 279\ ksi$
$\epsilon_y^* = 0.00838$	$\epsilon_s' = 0.0623$

Table 7.2 Conventional Reinforcement

$F_{sy} = 60\ ksi$	$F_{su} = 70\ ksi$
$\epsilon_{sy} = 0.0019$	$\epsilon_{su} = 0.21$

Table 7.3 Concrete

$f_c' = 5.5\ ksi$	$F_{cu} = 3.85\ ksi$
$\epsilon_{cc} = 0.002$	$\epsilon_{cu} = 0.004$

Table 7.4 Internal Tendon Bond-Slip

$\tau_o = 0.37\ ksi$	$\tau_y = 1.0\ ksi$	
$S_o = 0.0007\ inch$	$S_1 = 0.004\ inch$	$S_y = 0.2\ inch$

Table 7.5 External Tendon Bond-Slip

$\tau_y = 0.37\ ksi$	
$S_o = 0.004\ inch$	$S_y = 0.4\ inch$

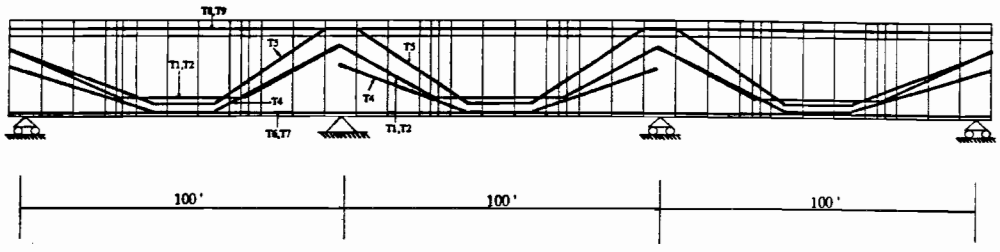

a) Bridge Elevation

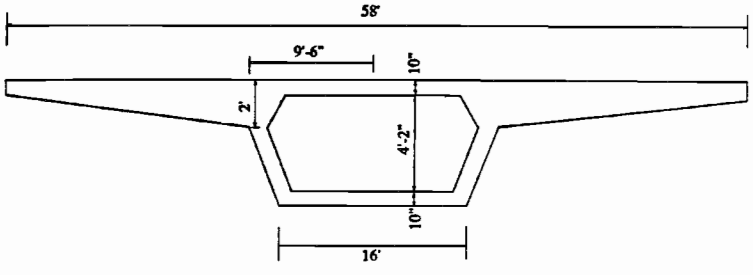

b) Cross Section

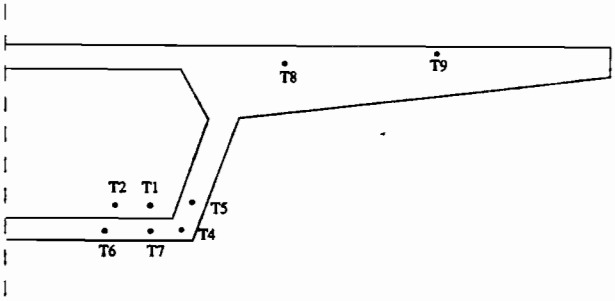

c) Section at Midspan

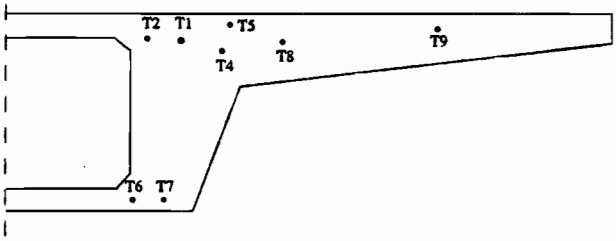

d) Section at Pier Segment

Figure 7.1 Bridge details.

except at the end diaphragms. This case would be pertinent for construction where a corrosion protection system such as grease or wax is used instead of a cement grout. Due to the deviation angle (change in tendon direction) at the deviators, the external tendons in both cases have friction between them and the deviators.

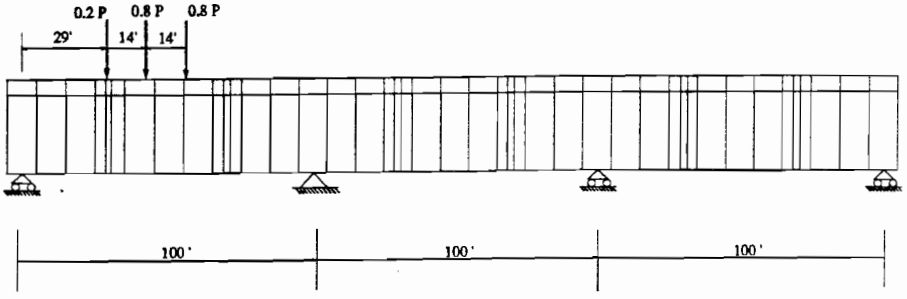

Loading Layout

HS 20-44
Bridge width =58 ft
4 Lane
Axle Load W = 40 Kip (HS 20-44)
Load P = 0.75*4 (Lane)* 40* Impact factor
Impact factor = 1.222
P=146.66 kip

Figure 7.2 Bridge loads.

Table 7.6 Tendon Composition

Case	Internal Tendons	External Tendons
1	T4,T5,T6,T7,(T8+T9)	T1,T2
2	T6,T7,(T8+T9)	T1,T2,T5,T4
3	NONE	ALL

7.2.1 Case One. In this case ten internal tendons and four external tendons were assumed for the bridge as shown in Table 7.6. The external tendons provide about 34 percent of the total prestress area in this case, while the remaining prestress is provided by grouted internal tendons. Figures 7.3 through 7.6 show the different bridge responses for the discretely bonded and the unbonded analyses. In the discretely bonded analysis, the external tendons were assumed to be bonded at the intermediate diaphragms, while they were assumed to be unbonded in the second analysis. Figure 7.3 shows that there is relatively little difference in the load-displacement relation between these analyses. The

Table 7.7 Percentage of External Tendons

Case	% of Total Prestress Steel Area Used as External Tendons
1	34
2	69
3	100

ultimate live load capacity of the structure in the discretely bonded case was about 5 percent higher than for the unbonded case. The ultimate live load displacement for the discretely bonded case was about 4 percent greater than for the unbonded case. The effect of discrete bonding at the deviators was noticed only at loads higher than the load at which the internal tendons yielded as shown in Fig 7.3. The internal tendons yielded at a load of 6.75*(LL+I) as shown in Fig 7.4. As the internal tendons yielded, the effect of bonding the external tendons became important because the effect of internal tendons on the critical joint stiffness disappeared as soon as the internal tendons yielded (if strain hardening of the internal tendon is neglected). In this case, bonding of external tendons increases the critical joint stiffness which attracts more external force moment to the critical region. As the external moment increases, the opening of adjacent joints (adjacent to the critical joint) also increases. Higher adjacent joint opening results in higher total joint opening (as shown in Fig. 7.6) and higher external tendon stress (as shown in Fig. 7.5) in the discretely bonded case than in the unbonded case. Higher external tendon stress change was due to shorter unbonded tendon length for the discretely bonded case. The maximum increase in the external tendon stress was 65 ksi for the discretely bonded case and 35 ksi for the unbonded case. A major change in tendon stress (from 35 to 65 ksi) had small effect on the strength due to relatively small change in tendon force (depends on initial prestress and tendon area). The critical joint opening for the unbonded case increased at a higher rate after yielding of the internal tendon than for the discretely bonded case as shown in Fig 7.6. The higher critical joint opening for the unbonded case caused failure of the concrete at a lower load and displacement than for the discretely bonded case. This resulted in the lower strength and ductility for the unbonded case as shown in Fig 7.3.

Table 7.8 Number of Strands in Tendon

T1	T2	T4	T5	T6	T7	T8	T9
19	19	19	19	12	12	7	3

7.2.2 Case Two. The second analysis case was carried out assuming six internal tendons and eight external tendons as shown in Table 7.6. The external tendons provide approximately 69 percent of the total prestress area. Figures 7.7 through 7.10 show the response of the structure to the applied loads. In this case there is much more evidence of the efficiency of discrete bonding of the external tendons at the intermediate diaphragms. Discrete bonding of the external tendons caused an increase of 16 percent in the ultimate live load capacity of the structure and 37 percent increase in the ultimate live load displacement as shown in Fig 7.7. The internal

tendons yielded at a load of 5.75*(LL+I) as shown in Fig 7.8. Above this load, the effect of discrete bonding was noticed. Discrete bonding increased the critical joint stiffness which attracted more moment in that region. This increased the opening of the adjacent joints which were already open. The change in stresses developed in the external tendons were substantially higher in the discretely bonded case as shown in Fig 7.9.

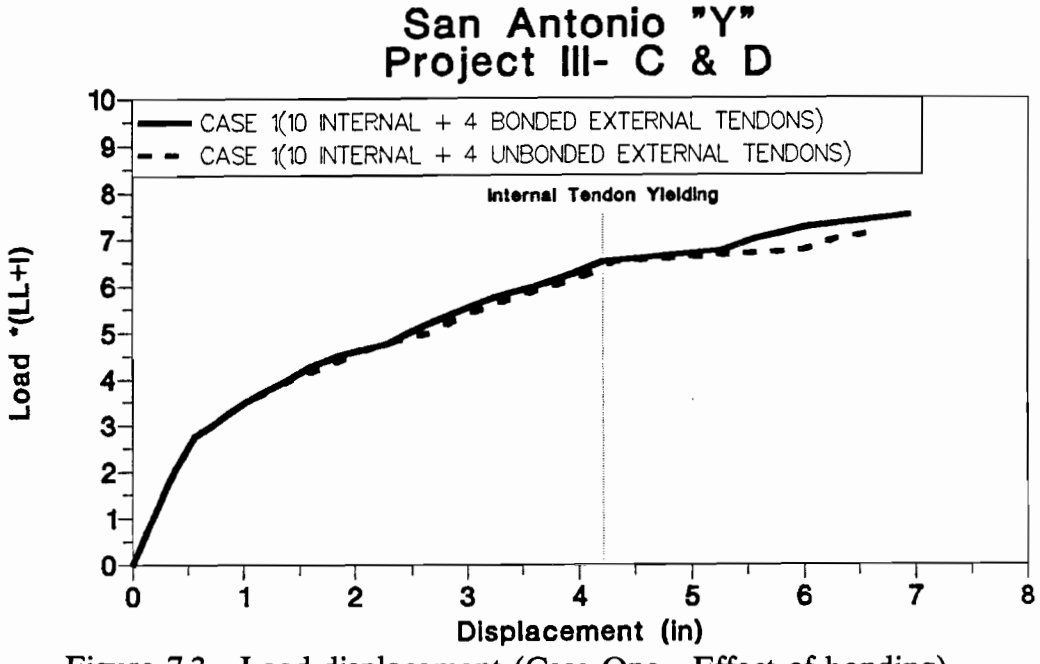

Figure 7.3 Load-displacement (Case One - Effect of bonding).

The maximum increase in the external tendon stress was 62 ksi in the discretely bonded case and only 26 ksi in the unbonded case. This difference in external tendon stress leads to the difference in the ultimate live load capacity of the structure because the internal tendons yielded in both cases. As the internal tendons yielded, the critical joint started opening at a higher rate for the unbonded case than for the discretely bonded case as shown in Fig 7.10. This caused the critical joint to fail at a lower ultimate load and displacement for the unbonded case.

7.2.3 Case Three. In the third case, all tendons were assumed to be external tendons. The six straight tendons in the top and bottom flanges were assumed to be ungrouted in their ducts and, thus, behave essentially as unbonded external tendons. These six tendons were assumed to be unbonded in the two cases because while they can be continuously grouted to the ducts, they cannot be discretely bonded only at the intermediate diaphragms and the purpose of the analysis was to illustrate the effect of discrete bonding at the diaphragms. The eight draped tendons were assumed to be discretely bonded only at the intermediate diaphragms in the first analysis and to be unbonded in the second analysis. Figures 7.11 through 7.14 show the responses of the structure to the load. The

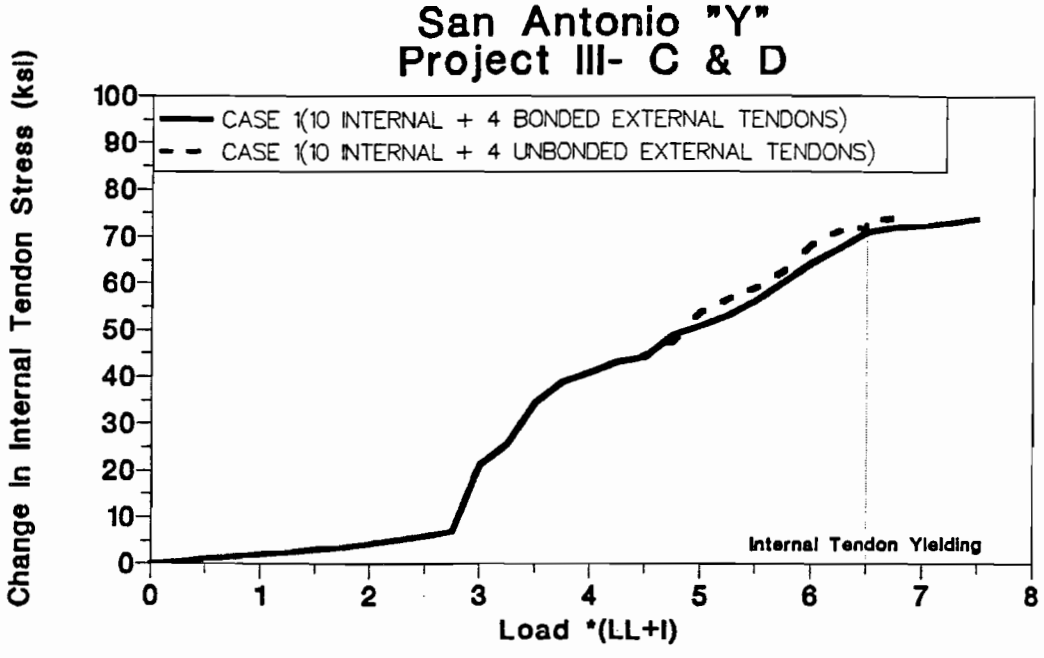

Figure 7.4 Internal tendon stress (Case One - Effect of bonding).

ultimate live load capacity of the structure for the discretely bonded case was 16 percent higher than for the unbonded case as shown in Fig 7.11. The ultimate live load displacement for the discretely bonded case was 35 percent higher than for the unbonded case. The change in stress in the ungrouted tendons (which are assumed in this case to behave as unbonded external tendons) was less than 10 ksi as shown in Fig 7.12. Stress changes in the external tendons for the discretely bonded case were higher than for the unbonded case as shown in Fig 7.13. This was the cause for the difference in the live load capacity of the structures. The maximum change in external tendon stress was 70 ksi for the discretely bonded case and 27 ksi for the unbonded case. The critical joint opening for the unbonded case was higher than for the discretely bonded case as shown in Fig 7.14. The higher joint opening and consequent higher concrete strains for the unbonded case caused a failure of the concrete at lower load and displacement.

7.2.4 Summary. Table 7.9 compares the effect of bonding on strength, ductility, and external tendon stress for the three cases. The changes are not measured from a common reference case but are relative changes between the discretely bonded and unbonded cases.

The effect of discrete bonding of external tendons in case one was smaller than the other two cases due to two reasons. The first reason is that the percentage of external tendons in case one was substantially smaller than the other two cases as shown in Table 7.7. The second reason is that the use of grouted internal tendons substantially improved

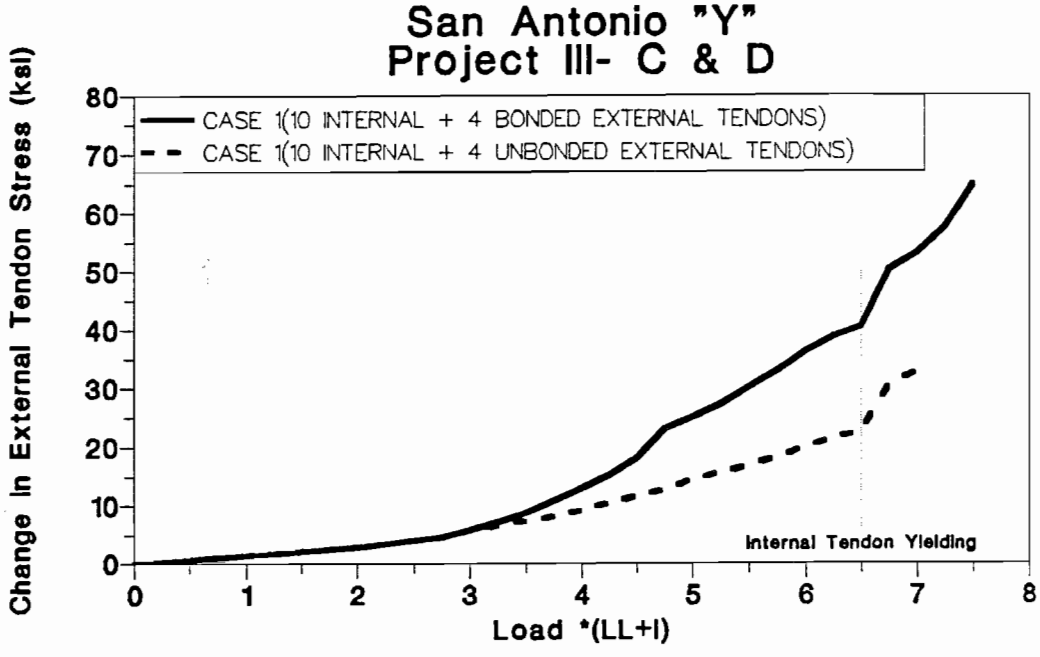

Figure 7.5 External tendon stress (Case One - Effect of bonding).

the strength and ductility of the girder without discrete bonding of external tendons so that the effect of discrete bonding of the external tendons was clear only after the internal tendons yielded.

The load level is in excess of 5(LL+I) before these differences are noted, but the effect of bonding at high overloads is clearly demonstrated by the analyses. Strength, ductility, and external tendon stress are increased by bonding as shown by the analyses.

Figure 7.15(a) shows the response as affected by varied percentage of unbonded external tendons and grouted internal tendons. In order to substantially improve the strength and ductility of the structure, the percentage of internal tendons used must be high. Figure 7.15(b) shows that discretely bonding external tendons is effective in increasing strength and ductility even if no internal tendons are used (as with case 3). Using a mixture of discretely bonded external tendons and grouted internal tendons improves the strength and ductility somewhat more.

Table 7.9 shows that discrete bonding of the external tendons and/or using grouted internal tendons increases strength and ductility up to a certain level after which the efficiency of additional bonding reduces. Discretely bonding 69 percentage of the external tendons (case two) increases the live load capacity by 16 percent and the ultimate displacement by 37 percent. This gives a ratio of percentage increase in displacement to

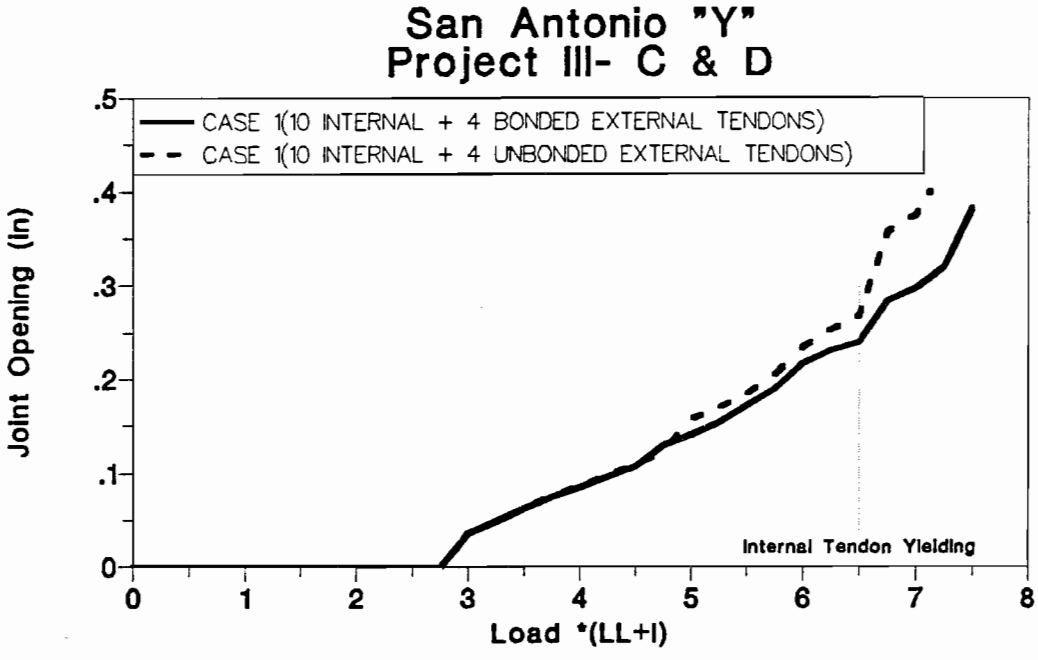

Figure 7.6 Joint opening (Case One - Effect of bonding).

percentage of bonded tendon of 0.523. In case one (34 percent of the external tendons discretely bonded), the percentage increase in live load capacity is only 5 percent, while the displacement increases by only 4 percent. The ratio of percentage increase in displacement to percentage of discretely bonded tendon is 0.11 which is much lower than in case two. Comparing the ratios for case one and two indicates that the efficiency of bonding is higher in case two than case one. The 66 percent of grouted internal tendons assumed in case one is enough to substantially increase the strength and ductility so that the efficiency of incremental bonding the external tendons is greatly reduced.

Table 7.9 Bonding Effects

Case	% Bonded External	% Grouted Internal	Ultimate Strength	Ultimate Displacement	External Tendon Stress
1	34	66	+5%	+4%	+30 ksi
2	69	31	+16%	+37%	+38 ksi
3	69	0	+16%	+35%	+43 ksi

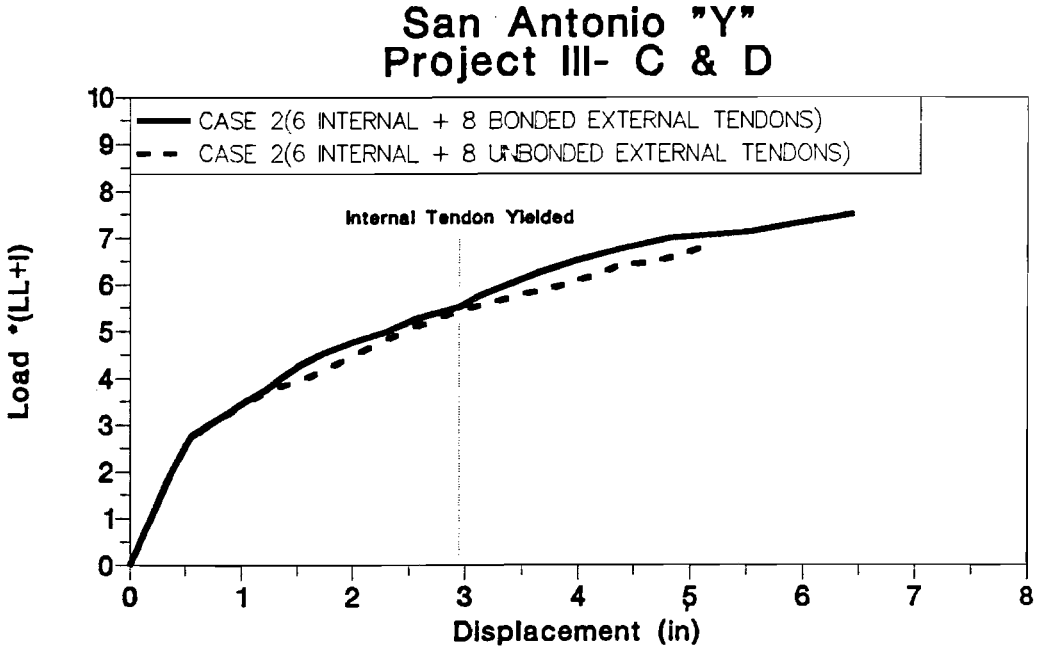

Figure 7.7 Load-displacement (Case Two - Effect of bonding).

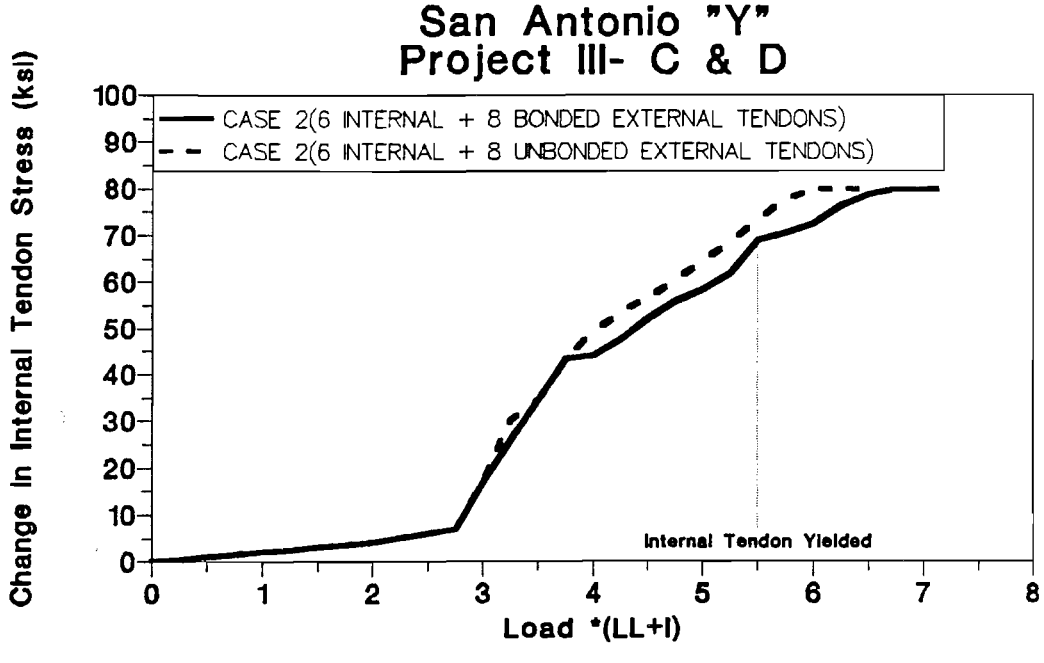

Figure 7.8 Internal tendon stress (Case Two - Effect of bonding).

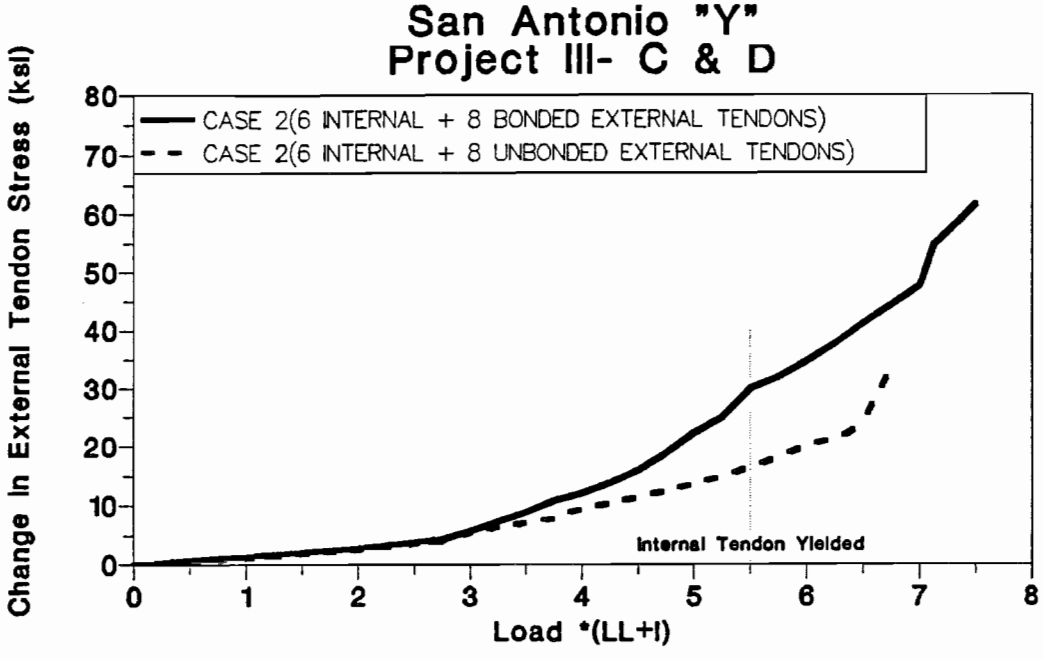

Figure 7.9 External tendon stress (Case Two - Effect of bonding).

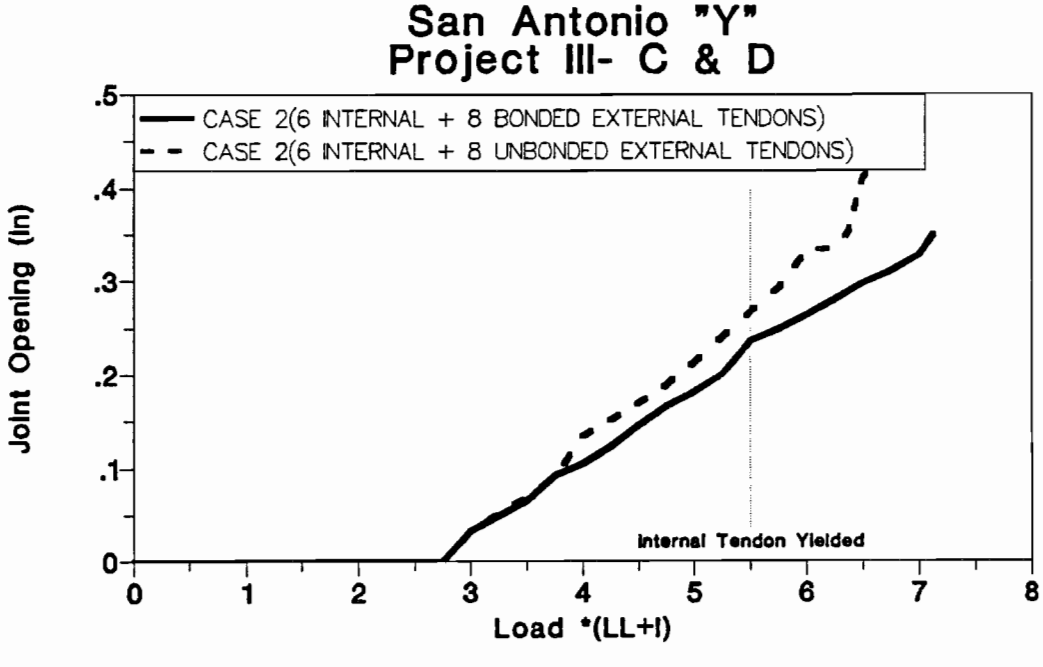

Figure 7.10 Joint opening (Case Two - Effect of bonding).

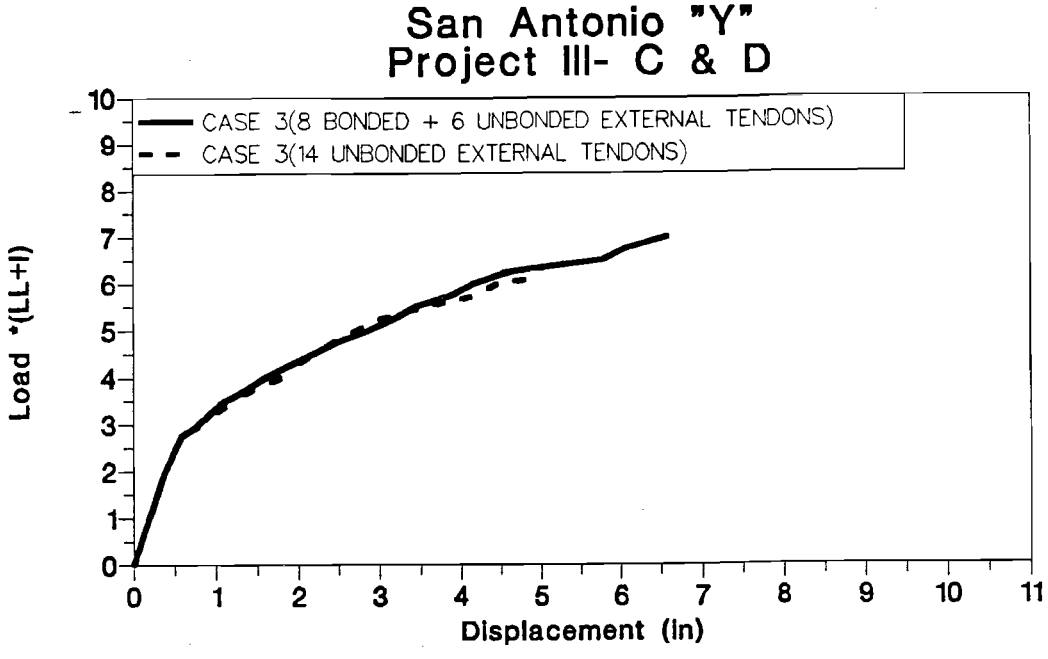

Figure 7.11 Load-displacement (Case Three - Effect of bonding).

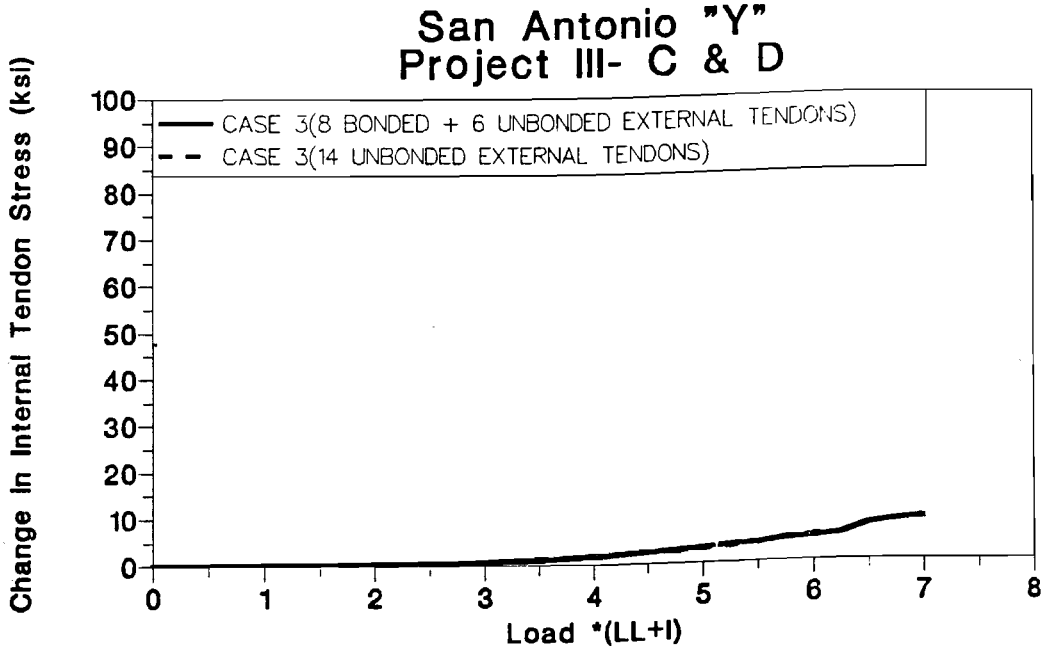

Figure 7.12 Internal tendon stress (Case Three - Effect of bonding).

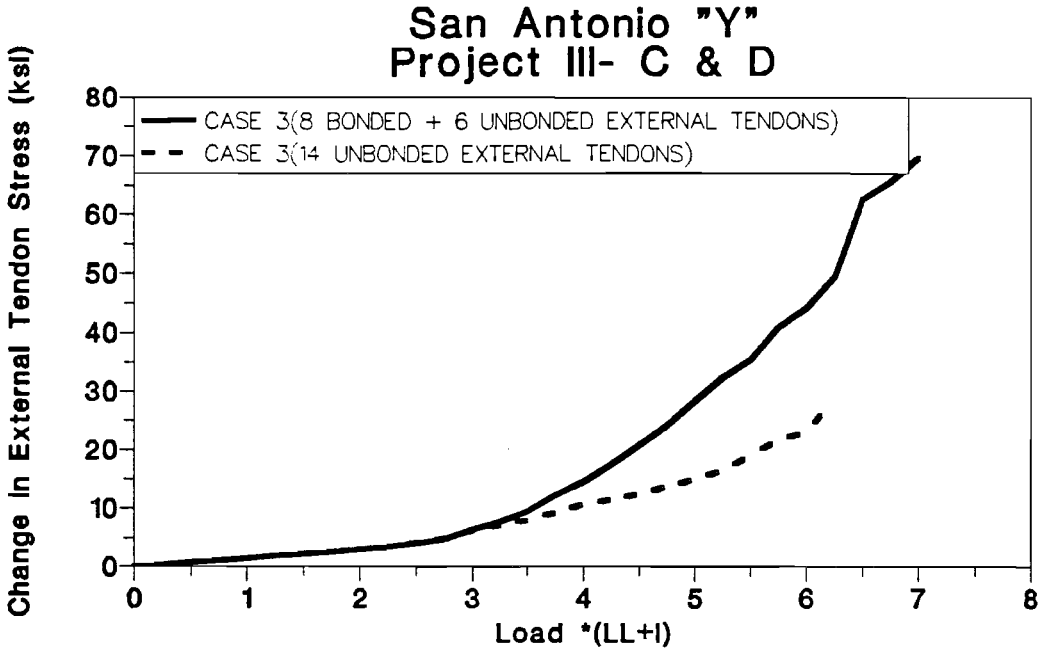

Figure 7.13 External tendon stress (Case Three - Effect of bonding).

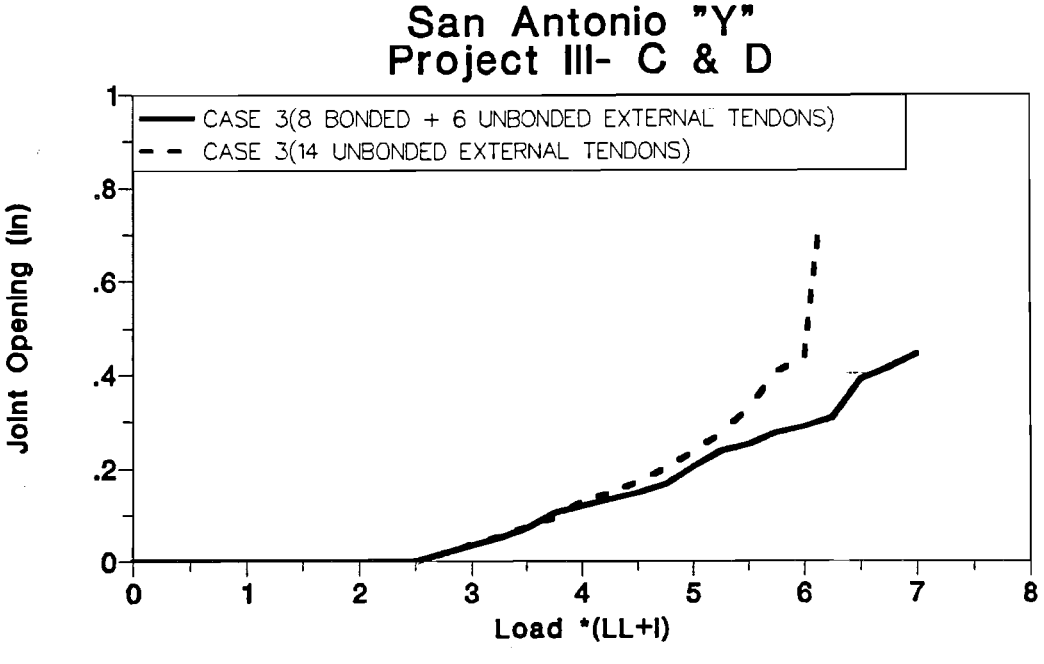

Figure 7.14 Joint opening (Case Three - Effect of bonding).

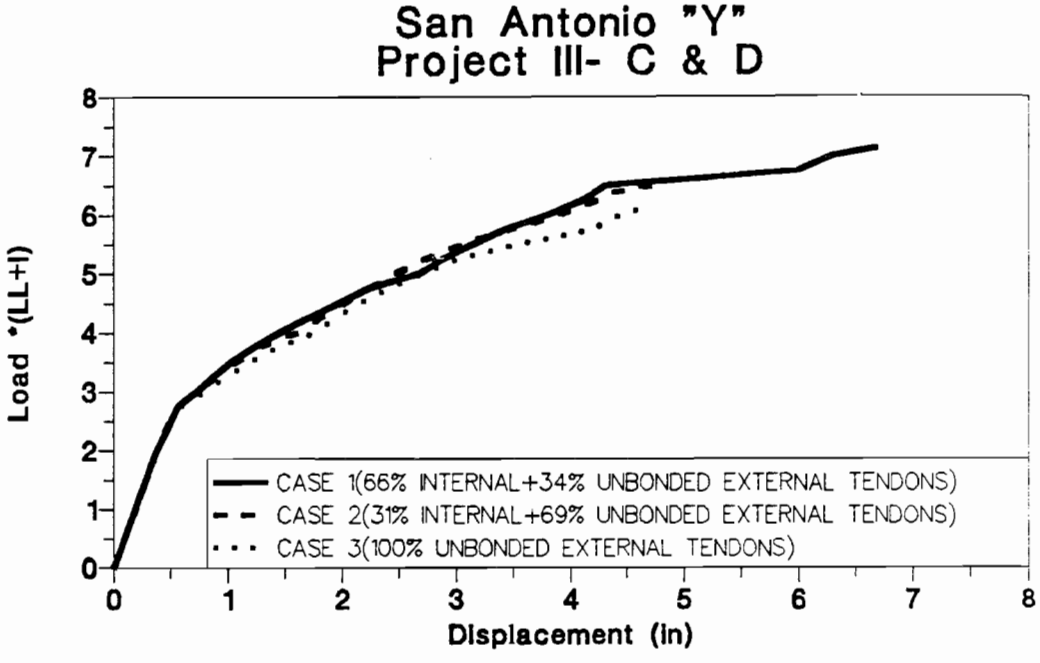

a) Load-displacement (unbonded external tendons)

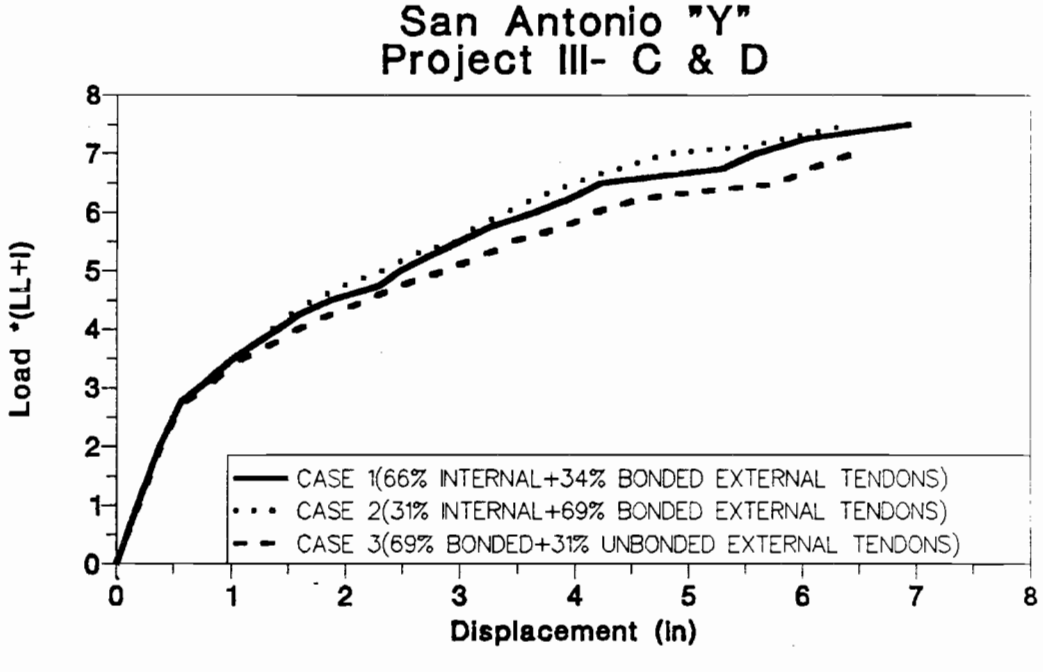

b) Load-displacement (bonded external tendons)

Figure 7.15 Load-displacement (effect of bonding).

7.3 Grouted Internal Tendons

The effect of grouted internal tendons was studied by analyzing the structure using three cases each with a different percentage of grouted internal tendons and external tendons. Table 7.6 shows the three cases used while Table 7.10 shows the percentage of the grouted internal tendon steel area as compared to the total prestress steel area. Two analyses were carried out for each of the three cases. In the first analysis, the external tendons were assumed to be discretely bonded to the two intermediate diaphragms in each span while in the second analysis the external tendons were assumed to be completely unbonded within the span.

Table 7.10 Percentage of Internal Tendons

Case	% of Total Prestress Steel Area Used as Grouted Internal Tendons
1	66
2	31
3	0

7.3.1 Grouted Internal Tendons with Unbonded External Tendons. Figures 7.16 through 7.19 show the calculated responses of the structure to the loads for the three cases with unbonded external tendons. Figure 7.16 shows the load-deflection predictions of the program for the three cases. The ultimate live load capacity for case two was 12.5 percent higher than for case three while the capacity for case one was 19 percent higher than for case three. The ultimate displacement for case two was 14 percent higher than for case three, while the ultimate displacement for case one was 50 percent higher than for case three. The internal tendons yielded for case two at a load 12 percent lower than for case one as shown in Fig 7.17. The maximum external tendon stress change for case two was 8 ksi higher than for case three while the stress change for case one was 13 ksi higher than case three as shown in Fig. 7.18. The maximum joint opening shown in Fig. 7.19 was highest for case three followed by case two and finally by case one.

7.3.2 Grouted Internal Tendons with Discretely Bonded External Tendons. Figures 7.20 through 7.23 show the calculated responses of the structure for different percentages of grouted internal tendons and external tendons discretely bonded at the two intermediate diaphragms in each span. Figure 7.20 shows that using a combination of internal tendons and some external tendons in case one and two increased the ultimate live load capacity by 10 percent over case three which uses a mixture of discretely bonded and unbonded external tendons only. The ultimate live load displacement for case one was 8 percent higher than those of case two and three. The internal tendons in case two yielded at a load 7 percent lower than the yielding load in case one as shown in Fig 7.21. The maximum external tendon stress increase developed in case three was 15 ksi higher than the stress increase developed in case one and two as shown in Fig 7.22. The maximum joint opening was highest for case three followed by case two and finally case one as shown in Fig 7.23.

Table 7.11 Grouted Internal Tendon Effects

	Unbonded External Tendons		Discretely Bonded External Tendons	
Case	1	2	1	2
% Internal Tendons	66	31	66	31
% Bonded External Tendons	0	0	34	69
Ultimate Strength	+19%	+12.5%	+10%	+10%
Ultimate Displacement	+50%	+14%	+8%	+0%
External Tendon Stress	-13ksi	+8ksi	-15ksi	-15ksi

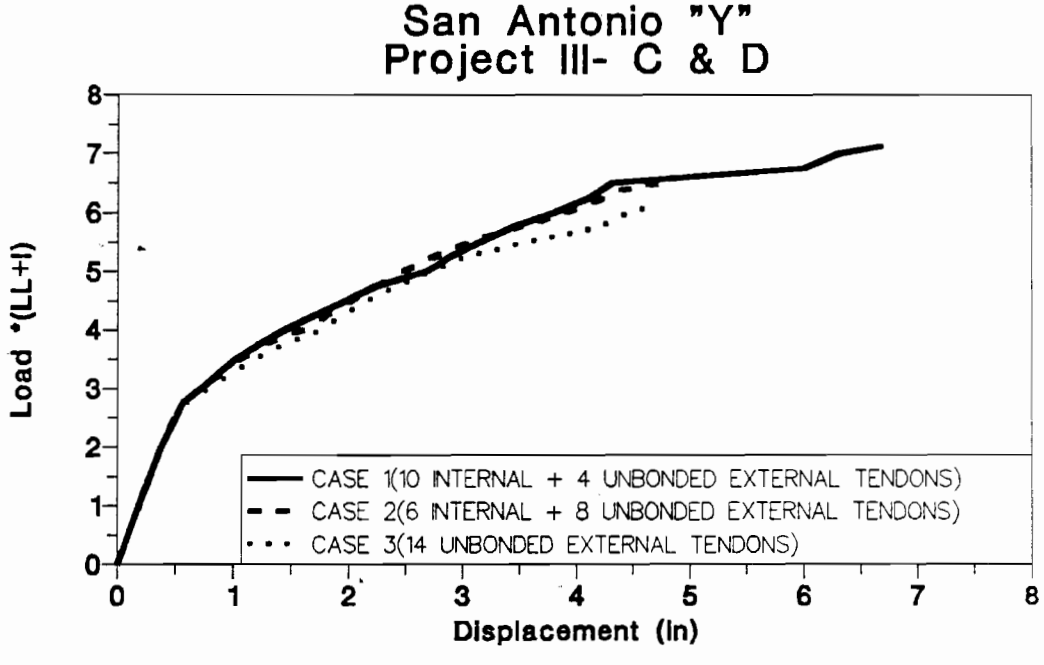

Figure 7.16 Load-displacement (effect of internal tendons - unbonded external tendons).

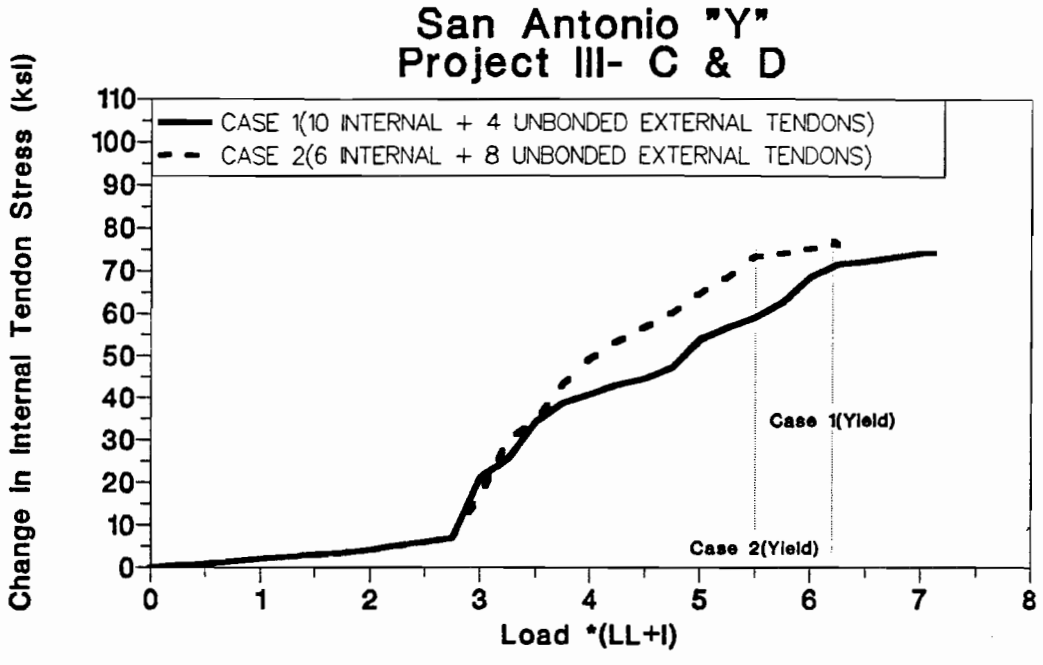

Figure 7.17 Internal tendon stress (effect of internal tendons - unbonded external tendons).

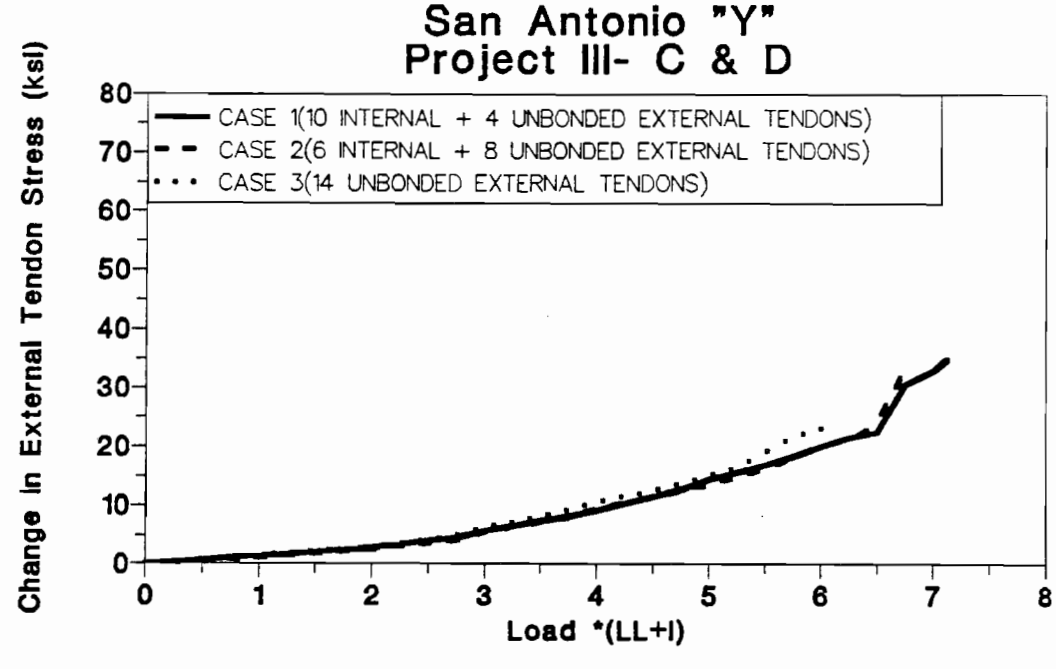

Figure 7.18 External tendon stress (effect of internal tendons - unbonded external tendons).

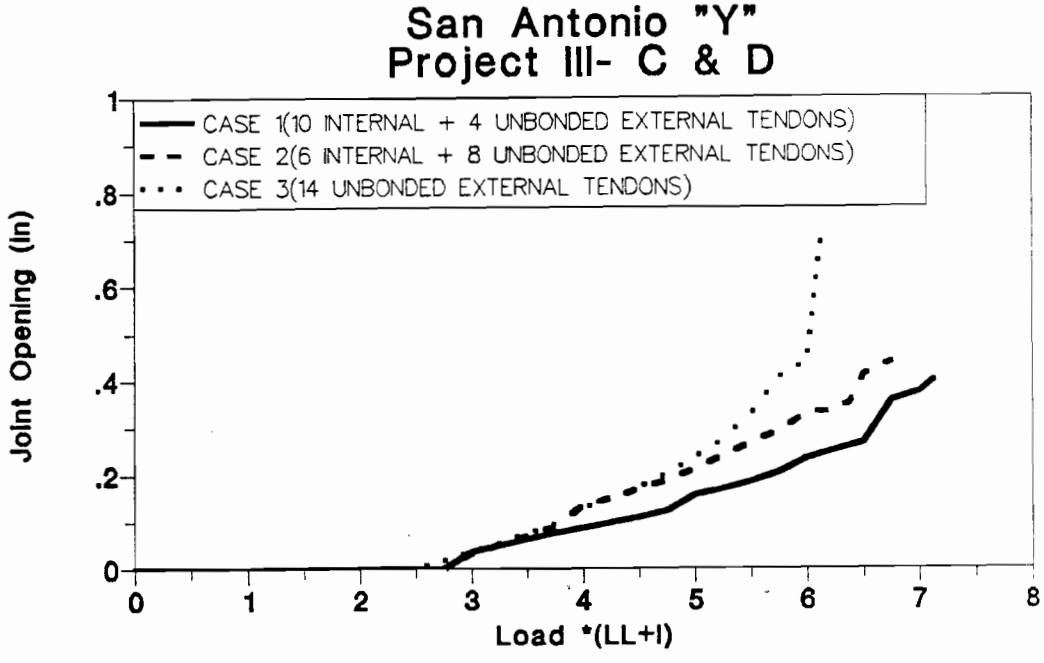

Figure 7.19 Joint opening (effect of internal tendons - unbonded external tendons).

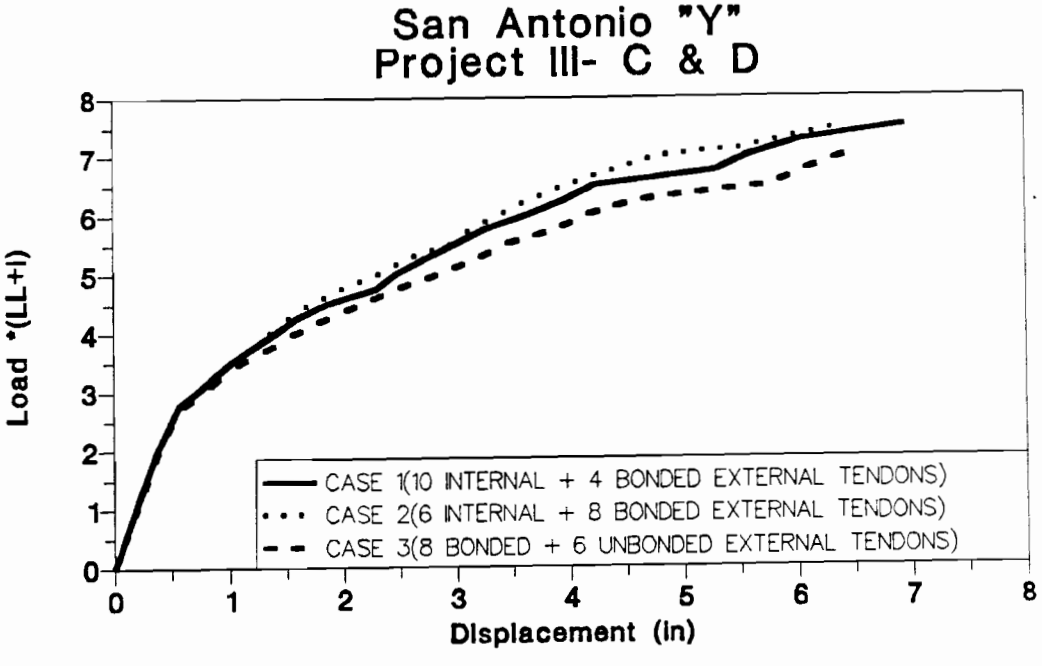

Figure 7.20 Load-displacement (effect of internal tendons - bonded external tendons).

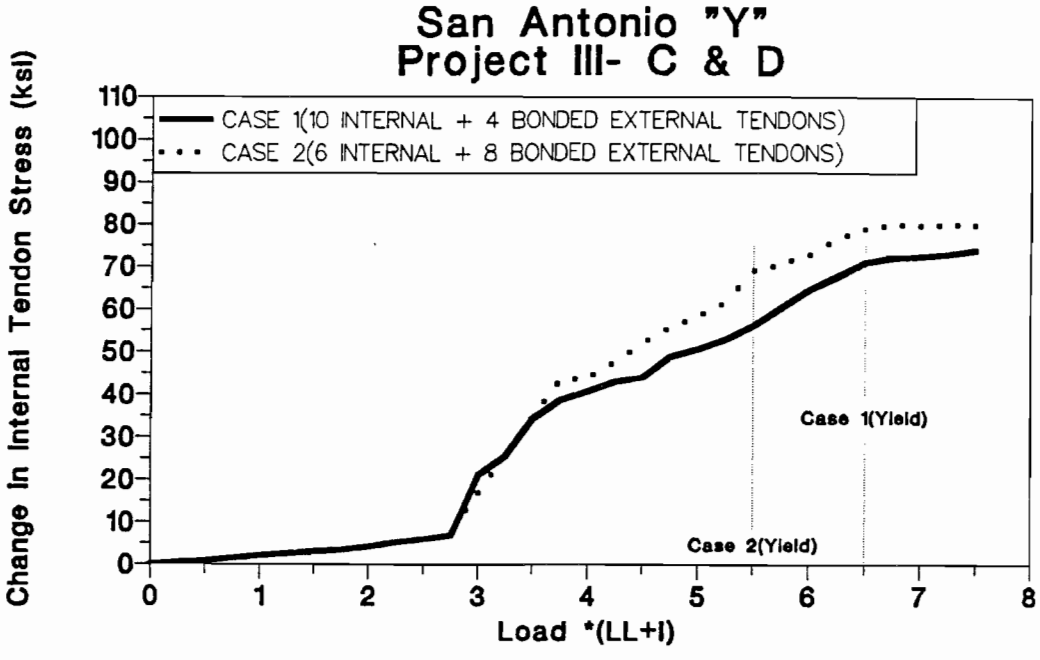

Figure 7.21 Internal tendon stress (effect of internal tendons - bonded external tendons).

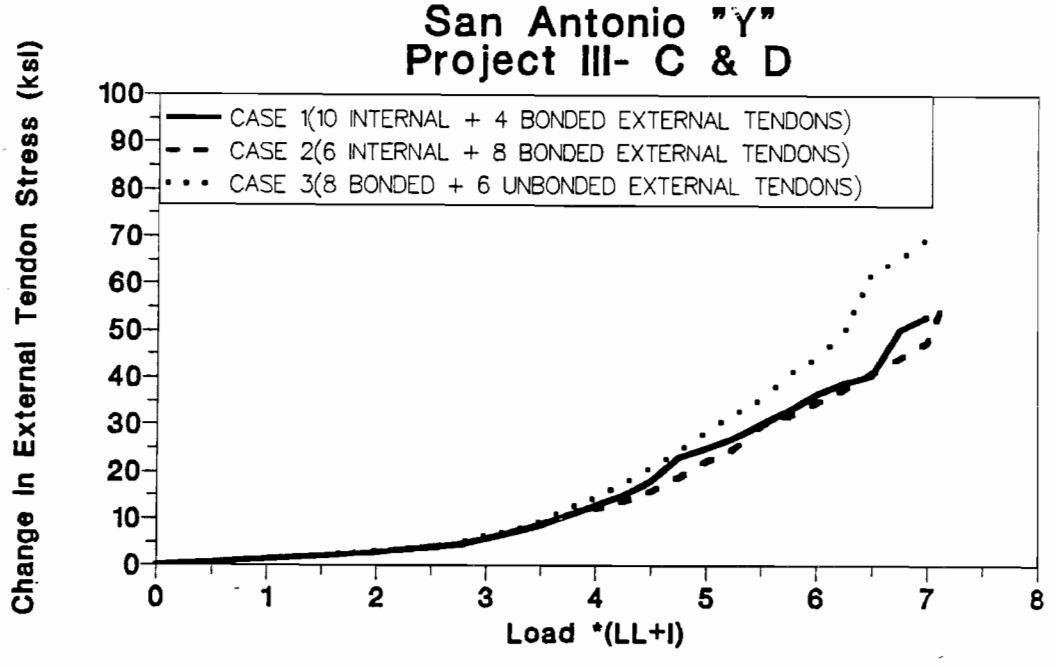

Figure 7.22 External tendon stress (effect of internal tendons - bonded external tendons).

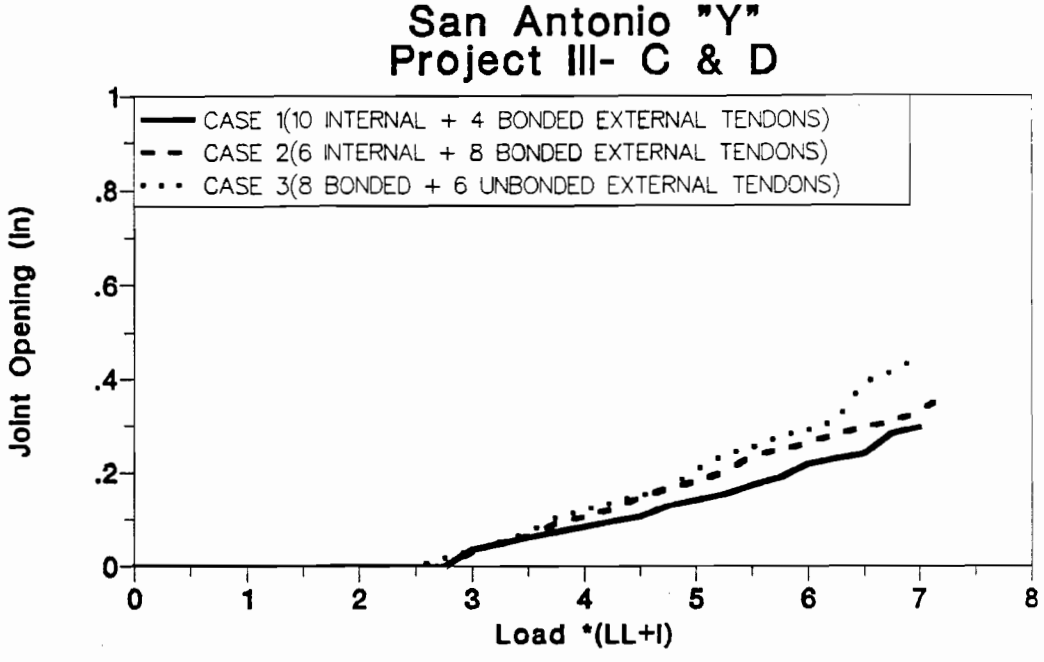

Figure 7.23 Joint opening (effect of internal tendons - bonded external tendons).

7.3.3 Summary. Table 7.11 shows the difference in response of cases one and two with respect to case three. Using grouted internal tendons increased the ultimate live load capacity and ductility. Using 31 percent (case two) of the total prestress area as grouted internal tendons with the remainder as unbonded external tendons was not enough to substantially increase the strength and ductility. However, using 66 percent (case one) of the prestress as internal tendons increased the ductility substantially. The effect of using grouted internal tendons with discretely bonded external tendons was less than in the cases with unbonded external tendons because the response was already greatly improved by discrete bonding of the external tendons.

7.4 Assumed Maximum Strain of Concrete

The maximum strain of the concrete at the joints can be increased by better confinement of the flanges. As discussed in Chapter Four, confinement can be improved by increasing the flange thickness or reducing the shear span (12). It is also believed that the use of epoxy joints leads to improved stress distribution at the joints by minimizing local contact stresses at surface irregularities. This seems to effectively increase the compressive strain that can be developed before joint spalling and crushing occur. As discussed in Chapter Four, use of epoxy joints increased the effective volume of the highly compressed region at the joint as evidenced by to the different lateral cracking pattern that formed in connection with the epoxy joints as compared to that with the dry joints. The effect of joint type is included in the method suggested by the author to calculate the maximum joint

opening by increasing the effective volume of the highly compressed region in the joint (see Chapter Four) and not by increasing the maximum concrete strain. In the Program Bridge, no special treatment was included for the different joint types and the effect of epoxy joints can be included by increasing the maximum concrete strain. Three analyses with different maximum compressive strain levels were carried out for the prototype structure. The three analyses were carried out for case one which was assumed to have 10 internal tendons and 4 discretely bonded external tendons. In the first analysis, the maximum concrete strain was assumed at an upper bound level of 0.006 which is very high and would be difficult to obtain. In the second analysis, the maximum concrete strain was assumed to be 0.004 which can probably be obtained by increasing the flange thickness or by using epoxy joints, while in the third analysis, the maximum concrete strain was assumed at the conventional code lower bound limit of 0.003. Figures 7.24 through 7.26 show the calculated response of the structure to loads for the three analyses.

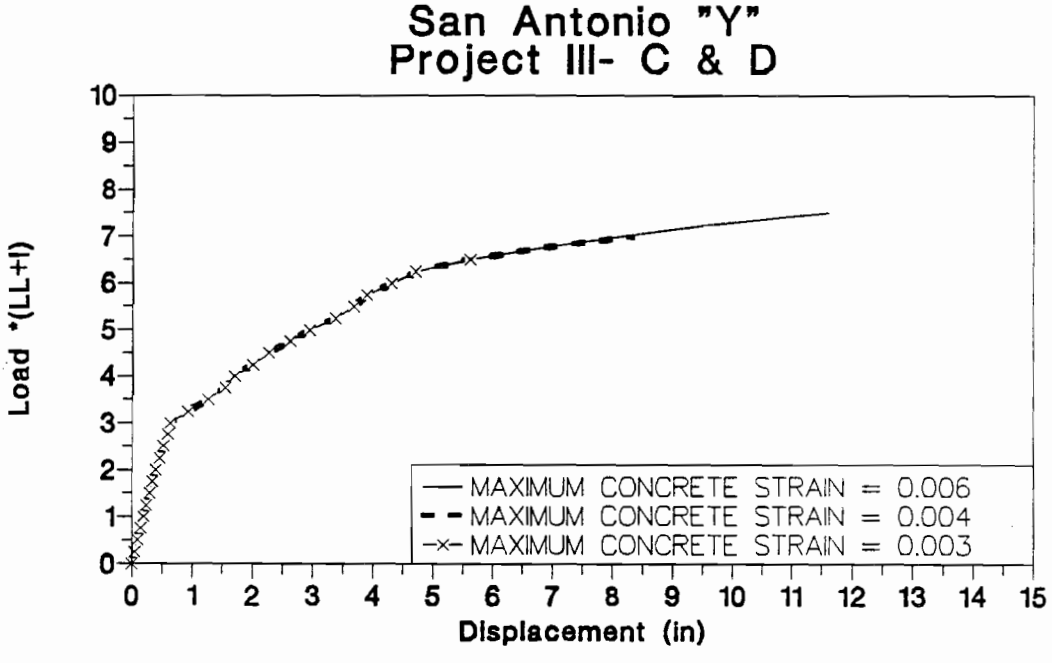

Figure 7.24 Load-displacement (maximum concrete strain).

Table 7.12 compares the ultimate live load capacity, ductility, external tendon stress increase, and joint opening for two cases where the maximum concrete strains are assumed to be 0.004 and 0.006 with the case where the maximum concrete strain is taken as 0.003. The ultimate live load capacity of the structure, when the maximum concrete strain is 0.006, is 15 percent higher than when the maximum strain is 0.003 as shown in Fig 7.24. The ultimate live load displacement increases by 100 percent if the maximum concrete strain increases from 0.003 to 0.006. This makes a great deal of sense since the deflection is proportional to the maximum curvature attainable which is essentially governed by the compressive strains attainable at the opening joints. The maximum change in external

Table 7.12 Concrete Strain Effects Increase Maximum Concrete Strain to Over 0.003

Assumed Maximum Concrete Strain	Ultimate Live Load Capacity	Ultimate Live Load Displacement	External Tendon Stress	Critical Joint Opening
0.006	+15%	+100%	+30 ksi	+100%
0.004	+8%	+42%	+10 ksi	+50%

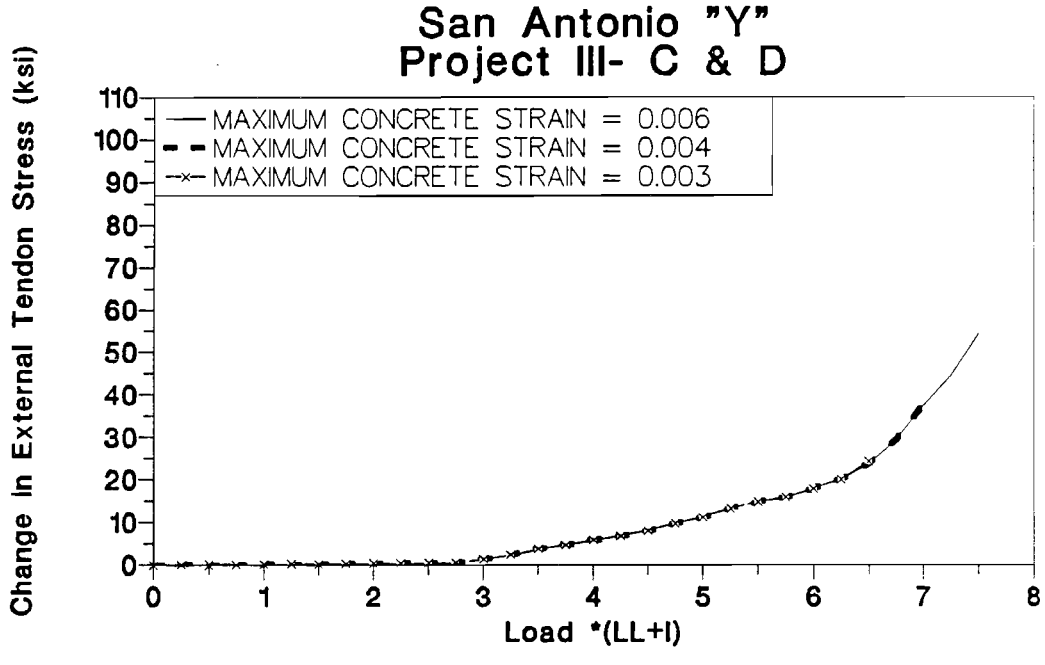

Figure 7.25 External tendon stress (maximum concrete strain).

tendon stress is increased by 30 ksi when the maximum concrete strain limit is increased from 0.003 to 0.006 as shown in Fig 7.25. The maximum joint opening is increased by 100 percent when the maximum concrete strain limit is increased from 0.003 to 0.006 as shown in Fig 7.26.

It should be possible to increase the maximum concrete strain limit from 0.003 to 0.004 by increasing the flange thickness or by reducing the shear span. This increase in concrete strain increased the live load capacity by 8 percent and increased the ultimate live load displacement by 42 percent. The corresponding increase in the maximum joint opening and external tendon stress were 50 percent and 10 ksi.

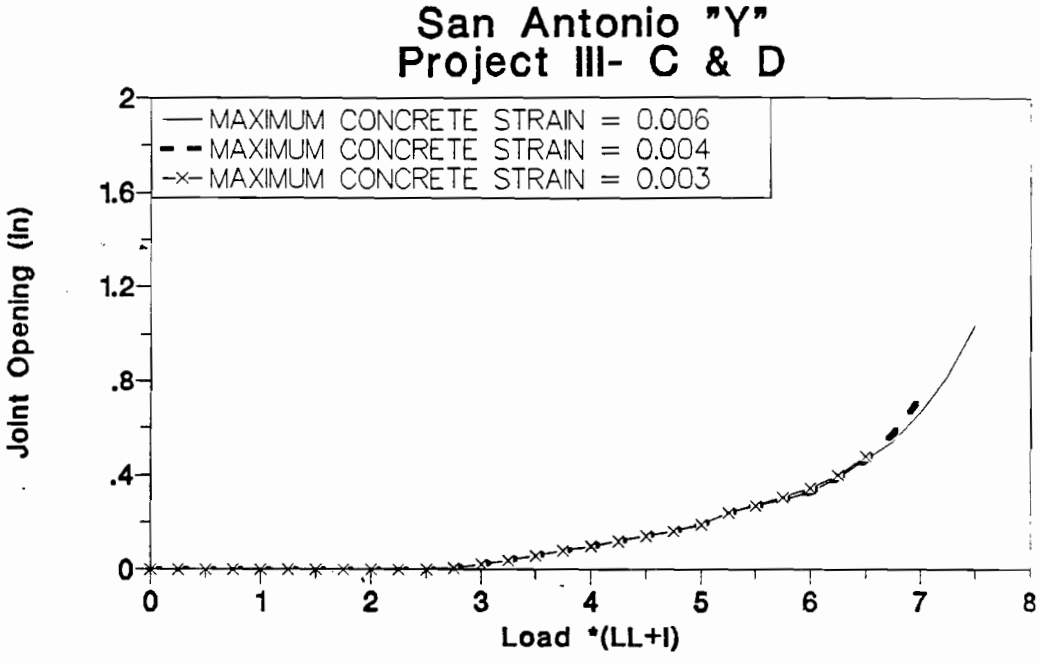

Figure 7.26 Joint opening (maximum concrete strain).

7.5 Incremental Bonding of External Tendons

Incremental bonding of external tendons was studied for case three (100 percent external tendons) of Section 7.2. Three analyses were carried out on the prototype model to see the effect of the degree of incremental bonding on the flexural behavior of the bridge. The six straight tendons in the top and bottom flanges were assumed as ungrouted in their ducts and ,thus, they behave essentially as unbonded tendons. These six tendons were assumed to be unbonded in all three analyses. The remaining eight draped external tendons made up about 69 percent of the total prestress. In the first analysis, the eight draped external tendons were assumed to be discretely bonded to a fictitious diaphragm in all segments as shown in Fig. 7.27(b). In the second analysis, the eight tendons were assumed to be discretely bonded to the pier segments and at two deviation locations in each span as shown in Fig. 7.27(a). In the third analysis, the eight external tendons were assumed to be unbonded tendons except at the pier segments. In all three analyses, the tendons were assumed to have friction at the deviation locations shown in Fig. 7.27(a).

Figures 7.28 through 7.31 show the calculated response of the structure to the loads for the three analyses. Figure 7.28 shows the load-deflection behavior, while Fig. 7.29 shows the change in external tendon stress with load. Figure 7.30 shows the critical joint opening response versus load. The critical joint for the three analyses was joint(4,5). Figure 7.31 shows the adjacent joint(5,6) opening as a function of the load. In the second and third analyses, the external tendons were unbonded at segment 5 (between the critical joint and the adjacent joint) as shown in Fig. 7.27(a). Table 7.13 shows the increase in strength,

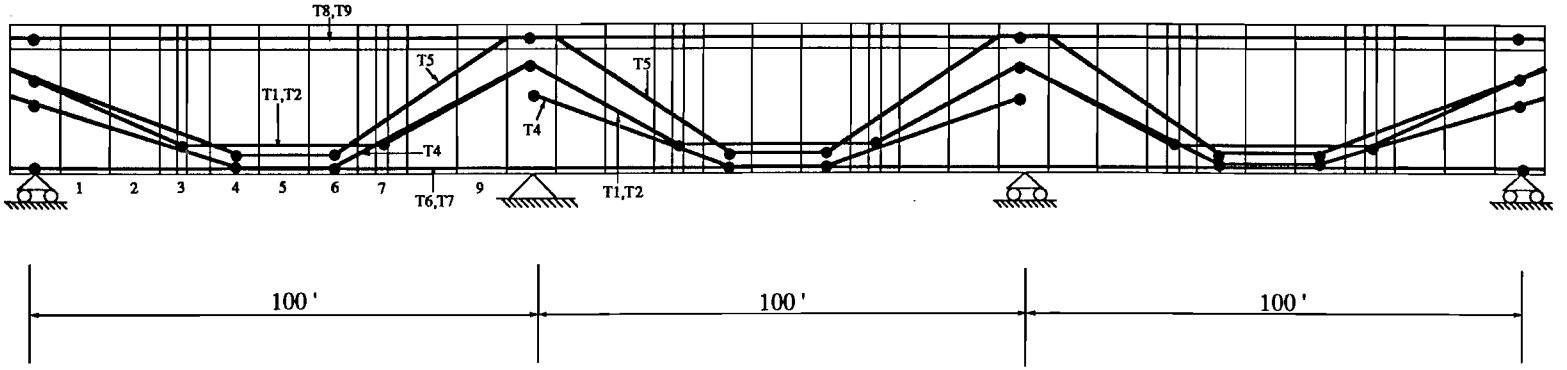

a) External Tendons Bonded at Two Intermediate Diaphragms in each Span

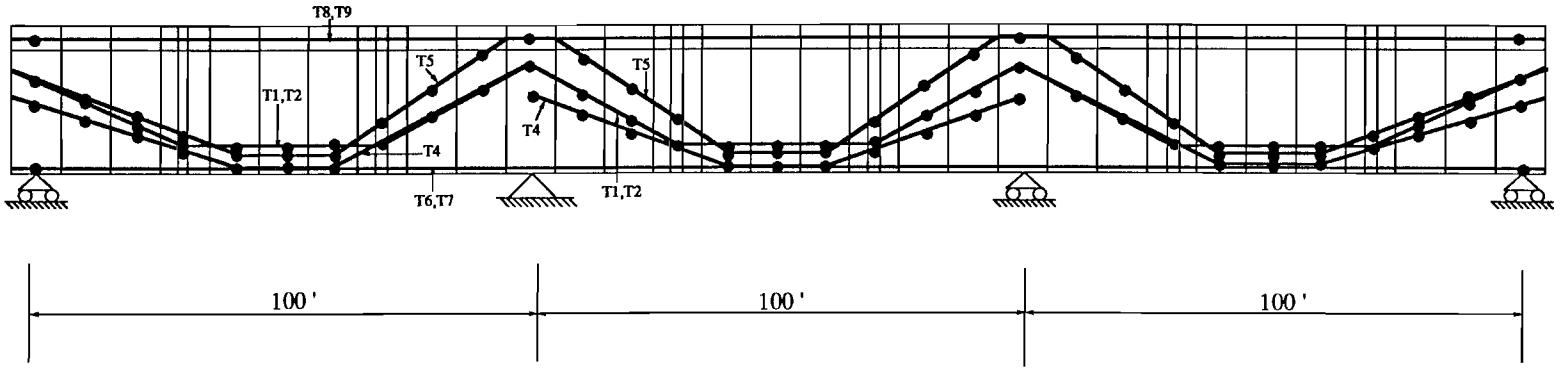

b) External Tendons Bonded at All Intermediate Diaphragms

• : Bonded Location

Figure 7.27 Bonding locations.

displacement, and external tendon stress for the first (all diaphragms bonded) and second (two diaphragms bonded) analyses with respect to the third analysis (unbonded).

Figure 7.28 and Table 7.13 show that strength and ductility were increased by increasing the number of diaphragms at which the external tendons were discretely bonded. The strength and ductility for the first analysis (all diaphragms bonded) were increased by 28 and 48 percent respectively. However, strength and ductility were increased by 16 and 35 percent for the second analysis (two diaphragms bonded). Thus, the substantial additional tendon bonding associated with the first analysis had only a relatively small effect on increasing ductility over what is gained by bonding at few deviators in the second analysis. The change in external tendon stresses was increased with the number of bonded locations as shown in Fig. 7.29 and Table 7.13. Critical joint opening reduced with the number of bonded diaphragms as shown in Fig. 7.30. Figure 7.31 shows the opening of the adjacent joint(5,6). There was no bonded diaphragm between the critical joint and the adjacent joint in the second (two bonded diaphragms in each span) and the third (unbonded external tendon) analyses. In the second and third analyses, the adjacent joint opened and the external tendon stress increased over the critical joint and the adjacent joint by the same amount. This forced the adjacent joint to reduce its opening. In the first analysis with tendons bonded discretely to all diaphragms, the adjacent joint continued opening until failure of the critical joint.

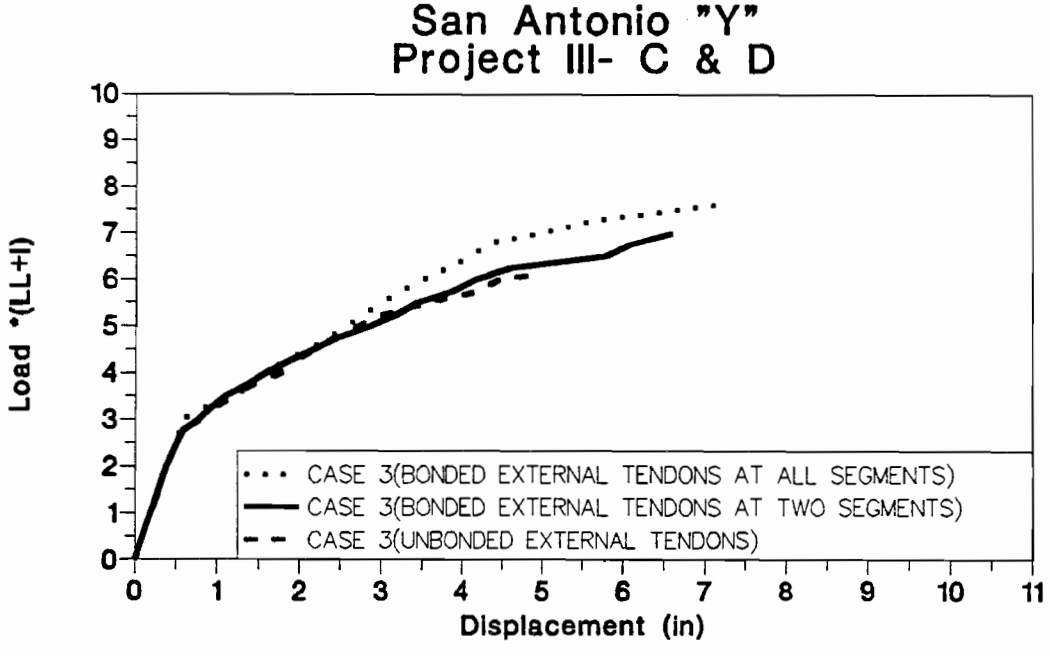

Figure 7.28 Load-deflection (incremental bonding effects).

Table 7.13 Incremental Bonding Effects

Diaphragms Bonded in each Span	Ultimate Live Load Capacity	Ultimate Live Load Displacement	External Tendon Stress
Two bonded	+16%	+35%	+43 ksi
All Bonded	+28%	+48%	+60* ksi
* Tendons were yielded			

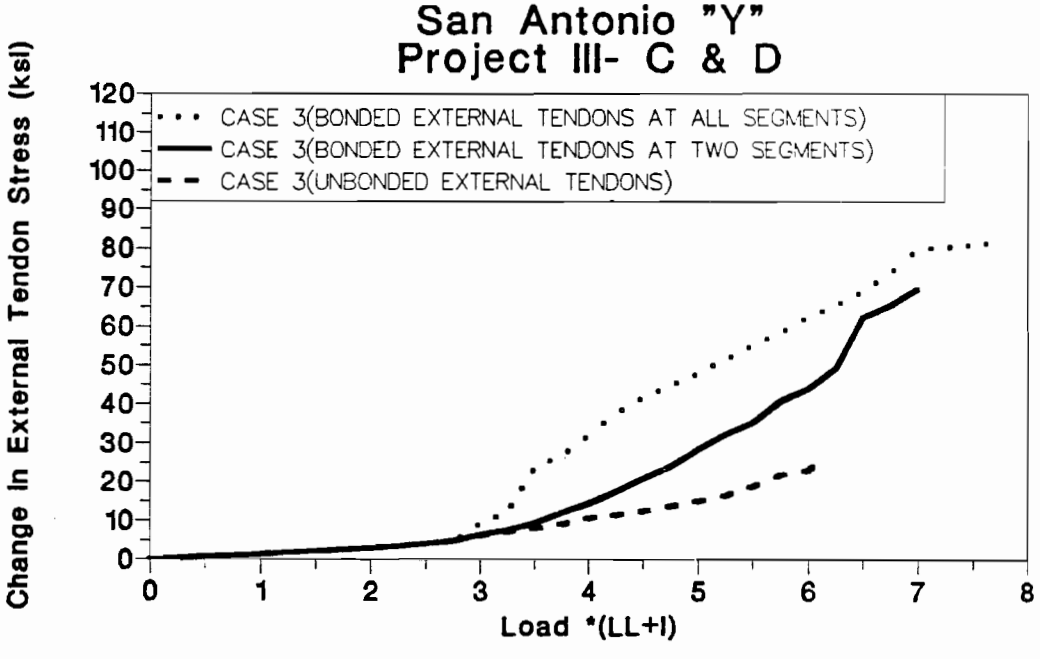

Figure 7.29 External tendon stress (incremental bonding effects).

The adjacent joint opening increased in the first analysis due to different tendon stress at the critical joint and at the adjacent joint. Lower tendon stress at the adjacent joint reduced the moment required to increase the adjacent joint opening. At the same time, bonding at diaphragms reduced the unbonded length of the tendons. Discrete bonding increased the critical joint stiffness and strength. Higher critical joint stiffness attracted higher external moment to the critical region and forced the adjacent joints to open widely. Higher strength delays failure of the critical joint and results in a larger loading range to increase the adjacent joint openings. These reasons increased the adjacent joint openings and resulted in higher total joint opening in the critical region. Higher total joint opening increased the change in tendon length. Higher change in tendon length over a shorter

unbonded length (due to discrete bonding) resulted in higher tendon stress. Higher tendon stress at the critical joint increased the structure strength. Higher total joint opening increased the ultimate displacement.

The main effects of discrete bonding are that discrete bonding creates a different external tendon stress at the critical joint than at the adjacent joints and reduces the unbonded tendon length. For higher strength and ductility, the external tendons should be discretely bonded to the diaphragms at the two sides of the critical joint because this bonding reduces the unbonded tendon length to its minimum and increases the difference in tendon stresses between the critical joint and the adjacent joints to its maximum.

If external tendons are discretely bonded to a diaphragm in each segment, it will maximize the strength and ductility of all joints of the bridge. However, if only two diaphragms or deviator blocks are used in each span to deviate the external tendons and if tendons are to be discretely bonded only at these deviators, the location of these two diaphragms should be selected to be close to the most critical joints (joints which control the design) in that span. Due to the nature of the loads (moving loads) on the bridge, each joint of the span is critical under certain load positions. Thus it is safer to take all the joints as critical joints and to place the two diaphragms at the third points of the span. In this case, the three segments of the external tendons have approximately the same unbonded effective length.

7.6 Fretting Fatigue

The three factors which must be present for fretting fatigue to occur are high lateral bearing pressure between the materials in contact, shear stresses, and slip movement between the two surfaces. An external tendon deviated at a diaphragm has high bearing pressure as a result of the deviation angle. Shear stresses can be created by the difference in external tendon forces at the two ends of the diaphragm due to friction between the tendon and the grout or the duct. Slip was not apparent in the tests at the design live load plus impact load level. The program analysis results show that small slip can occur at the design live load plus impact load level. The bond-slip relationship for external tendons obtained by Radloff (10) from tests conducted as part of this study and used in the computer program shows that no bond stress can be developed at the diaphragm unless small slip takes place. At deviators with a small deviation angle (small friction forces), the program results indicated a small slip at the design live load level. Fretting fatigue would be aggravated by slip at the deviators. A more comprehensive study is needed to assess the effect of fretting fatigue of external tendons.

7.7 Recommendations

7.7.1 Percentage of Grouted Internal or Bonded External Tendons. Using grouted internal tendons or discretely bonded external tendons improved the strength and ductility of the structure as discussed in Chapter Four and Sections 7.2 and 7.3. These two methods improve the strength and ductility by increasing the number of joints which open during loading of the structure. The author recommends that at least a second joint adjacent to the critical joint should open before the critical joint fails.

A second joint opens when the external moment applied at the joint section adjacent to the critical joint is higher than the moment required to open that joint. The adjacent joint opens when the external moment is higher than the cracking moment (for an epoxy joint) or joint opening moment (for a dry joint). The way to achieve this is to increase the applied moment on the adjacent joint by increasing the ultimate moment capacity of the critical joint and/or reducing the moment required to open the adjacent joint.

Using grouted internal tendons and/or discretely bonded external tendons helps in these two objectives as discussed in Chapter Four. Using grouted internal tendons and/or discretely bonded external tendons increases the stiffness of the opened joint which attracts higher external moments in that region. It increases the critical joint capacity due to the higher tendon stress which can be developed due to bonding of the tendon. This delays crushing of the critical joint. By bonding the external tendons to the diaphragm between the critical joint and the second opening joint, a difference in external tendon stress is created between these two joints. This causes a lower external tendon stress at the adjacent joint and reduces the moment required to open that joint. In the same way, using grouted internal tendons increases the critical joint stiffness and reduces the tendon stress at the adjacent joint. In order to check if this second joint will open, a relatively simple calculation procedure is possible. The basic procedure is to calculate the moment at the adjacent joint when the critical joint is close to its ultimate capacity. This moment should be higher than the moment required to open a dry joint or crack an epoxy joint. The second joint opens when the external moment is higher than the cracking moment in an epoxy joint or higher than the joint opening moment in a dry joint. In this section, a calculation procedure will be presented for dry joints. A similar procedure could be developed for epoxy joints by considering the extra cracking moment capacity of such joints.

The procedure for calculating the required percentage of grouted internal tendons or discretely bonded external tendons to ensure that a second dry joint would open is shown in Fig 7.32, 7.33, and 7.34. In this procedure, a single concentrated load is assumed to simplify the calculation procedure and to take into consideration the worst loading condition. The dead load moment diagram is assumed to have the same shape as the diagram for the concentrated load in order to simplify the calculations and to conservatively predict the required percentage of discretely bonded external tendons or grouted internal tendons. The procedure is based on the assumption that a second joint will open as soon as the internal tendons yield at the critical joint or when the discretely bonded external

tendon stress change is the calculated (calculated by the procedure presented in this chapter) ultimate change in external tendon stress. The second joint should open before the structure fails so that it has a chance to open widely before the critical joint fails. Strain hardening of the internal tendons at the critical joint increases the critical joint strength and causes the adjacent joint to open widely before the structure fails. The ultimate change in stress calculated by the procedure presented in this chapter is conservative. The actual change in tendon stress in the structure would be higher (as discussed in this chapter) which causes the adjacent joint to open widely before the structure fails.

Figure 7.32 shows the notation for the variables used. Figure 7.33(a) shows the derivation of the procedure for an exterior span, while Fig. 7.33(b) shows the equations for the required percentage for three different tendon combination cases in a dry joints span. Figure 7.34(a) shows the derivation for interior spans and Fig 7.34(b) shows the equations for three different tendon combination cases in a dry joints span.

The first case discussed is when internal tendons are used with unbonded external tendons. In this case the joint adjacent to the critical joint opens as a second joint (n=1). The second case is when internal tendons are used with discretely bonded external tendons. In this case, the joint adjacent to the critical joint opens as a second joint (n=1). The third case is when discretely bonded external tendons are used with unbonded external tendons. The joint which is separated from the critical joint by a diaphragm discretely bonded to the external tendons is the next joint to open after the critical joint and (n) will be the number of segments between the two joints. In this procedure the unbonded external tendons are assumed to have the same stress at all joints. Any external tendon with a different stress at the critical joint from that in the next joint due to bond and/or friction is assumed to be a discretely bonded external tendon. The ultimate change in external tendon stress is obtained from the calculation procedures discussed in this chapter. The internal tendon stress in the adjacent joint is assumed to be the effective prestress when the internal tendons yield at the critical joint.

Figures 7.30 and 7.31 show the simplified equations for case one and three for exterior and interior dry joint spans respectively. The most influential factor is the ratio of segment length to span length (S/L). As (S/L) increases the percentage of internal tendons required to open a second joint also increases.

As an example, this procedure was used to calculate the percentage of internal tendons required to ensure opening of an adjacent joint prior to failure.

$$R_i = \frac{4.6 * \frac{S}{L}}{\left(1 - 2.5 * \frac{S}{L}\right)}$$

(From Fig. 7.30)

$\frac{S}{L} = 0.1$ (10 segments in each span)

$R_i \geq 0.61$

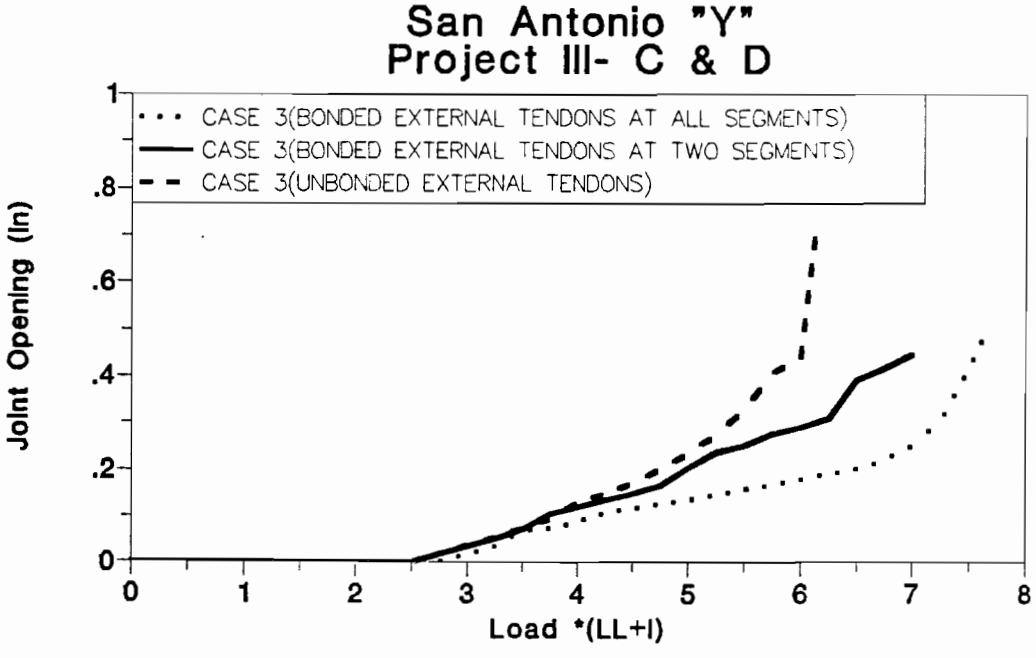

Figure 7.30 Joint opening (incremental bonding effects).

The predicted percentage of internal tendons required to ensure adjacent joint opening for case one (with unbonded external tendons) of the analysis carried out for the San Antonio 'Y' project was 61 percent. Thus, the calculation says that 61 percent of the positive moment prestress should be provided as grouted internal tendons. Table 7.14 shows that case one of the Section 7.3.1 example has 62 percent of its positive moment prestress as grouted internal tendons while case two and three have less internal tendons than what this calculation procedure suggests. Figure 7.16 and Table 7.11 show that the ultimate live load capacity of case one was 19 percent higher than case three while the case one ultimate live load displacement was 50 percent higher than case three. Case one had the highest strength and ductility of the three cases. Clearly the percentage of internal tendons calculated by this suggested procedure is adequate.

The second example for this calculation procedure is the case three analysis with bonded external tendons of Section 7.3.2 which showed good strength and ductility as compared to the other two cases as shown in Fig 7.20. The calculation procedure predicted that having 75 percent of the tendons being discretely bonded external tendons should be enough to substantially increase the strength and ductility. The actual percentage of discretely bonded external tendons used in the analysis for case three of Section 7.3.2 was 76 percent. Again, very good agreement is shown.

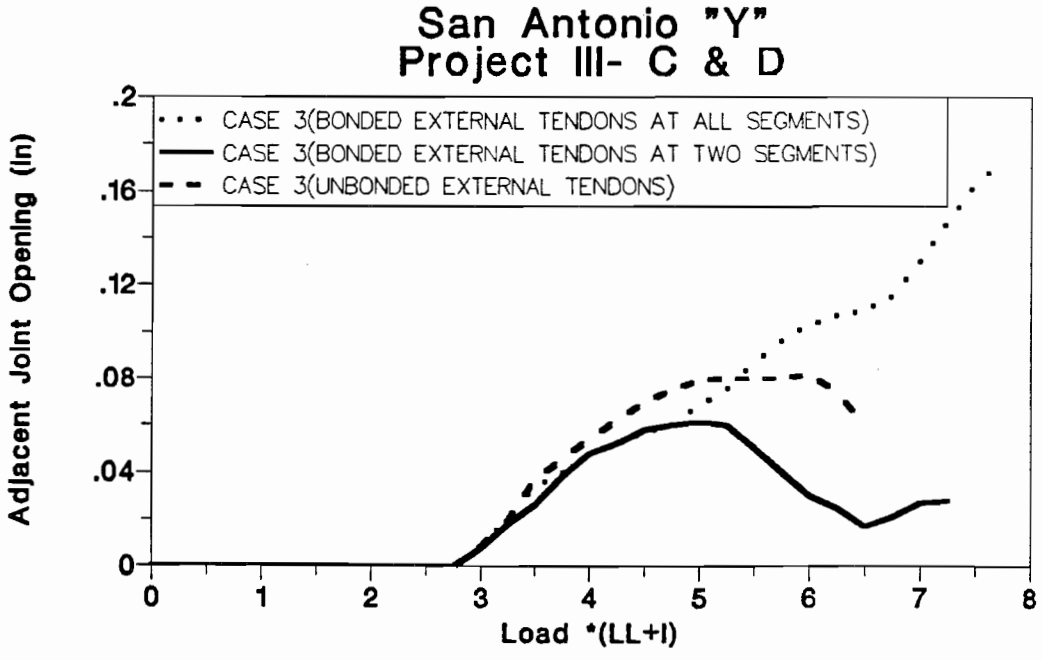

Figure 7.31 Adjacent joint opening (incremental bonding effects).

Table 7.14 Percentage of Internal Tendons

Case	% of Positive Prestress Steel Area as Grouted Internal Tendons
1	62
2	24
3	0

The calculation procedure was also applied for the flexural tests carried out in the dry joints span in the first and second part of this study. In these tests, only discretely bonded external tendons were used (see Chapter Three and Four). In the initial tests performed by MacGregor(1), all (100%) external tendons were bonded to a maximum of four deviators in each span. Four tendons were bonded to the pier segments and to four interior diaphragms, while two tendons were bonded to the pier segments and to two interior diaphragms in each span as shown in Figure 4.16. In this case n=2. The calculation procedure indicated that 170 percent of the external tendons should be bonded. This is not physically possible. During these initial tests, the joint rotation was concentrated in the critical joint and the structure failed prematurely with a relatively small displacement (See Chapter Four). A second joint opened in these tests but its opening remained small until the end of the test. The second joint opened in these tests due to higher dead load moment on the second joint than that on the critical joint. This caused the second joint to open but it did not open widely as indicated by the calculation procedure that no second joint will open widely. The current tests were carried out when all (100%) external tendons were bonded to all ten diaphragms as shown in Figure

F_{su} : Stress of unbonded external tendon when new joint opens
F_{sbc} : Stress of bonded external tendon at critical joint when new joint opens
F_{sbn} : Stress of bonded external tendon at new joint
F_{sic} : Stress of tendon at critical joint when new joint opens
F_{sin} : Stress of internal tendon at new joint
A_b : Area of bonded external tendon
A_i : Area of internal tendon
A_u : Area of unbonded external tendon
D_{euc} : Effective depth of unbonded external tendons at critical joint
D_{eun} : Effective depth of unbonded external tendons at new joint
D_{ebc} : Effective depth of bonded external tendons at critical joint
D_{ebn} : Effective depth of bonded external tendons at new joint
D_{eic} : Effective depth of internal tendons at critical joint
D_{ein} : Effective depth of internal tendons at new joint
M_c : Moment at critical joint when new joint opens
M_a : Moment required to open the new joint

R_b : Ratio of bonded external tendons = $\dfrac{A_b}{A_i + A_b + A_u}$

R_u : Ratio of unbonded external tendons = $\dfrac{A_u}{A_i + A_b + A_u}$

R_i : Ratio of internal tendons = $\dfrac{A_i}{A_i + A_b + A_u}$

L_1 : Length to the critical joint
L : Span length
S : Length of segment
n : Number of segments to where the new joint is to be opened.

Figure 7.32 Notation

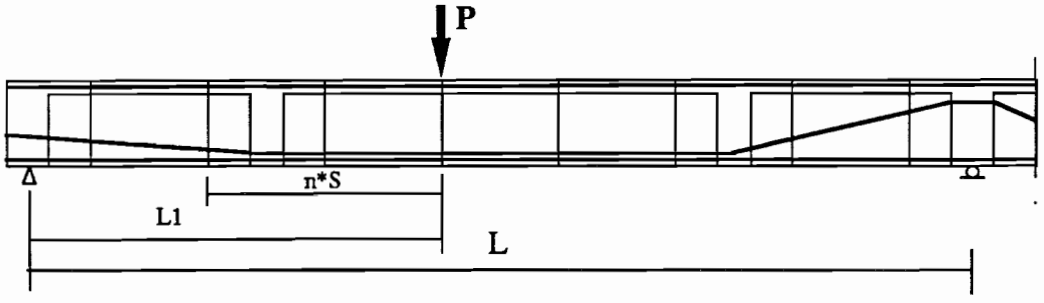

Exterior Span Elevation

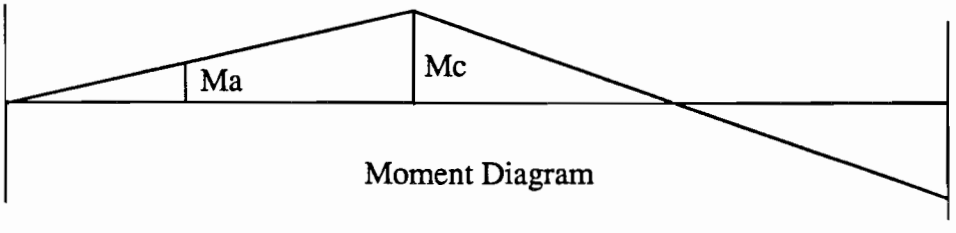

Moment Diagram

As the joint opens, the compressive force concentrates in the top fiber of the top flange, then:

$$M_c = F_{sic}*A_i*D_{eic} + F_{sbc}*A_b*D_{ebc} + F_{su}*A_u*D_{euc}$$

$$M_a = F_{sia}*A_i*D_{eia} + F_{sba}*A_b*D_{eba} + F_{su}*A_u*D_{eua}$$

Assume that at least one adjacent joint opens in addition to the critical joint to improve ductility and strength

$$M_c * \frac{L_1 - n*S}{L_1} \geq M_a \qquad (1)$$

$$(F_{sic}*A_i*D_{eic} + F_{sbc}*A_b*D_{ebc} + F_{su}*A_u*D_{euc}) * \frac{L_1 - n*S}{L_1} \geq (F_{sia}*A_i*D_{eia} + F_{sba}*A_b*D_{eba} + F_{su}*A_u*D_{eua})$$

Dividing by total area of tendons, gives:

$$(F_{sic}*R_i*D_{eic} + F_{sbc}*R_b*D_{ebc} + F_{su}*R_u*D_{euc}) * \frac{L_1 - n*S}{L_1} \geq (F_{sia}*R_i*D_{eia} + F_{sba}*R_b*D_{eba} + F_{su}*R_u*D_{eua}) \qquad (2)$$

$$R_i + R_b + R_u = 1 \qquad (3)$$

Figure 7.33 Exterior span tendon ratios.

Case 1

Internal tendon with unbonded external tendon

$R_b = 0 \qquad n=1$

$$(F_{sic}*R_i*D_{eic} + F_{su}*(1-R_i)*D_{euc})*\frac{L_1 - S}{L_1} \geq (F_{sia}*R_i*D_{eia} + F_{su}*(1-R_i)*D_{eua})$$

$$R_i \geq \frac{(D_{eua}*F_{su} - D_{euc}*F_{su}*(1-\frac{S}{L_1}))}{((D_{eic}*F_{sic} - D_{euc}*F_{su})*(1-\frac{S}{L_1}) - D_{eia}*F_{sia} + D_{euc}*F_{su})}$$

Case 2

Internal tendon with bonded external tendon

$R_u = 0 \qquad n=1$

$$(F_{sic}*R_i*D_{eic} + F_{sbc}*(1-R_i)*D_{ebc})*\frac{L_1 - S}{L_1} \geq (F_{sia}*R_i*D_{eia} + F_{sba}*(1-R_i)*D_{eba})$$

$$R_i \geq \frac{(D_{eba}*F_{sba} - D_{ebc}*F_{sbc}*(1-\frac{S}{L_1}))}{((D_{eic}*F_{sic} - D_{ebc}*F_{sbc})*(1-\frac{S}{L_1}) - D_{eia}*F_{sia} + D_{ebc}*F_{sbc})}$$

Case 3

Bonded external tendon with unbonded external tendon

$R_i = 0$

$$(F_{sbc}*R_b*D_{ebc} + F_{su}*(1-R_b)*D_{euc})*\frac{L_1 - n*S}{L_1} \geq (F_{sba}*R_b*D_{eba} + F_{su}*(1-R_b)*D_{eua})$$

$$R_b \geq \frac{(D_{eua}*F_{su} - D_{euc}*F_{su}*(1-\frac{n*S}{L_1}))}{((D_{ebc}*F_{sbc} - D_{euc}*F_{su})*(1-\frac{n*S}{L_1}) - D_{eba}*F_{sba} + D_{euc}*F_{su})}$$

b) Cases

Figure 7.33 Exterior span tendon ratios (continued).

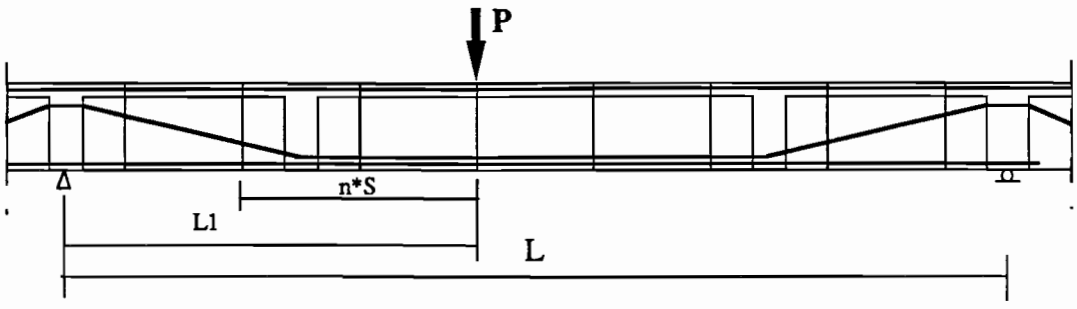

Interior Span Elevation

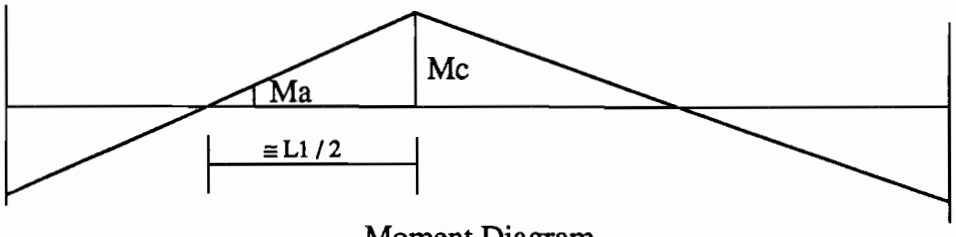

Moment Diagram

As the joint opens, the compressive force concentrates in the top fiber of the top flange, then:

$$M_c = F_{sic}*A_i*D_{eic} + F_{sbc}*A_b*D_{ebc} + F_{su}*A_u*D_{euc}$$

$$M_a = F_{sia}*A_i*D_{eia} + F_{sba}*A_b*D_{eba} + F_{su}*A_u*D_{eua}$$

Assume that at least one adjacent joint opens in addition to the critical joint to improve ductility and strength

$$M_c * \frac{0.5*L_1 - n*S}{0.5*L_1} \geq M_a \qquad (1)$$

$$(F_{sic}*A_i*D_{eic} + F_{sbc}*A_b*D_{ebc} + F_{su}*A_u*D_{euc}) * \frac{0.5*L_1 - n*S}{0.5*L_1} \geq (F_{sia}*A_i*D_{eia} + F_{sba}*A_b*D_{eba} + F_{su}*A_u*D_{eua})$$

Dividing by total area of tendons, gives:

$$(F_{sic}*R_i*D_{eic} + F_{sbc}*R_b*D_{ebc} + F_{su}*R_u*D_{euc}) * \frac{0.5*L_1 - n*S}{0.5*L_1} \geq (F_{sia}*R_i*D_{eia} + F_{sba}*R_b*D_{eba} + F_{su}*R_u*D_{eua}) \qquad (2)$$

$$R_i + R_b + R_u = 1 \qquad (3)$$

Figure 7.34 Interior span tendon ratios.

Case 1

Internal tendon with unbonded external tendon

$R_b = 0 \qquad n=1$

$$(F_{sic}*R_i*D_{eic} + F_{su}*(1-R_i)*D_{euc})*\frac{0.5*L_1 - S}{0.5*L_1} \geq (F_{sia}*R_i*D_{eia} + F_{su}*(1-R_i)*D_{eua})$$

$$R_i \geq \frac{(D_{eua}*F_{su} - D_{euc}*F_{su}*(1-\frac{2*S}{L_1}))}{((D_{eic}*F_{sic} - D_{euc}*F_{su})*(1-\frac{2*S}{L_1}) - D_{eia}*F_{sia} + D_{euc}*F_{su})}$$

Case 2

Internal tendon with bonded external tendon

$R_u = 0 \qquad n=1$

$$(F_{sic}*R_i*D_{eic} + F_{sbc}*(1-R_i)*D_{cbc})*\frac{0.5*L_1 - S}{L_1} \geq (F_{sia}*R_i*D_{eia} + F_{sba}*(1-R_i)*D_{eba})$$

$$R_i \geq \frac{(D_{eba}*F_{sba} - D_{ebc}*F_{sbc}*(1-\frac{2*S}{L_1}))}{((D_{eic}*F_{sic} - D_{ebc}*F_{sbc})*(1-\frac{2*S}{L_1}) - D_{eia}*F_{sia} + D_{ebc}*F_{sbc})}$$

Case 3

Bonded external tendon with unbonded external tendon

$R_i = 0$

$$(F_{sbc}*R_b*D_{ebc} + F_{su}*(1-R_b)*D_{euc})*\frac{L_1 - 0.5*n*S}{L_1} \geq (F_{sba}*R_b*D_{eba} + F_{su}*(1-R_b)*D_{eua})$$

$$R_b \geq \frac{(D_{eua}*F_{su} - D_{euc}*F_{su}*(1-\frac{2*n*S}{L_1}))}{((D_{ebc}*F_{sbc} - D_{euc}*F_{su})*(1-\frac{2*n*S}{L_1}) - D_{eba}*F_{sba} + D_{euc}*F_{su})}$$

b) Cases

Figure 7.34 Interior span tendon ratios (continued).

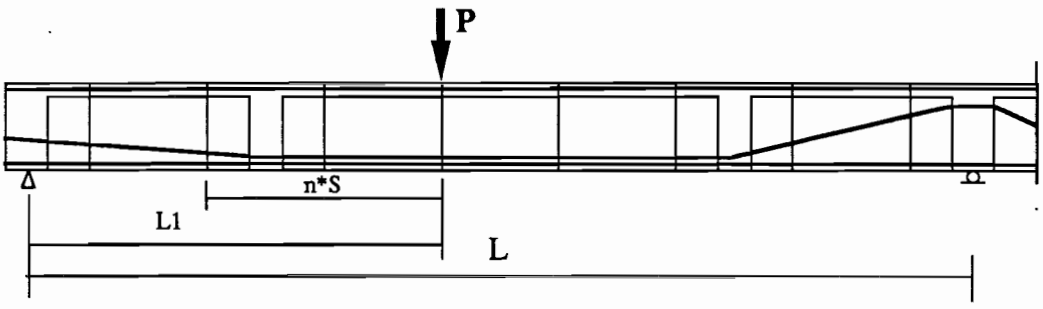

Exterior Span Elevation

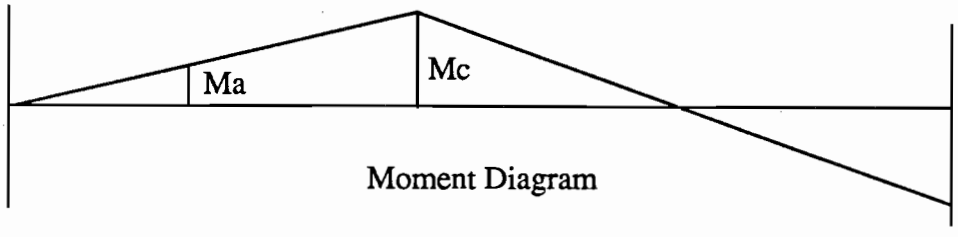

Moment Diagram

To Simplify:

Assume

$D_{eic} = D_{ebc} = D_{euc} = D_{eia} = D_{eba} = D_{eua} = D$

Internal tendon yield at critical joint $(F_{sic} = F^*_y)$

Internal tendon stress at next joint is effective stress $(F_{sia} = 0.65\ F^*_y)$

$L_1 = 0.4 * L$

Case 1 (Internal tendon with unbonded external tendon)

Assume very small change in unbonded external tendon stress $(F_{su} = F_{sia})$

$$R_i \geq \frac{4.6 * \frac{S}{L}}{(1 - 2.5 * \frac{S}{L})}$$

Case 3 (Bonded external tendon with unbonded external tendon)

Assume $F_{sba} = F_{su}$

Find F_{sbc}, F_{su}

$$R_b \geq \frac{(F_{su} * \frac{2.5n * S}{L})}{((F_{sbc} - F_{su}) * (1 - \frac{2.5n * S}{L}))}$$

Figure 7.35 Simplified exterior span tendon ratio (dry joints).

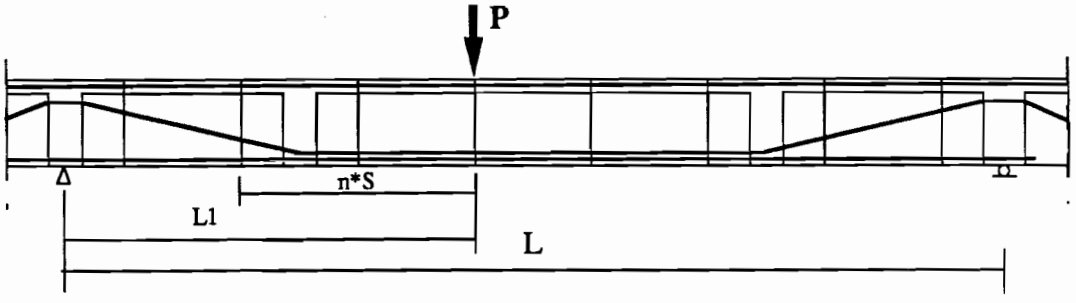

Interior Span Elevation

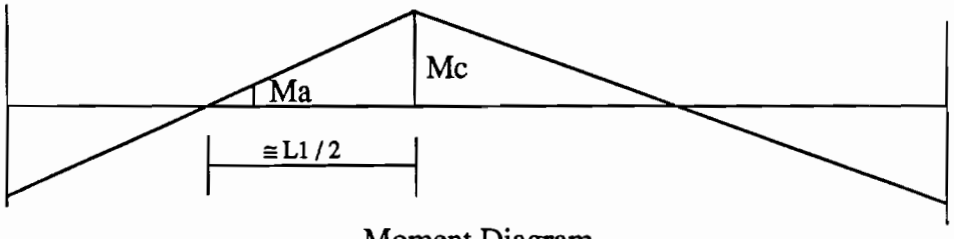

Moment Diagram

To Simplify:

Assume $L_1 = 0.5 * L$

$D_{eic} = D_{ebc} = D_{euc} = D_{eia} = D_{eba} = D_{eua} = D$

Internal tendon yield at critical joint $(F_{sic} = F^*_y)$

Internal tendon stress at next joint is effective stress $(F_{sia} = 0.65\ F^*_y)$

Case 1 (Internal tendon with unbonded external tendon)

Assume very small change in unbonded external tendon stress $(F_{su} = F_{sia})$

$$R_i \geq \frac{7.3 * \frac{S}{L}}{(1 - 4 * \frac{S}{L})}$$

Case 3 (Bonded external tendon with unbonded external tendon)

Assume $F_{sba} = F_{su}$

Find F_{sbc}, F_{su}

$$R_b \geq \frac{(F_{su} * \frac{4n*S}{L})}{((F_{sbc} - F_{su}) * (1 - \frac{4n*S}{L}))}$$

Figure 7.36 Simplified interior span tendon ratio (dry joints).

4.16. In this case n=1. The calculation procedure indicated that 70 percent of the external tendons should be bonded to improve strength and ductility. The indicated theoretical percentage of bonded external tendons (70%) is lower than the percentage of the external tendons actually bonded (100%). The ultimate live load capacity in the latter tests were 23 percent higher than in the initial tests. The ultimate displacement in the latter tests was 47 percent higher than in the initial tests as discussed in Chapter Four (Fig. 4.25). Again, providing a discretely bonded external tendon percentage higher than the suggested procedure indicated percentage gave a substantially higher strength and ductility.

The examples discussed in this section show that the calculation procedure presented in this study correctly indicated the percentage of discretely bonded external tendons or fully grouted internal tendons required to substantially improve strength and ductility.

7.7.2 Maximum Joint Opening. Section 4.6.2 discussed the Author's recommendation for a new method to calculate the maximum allowable joint opening for dry and epoxy joints which is based on the actual behavior of the segments observed during testing (see Chapter Four). This method takes into consideration the difference between the cracking pattern observed around epoxy joints and dry joints. Table 7.15 shows a comparison between the measured joint openings and the openings predicted by the two differing procedures suggested by the author and by Virloguex (13). The ratios of the measured to predicted joint opening were 1.05 to 1.40 and averaged 1.20 for the author's method. They were 1.82 to 2.6 (an average of 2.05 for the Virloguex method. The predictions by the method suggested by the author were much closer to the measured joint opening than were by the Virloguex method. Importantly, they were still conservative.

Table 7.15 Maximum Joint Opening

	Current Test		C.E.B.T.P		Average
Test	Epoxied	Dry	NM3	NM4	
Measured (in)	0.37	0.30	0.33	0.42	
Author (in)	0.35	0.28	0.26	0.29	
	1.05	1.07	1.26	1.40	1.20
Virlogeux (in)	0.14	0.14	0.20	0.23	
	2.60	2.10	1.65	1.82	2.05

7.7.3 Second Order Effect. The second order moment resulting from change in the position of the external tendon with respect to the deformed concrete is significant in beams without intermediate diaphragms as shown in Fig. 5.13. Using intermediate diaphragms reduces the second order moment. In calculating the change in tendon stress or the

ultimate moment capacity of the section, the correct position of the external tendon at the critical joints must be used. Knowing the rotation of the critical joint and the deformed shape of the structure, the position of the external tendon at the critical joint can be calculated from the deformed geometry of the structure. The deformed geometry of the structure can be obtained as discussed in Section 7.6.4.

7.7.4External Tendon Stress. Many methods are currently available to predict the ultimate external tendon stress. Each method calculates the ultimate stress as the sum of the effective prestress plus a predicted change in external tendon stress under load. Several methods are reviewed in the following sections.

7.7.4.1 Author. The author recommends a new method to calculate the change in external tendon stress taking into consideration the bonding condition of the external tendon at intermediate diaphragms. The procedure discussed in Section 4.10 for calculating external tendon stress at ultimate is based on two assumptions. First, the model is based on a rigid body mechanism which means that there is no increase in tendon stress until the joint starts opening. Second, the model assumes that a single joint opens in each hinge region.

An ideal rigid body mechanism can be used by assuming that there is no limit on the rotation capacity of the hinges. In this case, a full plastic mechanism is assumed and a plastic mechanism analysis is conducted to obtain the plastic hinge locations. In actual concrete structures, the maximum rotation is limited by the curvature capacity of the reinforced segment. For that reason, this model represents an upper bound limit to the true strength of the structure.

Instead of allowing unlimited rotation of the plastic hinge, the maximum calculated rotation (which can be calculated from the procedure presented in this chapter) can be used to define the limit for the deflection of the structure. In this case, no hinge is allowed to have a rotation higher than its maximum rotation. In this case, the number of hinges which can reach their ultimate rotation capacity is less than the number of hinges required to form full mechanism (Degree of indeterminacy plus one). For an internal span, the number of degrees of indeterminacy equals two. Therefore, less than three hinges can reach their ultimate rotation. One hinge usually reaches its maximum rotation while the other hinges have lower rotations than their maximum allowable rotation. This theory is called the Lower Bound Theory and represents a lower bound limit to the true strength of the structure. This method will yield a conservative estimate of the ultimate external tendon stress.

In order to comply with the lower bound theory, the maximum allowable rotation is assumed to occur only at the critical joint (joint to be designed). From the geometry of the deflected structure, the rotation at the other hinge locations can be obtained. These hinge rotations must be lower than their maximum allowable rotations. The maximum allowable rotation is calculated in a similar manner to the calculation of the maximum joint opening

as shown in Fig. 7.37. If the rotation of any hinge is higher than its maximum rotation, that hinge will fail before the assumed critical joint.

The change in tendon length can be obtained from the deflected shape of the structure in compliance with the lower bound theory. The change in tendon length is equal to the sum of the joint openings at the level of the tendon in these joints. No change in tendon length is added if the tendon does not pass through the opened joint or if it passes through the compression part of the opened joint.

The assumption of having a single joint open in each critical zone will conservatively estimate the external tendon stress because usually more than one joint opens in each hinge region. The number of opening joints depends on many factors such as the percentage of grouted internal tendons and the bonding condition of the external tendons. The procedure for calculating the change in external tendon stress is as follow:

a) A plastic mechanism analysis is conducted to determine the critical mechanism joint locations.

b) The maximum joint rotations and openings at all hinge locations are calculated as discussed in Section 7.7.2 of this chapter and in Chapter Four.

c) The change in tendon length is calculated from the deflected shape of the structure in compliance with the lower bound theory as discussed above. The change in stress of the external tendon is calculated from the change in tendon length between the bonded diaphragms or anchors.

d) The bond strength at the bonded diaphragms is checked. If the maximum bond strength is exceeded, the change in tendon stress is recalculated taking into consideration the fact that part of the elongation will be distributed over a longer length of the tendon (length between the next diaphragms) as discussed in Chapter Four.

To simplify the procedure for calculating the tendon stress, the equations in Fig 7.38 were derived. In this simplified procedure, the effect of joint type on maximum joint opening is neglected. The bonding condition was neglected by using the full tendon length between anchors instead of the length between the intermediate bonded points.

Two calculations were performed using this method. Results are given in Table 7.16. The first calculation was done using the original method which takes into consideration the bonding condition of the external tendons and the joint type effect. The second calculation, which neglects the bond and joint type effect, is simpler and much easier to use. However, the predicted stresses are more conservative than the first calculation.

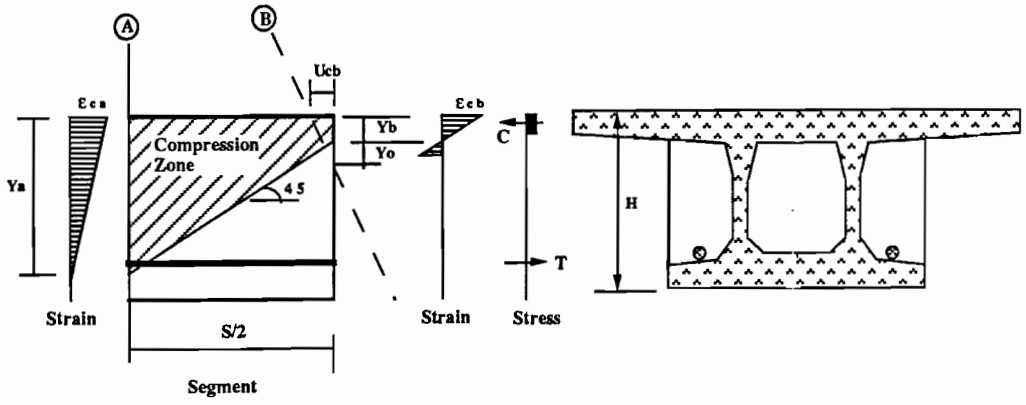

Section A : Segment Section
Section B : Deformed Joint Between Two Segments
S : Segment Length
H : Depth of Cross Section
ε_{cb} : Maximum Concrete Strain at the Joint
ε_{ca} : Top Fiber Concrete Strain at Section A
U_{cb} : Top Fiber Displacement at the Joint
Y_a : Neutral Axis Depth at Section A
Y_b : Neutral Axis Depth at Section B
Y_o : Depth from Neutral Axis to Center of Rotation
T : Tension Force assuming all Tendons Yielded
b_e : Effective Width (calculated according to AASHTO)
L_c : Length of Compression Zone between A @ B

$$L_c = \frac{S}{2} \qquad \text{if } H > \frac{S}{2}$$

$$L_c = H \qquad \text{if } H < \frac{S}{2}$$

$$U_{cb} = \int \varepsilon_c \, dx$$

$$U_{cb} = \frac{\varepsilon_{ca}+\varepsilon_{cb}}{2} * L_c$$

Assume $\varepsilon_{ca} << \varepsilon_{cb}$ Then

$$U_{cb} = \frac{\varepsilon_{cb}}{2} * L_c$$

$$Y_b = \frac{T}{\beta_1 * 0.85 * f'_c * b_e}$$

Find Y_a from geometry $\qquad Y_a = Y_b + L_c$

$$Y_o = \frac{(Y_b)^2 * (Y_a - Y_b)}{((Y_a)^2 + (Y_b)^2)} \qquad \text{(see Eq. 5.28)}$$

$$\text{Maximum Joint Rotation} = 2 * \frac{U_{cb}}{(Y_o+Y_b)} = \frac{\varepsilon_{cb} * L_c}{(Y_o+Y_b)}$$

a) Dry Joints

Figure 7.37 Prediction of joint rotation.

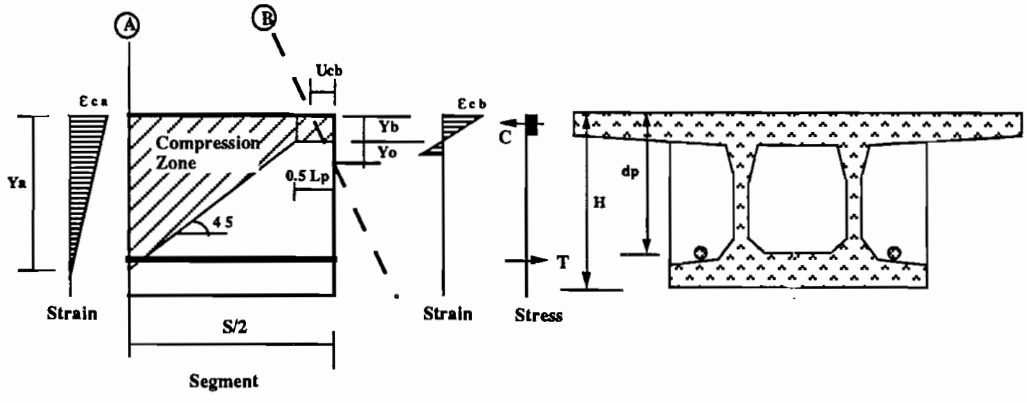

Section A	: Segment Section
Section B	: Deformed Joint Between Two Segments
S	: Segment Length
H	: Depth of Cross Section
ε_{cb}	: Maximum Concrete Strain at the Joint
U_{cb}	: Top Fiber Displacement at the Joint
Y_b	: Neutral Axis Depth at Section B
Y_o	: Depth from Neutral Axis to Center of Rotation
L_c	: Length of Compression Zone between A @ B
L_p	: Length of Plastic Region Assume = $\frac{d_p}{2}$
d_p	: Depth to Prestress Steel

$$L_c = \frac{S}{2} \qquad \text{if } H > \frac{S}{2}$$

$$L_c = H \qquad \text{if } H < \frac{S}{2}$$

$$U_{cb} = \frac{\varepsilon_{cb}}{2} * (L_c - 0.5 * L_p) + \varepsilon_{cb} * 0.5 * L_p$$

$$\text{Maximum Joint Rotation} = 2 * \frac{U_{cb}}{(Y_o + Y_b)}$$

b) Epoxy Joints

Figure 7.37 Prediction of joint rotation (continued).

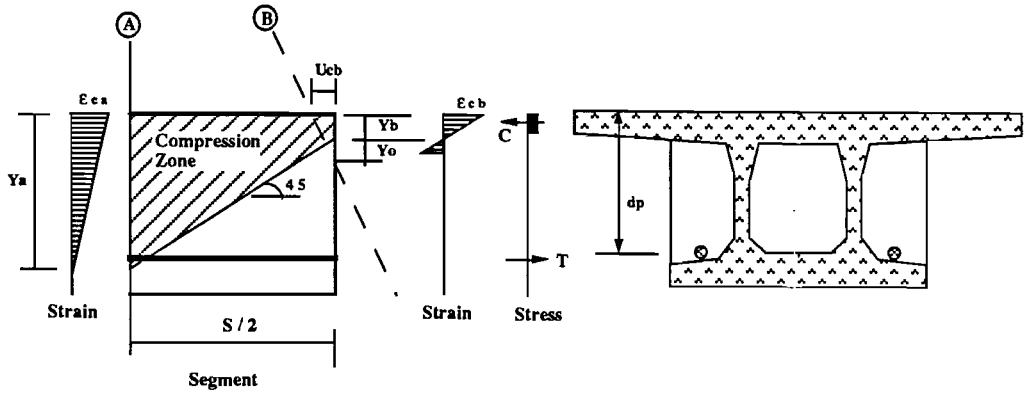

Section A : Segment Section

Section B : Deformed Joint Between Two Segments

S : Segment Length

H : Depth of Cross Section

Y_a : Neutral Axis Depth at Section A

Y_b : Neutral Axis Depth at Section B

Y_o : Depth from Neutral Axis to Center of Rotation

T : Tension Force assuming all Tendons Yielded

b_e : Effective Width (calculated according to AASHTO)

L_c : Length of Compression Zone between A @ B

L : Length of Tendon

$$L_c = \frac{S}{2} \qquad \text{if } H > \frac{S}{2}$$

$$L_c = H \qquad \text{if } H < \frac{S}{2}$$

$$Y_b = \frac{T}{\beta_1 * 0.85 * f'_c * b_e}$$

Find Y_a from geometry $\quad Y_a = Y_b + L_c$

$$Y_o = \frac{(Y_b)^2 * (Y_a - Y_b)}{((Y_a)^2 + (Y_b)^2)} \qquad \text{(see Eq. 5.28)}$$

$$\text{Change in Tendon Length} = 0.003 * L_c * \frac{(d_p - (Y_o + Y_b))}{(Y_o + Y_b)}$$

$$\text{Change in Tendon Stress} = 80 * \frac{L_c}{L} * \frac{(d_p - (Y_o + Y_b))}{(Y_o + Y_b)}$$

Figure 7.38 Simplified method for predicting ultimate tendon stress.

Table 7.16 External Tendon Change in Stress

	Current Test		C.E.B.T.P		Average
Test	Epoxied	Dry	NM3	NM4	
Measured (ksi)	70	50	38	40	
Author* (ksi)	52	45.5	32	36	
$\frac{Predicted(A^*)}{Measured}$	0.75	0.91	0.84	0.90	0.85
Author** (ksi)	27	27	32	36	
$\frac{Predicted(A^{**})}{Measured}$	0.39	0.54	0.84	0.90	0.66
CSA (ksi)	26	26	48	49	
$\frac{Predicted(CSA)}{measured}$	0.37	0.52	1.26	1.22	0.84
ACI (ksi)	36	36	35	36	
$\frac{Predicted(ACI)}{Measured}$	0.51	0.72	0.92	0.90	0.76
AASHTO (ksi)	15	15	15	15	
$\frac{Predicted(AASHTO)}{Measured}$	0.21	0.30	0.39	0.37	0.32

* Bonding and joint type effect included
** Bonding and joint type effect neglected

7.7.4.2 CSA. The Canadian Standards Association (CSA)(14) specifies a method for calculating the unbonded tendon stress as shown in Fig 7.39(a). Two corrections are needed in this method.

The first correction is that the Code specifies that tendon effective length(L_e) is equal to the tendon length divided by the number of plastic hinges required to form a mechanism in the span without mentioning that these hinges must intersect the tendon and cause an increase in tendon length.

The second correction is that the number of hinges used in calculating the effective length must take into consideration the rotation in each hinge. Only one hinge develops the full ultimate rotation while the other hinges have partial rotations according to the deflected structure. In the CSA procedure, three hinges must form in an interior span to form a mechanism and the length must be divided by three. In actual behavior, the support hinges rotate only half of the midspan hinge rotation. This means that the length must be divided by two instead of three. These corrections do not make any difference in a simply supported structure but do in a continuous structure. Results using this calculation (with the corrections mentioned above) are shown in Table 7.16.

7.7.4.3 ACI. The ACI Building Code (9) specifies equations for ultimate unbonded tendon stress as shown in Fig 7.39(b). Two equations are suggested for unbonded tendons depending on the slenderness of the girder. Results using these equations are shown in Table 7.16.

7.7.4.4 AASHTO. AASHTO (15) limits the stress increase to 15 ksi in bridge structures as shown in Fig 7.39(c). Results using the AASHTO method are shown in Table 7.16.

7.7.4.5 Comparison of Predictions with Test Data. Table 7.16 and Fig 7.40 show the comparison between the measured changes in external tendon stress and the predicted changes in tendon stress using the four methods discussed in this Section.

The method recommended by the author predicts the measured tendon stress with ratios of predicted to measured from 0.75 to 0.91. The method underestimates the tendon stress in all cases due to the assumption of a single joint opening and lower bound rigid body mechanism.

The CSA method seriously underestimates the tendon stress in the bonded tendons in the structure tested in this study with ratios of predicted to measured of 0.37 to 0.52, while it overestimates the tendon stress in the C.E.B.T.P. tests with ratios of 1.22 to 1.26.

The ACI method conservatively predicts the change in tendon stress with predicted to measured ratios of 0.51 to 0.92. AASHTO severely underestimates the change in tendon stress with predicted to measured ratios of 0.21 to 0.39.The predictions by the procedure

$$f_{ps} = f_{pe} + 725 * \left(\frac{d_p - c_y}{l_e}\right)$$

c_y : Neutral axis depth assuming tendons yielded

l_e : Length of tendon between anchors divided by number of plastic hinges required to develope a mechanism in the span under consideration

a) CSA

Span / Depth $\leq$ 35 Use lesser of

$$f_{ps} = f_{pe} + 10000 + \frac{f'_c}{100 * \rho_p}$$

$$f_{ps} = f_{pe} + 60000$$

$$f_{ps} = f_{py}$$

Span / Depth $\geq$ 35 Use lesser of

$$f_{ps} = f_{pe} + 10000 + \frac{f'_c}{300 * \rho_p}$$

$$f_{ps} = f_{pe} + 30000$$

$$f_{ps} = f_{py}$$

b) ACI

$$f_{ps} = f_{pe} + 15000$$

c) AASHTO

Figure 7.39 Methods for calculating unbonded tendon stress.

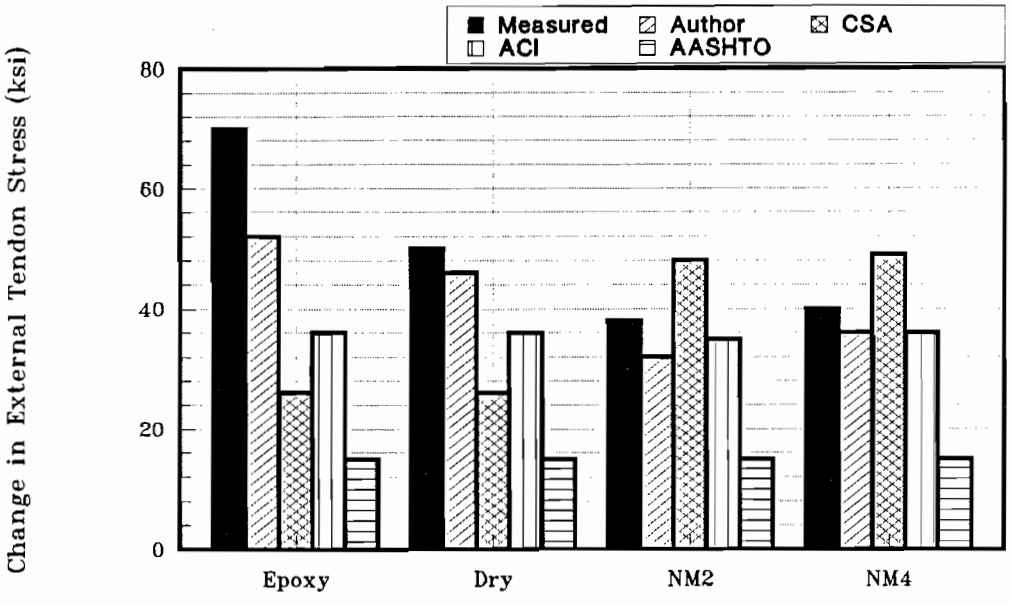

Figure 7.40 Prediction of external tendon stress.

recommended by the author were conservative , closer to the measured values than the other methods, and take into consideration the actual behavior of the segments and bonding condition of the tendon.

7.7.5 Internal Tendon Strain. The ultimate external tendon stress depends on the change in the length of the tendon. The change in tendon length can be obtained from the deflected shape of the structure. The maximum deflection of the structure depends on the allowable joint opening or rotation. The maximum joint opening can be calculated from the procedure presented in this chapter and in Chapter Four and it is controlled by the concrete stress and strain. At the same time, the joint opening should not cause any damage to the grouted internal tendons passing through that joint. The grouted internal tendons are checked by calculating their maximum strain resulting from the joint opening. The calculation procedure for the maximum tendon strain resulting from the joint opening is shown in Fig. 7.41. In this calculation procedure, the development length over which slip takes place is calculated from the increase in tendon stress and average bond strength obtained from Trost(11). The shape of the slip curve along the tendon depends on the bond-slip relationship. Chapter Five discusses the bond-slip relationship assumed in this study and the procedure to obtain the slip at any point along the tendon using the slip differential equation derived. In this calculation, a parabolic slip curve is assumed along the tendon to simplify the calculation. From the slip curve shape, an effective unbonded tendon length is assumed. The change in grouted tendon strain is calculated using the unbonded tendon length and the joint opening at the level of tendon. The internal tendon strain

should be lower than the ultimate strain of the prestressing steel otherwise the grouted tendon will fail before the joint reaches its maximum opening.

As an example, this procedure was used to calculate the internal tendon strain at the end of the flexural test carried out on the epoxy jointed exterior span.

$$D_e = 0.465\ in.$$

$$\Delta F_s = 120\ ksi$$

$$L_d = \frac{120 * 0.465}{4} * 1.0 = 14\ in. > \frac{Segment\ Length}{2}\ (13.5\ in.)$$

$$Tendon\ Strain = \frac{f_{pe}}{E} + \frac{3 * \delta}{2 * l_d}\quad (Figure\ 7.41)$$

$$= \frac{160}{27000} + \frac{3 * 0.37}{2 * 13.5} = 0.0427 < 0.0623\quad O.K.$$

The procedure predicted that the maximum internal tendon strain is 0.0427 which is lower than the ultimate strain of the prestressing steel (0.0623). The test results confirmed this calculated behavior (see Chapter Three).

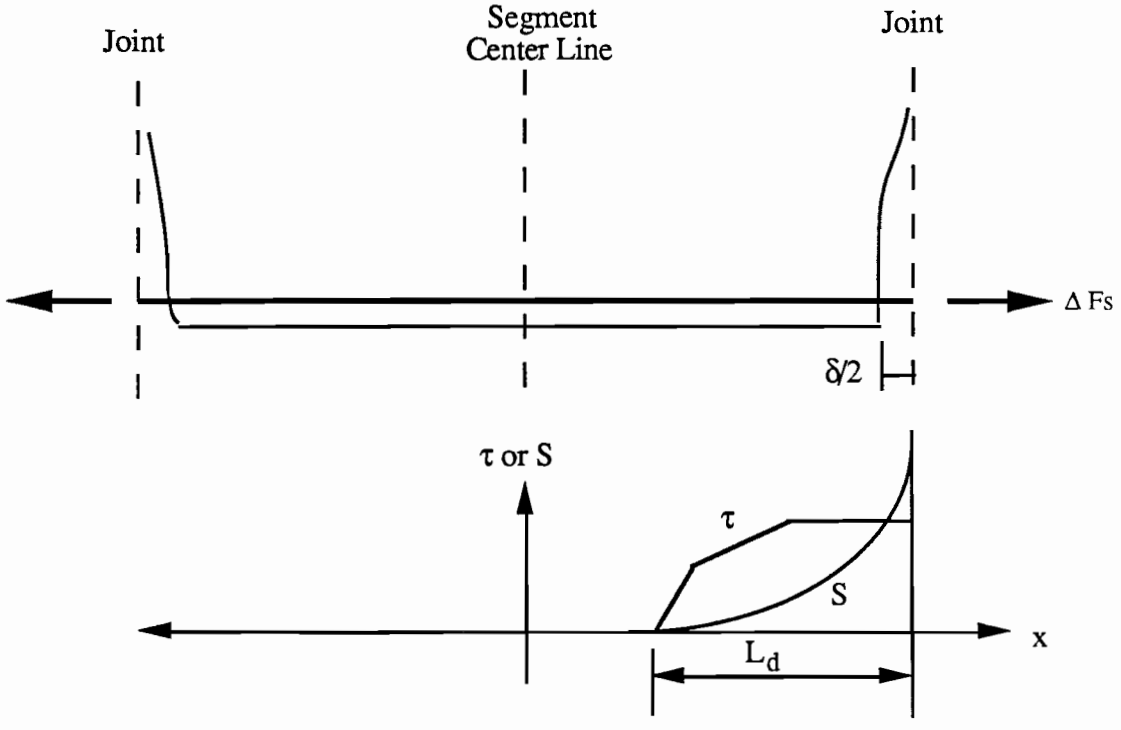

Bond & Slip along the segment

L_d :Development Length for Prestress Increase in Grouted Internal Tendon
S :Slip along the tendon
τ :Bond Strength along the Tendon
ΔF_s :Change in Grouted Internal Tendon Stress
D_e :Effective Strand Diameter (Calculated from Tendon Area)
δ :Maximum Joint Opening at Tendon Level

Assume ΔF_s= Ultimate Tendon Stress (f'_s) - Effective Prestress (f_{pe})
average τ from Bond-Slip Relation = 1.0 ksi (From Trost (11))

Calculate L_d from ΔF_s and τ

$$L_d = \frac{\Delta F_s * D_e}{4*\tau} \leq \text{Half the segment length}$$

Assume Joint opening distributed over $\frac{L_d}{3}$ in each segment

Calculate Change in Tendon Strain $= \frac{3*\delta}{2*L_d}$

$$\text{Tendon Strain} = \frac{f_{pe}}{E} + \frac{3*\delta}{2*L_d} \leq \text{Ultimate Steel Strain}$$

Figure 7.41 Ultimate strain of grouted internal tendon.

CHAPTER EIGHT

CONCLUSIONS & RECOMMENDATIONS

8.1 Introduction

An experimental and analytical investigation was conducted to determine the effect of using external tendons discretely bonded at intermediate diaphragms or using supplementary grouted internal tendons on the strength and ductility of external tendon bridges. A three-span reduced-scale segmental box girder bridge model had been constructed and tested in an earlier part of this overall program by MacGregor (1). Flexural and shear strength tests were conducted in that part of the program to examine the effect of joint type (epoxy vs dry joints) on the stiffness, strength, and ductility of the model. The current portion of the program consists of further experimental tests with improved bonding techniques, tests with supplemental internal tendons, and analytical examination of these effects.

The current experimental studies were performed in three phases. In the first phase, a complete evaluation and repair was carried out to determine the condition of the previously overloaded model and to restore it to a good condition before the beginning of further testing. In the second phase, flexural tests were conducted on the model to examine the effect of incremental discrete bonding of the external tendons to intermediate diaphragms. Flexural strength tests were conducted at the end of the second phase to examine the effect of discrete bonding of the external tendons to all (10) intermediate diaphragms in each span on the strength and ductility of the model. In the third phase, flexural strength tests were conducted to examine the effect of supplementary ungrouted or grouted internal tendons on the strength and ductility of this kind of structure. The experimental portion of the study was presented in Chapters Two, Three, and Four.

The analytical study was also carried out in three stages. In the first stage, a non-linear finite element computer program which modelled the effects of concrete cracking and slipping of external and internal tendons was developed and implemented by the author. In the second stage of the analytical study, the analytical model was verified by comparing the program predictions with experimental measurements from the current study as well as results of tests reported in the literature. In the third stage, an analytical examination of a range of critical variables was carried out. The analytical portion of the study was presented in Chapters Five, Six, and Seven.

The conclusions and design recommendations presented in this chapter are based on experimental test results and analytical studies of span-by-span segmental construction with external or mixed (external and internal) tendons. Their applicability may be limited to span-by-span segmental construction, although some of the general characteristics should also apply to cantilever-constructed bridges. The tests and computer program results

indicated that both discrete bonding of external tendons and/or using grouted internal tendons improved the strength and ductility of this type of construction.

In this chapter, behavior observations and conclusions are summarized from the test data and analytical results. Finally, design recommendations and primary conclusions are presented to assist designers in the development of improved structures.

8.2 Behavior

The following observations and detailed conclusions are drawn from the tests and analytical studies which examined and documented the full range of behavior of a typical span-by-span constructed three-span segmental box girder bridge with external or mixed (external and internal) tendons.

8.2.1 Observations.

1) The epoxied-joint exterior span was uncracked at service load levels and a design live-load-plus-impact deflection of 0.049 in. (span/6122) was measured. The dry-joint exterior span had no joints open at service-load levels and a design live-load-plus-impact deflection of 0.055 in. (span/5455) was measured in the test. The live load deflection of the epoxied-joint exterior span was 12 percent lower than the dry-joint exterior span. The difference in the live load deflections was most probably due to partial contact between match-cast segments due to differential shrinkage in the segments in the dry-joint span. However, in the epoxied-joint span the epoxy filled these spaces and restored the contact area between the segments in the epoxied-joint span resulting in a higher effective stiffness.

2) Under the application of design live loads, the measured tendon stress changes in the midspan region were less than 2.5 ksi even when the external tendons were bonded to all intermediate diaphragms. Tendon slip was not noticed at service load levels during testing but the computer analysis predicted some small tendon slip at design live load levels. The bond-slip relationship for external tendons obtained by Radloff (10) from tests conducted as part of this study was used in the analytical studies. It assumes that no bond stress can be developed at the diaphragm unless small slip occurs. At deviators with small deviation angles (small friction forces), the analytical results indicated a small slip at design live load levels.

3) The repaired epoxied-joint exterior span cracked adjacent to the critical joint and not through the epoxy material itself at a live load approximately 1.8 times the load at which the previously cracked joint opened in the same span. This indicates substantial reserve capacity against cracking in the epoxied-joint construction as well as the efficacy of the crack injection processes used in the repair.

4) Failure of each of the exterior spans in flexure due to crushing of the top flange occurred only after development of a lower-bound plastic mechanism in which the critical joint in the midspan region of the exterior span reached its ultimate rotation capacity and crushed, while the joint in the center span at the interior face of the interior pier segment opened but to less than its maximum rotation capacity.

5) The concrete compressive strains at the joints were higher than those away from the joints along the length of the segments. Crushing of the concrete at the joints in all flexural strength tests indicated that the compressive strains in these joints were much more critical than those in the segments.

6) Discrete bonding of external tendons at deviators and pass-through location in diaphragms increased the number of opening joints in the midspan region of the two exterior spans during flexural strength tests. In the epoxied-joint exterior span, one joint opened (test performed by MacGregor(1)) in the partially bonded case (4 external tendons were discretely bonded to four deviators while two external tendons were discretely bonded to two deviators in each span). In this series of tests, three joints opened for the fully-bonded case (all external tendons were discretely bonded to all intermediate diaphragms). In the dry-joint exterior span, two joints opened in the partially-bonded case, while three joints opened in the fully-bonded case.

8.2.2 Detailed Conclusions.

1) Discrete bonding of external tendons and/or using grouted internal tendons increased the number of opening joints or wide cracks by increasing the critical joint stiffness and strength and reducing the opening moment or cracking moment of the adjacent joints (adjacent to the critical midspan joint). Discretely bonded external tendons or grouted internal tendons increased the joint stiffness due to the reduction in the effective unbonded tendon length which resulted in higher moment capacity being developed for the same joint rotation. Increasing the midspan stiffness relative to the support joint stiffness attracted higher moments to the midspan region. Higher critical joint strength delayed the critical joint crushing and gave the adjacent joints a better chance to open widely before failure of the critical joint. The stress change in a discretely bonded external tendon depends on the concrete deformation (sum of the joint openings) between the bonded points (if slip effect is neglected). Thus, discretely bonded and/or grouted tendons could develop higher stresses at the opened joint and lower stresses at the adjacent unopened joints. The higher tendon stress at the critical joint was due to lower effective unbonded length, while the lower tendon stress at the adjacent joint was due to lower concrete deformation (adjacent joint opening). The lower tendon stresses at the adjacent joints resulted in lower cracking or joint opening moment in the adjacent joints. Higher external moments and lower joint opening or cracking moments resulted in a larger number of opening joints and larger total joint opening in the midspan region.

2) Ductility increased substantially with the increasing percentage of discretely bonded external tendons and/or grouted internal tendons. Discrete bonding of external tendons increased the ductility by 75 percent in the epoxied-joint exterior span and by 47 percent in the dry-joint exterior span. The bonded or grouted tendons increased the number of opening joints which resulted in higher total joint opening in the midspan region and higher midspan deflection.

3) Ductility was increased appreciably with increasing percentage of discretely bonded external tendons or grouted internal tendons, to a certain point. A relatively simple procedure was developed to calculate this critical percentage of discretely bonded tendons or grouted internal tendons (see Recommendation No. 1). Above that value, the efficiency of increasing the ductility by using further bonded or grouted tendons was reduced. The increase in maximum deflection was due to the increase in total joint opening in the midspan region. Increasing the number of bonded or grouted tendons above the number required to open all possible opening joints had only a small effect in increasing the total joint opening. Since all possible joints were already opened, the increase in number of bonded tendons would not increase the number of opening joints but might slightly increase the amount of the joint openings. In fact, the increase in the number of bonded or grouted tendons increases the ultimate compressive force (bonded or grouted tendons reach a much higher stress at ultimate than unbonded tendons) in the joint section and reduces the maximum joint rotation which resulted in some reduction in ductility.

4) Discretely-bonded external tendons and/or grouted internal tendons increased the possible change in external tendon stress under ultimate loading. Discretely-bonded external tendons or grouted internal tendons increased the maximum total joint opening in the midspan region which resulted in greater changes in tendon length. Discrete bonding of the external tendons or grouting the internal tendons reduced the effective unbonded tendon length. Greater changes in tendon length with smaller unbonded length resulted in much higher tendon stresses being developed.

5) Strength was increased substantially by discrete bonding of the external tendons and/or using grouted internal tendons. Bonding the external tendons increased the live load capacity by 33 percent in the epoxied-joint exterior span and by 23 percent in the dry-joint exterior span. Discretely-bonded external tendons or grouted internal tendons increased the total joint opening in the midspan region which resulted in larger increases in the tendon length and higher tendon stresses. Higher tendon stresses resulted in higher moment capacity and higher strength.

6) Maximum joint opening or rotation was higher in the epoxied-joint span than in the dry-joint span. Crack patterns in the epoxied-joint span were different than those in the dry-joint span which caused a larger effective volume of the highly compressed region to be mobilized with a consequent reduction in the concentration of the

compressive strain. At maximum concrete strain, the flange compressive deformation was increased and resulted in greater joint rotation (Section 4.6.1).

7) Maximum allowable joint openings or rotations were reduced with the increase in compressive forces in the joint section. Higher compressive force increased the depth to the neutral axis and reduced the maximum joint rotation.

8) Maximum allowable joint rotation depended on the segment dimensions (segment depth (H) and segment length (S)), depth to the neutral axis, maximum concrete strain (which is affected by the level of confinement in the compression zone), section effective depth (d_p), and joint type (dry joints or epoxy joints)(Section 4.6.2.2).

9) Epoxy joints affect the ductility and strength of segmental bridges. Epoxy joints had two almost opposing effects on strength and ductility. The first effect seemed to be due to the cracking patterns in the epoxy joints (see Item No. 6) and the ability of the epoxy to smooth out local contact stresses between the match cast segments. These effects seemed to allow the epoxy joint to develop a higher maximum concrete strain, and hence, higher joint rotations than the dry joints. This resulted in higher total joint opening in the midspan region which resulted in higher external tendon stresses, strength, and ductility. The second effect was due to the fact that the cracking moments at the epoxy joints are higher than the joint opening moments of the dry joints. This resulted in delaying the joint opening until higher load levels, and sometimes, in reducing the number of opened joints. This effect tended to reduce the total joint opening, external tendon stress, strength, and ductility.

10) The net effect of using epoxy joints depends on the percentage of discretely bonded external tendons or grouted internal tendons. Discretely bonded external tendons or grouted internal tendons reduce the second effect of using epoxy joints by forcing the adjacent joints to open widely before the critical joint fails. The second effect (see No. 9) seemed to dominate in the tests performed by MacGregor(1) (external tendons discretely bonded to only two or four diaphragms in each span) because only one joint opened in the mid-span region during those tests. The first effect (see No. 9) seemed to dominate in the current tests because the external tendons were discretely bonded to all ten intermediate diaphragms in each span and three joints opened in the mid-span region during these tests.

11) Discretely bonded external tendons or grouted internal tendons increased the moment redistribution in these continuous structures. Discretely bonded or grouted tendons increased the total joint opening in the critical region which resulted in higher moment redistribution from the critical region to other sections.

12) Discrete bonding of external tendons at two deviators in each span substantially increased the strength and ductility. Further discrete bonding of external tendons to

a single diaphragm in each segment caused a relatively small increase in the strength and ductility. Due to the nature of the loads (moving loads), each joint can be critical under some possible placement of loads. Thus, discrete bonding should be provided in such a way as to increase the strength and ductility of all joints. Discrete bonding to a diaphragm in each segment should improve the strength and ductility of all joints by reducing the effective unbonded tendon length at all the joints. However, if only two diaphragms or deviator blocks are used in each span to deviate the external tendons, and if tendons are to be discretely bonded only at these deviators, the location of these two diaphragms should be selected to divide the tendon length into approximately equal pieces. This should result in improving the strength and ductility of all the joints.

8.3 Analysis

The following observations and detailed conclusions are drawn from the analytical model incorporated in the computer program Bridge, its prediction of the model behavior, and its use to study a range of variables. The program was verified by comparing its predictions with the data obtained in this study and with the results of the CEBTP tests (4) conducted in France.

8.3.1 Observations.

1) The analysis developed by the author and presented in Chapter Five predicted the load-deflection behavior of the three-span segmental girder in a very precise manner up to the load at which a flexural crack or joint started opening. In this part of the analysis, the modelling was performed using classical non-linear finite element analysis. The modelling included slip of the external tendons based on an empirically obtained bond-slip relation, and excluded cracking of the concrete.

2) The analysis predicted the ultimate behavior of the beams very well. The program predicted load capacity within 10 percent of the measured strength, while it predicted the ultimate displacement within 15 percent of the measured ultimate displacement. The program predicted ultimate external tendon stresses with a maximum difference of 12 ksi from the measured values. The program predictions for changes in external tendon stresses were a substantial improvement over current design code values.

8.3.2 Detailed Conclusions.

1) The assumption used for the limiting concrete strain plays a major role in predicting the ultimate behavior of the structure which is terminated at the stage at which critical joints crush. Due to concentration of rotations at the critical joints, externally post-tensioned segmental structures have the possibility of premature failure at these joints. The ultimate concrete strain determines when the structure will fail. The

ultimate concrete strain limit should be chosen taking into consideration the confinement of the concrete flanges and the type of joint. Unless confinement of the flanges is examined in more detail, the maximum concrete strain should be assumed as 0.003 for dry joints and 0.0035 for epoxy joints.

8.4 Design Recommendations

1) Maximum allowable joint opening or rotation can be calculated by the procedures suggested by the author in Sections 7.7.2 and 4.6.6.2. The calculation methods are based on the actual behavior of the segments observed during testing. The two calculation methods, one for epoxy joints and the other for dry joints, take into consideration the difference between the cracking pattern for epoxy joints and dry joints. The predictions of the methods were very close to the measured maximum joint openings from the current study and from the CEBTP(4) tests carried out in France. The average ratio of the measured to predicted joint opening was 1.2. In addition it is important to note that all predictions were conservative.

2) The ultimate external tendon stress corresponding to nominal flexural strength (f_{ps}) is dependant on many factors. The effective prestress (f_{pe}) after allowance for all prestress losses is the primary variable. Other factors that may influence (f_{ps}) in segmental construction are: the maximum joint opening or rotation, the number of opening joints in the critical region, and the ratio of the section effective depth to the effective unbonded tendon length.

3) The method recommended for predicting the ultimate external tendon stress (f_{ps}) is based on these assumptions:

   i. Rigid Body Mechanism.

      The structure can be modeled as rigid segments connected by hinges at the opened joints. The structure has no deformation unless a joint is opened and a hinge is formed. The elastic curvature is neglected and the joint openings provide the only increase in tendon length.

   ii. Single Joint Openings.

      It can be assumed that a single joint opens in the critical hinge region. This assumption will result in a conservative estimate of ultimate tendon stress since, in some cases, more than one joint opens in each hinge region. The number of opening joints depends on the discrete bonding conditions of the external tendons, percentage of discretely bonded external tendons, percentage of grouted internal tendons, and segment length.

iii. Lower Bound Theorem.

In actual concrete structures, the maximum rotation capacity of the plastic hinges is limited by the curvature capacity of the segments. An ideal rigid body mechanism cannot be used since it assumes unlimited joint rotation and represents an upper bound limit to the true strength. A lower bound theorem, in which one hinge (critical opened joint) is allowed to reach its maximum strength and rotation while the other hinge locations (opened joints) have rotations less than their maximum rotation, can be used to obtain the deflected shape of the structure.

The change in tendon length can be calculated from the deflected shape of the structure. Joint openings at the level of the tendon are the only increase in tendon length. These openings can be calculated from the joint rotations obtained from the deflected shape of the structure(Lower bound theory). The change in external tendon stress can be calculated from the change in tendon length and the effective unbonded tendon length (distance between the anchorages or the discretely bonded points). For more details and examples see Sections 7.7.4.1 and 4.10.

4) The following simplified design method can be used to calculate the ultimate external tendon stress.

$$f_{ps} = f_{pe} + 80 * \frac{L_c}{L_e} * \frac{(d_p - (Y_o + Y_b))}{(Y_o + Y_b)} \quad (ksi)$$

but not to exceed f_{py}.

where

f_{ps} = the tendon stress corresponding to nominal strength (ksi).

f_{pe} = effective stress in the prestressed tendon after allowance for all prestress losses (ksi).

f_{py} = yield stress of the prestress steel (ksi).

d_p = distance from the extreme compression fiber to center of prestress tendon (in.).

Y_b = distance from extreme compression fiber to the neutral axis in the joint section calculated using factored material strengths and assuming the tendon prestress has yielded (in.).

L_c = length of compression zone in the segment taken as equal to the lesser of section depth or half segment length (see Section 4.6.2.2) (in.).

Y_a = distance from extreme compression fiber to the neutral axis in the segment section (in.). $Y_a = Y_b + L_c$

Y_o = distance from the neutral axis to the center of rotation of the joint (in.) and calculated from (see Equation 5.28 Chapter Five):

$$Y_o = \frac{(Y_b)^2 * (Y_a - Y_b)}{((Y_a)^2 + (Y_b)^2)}$$

L_e = effective length of the tendon

$$L_e = \frac{L}{(1 + \frac{N_s}{2})} \quad (in.)$$

where

L = length of tendon between anchorages or discretely bonded points (in.)

N_s = number of support hinges crossed by the tendon between the anchorages or the discretely bonded points.

This simplified method neglects the effect of joint type on the maximum joint opening. It assumes that the effective depth of the tendon (d_p) is the same at all hinge locations. The method discussed in item No. 3 is more general.

5) The calculation procedure for the ultimate tendon stress presented in Items No. 3 and 4 is based on the assumption that no slip occurs at the discretely bonded points. If the stress difference across the diaphragm is higher than the ultimate bond strength, appreciable slip between the tendon and diaphragm takes place and a stress correction is needed. In this case, part of the change in tendon length will be distributed over a longer length (the effective tendon length between the adjacent discretely bonded diaphragms) (see Sections 7.7.4.1 and 4.10).

6) The maximum strain in internal tendons passing through an open joint depends on the maximum joint opening and the bond-slip relation. The joint opening should not cause any damage to the grouted internal tendon, and the tendon strain should be lower than the ultimate strain of the prestressing steel. A simple calculation procedure for the internal tendon strain is presented in Section 7.7.5.

7) The percentage of grouted internal tendons or discretely bonded external tendons to be used in the critical region should be high enough to force a second joint in the critical region to open widely before the critical joint fails. This recommendation is based on the test observation that discretely bonded external tendons or grouted internal tendons increased strength and ductility by increasing the number of opening joints. The second joint opens when the external applied moment on the joint section is higher than the joint opening moment of the dry joint or the cracking moment of the epoxy joint. The basic procedure is that the calculated moment at the adjacent joint when the critical joint is close to its ultimate capacity must be higher than the cracking or the joint opening moment of the adjacent joint. Section 7.7.1 presents a detailed calculation procedure and gives a full derivation for the required percentage of discretely bonded or grouted tendons in a dry-joint span in order to insure that a second joint will open.

8.5 Primary Conclusions

Based on this experimental and analytical study of segmental box-girder construction with external or mixed tendons reported in this dissertation, the primary conclusions are:

1) Discretely bonded external tendons and/or grouted internal tendons substantially increased the strength and ductility of the three-span segmental model.

2) The percentage of discretely bonded external tendons or grouted internal tendons provided should be enough to insure that a second joint in the critical region will open prior to complete failure. This will ensure higher external tendon stress, strength, and ductility.

3) The span with epoxy joints exhibited cracking patterns which resulted in higher maximum joint rotations than were experienced in the dry-joint span. The crack patterns in the epoxied-joint span also permitted use of a somewhat higher compression strain limit (0.0035 rather than 0.003) resulting in higher strength and ductility for the epoxied-joint span.

4) Discrete bonding of external tendons at the piers and at two locations in each span will generally improve ductility by forcing more than a single joint to open in the critical region.

REFERENCES

1. MacGregor, R.J., Kreger, M.E. and Breen, J.E., "Evaluation of Strength and Ductility of a Three-Span Externally Post-Tensioned Box Girder Bridge Model," unpublished Ph.D. Dissertation, The University of Texas at Austin, August 1989.

2. Powell, L.C., Kreger, M.E., and Breen, J.E., "State of the Art for Externally Post-Tensioned Bridges with Deviators," The University of Texas at Austin, Center for Transportation Research, Research Report 365-1, June 1988.

3. VSL External Post-Tensioning, April 1988, VSL International Ltd., Berne, Switzerland.

4. Foure, B., and Martins, P., "Flexural Behavior up to Failure of Externally Prestressed Concrete Beams," Proceedings of XI FIP Congress, June 1990, Hamburg, pp. 195-215.

5. El-Habr, K.C., "Finite Element Analysis of Externally Prestressed Segmental Construction," Unpublished M.S. Thesis, The University of Texas at Austin, May 1988.

6. Muller, J., and Gauthier, Y., "Ultimate Behavior of Precast Segmental Box-Girders with External Tendons," Proceedings of the International Symposium on External Post-Tensioned Bridges, Houston, Texas, October 1988.

7. Giuriani, E., "Theoretical Analysis of the Early Stage in Reinforced Concrete Beams," C.E.B. Bulletin No. 153, 1982.

8. Mattock, A.H., Kriz, L.B., and Hognestad, E., "Rectangular Concrete Stress Distribution in Ultimate Strength Design," ACI Journal, Proceedings 1961, Vol. 57, pp. 877-928.

9. American Concrete Institute Committee 318, "Building Code Requirements for Reinforced Concrete (ACI 318-89)," American Concrete Institute, Detroit, Michigan, 1989.

10. Radloff, B., "Bonding of External Tendons at Deviators," unpublished M.S. Thesis, The University of Texas at Austin, December 1990.

11. Trost, H., Cordes H., Thormahln, U., and Hagen, H., "Verbundfestigkeit von Spanngliedern und ihre Bedeutung fur Ribbilung und Ribbreietenbeschrankung," Deutscher Ausschuss Fur Stahlbeton, Heft 310, W. Ernst and Sohn, Berlin, West Germany, 1980.

12. Ford, J.S., and Breen, J.E., "Behavior of Unbraced Columns in Unbraced Multipanel Frames," unpublished Ph.D. Dissertation, The University of Texas at Austin, December 1977.

13. Virlogeux, M., "Non-linear Analysis of Externally Prestressed Structures," Proceedings of XI FIP Congress, June 1990, Hamburg, pp. 165-193.

14. Canadian Standards Association Committee A23.3, "Design of Concrete Structures for Buildings CAN3-A23.3-M84," Canadian Standards Association, Ottawa, Ontario, 1984.

15. AASHTO, "Standards Specifications for Highway Bridges," 14th Edition, American Association of State Highway and Transportation Officials, 1989.

16. Post-Tensioning Institute, "Design and Construction Specifications for Segmental Concrete Bridges," Final Report on NCHRP Project 20-7/32, February 1988.

17. Sowlat, K., and Rabbat, B.G., "Testing of Segmental Girders," Final Report to Figg and Muller Engineers, Inc., Project No. 0217, July 1984.

18. Naaman, A.E., "Partially Prestressed Concrete: Review and Recommendations," PCI Journal, Vol. 30, No. 6, Nov. 1985, pp. 30-71.

19. Mattock, A.H., Yamazaki, J., and Kattula, B.T., "Comparative Study of Prestressed Concrete Beams with and Without Bond," ACI Journal, No. 2, Vol. 68, Feb. 1971, pp. 116-125.

20. Beaupre, R.J., Powell, L.C., Breen, J.E., and Kreger, M.E., "Deviation Saddle Behavior and Design of Externally Post-Tensioned Bridges," The University of Texas at Austin, Center for Transportation Research, Research Report 365-2, July 1988.

21. Virlogeux, M., "Non-Linear Analysis of Externally Prestressed Structures," Proceedings of the FIP Symposium, Jerusalem, September 1988.

22. Sowalt, K., and Rabbat, B.G., "Testing of Segmental Concrete Girders with External Tendons," PCI Journal, March-April 1987, pp. 86.

23. Trost, H., Cordes, H., Thormahln, U., and Hagen H., "Auswirkungen des Verbundverhaltens Zwischen Spannglied und Einpressmoretel Bei Verwendung Von Spanngliedern Mit Uber 1500 Kn Zulassiger Spannkraft," Technischen Hochschule Aachen, July 1978.

24. Martins, R., "Modelisation du comportement jusqu's la rupture en flexion de poutres en beton a precontrainte exterieure ou mixte," These de Doctorate de l'Ecole Centrale de Paris, September 1989.

25. Eibl, J., "On Some External Prestressed Bridges in Germany," FIL-Xith International Congress on Prestressed Concrete, Hamburg, 4-9 June 1990, pp. B69-B74.

26. Naaman, A.E., "An Approximate Nonlinear Design Procedure for Partially Prestressed Concrete Beams," Computers & Structures, Vol. 17, No. 2, 1983, pp. 287-299.

27. Naaman, A.E., "Ultimate Analysis of Prestressed and Partially Prestressed Sections by Strain Compatibility," PCI Journal, Jan. 1977, Vol. 22, No. 1, pp. 32-51.

28. Naaman, A.E., "Proposal to Extend Some Code Provisions on Reinforcement to Partial Prestressing," PCI Journal, Vol. 26, No. 2, March 1981, pp. 74-91.

29. MacDonald, J.E., "Epoxy Injection of A Gate Pier," Concrete International, August 1986, pp. 34-38.

30. Trout, J.F., and Santangelo, S., "Epoxy Injects New Life into Bridge Pier," Concrete International, August 1986, pp. 39-43.

31. Ojha, S., "Rehabilitation of a Parking Garage," Concrete International, April 1986, pp. 24-28.

32. Guedelhoefer, O.C., and Krauklis, A.T., "To Bond or Not to Bond," Concrete International, August 1986, pp. 10-15.

33. Pashina, B.J., "Crack Repair of Precast Concrete Panels," Concrete International, August 1986, pp. 22-26.

34. Popovics, S., "A Review of Stress-Strain Relationships for Concrete," ACI Journal Proceedings 1970, Vol. 67, No. 3, pp. 243-248.

35. Lin, T.Y., and Burns N.H., Design of Prestressed Concrete Structures, Third Edition, John Wiley, 1981.

36. Libby, J.R., Modern Prestressed Concrete: Design Principles and Construction Methods, Van Nostrand Reinhold Col., N.Y. 1984.

37. Weaver, J.W., and Johnston, P.R., Finite Elements for Structural Analysis, Prentice Hall, Englewood Cliffs, N.J., 1984.

38. Zienkiewicz, O.C., The Finite Element Method, 3rd Edition, MacGraw-Hill Ltd., London, 1977.

39. Bathe, K.J., Finite Element Procedures in Engineering Analysis, Prentice Hall, Englewood Cliffs, N.J., 1982.

40. Shanafelt, G.O., and Horn, W.B., "Damage Evaluation and Repair Methods for Prestressed Concrete Bridge Members," National Cooperative Highway Research Program, Report No. 226.

41. Shanafelt, G.O., and Horn, W.B., "Guidelines Evaluation and Repair for Prestressed Concrete Bridge Members," National Cooperative Highway Research Program, Report No. 280, 1985.

42. Hindi, Azez Nefei A., "Enhancing the Strength and Ductility of Post-Tensioned Segmental Box-Girder Bridges," unpublished Ph.D. Dissertation, The University of Texas at Austin, December 1990.